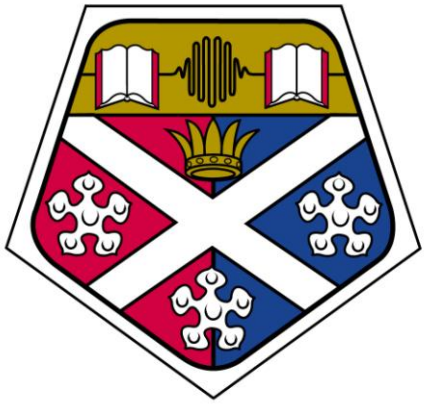

Identification of electric power system dynamic equivalent

A thesis submitted for the degree of
Doctor of Philosophy
at the University of Strathclyde

by

Thamvarit Singhavilai

Supervisor: Professor K. L. Lo

Power Systems Research Group
Department of Electronic and Electrical Engineering
University of Strathclyde
Glasgow, United Kingdom

January 2011

Declaration of author's rights

This thesis is the result of the author's original research. It has been composed by the author and has not been previously submitted for examination which has led to the award of a degree.

Signed: Date:

Acknowledgements

First, I would like to thank my principal supervisor Professor K. L. Lo in providing guidance and useful comments throughout my PhD study. Without Professor Lo, my goal of submitting my thesis would not have been accomplished. Thanks also to my second supervisor Dr.Olympo Anaya-Lara for his guidance and support.

Second, I would like to thank the Royal Thai Government and Faculty of Engineering, Mahidol University for the scholarship and their financial support.

Third, special thanks to Assistance Professor Somchai Chatrattana for the inspiration to pursue my study in the area of power system. Many thanks to Nattaka Yokakul and her family for their emotional support and encouragement during my study.

Last but not least, I am very grateful to thank my parents back home, my mother (Arpha) and my father (Chaiwat), for their understanding, support, caring thought and greatest love.

Thamvarit Singhavilai

17 January 2010

Abstract

This thesis is devoted to the identification of electric power system dynamic equivalent for online application which calls for the equivalent featuring high reliability but limited modelling data use. The aim is to develop dynamic equivalent based on grey-box approach where recorded responses at boundaries are used together with partial modelling data (i.e. only power flow modelling data) to construct the dynamic equivalent.

The proposed identification-based dynamic equivalencing method consists of three major steps: coherent generator identification from power flow modelling data, determination of an appropriate model structure for the equivalent of the external part (i.e. a reduced set of equations without the values of their coefficient) from the knowledge of coherent generators, and parameter identification of the model structure without a complete system simulation. The obtained equivalent is modelled by a combination of equivalent generators, equivalent transmission lines, and equivalent shunts. Therefore, it can be directly implemented into conventional power system software without any modification.

A node weighted graph model and its coherency theorem are employed to develop the coherent generator identification. The node weighted graph model represents power system dynamic model in the way that parameters of generators and of transmission network are presented in different components of the graph. Therefore it allows making an assumption to identify coherent generator by using only power flow modelling data.

An aggregation process of coherency-based dynamic equivalent is adapted to develop a procedure to determine the model structure for the equivalent of the external part. The procedure is straightforward except that no generator parameters are used. This results in the sets of equations which represent the model structure preserving the form of conventional power system components (i.e. equivalent generator, reduced transmission lines, and equivalent shunts). As the model structure for the equivalent is determined based on knowledge of coherent generator rather than an intuitive choosing, the obtained dynamic equivalent would be more reliable.

The values of the parameters of the model structure, in particular the parameters of equivalent generators, are identified by using non-linear optimisation technique to fit the responses of the reduced model (i.e. internal part and external equivalent) with

that of the original system. In order to reduce the time usage during the parameter identification process, the parameter identification technique that does not require a complete system simulation is developed. The technique is based on re-formulation of the obtained model structure as the input-output model. One set of recorded responses at boundaries is used as the input while another set is used as the original response for fitting. By using this technique, only external equivalent is needed to be simulated during fitting process. Therefore, the total usage time would be greatly reduced.

Finally, the proposed identification-based dynamic equivalencing method has been applied to IEEE39 bus and IEEE118 bus system for extensive performance evaluation.

Publications

Singhavilai, T., Anaya-Lara, O., Lo, K. L., "Identification of dynamic equivalent of a power system," in the proceedings of 44th Universities Power Engineering Conference (UPEC), Glasgow, 2009.

Lo, K. L., Singhavilai, T., Anaya-Lara, O., "Identification-based dynamic equivalent of power system". Under preparation for submit to IET journal.

Singhavilai, T., Anaya-Lara, O., Lo, K. L., "Graph model-based coherent generator identification". Journal paper, under preparation.

Singhavilai, T., Anaya-Lara, O., Lo, K. L., "Parametric identification of dynamic equivalent". Journal paper, under preparation.

Singhavilai, T., Anaya-Lara, O., Lo, K. L., "Identification of equivalent generator paramters without full system simulation". Journal paper, under preparation.

Table of contents

List of tables

List of figures

CHAPTER 1

INTRODUCTION

1.1 Introduction

External equivalent is a simplified model for replacing an uninterested part, known as an external part, of a power system model. This replacement aims to reduce the dimension of the original model whilst the part of interest remains unchanged. The model reduction through using equivalent expects to provide a reduced model that can perform detailed studies of the interested part in cost-effective way, for instance requiring less computing resources (time and memory) while retaining acceptable accuracy. Hence, more analysis can be performed within available resources [1].

According to type of analysis, there are two kinds of equivalents known as Static Equivalent and Dynamic Equivalent. The static equivalent is an equivalent model applied in steady state analysis, in particular power flow analysis. The dynamic equivalent is an equivalent model applied in dynamic analysis and may be further divided into three broad categories according to their dynamics of interest: high frequency equivalent, low frequency equivalent, and wide-band equivalent[2]. The first two categories correspond to the equivalents of electromagnetic transient model and electromechanical transient model, respectively, while the equivalent that is able to represent both high and low frequency dynamics of power system falls into the wide-band category. The problem of deriving and utilising static equivalent is practically solved and the reviews of major techniques are documented [3-6]. However, there is still need for the dynamic equivalent, especially the low frequency equivalent.

The low frequency equivalent or electromechanical equivalent has received high attention as it benefits the angle stability analysis of a power system; and it has been extensively developed since 1960s. Despite a long development in conjunction with

a dramatic progress in computer performance, the need for further research in dynamic equivalent is still required.This is because a recently arising unconventional power system model from connection of power electronics [2, 7] as well as a changing of analysis environments towards online that place more constraints on equivalencing method and its equivalent model[8]. In this thesis, attention is directed to the second topic - for online application.

This chapter set out to give an overview of dynamic equivalent. Equivalencing approach and equivalent model are firstly reviewed, and then the challenging issues are addressed. Research aim and objectives, research methodology, and contribution of thesis are next discussed. Finally, the organisation for the rest of thesis is given.

1.2 Review of dynamic equivalent

This review is divided into two parts. The first part discusses equivalencing approach and equivalent models as these are fundamental aspects of dynamic equivalencing. Instead of focusing on the development and the details of well accepted methods, selected literatures are brought to show a variety of equivalencing methods and equivalent models. The second part addresses the challenging issues involving the current need of development, in particular dynamic equivalent for online application, and discusses the possible solutions of these challenging issues.

1.2.1 Equivalencing approach and Equivalent model

From the modeling point of view[9], the dynamic equivalent may be constructed by following two distinct frameworks: Analytical framework and Identification framework. In the analytical framework, the construction of dynamic equivalent is based on an application of laws from various disciplines such as mathematics, linear system theory, and non-linear system theory to reduce an original model. By contrast, the dynamic equivalent is determined by adjusting an assumed model until its response matches the response from the original model or field measurements when using identification framework approach. From these two distinct frameworks

and their combinations, a variety of dynamic equicalencing has been developed and may be classified into three approaches, similar to the classification of modelling[10], and can be named as White box approach, Black box approach and Grey box approach as shown in Figure 1.

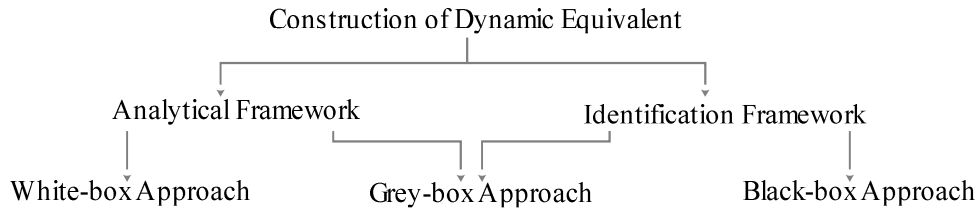

Figure 1.1 Overview of construction of dynamic equivalent

The white box approach is purely based on the analytical framework. It is normally applies when a complete set of modelling data (e.g. model, parameter values, and operating status) is available and the parts to be equivalenced are represented by simple models. Most researchers have paid attention on this approach because the obtained dynamic equivalent is reliable and has a high possibility of keeping physical insight. Two of the well accepted methods are Coherency-based methods [11-14] and Modal-based methods [15, 16].

The black box approach is purely based on identification framework. It applies when the access to the modelling data is limited or the parts to be equivalenced are represented by more complex models and where there is a lack of analytical techniques. Even though it sounds practical, research works based on this approach are much fewer than the previous approach and are quite diverse due to different opinions on choosing the type of model representing the equivalent. Many types of models, such as differential equation model in fictitious generator formulation [17], stochastic model [18], and nonparametric model based on artificial neural network [19], have been tried and claimed successful results. However, since the part to be equivalenced is treated as unknown, their true capability and validity are difficult to justify because there are no any other evidences to prove except a testing on different set of training data.

The grey box approach is a combination of the white box and black box approaches to compromise for a particular practical solution. A traditional combination mentioned in [10] and may be well applied to the context of equivalencing is that the model type and the model structure of the part to be equivalenced are determined from the white box approach, whilst its parameters are determined from the black box approach. However, an implementation of grey-box equivalencing method is rather complicated and is problem dependent. Furthermore, it requires good experience in power system modelling and system dynamics of the part to be equivalenced as well as a familiarity with existing equivalencing methods. For example, dynamic equivalent for extended time simulation in DYNRED software [1] is composed of two parts regarding to their impacts of different time. The first part, fundamental part (reduced network and equivalent generators), is constructed by Coherency-based method. The second part, extended part (excitation system), is constructed by identification technique based on sensitivity method due to its nonlinearity and multitude of excitation system models.

Apart from focusing on approach, the study also concerns the model formulation as it determines permissible analysis tasks (time domain simulation and linearised analysis), compatible power system analysis software, and applicable equivalencing techniques. The equivalent model may be classified into two classes which are power system component respectively preserved equivalents and non-power system component preserved equivalents. The former represents the equivalent by a combination of conventional power system components such as transmission lines, shunt reactance, and generators; but the latter represents the equivalent by other models such as state equation, differential algebraic equation (DAE), and artificial neural network. In some literatures[20], the equivalent represented by DAE is called power system structure preserved equivalent because it preserves the structure of the power system model which consist of dynamic devices (differential equation) and transmission network (algebraic equation). However, the zero entries of matrices are not retained so these equivalents cannot be reformulated back to power system components. Figure 2 shows an overview of model formulation for dynamic equivalent as mentioned above. So far the power system component preserved equivalents have received wide acceptance, especially those obtained by Coherency-

based method, because they have physical meaning and is compatible with most of power system analysis software, and can be performed in both time domain simulation and linearised analysis.

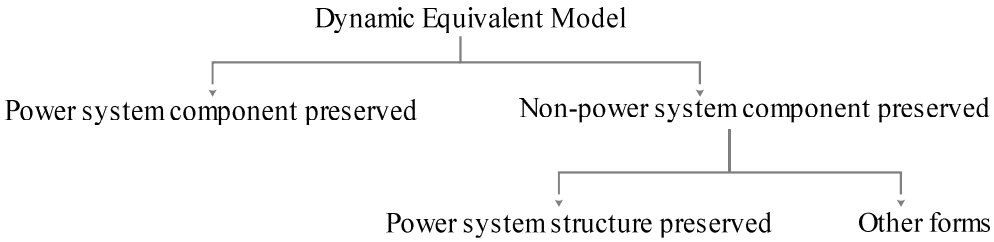

Figure 1.2 Overview of model formulation for dynamic equivalent

1.2.2 Challenging issues of dynamic equivalent for online application

Basically, online analysis [21] is performing analyses on a snapshot of current system condition. The main aim is to obtain the results of analyses from accurate system condition than those based on forecasting condition under offline condition. However, online analysis requires an extensive computation power and up-to-date model, and hence restricts its implementation due to the limited computational resources of an installed system and a lack of real-time detailed modeling data of neighbouring system[8]. A reduced external system has been considered as one way to overcome these difficulties by reducing the size of the overall system and decreasing the amount of real-time data required. This, therefore, makes dynamic equivalent more involved and faced a number of challenging issues.

There are three major challenging issues towards online application, namely modeling data, validity of equivalent, and compatibility of software. Firstly, modeling data (both offline data and real time data) may not be completely accessible, thus restricting an applicable equivalencing approaches (black-box or grey-box). Secondly, as the analyses are normally a predictive type, an equivalent itself must be valid for various circumstances such as various types of faults, various locations of faults, and various operating conditions. Thirdly, the equivalent should be formulated in conventional power system component models so as to be compatible with various existing software and applications.

Accordingly, many research works on dynamic equivalent aiming for online application have been conducted and at least two main schemes have commonly been found in the literatures. The first scheme focuses on an offline construction of a robust equivalent which could cover wide circumstance of validity. By contrast, the second scheme is more like a tailor-made model where the equivalent is reconstructed or partly updated for each particular circumstance such as a new operating condition or a new zone of contingencies[22] before performing analyses.

In the first scheme, an artificial neural network-based dynamic equivalent [19, 23-25] is a promising solution as it can capture a wide range of system dynamics. However, the main objection is its incompatibility with many commercial power system software and applications. With respect to compatibility issue, the second scheme is more appealing as it can generally apply to many equivalent models based on identification framework (either black box approach or grey box approach), especially those using conventional model of power system components.

However, identification-based dynamic equivalent intended for use in the second scheme requires further investigation and improvement in two aspects: its validity and its construction time. The validity of equivalent determines what studies within the internal part (illustrated by a box with upward diagonal pattern in Figure 3) can be accurately performed, while the construction time determines how frequently the equivalent can be reconstructed or updated. These two aspects affect effectiveness and efficiency of the scheme.

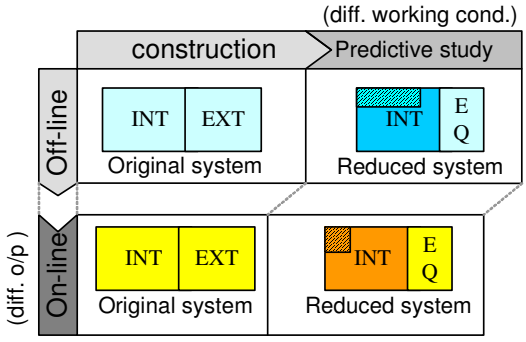

Figure 1.3 Second implementation scheme of dynamic equivalent for online application

Until now, the identification-based dynamic equivalent (either black-box or grey-box approaches) has no clear answer about a selection of an appropriate model structure corresponding to a chosen model type. For example, in the case of fictitious generator model type, the choice of a suitable number of fictitious generators and their proper way of interconnection are still not solved; and, attaching one fictitious generator to each boundary buses is simply used among the literatures. This may cause an inappropriate model structure and hence deteriorating the validity of the obtained equivalent. The possible consequence is that the study, which can be performed with an acceptable accuracy, on a resultant reduced system would be very limited and unpredictable. Another concern is a time usage during parameter identification process as it usually involves a non-linear optimization that requires a simulation of a full system (i.e. internal part and the equivalent) every time parameters adjusted to produce the responses of the reduced system for a comparison with those of the original system. The repetitive full system simulation is a time consuming process, especially when the internal part is very large or is modelled in great detail. This may result in a long construction time that is unable to fit to an allocated time during online construction stage.

1.3 Research aim and objectives

The aim of this thesis is to develop dynamic equivalent for online applications based on the second scheme mentioned in the previous section. In order to achieve this aim, the identification-based dynamic equivalent (grey box approach) having the following three properties is being developed:

- Compatible with conventional power system software
- More reliable (i.e. the model structure relies on the modelling data rather than iterative process), and
- Fast construction time.

1.4 Research methodology

The methodology used to develop identification-based dynamic equivalent for online applications is divided into two major phases: development phase and evaluation phase. The development phase comprises of the three following steps:

1. Study the feasibility of the determination of a suitable model structure from limited data of the part to be equivalenced.
2. Develop a procedure to identify the equivalent based on the obtained model structure.
3. Develop a procedure to identify parameters of an equivalent without full system simulation.

In the evaluation phase, the key performances of the developed equivalent are examined as follows:

1. the validity of the equivalent by a study of a full system under various conditions
2. the improvement in reliability by a comparison with full system study formed by other equivalents
3. the improvement in construction time by a comparison with the procedure that requires full system simulation

1.5 Contributions of the thesis

The major contributions of this thesis are fourfolds:

1. Development and verification of a new methodology for constructing identification-based dynamic equivalent based on grey-box approach

2. Development and verification of a new methodology for coherent generator identification based on graph model

3. Development and verification of a new methodology for parameter identification without full system simulation.

4. Application of the developed computer programs based on the above methodologies of (1), (2), and (3) to IEEE 39 bus system and IEEE 118 bus system.

1.6 Organisation of the thesis

The thesis is organised in seven chapters. Chapter 2 is a mathematical survey of dynamic equivalent to investigate the applicability to the development of dynamic equivalents for online application.

Chapter 3 describes the identification of coherent generator based on Graph model. The related graph theorems and their application to identify coherent generators together with test results are included. Moreover, an extension for coherent generator identification without parameters of generators is discussed.

By using a structure of equivalent based on the knowledge of coherent generator provided from the above technique, the procedure to construct more reliable identification-based dynamic equivalent that requires only power flow modeling data and measurements at boundary buses is explained and illustrated in Chapter 4.

In order to reduce the construction time of the procedure in Chapter 4, Chapter 5 provides the modified parameter identification technique that requires no simulation of complete system. Test results are also discussed in this chapter.

Combining the parametric identification of dynamic equivalent and the modified parameter identification technique described in Chapter 4 and 5 respectively, a procedure for constructing identification-based dynamic equivalent aiming for online application is developed. Chapter 6 is devoted to the applications of the procedure to the two case studies (IEEE 39 bus system and IEEE 118 bus system).

Finally, Chapter 7 is the conclusion and suggestion for future work.

1.7 References

[1] GE Electrical distribution and control, "Improved dynamic equivalencing software," EPRI EPRI Final Report, EPRI TR-105919, December 1995.

[2] U. D. Annakkage, N. K. C. Nair, A. M. Gole, V. Dinavahi, T. Noda, G. Hassan, and A. Monti, "Dynamic system equivalents: A survey of available techniques," in *Power & Energy Society General Meeting, 2009. PES '09. IEEE*, 2009, pp. 1-5.

[3] S. Deckmann, A. Pizzolante, A. Monticelli, B. Stott, and O. Alsac, "Studies on Power System Load Flow Equivalencing," *Power Apparatus and Systems, IEEE Transactions on,* vol. PAS-99, pp. 2301-2310, 1980.

[4] S. Deckmann, A. Pizzolante, A. Monticelli, B. Stott, and O. Alsac, "Numerical Testing of Power System Load Flow Equivalents," *Power Apparatus and Systems, IEEE Transactions on,* vol. PAS-99, pp. 2292-2300, 1980.

[5] F. F. Wu and A. Monticelli, "Critical review of external network modelling for online security analysis," *International Journal of Electrical Power & Energy Systems,* vol. 5, pp. 222-235, 1983.

[6] J. Machowski, J. W. Bialek, and J. R. Bumby, *Power System Dynamics and Stability*: John Wiley & Sons Ltd., 1997.

[7] F. O. Resende and J. A. Pecas Lopes, "Development of Dynamic Equivalents for MicroGrids using System Identification Theory," in *Power Tech, 2007 IEEE Lausanne*, 2007, pp. 1033-1038.

[8] Y. Ziwen, A. Steed, G. Dwernychuk, and D. Cave, "A model for all seasons," *Power and Energy Magazine, IEEE,* vol. 8, pp. 54-60, 2010.

[9] T. Soderstrom and P. Stoica, *System Identification*: Prentice Hall International (UK) Ltd, 1989.

[10] O. Nelles, *Nonlinear system identification: from classical approaches to neural networks and fuzzy models*: Springer-Verlag Berlin Heidelberg, 2001.

[11] A. Chang and M. M. Adibi, "Power System Dynamic Equivalents," *Power Apparatus and Systems, IEEE Transactions on,* vol. PAS-89, pp. 1737-1744, 1970.

[12] R. Podmore, "A Comprehensive Program For Computing Coherency-based Dynamic Equivalents," in *Power Industry Computer Applications Conference, 1979. PICA-79. IEEE Conference Proceedings*, 1979, pp. 298-306.

[13] Z. Z. Qi, "Coherency based dynamic equivalence of power systems." vol. Ph.D.: University of Strathclyde, 1994, p. 184.

[14] K. L. Lo, Z. Z. Qi, and B. Urqhart, "Dynamic Network Equivalents for Analysis and Control of Large-Scale Power Systems," in *IEE International Conference on Power System Control, Operation & Management, Invited Plenary Paper,* Hong Kong, 1995.

[15] J. M. Undrill, J. A. Casazza, E. M. Gulachenski, and L. K. Kirchrnayer, "Electromechanical Equivalent for Use in Power System Stability Studies," *Power Apparatus and Systems, IEEE Transactions on,* vol. PAS-90, pp. 2060-2071, 1971.

[16] J. M. Undrill and A. E. Turner, "Construction of Power System lectromechanical Equivalents by Modal Analysis," *Power Apparatus and Systems, IEEE Transactions on,* vol. PAS-90, pp. 2049-2059, 1971.

[17] Y. Yao-nan and M. A. El-Sharkawi, "Estimation of External Dynamic Equivalents of a Thirteen-Machine System," *Power Apparatus and Systems, IEEE Transactions on,* vol. PAS-100, pp. 1324-1332, 1981.

[18] W. P. William, C. S. Fred, M. G. Edward, and F. S. Robert, "Maximum likelihood identification of power system dynamic equivalents," in *Decision and Control including the 13th Symposium on Adaptive Processes, 1974 IEEE Conference on*, 1974, pp. 579-586.

[19] A. M. Stankovic, A. T. Saric, and M. Milosevic, "Identification of nonparametric dynamic power system equivalents with artificial neural networks," *Power Systems, IEEE Transactions on,* vol. 18, pp. 1478-1486, 2003.

[20] G. N. Ramaswamy, L. Rouco, O. Fillatre, G. C. Verghese, P. Panciatici, B. C. Lesieutre, and D. Peltier, "Synchronic modal equivalencing (SME) for structure-preserving dynamic equivalents," *Power Systems, IEEE Transactions on,* vol. 11, pp. 19-29, 1996.

[21] K. Morison, W. Lei, and P. Kundur, "Power system security assessment," *Power and Energy Magazine, IEEE,* vol. 2, pp. 30-39, 2004.

[22] J. M. Ramírez Arredondo, "Obtaining dynamic equivalents through the minimization of a line flows function," *International Journal of Electrical Power & Energy Systems,* vol. 21, pp. 365-373, 1999.

[23] H. Chen, C. Deng, and D. Li, "Recurrent Neural Network-based Dynamic Equivalencing in Power System," in *Control and Automation, 2007. ICCA 2007. IEEE International Conference on*, 2007, pp. 2396-2399.

[24] O. C. Y. Lino, "Robust recurrent neural network-based dynamic equivalencing in power system," in *Power Systems Conference and Exposition, 2004. IEEE PES*, 2004, pp. 1068-1077 vol.2.

[25] A. M. Stankovic and A. T. Saric, "Transient power system analysis with measurement-based gray box and hybrid dynamic equivalents," *Power Systems, IEEE Transactions on,* vol. 19, pp. 455-462, 2004.

CHAPTER 2

MATHEMATICAL SURVEY OF DYNAMIC EQUIVALENT

2.1 Introduction

Derivation of dynamic equivalent was initially based on empirical method. For example, a transmission network and loads are reduced by a method of static equivalent while all external generators are simply replaced by one equivalent generator [1] or by equivalent generators whose inertias are allocated following the distribution factor [2]. An accuracy of dynamics study by using these equivalents may not be adequate because the equivalencing procedures do not directly focus on the actual impact of dynamics interaction between the part being retained (the internal part) and the part being equivalenced (the external part). Therefore, more sophisticated methods have been proposed and studied to obtain a better performance of dynamic equivalent including additional features such as a short construction time, less modeling data required, and a power system structure preserved. Over past four decades, a number of dynamic equivalencing methods have been developed. Among them are three classes of methods dominated, namely Modal-based method, Coherency-based method, and identification-based method. Understanding of these methods (e.g. their key concepts, properties, and progress) is not only necessary for using but also useful for further developing.

This chapter provides a mathematical survey of dynamic equivalent, in particular Modal-based method, Coherency-based method, and identification-based method. First, the individual method and its variations are reviewed. Afterward, their applicability to the development of identification-based dynamic equivalent for online application is discussed.

2.2 Modal-based methods

The key concept of modal-based method is that some modes of responses of the external part, such as fast decay modes, have negligible effect on the internal part. Thus, they could be eliminated in order to obtain the reduced order model of the

external part. According to this concept, Undrill et al. [3, 4] utilised the linear modal analysis of the external part to identify the insignificant modes from its eigenvalues and proposed the equivalencing method that could be summarized into four major steps as shown in Figure 2.1.

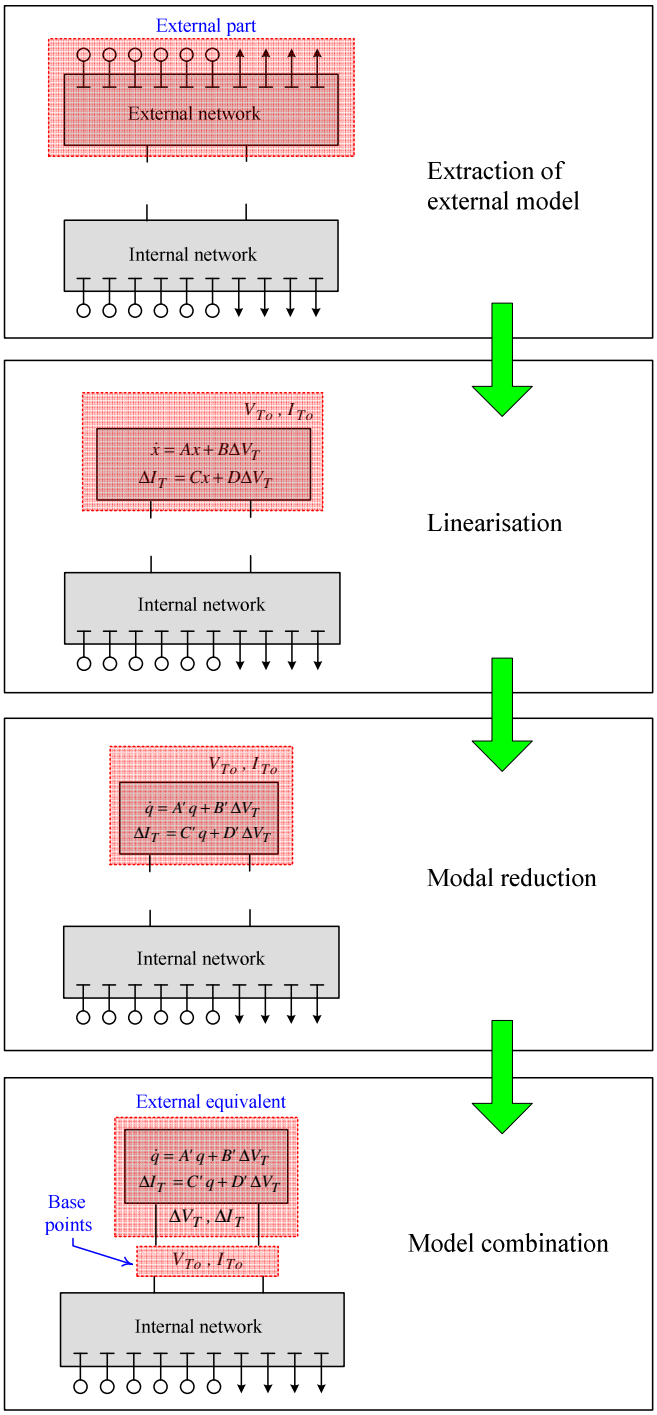

Figure 2.1 Summarized procedure for constructing Modal-based dynamic equivalent by Undrill et al.

In the first step, the equations of transmission network, loads, and generating units, which belong to the external part, are extracted from the entire power system model. Next, these equations are linearised and reformulated into a linearised state equation form in the second step. Afterward, in the third step, the linearised state equation form is transformed into the canonical form for a separation of natural modes of the responses; and then, the selected natural modes (such as large negative eigenvalues corresponding to fast decay modes) are deleted for the order reduction of the canonical form equation. Finally, the fourth step combines the reduced canonical form equation and the nonlinear differential equations of the internal part to form a reduced system for the dynamics simulation. In this step, the based points of terminal voltages and currents are needed to be included as the reduced canonical form equation of the external part is a small-signal model type (a linearised model).

A modal-based equivalent method was successful implemented and tested on a large-scale system (1323 bus system) [5, 6] and revealed that, even the equivalent was for a small-signal type, the obtained reduced system is able to perform with sufficient accuracy for large-signal time domain simulation (i.e. transient stability) under numerous fault locations, as long as, the faults are far from the boundary. However, the implementation of modal-based equivalent requires a time-consuming Eigen analysis and some modification of the main simulation program. It also appears that elimination of selected modes following the authors' proposed criteria could give unacceptable equivalent and further research on mode-selection is required The authors, therefore, suggest using the original unreduced canonical state equation in order to avoid degradation of accuracy resulting from improper selection of modes. This would not significantly affect the benefit of using equivalent because the obtained unreduced canonical state equation of the external part is computationally efficient due to its diagonalised structure. In addition, the effectiveness of this modal-based method was confirmed by the testing in [7].

Furthermore, Takeda et al. [8] proposed a modal-based dynamic equivalent having a model in a parallel-generator formation. The general idea of deriving the equivalent is similar to Undrill's method [3, 4] except that the related equations of the external part are formulated in the term of transfer function to neglect terms having small

coefficients and an extra step to re-compose the reduced transfer function to generator formation is introduced. Afterward, de Oliveira et al [9, 10] extended above method and developed the dynamic equivalent in generator formation, called Modal-generator, where one of the modal-generators corresponds to one retained mode of oscillation. By including the base points as constant admittances, both methods need no modification of the main simulation program. The difficulty in mode selection is not reported as the reduction is directly considered from explicit expression between outputs and inputs. Their test results show good quality of the equivalents and both methods can be applied to a more complicated generator model. However, the obtained equivalents are artificial generators having no physical meaning.

Yu-Ken et al. [11] also proposed the equivalencing method which produces the equivalent in power system component. However, the major difference of their method is that linear analysis is applied to the entire power system model rather than the extracted external equations. The concepts of Reachability Grammian and Singular value decomposition are utilized for order reduction, which is confined to the part belonging to the external. The final equivalent model in the form of generators and power network is then synthesized from the corresponding terms of the reduced equations. The authors also suggested the technique for matching power flows at boundaries in order to connect the obtained equivalent with the detailed model of the internal part for transient stability analysis. Even though this method is developed from a rigorous mathematical technique, it is limited to a classical generator model for the external part and no numerical testing results are presented.

In addition, Perez-Arriaga et al. [12, 13] introduced a new framework for physically-based model reduction called Selective Modal Analysis (SMA). The basic concept is to perform the model reduction on the original state equation setting, which has a physical meaning, rather than the transformed version (e.g. diagonalised state equation). In order to achieve the model reduction based on this concept, the portion of model and its states variables significantly involved with the modes being retained are first identified; and then, the remaining part and its associated states (less relevant states) are collapsed in the way that do not affect the retained dynamics. Although an

iterative algorithm for performing the model reduction following this framework has been proposed, its application in dynamic equivalent of power system has not received much attention. This is because of the difficulty in finding the suitable modes being retained (and accordingly their relevant states).

Ramawamy et al. [14, 15] later proposed a Synchronic Modal Equivalencing (SME) which grows out of Slow-coherency and SMA frameworks. The method is composed of two phases: a structuring phase and a modal equivalencing phase. In the structuring phase, an analysis of modal structure is performed on a simple model (e.g. linearised swing-equation model) of the entire original system to cluster the generators into decomposable groups, called Synchronic groups. Then, in the equivalencing phase, one of these groups is chosen as a study system while others are equivalenced in SMA style by considering states of one generator in each group as relevant states. Although a full detailed model of the original system is resumed during this phase, the equivalencing based on SMA framework gives an equivalent in a small-signal type represented by a linear multi-port admittance. In order to use the equivalent in non-linear time domain simulation, the based-points (corresponding to the nominal steady-state condition) are included by using a constant current source. The testing with intermediate-sized model for various perturbations in the study system [16] showed promising results except when the perturbation is at the transmission line connected between different groups of synchrony. Therefore, the further research is still needed.

2.3 Coherency-based methods

Coherency-based method was originally introduced by Chang et al. [17]. The derivation of equivalent was based on the condition that there exist groups of generators oscillating in cohesion, known as *Coherent*, which is defined in (1).

$$\delta_i(t) - \delta_j(t) \cong C_{ij}, \qquad 0 \le t \le t_{max} \tag{1}$$

Where $\delta_i(t)$ and $\delta_i(t)$ are the rotor angle of *i*-th and *j*-th generators at time t respectively and C_{ij} is a constant.

The existence of this condition results in a reasonably mathematical approximation of each group of coherent generators by one set of generator equation. However, in this original method, the derivation is based on a time-varying current source representing generator which is uncommon for the main simulation program (see [17] for details).

This concept is further developed by Podmore et al. [18-20]and leads to the coherency-based method that provides an equivalent in a conventional power system component representation. The method is composed of four main steps: coherency identification, generator bus reduction, load bus reduction, and dynamic aggregation of generating unit models (see figure 2.2).

From Figure 2.2, the groups of coherent generators are first identified from swing curves obtained by time domain simulation of the full system for a particular fault. Next, the coherent generators of each group are transferred to the equivalent buses via ideal phase-shift transformers; and then, their terminal buses are eliminated in the second step. The third step is load bus reduction and is often based on technique of network equivalent (such as Ward method). For example, the loads are represented by constant impedances and then Gaussian elimination is performed to eliminate the buses. Finally, the dynamic models of generating units for each coherent group are aggregated.

Similar to Chang's concept, the derivation of the equivalent relies on justification for simplifying or approximating parts of model when the coherent condition exists. In fact, there are two types of coherencies (the generator terminal bus coherency and the generator internal bus coherency) sequentially identified in this method during the first step. The former coherency gives the condition to obtain an approximately constant transformation ratio of phase-shift transformer for transferring (terminal bus) coherent generators to the same equivalent bus. The later coherency is the condition to ensure that generators have a similar dynamics and hence allowing the aggregation of their dynamic models.

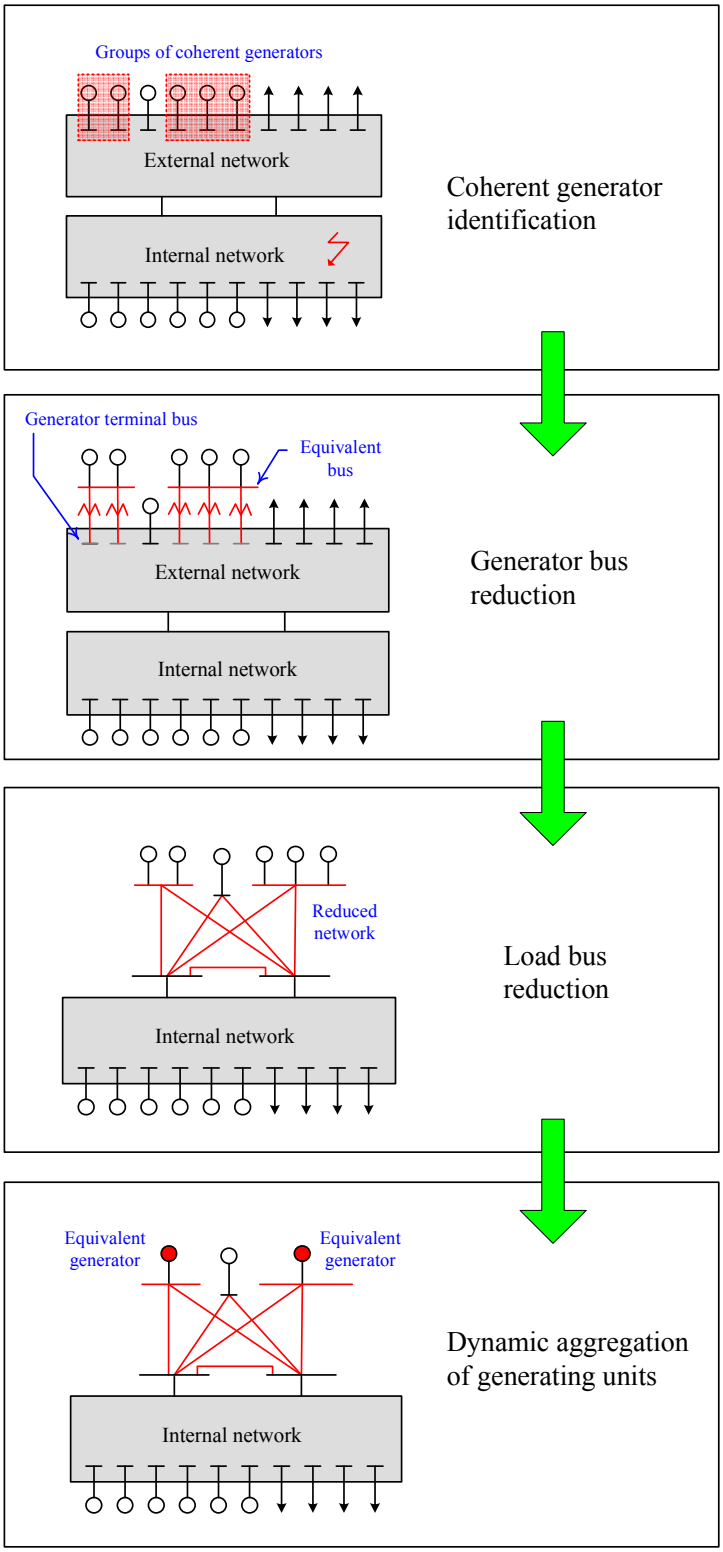

Figure 2.2 Summarized procedure for constructing coherency-based dynamic equivalent by Podmore et al.

The coherency-based method developed by Podmore et al. has two interesting features summarized as follows:

- The equivalent is a large-signal type and it is represented by conventional power system components with their physical meaning preserved.
- The equivalencing method decouples the construction of the static part of equivalent (transmission network) from the construction of the dynamic part of the equivalent (generating units).

According to these interesting features, the coherency-based method has been widely acknowledged. A large effort has been paid to improve the identification of coherent generators and the aggregation of generating unit models as they largely determine the performance of the obtained equivalent. The following two sub-sections give reviews on these two topics.

2.3.1 Identification of coherent generators

Originally, the coherent generators were identified by examining the angle variations of generator buses obtained from a time domain simulation of the detailed power system model for a particular fault. This method is straightforward and can accurately identify coherent generators including non-linear effects. However, it is time-consuming process and the identified coherent groups are fault-dependent. A large initial effort, therefore, is required during construction of equivalent but the resultant equivalent has a very limited use. In this regard, many research works on coherent-generator identification have been attempting to improve this inefficiency.

The first group of works has emphasized on the improvement in computational expense. Lee and Schweppe [21] first developed the method utilizing the concept of pattern recognition. The method was very fast but its recognition criteria produced by observations from one simple system may affect accuracy and confident of results. Spalding et al. [22] later proposed the method based on comparison of machine angles at two steady-state operating points (stable and unstable points). This method

is less empirical than previous methods, but the major difficulty is the determining the unstable operating point.

Concerning accuracy, Podmore [18]went back to the direct method where the rotor angle time response of generators obtained from numerical integration are compared. However, to decrease the computational time and memory usage, the author used a linearised swing equation model of power system rather than non-linear detailed model. Hiyama [23] also considered the identification of coherent generators from comparison of rotor angle responses. In order to further improve the speed of calculation, the modeling of power system, solving for its solution, and identifying coherent generators are performed in frequency domain as the differential equations become algebraic equations.

Regarding to above drawbacks (either using only steady-state information or integrating over long interval), Rudnick [24] proposed the method utilized machine conditions at initial steady-state and at the critical clearing time for identifying coherent generators. This method still requires numerical integration for calculating machine conditions during fault, but its interval is much shorter (up to the critical clearing time) and may be obtained from transient stability simulation when accuracy is of major concern. However, the critical clearing time must be known priory.

Furthermore, Haque et al. [25] identify coherent generators by using a combination of faulted and post-fault rotor angles, and the electric coupling between generators. The rotor angles are approximated by Taylor series expansion so it is faster than direct integration and could preserve the non-linearity of power-system model by using higher order of Taylor series. Later in [26], the same authors introduced another method using energy function for checking the coherent generators at post-fault condition while the coherent generators during faulted period are still identified from comparison of rotor angles approximated by Taylor series. The groups of coherent generators identified from these two conditions are checked for agreement to finalise the coherent generators of the system. This method considerably minimize the computation required than their previous method as the calculation of high order Taylor series at post-fault is no required. Haque [27] finally combines the strengths

from the previous two methods and proposed a method for coherent generator identification using information during three periods: faulted period, early part of post-fault period and later part of post-fault period. By contrast, Lo et al. [28, 29] proposed the method based on concept of predicting rotor angles by Taylor series but they emphasize on improving the accuracy rather than minimizing the computation. This is achieved by using multi-step Taylor series expansion and that the coefficients are recalculated at each time-step; and comparing the predicted angles in the frequency domain as it is barely perceptible.

Apart from numerical solution, Gallai and Thomas [30] solved a linearised power system model after disturbance for close-form solution using Cayley-Hamilton theorem and proved the condition for coherency. This condition leads to the development of a coherent generator identification method that requires no numerical integration. However there is an additional burden of computation for coefficients which represent matrix exponential. Similarly, Al Fuhaid [31] also proposed the coherent identification based on the condition derived from the close form solution. However, the condition is slightly different as the author defines the coherent of generators in term of mean-square error rather than absolute error.

The attempt to decrease the computation expense during the identification of coherent generator has a great benefit to the utilization of coherency-based equivalent. However, a unique equivalent must be constructed for each fault as the coherent generators identified by above methods are fault-dependent. For this reason, the second group of works has paid attention to study and to develop the identification of fault-independent coherent groups.

Lawler et al. [32] developed the coherent identification method based on applying a probabilistic disturbance to all mechanical inputs of linearised power system model. By using a root-mean-square (RMS) coherency measure and more specific probabilistic disturbance (i.e. a zero mean and a variance proportional to the square of the generator inertia), the coherent measure can be determined from the system parameters hence making disturbance-independent. Besides the theoretic

development, the authors also provided algorithm and numerical results in [33]. Although the authors claimed this kind of disturbance could represent many classes of practical fault, its analytic relation is difficult to verify.

Wu et al. [34] studied the conditions for exact coherent of generators, in terms of controllability subspace, according to both a single disturbance and a set of disturbances. The model used for the study is based on incorporating fault model (load shedding, generator dropping, and line switching) into a linearlised swing equation model of power system. An algebraic characterization of coherency revealed from the study is used to develop the coherent generator identification algorithm. Later in Wu et al. [35] extend the method for more practical situation where coherent condition need not to exactly adhered to but allow for a small difference However, both works involved many matrix-operations and no numerical evaluations were reported.

Chow [36] introduced Slow coherency method in which coherent generators are identified by examining the dependency of slow-eigenvector basis of linearised power system model. The author formulated the grouping of dependent row eigenvectors as an optimization problem and proposed a finite-step algorithm based on Gaussian elimination to approximate the solution for this problem. As the eigenvector basis is calculated from the linearised model before fault, the identified coherent generators are fault location independent. In addition to the closeness of rotor angle time response when low frequencies of oscillation are considered, another appealing property is that it allows the linearised model to be partitioned following slow coherent group aggregability. This reason reinforces the justification of the dynamic aggregation of generator unit models and makes the method widely accepted even time-consuming Eigen analysis required. Chow et al. [37] later improved a condition of the method that has a tendency to obtain a large-size group containing less coherent generators, especially for a large scale system, by removing the restriction on equality between number of coherent groups and number of slow modes and introducing loose and tight coherent concept. However, the key idea of identification still relies on examining the dependency of slow-eigenvector basis. To

further improve the accuracy, Joo et al. [38] incorporate voltage dynamics in the identification of coherent generators by adding the modes involving AVR action based on participation factors to the eigenvector basis being examined and clustering groups by K-mean algorithm.

Moreover, Geeves [39] proposed the coherent generator identification based on examining modal-contents of simplified linearised power system model before fault. The basic concept is to display modal data as hierarchical tree structure, called Modal tree. The root of modal tree represents the mode that all generators are in phase while each branch represents the particular mode and sub-group of generators which are in phase for that mode. Any generators under the same sub-tree are identified as a group of coherent generators. By using modal tree, the group of coherent generators could preserve high frequency modes. However, in term of computation, the creation of modal tree requires the graph clustering which may be an additional time-consuming routine besides the Eigen analysis.

Apart from the solution of model (either analytical or numerical), Lamba et al. [40] identify coherent generators by investigating the weak coupling structure in the matrix of linearised swing equation model as it causes the slow coherency. The authors introduced the ratio of off-diagonal block-matrix norms to diagonal block-matrix norms, called “Coupling Factor”, as the coupling measure and proposed the ordering algorithm to arrange the sub-matrices (representing generators) in the relative coupling order. The plot of the coupling factor versus the ordered sub-matrices (generators) is used for the identification of weak coupling areas and hence the coherent generators. The weak coupling method is further improved by Nath et al. [41]. Another plot of the change of coupling factor called Grouping bar chart was introduced in order to allow the method to be able to identify the weak coupling areas consisting of only one generator. Furthermore, Lo et al. [42] modified the weak coupling method by using the Taylor series expansion of the swing equation model of the power system up to the second order terms rather than using the linearised model. The test results showed that this modified method which takes account of the nonlinearity is highly effective and more accurate to identify the coherent groups.

In addition, Gacic [43] also proposed the identification of coherent generators based on identifying weak coupling structure in dynamic system. The author decided to identify such a structure from the Jacobian matrix by using Epsilon decomposition. The reason to use the Jacobian matrix is due to its availability in most standard power system program. However, the identification process is not straightforward because the variables associated with generators are indirectly linked. Recently, De Tuglie et al. [44] developed the method based on applying Epsilon decomposition using their formulated matrix which represented direct coupling among generators. This direct coupling is quantified from the linearised algebraic equations that describe the system connection. Even though the way to build the matrix is reasonable, the link with the real structure in the dynamic model that causes the coherency is weak.

2.3.2 Dynamic Aggregation of generating unit models

The dynamic aggregation of generating unit models is a determination of a representative generating unit model for the generators within the coherent group. Several researchers have developed the methods based on the concept of transferring coherent generators to a common terminal bus introduced by Podmore [20]. By this concept, the coherent generators are at the same terminal voltage and at the same speed. The inertia constant and damping factor of the representative generator, therefore, are the sum of their individual inertia constants and individual damping factor, respectively. For other parameters, the calculations are not uniform and are dependent on the methods used. DeMello and Podmore [45,cited in [44]] proposed the weight logarithmic average method. The equivalent transient reactance is calculated as a parallel of individual while the other parameters of synchronous generators and their controls are calculated based on weight logarithmic average by the rated output. The only limitation of this method is that the generating units must be represented by the same type of model. Later in [19], Germond and Podmore developed a method that allows aggregation of different model types. However, the method is time-consuming as it is based on iterative process for fitting of transfer

functions in the frequency domain. Additionally, Galarza et al. [46] developed a sensitivity method to determine the parameters of the aggregated exciter model. The method is based on tuning of the exciter parameters until the boundary bus voltages of the reduced model and the full model are matched.

Nath and Lamba [47] proposed a method based on time-domain aggregation using structure constraints. In this method, the equivalent parameters of synchronous machine and excitation system are determined by structure preservation of the coefficient matrices. Although this method can be applied to the same types of model, the method is less heuristic comparing with [45, cited in [44]] and requires no iteration. Lo. et al [48] and Qi [49] further extended Nath's and Lambda's method to include turbine governor system and power system stabilizer (PSS). Moreover, this extended method requires no matrix inversion. In addition to the concept of transferring coherent generators to a common terminal bus, Ghafunrian and Berg [50] proposed a dynamic aggregation of generating units based on retaining terminal bus and equation of one generator in each coherent group. This result of aggregation is reached by using coherency conditions to eliminate terminal buses and equations of other generators within the coherent group.

Furthermore, Chow et al. [51] introduced another two dynamic aggregations: inertial aggregation and slow coherency aggregation. These two aggregations improve the stiff problem in Podmore's methods by performing the aggregation at generator internal buses. However, these two techniques are limited to only classical model of generator.

2.4 Identification-based methods

The identification-based method is another dominating method for construction of dynamic equivalent. This method is based on either black-box approach or grey-box approach mentioned in chapter 1. The essence of the method is to incorporate measurement for adjusting the assumed model; and only the methods taking measurement outside the part to be equivalent (external part) are discussed in this

thesis. From the implementation aspect, there are two schemes commonly found in the literature on identification-based dynamic equivalent.

The first scheme, see Figure 2.3, requires a simulation of full system (internal part and equivalent). The recorded responses from the internal part of the original system are compared with the simulated responses from the reduced system under the same condition of disturbance; and then, the equivalent model (e.g. parameters, order, and structure) are adjusted until the pre-defined criteria are satisfied.

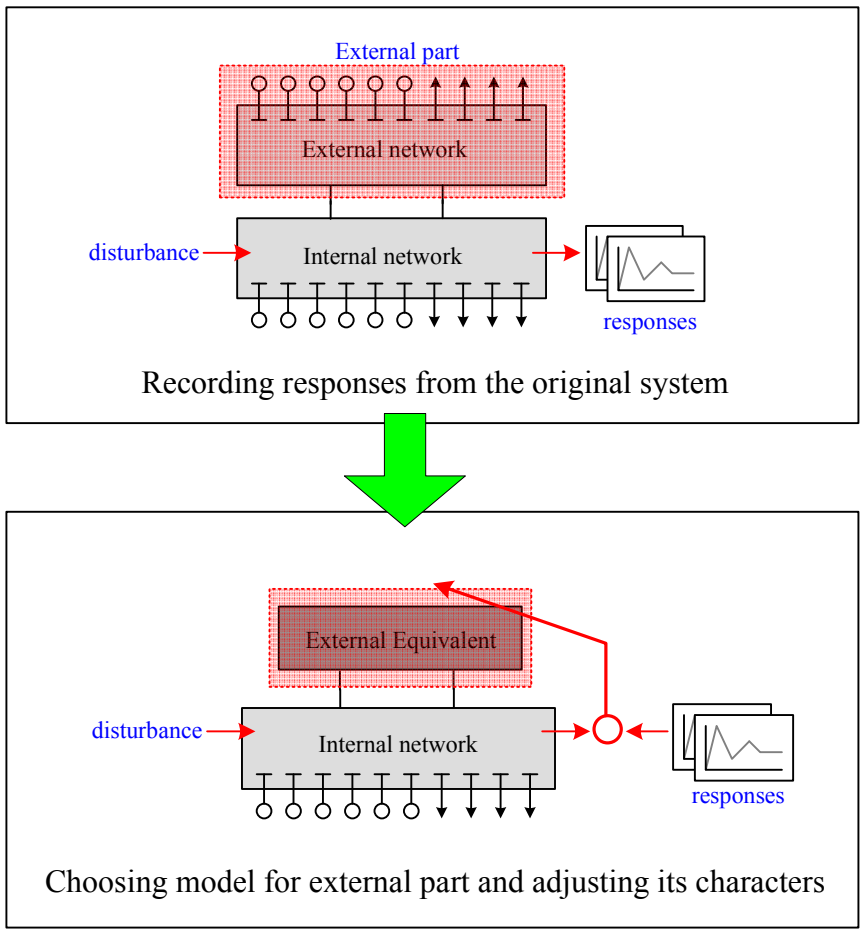

Figure 2.3 First scheme for implementation of identification-based dynamic equivalent

The full system simulation in this scheme is time-consuming and, moreover, the implementation of disturbance for the reduced system having the same condition as it

occurs in the original system is rather difficult, especially when the natural fluctuation of loads is considered as disturbance [52]. However, the great benefit of using this scheme is that the reduced system is obtained at the same time as the adjusting process finished.

According to this scheme of implementation, Price et al. [52] proposed the mathematical development of maximum likelihood technique to identify the equivalent from natural fluctuation of power system. The key concept is to compare the recorded responses with the simulated responses from the reduced system (the assumed external equivalent and the internal part) formulated as a Kalman Filter estimator. Price et al. [53] later showed the feasibility of the method by using the external equivalent having the same structure as the unreduced external part. In order to reduce the dimension of external part, the authors suggested using knowledge of coherent generators from the off-line data for the derivation of the assumed model structure.

Furthermore, Yao-nan and El-Sharkawi [54] proposed the identification-based dynamic equivalent using differential equations in fictitious generator formulation as the model for the equivalent. Each individual fictitious generator was directly connected to each boundary bus and its parameters were identified by fitting the responses of one particular generator within the internal part. Moreover, the authors provided a guideline for choosing an appropriate model order by observing the uniqueness of the minimum cost function values. Next, Ramrez Arredondo [55] also proposed a method that utilized the fictitious generator model. However, the author used a different criterion (based on active power flow transients) and introduced the concept of using different set of values of parameters for different zones of contingency. The zone of contingency is calculated through using a composite electromechanical distance [56]. In addition, Ramirez and Valle [57] developed the fictitious generator dynamic equivalent as well; but the major difference is in the criterion that takes operating conditions into account. The authors proposed the criterion based on difference between eigen-values of original system and eigen-

values of reduced system for the set of operating conditions under study; and used Genetic algorithm (GA) to identify the parameters.

In the second scheme (see Figure 2.4), it requires only a simulation of the equivalent. This is achieved by the modelling the equivalent in an input/output formulation so that one set of recorded responses from the original system is used as input to the equivalent while the rest is used for a comparison with those obtained from the simulation of the equivalent.

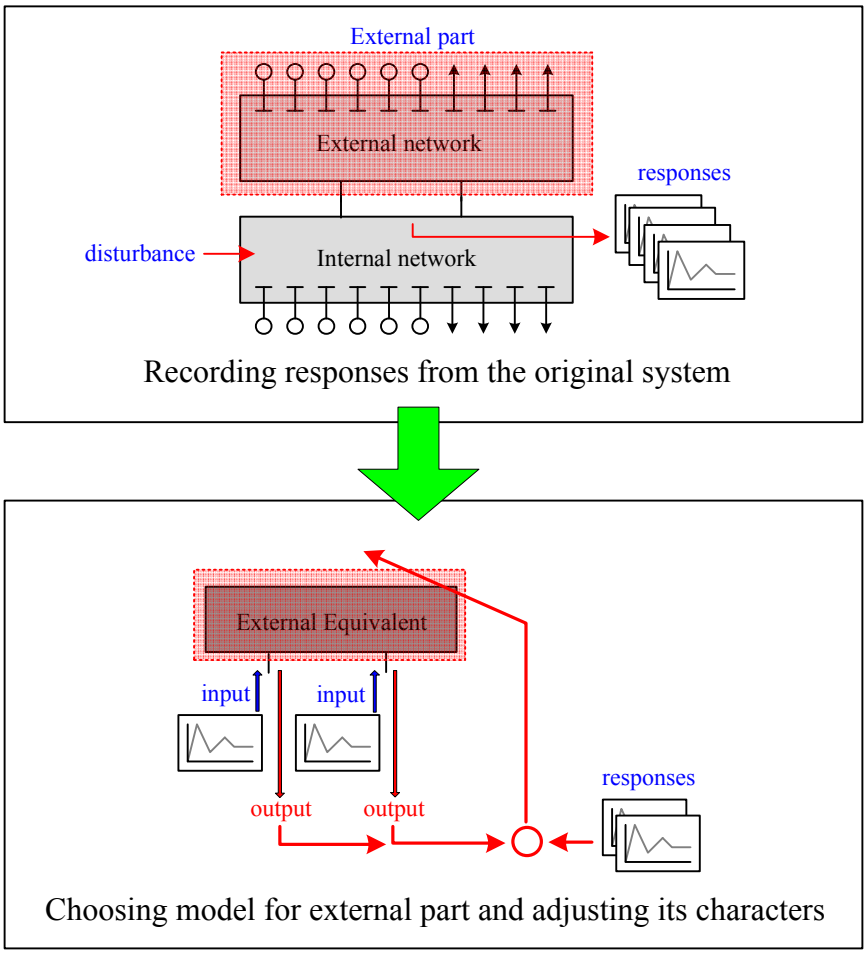

Figure 2.4 Second scheme for implementation of identification-based dynamic equivalent

Apart from much smaller in dimension of the model required for simulation, another advantage of the second implementation scheme is that a standard system identification package could be employed (depending on how the external equivalent is modeled) since the requirement of power system simulator for the internal part is no longer needed. At these points, the second scheme is considerably superior. However, the adjusting process may not converge or it may produce a poor final equivalent. This is because the input to the external equivalent (Figure2.4) is not actually the true cause of the external part producing the response but it is the response caused by dynamics interaction from both internal part and external part. Moreover, a modification of the power system simulation program may be required for interfacing the obtained equivalent with the internal part.

Based on the second implementation, Ibrahim et al. [58] proposed the black-box method by choosing a combination of a reduced network and stochastic linear difference equations as the model for the dynamic equivalent. The reduced network represents the quasi-steady state performance while the stochastic linear difference equations represent the dynamic changes of voltages at boundaries. The parameters of these two components could be identified from the measurements taken at the boundaries based on least square technique. However, in the demonstration, the reduced network was obtained from a network reduction technique so it was slightly based on a grey-box approach. In addition, this dynamic equivalent was tested by Lo. and Al-Ghafri [59]. The results confirmed the good performance of the model.

Wilson and Aplevich [60] developed the method utilised the linear transfer function between voltages and currents at boundaries for the assumed model of the external part and used least square technique for its parameters identification. Besides the identification of parameters, the author also estimated the model order by using different orders of transfer function and chose the lowest order that satisfied the criteria. In order to form the reduced model for non-linear time domain simulation, the author reformulated the obtained equivalent into the state-space formulation and connected it with the internal part by simply adding based-points of voltages and currents. However, this equivalent is a small-signal type.

Ju et al. [61] proposed the equivalent having a form of fictitious generator (third order model) and a electric load in parallel and provided a proof of the identifiability of parameters. The proof showed that all parameters of the assumed model are identifiable when pre-steady, dynamic and post-steady responses are all used for the parameter identification. Ju et al. [62] further validated their proposed equivalent with field tests. Although a comparison of time responses and a comparison of maximum clearing times are close, the identified parameters of the equivalent are much dependent on fault location. This may infer unsuitable model structure and model order.

Another group of works that employ the second scheme of implementation is based on modelling external equivalent by artificial neural network (ANN) and it is trained by a supervised learning technique. Stankovic et al. [63] proposed the ANN-based equivalent composed of two stages. The first stage is a bottleneck type used for extracting estimates about states and the second stage is a recurrent type used for approximating the right-hand side of a continuous-time system. These two stages actually emulate a structure of solver for numerical solution of multi-machines model [64]. Recorded voltages and currents at the boundaries are used for training the ANN. However, these recorded data are not separately used as input and output. The values of both voltage and current at current time are considered as inputs and their values at the next time step are considered as outputs. Stankovic et al. [65] further proposed the hybrid implementation of ANN-based and Coherency-based equivalent. However, Shakouri and Radmanesh [66] claimed that the methods proposed in [63, 65] are one-way interaction between the internal part and the external equivalent. Also, the methods may have some deficiency in simultaneously solving the internal part and the external equivalent, because there is no emphasis on the implementation given. Shakouri and Radmanesh developed a two-way interaction ANN-based equivalent having currents and voltages at boundaries as inputs and outputs, respectively. In addition to these methods, ANN-based equivalents having different ANN-type and ANN-structure have been proposed in [67, 68]. Although all the references mentioned here showed promising results of reproducing the responses at boundaries, the implementation of reduced system and the compatibility with standard power system software are the main objections. Evidently, there are no any

references showing the simulation results within the internal system (such as rotor angle of internal generators) by using the equivalent.

2.5 Applicability to the development of identification-based dynamic equivalent for online applications

As mentioned in Chapter 1, the development of dynamic equivalent for online application has been facing three major challenging issues which are modeling data, validity of equivalent, and compatibility of software. These challenging issues necessitate further investigating and improving identification-based dynamic equivalent having a model with conventional power system components in two aspects: its validity and its computational time.

The validity of identification-based dynamic equivalent could be improved by a selection of suitable model structure (and order) corresponding to the chosen model type. This might be achieved by either adding a cascade-loop for model structure selection over parameter identification-loop or deriving a suitable structure from available modelling data. The former is a time-consuming iterative process but it requires no modeling data of the part to be equivalenced. By contrast, the later relies on an experience of power system dynamic model as well as an availability of modelling data.

From the previous section, the suggestion of using knowledge of coherent generators in the derivation of the assumed model structure for the external part from off-line modelling data [53] is very interesting because the obtained model structure is in conventional power system components and preserves a physical-meaning (e.g. equivalent generators, reduced transmission network, and constant impedance loads). However, the identification of coherent generator requires a complete set of dynamic modelling data (e.g. topology of transmission network and its parameters, model of generator and its parameters, and operating states) at least for a swing equation model. This could be a deadlock since we are looking for the procedure that could provide a model structure without such a complete data requirement, even they are

from the offline data, otherwise modal-based equivalents or coherency-based equivalents can be applied.

As the derivation of model structure based on the knowledge of coherent generators is intended to provide a better model structure for identification-based dynamic equivalent, an idea of using approximate information about coherent generators is justified to compromise on the required modelling data. Taylor et al. [69] proposed an approximation of coherent generator based on synchronization coefficient that requires only power-flow modelling data. The synchronization coefficient reflects strength of dynamic coupling between generators and its weak connections causes an approximate time-scale separation, hence slow coherency of generators. Although the authors gave a reasonable explanation referring to theoretical development in [36] and showed a feasibility of the method on a 179bus test system, yet more evaluation of the performance is needed. Moreover, the calculation of the synchronization coefficient requires not only power-flow modelling data but also transient reactance of generator. Therefore, the piece of modelling information that is actually neglected is only the inertia of generator.

Instead of conducting more extensive evaluation of the method above, in this thesis the explanation of coherency phenomenon based on graph model [70] is adopted for developing new coherent generator identification technique. It will be discussed in the next chapter that the coherent generator identification based on graph model could provide an aid to interpretation and allow to make a reasonable assumption for identification of coherent generators using only power-flow modelling data.

For the computational time, the implementation scheme of identification-based dynamic equivalent that requires no full system simulation is preferred. The key concept is to formulate the assumed model of the external part into input/output formulation. As our assumed model has a power system structure, the technique for reformulation from modal-based methods in [3, 4] is adapted to be used in this thesis. The criterion based on recorded responses of active power flow in the transmission lines at boundaries [55] is chosen as it has high possibility for further practical development by using online measurements. However, the recorded responses will

be taken from a simulation of original system in this thesis. The detail of implementation will be explained in Chapter 5.

The development framework of dynamic equivalent for online application in this thesis could be summarized in Figure 2.5.

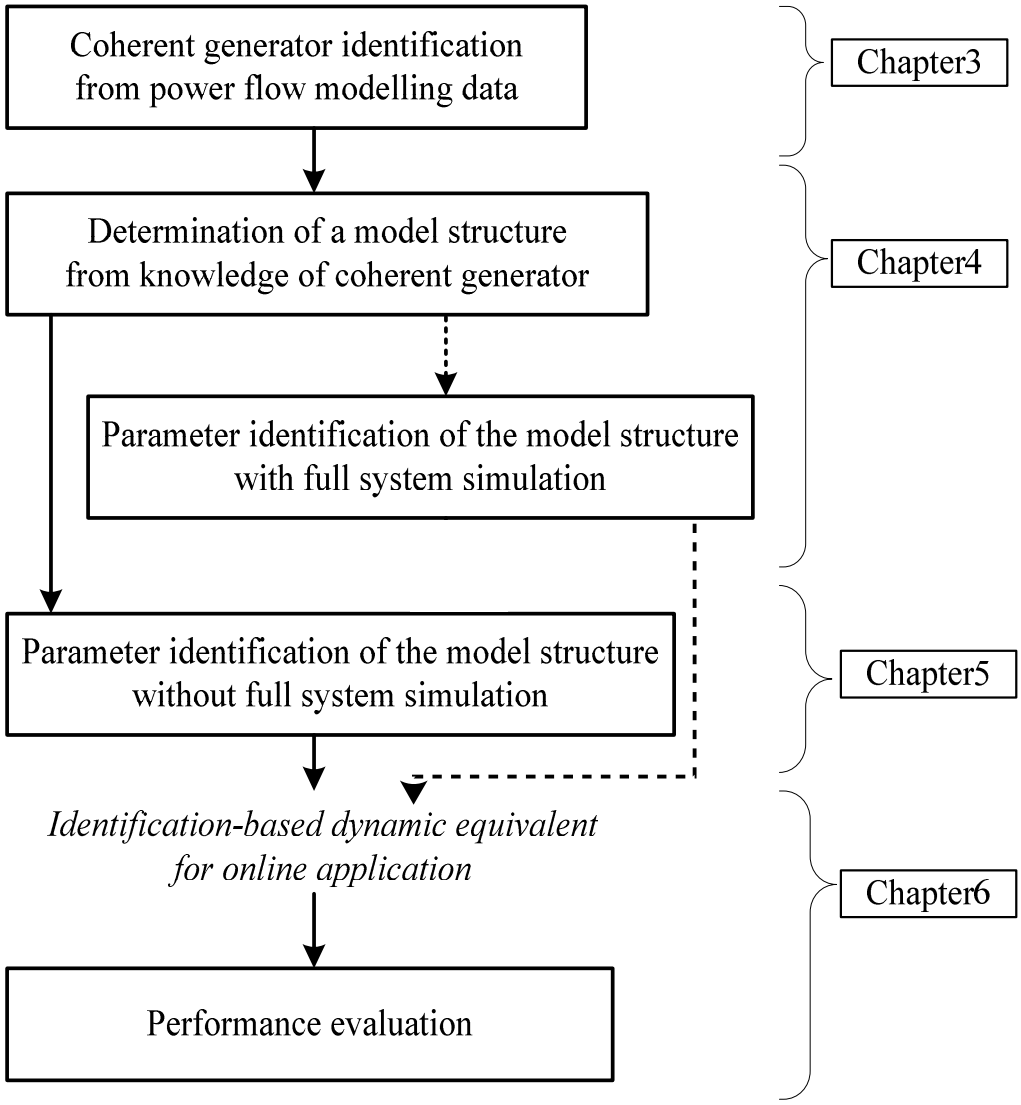

Figure 2.5 Development framework of dynamic equivalent for online application of this thesis

2.6 Conclusion

In this chapter, modal-based methods, coherency-based methods, and identification-based methods of dynamic equivalencing have been reviewed. Modal-based equivalent methods rely on applying technique of linear system to eliminate less significant modal contents of the external part for order reduction. These methods provide an equivalent model in a small-signal type; however it could be used for non-linear time domain simulation as long as faults are far from boundaries. Coherency-based methods rely on justification for simplifying or approximating parts of model when the coherent condition exists. There are two key steps of coherency-based methods which are coherent generator identification and dynamic aggregation of generating unit model. Both are reviewed in this chapter. The equivalent obtained from coherency-based methods is a large-signal type and is represented by a conventional power system components with physical meaning preserved. Identification-based methods rely on either back-box approach or grey-box approach; and two implementation schemes (with full system simulation and without full system simulation) have been reviewed. However, several diverse methods of identification-based dynamic equivalent have been proposed due to different opinions on choosing the assumed model and the recorded measurements.

In addition, the applicability to the development of identification-based dynamic equivalent for online application has been discussed with respect to the issues of validity and computational time, respectively. This leads to the proposed identification-based method that utilizes knowledge of coherent generator and technique of adjusting model without full system simulation for deriving the assumed model and identifying the parameters, respectively. This proposed identification-based dynamic equivalencing method requires only the power-flow modelling data and the recorded measurements at boundaries; and it is expected to have an improvement in its reliability and its construction time.

2.7 References

[1] W. T. Brown and W. J. Cloues, "Combination Load-Flow and Stability Equivalent for Power System Representation on A-C Network Analyzers," *Power Apparatus and Systems, Part III. Transactions of the American Institute of Electrical Engineers,* vol. 74, pp. 782-787, 1955.

[2] H. E. Brown, R. B. Shipley, D. Coleman, and R. E. Nied, "A Study of Stability Equivalents," *Power Apparatus and Systems, IEEE Transactions on,* vol. PAS-88, pp. 200-207, 1969.

[3] J. M. Undrill, J. A. Casazza, E. M. Gulachenski, and L. K. Kirchrnayer, "Electromechanical Equivalent for Use in Power System Stability Studies," *Power Apparatus and Systems, IEEE Transactions on,* vol. PAS-90, pp. 2060-2071, 1971.

[4] J. M. Undrill and A. E. Turner, "Construction of Power System lectromechanical Equivalents by Modal Analysis," *Power Apparatus and Systems, IEEE Transactions on,* vol. PAS-90, pp. 2049-2059, 1971.

[5] W. W. Price, E. M. Gulachenski, P. Kundur, F. J. Lange, G. C. Loehr, B. A. Roth, and R. F. Silva, "Testing of the Modal Dynamic Equivalents Technique," *Power Apparatus and Systems, IEEE Transactions on,* vol. PAS-97, pp. 1366-1372, 1978.

[6] W. W. Price and B. A. Roth, "Large-Scale Implementation of Modal Dynamic Equivalents," *Power Apparatus and Systems, IEEE Transactions on,* vol. PAS-100, pp. 3811-3817, 1981.

[7] K. L. Lo and J. J. Mohammed, "Modal Analysis for Power System Network Equivalence," in *20th Universities Power Engineering Conference*, 1985.

[8] S. Takeda, S. Nishida, and T. Yamaguchi, "Derivation of dynamic equivalents for stability analysis," *International Journal of Electrical Power & Energy Systems,* vol. 2, pp. 96-102, 1980.

[9] S. E. M. de Oliveira and J. F. de Queiroz, "Modal dynamic equivalent for electric power systems. I. Theory," *Power Systems, IEEE Transactions on,* vol. 3, pp. 1723-1730, 1988.

[10] S. E. M. de Oliveira and A. G. Massaud, "Modal dynamic equivalent for electric power systems. II. Stability simulation tests," *Power Systems, IEEE Transactions on,* vol. 3, pp. 1731-1737, 1988.

[11] T. Yu-Kun, N. Narasimhamurthi, and F. Wu, "Structure-preserving model reduction with applications to power system dynamic equivalents," *Circuits and Systems, IEEE Transactions on,* vol. 29, pp. 525-535, 1982.

[12] I. J. Perez-Arriaga, G. C. Verghese, and F. C. Schweppe, "Selective Modal Analysis with Applications to Electric Power Systems, PART I: Heuristic Introduction," *Power Apparatus and Systems, IEEE Transactions on,* vol. PAS-101, pp. 3117-3125, 1982.

[13] G. C. Verghese, I. J. Perez-Arriaga, and F. C. Schweppe, "Selective Modal Analysis With Applications to Electric Power Systems, Part II: The Dynamic Stability Problem," *Power Apparatus and Systems, IEEE Transactions on,* vol. PAS-101, pp. 3126-3134, 1982.

[14] G. N. Ramaswamy, L. Rouco, O. Fillatre, G. C. Verghese, P. Panciatici, B. C. Lesieutre, and D. Peltier, "Synchronic modal equivalencing (SME) for

structure-preserving dynamic equivalents," *Power Systems, IEEE Transactions on,* vol. 11, pp. 19-29, 1996.

[15] G. N. Ramaswamy, G. C. Verghese, and B. C. Lesieutre, "Multi-dimensional synchrony and dynamic equivalence," in *Control Applications, 1995., Proceedings of the 4th IEEE Conference on*, 1995, pp. 605-610.

[16] G. N. Ramaswamy, C. Evrard, G. C. Verghese, O. Fillatre, and B. C. Lesieutre, "Extensions, simplifications, and tests of synchronic modal equivalencing (SME)," *Power Systems, IEEE Transactions on,* vol. 12, pp. 896-905, 1997.

[17] A. Chang and M. M. Adibi, "Power System Dynamic Equivalents," *Power Apparatus and Systems, IEEE Transactions on,* vol. PAS-89, pp. 1737-1744, 1970.

[18] R. Podmore, "Identification of Coherent Generators for Dynamic Equivalents," *Power Apparatus and Systems, IEEE Transactions on,* vol. PAS-97, pp. 1344-1354, 1978.

[19] A. J. Germond and R. Podmore, "Dynamic Aggregation of Generating Unit Models," *Power Apparatus and Systems, IEEE Transactions on,* vol. PAS-97, pp. 1060-1069, 1978.

[20] R. Podmore, "A Comprehensive Program For Computing Coherency-based Dynamic Equivalents," in *Power Industry Computer Applications Conference, 1979. PICA-79. IEEE Conference Proceedings*, 1979, pp. 298-306.

[21] S. T. Y. Lee and F. C. Schweppe, "Distance Measures and Coherency Recognition for Transient Stability Equivalents," *Power Apparatus and Systems, IEEE Transactions on,* vol. PAS-92, pp. 1550-1557, 1973.

[22] B. D. Spalding, H. Yee, and D. B. Goudie, "Coherency recognition for transient stability studies using singular points," *Power Apparatus and Systems, IEEE Transactions on,* vol. 96, pp. 1368-1375, 1977.

[23] T. Hiyama, "Identification of coherent generators using frequency response," *Generation, Transmission and Distribution, IEE Proceedings C,* vol. 128, pp. 262-268, 1981.

[24] H. Rudnick, R. I. Patino, and A. Brameller, "Power-system dynamic equivalents:coherency recognition via the rate of change of kinetic energy," *Generation, Transmission and Distribution, IEE Proceedings C,* vol. 128, pp. 325-333, 1981.

[25] M. H. Haque and A. H. M. A. Rahim, "An efficient method of identifying coherent generators using Taylor series expansion," *Power Systems, IEEE Transactions on,* vol. 3, pp. 1112-1118, 1988.

[26] M. H. Haque and A. H. M. A. Rahim, "Identification of coherent generators using energy function," *Generation, Transmission and Distribution, IEE Proceedings C,* vol. 137, pp. 255-260, 1990.

[27] M. H. Haque, "Identification of coherent generators for power system dynamic equivalents using unstable equilibrium point," *Generation, Transmission and Distribution, IEE Proceedings C,* vol. 138, pp. 546-552, 1991.

[28] K. L. Lo, Z. Z. Qi, and D. Xiao, "Identification of coherent generators by spectrum analysis," *Generation, Transmission and Distribution, IEE Proceedings-,* vol. 142, pp. 367-371, 1995.

[29] K. L. Lo, D. Xiao, and Z. Z. Qi, "Spectrum Analysis with Applications to Transient Stability Equivalents," in *26th Universities Power Engineering Conference*, 1991.
[30] A. Gallai and R. Thomas, "Coherency identification for large electric power systems," *Circuits and Systems, IEEE Transactions on,* vol. 29, pp. 777-782, 1982.
[31] A. S. Al Fuhaid, "Coherency identification for power systems," *International Journal of Electrical Power & Energy Systems,* vol. 9, pp. 149-156, 1987.
[32] J. Lawler, R. A. Schlueter, P. Rusche, and D. L. Hackett, "Modal-Coherent Equivalents Derived from an RMS Coherency Measure," *Power Apparatus and Systems, IEEE Transactions on,* vol. PAS-99, pp. 1415-1425, 1980.
[33] J. S. Lawler and R. A. Schlueter, "Computational Algorithms for Constructing Modal-Coherent Dynamic Equivalents," *Power Apparatus and Systems, IEEE Transactions on,* vol. PAS-101, pp. 1070-1080, 1982.
[34] F. Wu and N. Narasimhamurthi, "Coherency identification for power system dynamic equivalents," *Circuits and Systems, IEEE Transactions on,* vol. 30, pp. 140-147, 1983.
[35] F. Wu and T. Yu-Kun, "Identification of groups of ε-coherent generators," *Circuits and Systems, IEEE Transactions on,* vol. 30, pp. 234-241, 1983.
[36] J. H. Chow, *Time-scale modeling of dynamic networks with application to power systems*: Springer-Verlag, 1983.
[37] J. H. Chow, P. V. Kokotovic, and R. J. Thomas, *New algorighms for slow coherency aggregation of large power systems* vol. 64: Springer-Verlag, 1995.
[38] S. K. Joo, C. C. Liu, L. E. Jones, and J. W. Choe, "Coherency and aggregation techniques incorporating rotor and voltage dynamics," *Ieee Transactions on Power Systems,* vol. 19, pp. 1068-1075, May 2004.
[39] S. Geeves, "A modal-coherency technique for deriving dynamic equivalents," *Power Systems, IEEE Transactions on,* vol. 3, pp. 44-51, 1988.
[40] S. S. Lamba and R. Nath, "Coherency identification by the method of weak coupling," *International Journal of Electrical Power & Energy Systems,* vol. 7, pp. 233-242, 1985.
[41] R. Nath, S. S. Lamba, and K. S. Prakasa Rao, "Coherency Based System Decomposition into Study and External Areas Using Weak Coupling," *Power Apparatus and Systems, IEEE Transactions on,* vol. PAS-104, pp. 1443-1449, 1985.
[42] K. L. Lo, Z. Z. Qi, and A. Danielsen, "Coherency Identification for Power System Dynamic Equivalents," in *26th Universities Power Engineering Conference*, 1991.
[43] N. Gacic, A. I. Zecevic, and D. D. Siljak, "Coherency recognition using epsilon decomposition," *Power Systems, IEEE Transactions on,* vol. 13, pp. 314-319, 1998.
[44] E. De Tuglie, S. M. Iannone, and F. Torelli, "A Coherency Recognition Based on Structural Decomposition Procedure," *Power Systems, IEEE Transactions on,* vol. 23, pp. 555-563, 2008.
[45] R. W. deMello, R. Podmore, and K. N. Stanton, "Coherency-based dynamic equivalents: applications in transient stability studies," in *PICA conference* New Orleans, 1975.

[46] R. J. Galarza, J. H. Chow, W. W. Price, A. W. Hargrave, and P. M. Hirsch, "Aggregation of exciter models for constructing power system dynamic equivalents," *Power Systems, IEEE Transactions on,* vol. 13, pp. 782-788, 1998.

[47] R. Nath and S. S. Lamba, "Development of coherency-based time-domain equivalent model using structure constraints," *Generation, Transmission and Distribution, IEE Proceedings C,* vol. 133, pp. 165-175, 1986.

[48] K. L. Lo, Z. Z. Qi, A. Danielsen, and D. Royston, "Development o Dynamic Equivalents for Generating Units," in *the 25th Univeresities Power Engineering Conference* 1990.

[49] Z. Z. Qi, "Cohrency based dynamic equivalence of power systems." vol. Ph.D.: University of Strathclyde, 1994, p. 184.

[50] A. Ghafurian and G. J. Berg, "Coherency-based multimachine stability study," *Generation, Transmission and Distribution, IEE Proceedings C,* vol. 129, pp. 153-160, 1982.

[51] J. H. Chow, R. Galarza, P. Accari, and W. W. Price, "Inertial and slow coherency aggregation algorithms for power system dynamic model reduction," *Power Systems, IEEE Transactions on,* vol. 10, pp. 680-685, 1995.

[52] W. P. William, C. S. Fred, M. G. Edward, and F. S. Robert, "Maximum likelihood identification of power system dynamic equivalents," in *Decision and Control including the 13th Symposium on Adaptive Processes, 1974 IEEE Conference on*, 1974, pp. 579-586.

[53] W. W. Price, D. N. Ewart, E. M. Gulachenski, and R. F. Silva, "Dynamic equivalents from on-line measurements," *Power Apparatus and Systems, IEEE Transactions on,* vol. 94, pp. 1349-1357, 1975.

[54] Y. Yao-nan and M. A. El-Sharkawi, "Estimation of External Dynamic Equivalents of a Thirteen-Machine System," *Power Apparatus and Systems, IEEE Transactions on,* vol. PAS-100, pp. 1324-1332, 1981.

[55] J. M. Ram□rez Arredondo, "Obtaining dynamic equivalents through the minimization of a line flows function," *International Journal of Electrical Power & Energy Systems,* vol. 21, pp. 365-373, 1999.

[56] R. Belhomme and M. Pavella, "A composite electromechanical distance approach to transient stability," *Power Systems, IEEE Transactions on,* vol. 6, pp. 622-631, 1991.

[57] J. M. A. Ramirez and R. J. G. Valle, "Identification of dynamic equivalents preserving the internal modes," in *Power Tech Conference Proceedings, 2003 IEEE Bologna*, 2003, p. 6 pp. Vol.2.

[58] M. A. H. Ibrahim, O. M. Mostafa, and A. H. El-Abiad, "Dynamic equivalents using operating data and stochastic modeling," *Power Apparatus and Systems, IEEE Transactions on,* vol. 95, pp. 1713-1722, 1976.

[59] K. L. Lo and A. H. Al-Ghafri, "Identification of Power System Dynamic Eqiuvalents from on-line Estimation by using Stochastic Modelling and Least Squares," in *26th Universities Power Engineering Conference*, 1991.

[60] W. J. Wilson and J. D. Aplevich, "Dynamic Equivalent Power System Models," *Power Apparatus and Systems, IEEE Transactions on,* vol. PAS-102, pp. 3753-3760, 1983.

[61] P. Ju, L. Q. Ni, and F. Wu, "Dynamic equivalents of power systems with online measurements. Part 1: Theory," *Generation, Transmission and Distribution, IEE Proceedings-,* vol. 151, pp. 175-178, 2004.

[62] P. Ju, F. Li, N. G. Yang, X. M. Wu, and N. Q. He, "Dynamic equivalents of power systems with online measurements Part 2: Applications," *Generation, Transmission and Distribution, IEE Proceedings-,* vol. 151, pp. 179-182, 2004.

[63] A. M. Stankovic, A. T. Saric, and M. Milosevic, "Identification of nonparametric dynamic power system equivalents with artificial neural networks," *Power Systems, IEEE Transactions on,* vol. 18, pp. 1478-1486, 2003.

[64] P. W. Sauer and M. A. Pai, *Power system Dynamics and Stability*: Prentice-Hall, Inc., 1998.

[65] A. M. Stankovic and A. T. Saric, "Transient power system analysis with measurement-based gray box and hybrid dynamic equivalents," *Power Systems, IEEE Transactions on,* vol. 19, pp. 455-462, 2004.

[66] H. Shakouri G and H. R. Radmanesh, "Identification of a continuous time nonlinear state space model for the external power system dynamic equivalent by neural networks," *International Journal of Electrical Power & Energy Systems,* vol. 31, pp. 334-344, 2009.

[67] O. C. Y. Lino, "Robust recurrent neural network-based dynamic equivalencing in power system," in *Power Systems Conference and Exposition, 2004. IEEE PES*, 2004, pp. 1068-1077 vol.2.

[68] M. A. E. A. Abd-Ei-Rehim, I. D. Helal, and M. A. H. Omar, "Multi-machine power system dynamic equivalents using artificial intelligence (ANN)," in *Power Systems Conference, 2006. MEPCON 2006. Eleventh International Middle East*, 2006, pp. 197-207.

[69] J. A. Taylor and S. M. Halpin, "Approximation of Generator Coherency Based on Synchronization Coefficients," in *System Theory, 2007. SSST '07. Thirty-Ninth Southeastern Symposium on*, 2007, pp. 47-51.

[70] B. Ayazifar, "Graph Spectra and Modal Dynamics of Oscillatory Networks." vol. Ph.D.: Massachusetts Institute of Technology, 2002, p. 191.

CHAPTER 3

GRAPH MODEL-BASED COHERENT GENERATOR IDENTIFICATION

3.1 Introduction

Identification of coherent generators could be classified into two major approaches: an effect-based approach and a cause-based approach. The former identifies coherent generators by an observation of their influences on power system, e.g. a relatively constant between rotor angle (or speed) variations[1], a row-dependency of basis-eigenvectors [2], and an equality of rotor angle deviation from a reference generator at both a stable operating point and an unstable operating point [3]. The latter identifies coherent generators by an inspection of a particular structure of power system that causes a coherency, e.g. a weak coupling between diagonal blocks inside a model matrix [4], and an equality of a ratio of admittance (between generator and fault) to inertia [5].

The graph model-based method proposed in this chapter is the cause-based approach where the coherent generators are identified from a particular structure of the graph model causing the coherency. By using the graph model, it helps the interpretation of and could make a reasonable approximation for identifying the coherent generators without parameters of generators. Although there are developments of power system partitioning based on graph model [6-8], their aim is for islanding and require initialising groups obtained from the slow coherency based method. Moreover, those graph models are not directly built from dynamic model of power system.

This chapter presents the identification of coherent generator based on the graph model. The graph model, in particular a node-weight graph type, of oscillatory network and its related coherency theorems are first described. Next, their application to identify coherent generators of power system is explained. Afterward, three proposed techniques (based on a visual inspection, a weak coupling technique, and an epsilon decomposition technique) are developed and evaluated. Finally, an extension to identify coherent generators without generator parameters is discussed.

3.2 Graph model and its coherency

Ayazifar [9] has modelled a class of dynamic systems called oscillatory network by a node-weighted graph model and has studied the mutual influence between a structure of graph and its dynamic behaviour, in particular coherency phenomenon. In this section, a representation of oscillatory network by the node-weighted graph model is first presented; and then, the related coherency theorems will be summarised.

3.2.1 Node-weighted graph representation of oscillatory network

The oscillatory network is a network comprising dynamic and static elements such as LC-circuit, mass-spring systems, and electric power system which behaves according to equation (1).

$$\mathbf{M}\ddot{\mathbf{y}}(t) + \mathbf{L}\mathbf{y}(t) = \mathbf{0} \tag{1}$$

Where **M** is a diagonal matrix, **L** is a matrix whose off-diagonal entries are symmetry and a diagonal entry is a negative sum of off-diagonal entries in the same row (known as Laplacian matrix), and **y(t)** is a displacement vector.

According to this equation, its node-weighted graph model can be established by associating nodes, edges and weights with the entries of the matrices in eqn. (1) as shown in figure 3.1.

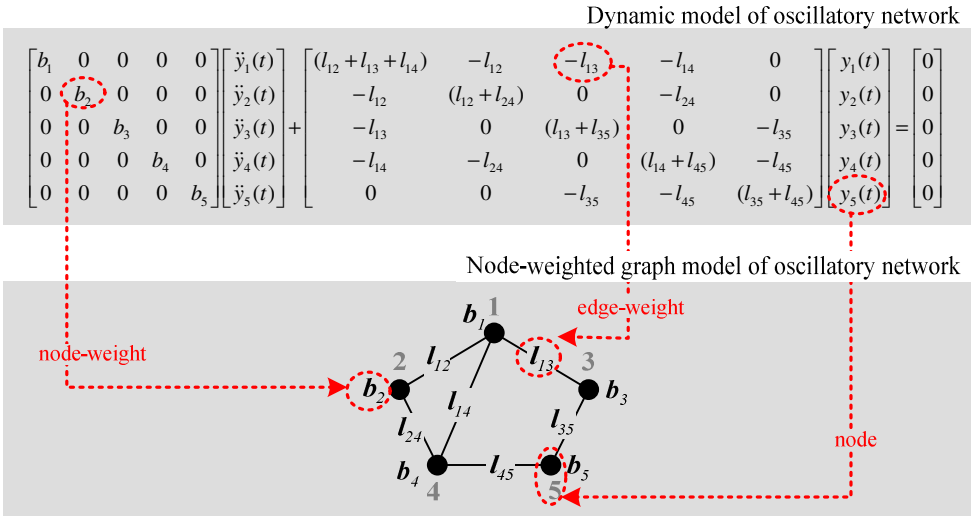

Figure 3.1 Establishing a node-weighted graph model of oscillatory network

From figure 3.1, the elements of y denote the nodes whose weights correspond to the diagonal entries of matrix **M**. The nodes are connected by the edges according to the existence of the off-diagonal entries of the **L** matrix and the edge-weights are denoted by those entries.

In addition to straightforward establishing the graph, system dynamics of oscillatory network could be deduced from the representation of eqn (1). This is because a generalized eigen-problem defined directly on **L**-matrix and **M**-matrix following eqn (2) gives the solutions, eigenvalue (ω^2) and eigenvector ($\mathbf{\upsilon}$), that characterize the time response of oscillatory network ($\mathbf{y}(t)$) according to eqn (3).

$$\mathbf{L}\mathbf{\upsilon} = \omega^2\mathbf{M}\mathbf{\upsilon} \tag{2}$$

$$\mathbf{y}(t) = ce^{j\omega t}\mathbf{\upsilon} \tag{3}$$

where c is a constant from initial condition. Consequently, the mutual influence between a structure of graph and its dynamic behaviour can be studied.

3.2.2 Coherency in term of node-weighted graph

Coherency studied by Ayazifar [9] is based on characterizing the time response by eigenvalue and eigenvector. This make coherency could be observed from the dependency between rows of basis eigenvector-matrix in the same manner as slow coherency introduced by Chow [2]. However, Ayazifar has employed a matrix perturbation approach and a generalised eigenvalue technique so that the study of coherency phenomena is conduced on the original **M** and **L** matrices setting, hence connecting with the node-weighted graph model.

There are two major proofs of coherency in terms of the node-weighted graph introduced by Ayazifar. These proofs cover the case of the graph having both zero weighted node (called L-node) and non-zero weighted node (called G-node). The first proof is *Slow-coherency* while the second proof is *Exact-Coherency*. However, only the *Slow-coherency* theorem is mentioned here because it is needed to

understand our development of the coherent generator identification method. The Slow-Coherency in Graph Theoretic Terms states that:

> '*Consider a graph G with n vertices, Laplacian matrix L, and vertex weight matrix M. Let the graph have a q-partition* $v_q = \{V_1, \ldots, V_q\}$, *where each cluster* $G(V_i)$ *contains at least one G-node. The intra-area weights are of order* $O(1)$, *while the inter-area link strengths are of order* $O(\varepsilon)$. *Then*
>
> 1. *the fastest* n_G*-q eigenvalues of (**L**,**M**) are of order* $O(1)$.
> 2. *the slowest q eigenvalues of (**L**,**M**) are of order* $O(\varepsilon)$.
> 3. *the slowest q eigenvectors of (**L**,**M**) exhibit approximate coherency, i.e., they are approximately constant over any given area* $G(V_i)$, *i=1,…,q.'*
>
> *Theorem 5.3, p.98-99, Ayazifar[9]*

According to this theorem, each cluster of the nodes are slow coherent (i.e. coherency occurs in the slow modes of an oscillations) if the intra-area edge weights are of order O(1), while the inter-area edge weights are of order O(ε) provided that each cluster contains at least one non-zero weighted node. The ε is a small number approaching zero. The intra-area edge weight is the weight of edge which connects between the nodes in the same cluster (or group). The inter-area edge weight is the weight of edge which connects between the nodes of different clusters (or groups). Therefore, the groups of coherency can be identified by looking for the particular structure of the graph, in which the groups of coherent nodes have the strong connections between nodes within their group and have the weak connections among nodes of other groups. It is note that this theorem requires no value of node weight for the identification of coherent nodes.

3.3 Coherent Generator identification from Graph model

The graph model-based coherent generator identification is composed of two successive steps: establishing node-weighted graph model of power system and identifying groups of strong-intra linked nodes and weak-inter linked nodes, respectively. These two steps are described in the following two subsections.

3.3.1 Node-weighted graph model of power system

In electric power system, a particular dynamics whose model fits to the representation of eqn (1) is the small-signal rotor angle dynamics.

$$\begin{bmatrix} \mathbf{J} & \mathbf{0} \\ \mathbf{0} & \mathbf{0} \end{bmatrix} \begin{bmatrix} \Delta\ddot{\boldsymbol{\delta}}_G \\ \Delta\ddot{\boldsymbol{\delta}}_L \end{bmatrix} + \begin{bmatrix} \mathbf{L}_{GG} & \mathbf{L}_{GL} \\ \mathbf{L}_{LG} & \mathbf{L}_{LL} \end{bmatrix} \begin{bmatrix} \Delta\boldsymbol{\delta}_G \\ \Delta\boldsymbol{\delta}_L \end{bmatrix} = \mathbf{0} \tag{4}$$

$$[\mathbf{L}]_{ij} = \begin{cases} v_i v_j S_{ij} \cos(\delta_i - \delta_j) & \text{if } i \neq j \\ \sum_{l=1, l\neq i}^{n} [\mathbf{L}]_{il} & \text{if } i = j \end{cases} \tag{5}$$

Where $\mathbf{J}$ is the matrix of normalized generator inertias, $\boldsymbol{\Delta\delta}$ is the displacement vector of bus voltage phase angle from a specific operating point (subscript G for a generator internal voltage bus and L for a load bus including a generator terminal voltage bus), v_i is the ith bus voltage magnitude, δ_i is the ith bus voltage angle, and S_{ij} is the transmission line susceptance between buses i and j. As the displacement variables (nodes) are bus-angles, the coherent groups of nodes identified here are the coherent groups of generators in the context of coherency-based equivalent.

The node-weighted graph model of the power system dynamic model eqns (4)-(5) can be established by the same procedure previously described in the section 3.2.1. Alternatively, it could be directly established from a one line diagram and power-flow solutions as shown in Figure 3-2.

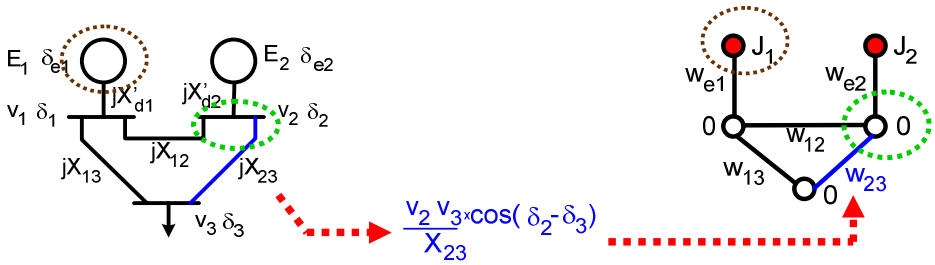

Figure 3.2 Establishing the node-weighted graph model of power system from a one line diagram and power-flow solutions

From Figure 3.2, the left hand side shows a single line diagram of power system where v_i is the i[th] bus voltage magnitude, δ_i is the i[th] bus voltage angle, where E_i is the i[th] generator internal bus voltage magnitude, δ_{ei} is the i[th] generator internal bus voltage angle, and X_{ij} is the reactance of transmission line between the i-th bus and the j-th bus. The right hand side shows the node-weighted graph model of the system on the left hand side where w_{ij} is the edge weight between the i-th node and the j-th node, J_i is the weight of i-th non-zero weighted node.

The nodes and the edges of the graph correspond to the buses and the transmission lines of power system, respectively. The load buses and generator terminal buses are the zero-weighted node type (represented by un-filled circles), while the generator internal buses are the nonzero-weighted node type (represented by filled circles). The edge-weights are calculated from a reactance of associated transmission lines and voltages at its two ends. For example, the edge-weight between node 2 and node 3 is $w_{23} = \frac{v_2 v_3}{X_{23}} \cos(\delta_2 - \delta_3)$. The weight of the generator internal node (bus) equals the normalized inertia of generator at that node (bus). For example, the node-weight of the generator internal node 1 is $J_1 = \frac{2H_1}{2\pi f}$, where H is the inertia constant in kWs/kVA and f is the frequency in Hertz.

However, the node weights need not be calculated as their values are not used according to the theorem in the section 3.2.2. The inertia of generator, therefore, is not required. Moreover, if the edge weight between the generator terminal and internal nodes is assumed to be strong, the coherent groups can be identified without the necessity of parameters of generators.

3.3.2 Identification of strong intra-linked nodes and weak inter-linked nodes

There are three techniques to identify the groups of strong intra-linked nodes among weak inter-link nodes proposed in this section, which are a visual inspection, an

applied weak coupling, and an applied epsilon decomposition techniques, respectively.

3.3.2.1 Visual inspection technique

This technique is based on a direct inspection on a drawing of graph model whose edges are drawn by a line of two-different thicknesses. Edges whose weight is strong will be drawn by a thick line while other edges, whose weights are weak, will be drawn by a thin line. This drawing of graph model provides a visual aid to identify the groups of strong intra-linked nodes among weak inter-linked nodes. However, the decision is human. In this thesis, the drawing of graph model with two levels of edge thickness is drawn by the following process.

Drawing of a graph model with two levels of edge thickness

Step 1: Set a strength threshold, (e.g. in a percent of the maximum value of the edge-weight in the graph model), to differentiate between strong and weak.

Step 2: Draw a thick line for the edge whose weight is greater than or equal the threshold; and drawn a thin line for others.

3.3.2.2 Applied weak coupling technique

The second technique is based on an application of the Weak Coupling method [4, 10, 11] to a matrix of edge weight, which is a Laplacian matrix whose diagonal entries are set to zero. The weak coupling method was developed to identify sub-matrices which are internally strong but externally weak coupling. By applying the weak coupling method to the matrix of edge weight, the identified sub-matrices would mean the groups of strong intra-linked nodes among weak inter-linked nodes.

The key idea of Weak Coupling method is to quantify the relative strength of the connections between groups of sub-matrices (nodes) by ‘Coupling Factor’, which is a ratio of a summation of their off-diagonal entries to a summation of their diagonal

entries as depicted in Figure 3.3 (a). The Weak Coupling method uses this Coupling Factor to reorder sub-matrices according to their relative coupling by a successive inclusion of another node that gives a minimum value of Coupling Factor as depicted in Figure 3.3 (b). Then, the groups of strong internal connections among weak external connections are identified by investigating the changes in Coupling Factor versus the re-ordered sub-matrices with the aid of two plots, namely the coupling graph and the grouping bar chart as depicted in Figure 3.3 (c).

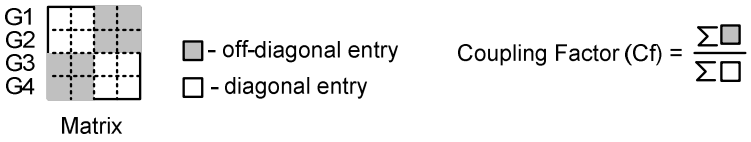

(a)

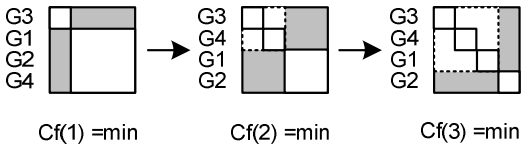

(b)

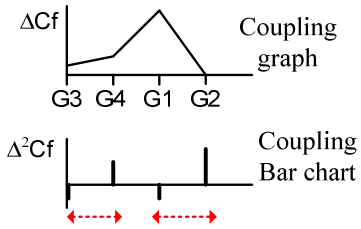

(c)

Figure 3.3 Weak Coupling method

In this thesis, the re-ordering algorithm are adopted from [11] with minor modifications to neglect the second order term and to exclude the diagonal entries of matrix, since the diagonal entries are not related to any particular edge-weight. In order to ensure that the identified groups are coherent groups (i.e. each group contains at least one non-zero weighted-node), the matrix of edge-weight of a reduced graph model whose all zero weighted nodes are eliminated should be used. The elimination of nodes could be performed by Gaussian elimination.

Node (Generator) Ordering Algorithm

Step1: Divide the matrix (L-matrix whose the diagonal entries are set to zeros) into two sub-matrices with the first one containing an arbitrarily chosen node (generator) "i", so that n_1=1. The second one contains the remaining (n-1) nodes.

Step2: Calculate

$$S_{S1} = \sum_{j=n_1+1}^{n} \sum_{i=1}^{n_1} \left|L_{ij}\right| + \sum_{j=1}^{n_1} \sum_{i=n_1+1}^{n} \left|L_{ij}\right| \tag{4}$$

$$S_{T1} = \sum_{j=1}^{n} \sum_{i=1}^{n} \left|L_{ij}\right| \quad , for \ i \neq j \tag{5}$$

$$S_{N1} = S_{T1} - S_{S1} \tag{6}$$

Step3: Calculate the coupling factor, $C_f = C_f(n_1)$ by

$$C_f = \frac{S_{S1}}{S_{N1}} \tag{7}$$

and set $C_{f\,min} = C_f(n_1)$, $L(n_1) = i$

Step4: Substitute node "i" in the first subsystem by any one nodes from the second sub-matrix. Calculate the corresponding $C_f = C_f(n_1)$

Step5: If $C_f(n_1) < C_{f\,min}$, Reset $C_{f\,min}$ and $L(n_1)$

Step6: Repeat Step 4 and 5 for all the remaining nodes in the second sub-matrix. Then from Step 5 the node $L(n_1)$ corresponding to the minimum coupling factor can be identified.

Step7: Divide the total matrix into two sub-matrices with the first one consisting of nodes $L(1), L(2), \ldots, L(n_1)$ that have been identified in Step 6 together with an arbitrarily chosen node "i". Thus $n_1 = n_1 + 1$ and the second one contains the remaining $(n - n_1)$ nodes.

Step8: Go to Step 3 if $n_1 < n$ and stop if $n_1 = n$.

Two plots for helping the identification of the groups of strong internal connections among weak external connections are defined below.

Coupling Graph:

A plot of $C_f(m)$ *against* $L(m)$ *(m=1, 2,…, n).*

Grouping Bar Chart:

A bar plot of $\Delta^2 C_f(m)$ *against* $L(m)$ *(m=1, 2,…, n), where* $\Delta^2 C_f(m)$ *can be calculated as follows*[11].

$$\Delta^2 C_f(m) = \begin{cases} C_f(2) - 2C_f(1), & m = 1 \\ C_f(m+1) - 2C_f(m) + C_f(m-1), & 1 < m < n \\ C_f(n-1), & m = n \end{cases} \tag{8}$$

The slope of the coupling graph indicates a coupling between a node and sub-matrices. It shows that, if $\Delta C_f(m) = C_f(m+1) - C_f(m) < 0$, a node $L(m+1)$ is stronger coupling with the first sub-matrix but the second sub-matrix if $\Delta C_f(m) > 0$. Therefore, the relative minima points could divide the nodes into groups that are weakly coupled.

On the other hand, the grouping bar chart provides a coupling between two successive nodes. A node $L(m+1)$ is weakly coupled to node $L(m)$ if $\Delta^2 C_f(m) > 0$ but it is strongly coupled to node $L(m)$ if $\Delta^2 C_f(m) < 0$, while the magnitude of bar indicates its strength. Hence, a group of strongly coupled nodes begins at a negative bar after a positive bar and ends at the next positive bar. Furthermore, the group of one node is indicated by a positive bar after a positive bar. However, these indicators must be used in conjunction with the positive slope ($\Delta C_f(m) > 0$) of the coupling graph (as shown in figure 3-4). This is because the grouping bar chart shows local

information (i.e. a relative coupling between two successive nodes) and the nodes may be considerably strong coupled as a whole (i.e. $\Delta C_f(m) < 0$).

Accordingly, the coupling graph and the grouping bar chart must be used together for an efficient identification of the groups of strong internal connections among weak external connections.

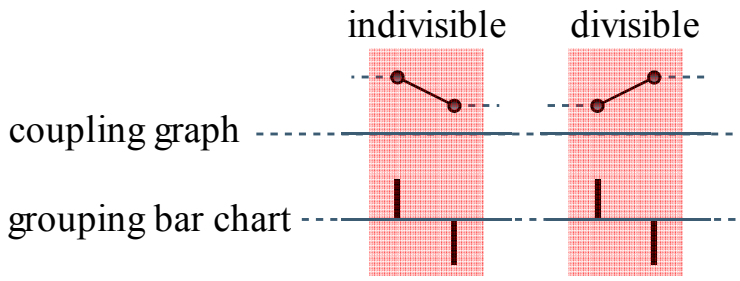

Figure 3.4 Indicators on the coupling graph and the grouping bar chart for the division of group.

3.3.2.3 Applied epsilon decomposition technique

The third technique is based on an application of Epsilon Decomposition [12] to the matrix of edge weight. The Epsilon Decomposition was also developed to identify the sub-matrices which are internally strong but externally weak connected. However, the key idea to quantify the strength of connection and the process to identify the sub-matrices are quite different from the Weak Coupling method.

In this technique, the strength of connection (i.e. off-diagonal entries of matrix) is quantified by a comparison to a pre-defined number, called 'Epsilon'. The connection is strong if its value greater than the Epsilon, otherwise it will be considered as weak. The procedure to identify the internally strong but externally weak connected sub-matrices by using the Epsilon Decomposition is simply depicted in Figure 3.5.

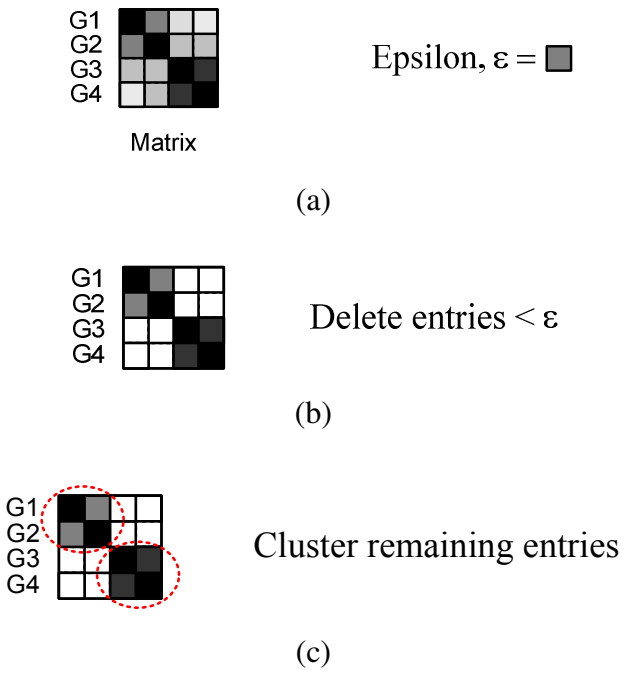

Figure 3.5 Epsilon decomposition method

From Figure 3.5 (a), the value of the off-diagonal entry is depicted by a filled box with a different darkness. The off-diagonal entries of matrix having value (weight) less than 'Epsilon' will be deleted (Figure 3.5 (b)) and the disjoint clusters of the remaining will be identified as the groups of coherent nodes (Figure 3.5 (c)).

Due to the algorithm in [12] is designed for a directed graph and rather complex to understand, the clustering method in [13] is alternatively chosen for this task. However, it is modified to include the case of non-symmetrical matrix as shown below.

Epsilon Decomposition Algorithm

Step1: Normalise entries of the matrix by its maximum entry and set the entries having values smaller than the value of a pre-assigned Epsilon to zero.

Step2: Start searching the first row not yet covered to its right and records the column numbers if non-zero entries are found.

Step3: Each individual recorded column (not yet covered) searches its down and records the row numbers if non-zero entries are found.

Step4: Go to Step 7 if all recorded row is covered, otherwise continues Step 5.

Step5: Each individual recorded row (not yet covered) searches its right and records the column number if non-zero entries are found.

Step6: Go to Step 7 if all recorded column is covered, otherwise continues Step 3.

Step7: Create a non-redundant set of recorded rows and recorded columns as one of disjoint cluster for the matrix.

Step8: Stop if all row and all column are covered, otherwise go to Step 2.

3.4 Test results and discussion

There are two types of system studied here which are an artificial system and a real power system. The former aims to provide a proof of a concept and a consistency of the coherent group identification based on the graph model when the system is ideal (strong-intra group and vanishingly weak-inter group connections). The latter aims to assess performance of graph model-based coherent generator identification when conditions of the studied system are more practical and gradually deviate from the ideal system. For example, there is an inclusion of the resistance of transmission line. Furthermore, the coherent generator identification by using only the power-flow modelling data is studied. All case studies are summarised below.

A. Artificial system cases *(an ideal system)*

Case 1: Consistency between the coherent groups identified by the graph-based method and other methods (the slow coherency and the weak coupling).

- A twelve-node system (i.e. six non-zero weighted nodes and six zero weighted nodes)

Case 2: Performance of the coherent group identification based on the applied weak coupling technique and the applied epsilon decomposition technique.

- A twelve non-zero weighted node system

B. Power system case*s*

Case 3: Feasibility of the identification of coherent generators by the graph-based method.

- Nine bus power system [14] *(no assumption of strong internal edge-weight)*

Case 4: Consistency between the coherent groups identified by the graph-based method and other methods. (the tolerance-based slow coherency method, and the weak coupling method).

-IEEE 39 bus system [15] *(no assumption of strong internal edge-weight)*

Case 5: Effect of the assumption on the strong internal generator edge-weight

-IEEE 39 bus system *(with assumption of strong internal edge-weight)*

All studies have been conducted on MATLAB[16] and Power System Analysis Toolbox (PSAT)[17]. The related coherency identification techniques have been coded in MATLAB's m-file based-on algorithms provided in this chapter and appendixes.

Case 1: The system for this case study is shown in Figure 3.6. It is composed of twelve nodes (i.e. six non-zero weighted nodes and six zero weighted nodes). The non-zero weighted node is denoted by a filled-circle while the zero weighted-node is denoted by an unfilled circle. All weights of non-zero nodes are 10 units and they are shown beside the filled circle. The edge-weight is shown in the middle of each edge.

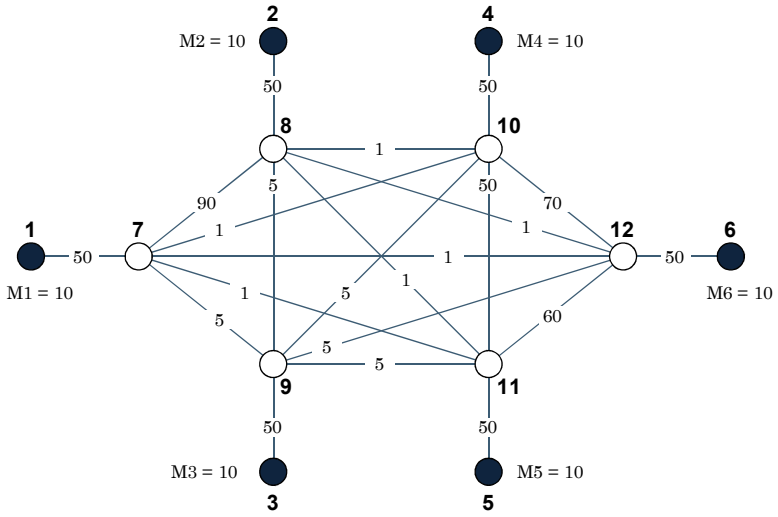

Figure 3.6 Artificial test system 1

The matrix of mass (**M**) and the matrix of connection (**L**-laplacian matrix) that describe this system ($\mathbf{M}\ddot{\mathbf{y}}(t)+\mathbf{L}\mathbf{y}(t)=\mathbf{0}$) are shown below:

```
M =

    10     0     0     0     0     0     0     0     0     0     0     0
     0    10     0     0     0     0     0     0     0     0     0     0
     0     0    10     0     0     0     0     0     0     0     0     0
     0     0     0    10     0     0     0     0     0     0     0     0
     0     0     0     0    10     0     0     0     0     0     0     0
     0     0     0     0     0    10     0     0     0     0     0     0
     0     0     0     0     0     0     0     0     0     0     0     0
     0     0     0     0     0     0     0     0     0     0     0     0
     0     0     0     0     0     0     0     0     0     0     0     0
     0     0     0     0     0     0     0     0     0     0     0     0
     0     0     0     0     0     0     0     0     0     0     0     0
     0     0     0     0     0     0     0     0     0     0     0     0
```

L =

-50	0	0	0	0	0	50	0	0	0	0	0
0	-50	0	0	0	0	0	50	0	0	0	0
0	0	-50	0	0	0	0	0	50	0	0	0
0	0	0	-50	0	0	0	0	0	50	0	0
0	0	0	0	-50	0	0	0	0	0	50	0
0	0	0	0	0	-50	0	0	0	0	0	50
50	0	0	0	0	0	-148	90	5	1	1	1
0	50	0	0	0	0	90	-148	5	1	1	1
0	0	50	0	0	0	5	5	-75	5	5	5
0	0	0	50	0	0	1	1	5	-177	50	70
0	0	0	0	50	0	1	1	5	50	-167	60
0	0	0	0	0	50	1	1	5	70	60	-187

The coherent nodes, in particular the non-zero weighted nodes, of the artificial test system 1 are identified by three methods: the slow-coherency method [2], the weak coupling method [11] and the graph model-based method. For the graph model-based method, three techniques (the visual inspection, the applied weak coupling technique, and the applied epsilon decomposition) are illustrated under two conditions: with and without assumption of strong internal edge-weight. To ensure that each identified group contains at least one non-zero weighted node, the applied weak coupling technique and the applied epsilon decomposition are applied to a reduced graph, i.e. a graph model where its zero-weighted nodes are all eliminated. The study of coherent node identification for this artificial system is summarized below.

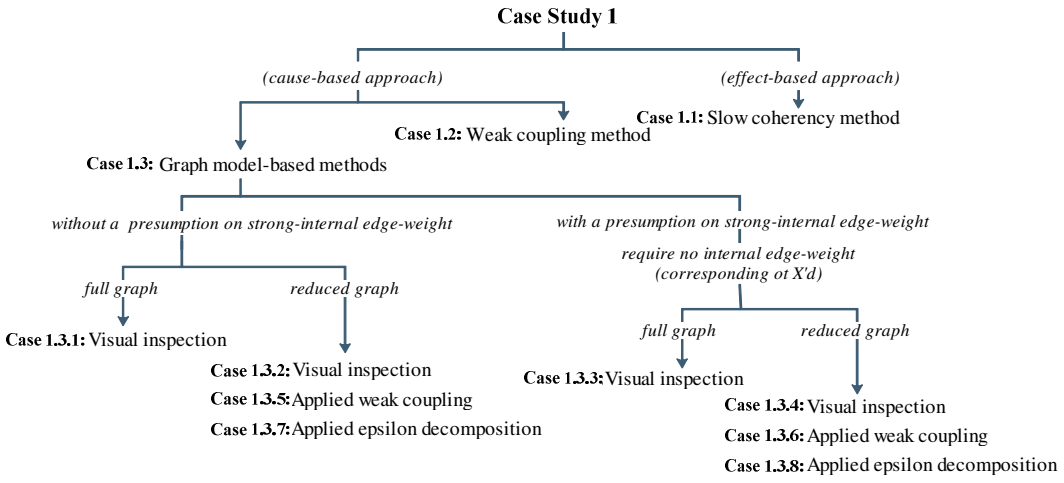

Figure 3.7 Summary of case study 1

Case 1.1: The slow-coherency method:

Step1: apply Gaussian elimination to eliminate the zero-weighted nodes. The reduced zero-weighted node graph model (see Figure 3.8) and its associated matrices are shown below.

Mred =

10	0	0	0	0	0
0	10	0	0	0	0
0	0	10	0	0	0
0	0	0	10	0	0
0	0	0	0	10	0
0	0	0	0	0	10

Lred =

-22.8729	16.6229	3.1250	1.0417	1.0417	1.0417
16.6229	-22.8729	3.1250	1.0417	1.0417	1.0417
3.1250	3.1250	-15.6250	3.1250	3.1250	3.1250
1.0417	1.0417	3.1250	-27.9993	10.9480	11.8430
1.0417	1.0417	3.1250	10.9480	-27.5519	11.3955
1.0417	1.0417	3.1250	11.8430	11.3955	-28.4468

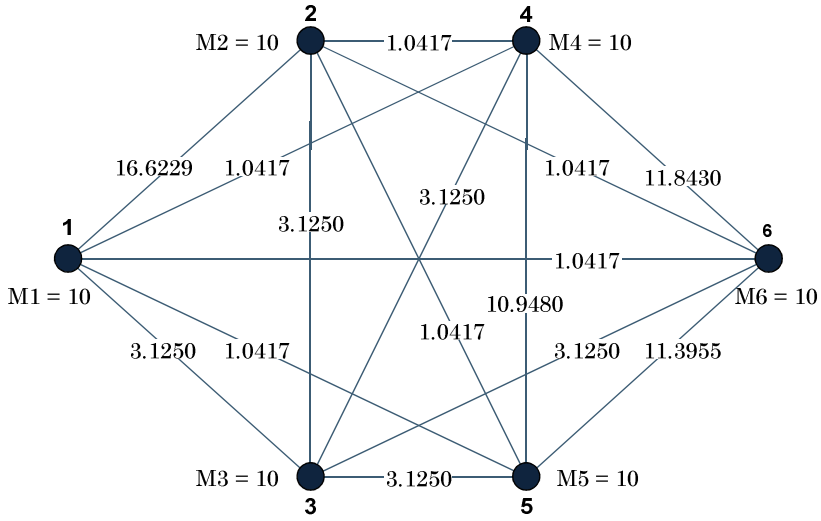

Figure 3.8 Artificial test system 1 after an elimination of the zero-weighted nodes

Step2: re-write the reduced graph model ($\mathbf{M}\ddot{\mathbf{y}}(t)+\mathbf{L}\mathbf{y}(t)=\mathbf{0}$) in a normal form of second order state-model ($\ddot{\mathbf{x}}=\mathbf{A}\mathbf{x}$) by multiplying **L**red-matrix with the inverse of **M**-matrix.

```
A =

   -2.2873    1.6623    0.3125    0.1042    0.1042    0.1042
    1.6623   -2.2873    0.3125    0.1042    0.1042    0.1042
    0.3125    0.3125   -1.5625    0.3125    0.3125    0.3125
    0.1042    0.1042    0.3125   -2.7999    1.0948    1.1843
    0.1042    0.1042    0.3125    1.0948   -2.7552    1.1396
    0.1042    0.1042    0.3125    1.1843    1.1396   -2.8447
```

Step3: specify the number of the slow modes (groups) and apply the slow-coherency algorithm (see Appendix E) to identify the coherent nodes. The calculation was performed up to the fourth step of those presented in Appendix E as $\mathbf{L}_d = \mathbf{V}_2\mathbf{V}_1^{-1}$ is enough to provide information of the slow coherent groups. The entry of i-th row and j-th column of $\mathbf{L}_d$ matrix show a degree of coherency between the i-th reference node and the j-th non-reference node. The more the value of entry closes to one, the more the j-th non-reference node and the i-th reference node are coherent. The entries of $\mathbf{L}_d$ matrix are shown in Table 3.1 below when the number of the slowest modes is chosen as three.

Table 3.1 Slow coherency of artificial test system A

Non-reference nodes	Reference nodes		
	3	2	6
1	-0.00	1.00	-0.00
4	0.00	-0.00	1.00
5	0.00	0.00	1.00

From table 1, the (slow) coherent nodes are (1, 2), (3), and (4, 5, 6) based on this result.

Case 1.2: The weak coupling method:

The simplified version of the weak coupling technique proposed in [11] (neglecting the second order terms, described in section 3.3.2.2) is applied to **A**-matrix (including its diagonal entries) and then the coupling graph and the grouping bar chart are plotted following the method mentioned in section 3.3.2.2. The plots are shown in Figure 3.9.

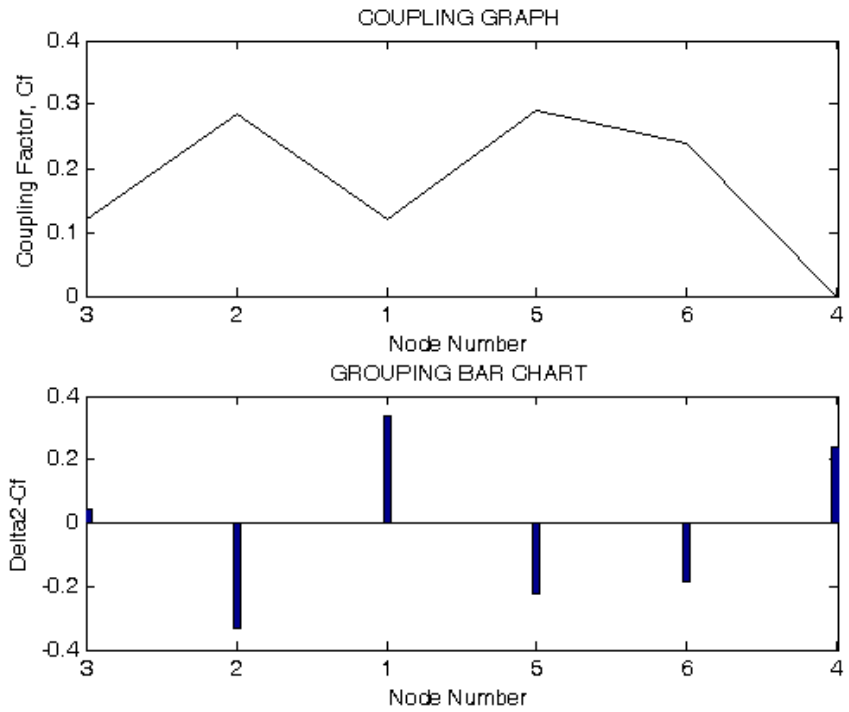

Figure 3.9 Coupling graph and the grouping bar chart of the **A**-matrix of the artificial test system 1

The coupling graph (Figure 3.9 (top)) shows the coupling factor against the node while the grouping bar chart (Figure 3.9 (bottom)) shows the change in the coupling factor against the node. The coherent groups can be determined from the grouping bar chart by examining the groups of nodes that begins at a negative bar after a positive bar and ends at the next positive bar. The negative bar after the positive bar must occur under a positive slope of the coupling graph to ensure that these two successive nodes are divisible (as shown in Figure 3.4). From the coupling graph (Figure 3.9(top)) and the grouping bar chart (Figure 3.9(bottom)), the coherent groups are nodes (2, 1) and nodes (5, 6, 4).

Case 1.3: The graph model-based method:

As shown in Figure 3.7, eight sub-cases of the graph model-based method (case 1.3.1 – case 1.3.8) were studied. These cases correspond to four categories of using information on L-matrix of the graph model which are: (1) a full graph model with complete information; (2) a reduced graph model with complete information; (3) a

full graph model with partial information; and (4) a reduced graph model with partial information. In the categories of using complete information, all modelling data contained in the L-matrix were used for the identification of coherent nodes, while only modelling data that related to the edge-weight of the non-zero weighted node were used in the categories of using partial information. This partial modelling data usage corresponds to an adoption of the assumption of strong edge-weight between the zero-weighted node and the non zero-weighted node.

The graph models and their associated part of L-matrices for each category are shown in Figures 3.10-3.13, respectively.

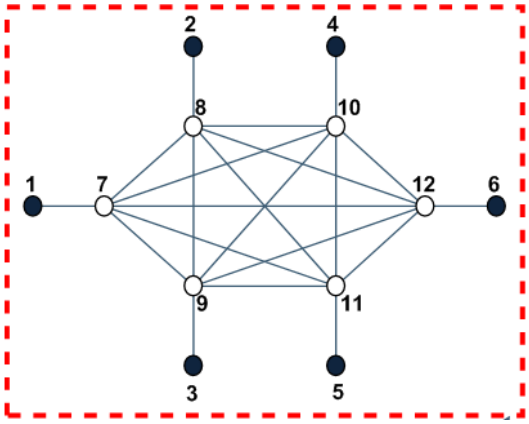

(a)

L =

-50	0	0	0	0	0	50	0	0	0	0	0
0	-50	0	0	0	0	0	50	0	0	0	0
0	0	-50	0	0	0	0	0	50	0	0	0
0	0	0	-50	0	0	0	0	0	50	0	0
0	0	0	0	-50	0	0	0	0	0	50	0
0	0	0	0	0	-50	0	0	0	0	0	50
50	0	0	0	0	0	-148	90	5	1	1	1
0	50	0	0	0	0	90	-148	5	1	1	1
0	0	50	0	0	0	5	5	-75	5	5	5
0	0	0	50	0	0	1	1	5	-177	50	70
0	0	0	0	50	0	1	1	5	50	-167	60
0	0	0	0	0	50	1	1	5	70	60	-187

(b)

Figure 3.10 Modelling data for the first category showing (a) the graph model and (b) its associated part on L-matrix

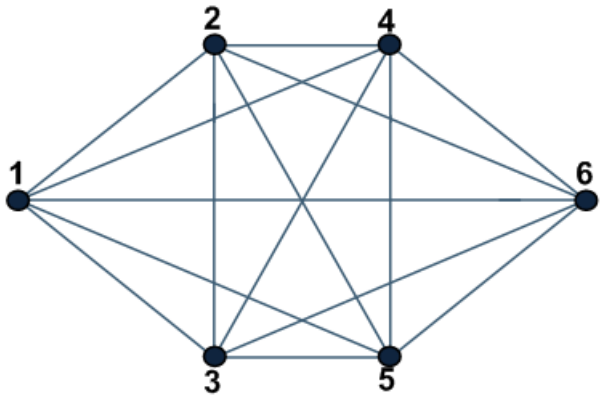

(a)

Lred =

-22.8729	16.6229	3.1250	1.0417	1.0417	1.0417
16.6229	-22.8729	3.1250	1.0417	1.0417	1.0417
3.1250	3.1250	-15.6250	3.1250	3.1250	3.1250
1.0417	1.0417	3.1250	-27.9993	10.9480	11.8430
1.0417	1.0417	3.1250	10.9480	-27.5519	11.3955
1.0417	1.0417	3.1250	11.8430	11.3955	-28.4468

(b)

Figure 3.11 Modelling data for the second category showing (a) the part of the graph model and (b) its associated part on L-matrix.

From Figure 3.11, the reduced graph model and the reduced L-matrix are obtained by applying Gaussian elimination to eliminate the zero-weighted nodes of the graph model inside a dashed box of Figure 3.10.

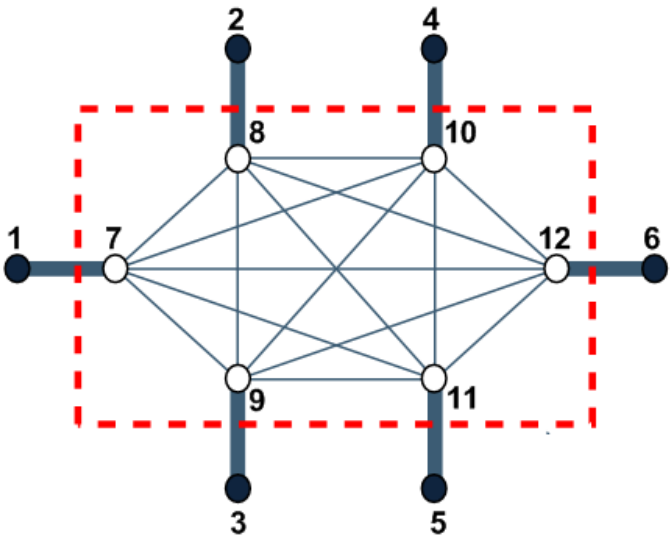

(a)

L =

-50	0	0	0	0	0	50	0	0	0	0	0
0	-50	0	0	0	0	0	50	0	0	0	0
0	0	-50	0	0	0	0	0	50	0	0	0
0	0	0	-50	0	0	0	0	0	50	0	0
0	0	0	0	-50	0	0	0	0	0	50	0
0	0	0	0	0	-50	0	0	0	0	0	50
50	0	0	0	0	0	-98	90	5	1	1	1
0	50	0	0	0	0	90	-98	5	1	1	1
0	0	50	0	0	0	5	5	-25	5	5	5
0	0	0	50	0	0	1	1	5	-127	50	70
0	0	0	0	50	0	1	1	5	50	-117	60
0	0	0	0	0	50	1	1	5	70	60	-137

(b)

Figure 3.12 Modelling data for the third category showing (a) the part of the graph model and (b) its associated part on L-matrix.

From Figure 3.12 (b), the diagonal-entries of the part of the L-matrix inside the dashed box are modified to exclude the effect of the off-diagonal entries outside the dashed box.

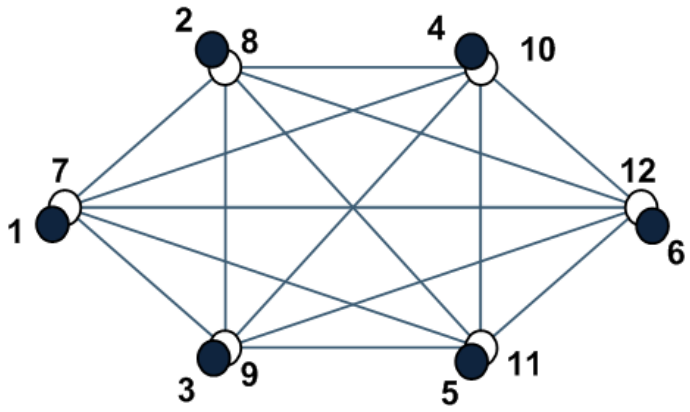

(a)

-98	90	5	1	1	1
90	-98	5	1	1	1
5	5	-25	5	5	5
1	1	5	-127	50	70
1	1	5	50	-117	60
1	1	5	70	60	-137

(b)

Figure 3.13 Modelling data for the fourth category showing (a) the part of the graph model and (b) its associated part on L-matrix.

From Figure 3.13, the reduced graph model and the reduced L-matrix are obtained by applying Gaussian elimination to eliminate the zero-weighted nodes of the graph model inside a dashed box of Figure 3.12. However, in this case, the zero weighted nodes inside the dashed box are all the representatives of the non-zero weighted nodes (denoted by the filled-node over the unfilled-node). Therefore, the reduced graph and its reduced L-matrix contain the same information as in Figure 3.12.

-The visual inspection technique (Case 1.3.1-Case1.3.4)

In this technique, the coherent groups are identified from the node-weighted graph representation by using two levels of line thickness under various edge-weight thresholds. Edges whose weights are above the threshold will be considered as strong and drawn by thick line while the others are considered as weak and drawn by thin line (as mentioned in section 3.3.2.1). The results shown in Figure 3.14, Figure 3.15 and Figure 3.16 are obtained when the threshold of 10 units is chosen. These results correspond to the cases 1.3.1, 1.3.2, and 1.3.3, respectively. Figure 3-16 also presents the result the case 1.3.4. It is clearly seen from the figures that they give the same coherent groups which are (1, 2), (3), and (4, 5, 6).

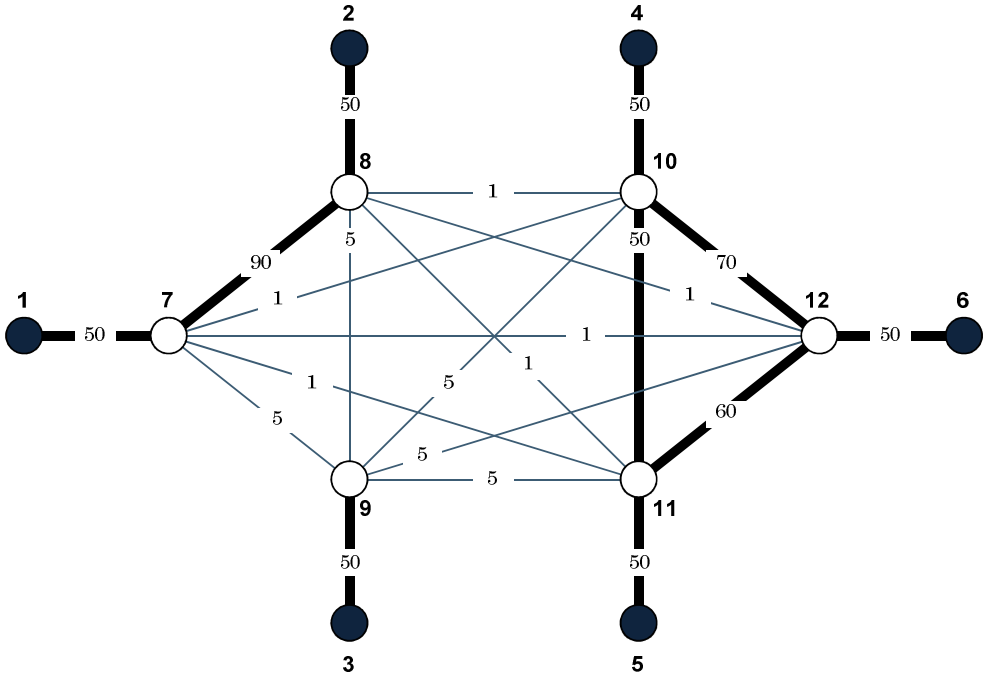

Figure 3.14 Two levels of line thickness plot of the full graph model without the assumption of strong internal edge-weight at threshold of 10 units

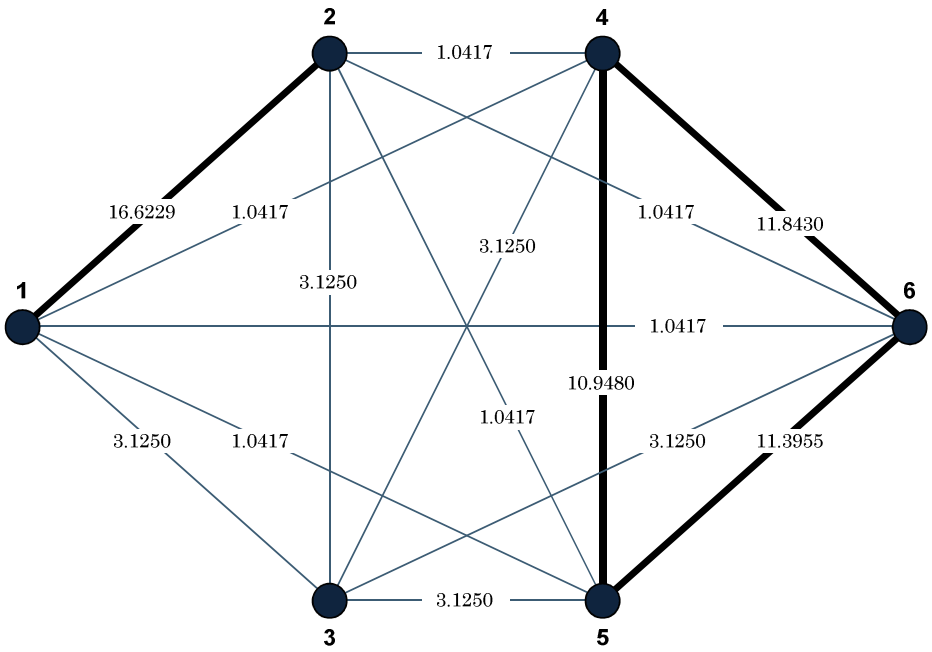

Figure 3.15 Two levels of line thickness plot of the reduced graph model without the assumption of strong internal edge-weight at threshold of 10 units

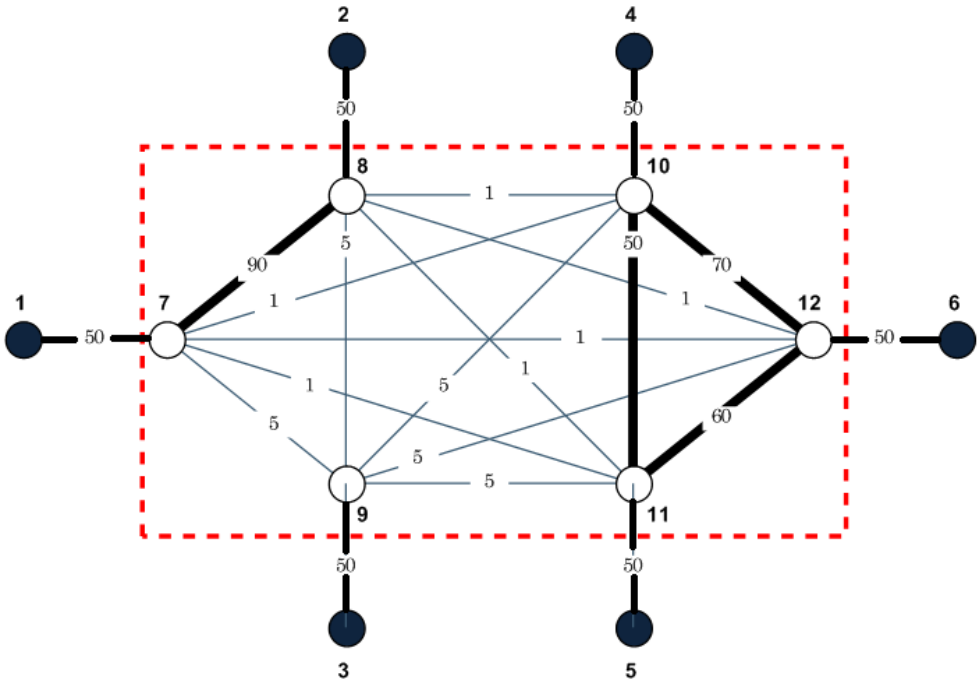

Figure 3.16 Two levels of line thickness plot of the full graph model (inside red-dashed box) with the assumption of strong internal edge-weight at threshold of 10 units

The applied weak coupling technique (Case 1.3.5 and Case 1.3.6)

Step1: Select the part of **L**-matrix according to each case (complete information or partial information of **L**-matrix) and set the diagonal entries to zero because they do not involve any particular edge-weights. In power system model, the off-diagonal entries of L-matrix which are irrelevant to generator internal buses (the partial information case here) can be calculated from the power flow model and its solutions (no need generator parameters).

Step2: apply the weak-coupling technique (as mentioned in section 3.3.2.2) to the above modified matrix in order to identify the strong-intra and weak-inter connected nodes. For both cases, the coherent nodes are (1, 2), (3), and (4, 5, 6), shown in Figures 3.17 and 3.18.

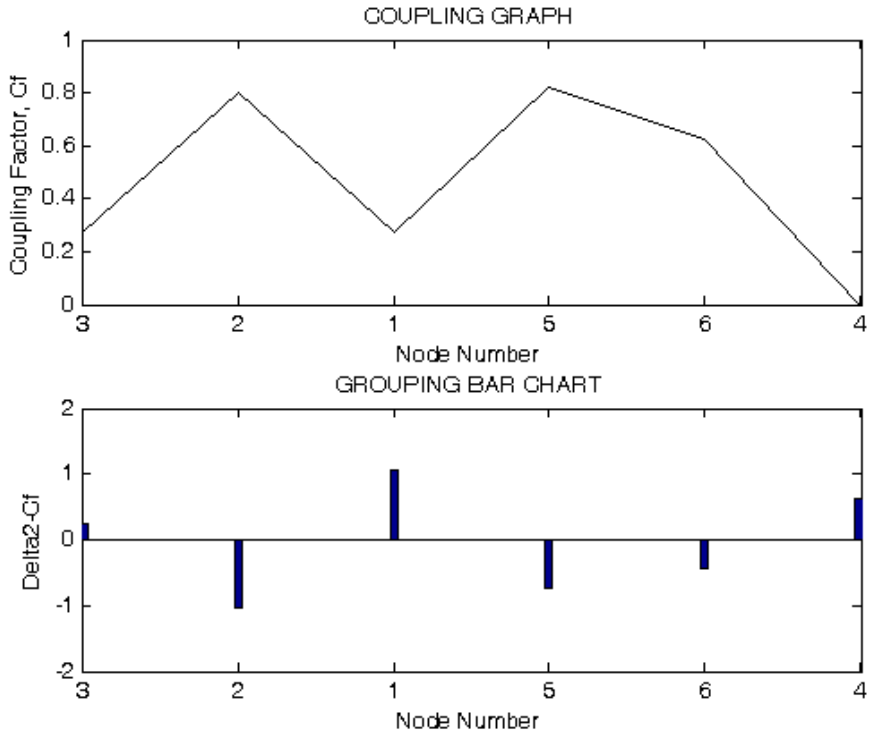

Figure 3.17 Coupling graph and coupling bar chart from complete information on **L**-matrix of the artificial test system 1.

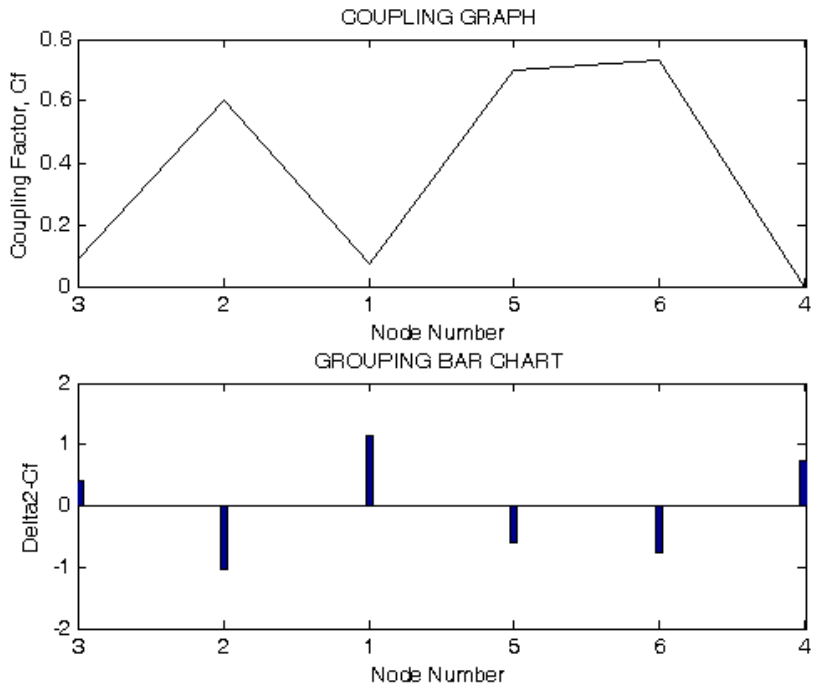

Figure 3.18 Coupling graph and coupling bar chart from partial information on L-matrix of the artificial test system 1.

The applied epsilon decomposition technique (**Case 1.3.7 and Case 1.3.8**)

Step1: Select the part of **L**-matrix according to each case (complete information or partial information of **L** matrix) and set the diagonal entries to zero because they do not involve any particular edge-weights.

Step2: apply the epsilon-decomposition technique (as mentioned in section 3.3.2.3) to the above modified matrix in order to identify the strong-intra and weak-inter connected nodes

The images of the modified matrices after a permutation of their rows and columns until nodes in the same group are next to each other are shown in Figure 3.19 and 3.20. The off-diagonal entries having magnitude less than the epsilon (0.5 units in this case) are shown in white while the others are shown in different level of darkness corresponding to their magnitudes. The coherent nodes are (1, 2), (3), and (4, 5, 6) for both cases.

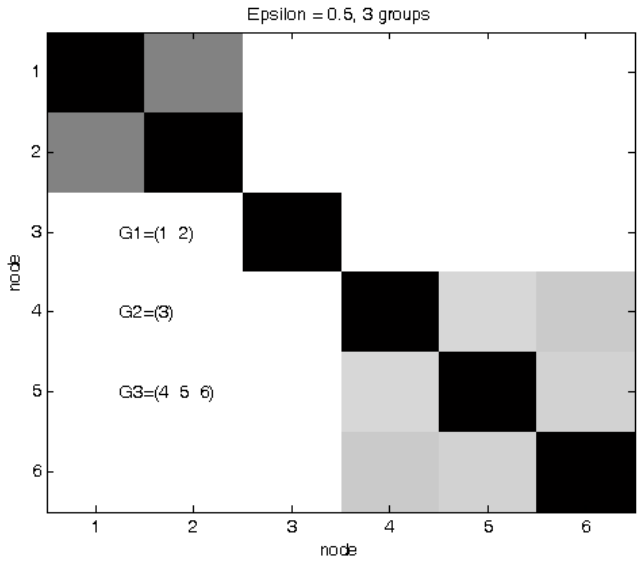

Figure 3.19 Image of normalised complete L-matrix of the artificial test system 1 for the epsilon of 0.5 units

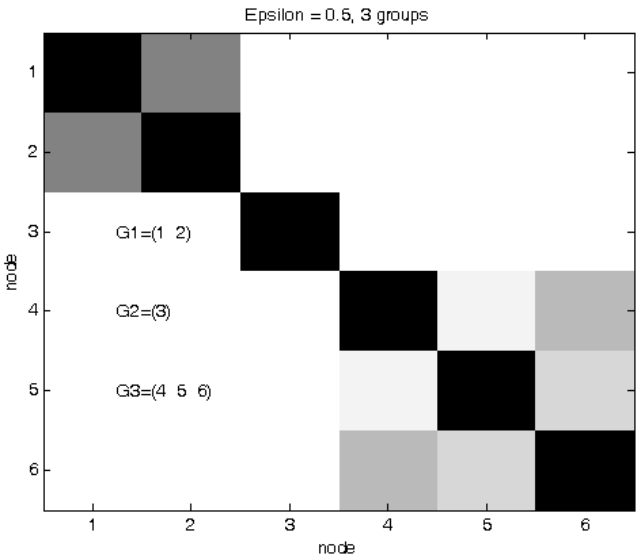

Figure 3.20 Image of normalised partial L-matrix of the artificial test system A1 for the epsilon of 0.5 units

Although the different groups of the coherent nodes (with different strength of coherency) could be obtained by setting a different value of the epsilon, an epsilon values of 0.5 units is chosen here to show a consistency of the result.

Case 2: This example is to show a better performance of the applied epsilon decomposition technique over the applied weak-coupling technique, considering information about degree of coherency versus size of group provided by these two methods. The example system ($\ddot{\mathbf{x}} = \mathbf{A}\mathbf{x}$) here is described by **A**-matrix below.

$$A = \begin{bmatrix} -105 & 90 & 5 & 5 & 1 & 1 & 0.5 & 0.5 & 0.5 & 0.5 & 0.5 & 0.5 \\ 90 & -105 & 5 & 5 & 1 & 1 & 0.5 & 0.5 & 0.5 & 0.5 & 0.5 & 0.5 \\ 5 & 5 & -25 & 10 & 1 & 1 & 0.5 & 0.5 & 0.5 & 0.5 & 0.5 & 0.5 \\ 5 & 5 & 10 & -25 & 1 & 1 & 0.5 & 0.5 & 0.5 & 0.5 & 0.5 & 0.5 \\ 1 & 1 & 1 & 1 & -12 & 5 & 0.5 & 0.5 & 0.5 & 0.5 & 0.5 & 0.5 \\ 1 & 1 & 1 & 1 & 5 & -12 & 0.5 & 0.5 & 0.5 & 0.5 & 0.5 & 0.5 \\ 0.5 & 0.5 & 0.5 & 0.5 & 0.5 & 0.5 & -156 & 135 & 7.5 & 7.5 & 1.5 & 1.5 \\ 0.5 & 0.5 & 0.5 & 0.5 & 0.5 & 0.5 & 135 & -156 & 7.5 & 7.5 & 1.5 & 1.5 \\ 0.5 & 0.5 & 0.5 & 0.5 & 0.5 & 0.5 & 7.5 & 7.5 & -36 & 15 & 1.5 & 1.5 \\ 0.5 & 0.5 & 0.5 & 0.5 & 0.5 & 0.5 & 7.5 & 7.5 & 15 & -36 & 1.5 & 1.5 \\ 0.5 & 0.5 & 0.5 & 0.5 & 0.5 & 0.5 & 1.5 & 1.5 & 1.5 & 1.5 & -16.5 & 7.5 \\ 0.5 & 0.5 & 0.5 & 0.5 & 0.5 & 0.5 & 1.5 & 1.5 & 1.5 & 1.5 & 7.5 & -16.5 \end{bmatrix}$$

This system represents a graph model of twelve non-zero weighted nodes and **A**-matrix here can also be considered as **L**-matrix of a reduced graph to their internal non-zero weighted-nodes. With representing the magnitude of each entry by different level of darkness, it is obviously seen that the degree of coupling between the nodes are a nest-structure (see Figure 3.21).

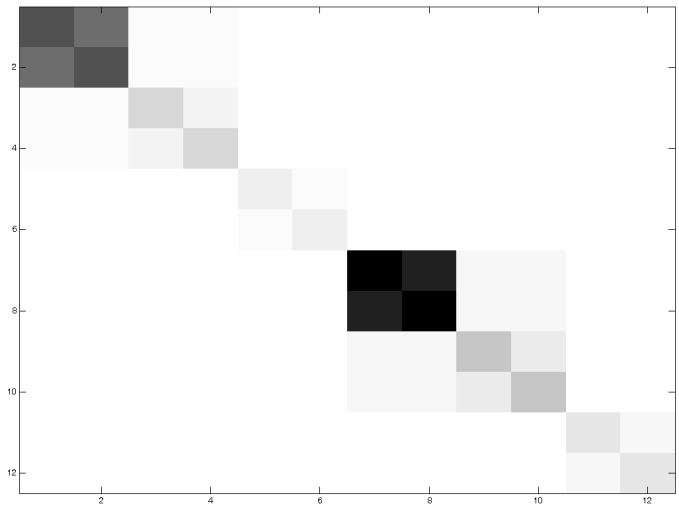

Figure 3.21 Image of **A**-matrix of the study case 2

Firstly, the coherent nodes are identified by the applied weak coupling technique (with the diagonal entries set to zero) and the result is shown in Figure 3.22.

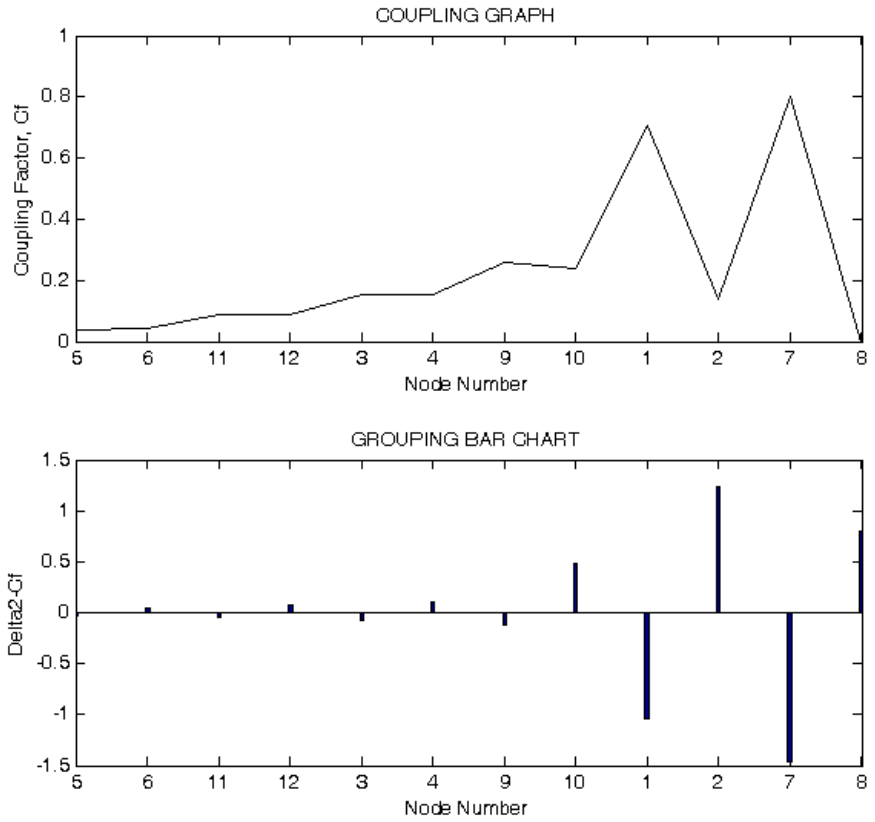

Figure 3.22 Coupling graph and grouping bar chart of **A**-matrix in the study case2

From the grouping bar chart (Figure 3.22), the coherent nodes are (5,6), (11,12), (3,4), (9,10), (1,2), and (7,8). In order to compromise between accuracy and computational resources (memory and time) of a subsequent reduced system, the coherent identification method should reasonably provide the flexibility in varying group size. In [10], the authors suggested that the different sizes of groups (according to different strength of coherency) could be determined from the grouping bar chart when the divisions according to the small magnitudes of the positive $\Delta^2 S$ are neglected. By setting $\Delta^2 S > 0.25$ as a criterion for the division, the groups of (5, 6, 11, 12, 3, 4, 9, 10), (1, 2), and (7, 8) are identified as weakly coherent groups.

Although the nodes (non-zero weighted nodes) in each weakly coherent groups are less coherent, the more proper groups of weakly coherent should be (1, 2, 3, 4), (7, 8, 9, 10), (5, 6), and (11, 12) as obviously seen on the image of the **A**-matrix in figure 3.21. These observations are also supported by time responses of the system ($\ddot{x} = Ax$) formed by the above **A**-matrix.

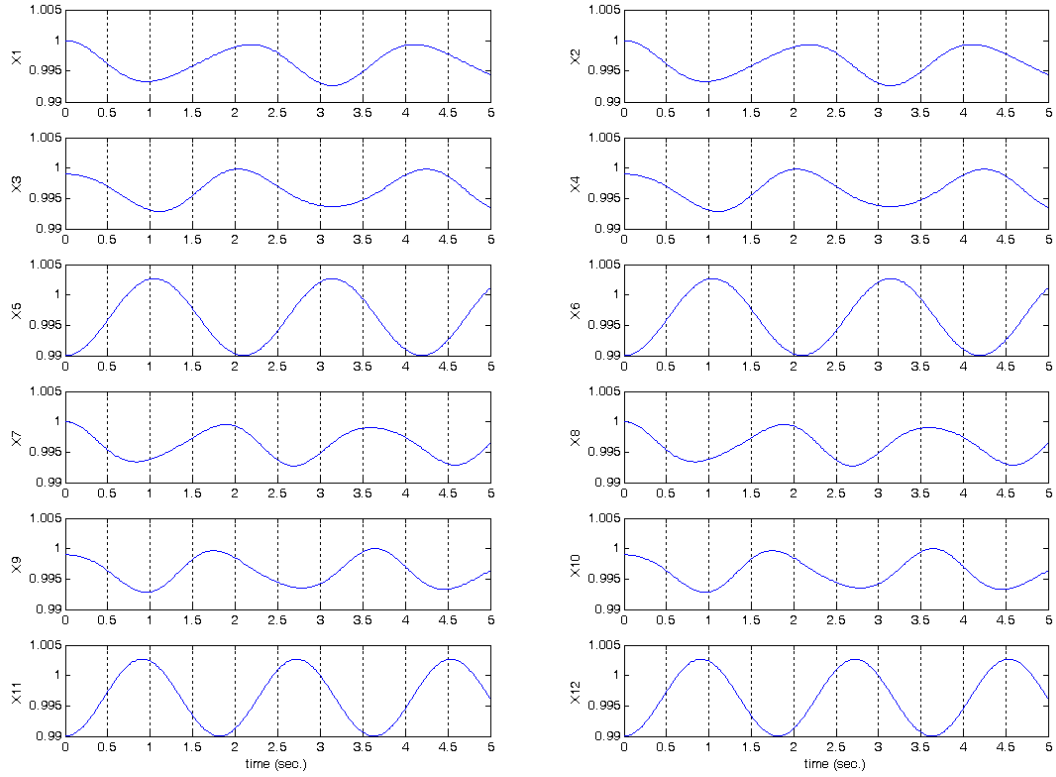

Figure 3.23 Time responses of the twelve states of the dynamic system formed by A-matrix ($\ddot{x} = Ax$) of the case study 2 when the initial states are all excited slightly different (1, 1, 0.999, 0.999, 0.99, 0.99, 1, 1, 0.999, 0.999, 0.99, 0.99)

From Figure 3.23, the clustering of weakly coherent responses according to groups of (1, 2, 3, 4), (7, 8, 9, 10), (5, 6) and (11,12) are more reasonable than the weakly coherent groups obtained from the grouping bar chart, (5, 6, 11, 12, 3, 4, 9,10), (1 2), and (7,8). Moreover, the contradiction between the responses within the weakly coherent groups identified from the coupling graph and the grouping bar chart, such as the responses of x3 and x5, is another indication of failure in varying a group size by this method.

In case of the applied epsilon decomposition technique, the groups of different size according to different degree of coherency can be identified by changing the value of epsilon. As shown in Figure 3.24, the applied epsilon decomposition method gives the idea of how groups should be according to their different degree of coherency close to the image of **A**-matrix (Figure 3.21); and, these results are also supported by the time responses in Figure 3.23.

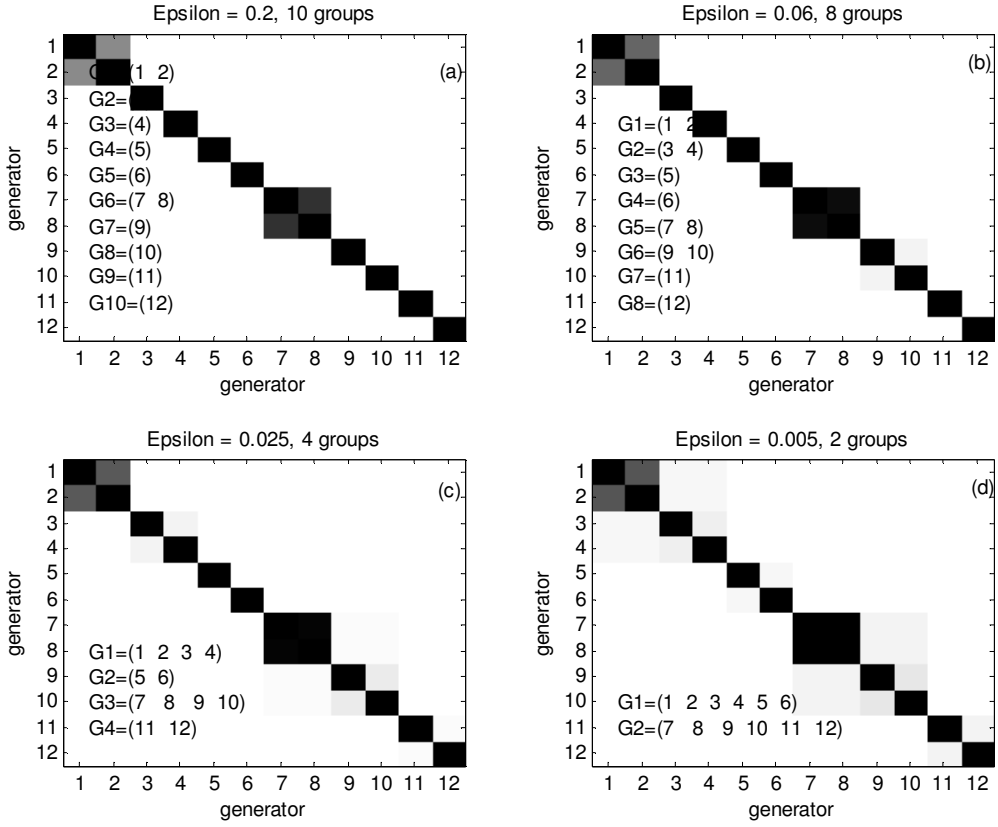

Figure 3.24 Images of normalized A-matrix of the case study 2 for the different values of epsilon: (a) epsilon=0.2; (b) epsilon=0.06; (c) epsilon=0.025; and (d) epsilon=0.005.

Case 3: This case study aims are to show a feasibility of identification of coherent generators by Graph model- based technique.

The procedure to identify coherent generators from the graph model of power system is composed of two successive steps: establishing node-weighted graph model of power system and identifying groups of strong-intra linked nodes and weak-inter linked nodes. However there are four assumptions not explicitly mentioned before the graph model is established. These assumptions (shown in Figure 3.25) cause the graph model to be departed from its original power system where the coherent generators are going to be identified.

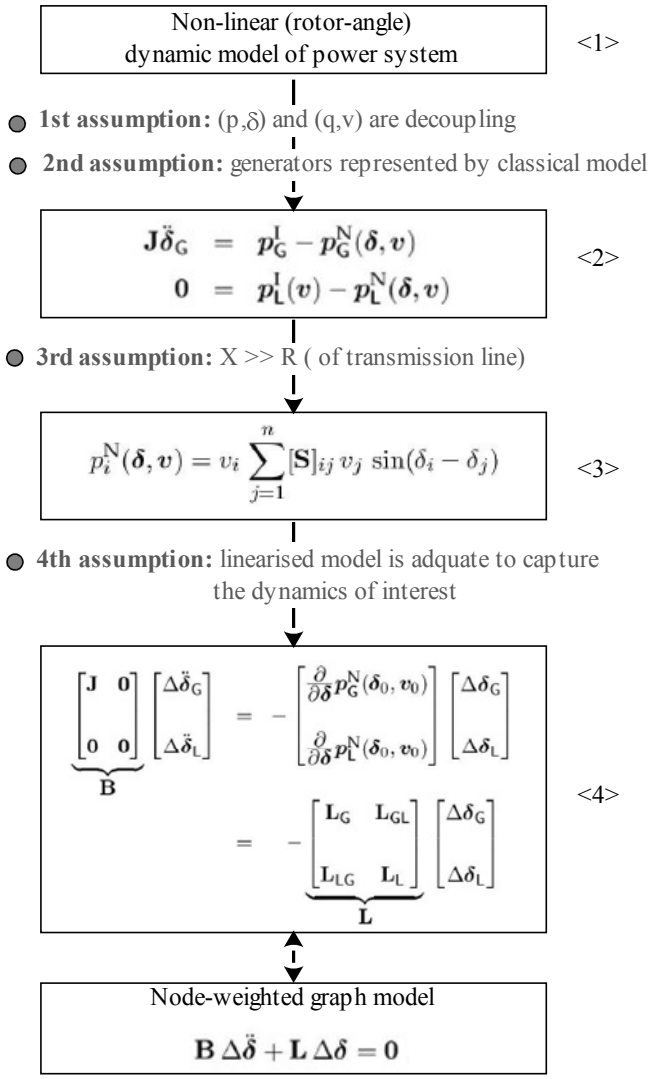

Figure 3.25 Four assumptions for establishing a node-weighted graph model of power system

The procedure and its related data to establish the node-weighted graph model are shown with the case of nine bus power system of Figure 3.26.

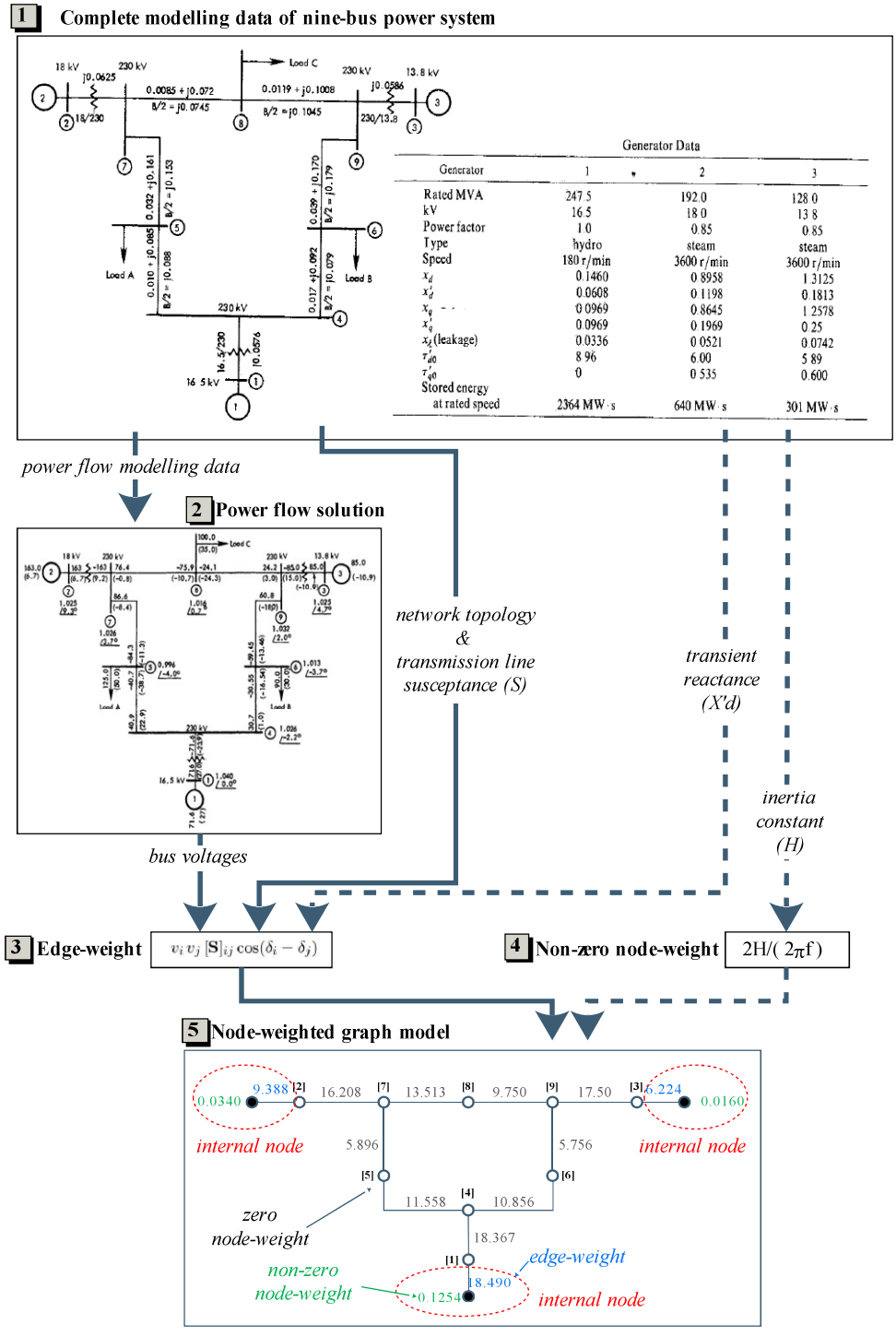

Figure 3.26 Calculations and their related data for establishing the node-weighted graph model.

From Figure 3.26, the modelling data of nine bus power system are divided into two major groups in the first step. The first group is static modelling data which involve the calculation through the solid-line paths. The second group is dynamic modelling data which involve the calculation through the dashed-line paths. In the second step, the static modelling data (i.e. power flow modelling data) is used to calculate the power flow solution, in particular bus voltages. Then, the bus voltages (both magnitude and angle) are used together with the susceptance of transmission line to calculate the edge-weight of the graph model in the third step. In this step, the transient reactance of generator and the additional routine to calculate the generator internal bus voltages are required for the calculation of the weight of edge between the generator terminal and internal buses. In the fourth step, the weights of nodes are calculated from the inertia constants of the generators. Finally, the node-weighted graph model is completely established in the fifth step.

However, to identify the coherent generators by the graph model method the inertia constants are no required and, therefore, the dashed-path along the forth step can be neglected. Moreover, based on the assumption of strong internal edge weight, the identification of coherent generator can be done without the value of transient reactance (no path of dashed-line to the third step).

To show the feasibility of coherent generator identification the visual inspection of the complete graph will be demonstrated first, while other techniques and consequence of neglecting generator parameters will be discussed in the next examples. From the graph model of the nine bus power system the groups of strong-intra linked nodes and weak inter-linked nodes can be easily identified by two levels of line thickness plot. As shown in Figure 3.27, the coherent generators are the generator 2 and the generator 3 when the thresholds of 6 are chosen.

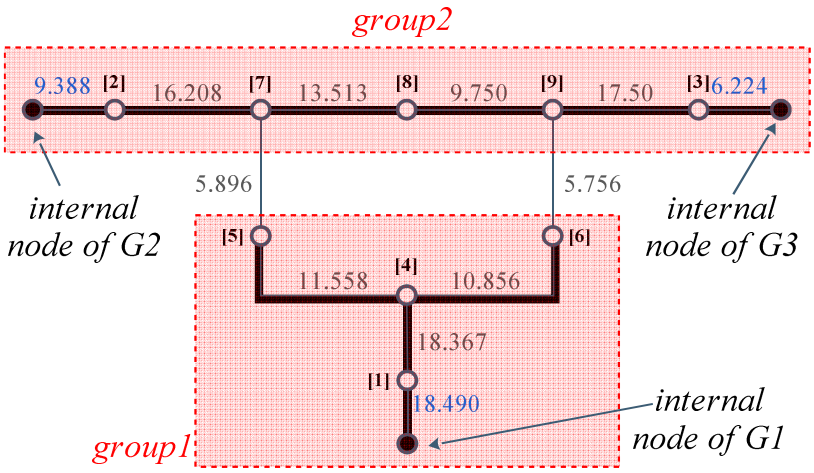

Figure 3.27 Two levels of line thickness plot of the node-weighted graph model of the nine-bus power system at the thresholds of 6 P.U.

These identified coherent generators (generator 2 and generator 3) are consistent with the results from Slow Coherency method as shown in Table 3.2 below. The reference generators are the generator 2 and 1 while the non-reference generator is the generator 3. As shown in the table, the non-reference generator is more correlates, 0.6871, to the generator 2 than the generator 1.

Table 3.2 Slow coherency of the nine bus power system

Non-reference nodes	Reference nodes	
	2	1
3	0.6871	0.3129

This result is obtained by applying the slow coherency method to the **A**-matrix of the nine-bus system which is calculated by using a procedure given in Appendix G. The calculation of the A-matrix is also based on the same assumptions in Figure 3.25. However, to provide a stronger verification, the non-linear time domain simulation of nine-bus system is performed and the rotor angles when a small fault is applied at bus 8 are given in Figure 3.28.

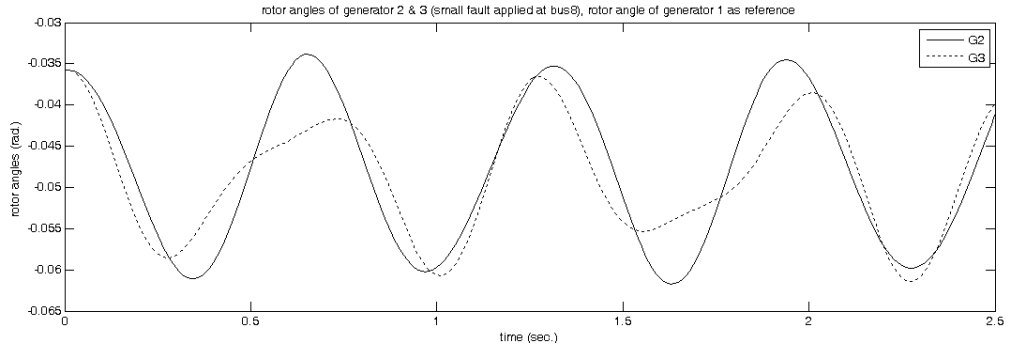

(a)

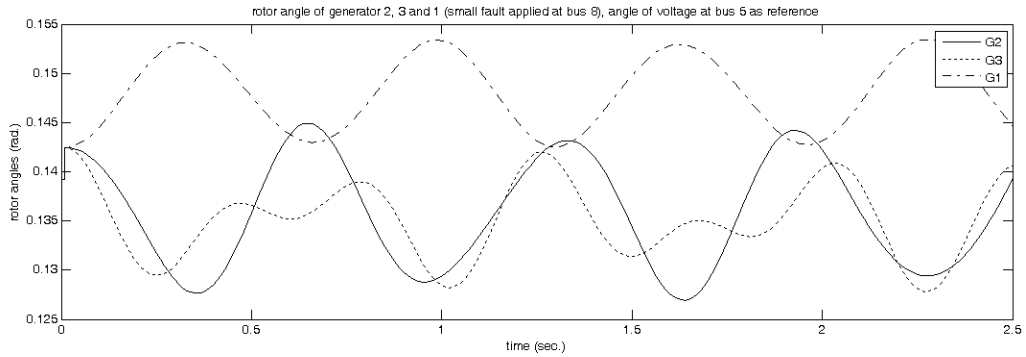

(b)

Figure 3.28 Deviation of rotor angle from the operating point when a fault with 10 PU impedances is applied at bus 8: (a) generator 2 & 3 when generator 1 is chosen as the reference; (b) generator 2, 3 and 1 when angle of voltage at bus 5 is chosen as the reference

From Figure 3.28, the deviations of rotor angle from the operating point confirm that the generator 2 and generator 3 are coherent in the slowest modes of oscillation. The reason for using the deviations of rotor angle from the operating point in the comparison because the definition of coherency here is given in term of the responses of linear model, so the deviations from the operating point have to be used when a linearlised model is considered.

Case 4: This case study aims to evaluate the performance of the graph model-based coherent generator identification (without the assumption of strong internal edge weight) by a comparison of its identified coherent groups with the groups obtained from other methods (the weak coupling method and the tolerance-based slow coherency method) that require the inertia of generators.

IEEE39 bus (with a classical generator model) is considered here as the test case. The identifications of coherent generators by the graph model-based method (the visual inspection, the applied weak coupling technique, and the applied epsilon decomposition technique) will be first demonstrated and then the evaluation of its performance will be discussed. In order to succeed in analyzing the results, the coherent groups identified through using an effect-based approach will be accepted as a standard for the comparison. Tolerance-based Slow Coherency method [18] is chosen here to provide this standard as it can specify the degree of coherency of the groups to be identified (see Appendix F). An outline of the experiment conducted for this case study is shown in Figure 3.29.

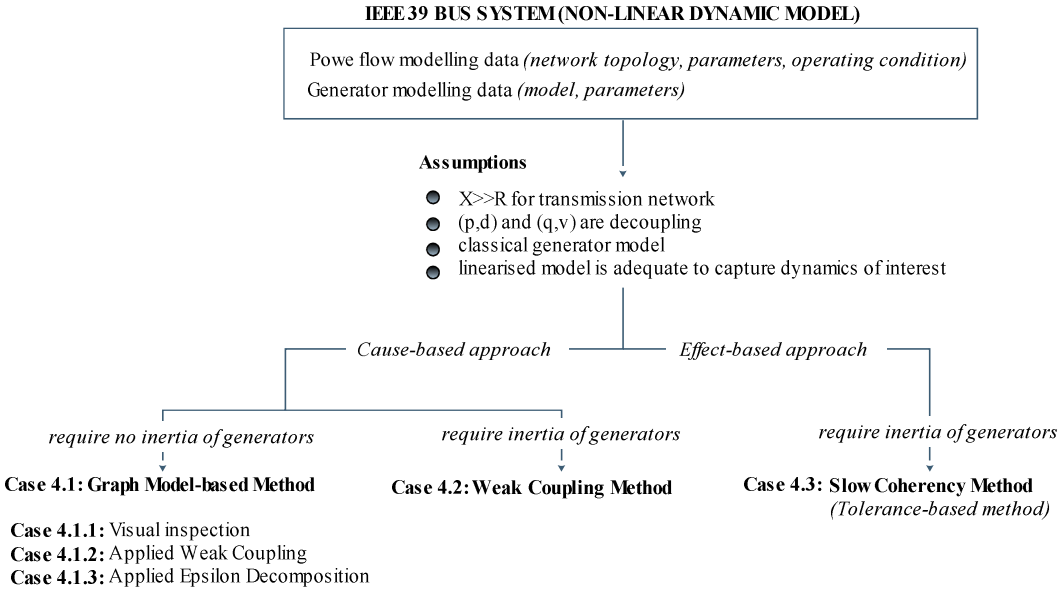

Figure 3.29 Outline of the study case 4

From Figure 3.29, all methods identify the groups of coherent generators based on the linearized model of power system, but they are different in an approach and a requirement of generator parameter, in particular the inertia of generator.

Case 4.1: the graph model-based method

Cased 4.1.1: the applied visual inspection technique

The node-weight graph model of IEEE 39 bus power system (Figure 3.30) is established and given in Figure 3.31.

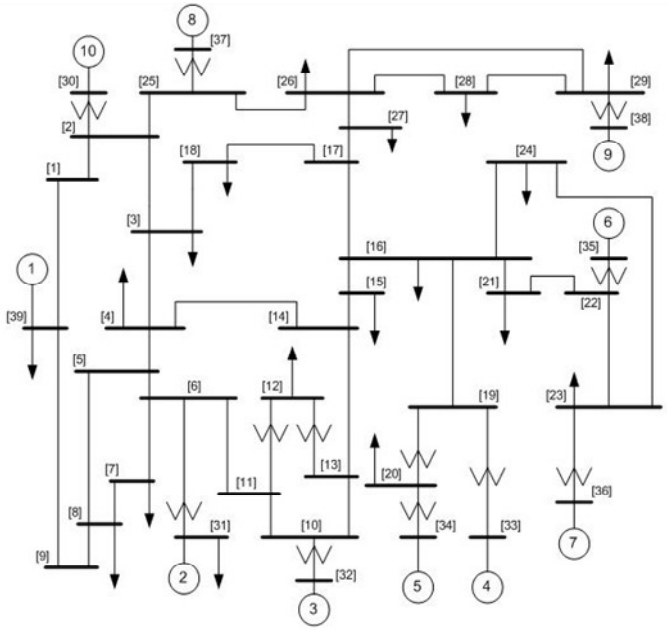

Figure 3.30 One line diagram of IEEE 39 bus system.

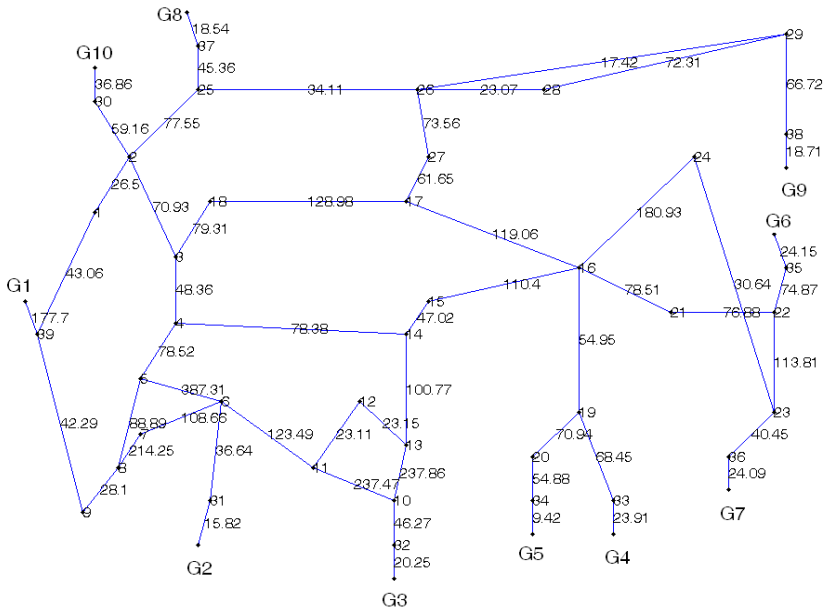

Figure 3.31 Node-weighted graph model of IEEE 39 bus system including the generator internal nodes (edge-weight shown in the middle of each edge).

The two levels of line thickness plot of the full node-weighted graph model of the IEEE 39 bus system for various thresholds in percent of the maximum values of edge weight is shown in Figure 3.32. The identification of strong-intra linked nodes and weak-inter linked nodes from the full node-weighted graph is not straightforward. For a high threshold level, the thick lines, which represent a strong-connection, are not connected to a generator bus. And for the low threshold levels when thick lines do actually connect to a generator, most of generators are accumulated in the same group.

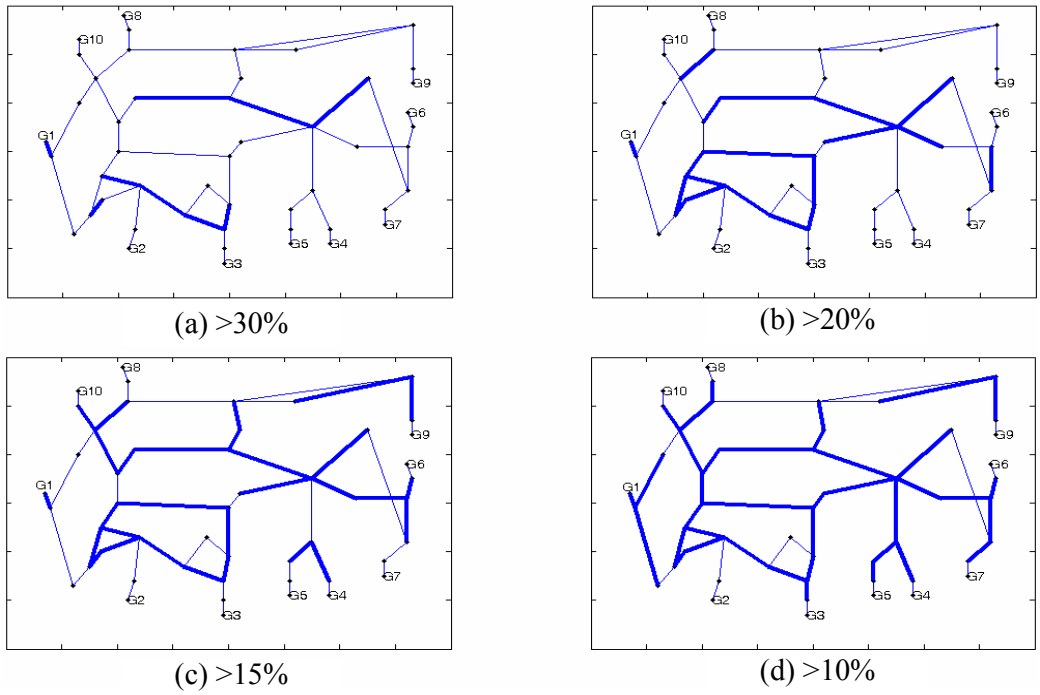

(a) >30% (b) >20%

(c) >15% (d) >10%

Figure 3.32 Two levels of line thickness plot of the node-weighted graph model of the IEEE 39 bus system for various thresholds

To avoid these difficulties, the reduced graph model to the generator internal bus (non-zero node weight) is used instead (see Figure 3.33). This reduced graph model is established from the one line diagram of IEEE39 that the load buses and the generator terminal buses are eliminated.

The two levels of line thickness plot of the reduced node-weighted graph model of the IEEE 39 bus system for various thresholds in percent of the maximum values of

edge weight is shown in Figure 3.34. This figure shows that various groups of strongly connected generator internal buses exist depending on threshold level. For example, if the thresholds above 50% of maximum edge weight are chosen, the coherent generators will be (G1, G2, G3, G8, G10), (G4, G5), (G6, G7), and (G9)

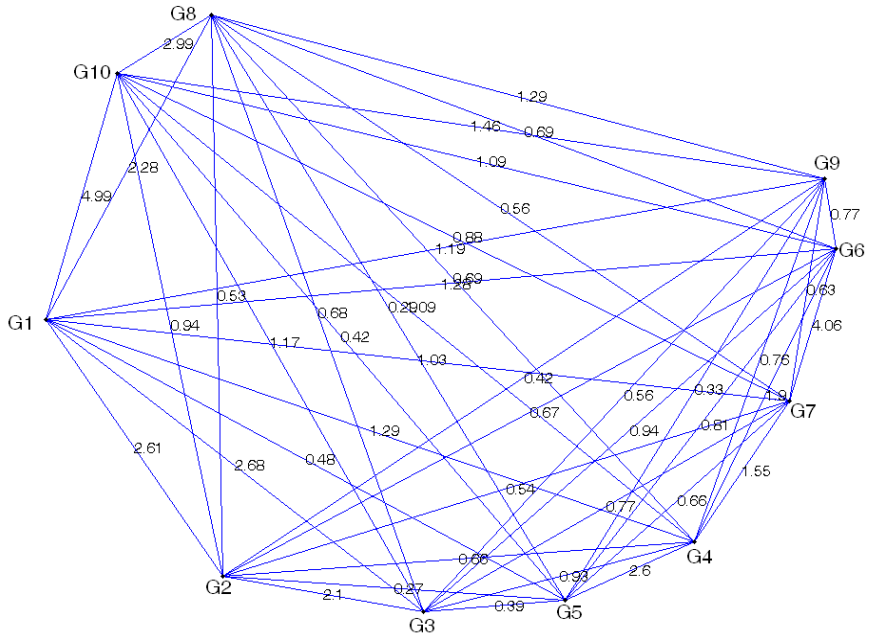

Figure 3.33 Reduced node-weighted graph model of the IEEE 39 bus system when the load buses and the generator terminal buses are eliminated.

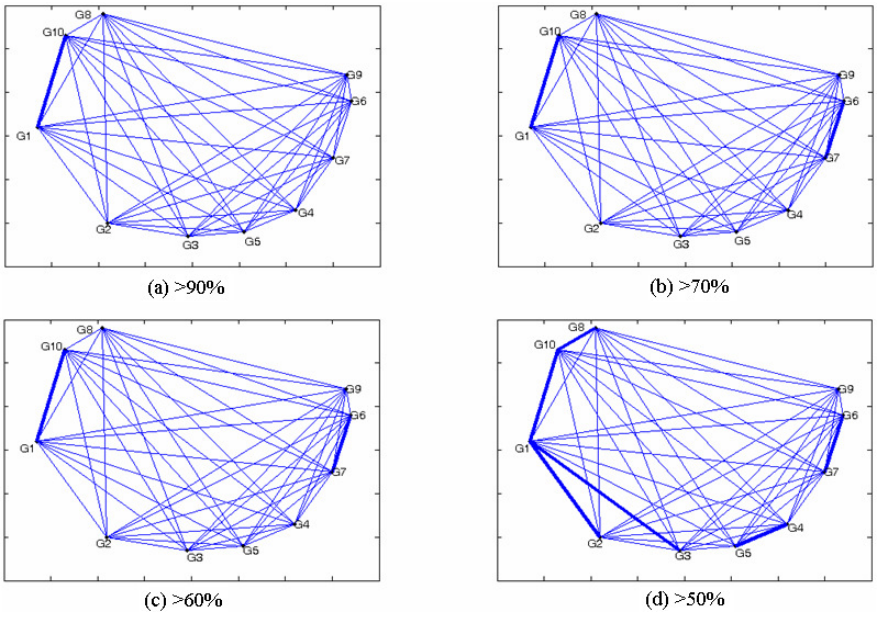

Figure 3.34 Two levels of line thickness plot of the reduced node-weighted graph model of the IEEE 39 bus system for various thresholds

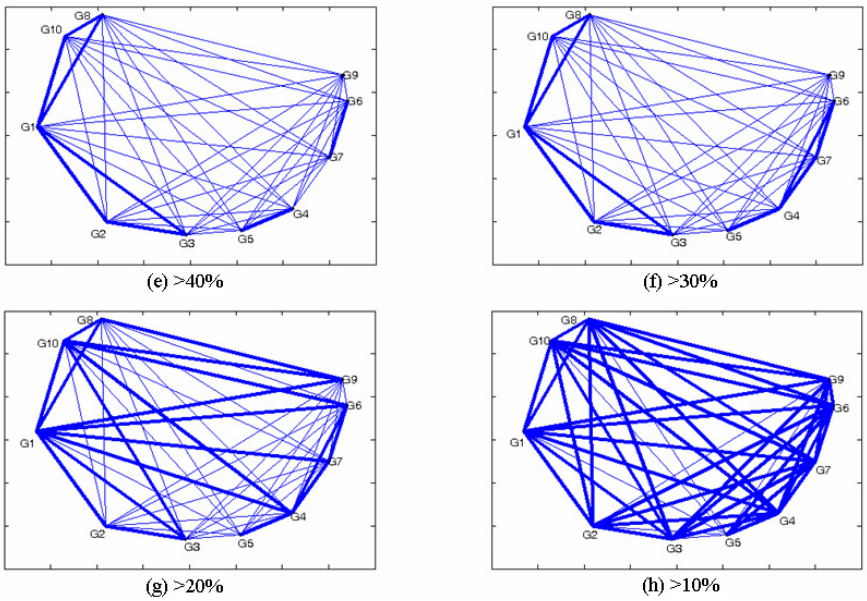

Figure 3.34 (cont.) Two levels of line thickness plot of the reduced node-weighted graph model of the IEEE 39 bus system for various thresholds

Case 4.1.2: the applied weak coupling technique

In this part, the reduced graph model where its zero-weighted nodes (load buses) are eliminated is used to ensure that each identified group contains at least one non-zero weighted node (generator internal bus). The weak coupling technique is applied to the **L**-matrix of the reduced graph model with its diagonal entries set to zero and the result indicates that the coherent nodes are (G5), (G4), (G9), (G6, G7), (G8, G10, G1), and (G3, G2), as shown in Figure 3.35.

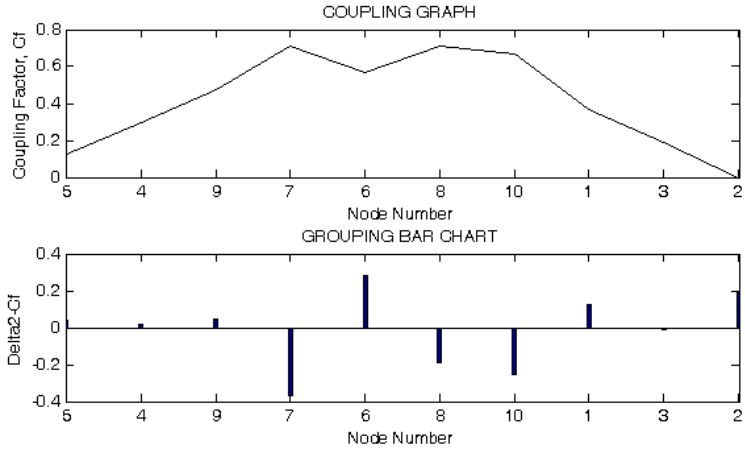

Figure 3.35 Coupling graph and grouping bar chart for the reduced L-matrix of IEEE39 bus system.

Case 4.1.3: the applied epsilon decomposition technique

The epsilon decomposition is applied to the same reduced L-matrix as in the case of applied weak coupling technique and the result is shown in Figure 3.36. The different groups of coherent nodes (shown on the figure) could be determined for the different values of epsilon.

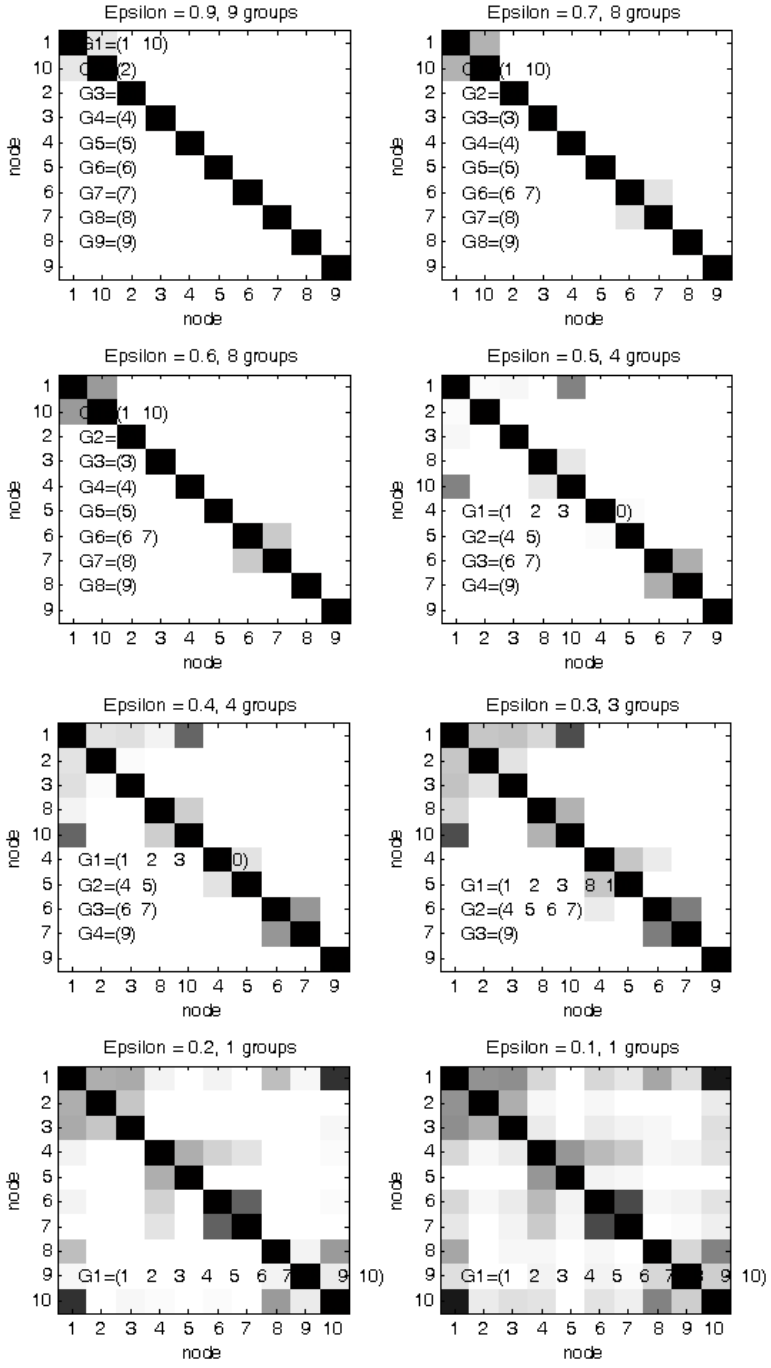

Figure 3.36 Images of normalized reduced L-matrix of IEEE39 bus system for the different values of epsilon.

Case 4.2: the weak coupling method

For this part, the weak coupling method is applied directly to A-matrix of the linearised model of IEEE 39 bus system. The derivation of A-matrix is the same procedure as those in Appendix G. The coupling graph and the grouping bar chart given in Figure 3.37 show the groups of coherent generators are (G9), (G5, G4), (G6, G7), and (G3, G2, G1, G10, G8).

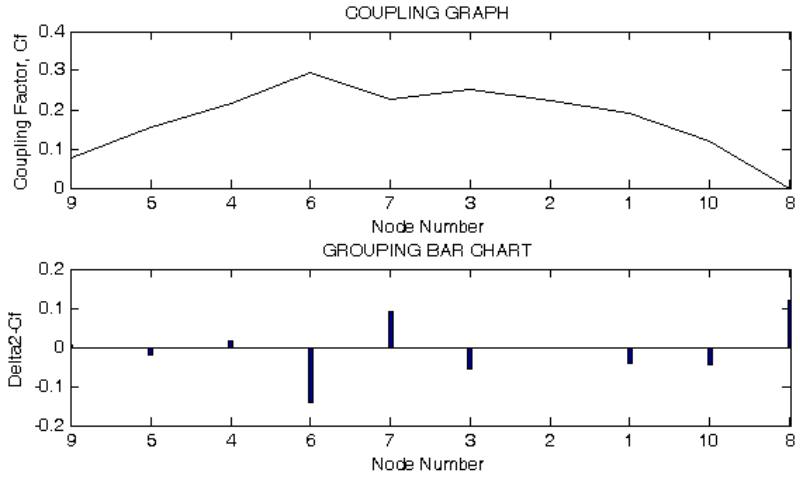

Figure 3.37 Coupling graph and grouping bar chart of the **A**-matrix of IEEE39 bus system.

Case 4.3: the tolerance-based slow coherency method

The tolerance-based slow coherency method identifies the groups of slow coherent generators based on the solutions (Eigenvalues and Eigenvectors) of a linearised power system model. Its specified parameters (number of slow modes and tolerance) of tolerance-base slow coherency algorithm can directly control the degree of closeness among the angle responses of generators to be accepted into the same groups. In other words, the tightness of coherency can be correctly implied from the results of this method as well. Table 3.3 and 3.4 show the results of the groups of coherent generators when the values of tolerance are 0.95 and 0.9 respectively. In each table, the coherent groups for different number of slow modes are given. The more number of slow modes is specified, the more closeness of angle responses are. Moreover, for each specified number of slow modes, the loos-coherent groups and their decomposition results to more tight-coherent groups are also given.

Table 3.3 Coherent groups of IEEE39 bus system identified by Tolerance-based slow coherency method with a tolerance of 0.95

Number of slow modes	Tight-coherent groups	Loose-coherent groups	Decomposition Of loose-coherent groups
10	G1, G2, G3, G4, G5, G6, G7, G8, G9, G10	-	-
9	G1, G2, G3, G4, G5, **(G6,G7)**, G8, G9, G10	-	-
8	G1, G2, G3, G4, G5, **(G6,G7)**, **(G8, G10)**,G9	-	-
7	G1, G2, G3, G4, G5, **(G6,G7)**, **(G8, G10)**,G9	-	-
6	G1, **(G2, G3)**, G4, G5, **(G6,G7)**, **(G8, G10)**,G9	-	-
5	G1, **(G2, G3)**, G4, G5, **(G6,G7)**, **(G8, G10)**,G9	-	-
4	G1, **(G2, G3)**, G4, G5, **(G6,G7)**, **(G8, G10)**,G9	-	-
3	G1, **(G2, G3, G8, G10)**, **(G4,G6,G7)**,G5 ,G9	-	-
2	G1, **(G2, G3, G4, G5, G6,G7, G8, G9, G10)**	-	-
1	**(G1,G2, G3, G4, G5, G6,G7, G8, G9, G10)**	-	-

Table 3.4 Coherent groups of IEEE39 bus system identified by Tolerance-based slow coherency method with a tolerance of 0.90

Number of slow modes	Tight-coherent groups	Loose-coherent groups	Decomposition Of loose-coherent groups
10	G1, G2, G3, G4, G5, G6, G7, G8, G9, G10	-	-
9	G1, G2, G3, G4, G5, **(G6,G7)**, G8, G9, G10	-	-
8	G1, G2, G3, G4, G5, **(G6,G7)**, **(G8, G10)**,G9	-	-
7	G1, G2, G3, G4, G5, **(G6,G7)**, **(G8, G10)**,G9	-	-
6	G1, **(G2, G3)**, G4, G5, **(G6,G7)**, **(G8, G10)**,G9	-	-
5	G1, **(G2, G3)**, G4, G5, **(G6,G7)**, **(G8, G10)**,G9	-	-
4	G1, **(G2, G3)**, G5, **(G4, G6,G7)**, **(G8, G10)**,G9	-	-
3	G1, G9	**(G2, G3, G4,G5,G6,G7, G8, G10)**	**(G4, G5), (G6, G7), (G2, G3,G8,G10)**
2	G1, **(G2, G3, G4, G5, G6,G7, G8, G9, G10)**	-	-
1	**(G1,G2, G3, G4, G5, G6,G7, G8, G9, G10)**	-	-

The major results are summarised in the following tables, Table 3.5 to Table 3.9, together with the rotor angle deviations of generators in the IEEE39 bus system for a discussion.

Table 3.5 Coherent groups obtained from Tolerance-based slow coherency technique with the tolerance of 0.90.

Degree of coherency	Coherent groups
Tight	(G6,G7)
.	(G6,G7), (G8, G10)
.	(G2, G3), (G6,G7), (G8, G10)
.	(G2, G3), (G4, G6,G7), (G8, G10)
	(G4, G5), (G6, G7), (G2, G3,G8,G10)
Loose	(G2, G3, G4, G5, G6,G7, G8, G9, G10)

Table 3.6 Coherent groups obtained from Weak coupling method.

Degree of coherency	Coherent groups
Tight	(G4, G5), (G6, G7), (G1,G2, G3,G8,G10)
	(G4, G5,G9), (G6, G7), (G1,G2, G3,G8,G10)
Loose	(G4, G5,G9, G6, G7), (G1,G2, G3,G8,G10)

Table 3.7 Coherent groups obtained from the graph model with the visual inspection technique.

Degree of coherency	Coherent groups
Tight	(G1,G10)
.	(G1,G10), (G6,G7)
.	(G1, G2, G3, G8, G10), (G4,G5), (G6,G7)
Loose	(G1, G2, G3, G8, G10), (G4,G5, G6,G7)

Table 3.8 Coherent groups obtained from the graph model with the applied weak coupling technique.

Degree of coherency	Coherent groups
Tight	(G2,G3), (G6,G7), (G1, G8, G10)
	(G2,G3, G1, G8, G10), (G6,G7)
Loose	(G2,G3, G1, G8, G10, G6,G7)

Table 3.9 Coherent groups obtained from the graph model with the applied epsilon decomposition technique.

Degree of coherency	Coherent groups
Tight	(G1,G10)
.	(G1,G10), (G6,G7)
.	(G1, G2, G3, G8, G10), (G4,G5), (G6,G7)
Loose	(G1, G2, G3, G8, G10), (G4,G5, G6,G7)

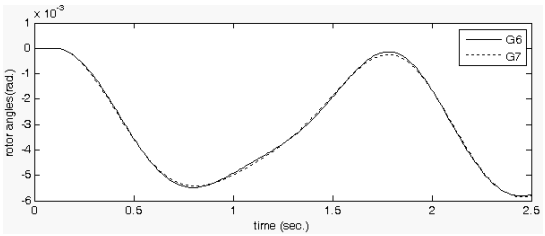

(a) G6 and G7

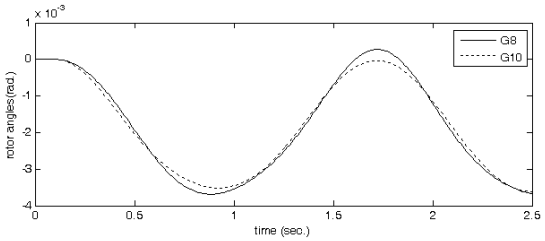

(b) G8 and G10

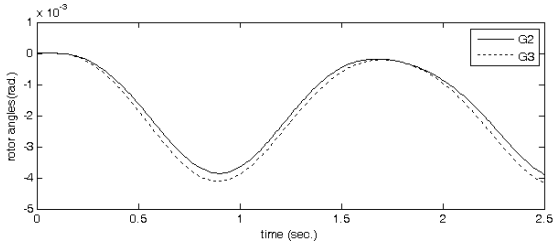

(c) G2 and G3

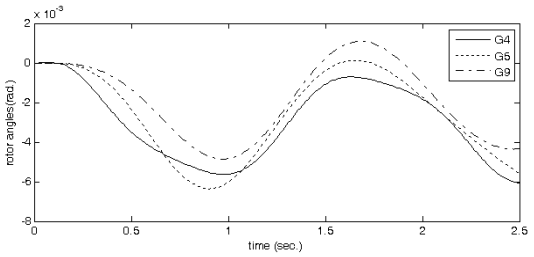

(d) G4, G5 and G9

Figure 3.38 Rotor angle deviations of IEEE39 bus system when a fault with 10 P.U. impedance is applied at bus 16 (generator 1 as reference).

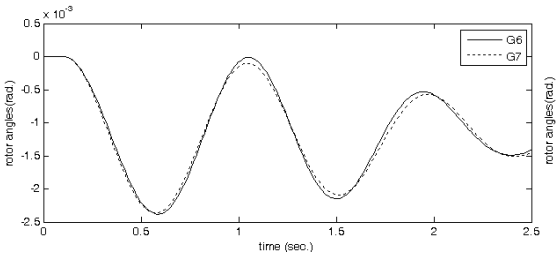

(a) G6 and G7

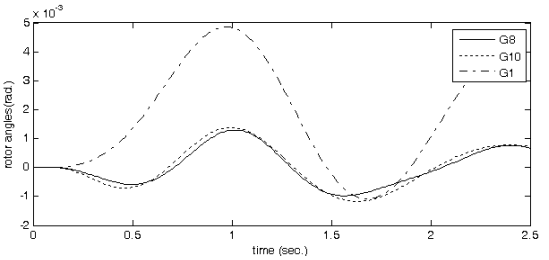

(b) G8, G10 and G1

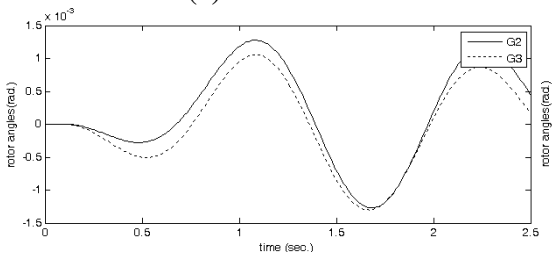

(c) G2 and G3

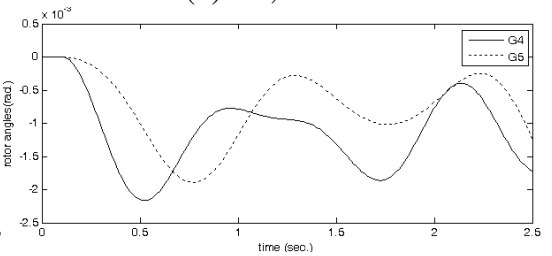

(c) G4 and G5

Figure 3.39 Rotor angle deviations of IEEE39 bus system when a fault with 10 P.U. impedance is applied at bus 16 (generator 9 as reference).

Regarding only the evaluation of results from the graph model-based methods, it is evidently that all techniques (the visual inspection, the applied weak coupling, and the applied epsilon decomposition) can identify the tightest coherent group of G6 and G7 (see Table 3.5, Figure 3.38 (a) and Figure 3.39 (a)) out of other groups. However, the coherent group of G6 and G7 does not appear as the tightest group in the visual inspection method and the applied epsilon decomposition method but the group of G1 and G10 does (see Table 3.7 and Table 3.9). Having a close look at the angle responses of G1 and G10 (see Figure 3.39 (b)), the closeness between them is larger when compared to the case of G6 and G7. This result indicates nothing wrong about the graph model of power system, the methods applied to identify the strong-intra and weak-inter linked node structure, or even the (slow) coherency theorem of graph. The graph model of IEEE39 bus system is correctly established. The G1 and G10 are linked by the edge having the strongest weight in the graph (see Figure 3.33) and they can be considered as coherent generators which is supported by the result from Weak Coupling method (see Table 3.6). The reason for identifying wrong order of coherent groups is that the coherency caused by the structure of strong-intra and weak-inter linked node is weaker than the coherency caused by the conditions of exact coherency theorem [9] (detail in Appendix D) where the group of G6 and G7 is fully satisfied. The exact coherency conditions are:

$$\tilde{\mathbf{L}}_i = \frac{\delta_i}{M[i]}\mathbf{M}_i \tag{6}$$

$$\tilde{\mathbf{L}}_{ij}\mathbf{1}_{nj} = -\frac{\xi_{ij}}{M[i]}\underbrace{\mathbf{M}_i\mathbf{1}_{ni}}_{\mathbf{m}_i} = -\frac{\xi_{ij}}{M[i]}\mathbf{m}_i \tag{7}$$

The two requirements for exact coherency in term of graph model given in eqn (6) and eqn (7) state that nodes will be exact coherent if their inter group part of **L**-matrix ($\tilde{\mathbf{L}}_i$) from the original graph (left hand side of the equations) have the values equal to those calculated from the condition on its aggregated graph (right hand side of the equations).The definitions and the calculation of the matrices and their entries are illustrated in Figure 3.40 for the case of node 6 and node7.

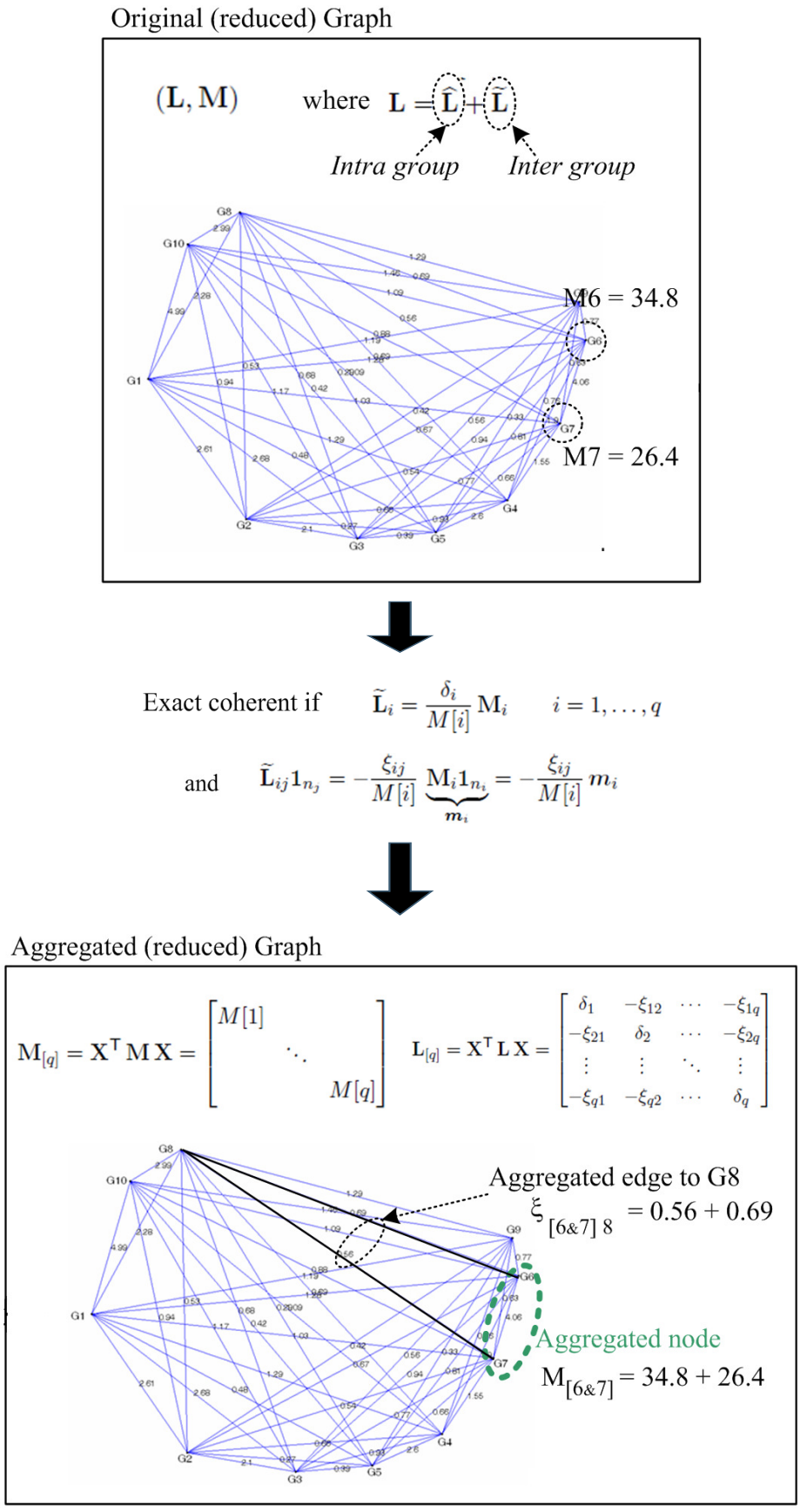

Figure 3.40 Reduced graph and its aggregated graph of node G6 and G7

Figure 3.40 shows how their matrices required for checking the exact coherency condition are calculated in case of node 6 and node 7. From the right hand side of eqn (6) and eqn (7) the requirements for G6 and G7 to be exact coherent are:

	(G6)	(G7)
(G6)	8.4017	0
(G7)	0	6.3737

	(G1)	(G2)	(G3)	(G4)	(G5)	(G8)	(G9)	(G10)
(G6)	-1.3153	-0.6862	-0.9713	-1.9608	-0.8338	-0.7136	-0.7977	-1.1231
(G7)	-0.9978	-0.5205	-0.7369	-1.4875	-0.6325	-0.5414	-0.6052	-0.8520

These requirements can be checked by a comparison with the values obtained from the original graph. By rearranging L-matrix of the original graph until first two rows and columns belong to G6 and G7, the actual values can be extracted from the diagonal block and off-diagonal block of inter group part as shown below.

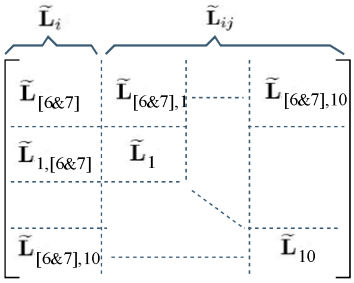

	(G6)	(G7)
(G6)	8.1519	0
(G7)	0	6.6236

	(G1)	(G2)	(G3)	(G4)	(G5)	(G8)	(G9)	(G10)
(G6)	-1.2792	-0.6655	-0.9419	-1.9016	-0.8076	-0.6921	-0.7727	-1.0912
(G7)	-1.0339	-0.5412	-0.7663	-1.5467	-0.6587	-0.5628	-0.6301	-0.8838

From the comparison between the requirement matrices and the actual matrices, it is clearly seen that the structure on the graph model related to G6 and G7 is very close to the requirements of exact coherent structure. On the other hand, even G1 and G10 having a strong-linked edge, the condition of exact coherency between them is not totally satisfied.

Requirement matrices for G1 and G10 to be exact coherent

	(G1)	(G10)
(G1)	21.1140	0
(G10)	0	1.7736

,

	(G2)	(G3)	(G4)	(G5)	(G6)	(G7)	(G8)	(G9)
(G1)	-3.2723	-3.5537	-2.1943	-0.8312	-2.1867	-1.7691	-4.8646	-2.4421
(G10)	-0.2749	-0.2985	-0.1843	-0.0698	-0.1837	-0.1486	-0.4086	-0.2051

Actual matrices for the group of G1 and G10

	(G1)	(G10)
(G1)	12.8362	0
(G10)	0	10.0514

,

	(G2)	(G3)	(G4)	(G5)	(G6)	(G7)	(G8)	(G9)
(G1)	-2.6066	-2.6835	-1.2862	-0.4778	-1.2792	-1.0339	-2.2803	-1.1886
(G10)	-0.9405	-1.1687	-1.0924	-0.4232	-1.0912	-0.8838	-2.9929	-1.4586

Actually not only the group of G6 and G7, the other group such as the group of G8 and G10 is also well satisfied the exact coherency conditions compare to the group of G1 and G10.

Requirement matrices for G8 and G10 to be exact coherent

	(G8)	(G10)
(G8)	6.9848	0
(G10)	0	12.0725

,

	(G1)	(G2)	(G3)	(G4)	(G5)	(G6)	(G7)	(G9)
(G8)	-2.6644	-0.5401	-0.6762	-0.6519	-0.2601	-0.6536	-0.5302	-1.0084
(G10)	-4.6051	-0.9335	-1.1687	-1.1267	-0.4495	-1.1297	-0.9164	-1.7430

Actual matrices for the group of G8 and G10

	(G8)	(G10)
(G8)	7.0097	0
(G10)	0	12.0477

,

	(G1)	(G2)	(G3)	(G4)	(G5)	(G6)	(G7)	(G9)
(G8)	-2.2803	-0.5330	-0.6762	-0.6861	-0.2863	-0.6921	-0.5628	-1.2928
(G10)	-4.9892	-0.9405	-1.1687	-1.0924	-0.4232	-1.0912	-0.8838	-1.4586

From these results, caution should be exercised when attempt to identify the coherent generators through using slow coherency theorem in term of graph. The obtained groups are coherent but they may be relatively weak if there are other groups that fully satisfy the exact coherency conditions. However, the identification of the exact or true tight coherent groups requires not only generator inertia but also a huge amount of computation. For example, calculating Eigenvalues/eigenvectors is required in case of Tolerance-based slow coherency technique; and a combinatorial search of proper criterion, such as those based on conditions of eqns (6) & (7), is required in case of graph model. Without these computations, tight and weak coherent generators can not be suitably distinguished as seen from the result of Weak coupling method (first row of Table 3.6) that the weakly coherent generator G1 is still included in the group considered as tight.

The conclusions that can be drawn about the performance of coherent generator identification based on slow coherency theorem in term of graph model are as follows.

-The three methods (visual inspection, applied weak coupling, and applied epsilon decomposition) can identify only the groups of coherent generators caused by strong-intra and weak-inter linked node structure in which the degree of coherency may not be strong if there are exact coherent structure hidden in the system.

- Although the visual inspection and applied epsilon decomposition give the same coherent groups in this case, they might give different results for other systems due to the grouping based on visual inspection is subjective.

Case 5: This case study aims to evaluate the performance of the graph model-based coherent generator identification when the strong edge weight between the generator internal bus and the generator terminal bus is assumed.

On this assumption, the nodes corresponding to the generator terminal buses are considered as the representatives for the nodes of the generator internal buses (similarly to Figure 3.13 of the case study 1). Therefore, establishing a node-weight graph model of IEEE39 bus system requires only power-flow modelling data. The full node-weight graph model and its two levels of line thickness plot are shown in Figure 3.41 and Figure 3.42, respectively.

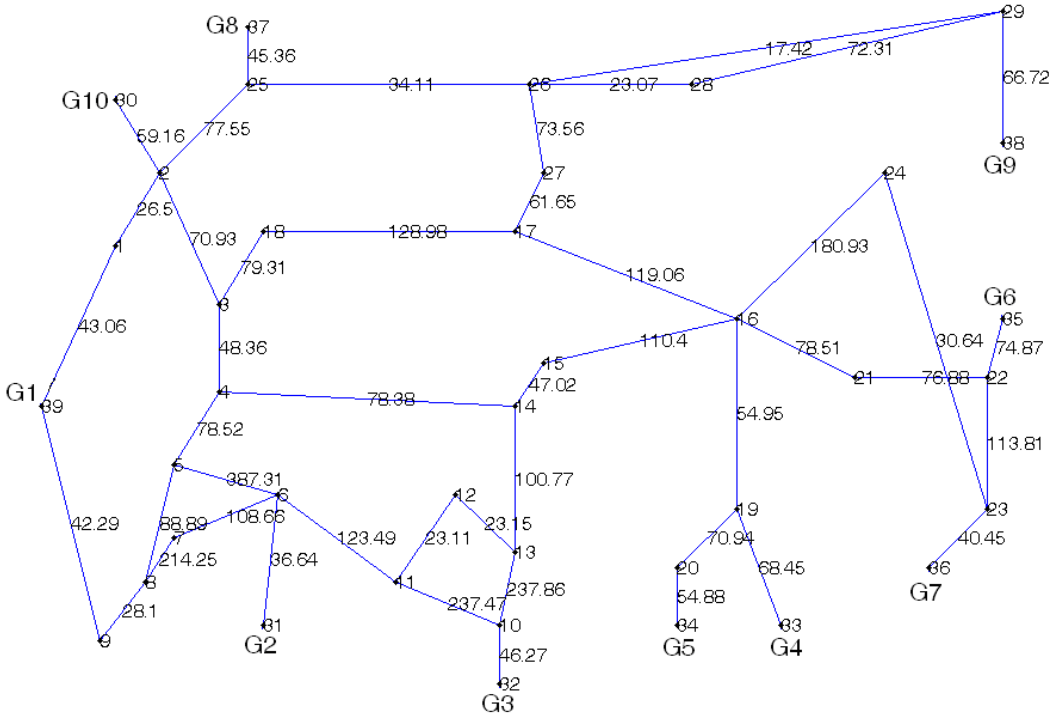

Figure 3.41 Node-weighted graph model of IEEE 39 bus system excluding the generator internal nodes (edge-weight shown in the middle of each edge).

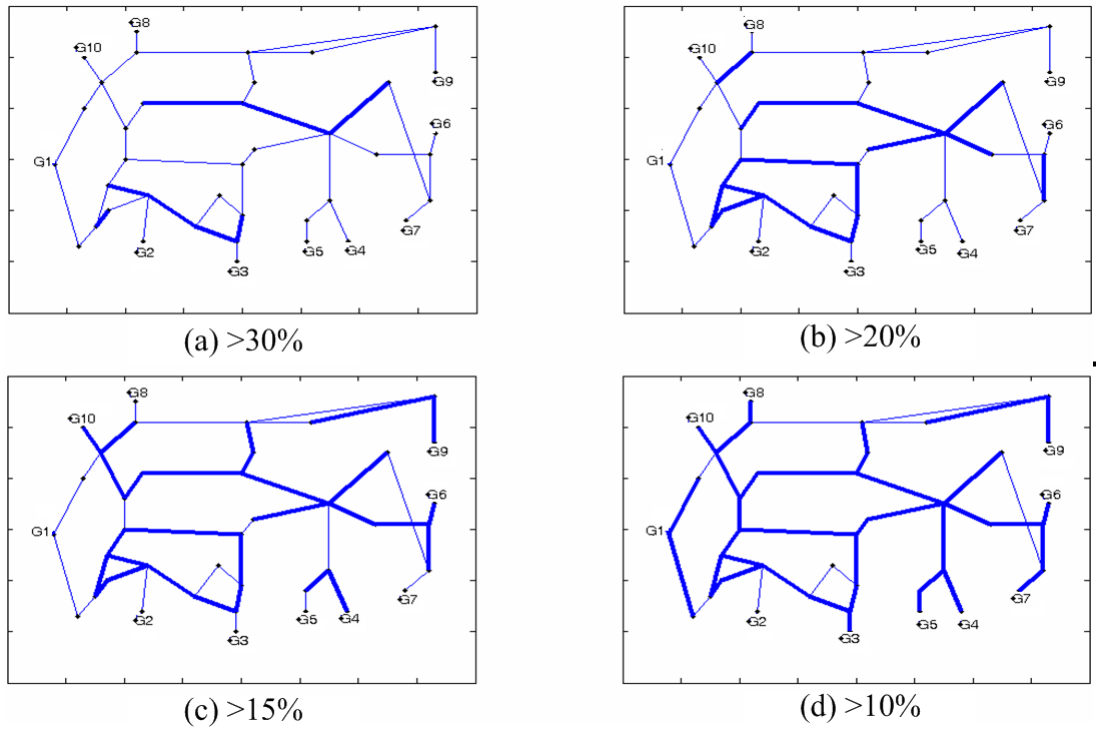

Figure 3.42 Two levels of line thickness plot of the node-weighted graph model of the IEEE 39 bus system excluding the generator internal nodes for various thresholds

From Figure 3.42, the identification of strong-intra linked nodes and weak-inter linked nodes from the full node-weighted graph is not straightforward as in the study case 4. For a high threshold level, the thick lines, which represent a strong-connection, are not connected to a generator bus. And for the low threshold levels when thick lines do actually connect to a generator, most of generators are accumulated in the same group.

To avoid these difficulties, the reduced graph model to the generator internal bus (non-zero node weight) is used instead (see Figure 3.43). This reduced graph model is established from the one line diagram of IEEE39 that only load buses are eliminated. The generator terminal buses are now considered as the representative of the generator internal buses. The resultant reduced node-weight graph model is given in Figure 3.43.

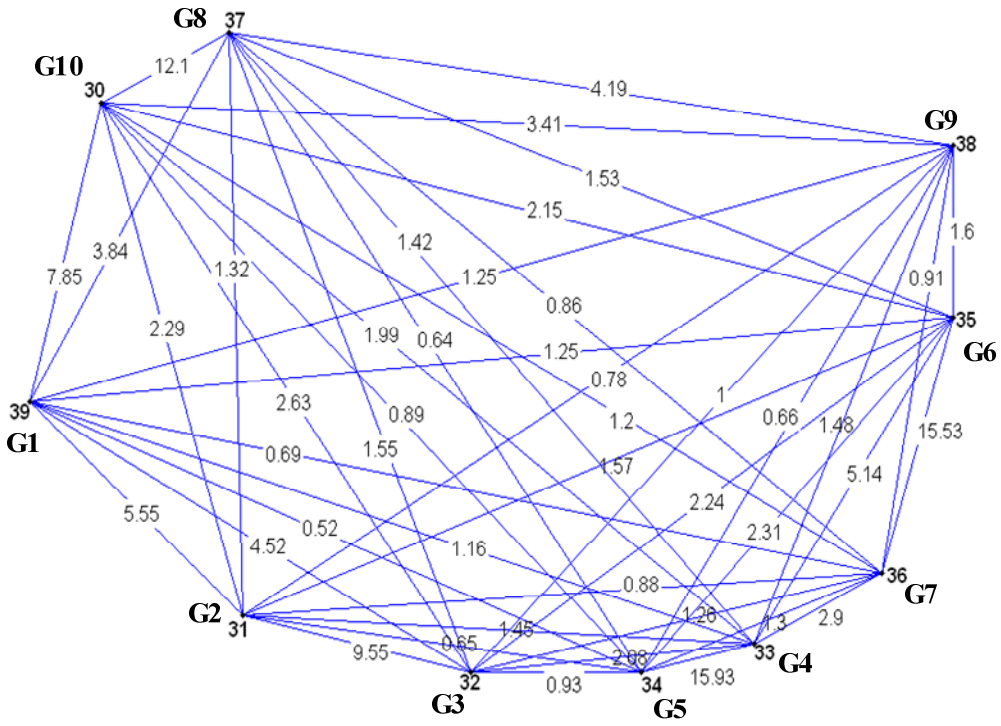

Figure 3.43 Reduced node-weighted graph model of IEEE 39 bus system when only load buses are eliminated (excluding the generator internal buses).

The coherent generators are identified by using three techniques (the visual inspection, the applied weak coupling, and the applied epsilon decomposition) as in the previous case study. The results obtained for each technique are shown in Figure 3.44, Figure 3.45, and Figure 3.46, respectively.

- The visual inspection technique

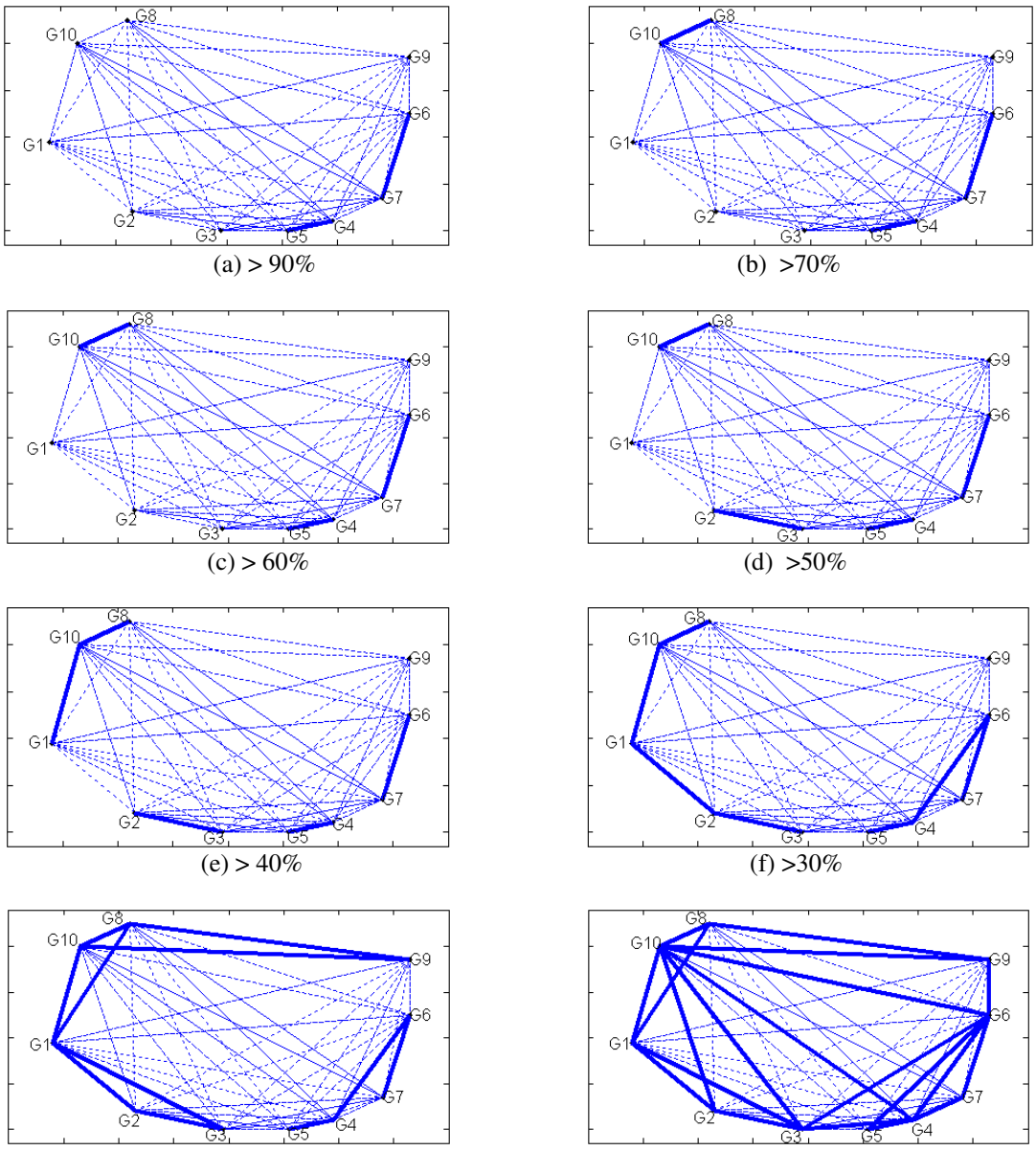

(a) > 90% (b) >70%

(c) > 60% (d) >50%

(e) > 40% (f) >30%

Figure 3.44 Two levels of line thickness plot of the reduced node-weighted graph model of the case 5 for various thresholds

- The applied weak coupling technique

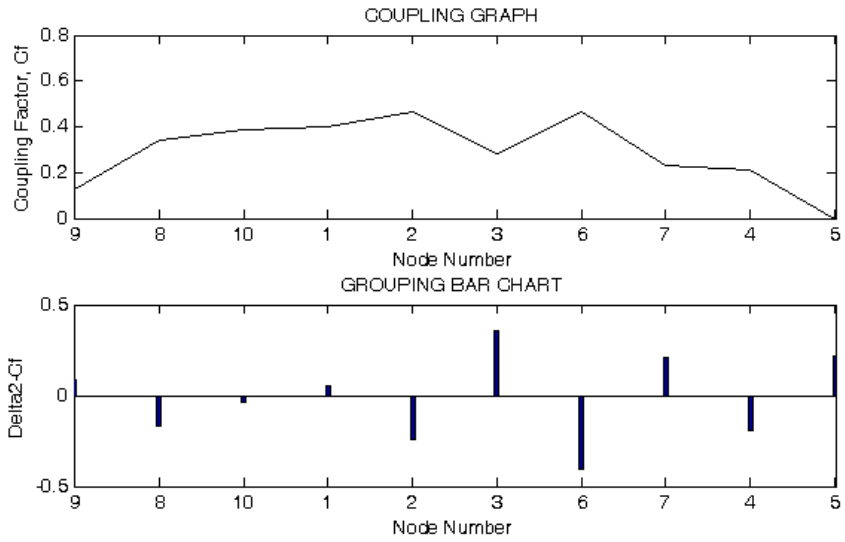

Figure 3.45 Coupling graph and the grouping bar chart for the **L**-matrix of the case 5

- The applied epsilon decomposition technique

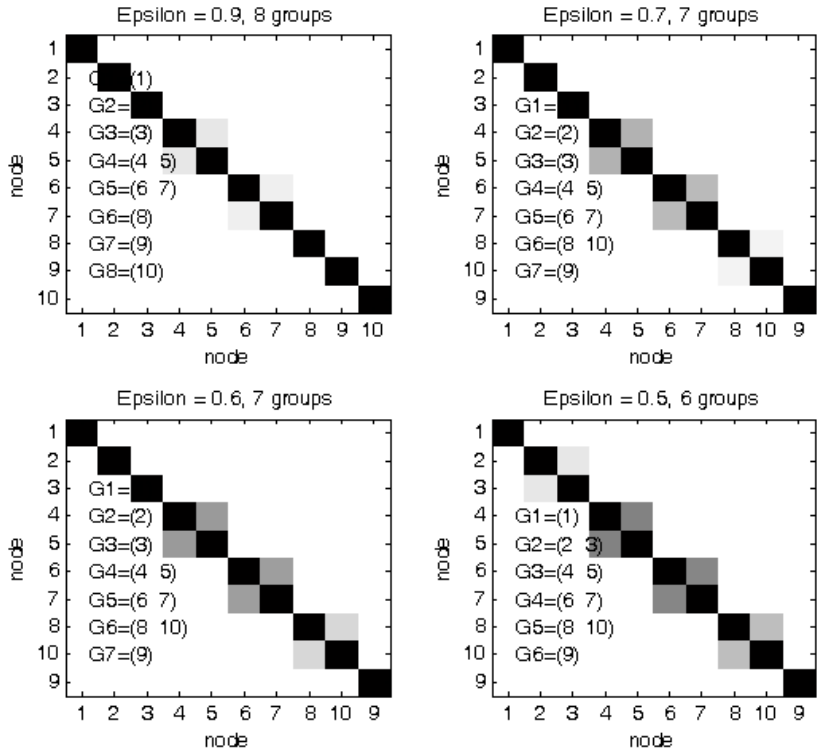

Figure 3.46 Images of normalized reduced L-matrix of the case 5 for the different values of epsilon.

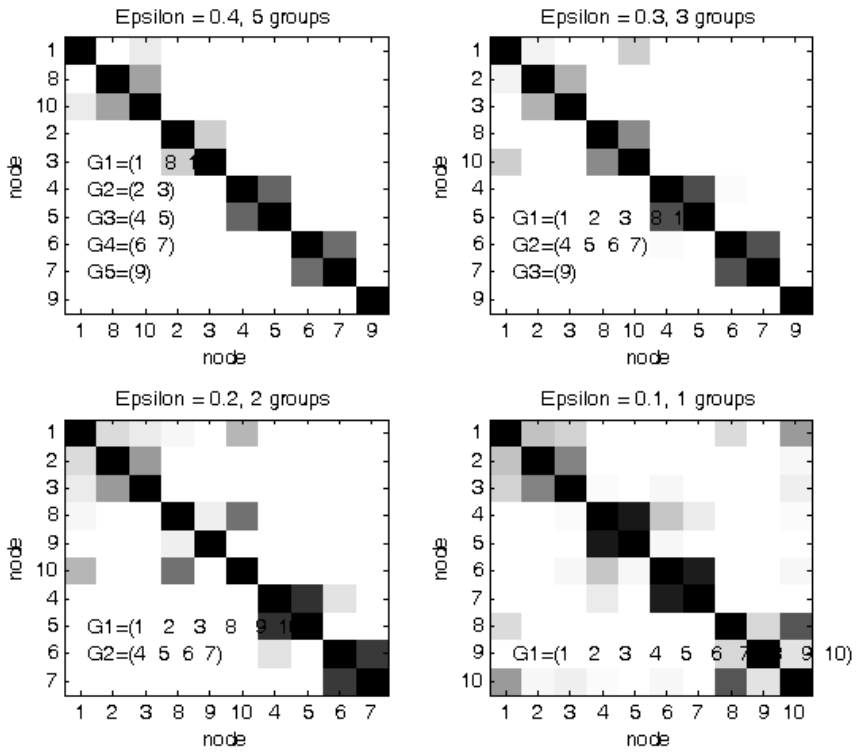

Figure 3.46 (cont.) Images of normalized reduced L-matrix of the case 5 for the different values of epsilon.

The identified coherent groups according to different levels of coherency for each individual technique are summarised in the Table 3.10, Table 3.11, and Table 3.12, respectively.

Table 3.10 Coherent groups obtained from the graph model with the visual inspection technique.

Degree of coherency	Coherent groups
Tight	(G4, G5), (G6,G7)
.	(G4,G5), (G6,G7), (G8, G10)
.	(G2, G3), (G4,G5), (G6,G7), (G8, G10)
	(G2, G3), (G4,G5), (G6,G7), (G1, G8, G10)
	(G1, G2, G3, G8, G10), (G4,G5, G6,G7)
Loose	(G1, G2, G3, G8, G9, G10), (G4,G5, G6,G7)

Table 3.11 Coherent groups obtained from the graph model with the applied weak coupling technique.

Degree of coherency	Coherent groups
Tight	(G2,G3), (G4, G5, G6,G7), (G1, G8, G10)
Loose	(G1,G2,G3, G8, G10), (G4, G5, G6,G7)

Table 3.12 Coherent groups obtained from the graph model with the applied epsilon decomposition technique.

Degree of coherency	Coherent groups
Tight	(G4, G5), (G6,G7)
.	(G4,G5), (G6,G7), (G8, G10)
.	(G2, G3), (G4,G5), (G6,G7), (G8, G10)
.	(G2, G3), (G4,G5), (G6,G7), (G1, G8, G10)
.	(G1, G2, G3, G8, G10), (G4,G5, G6,G7)
Loose	(G1, G2, G3, G8, G9, G10), (G4,G5, G6,G7)

In this case, the results obtained from the visual inspection technique are the same as those obtained from the applied epsilon decomposition technique; but, the results obtained from the applied weak coupling technique are a bit different and having less discrimination. However, in average, all the methods identify acceptable coherent groups. This could be confirmed from a comparison of the results in the Table 3.10, 3.11, and 3.12 respectively with the coherent groups identified by the tolerance-based slow coherency method of the previous case (Table 3.5). It can be seen that the similar generators are identified in the same group of coherent such as the group of G6 and G7. By contrast, no strong contradiction is presented such as grouping the incoherent generators together.

Compared with the results obtained from the graph model method of the previous study case, it shows some differences. However, this is not a result of the assumption. All the internal edge-weights are relatively strong compare to the other edges as shown in Figure 3.47. In fact, the differences are from using the different nodes of references in the identification of coherent generators. The previous case (case 4) uses the generator internal nodes of the reduced graph of IEEE 39 bus system when both the generator buses and the load buses are eliminated. This case

(case 5) uses the generator terminal nodes of the reduced graph of IEEE 39 bus system when only the load buses are eliminated.

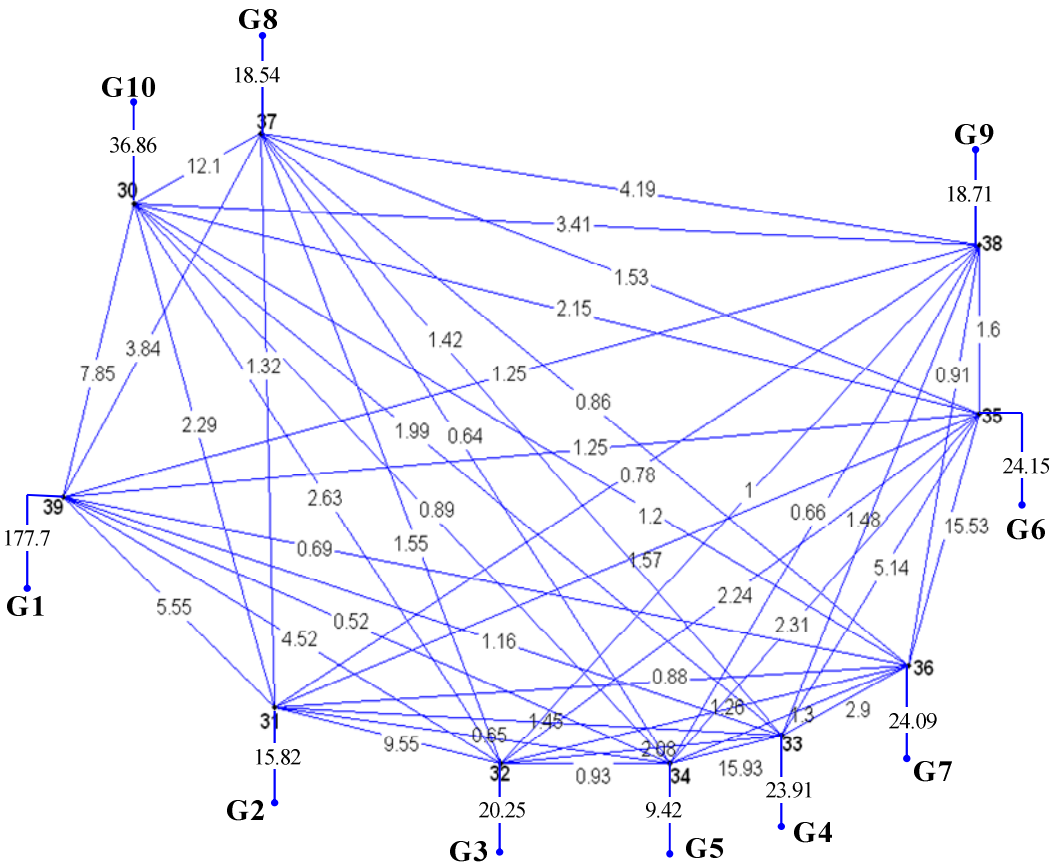

Figure 3.47 Reduced node-weighted graph model including the generator internal edges of IEEE 39 bus system when only load buses are eliminated.

3.5 Conclusion

The graph model-based coherent generator identification has been proposed in this chapter. The method is based on identifying the groups of coherent nodes of the corresponding node-weighted graph model of the power system. The groups of coherent nodes could be determined from the groups of nodes having strong intra group connections and weak inter group connections. In order to identify this

particular structure three techniques have been developed: the visual inspection, the applied weak coupling technique, and the epsilon decomposition technique.

The results from the study on the artificial system and the nine bus power system confirm that the proposed method is feasible. For these two cases, three techniques consistently identified the same groups of coherent generators. The performance of the proposed method then has been evaluated with the IEEE39 bus system. The three techniques have given slightly different results in this case. Moreover, the evaluation has also revealed that the coherent groups identified based on the structure of strong intra group connections and weak inter group connections could be weakly coherent if there exist the exact coherent structure for the different groups. However, to identify the coherent groups caused by the exact coherent structure, a combinatorial search for all possible combination of groups need to be performed.

Finally, the case of coherent generator identification by using only power flow modeling data has been studied. As the parameters of generators and of transmission network are presented in different components of the graph model, this allows making an assumption to identification to identify coherent generator by using only power flow modelling data. The coherent groups identified by three techniques are all acceptable, especially for providing the information about the model structure of identification-based dynamic equivalent.

3.6 References

[1] R. Podmore, "Identification of Coherent Generators for Dynamic Equivalents," *Power Apparatus and Systems, IEEE Transactions on,* vol. PAS-97, pp. 1344-1354, 1978.

[2] J. H. Chow, *Time-scale modeling of dynamic networks with application to power systems*: Springer-Verlag, 1983.

[3] B. D. Spalding, H. Yee, and D. B. Goudie, "Coherency recognition for transient stability studies using singular points," *Power Apparatus and Systems, IEEE Transactions on,* vol. 96, pp. 1368-1375, 1977.

[4] S. S. Lamba and R. Nath, "Coherency identification by the method of weak coupling," *International Journal of Electrical Power & Energy Systems,* vol. 7, pp. 233-242, 1985.

[5] F. Wu and N. Narasimhamurthi, "Coherency identification for power system dynamic equivalents," *Circuits and Systems, IEEE Transactions on,* vol. 30, pp. 140-147, 1983.

[6] X. Guangyue and V. Vittal, "Slow Coherency Based Cutset Determination Algorithm for Large Power Systems," *Power Systems, IEEE Transactions on,* vol. 25, pp. 877-884.

[7] X. Wang and V. Vittal, "System islanding using minimal cutsets with minimum net flow," in *Power Systems Conference and Exposition, 2004. IEEE PES*, 2004, pp. 379-384 vol.1.

[8] H. You, V. Vittal, and W. Xiaoming, "Slow coherency-based islanding," *Power Systems, IEEE Transactions on,* vol. 19, pp. 483-491, 2004.

[9] B. Ayazifar, "Graph Spectra and Modal Dynamics of Oscillatory Networks." vol. Ph.D.: Massachusetts Institute of Technology, 2002, p. 191.

[10] R. Nath, S. S. Lamba, and K. S. Prakasa Rao, "Coherency Based System Decomposition into Study and External Areas Using Weak Coupling," *Power Apparatus and Systems, IEEE Transactions on,* vol. PAS-104, pp. 1443-1449, 1985.

[11] Z. Z. Qi, "Coherency based dynamic equivalence of power systems." vol. Ph.D.: University of Strathclyde, 1994, p. 184.

[12] D. D. Siljak, *Decentralized control of complex systems*: Academic Press, Inc., 1991.

[13] J. Zaborszky, W. Keh-Wen, H. Garng, C. Luo-Jen, and L. Shin-Yeu, "A Clustered Dynamic Model for a class of LInear Autonomous Systems Unsing Simple Enumerative Sorting," *Circuits and Systems, IEEE Transactions on,* vol. 29, pp. 747-758, 1982.

[14] P. M. Anderson and A. A. Fouad, *Power System Control and Stability*: The Iowa State University Press, 1977.

[15] I. A. Hiskens, "Power System Test Cases [online] http://psdyn.ece.wisc.edu/IEEE_benchmarks/index.htm."

[16] The MathWorks Inc. , "MATLAB Programing," The MathWorks Inc., 2007.

[17] F. Milano, "Power System Analysis Toolbox (PSAT) ", 1.3.4 ed, 2006.

[18] GE Electrical distribution and control, "Improved dynamic equivalencing software," EPRI EPRI Final Report, EPRI TR-105919, December 1995.

CHAPTER 4

PARAMETERIC IDENTIFICATION OF DYNAMIC EQUIVALENT

4.1 Introduction

Parametric identification of dynamic equivalent is a modelling of the external part based on an appropriate model structure and measurements. It is typically composed of two sequential tasks similar to the parametric identification technique of the system identification framework [1]. The first task is to determine the appropriate model structure, a set of equations (without the values of their coefficients), that describes the dynamics of the external part. The second task is the identification of the parameters (or coefficients) of the appropriate model structure by using the measurements. These two tasks affect the performance of the equivalencing process and of the equivalent model itself. As for the result, they need to be well planned with a good justification of several fundamental issues, for examples, what types of equations and how many of them to be used; how the equations will be parameterised; and what is the criterion for parameter identification.

Accordingly, various existing methods of identification-based dynamic equivalent have been reviewed in Chapter 2; and the conclusion of using the model structure based on the knowledge of coherent generator and using the criterion based on the active power flow in the transmission lines at boundaries have been reached. The knowledge of coherent generator could lead to the reduced sets of differential algebraic equations (represented in the generator model and the transmission network model formulations, respectively) postulating the suitable model structure. With the graph model-based coherent generator identification techniques developed in Chapter 3, the identification-based dynamic equivalent that requires only power flow modelling data and measurements at boundaries is presented in this chapter. The details of two essential tasks, the model structure determination and the parameter identification, are explained in the next section. Afterward, the proposed procedure will be demonstrated with the nine bus power system and a short evaluation is also presented. Finally, the conclusions are drawn.

4.2 Identification procedure of dynamic equivalent

4.2.1 Model structure determination

The aim of this task is to arrive at the small set of equations (without the values of their coefficients) describing the dynamics of the external part by using the knowledge of coherent generator in power system component formulation. The determination process, therefore, is similar to the derivation of coherency-based dynamic equivalent taking incomplete generator modelling data into consideration. This could be summarised into five fundamental steps: establishing the node-weighted graph model, identifying coherent generator from the graph, aggregating of coherent generator buses, reducing the transmission network, and attaching the generator equations. The first two steps have been described in chapter 3. In this chapter, only the last three steps are explained.

The aggregation of coherent generator buses

As the parameters of generators may not be available, the aggregating of coherent generator buses should be performed at the terminal buses. Therefore, the method proposed in [2] is adopted with a minor modification. For each group of coherent generators, k-th group, a new common generator bus (or the aggregated bus) is first created with its voltage magnitude and its voltage angle calculated by eqn. (4.1) and eqn. (4.2), respectively. Here, the complex power magnitudes are chosen as the weights for averaging the angles rather than the inertia of each coherent generator, which is considered as unknown. All coherent generator terminal buses are then connected to the common bus via the ideal phase shift transformers having the voltage transformation ratios following eqn. (4.3). Finally, the power generations on the new common bus and on the coherent generator buses are adjusted by setting the values of the former to the total sum and the values of the later buses to zeros. At this stage, the coherent generator buses become the PQ-type buses.

$$\left|\vec{V}_{eq}(k)\right| = \frac{\sum_{i=1}^{n}\left|\vec{V}_i\right|}{n} \tag{4.1}$$

$$\theta_{eq}(k) = \frac{\sum_{i=1}^{n} |\vec{S}_i| \theta_i}{\sum_{i=1}^{n} |\vec{S}_i|} \tag{4.2}$$

$$\vec{a}_{i-k} = \frac{\vec{v}_i}{\vec{V}_{eq}(k)} \tag{4.3}$$

where

$\vec{V}_{eq}(k)$ is the k-th aggregated bus voltage

$\vec{v}_i$ is the i-th generator terminal bus voltage

$\theta_{eq}(k)$ is the k-th aggregated bus voltage angle

θ_i is the i-th generator terminal bus voltage angle

$\vec{a}_{i-k}$ is the ideal transformer from the i-th generator terminal bus to the k-th aggregated bus

$\vec{S}_i$ is the i-th complex power generation

n is the number of coherent generators of the k-th group

The reduction of transmission network

After the generator bus aggregation, all PQ-type buses of the external part can be eliminated for the reduction of transmission network size. There are many well developed techniques [3, 4] that could be employed to perform this task. The technique based on Ward injection method is briefly mentioned here. The key concept is to obtain the reduced transmission network from the admittance matrix when its rows and its columns corresponding to the external buses eliminated. This process starts from partitioning the admittance matrix of the complex current injection into internal part and external part, as shown in eqn. (4.4).

$$\begin{bmatrix} \vec{I}_{internal} \\ \vec{I}_{external} \end{bmatrix} = \begin{bmatrix} Y_{I,I} & Y_{I,E} \\ Y_{E,I} & Y_{E,E} \end{bmatrix} \begin{bmatrix} \vec{V}_{internal} \\ \vec{V}_{external} \end{bmatrix} \tag{4.4}$$

After elimination of the voltages belonging to the external part, the eqn. (4.5) are obtained.

$$\vec{I}_{internal} = \left(Y_{I,I} - Y_{I,E}Y_{E,E}^{-1}Y_{E,I}\right)\vec{V}_{internal} + Y_{I,E}Y_{E,E}^{-1}\vec{I}_{external} \tag{4.5}$$

From eqn. (4.5), the resultant of terms in the parenthesis represents the reduced admittance matrix of the system after the external buses are eliminated, while the second term inside the parenthesis represents new equivalent lines joining the boundary buses and shunts at the boundary buses. The second term of eqn. (4.5) represents equivalent current at boundary buses.

The attachment of the generator equation

What we have at this stage is the external part composed of the reduced network and the new common generator buses (or the aggregated buses). In order to complete the derivation of the model structure, the generator dynamic equations need to be attached to each common generator buses. For different problems, different degree of details of generator model may be used; and the justification could be based on either heuristics or iterative process such as the cost function sensitivity analysis method proposed in [5] (shown in Figure 4-1).

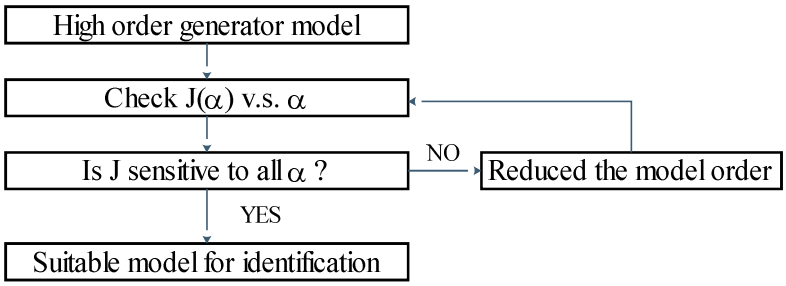

Figure 4.1 Procedure of the cost function sensitivity analysis

From Figure4.1, the process starts from the highest order model of generator. The sensitivity is justified by investigating the variation of the cost function $J(\alpha)$, defined in eqn. (4.6), under the perturbation of model parameters:

$$J(\alpha) = \int_{t_0}^{t_f} e^T(\alpha)e(\alpha)dt \tag{4.6}$$

where $e(\alpha)$ is the difference between the output of the original model and the output of the reduced model under α-th set of parameters. The current model will be replaced by the lower-order model if insensitivity is noticed. This process will continue until the cost function is sensitive to all parameters in the model.

4.2.2 Parameter identification

Since one of the objectives is to obtain the dynamic equivalent in power system component formulation, the implementation of the parameter identification in this thesis relies on a non-linear optimisation process where nothing alters the parameterisation of the model structure derived from the previous section. The parameters of the model structure, i.e. the equivalent generators' parameters, are directly identified by adjusting their values until the predefined criterion based on the difference between the responses from the reduced model and those from the original model is satisfied.

The transient responses of the active power flows from the i-th to the k-th bus [6] are selected, as discussed in Chapter 2, for the calculation of the error criterion:

$$J(x) = \sum_{i \in I} \sum_{k \in K} \left(P_{ik}^{original} - P_{ik}^{reduced}(x) \right)^2 \tag{4.7}$$

where I is the set of boundary buses and K is the set of buses in the internal system linked with the boundary buses.

In this chapter, only the parameter identification which requires a full system simulation (the first scheme described in Chapter 2) is presented (see Figure 4-2) while the method that requires no full system simulation will be discussed in Chapter 5. The procedure starts from the zero-th step where the corresponding time responses of the original system are simulated and recorded. Next, in step1, the power flow of the reduced system, which is created from the derived model structure of the external part (the external reduced network and the equivalent generator model without the values of parameters) and the model of the internal part, is simulated and recorded.

This power flow result is used with the initial guess of the generators' parameters (in the step 2) to calculate the initial conditions of the external generator model (in step 3) for the dynamic simulation in the step 4. The transient responses of the active power flows from the external to the boundaries obtained from the dynamic simulation in the step 4 are recorded and are compared with the records of the original system in the step 5. The comparison is justified by considering the error criterion (4.7). The process is stopped and the parameters are obtained if the error is less than the predefined tolerance, otherwise it continues through the route of the step 6.

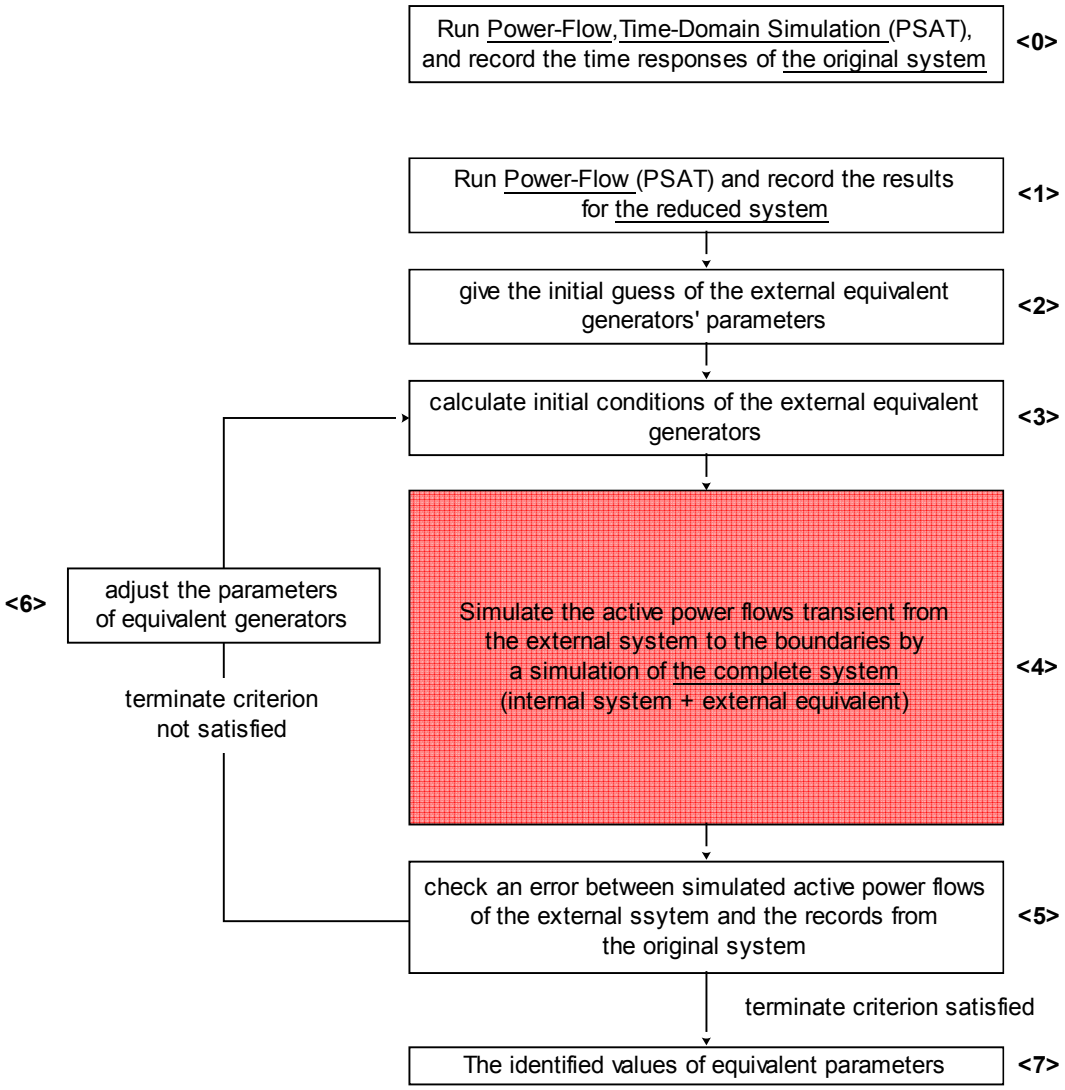

Figure 4.2 Proposed parameter identification procedure which require a full system simulation

4.3 Test results and discussions

The proposed method described in section 4.2 is demonstrated with the nine bus power system (shown in Figure 4-3).

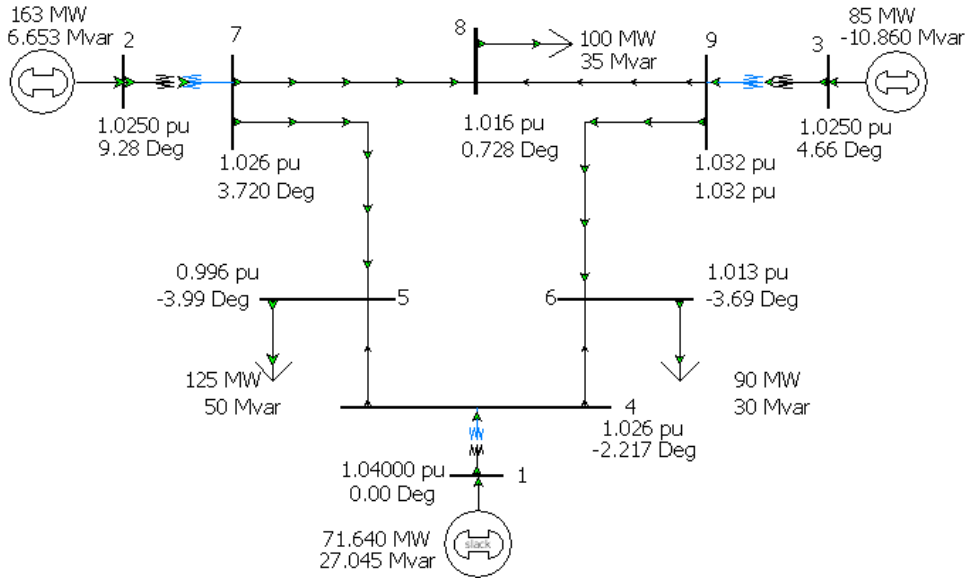

Figure 4.3 One line diagram of nine bus system

Step 1: Model structure determination

1.1 Establishing the node-weighted graph model

The node-weighted graph model of the nine bus power system is established by the same procedure as described in Chapter 3 and only the result (the graph model) is re-presented here in Figure 4.4. However, the node-weight of the generator internal bus and the weight of the edge between the generator internal bus and the generator terminal bus are not calculated; because the parameters of the generators are considered as unknowns.

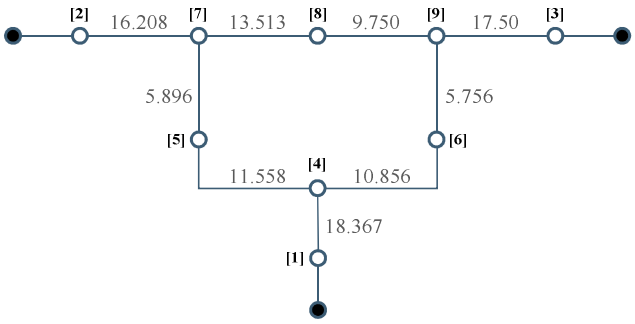

Figure 4.4 Graph model of nine bus power system

1.2 Identifying coherent generator

Based on the assumption of the strong internal edge-weight, the generator 2 and the generator 3 are identified as the coherent generators by using two levels of line-thickness plot (see Figure 4-5).

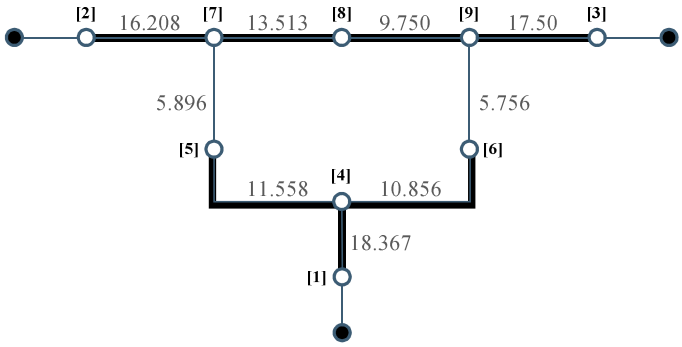

Figure 4.5 Two levels of line-thickness plot for the graph model of nine bus system

1.3 Aggregating of coherent generator buses

Firstly, the common generator bus for the coherent generator 2 and 3 is created. The voltage magnitude and angle are calculated from the power flow solutions (see Table 4-1) as following:

Aggregated active power = 163 + 85 = 248 MW.

Aggregated bus voltage magnitude = $\left|\vec{V}_{agg1}\right| = \frac{\left|\vec{V}_2\right| + \left|\vec{V}_3\right|}{2}$ =1.0250 P.U.

Aggregated bus voltage angle = $\theta_{agg1} = \frac{\left|\vec{S}_2\right|\theta_2 + \left|\vec{S}_3\right|\theta_3}{\left|\vec{S}_2\right| + \left|\vec{S}_3\right|}$ =7.6886 degree

Table 4.1 Power flow solutions of bus 2 and bus 3 of nine bus power system

Bus No.	Voltage magnitude (P.U.)	Voltage angle (degree)	Apparent power injection (MVA)
2	1.0250	9.28	163.1
3	1.0250	4.66	85.7

The generator buses of generator 2 and 3 are then connected to the common bus via the ideal phase-shift transformers whose transformation ratios are calculated by using eqn. (4.3).

Table 4.2 Ideal phase shift transformer for aggregation of bus 2 and bus 3 of nine bus power system

From bus – To bus	Transformation ratio
2 – agg1	1∠1.5914
3 – agg1	1∠ – 3.0286

Finally, generator 2 and 3 are deleted and the new equivalent generator is added to the common bus. The resultant one line diagram of the system when the coherent generator terminal buses are aggregated is shown in Figure 4.6.

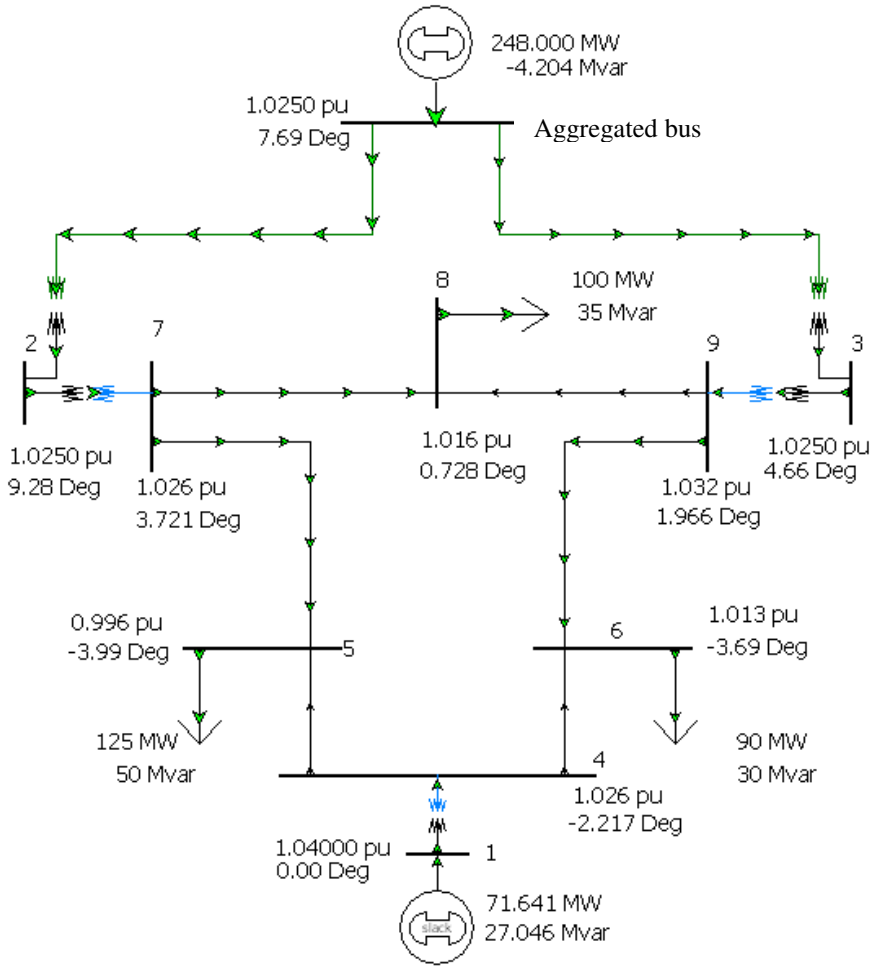

Figure 4.6 One line diagram of the nine bus system when coherent generator buses are aggregated

1.4 Reducing the transmission network

In this case the bus 1, bus 4, bus 5 and bus 6 are chosen as the internal part. The equivalencing tool of PowerWorld (which is based on Ward's method) is employed to eliminate the load buses of the external part (i.e. bus 2, 3, 7, 8, and 9). This results in the equivalent transmission lines and the equivalent shunts as shown in Table 4.3 and Table 4.4 respectively. The one line diagram of the static reduced system that combines the external equivalent and the internal part is given in Figure 4.7.

Table 4.3 Equivalent transmission lines for the external part of nine bus system

From bus	To bus	Resistance, R (P.U.)	Reactance, X (P.U.)
5	6	1.27336	3.53964
5	Agg1	0.02922	0.22170
6	Agg1	0.02549	0.23026

Table 4.4 Equivalent shunts for the external part of nine bus system

Bus	Shunt conductance, G (MW) (Actual / Nominal)	Shunt susceptance, B (MVar) (Actual / Nominal)
5	-8.03 / -8.101	19.41 / 19.584
6	-27.75 / -27.058	26.96 / 26.291
Agg1	-63.97 / -60.885	18.44 / 17.555

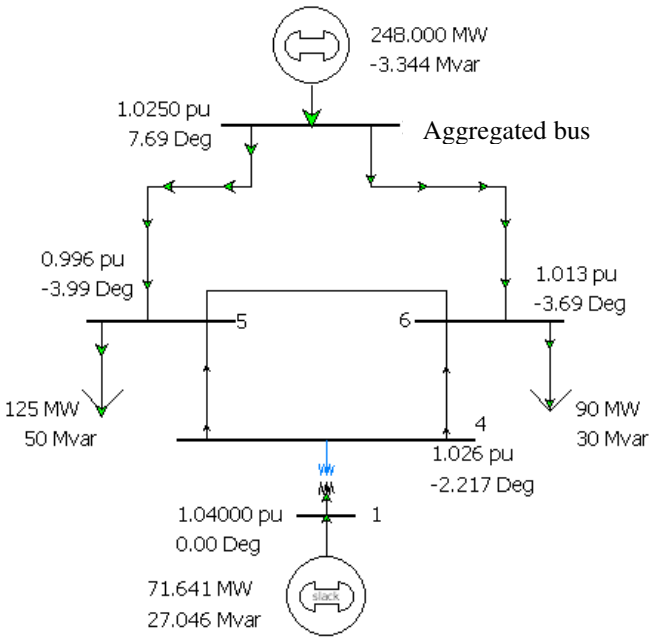

Figure 4.7 One line diagram of the nine bus system after coherent generator bus aggregation and load bus reduction

1.5 Attaching the generator equation

The last step is to attach the generator dynamic model to the static reduced system, shown in Figure 4.7. For the sake of simplicity, the classical generator dynamic model having only two parameters, transient reactance (X'_d) and inertia (H), is used.

Step 2: Parameter identification

The parameter identification as described in section 4.2.2 is implemented in MATLAB with the aid of Power System Analysis Tool box (PSAT) [7] and Optimisation Tool box [8]. The implementation is illustrated in Figure 4.8.

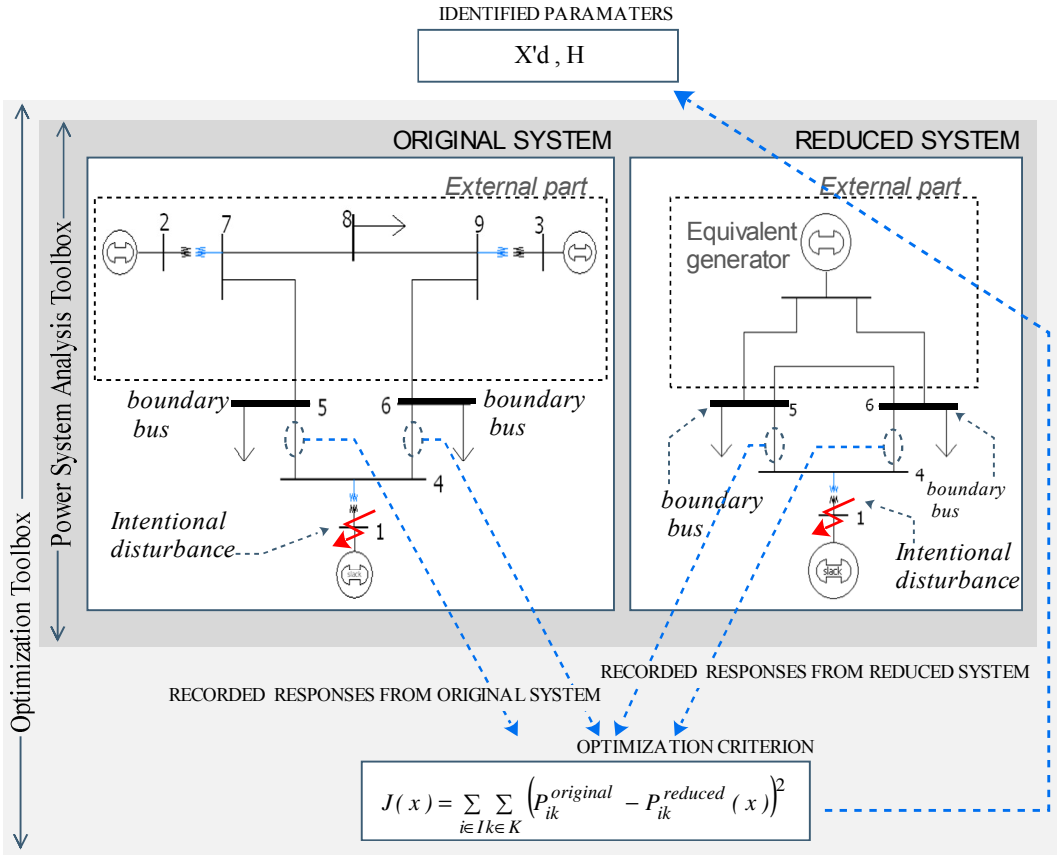

Figure 4.8 Parameter identification process implemented in MATLAB

From Figure 4.8, the power systems (the original system and the reduced system) are modelled and simulated by PSAT. The classical generator dynamic model is used for each generator of both systems where the generator data are obtained from [9].The relevant transient responses are the active power flows from bus 4 to bus 5 and bus 4 to bus 6 during a small fault applied at bus 1 (a fault with 10 P.U. resistance at

t=0.05s). The time duration for the records is 2.5 seconds. This is considered long enough to capture the slow rotor angle dynamics (0.4 Hz-0.7Hz) [10] and still is sufficiently short for the swing equation, which is a basis of graph model used for identifying coherent generators, to be valid. The discrepancy between the simulated responses of the reduced dynamic system under the current guessing parameters and those of the original system is improved by using new values of equivalent parameters supplied from a nonlinear optimisation routine of the Optimisation toolbox. The Levenberg-Marquardt algorithm is chosen throughout the thesis for the optimization. The fitting responses and the identified parameters of the equivalent generators after the termination criteria of the nonlinear optimisation routine satisfied are shown in Table 4.5 and in Figure 4.9, respectively.

Table 4.5 Identified parameters of the equivalent generator of the proposed reduced system

Equivalent Generator	Equivalent Parameters	Direct axis transient reactance (x'_d), p.u.	Inertia constant (H), kWs/kVA
Geq1	Initial Value	0.0500	10.0000
	Identified Value	0.0931	9.0438

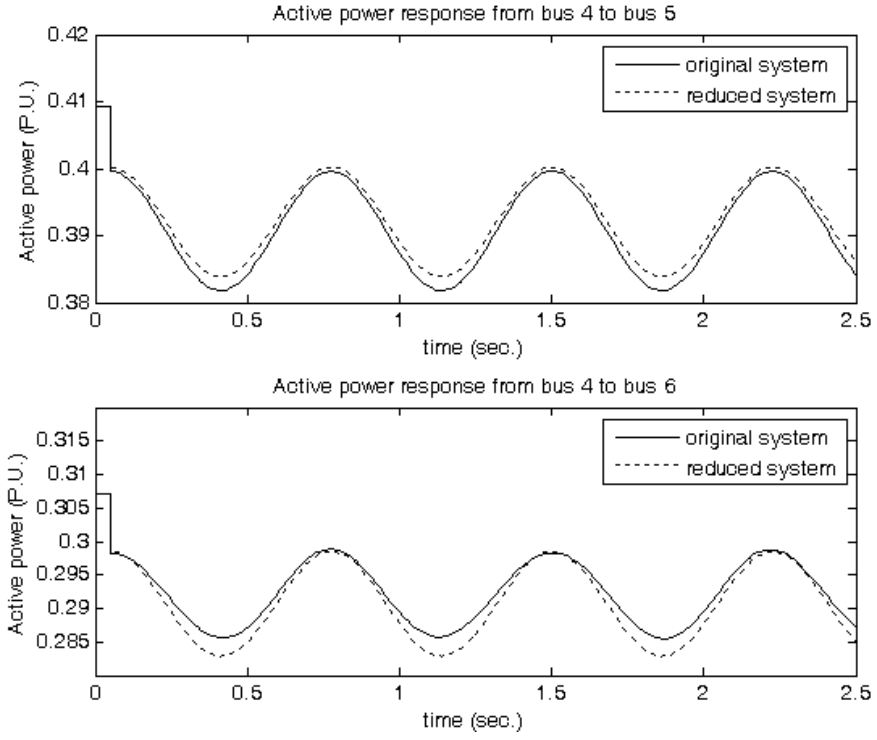

Figure 4.9 Active power responses of the original system and the proposed reduced system after the parameter identification is terminated.

The obtained equivalent is evaluated by the following comparisons. First, the simulated responses of the internal generator from the proposed reduced system (called the reduced system A) and those from the original system under various fault locations are compared. Besides the location of fault, the different types of fault are studied which consist of a small fault (a fault with 10 P.U. resistance) and a large fault (the solid fault applied at t=0.05 sec. and cleared at t=0.06 sec.). Second, another reduced system (called the reduced system B) which is based on a fictitious generator attached at each boundary bus is considered for comparison.

The reduced system B is formed by attaching two fictitious generators to bus 5 and bus 6, as shown Figure 4.10.

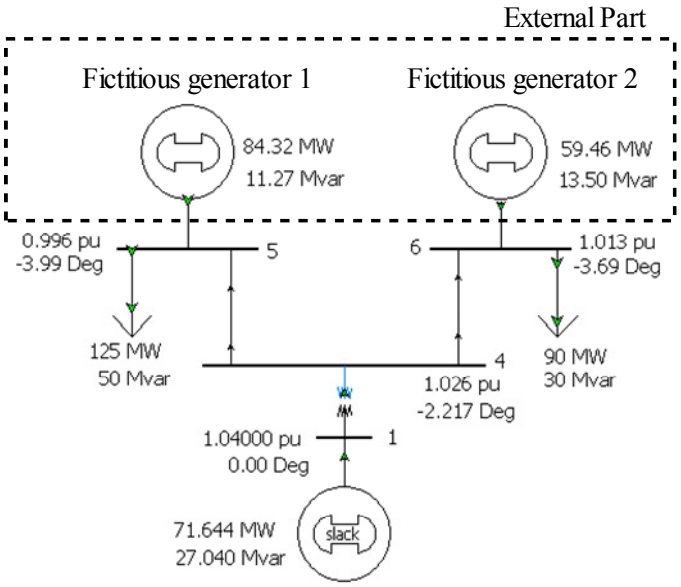

Figure 4.10 Reduced system B for the nine bus system

The static operating condition of the internal part is preserved by setting the power injection and the bus voltage magnitudes at the boundary buses (bus 5 and bus 6) equal to the values calculated by the power flow of the original system. The parameters of the fictitious generators are identified by the same process illustrated in Figure 4.8. The identified parameters of the fictitious generators and the responses at boundaries after process terminates are shown in the Table 4-6 and in the Figure 4-11, respectively.

Table 4.6 Identified parameters of the fictitious generators for the reduced system B of the nine bus system.

Fictitious Generator	Equivalent Parameters	Direct axis transient reactance (x'_d), p.u.	Inertia constant (H), kWs/kVA
FG1	Initial Value	0.5	0.3688
	Identified Value	5.0	5.4364
FG2	Initial Value	0.5	0.4993
	Identified Value	5.0	4.4080

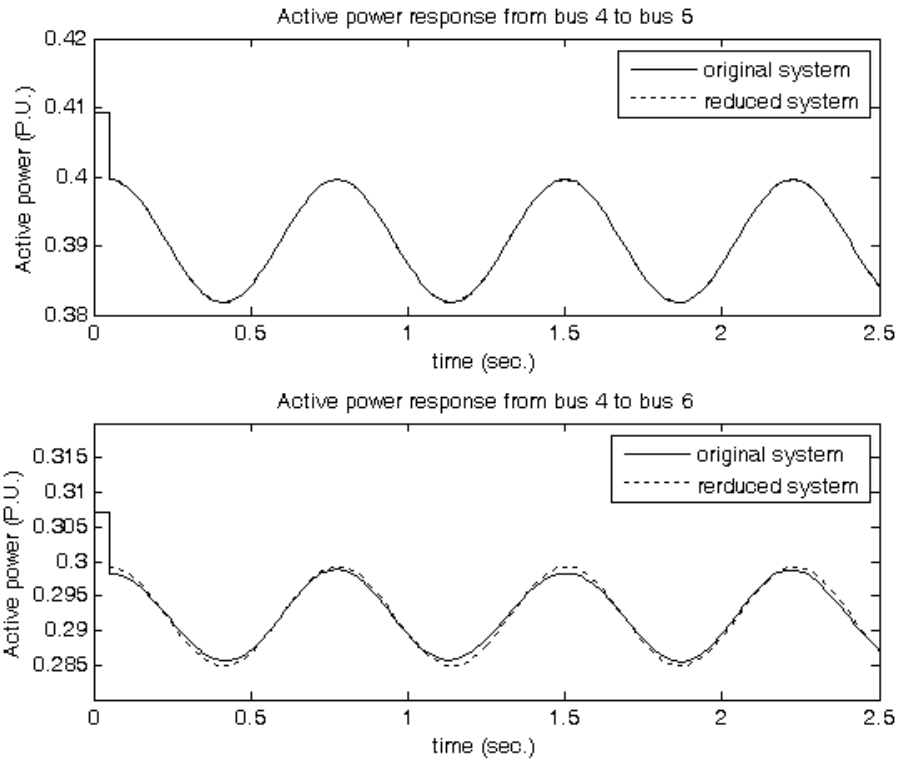

Figure 4.11 Active power responses of the original system and the reduced system B after the parameter identification is terminated.

Moreover, the simulated result from the reduced system when the group of coherent generators is replaced by the coherency-based dynamic equivalent [2] (called the reduced system D) is also presented. For this coherency-based equivalent, the inertia constants of corresponding coherent generators are used as the weights for the common bus angle average. The inertia constant of the equivalent generator is the sum of inertia constant of individual coherent generator. The direct axis transient reactance of the equivalent generator is calculated as transient reactance of the

individual generator in parallel. The reduced system D is shown in Figure 4.12 while its related components and the parameters are given in the Table 4.7 to Table 4.9 respectively.

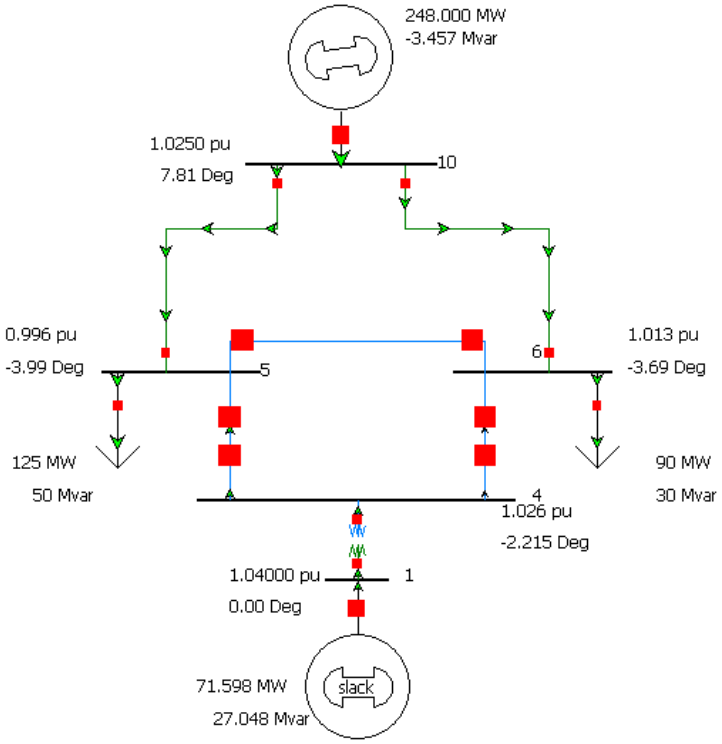

Fig. 4.12 Reduced system D for the nine bus system

Table 4.7 Equivalent transmission lines of the reduced system D

From bus	To bus	Resistance, R (P.U.)	Reactance, X (P.U.)
5	6	1.27335	3.53964
5	Agg1	0.02878	0.22176
6	Agg1	0.02503	0.23031

Table 4.8 Equivalent shunts of the reduced system D

Bus	Shunt conductance, G (MW) (Actual / Nominal)	Shunt susceptance, B (MVar) (Actual / Nominal)
5	-8.902 / -8.980	19.527 / 19.699
6	-28.620 / -27.909	27.056 / 26.384
Agg1	-62.171 / -59.175	19.080 / 18.161

Table 4.9 Equivalent parameters of the equivalent generator of the reduced system D

Equivalent Generator	Direct axis transient reactance (x'_d) p.u.	Inertia constant (H) kWs/kVA
Geq	0.0721	9.410

The calculated equivalent parameter in Table 4.9 is also used with the proposed equivalent to form another reduced system, called the reduced system C. All the reduced system are summarised as following:

- The reduced system A is constructed from the proposed equivalent
- The reduced system B is constructed from the fictitious generator equivalent.
- The reduced system C is constructed from the proposed equivalent with the parameters of equivalent generator from the calculation (Table 4.9).
- The reduced system D is constructed from the coherency-based equivalent.

These reduced systems are shown in Figure 4.13 below.

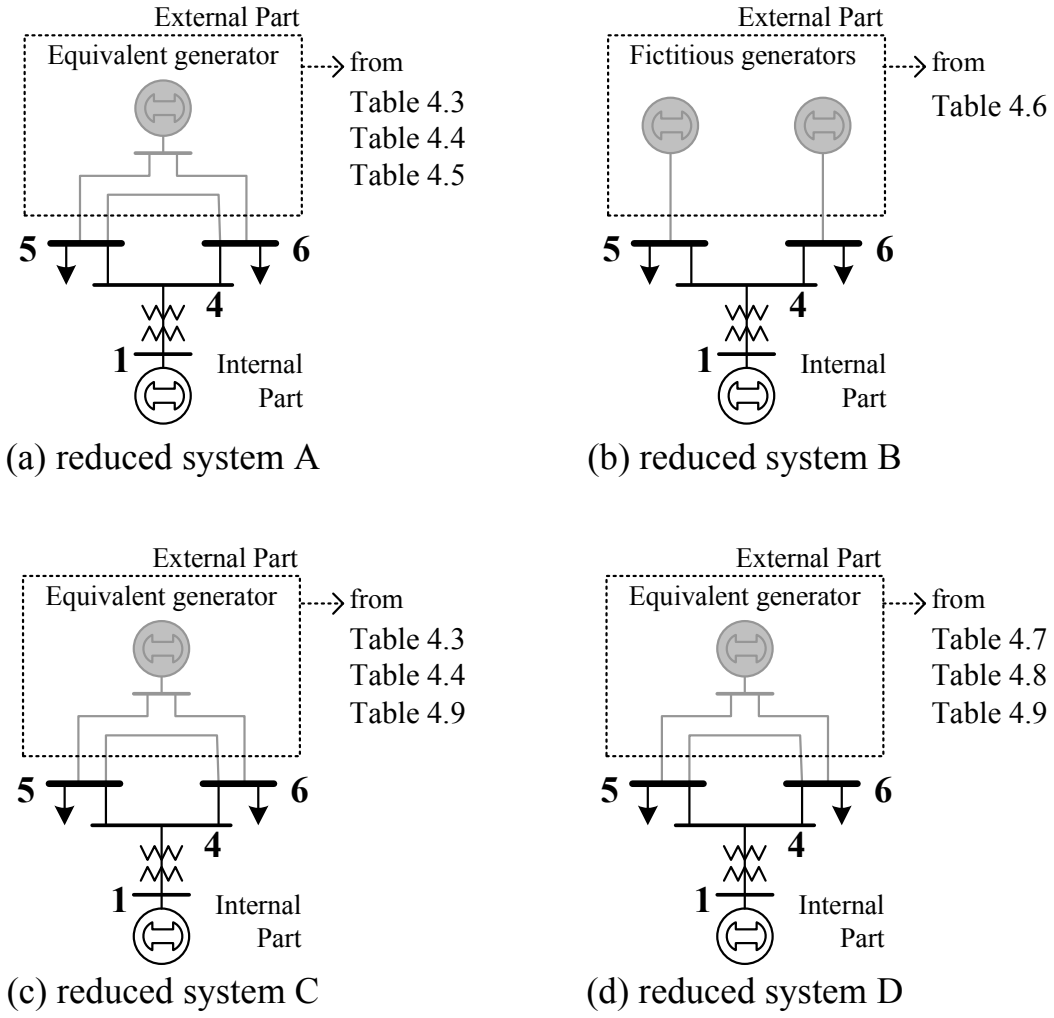

Figure 4.13 Summary of reduced systems studied in Chapter 4

The results of each reduced system and of the original system are presented together for each type of fault and each location of fault, respectively in Figure 4.14 to Figure 4.19.

From the results (each top sub-figure of the Figure 4.14 to Figure 4.19), the transient of rotor angle of the internal generator of the original system can be similarly reproduced by the reduced system A for all locations of fault and for both types of faults, especially the small fault. This is because the proposed model structure is derived from the knowledge of the coherent group that is independent to the fault location. Moreover, in the case of the small fault, the reduced system worked within the limit where its linearised model is good valid, thus giving a well condition for the equivalent model. However, the validity of the equivalent for all locations of fault do not assure because the parameters of the equivalent generator was not obtained by theoretical aggregation [11].

In comparison, the performance of the reduced system B (each second sub-figure from top of the Figure 4.14 to Figure 4.19) and the performance of the reduced system A are nearly the same, even the fitting results during the parameter identification of the reduced system A is poorer than those of the reduced system B (see Figure 4.9 and Figure 4.11). However the proposed equivalent has one fewer generator, hence producing the smaller size of the reduced system.

The poor result is not from the improper values of the identified parameters, but because it is the best performance that could be achieved by using the model structure based on the knowledge of the coherent generator. It can be clearly seen that the performance of the reduced system A is even better than those of the reduced system C and of the reduced system D (see each last two sub-figure of Figure 4.14 to Figure 4.19). The performance of this model structure largely relies on coherency between the generators, which depends on the character of each particular system. For this nine bus system, the coherency of the generator 2 and the generator 3 is not so tight (see Figure 3.28 of Chapter 3).

4.4 Conclusion

The development of a dynamic equivalent of a power system based on parametric identification has been presented in this Chapter. The model structure which largely determines the performance (i.e. accuracy, validity, and size) of the resultant reduced system is derived through using the knowledge of coherent generator. With the coherent generator identification technique proposed in Chapter 3, the model structure can be obtained without the parameters of the generators. The identification-based dynamic equivalencing method requires only power flow modelling data and measurements at the boundaries.

The nine bus power system was used to demonstrate the feasibility of this proposed method. Moreover, the proposed dynamic equivalent was also tested and compared with another equivalent to evaluate its validity and reliability. The results show good validity and reliability of the equivalent. However, further studies with a larger system were conducted in Chapter 6 to assess the real performance and the limitations of the proposed method.

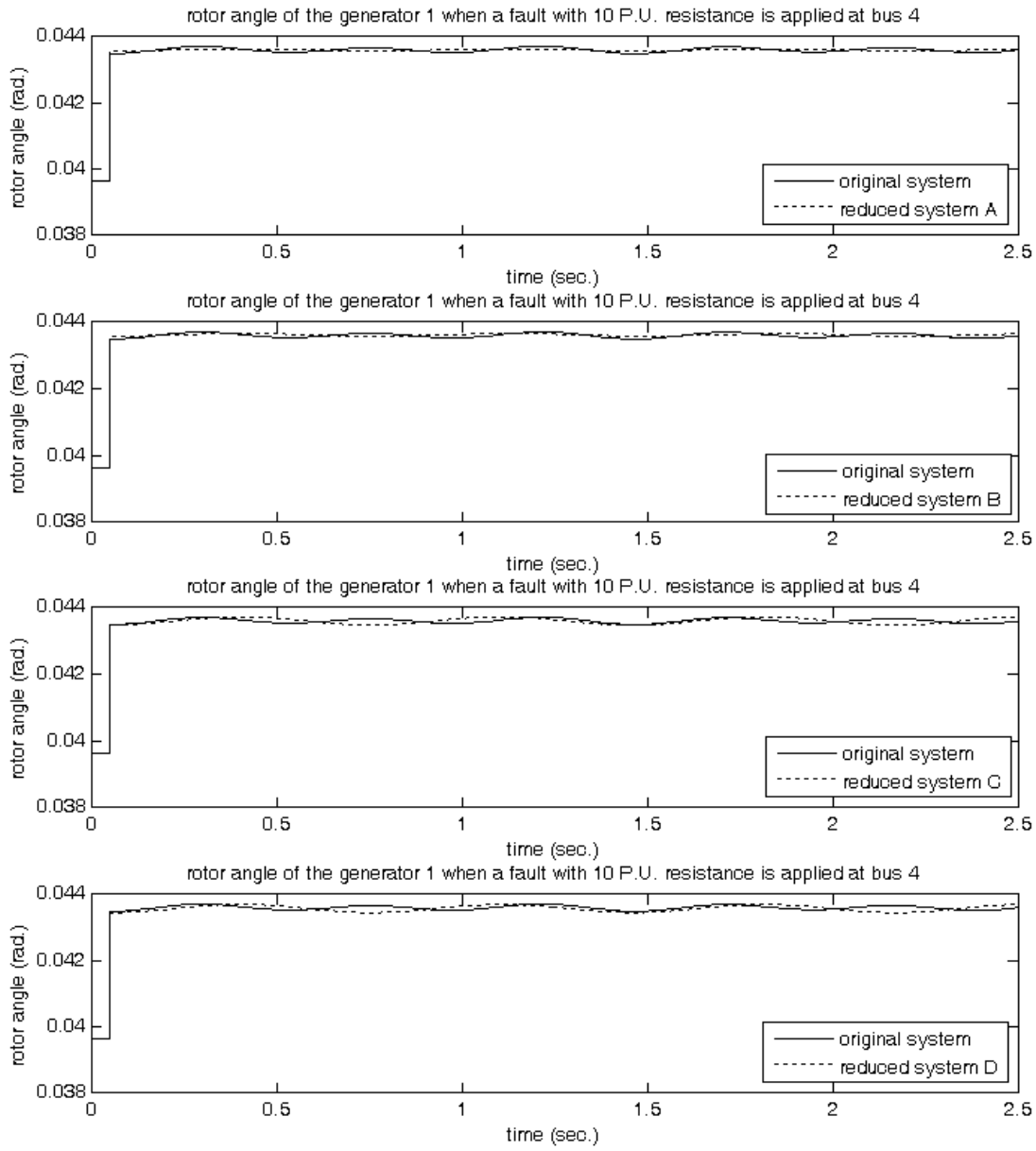

Figure 4.14 Rotor angles of the generator 1 from the reduced systems and the original system of the nine bus power system when a fault with 10 P.U. resistance is applied at bus 4.

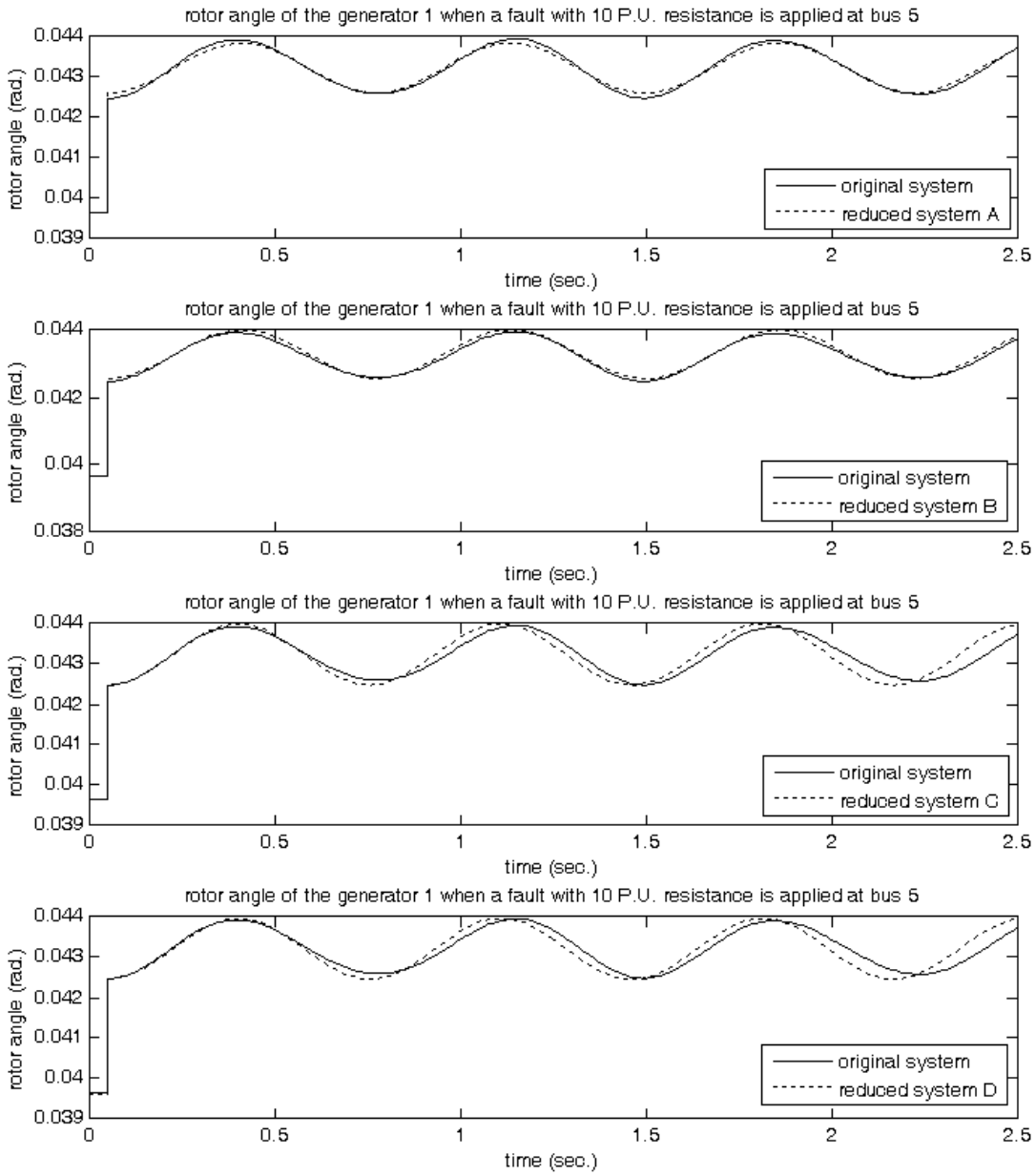

Fig 4.15 Rotor angles of the generator 1 from the reduced systems and the original system of the nine bus power system when a fault with 10 P.U. resistance is applied at bus 5.

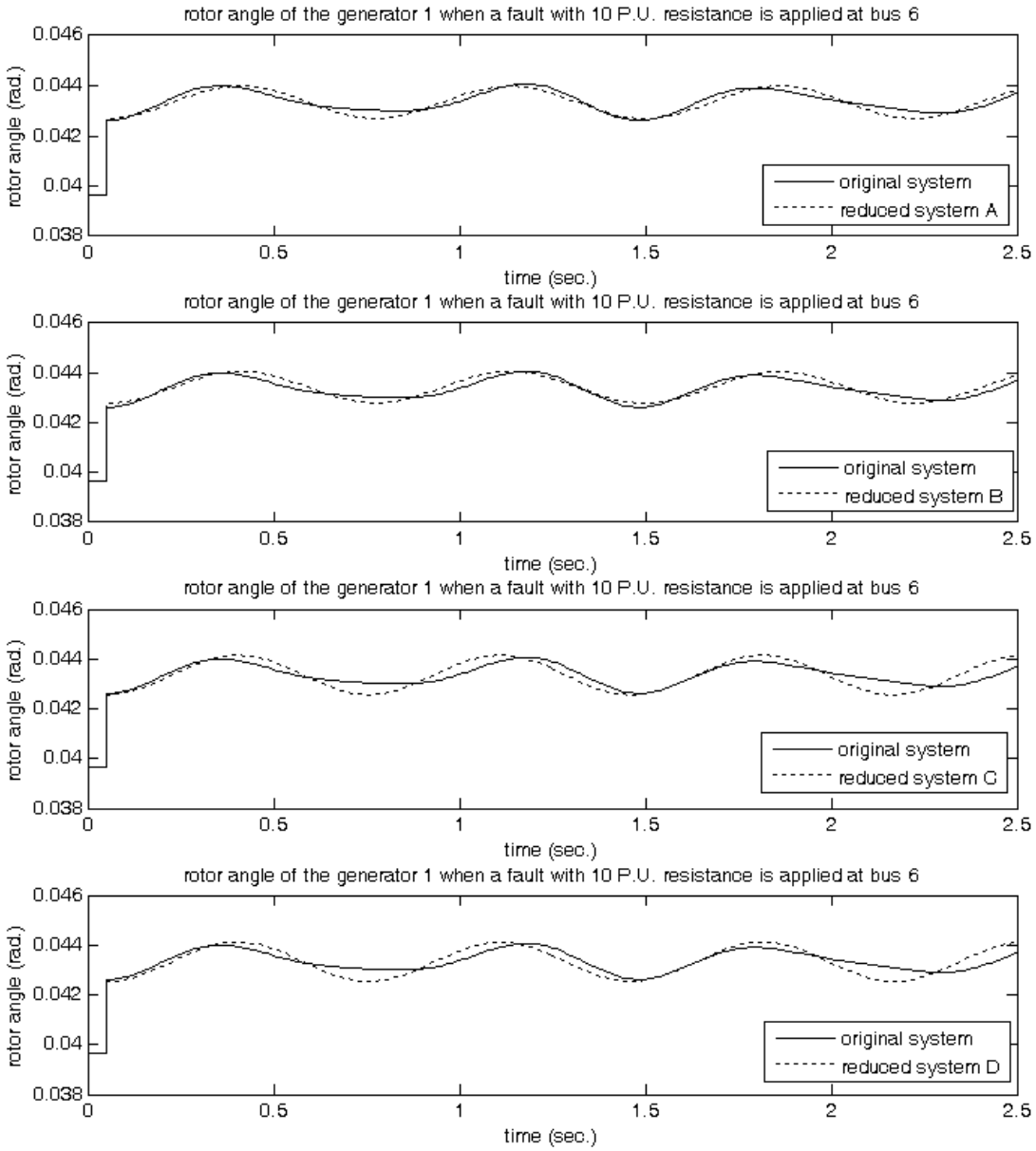

Figure 4.16 Rotor angles of the generator 1 from the reduced systems and the original system of the nine bus power system when a fault with 10 P.U. resistance is applied at bus 6.

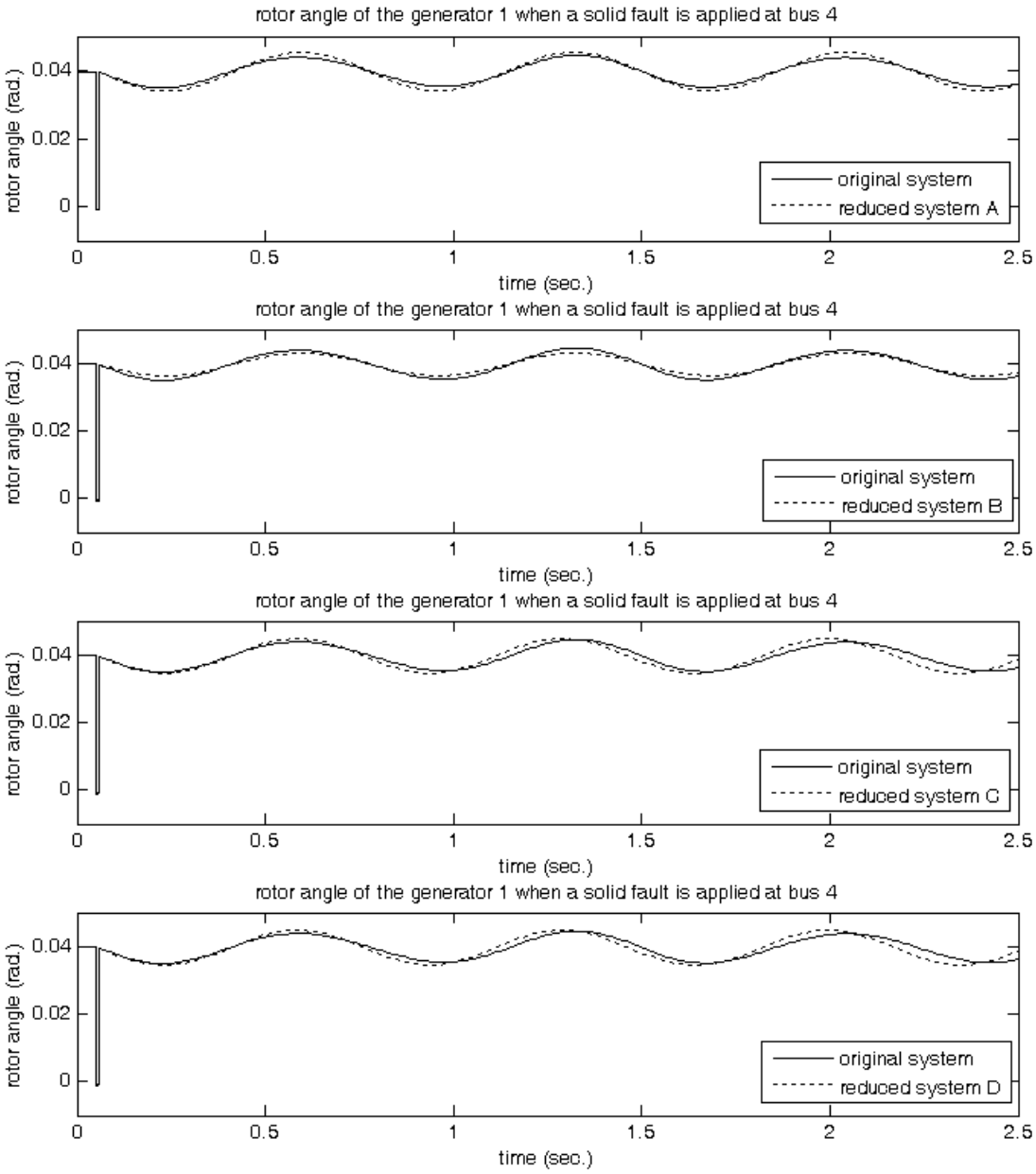

Figure 4.17 Rotor angles of the generator 1 from the reduced systems and the original system of the nine bus power system when a solid fault is applied at bus 4.

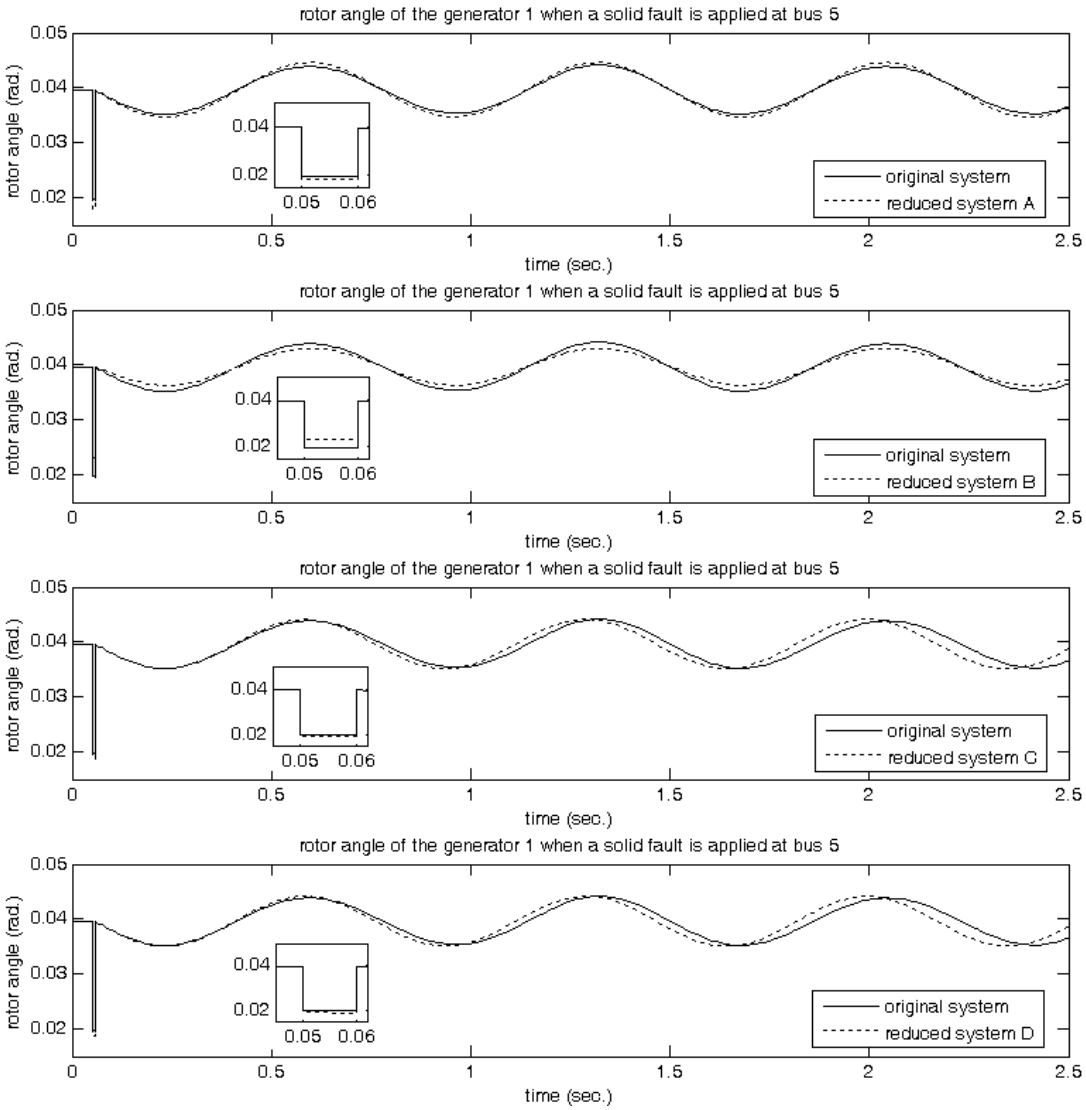

Figure 4.18 Rotor angles of the generator 1 from the reduced systems and the original system of the nine bus power system when a solid fault is applied at bus 5; the fault regions are magnified and shown in sub-figures.

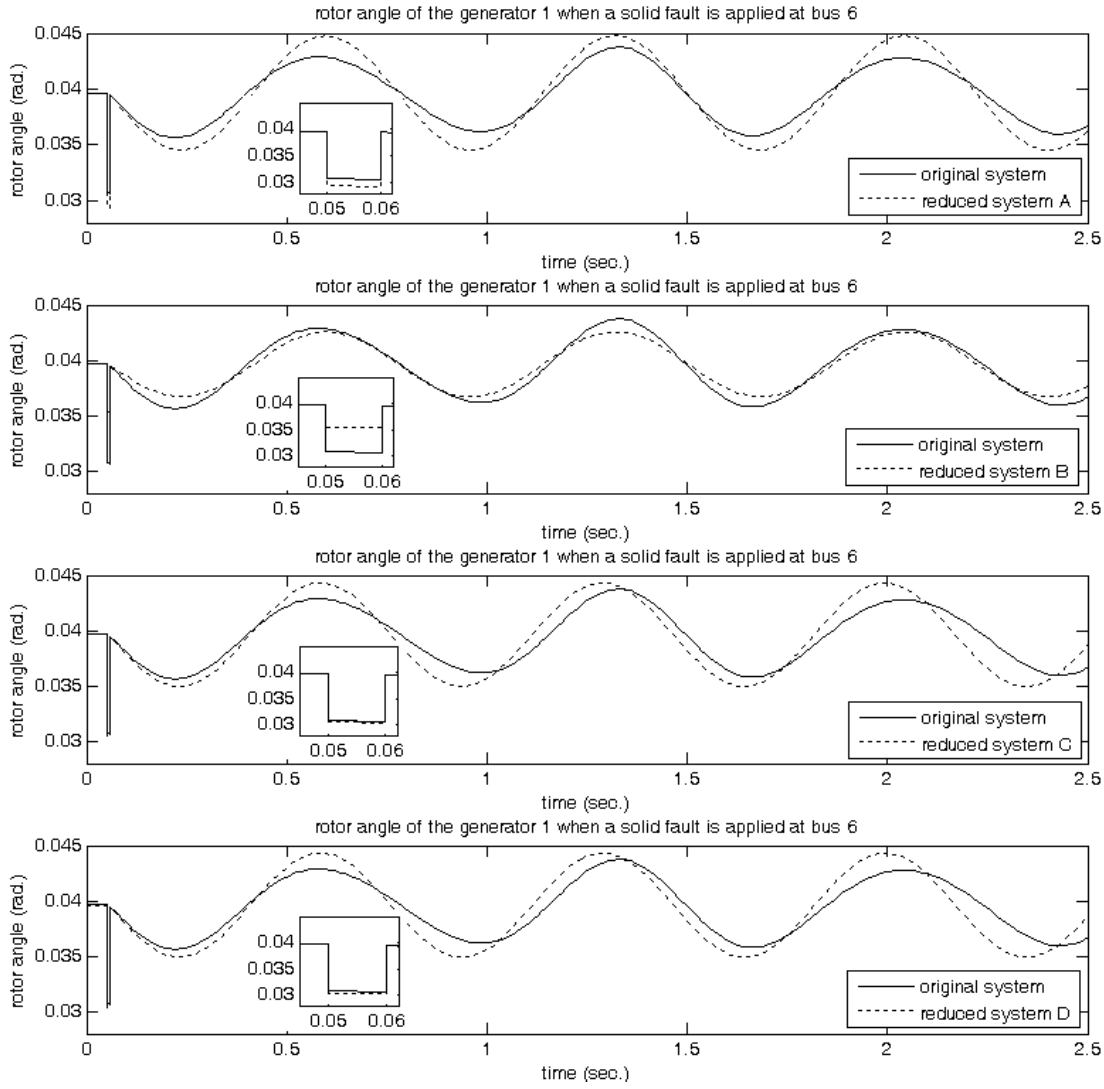

Figure 4.19 Rotor angles of the generator 1 from the reduced systems and the original system of the nine bus power system when a solid fault is applied at bus 6; the fault regions are magnified and shown in sub-figures.

4.5 References

[1] O. Nelles, *Nonlinear system identification: from classical approaches to neural networks and fuzzy models*: Springer-Verlag Berlin Heidelberg, 2001.

[2] Z. Z. Qi, "Coherency based dynamic equivalence of power systems." vol. Ph.D.: University of Strathclyde, 1994, p. 184.

[3] S. Deckmann, A. Pizzolante, A. Monticelli, B. Stott, and O. Alsac, "Studies on Power System Load Flow Equivalencing," *Power Apparatus and Systems, IEEE Transactions on,* vol. PAS-99, pp. 2301-2310, 1980.

[4] F. F. Wu and A. Monticelli, "Critical review of external network modelling for online security analysis," *International Journal of Electrical Power & Energy Systems,* vol. 5, pp. 222-235, 1983.

[5] M. A. El-Sharkawi, "Choice Of Model And Topology For External Equivalent Systems," *Power Apparatus and Systems, IEEE Transactions on,* vol. PAS-102, pp. 3761-3768, 1983.

[6] J. M. Ramírez Arredondo, "Obtaining dynamic equivalents through the minimization of a line flows function," *International Journal of Electrical Power & Energy Systems,* vol. 21, pp. 365-373, 1999.

[7] F. Milano, "Power System Analysis Toolbox (PSAT) ", 1.3.4 ed, 2006.

[8] The MathWorks Inc. , "MATLAB Programing," The MathWorks Inc., 2007.

[9] P. M. Anderson and A. A. Fouad, *Power System Control and Stability*: The Iowa State University Press, 1977.

[10] P. Kundur, *Power System Stability and Control*: McGraw-Hill, Inc., 1994.

[11] J. H. Chow, *Time-scale modeling of dynamic networks with application to power systems*: Springer-Verlag, 1983.

CHAPTER 5

IDENTIFICATION OF EQUIVALENT GENERATOR PARAMETERS WITHOUT FULL SYSTEM SIMULATION

5.1 Introduction

Parameter identification is one essential task for constructing identification-based dynamic equivalent. Its performance (i.e. accuracy and usage time) directly affects the efficiency of the dynamic equivalent especially when online application is concerned as discussed in Chapter 1. In this Chapter, the aim is directed to improve the usage time of the parameter identification process.

In general, the parameter identification could be formulated as an optimization problem [1] which can be further divided into linear and nonlinear optimization problems, respectively. These two sub-classes of optimization problem differ on how the error criterion is parameterized. In our case, the parameter identification falls into the latter as the consequence of a nonlinearity in parameters of the equivalent model. The total time used to solve this kind of problem largely depends on many factors [2] such as the chosen optimisation methods, the initial guessing parameters, and the character of the problem. The focus of this chapter is on the character of problem, in particular the reduction of the time to calculate the error criterion which is based on the difference between the recorded responses from the original system and the simulated responses from the reduced system under the current assuming parameter values. It is expected to have a large improvement; because, the simulation of the reduced system (i.e. the internal system together with the external equivalent) is a time consuming process and need to be repeated for each newly adjusted parameter during the optimisation process.

The parameter identification technique that requires no simulation of the complete system is presented in this chapter. This technique is modified from the previous parameter identification proposed in Chapter 4. Firstly, the input-output formulation of external part is described. Next, the modified parameter identification procedure is explained according to two schemes of implementation. In the first scheme,

parameters of equivalent generators are identified all at once while a set of parameters of each equivalent generator is individually identified in the second scheme. Finally, test results with IEEE39 bus system are discussed and the conclusions are drawn.

5.2 Input-output formulation of external system

The input-output formulation of external system here is adopted from [3, 4]. Electromechanical transient of the external system is modelled by three fundamental components (see Figure 5-1): a reduced transmission network of the external part, the generator dynamic equations in their coordinates, and the frame transformations.

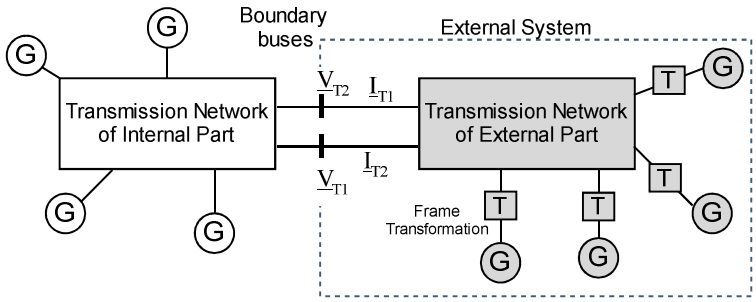

Figure 5.1 Components comprising the electromechanical transient model of power system

From Figure 5.1, the loads are represented by the constant admittances and are placed in the transmission network. The interfacing variables at the boundaries from the external system are the vectors of voltages and currents which are related to other components by the following sets of equations.

A. Reduced network equation of the external part

The derivation of the reduced network equation of the external part starts by rearranging the complete network equation (5.1) into a new order of bus as shown in eqn. (5.2)

$$[\underline{I}] = [\underline{Y}][\underline{V}] \tag{5.1}$$

$$\begin{bmatrix} \underline{I}_I \\ \underline{0} \\ \underline{I}_E \end{bmatrix} = \begin{bmatrix} \underline{Y}_{I,I} & \underline{Y}_{I,B} & \underline{0} \\ \underline{Y}_{B,I} & \underline{Y}_{B,B} & Y_{B,E} \\ \underline{0} & \underline{Y}_{E,B} & \underline{Y}_{E,E} \end{bmatrix} \begin{bmatrix} \underline{V}_I \\ \underline{V}_B \\ \underline{V}_E \end{bmatrix} \tag{5.2}$$

The underline denotes a complex variable. The sub-matrices inside a complex injection current are put in order with the injections of generator buses at the beginning, as eqn. (5.3). The zeros belong to the load injections which have been converted to the constant shunt admittances.

$$[\underline{I}] = \left[\underline{I_G} \quad \underline{0}\right]^T \tag{5.3}$$

The subscripts *I*, *B*, and *E* indicate that the matrix is related to internal bus, boundary bus, and external bus, respectively, while the subscript *G* denote the generator bus. After the parts associated with the external system are extracted (excluding the loads at boundaries) and load buses are eliminated, the reduced network equation of the external part is obtained as given in eqn. (5.4).

$$\begin{bmatrix} \underline{I_G} \\ \underline{I_B} \end{bmatrix} = \begin{bmatrix} \underline{Y_{GG}} & \underline{Y_{GT}} \\ \underline{Y_{TG}} & \underline{Y_{TT}} \end{bmatrix} \begin{bmatrix} \underline{V_G} \\ \underline{V_B} \end{bmatrix} \tag{5.4}$$

From eqn. (5.4), an occurrence of the complex injection currents at boundary buses ($\underline{I_B}$) is resulted from the separation at boundaries to balance those of the internal system.

B. Generator dynamic equations

For the sake of simplicity, the simplified classical generator dynamic model is used in this chapter. The related equations which are expressed in two-axis of individual machines co-ordinate are given below.

Stator voltage equation:

$$\left[\underline{V_m^i}\right] = \left[\underline{E'^i_m}\right] - \left[\underline{R_i}\right]\left[\underline{I_m^i}\right] - \left[\underline{PQ}\right]\left[\underline{X'_d}\right]\left[\underline{I_m^i}\right] \tag{5.5}$$

Electric torque equation:

$$T_{em}^i = -\left\{E'^i_q \, I_q^i + E'^i_d \, I_d^i\right\} \tag{5.6}$$

Rotor motion equations:

$$2H_i \frac{d\left\{\left(\omega_r^i - \omega_e\right)/\omega_b\right\}}{dt} = T_e^i + T_{mech}^i \tag{5.7}$$

$$\frac{d\delta^i}{dt} = \omega_r^i - \omega_e \tag{5.8}$$

Where

$\underline{I_m^i}, \underline{V_m^i}, \underline{E'^i_m}$ 2 element vectors containing d and q axis components of generator armature current, generator terminal voltage, and generator internal voltage.

T_{em}^i, T_{mech}^i an electrical and a mechanical torques of the i-th generator, p.u.

δ^i a rotor angle of the i-th generator, radians

ω_r^i a shaft speed of the i-th generator

H_i an inertia constant of the i-th generator

[PQ] permutation matrix, $\begin{bmatrix} 0 & -1 \\ 1 & 0 \end{bmatrix}$

C. Frame transformation

The individual set of generator equations and the equation of the reduced transmission network of the external part are worked together via the frame transformation of eqn. (5.9). The capital subscript denotes the network reference frame while the lower case subscript denotes the generator reference frame.

$$\underline{I_A^i} = \underline{T_i}\,\underline{I_a^i}, \qquad \underline{V_A^i} = \underline{T_i}\,\underline{V_a^i} \tag{5.9}$$

Where

$$\underline{T_i} = \begin{bmatrix} \cos\delta_i & -\sin\delta_i \\ \sin\delta_i & \cos\delta_i \end{bmatrix} \tag{5.10}$$

This frame transformation is based on the notation of generator and network axes shown in Figure 5.2.

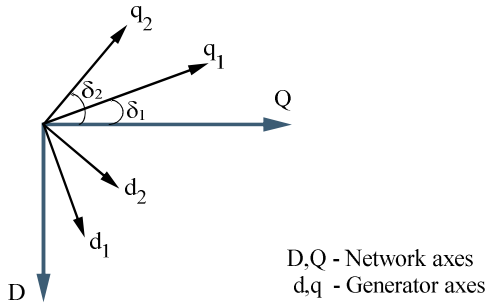

Figure 5.2 generator and network axes

By applying the frame transforms eqns. (5.9)-(5.10) to eqn. (5.5) and substitute into eqn. (5.4), the algebraic part of the external system dynamic model is obtained in eqn. (5.11).

$$\begin{bmatrix} \underline{1}+\underline{Y_{GG}}\left(\underline{R}+\underline{PQ}\,\underline{X'_d}\right) & \underline{0} \\ \underline{Y_{TG}}\left(\underline{R}+\underline{PQ}\,\underline{X'_d}\right) & \underline{1} \end{bmatrix}\begin{bmatrix} \underline{I_G} \\ \underline{I_T} \end{bmatrix}=\begin{bmatrix} \underline{Y_{GG}} & \underline{Y_{GT}} \\ \underline{Y_{TG}} & \underline{Y_{TT}} \end{bmatrix}\begin{bmatrix} \underline{TE'} \\ \underline{V_T} \end{bmatrix} \tag{5.11}$$

This equation can be reduced to eqn. (5.12) by a multiplying both sides of eqn. (5.11) with the inverse of its most left matrix.

$$\begin{bmatrix} \underline{I_G} \\ \underline{I_T} \end{bmatrix}=\begin{bmatrix} \underline{C'} & \underline{D'} \\ \underline{A'} & \underline{B'} \end{bmatrix}\begin{bmatrix} \underline{TE'} \\ \underline{V_T} \end{bmatrix} \tag{5.12}$$

Where $\underline{A}$', $\underline{B}$', $\underline{C}$', and $\underline{D}$' are the sub-matrices inside the resultant matrix obtained from the multiplication of the matrix of admittances on the right hand side of eqn. (5.11) by the inverse of the most left matrix of eqn. (5.11).

The equations (5.12) and (5.6)-(5.8) are the input-output formulation of dynamic model for the external part. The inputs are the voltages at boundary buses and the outputs are the injection currents at boundary buses from the external part.

As our recorded responses for the parameter identification are active power flows, another equation for the calculation of active power flow from the voltages and the currents at boundaries need to be included.

$$p_T = V_D I_D + V_Q I_Q \tag{5.13}$$

Where

V_D, V_Q D and Q axis components of voltages at boundaries

I_D, I_Q D and Q axis components of injection currents at boundaries

The idea to simulate the dynamic responses from the external part at boundaries without performing a full system simulation is tested with the IEEE39 bus system[5]. The external part and its corresponding inputs and outputs are defined in Figure 5-3.

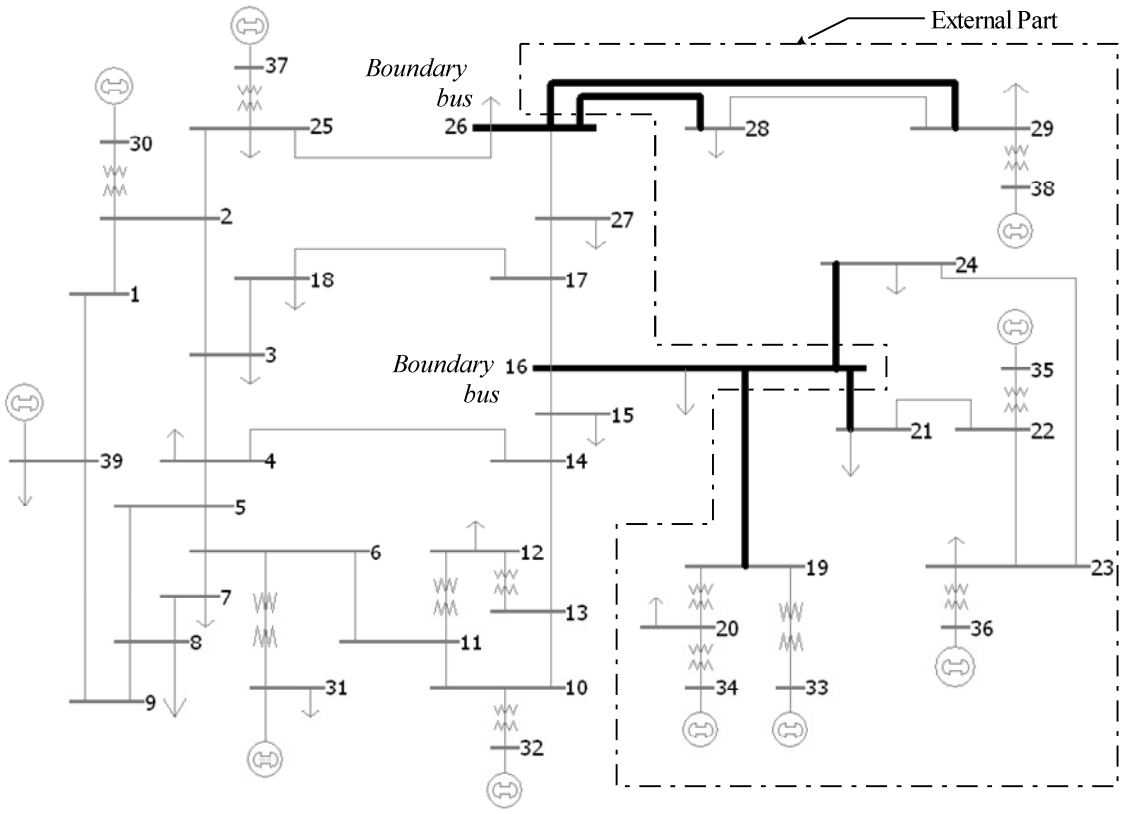

(a)

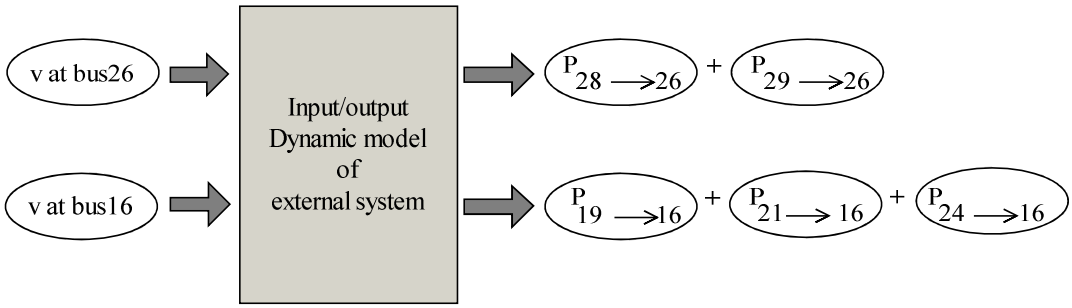

(b)

Figure 5.3 IEEE39 bus system: (a) single-line diagram with the external part inside dashed box (b) input-output model representation

From Figure 5.3 (a), the boundary buses are bus 16 and bus 26. The thick transmission lines inside the external part represent the lines that contribute the active power outputs of model. According to Figure 5.3 (a), the input-output model is summarised in Figure 5.3 (b).

The modelling techniques from [6, 7] are adapted for developing the dynamic model of the external system in Simulink/MATLAB [8]. The result of the developed model is shown in Figure 5.4.

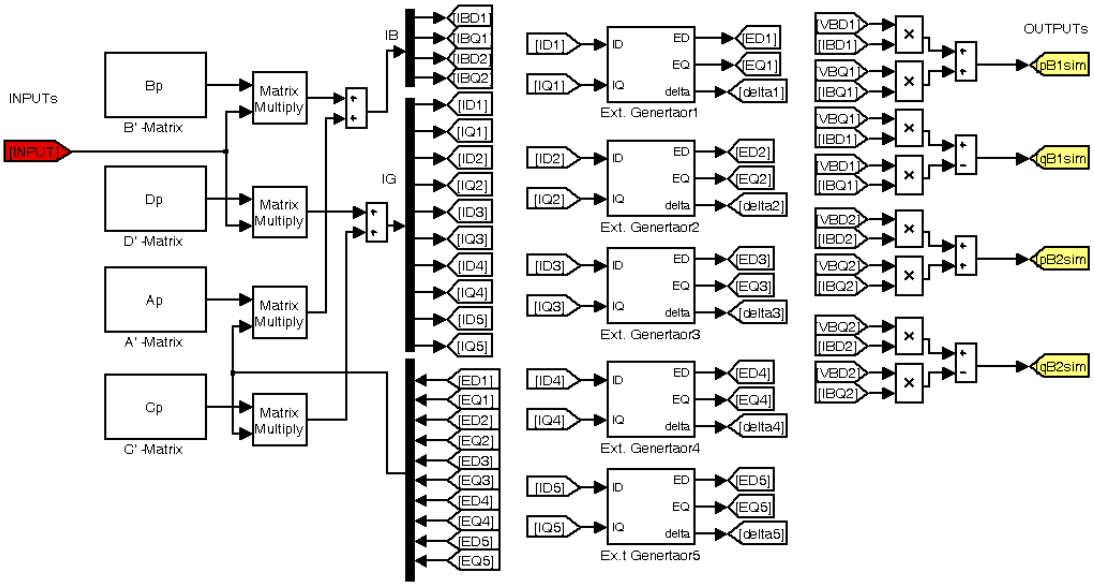

(a)

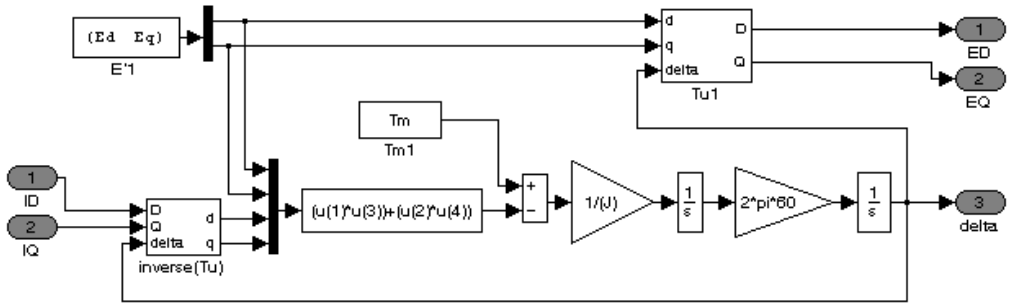

(b)

Figure 5.4 Simulink diagram (a) dynamic model of the external system (b) the details inside generator block.

From Figure 5.4 (a), the group of connected blocks on the left constitutes the equation (5.12), which represents the algebraic equations from the reduced network and the generator's stator. In the middle, each block is composed of the electric torque equation (eqn. (5.6)), the motion equations (eqns. (5.7) and (5.8)), and the frame transformation (eqn. (5.10)). The details inside each block are shown in Figure 5.4 (b). Finally, each group of connected blocks on the right corresponds to the equation (5.13) for calculating the active power outputs.

In order to validate the external dynamic model, the transient responses of the voltages (magnitude and angle) at boundary buses (bus 16 and bus 26) of the IEEE39 bus system when a small fault (a fault with 10 PU resistance) is applied at bus 18 are simulated by PSAT and the results are recorded in MATLAB workspace. After the recorded transient responses are transformed to DQ co-ordinate, by using equations (5.14)-(5.15), they are applied to the input terminals of simulink model (Figure 5.4 (a)).

$$V_D(t) = -\left|V_{boundary}(t)\right|\sin\left(\angle V_{boundary}(t)\right) \tag{5.14}$$

$$V_Q(t) = \left|V_{boundary}(t)\right|\cos\left(\angle V_{boundary}(t)\right) \tag{5.15}$$

Then the active power outputs from the simulink model are recorded and compare with those produced by PSAT. For each boundary bus, two groups of the recorded active power responses from PSAT are bought to compare. The first group is a summation of the active power flows in the lines from the external part to the boundary bus. The second group is a negative summation of the active power flows in the lines from the internal part to the boundary bus including that from the branch of the constant shunt admittance load. The comparisons in Figure 5.5 show good agreements.

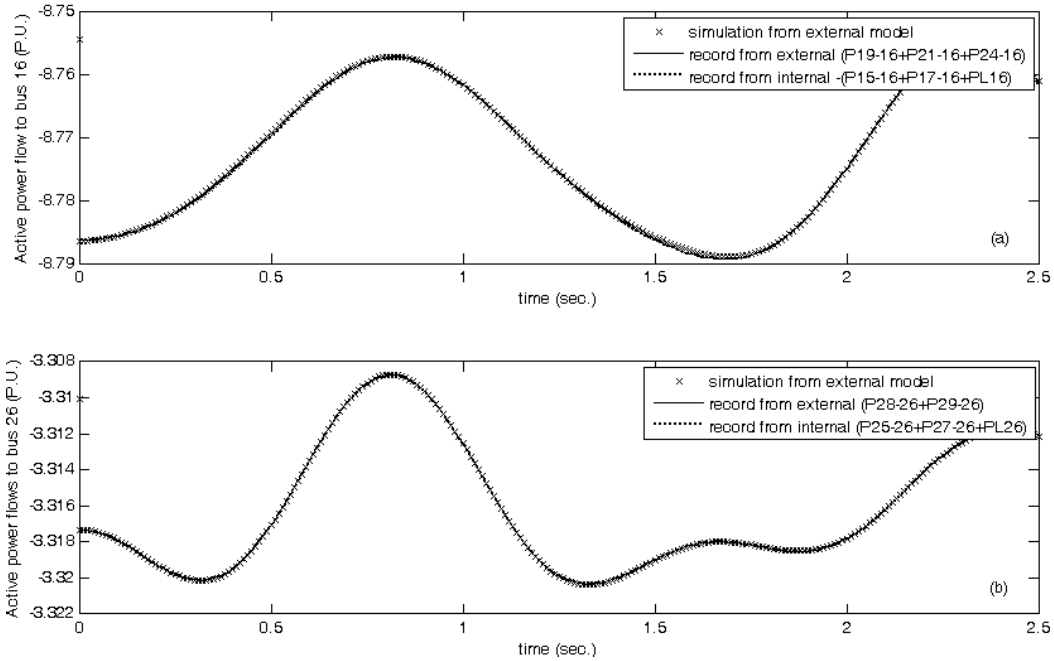

Figure 5.5 Active power flows (a) to boundary bus 16, and (b) to boundary bus 26

5.3 Modified parameter identification procedure

Based on the parameter identification procedure explained in Chapter 4 and the input-output formulation of the external system mentioned in the previous section, a modified parameter identification technique that does not require a full system simulation is shown in Figure 5-6.

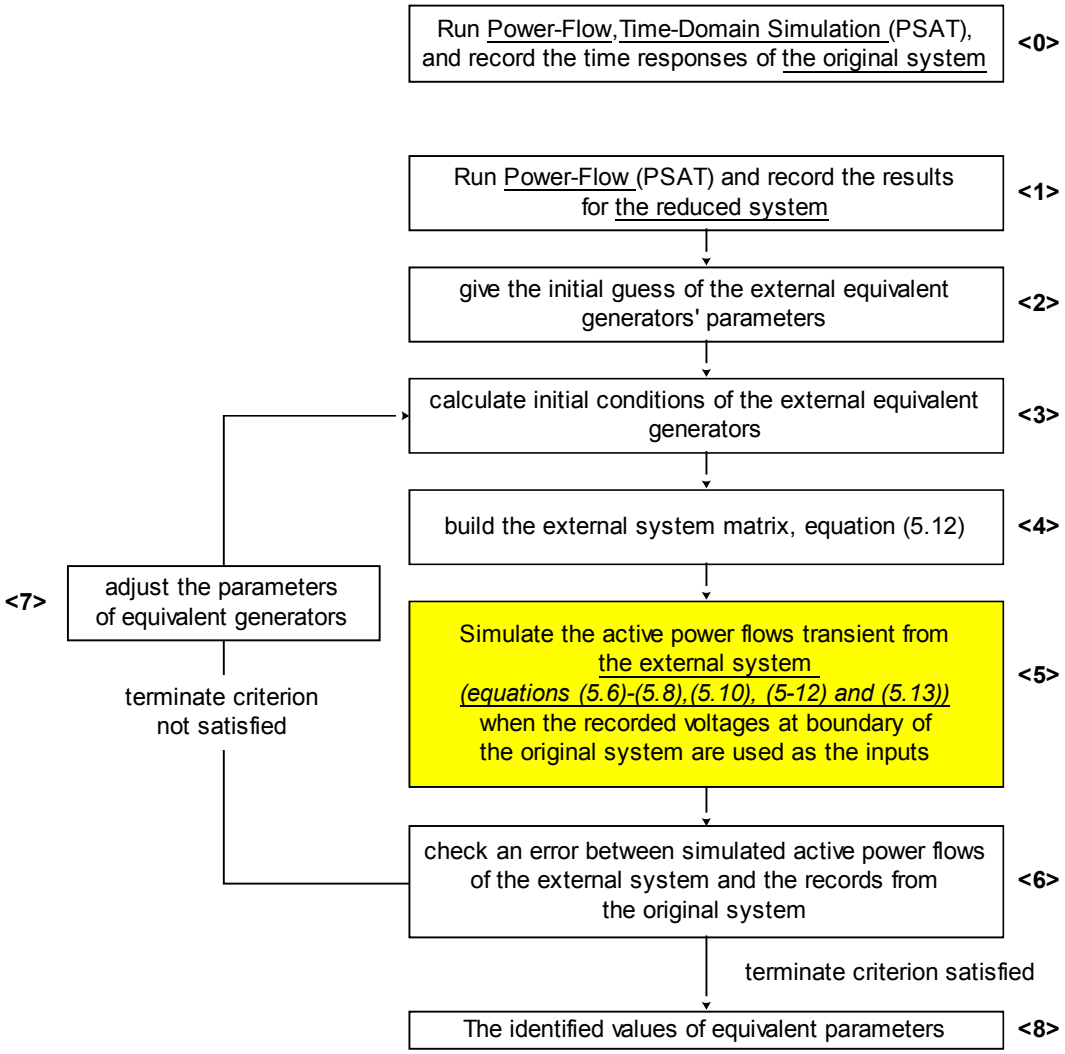

Figure 5.6 Parameter identification procedure which does not require a full system time domain simulation.

From Figure 5.6, the modified parameter identification procedure is similar to the parameter identification shown in Figure 4.2 except the fourth and the fifth steps. In

the fourth step of Figure 5.6, the initial guesses of the parameters of equivalent generators (from the second step) are used with the power flow modelling data and its solutions (from the first step) to calculate the values of entries (i.e. A',B',C', and D') in the matrix of equation (5.12). Next, in the fifth step, the dynamic model of the external part is built and its output responses are simulated following the method described in the previous section. The simulated responses are then compared with those recorded from the original system (from the zero-th step). The difference between them is examined to justify whether the process will be terminated or continue through to the seventh step.

By comparison with the previous procedure of Chapter 4 (Figure 4-2), the major expected reduction in the calculating time of this modified parameter identification procedure would be from the fifth step, which requires only the simulation of the external part of the reduced model to produce the responses at the boundaries.

It is worth mentioning that there are two possible schemes for implementation this modified parameter identification technique. The first scheme is to identify parameters of all generators together at the same time while the second scheme is to separately identify an individual set of parameters for each equivalent generator. The procedure shown in Figure 5.6 is applied equally to both schemes except for a difference in the extent of the internal and the external part. More details of these schemes are explained as follows.

5.3.1 Parameter identification for all equivalent generators

In this scheme, the partitioning between the internal part and the external part is defined in the way that all equivalent generators are together in the external part (see Figure 5.7). For this partitioning, the responses at boundary are contributed from all equivalent generators of the external part. As described in section 5.2, there are two possibilities of recording for use in the comparison with those simulated from the external dynamic model (see Figure 5.8).

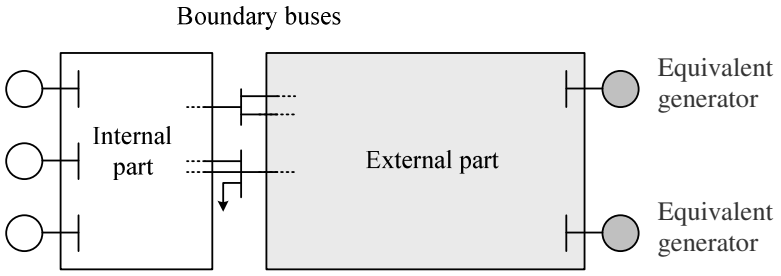

Figure 5.7 The partitioning for parameter identification of all equivalent generators

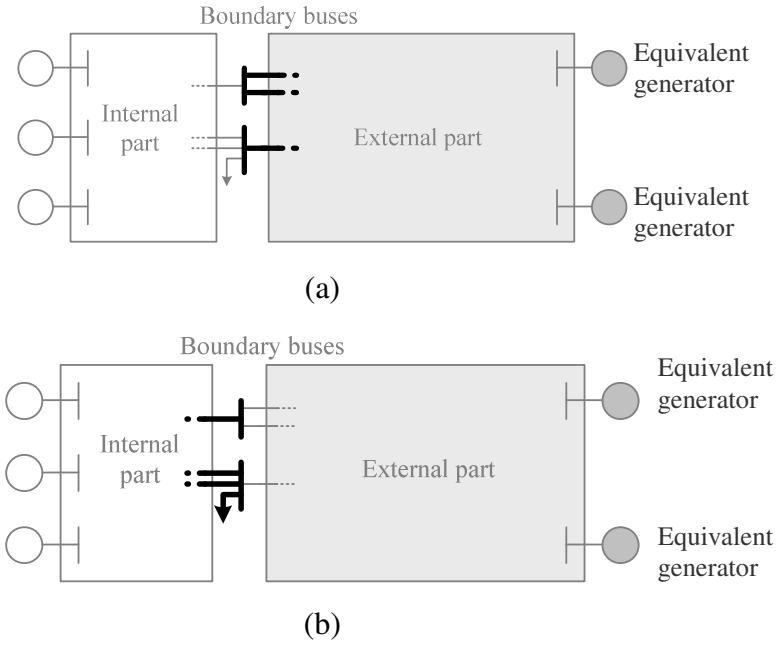

Figure 5.8 Two possibilities of responses recorded (a) from the internal side (b) from the external side.

The first possibility is to use the summation of the active power flows in the lines from the external part to the boundary buses (see Figure 5.8 (a)). The limitation for using this kind of records depends on the accessibility of the responses from the external part. However, the external part discussed in this section need not be the same as that drawn from the ownership boundary. One might re-define the partition so that the required responses are accessible.

The second possibility is to use the negative summation of the active power flows in the lines from the internal part to the boundary buses including that from branch of the constant shunt admittance loads. This method can be applied to the original partitioning of the system; however, the transient responses from the load branches at boundaries included in the internal side may add some difficulties. For example, these responses are not presented by the power system simulator (i.e. PSAT) and need to be separately calculated by an additional routine.

In addition to the partitioning, the load buses of the external part may be eliminated to reduce the size of the external network before performing the parameter identification, as shown in Figure 5.9. However, only the recorded responses from the internal side are justifiable for this case because the lines from the external part now become the artificial lines in which recording the responses may be impractical.

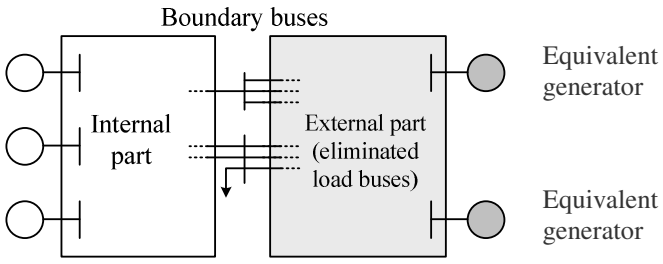

Figure 5.9 The partitioning for parameter identification of all equivalent generators when the external load buses are eliminated

5.3.2 Parameter identification for individual equivalent generator

This scheme partitions the internal part and the external part so that only equivalent generator whose parameters are to be identified contribute to the responses at boundaries from the external side, as shown in Figure 5-10.

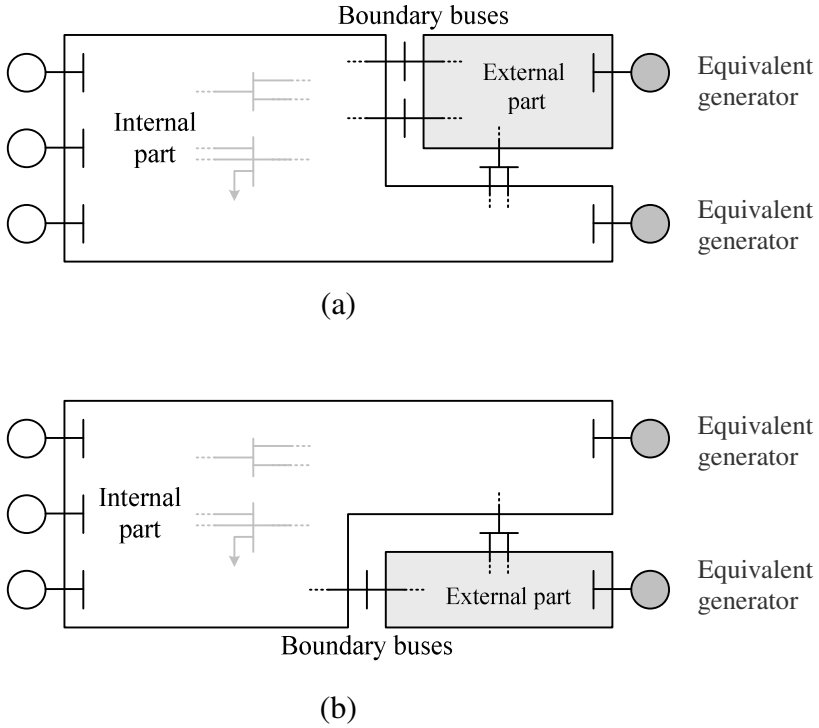

Figure 5.10 The partitioning for parameter identification of each equivalent generator

Different partitionings are needed for each particular equivalent generator (see Figure 5.10(a)-(b)). For each partitioning, the possibilities of either recording the responses at boundaries mentioned in previous sub-section could be applied. The applicability of the parameter identification for individual equivalent generator is subject to attaining the partition whose responses at boundaries from the external side are contributed by only one equivalent generator. Moreover, the corresponding responses must be accessible.

5.4 Test results and discussion

The modified parameter identification procedure has been developed on MATLAB with the aid of PSAT (Power System Analysis Toolbox) [9], Simulink, and Optimisation Toolbox. Its performance (i.e. accuracy and calculating time) is evaluated for both schemes described in the previous section with IEEE39 bus system.

The internal part and the external part are defined as shown in Figure 5.11. The groups of coherent generators according to the results in Chapter 3 (from the case study 5 by using two levels of line thickness plot with the thresholds > 50%) are also presented in the figure. Therefore, for this case, the parameters of three equivalent generators are needed to be identified. This corresponds to the reduced model shown in Figure 5.12. The external equivalent generator buses are aggregated as described in Chapter 4. The external network is reduced by using the Equivalencing tool of PowerWorld Simulator [10] with a default setting (a maximum per unit impedance for equivalent lines = 2.5).

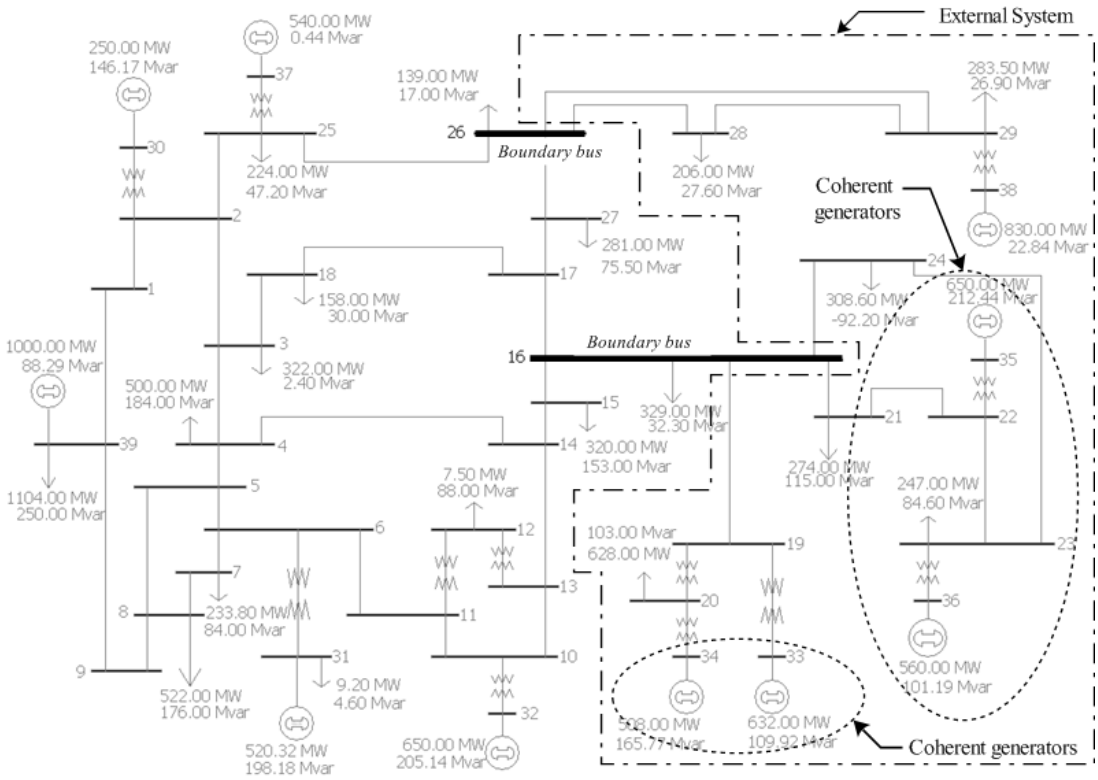

Figure 5.11 Single line diagram of IEEE39 bus system showing the external part including its groups of coherent generators

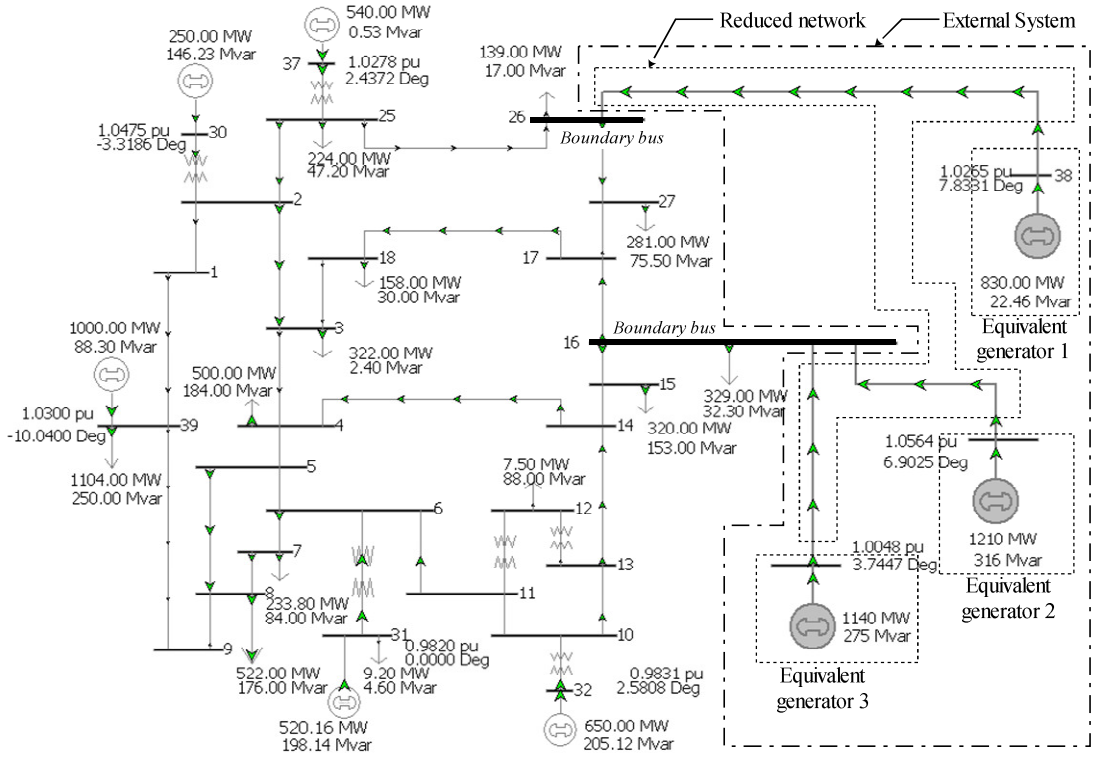

Figure 5.12 Single line diagram of the reduced model of IEEE39 bus system

Accordingly, fives study cases have been conducted. Case 1 is based on the parameter identification technique proposed in Chapter 4, while the others (case2-case5) are based on the parameter identification technique proposed in this Chapter. The details for each case are as follows.

-*Case 1:* the parameters of all equivalent generators are identified by using the techniques that requires a full system simulation. The model structure for this case is the same as shown in Figure 5.12 where the second-order of generator dynamic model with only two parameters (X'd and H) is attached for each equivalent generator. The relevant transient responses are the active power flows from bus 27 to bus 26, bus 25 to bus 26, bus 15 to bus 16, and bus 17 to bus 16 during a small fault applied at bus 18 (fault with 10 pu resistance at t=0.1s). For the same reason as explained in Chapter 4, all transient responses are recorded with the time durations of 2.5 seconds.

For case 2 to case 5, the modified parameter identification process is applied to the external part having the aggregation of coherent generator buses. The reason for not using the reduced network is because the power flows in the lines from the external side are our responses and are being recorded. Various components of model associated with the external generator(s) whose parameters are to be identified have to be defined for building the external system (the 4^{th}-step in Figure 5.6). These components are described below following the remaining four study cases.

The modified identification of the first scheme (all at once):

-*Case2* (see figure 5.13)

Parameters to be identified: *of equivalent generator 1, 2, and 3*

Inputs: *voltages (magnitude and angle) at boundary bus*

Input1=Voltage at bus 16

Input2=Voltage at bus 26

Outputs: *summations of active power transient in the line from bus → to bus*

Output1= P (19→16) +P (21→16) +P (24→16)

Output2= P (28→26) + P (29→26)

The modified identification of the second scheme (individual):

-*Case3* (see figure 5.14)

Parameters to be identified: *of equivalent generator 1*

Input: *voltage (magnitude and angle) at bus 26.*

Output: *P (28→26) + P (P29→26)*

-*Case4* (see figure 5.15)

Parameters to be identified: *of equivalent generator 2*

Input: *voltage (magnitude and angle) at bus 16.*

Output: *P (21→16) + P (24→16)*

-*Case5* (see figure 5.16)

Parameters to be identified: *of equivalent generator 3*

Input: *voltage (magnitude and angle) at bus 16.*

Output: *P (19→16)*

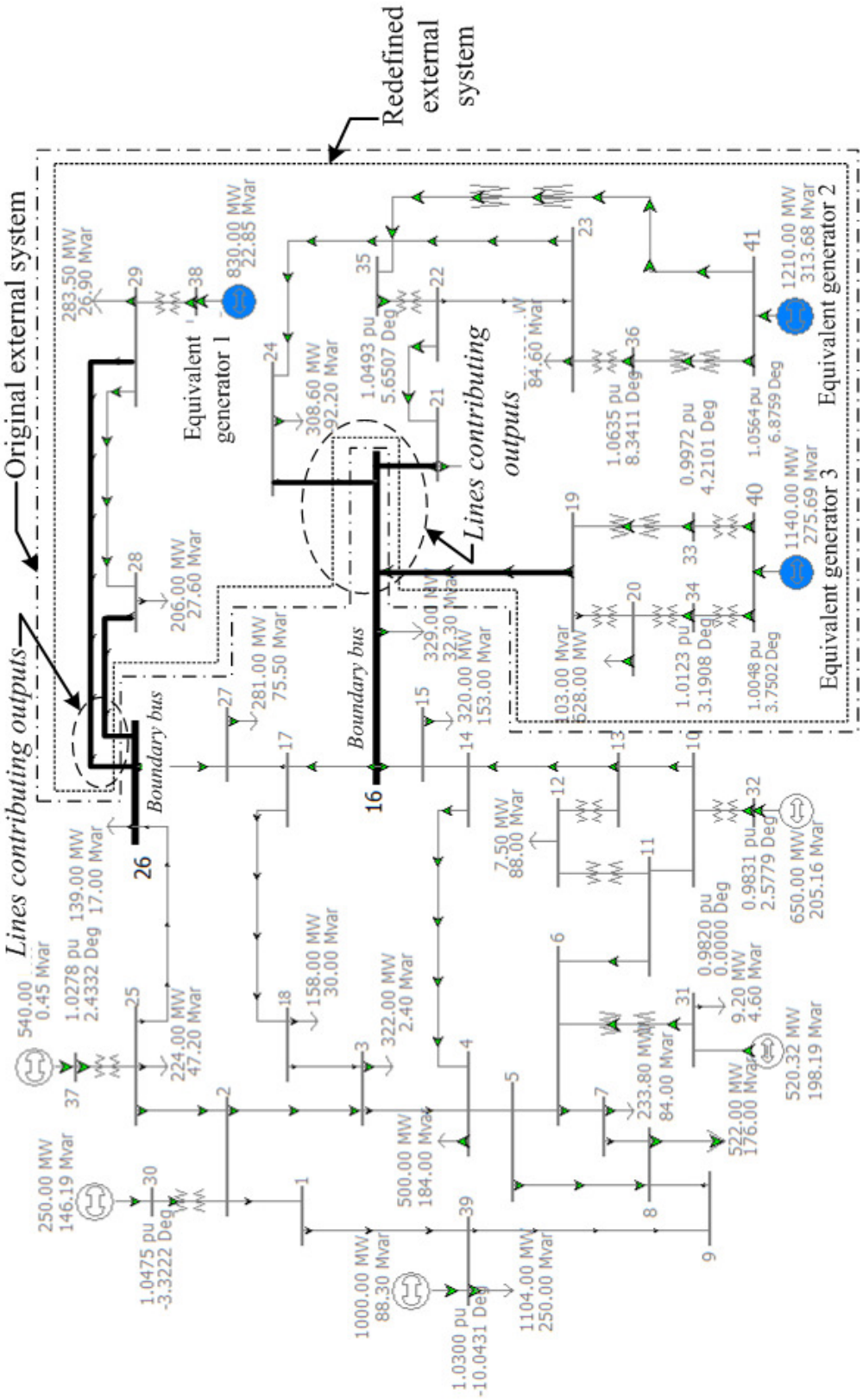

Figure 5.13 Single line diagram showing the external system for the case 2

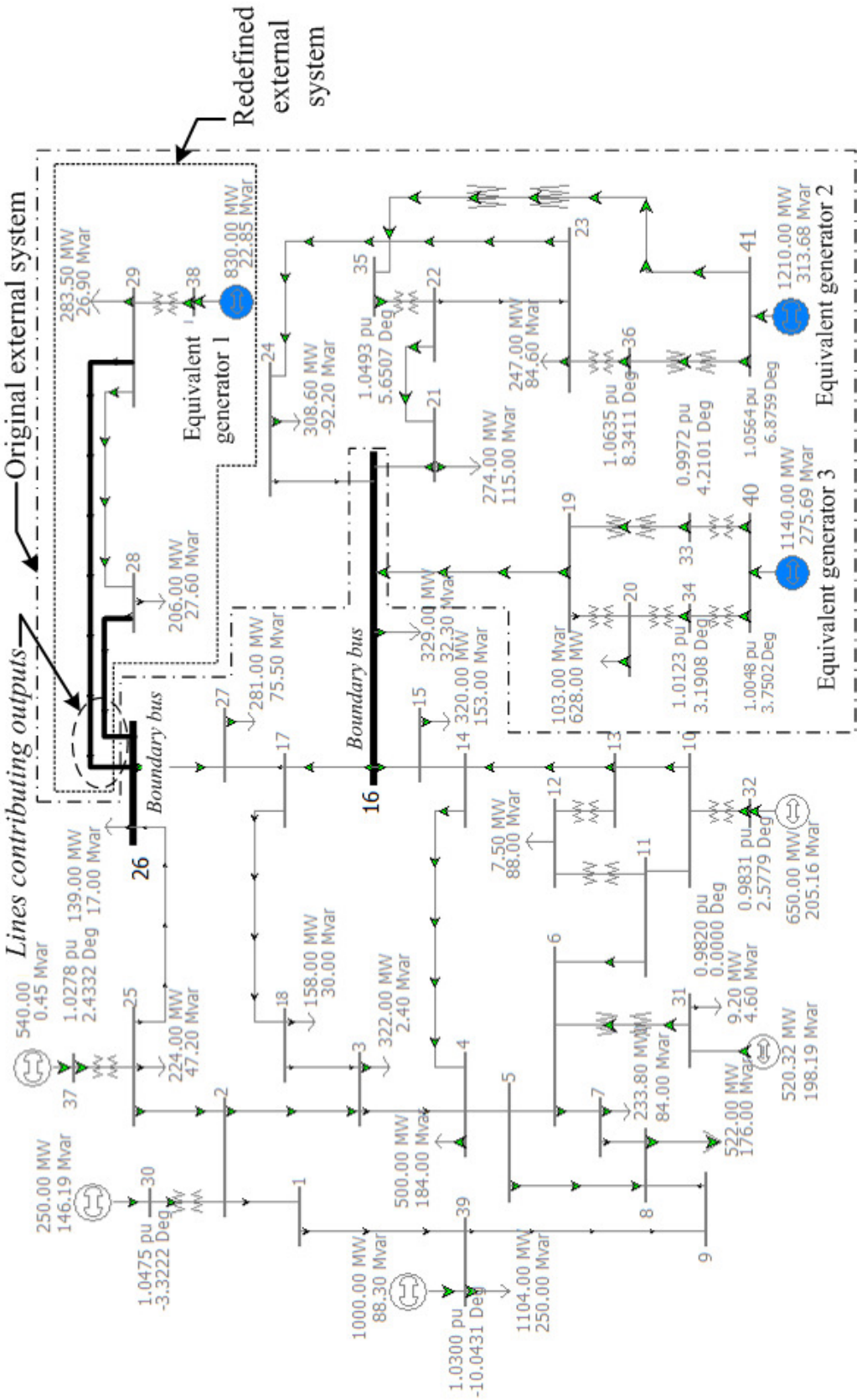

Figure 5.14 Single line diagram showing the external system for the case 3

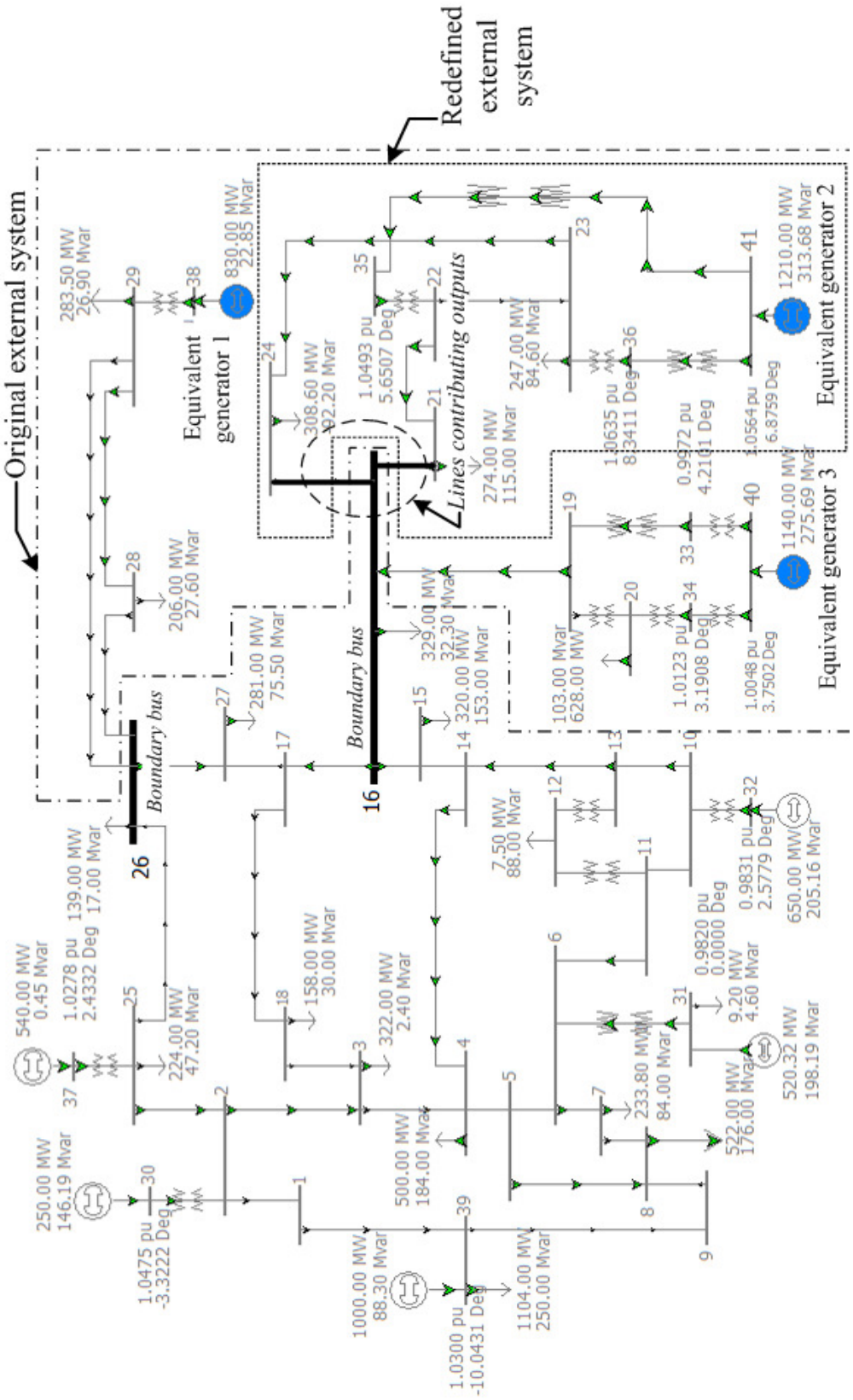

Figure 5.15 Single line diagram showing the external system for the case 4

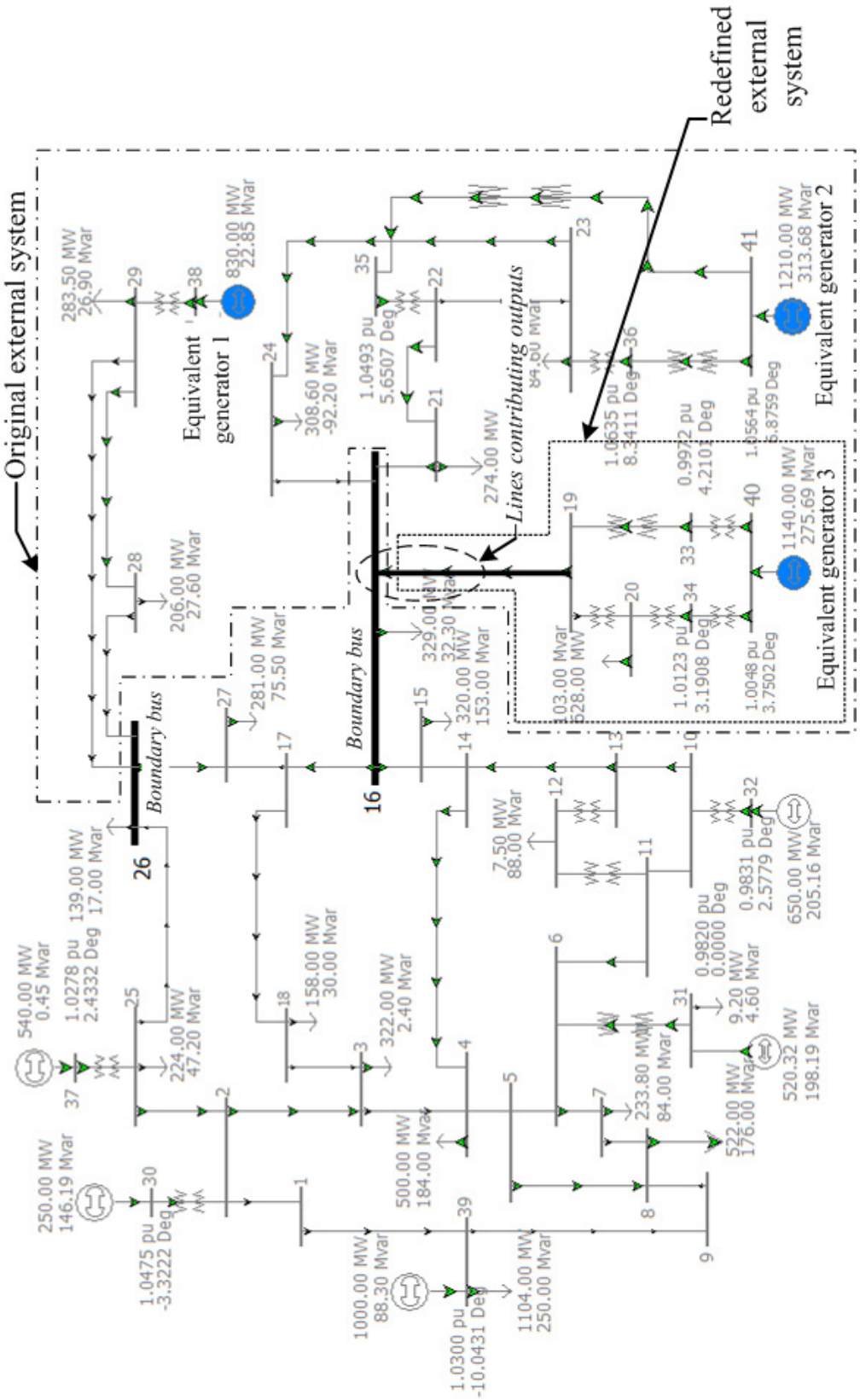

Figure 5.16 Single line diagram showing the external system for the case 5

All study cases have been carried out by using the same optimization technique (non-linear least square technique with Levenberg-Marquardt algorithm), termination criterion and set of initial guess parameters. The results are summarised and are given in two tables. The first table (Table 5.1) is to show a comparison of their identified parameters while the second table (Table 5.2) is to show a comparison of their calculating time. For the first table, the values of parameters obtained by using the structure preservation technique [11] are also included.

Table 5.1 Identified parameters of equivalent generators

Equivalent Parameters	Equivalent Generator1		Equivalent Generator2		Equivalent Generator3	
	X'_d	H	X'_d	H	X'_d	H
Initial values	0.050	50.00	0.050	50.00	0.050	50.00
Case 1	0.052	36.91	0.014	75.63	0.058	43.24
Case 2	0.054	36.65	0.021	68.35	0.044	60.59
Case 3/ Case 4/ Case 5	0.056	35.00	0.024	64.29	0.056	51.21
Structure preservation	0.057	34.50	0.025	61.20	0.035	54.60

Table 5.2 Calculating time of each parameter identification technique

Parameter Identification Method	Calculating time (sec.)		
	Equivalent Generator1	Equivalent Generator2	Equivalent Generator3
Case 1	197.90		
Case2	20.44		
Case 3/ Case 4/ Case 5	5.73	8.16	8.22

* The calculating times are measured by using “cputime” function in MATLAB

From Table 5.1, it shows that the values of parameters identified from the modified technique of both schemes (case2 and cases3-5) are within acceptable range when compared to the values calculated by using structure preservation technique [11]. The quality of these identified values is also evidenced by using them with the reduced system of Figure 5.12 to simulate swing curves of the internal generators. The plots of swing curves of the internal generators, when a fault with 10 p.u. resistance is applied at bus 18, for the original system and the reduced systems whose values of parameters of the external equivalent generators are from different techniques are given in the Table 5.1 and are shown in Figure 5.17.

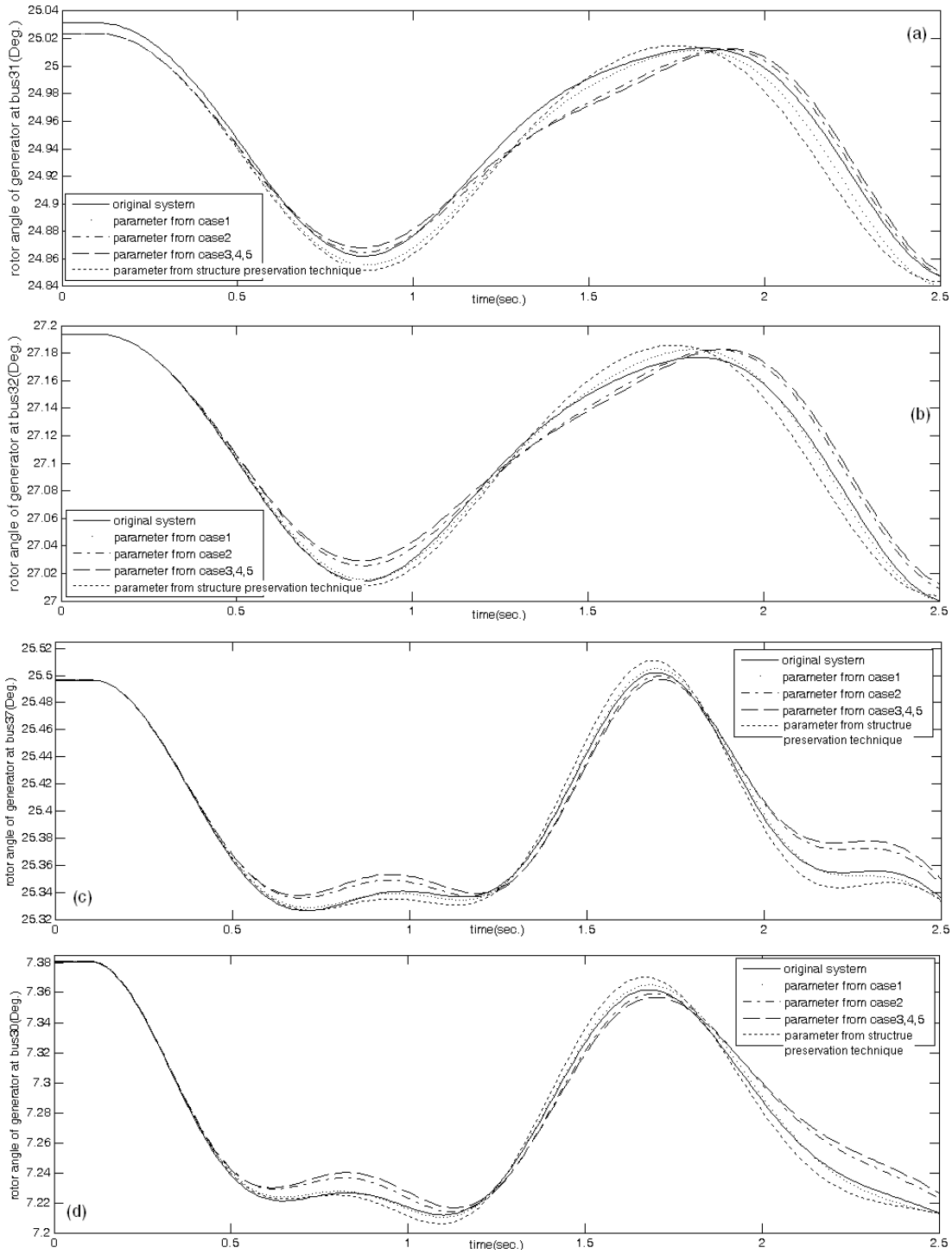

Figure 5.17 Swing curves of internal generators when a fault with 10 p.u. resistance is applied at bus 18 (a) generator at bus 31, (b) generator at bus 32, (c) generator at bus 37, and (d) generator at bus 30, (rotor angle of generator at bus 39 is the reference)

From Figure 5.17, the swing curves from the reduced system whose values of parameters of the external equivalent generators are from the first scheme of the modified technique (case2) are slightly better than those from the second scheme of the modified technique (cases3-5). However, the plots from both schemes show well agreement with those from the original system. This confirms that these values of parameters are acceptable and suitable to be the values of the parameters of equivalent generators of the reduced system in Figure 5.12.

Also from Figure 5.17, it can be seen that the swing curves from the reduced system using values of parameters from the technique that require a full system simulation (case1) is closer to the swing curves from the original system than those from the reduced systems using values of parameters from the modified identification technique (case2 and cases3-5). This shows that the values of parameters obtained from the modified parameter identification technique are less suitable than those obtained from the parameter identification technique that requires a full system simulation. The main reason that the modified parameter identification technique gives less suitable values of parameters is because the inputs to the external equivalent dynamic model (input/output formulation) during the parameter identification process are not quite correct. The correct inputs should be the voltages at boundaries recorded from the simulation of the reduced system (i.e. the internal part and the external equivalent) rather than those from the simulation of the original system (i.e. the internal part and the external part) of Figure 5.13. However, such reduced system does not happen beforehand, at least the parameter of the external part is about to be identified. Therefore, this is impractical.

Considering the calculating times (see Table 5.2), the modified identification technique show a big improvement. The total calculating times for the modified parameter identification of three equivalent generators are 20.44 seconds and 22.11 seconds for the first scheme and the second scheme, respectively. These calculating times are much shorter, compared to 197.90 seconds of the technique that require a full system simulation. The main reason of this big improvement for the modified parameter identification technique is that the largest computational expense is for the

sets of external equivalent generator equations only, in contrast to the previous identification technique where equations of all internal generators (normally represented in great details) and equivalent generators must be included. Moreover, with the second scheme of the modified parameter identification, the amount of time could be reduced to only 8.22 seconds if the three sets of parameters are identified in parallel on three different computers.

5.5 Conclusion

The modified parameter identification technique that requires no full system simulation has been developed. This technique could be implemented by two schemes. The first scheme is to identify parameters of all generators together at the same time while the second scheme is to separately identify an individual set of parameters for each equivalent generator.

The essence of the technique is the re-formulation of dynamics of the external part as the input-output dynamic model. By using this model formulation, the major calculation expense during each step of parameter adjustment is reduced because only the simulation of the input-output dynamic model is required for calculating value of the error criterion. This reduction greatly improves the computational time of the whole parameter identification process and saves memory needed for model storage during the identification process. However, the drawback of this technique is impractical to obtain the voltages at boundaries of the reduced system to be used as the inputs for the simulation of the external equivalent model and the nearest one recorded from the boundaries of the original system must be instead used.

The modified parameter identification technique and its performance (i.e. accuracy and usage time) have been studied and evaluated with the IEEE39 bus system. The results show the feasibility and good performance of this technique for both schemes of implementation.

5.6 References

[1] J. Sjъberg, Q. Zhang, L. Ljung, A. Benveniste, B. Delyon, P.-Y. Glorennec, H. Hjalmarsson, and A. Juditsky, "Nonlinear black-box modeling in system identification: a unified overview," *Automatica,* vol. 31, pp. 1691-1724, 1995.

[2] O. Nelles, *Nonlinear system identification: from classical approaches to neural networks and fuzzy models*: Springer-Verlag Berlin Heidelberg, 2001.

[3] J. M. Undrill, J. A. Casazza, E. M. Gulachenski, and L. K. Kirchrnayer, "Electromechanical Equivalent for Use in Power System Stability Studies," *Power Apparatus and Systems, IEEE Transactions on,* vol. PAS-90, pp. 2060-2071, 1971.

[4] J. M. Undrill and A. E. Turner, "Construction of Power System lectromechanical Equivalents by Modal Analysis," *Power Apparatus and Systems, IEEE Transactions on,* vol. PAS-90, pp. 2049-2059, 1971.

[5] I. A. Hiskens, "Power System Test Cases [online] http://psdyn.ece.wisc.edu/IEEE_benchmarks/index.htm."

[6] R. Patel, T. S. Bhatti, and D. P. Kothari, "MATLAB/Simulink-based transient stability analysis of a multimachine power system," *International Journal of Electrical Engineering Education, Manchester University Press,* vol. 39, pp. 320-336, 2002.

[7] C.-M. Ong, *Dynamic Simulation of Electric Machinery: Using MATLAB/SIMULINK*: Prentice Hall, 1997.

[8] The MathWorks Inc. , "MATLAB Programing," The MathWorks Inc., 2007.

[9] F. Milano, "Power System Analysis Toolbox (PSAT) ", 1.3.4 ed, 2006.

[10] PowerWorld Corporation, "PowerWorld Simulator version 14 [Online] Available at http://www.powerworld.com."

[11] Z. Z. Qi, "Coherency based dynamic equivalence of power systems." vol. Ph.D.: University of Strathclyde, 1994, p. 184.

CHAPTER 6

STUDY OF REDUCED SYSTEM

6.1 Introduction

The aim of this chapter is to describe the tests and to present the evaluation results of the proposed identification-based dynamic equivalent. This proposed equivalencing method is a combination of the parametric identification of dynamic equivalent and the modified parameter identification technique presented earlier in the previous two chapters; and, it could be summarised into the five steps below:

Step1: Identification of coherent generators based-on the node-weighted graph (chapter 3);
Step2: Aggregation of the coherent generator buses (chapter 4);
Step3: Reduction of the transmission network (chapter 4);
Step4: Attachment of the generator dynamic equation (chapter 4);
Step5: Parameter identification of the equivalent generator dynamic models (chapter 5).

The main objectives of the tests in this chapter are (a) to examine the validity of the proposed equivalent by a study of a complete system (i.e. internal part and external part) under various conditions, (b) to examine the reliability of the proposed equivalent by a comparison of complete system study formed by other equivalents, and (c) to examine the construction time by a comparison with the procedure that requires a complete system simulation. The tests were conducted on a medium size system (IEEE39 bus system) and a large size system (IEEE118 bus system).

This chapter is organised in four parts. The first part describes the procedure of tests. The second part presents the case study of IEEE39 bus system; and, the case study of IEEE118 bus system is presented in the third part. The details for each case study include the description of the system, the testing scenarios, the results and the discussions. Finally, the chapter is concluded in the last part.

6.2 Procedure of the Tests

To evaluate the performance of the proposed identification-based dynamic equivalent, three major tests, namely a test of validity, a test of reliability, and a test of construction time, are introduced in this section. All tests were conducted on MATLAB [1].

A) Test of validity

Once an external part is reduced it is necessary to test its accuracy. In this thesis it is termed as the validity of the equivalent. As the external part has been reduced to equivalent, the testing of validity is concentrated on the internal network. It is done by comparing the rotor angles of all internal generators before and after the reduction process. Therefore, the validity of equivalent here is an ability of the equivalent to form a reduced system (i.e. an internal part and an equivalent) which can reproduce an acceptable accuracy of responses of the internal part (i.e. the rotor angles of the internal generators) under each particular disturbance. A bus-fault is the only disturbance being studied. Accordingly, the accuracy measure, defined in eqn. (6.1), adapted from [2] is used in this chapter to quantify the accuracy of the reduced system under each fault location.

$$\max_{i \in G_I} \left| \delta(t)_i^{reduced} - \delta(t)_i^{original} \right|_{at\ fault\ j-th} < \delta_{tolerance}\ , \qquad 0 \le t \le t_{\max} \qquad (6.1)$$

where G_I is a set of internal generators ;and, $\delta(t)_i^{reduced}$ and $\delta(t)_i^{original}$ are the rotor angles at time t of i-th generators of the reduced system and of the original system, respectively. At the j-th bus, the equivalent is valid if the accuracy measure is less than a pre-defined tolerance ($\delta_{tolerance}$). Based on this accuracy measure, the test procedures are as follows:

1. Perform a transient stability simulation of the original system and record rotor angles of all internal generators.
2. Perform a transient stability simulation of the reduced system and record rotor angles of all internal generators.

3. Compute the accuracy measure of the reduced system by using eqn. (6.1) and check the value with the pre-defined tolerance if the reduced system is valid.

Throughout this chapter, t_{max} of 2.5 seconds is used in accordance with the time periods of recorded responses for parameter identification.

B) Test of reliability

The reliability of equivalent is the validity of the equivalent under various working conditions (e.g. different kind of fault and different location of fault). The more conditions the equivalent is valid, the more reliable equivalent is. The test of reliability is basically a repetitive validity test for all fault locations within the internal part. The test procedures are as follows:

1. Perform the validity test for all fault locations within the internal part.
2. Record the number of testing conditions for which the reduced system is valid and use this number as the reliability measure.

C) Test of construction time

The construction process of the equivalent involves five main steps as mentioned in the beginning of this chapter. However, in this thesis, the first four steps are not fully automated hence making it difficult to measure. Therefore, only the time usage during the parameter identification step (the fifth step) is considered here for an evaluation. The time will be recorded at the start of the parameter identification until the end of process when termination criterion is satisfied.

6.3 Case study 1: IEEE39 bus system

There are two studies presented in this section which are a reliability study and an order of equivalent generator dynamic model study. The former is to evaluate the reliability of the proposed equivalent in comparison with the traditional identification-based equivalent (i.e. a fictitious generator attached to each boundary

bus).The latter is to evaluate the validity of the proposed equivalent when different orders of the equivalent generator dynamic model are used.

6.3.1 Case study 1.1: Reliability study

6.3.1.1 Description of the test system and the testing scenarios

The IEEE39 bus system contains 39 buses, 46 branches, and 10 generators. The single line diagram of the system and the system data are given in Appendix B1. The generator is represented by the fourth order dynamic model. All the system data were originally from [3] except the resistances of the generators which are from [4]. However, to keep this study simple, only the second order of generator dynamic model with two parameters (i.e. X'_d and H) is used in this study for both the original model and the reduced model. The internal part and the external part of the system are defined according to Figure 6.1. The boundary buses are bus 16 and bus 26, respectively.

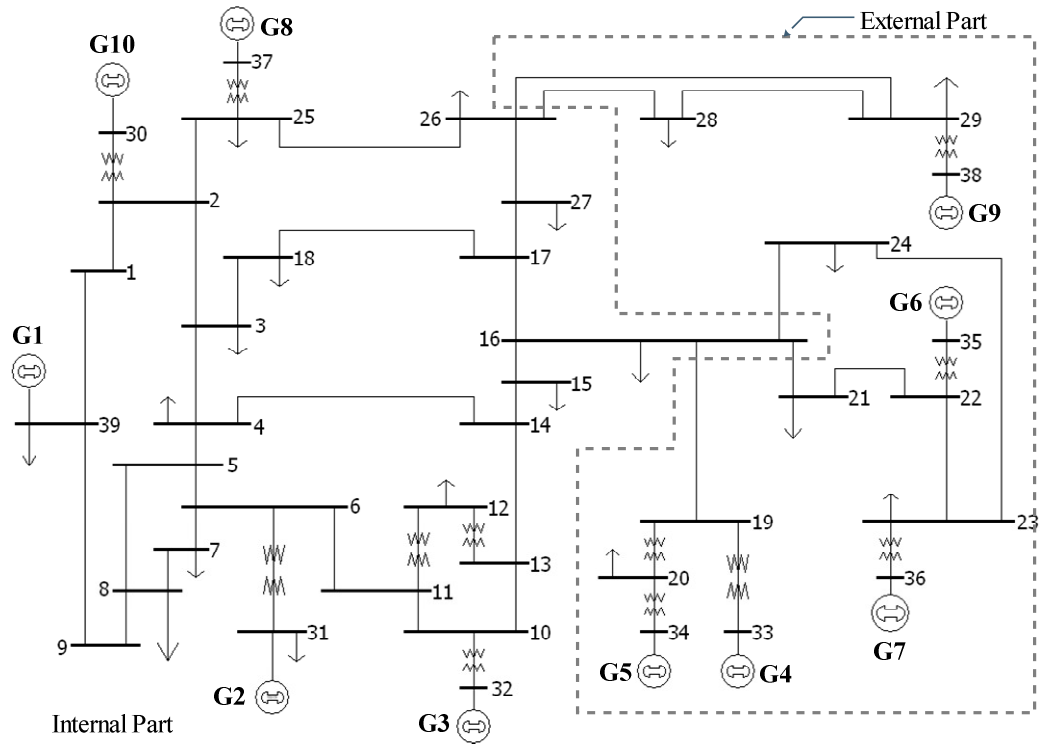

Figure 6.1 Test system for the case study 1.1

In order to assess the reliability, the reliability measure (described in the previous section) of the proposed equivalent and of the traditional identification-based equivalent are calculated and compared. The assessment is conducted for two scenarios of the proposed equivalent as follows.

Scenario 1: The proposed equivalent is constructed based on to the tight coherent groups

Scenario 2: The proposed equivalent is constructed based on to the loose coherent groups

6.3.1.2 Test results and discussions

The groups of coherent generators are identified from the node-weighted graph model by using the applied epsilon decomposition technique. The result of the identified coherent groups for different values of epsilon is summarised in Figure 6.2 by using contour lines.

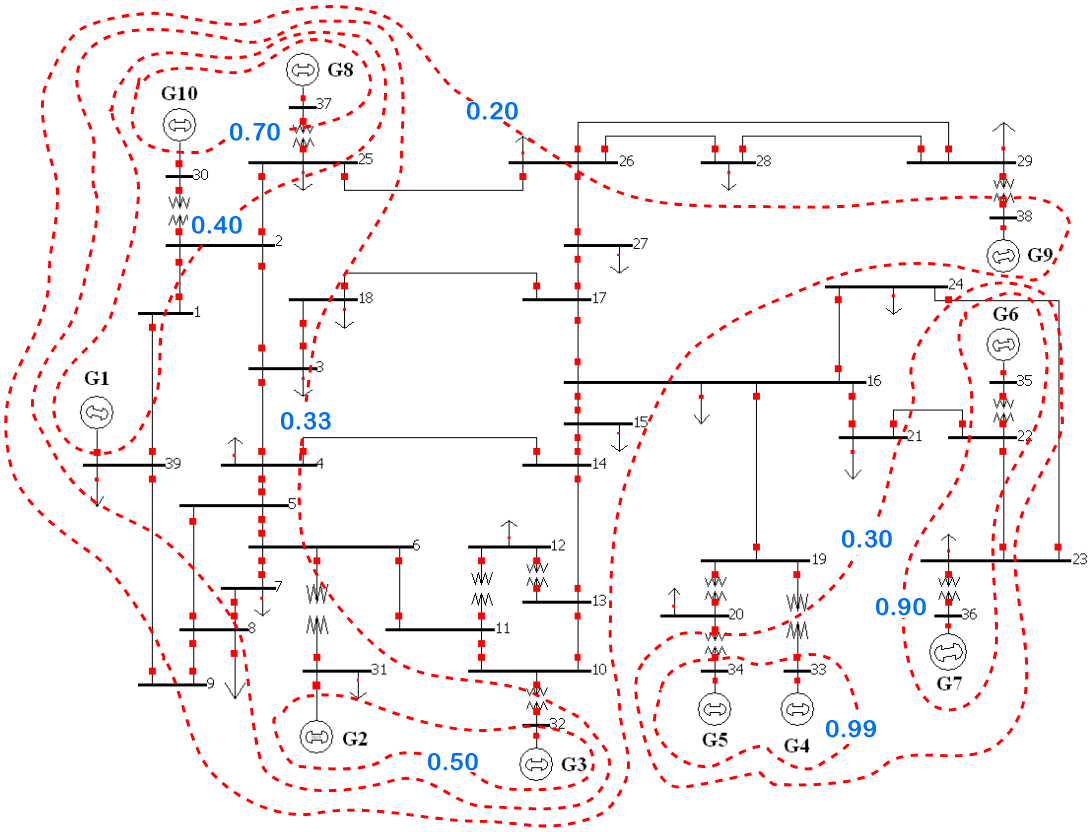

Figure 6.2 Coherent generators of the case study 1.1 for different values of epsilon

From Figure 6.2, a value on the contour line indicates the minimum value of epsilon. The generators contained in each contour are the coherent generators identified by using any values of epsilon which is greater than the value indicated on that contour line. For example, the group of generators2 and 3, the group of generators 4 and 5, the group of generators 6 and 7, and the group of generators 8 and 10 are the groups of coherent generators identified with the epsilon values greater than 0.5 units.

In this case study, the groups identified with the epsilon values greater than 0.5 units are considered as the tight coherent groups while the groups identified with the epsilon values greater than 0.3 units are considered as the loose coherent groups. These cause the external parts for the first scenario equivalent and the second scenario equivalent having three and two equivalent generators, respectively. Table 6.1 summarises the equivalent generators associated with the groups of coherent generators for both scenarios.

Table 6.1 Equivalent generators for the first and the second scenarios

Scenario	Equivalent generator 1	Equivalent generator 2	Equivalent generator 3
1	G9	(G6 - G7)	(G4 – G5)
2	G9	(G4 - G5 - G6 - G7)	-

After the aggregation of the coherent generator buses and the reduction of the external transmission network (using PowerWorld software [5] with a default setting), the single-line diagrams (see Tables A1.1-A1.4 for their parameters) of the reduced systems formed by the equivalents according to the scenario 1 and the scenario 2 are obtained as shown in Figures 6.3 (a) and (b), respectively.

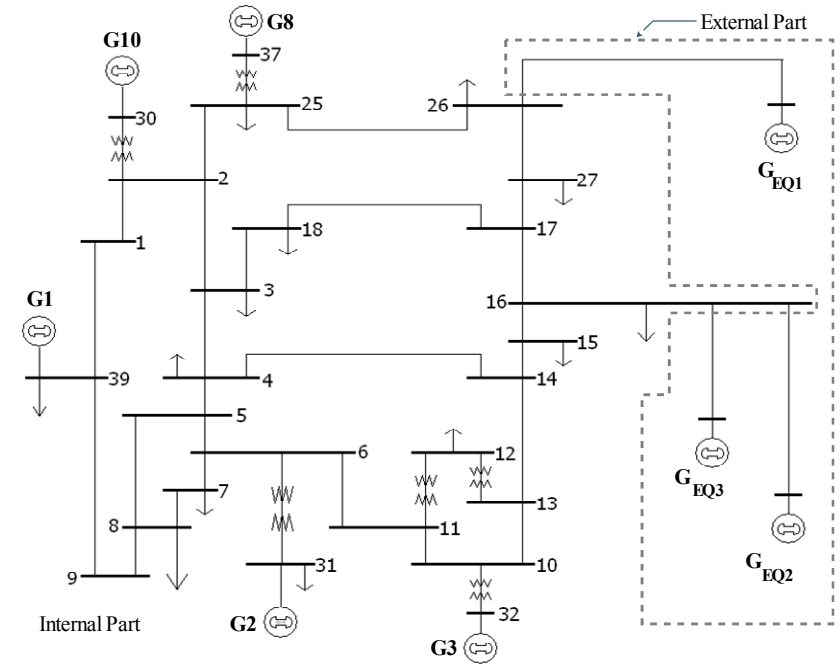

(a)

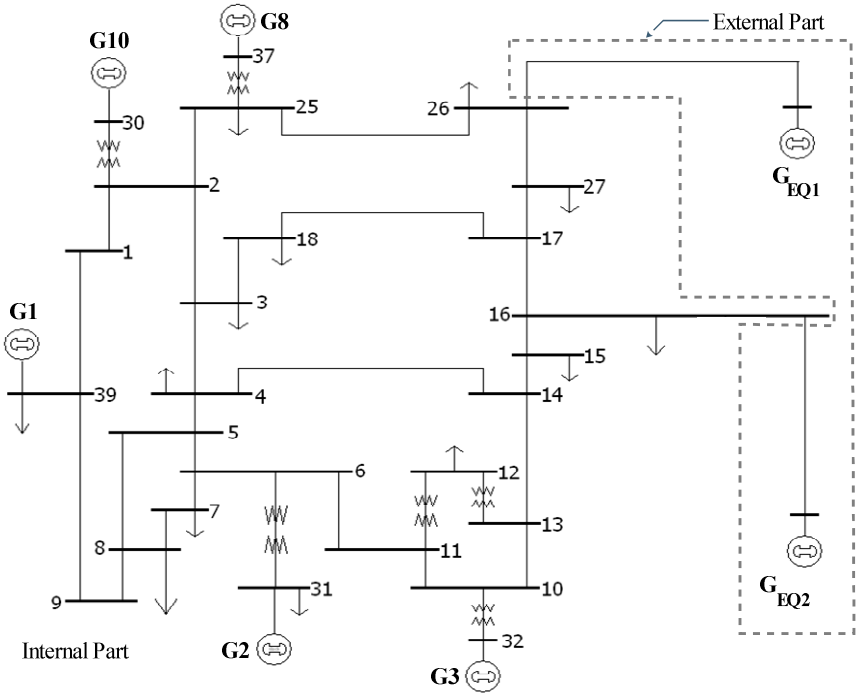

(b)

Figure 6.3 Single-line diagrams of the reduced systems for the case study 1.1: (a) based on tight coherent groups; and (b) based on loose coherent groups.

For the traditional identification-based equivalent, two fictitious generators are attached at bus 16 and bus 26 (see Figure 6.4), respectively. The static operating condition of the internal system is preserved by setting the complex power injection at the boundaries (bus 16 and 26) equal to the values calculated by the power flow of the original system [2]. The comparisons of the power flow results for these single-line diagram (power flow model) to that of the original are given in Tables A1.10-A1.12.

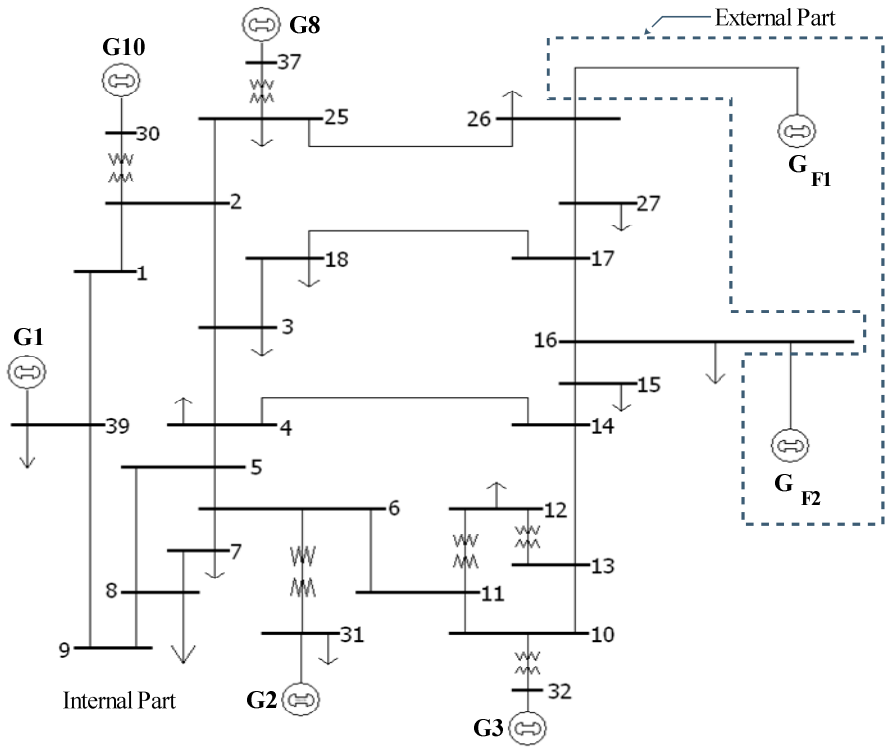

Figure 6.4 Single-line diagram of the reduced system based on two fictitious generators for the case study 1.1.

According to the single-line diagrams, five dynamic reduced systems (see Table 6-2) are actually constructed for a comparison of their reliability. The identified values of the parameters for each reduced system are given in Tables A1.5-A1.6. These parameters were identified based on an intentional small fault (a fault with 10 p.u. resistance) applied at bus 18 without remove.

Table 6.2 Details of the reduced systems for the case study 1.1

Reduced System	External Equivalent	Parameter identification
A	-Two fictitious generators	-Full system simulation (Chapter 4)
B	-Two equivalent generators -Equivalent transmission lines -Equivalent Shunt (scenario1)	-Without full system simulation (Chapter 5)
C	-Three equivalent generators -Equivalent transmission lines -Equivalent Shunt (scenario2)	-Without full system simulation (Chapter 5)
D	-Two equivalent generators -Equivalent transmission lines -Equivalent Shunt (scenario1)	-Full system simulation (Chapter 4)
E	-Three equivalent generators -Equivalent transmission lines -Equivalent Shunt (scenario2)	-Full system simulation (Chapter 4)

The reliability test was conducted on these reduced systems by applying two kinds of faults (a small fault and a large fault) in rotation of all 26 internal buses (including the boundary buses). The small fault is a fault with 10 p.u. resistance which is applied at 0.1 second without a clearance. The large fault is a solid fault which is applied at 0.1 second and cleared at 0.2 second. The numerical values of the maximum angle difference are given in Table A1.13.

The performance of the reduced systems could be assessed by a comparison of the testing conditions (i.e. locations of fault) for which the reduced systems are valid at specific acceptable level of accuracy. For example, at accuracy < 0.02 degree for the small fault and at accuracy < 2 degree for the large fault, the testing conditions for which the reduced systems are valid and invalid can be illustrated by a check and cross marks on the internal part of each reduced system, respectively (see Figures 6.5-6.9).

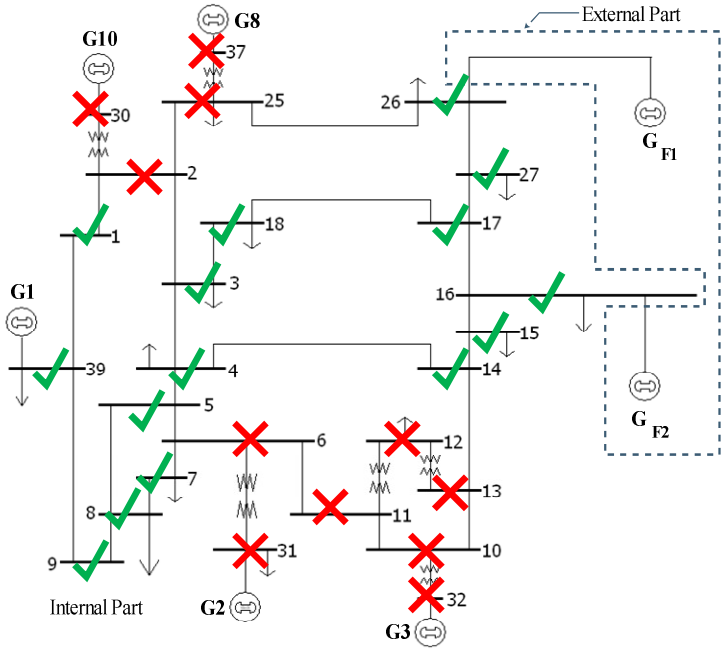

(a)

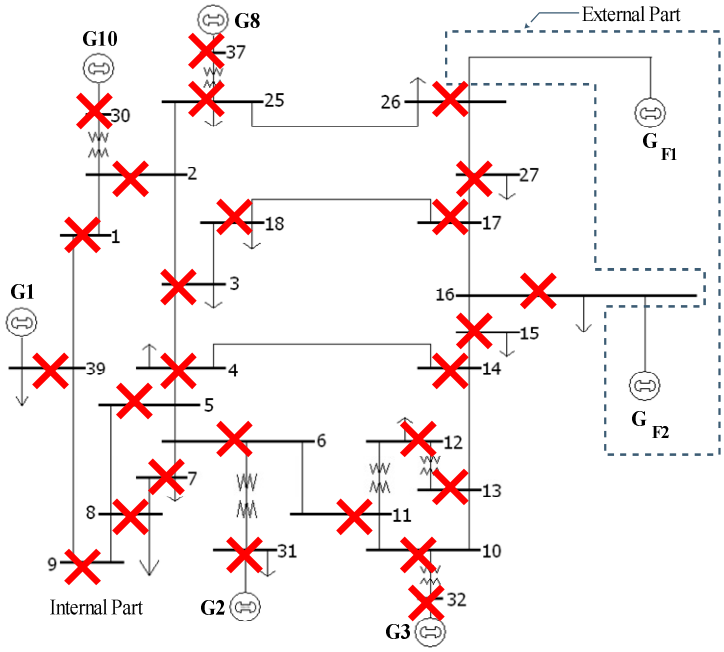

(b)

Figure 6.5 Reduced system A showing the testing condition (locations of buses) for which the reduced system is valid by the checking mark and invalid by the cross mark; (a) for the small fault with the accuracy <0.02 degree and (b) for the large fault with accuracy < 2 degree

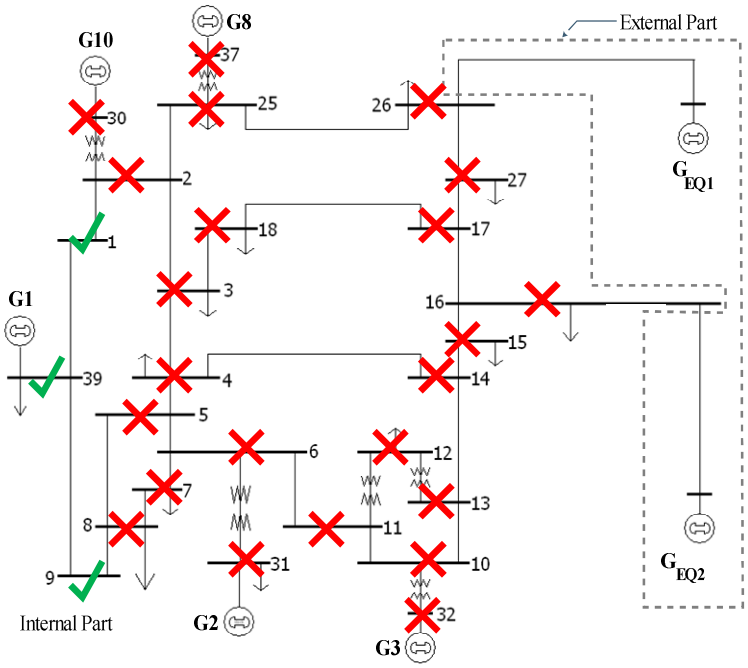

(a)

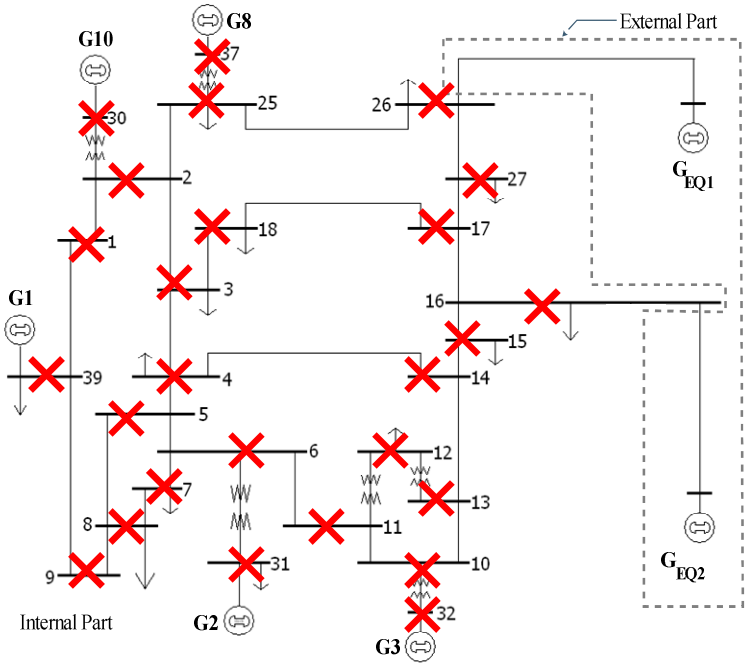

(b)

Figure 6.6 Reduced system B showing the testing condition (locations of buses) for which the reduced system is valid by the checking mark and invalid by the cross mark; (a) for the small fault with the accuracy <0.02 degree and (b) for the large fault with accuracy < 2 degree

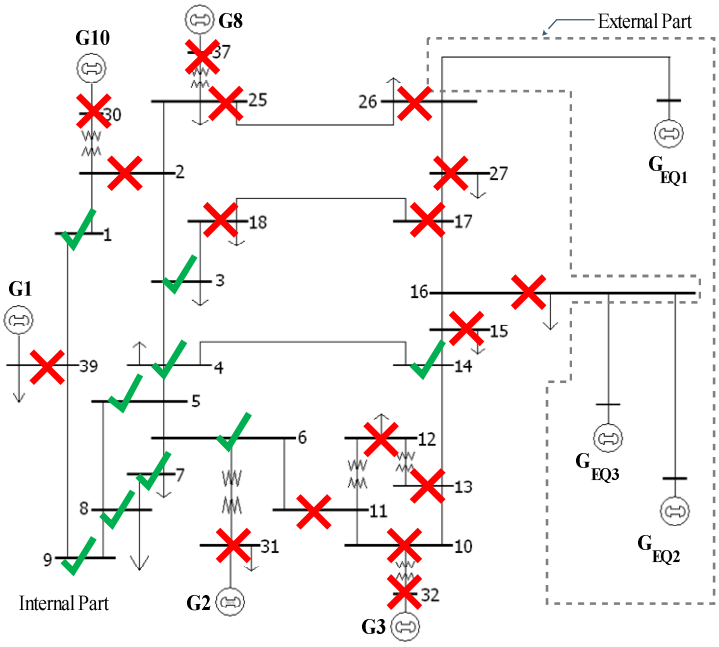

(a)

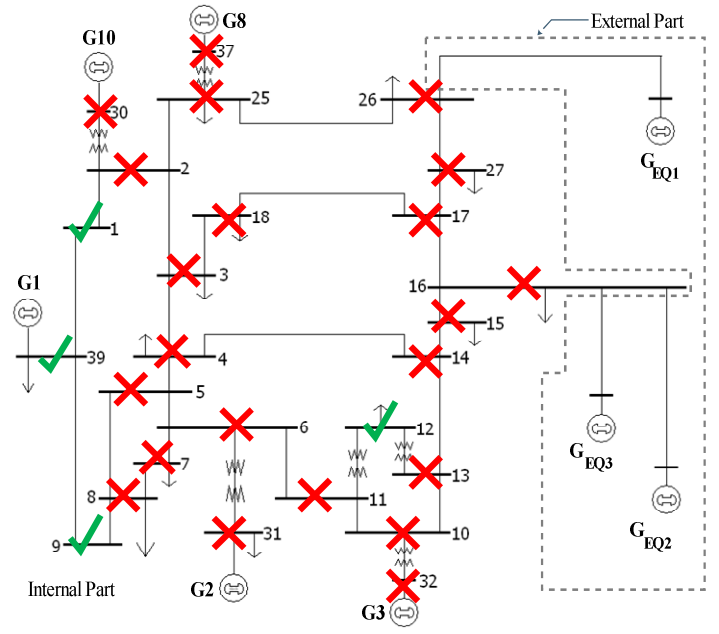

(b)

Figure 6.7 Reduced system C showing the testing condition (locations of buses) for which the reduced system is valid by the checking mark and invalid by the cross mark; (a) for the small fault with the accuracy <0.02 degree and (b) for the large fault with accuracy < 2 degree

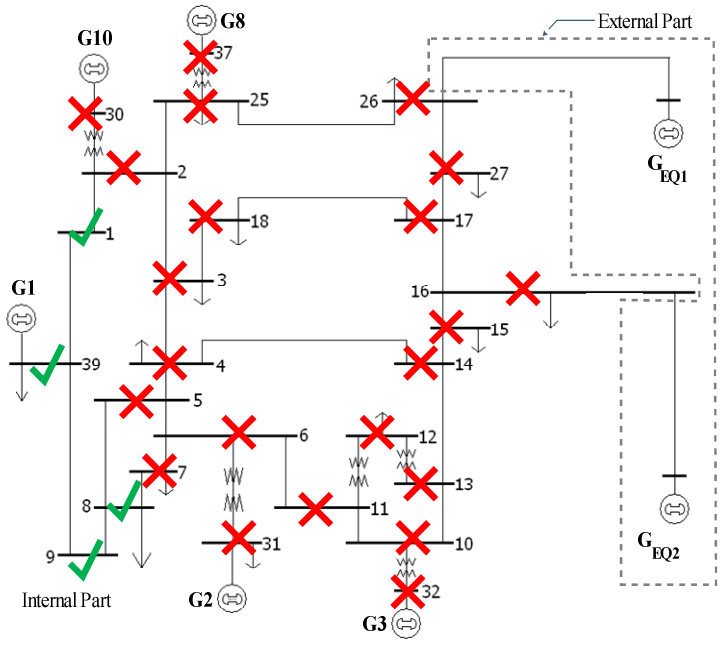

(a)

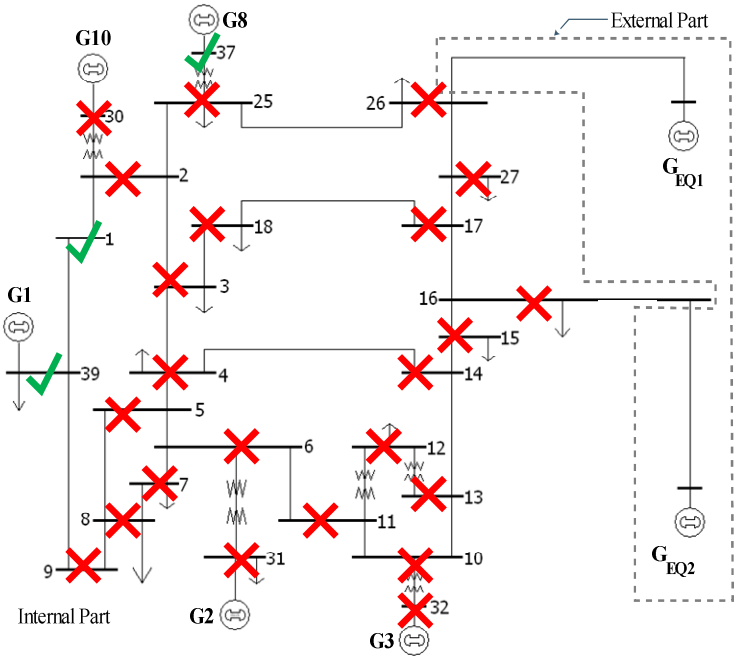

(b)

Figure 6.8 Reduced system D showing the testing condition (locations of buses) for which the reduced system is valid by the checking mark and invalid by the cross mark; (a) for the small fault with the accuracy <0.02 degree and (b) for the large fault with accuracy < 2 degree

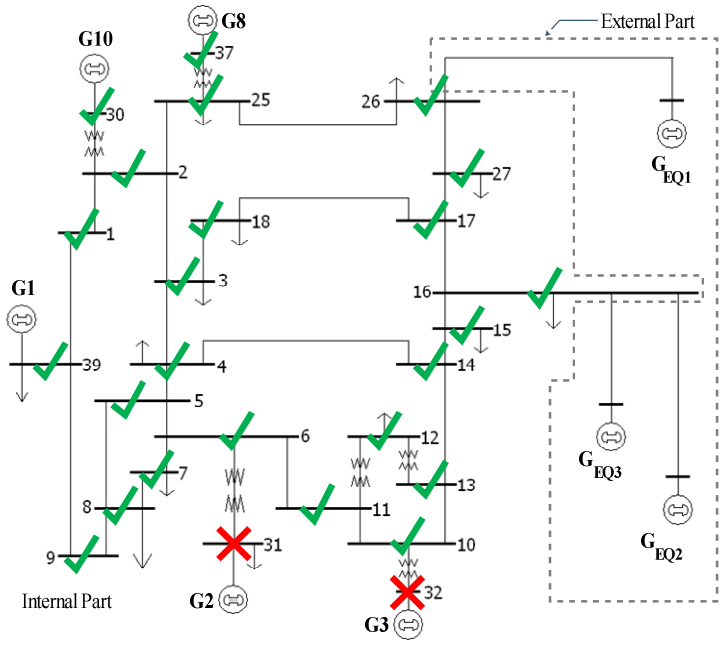

(a)

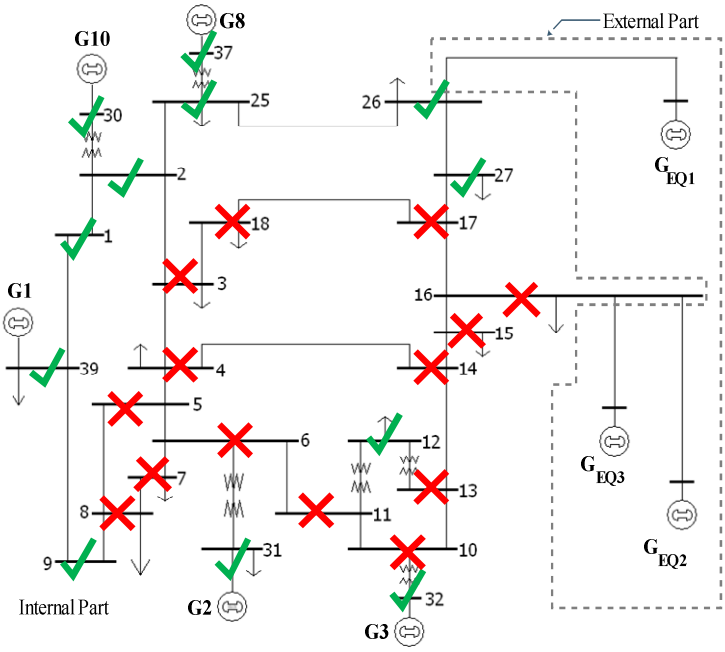

(b)

Figure 6.9 Reduced system E showing the testing condition (locations of buses) for which the reduced system is valid by the checking mark and invalid by the cross mark; (a) for the small fault with the accuracy <0.02 degree and (b) for the large fault with accuracy < 2 degree

For the small fault with accuracy < 0.02 degree, the numbers of testing conditions for which the reduced systems A, B, C, D, and E are valid are fifteen, three, nine, four, and twenty-four respectively. Although the numbers of testing conditions for which the reduced systems B, C, and D (which are constructed by the proposed equivalencing method) are less than that of the reduced system A, the equivalents B, C, and D are still acceptable to represent the external part but at lower accuracy level (e.g. accuracy < 0.03 degree). This can be seen from the simulation of the swing curves of the internal generators at testing condition for which the reduced systems (B, C, and D) are invalid, such as at bus 27 (as shown in Figures 6.11-6.13). The swing curves obtained from the simulation of these reduced systems (B, C, and D) are still similar to the swing curves of the original system. The swing curves of internal generators obtained from the simulation of the reduced systems A and E are also given in Figure 6.10 and 6.14, respectively, to confirm their validity at accuracy level < 0.02 degree.

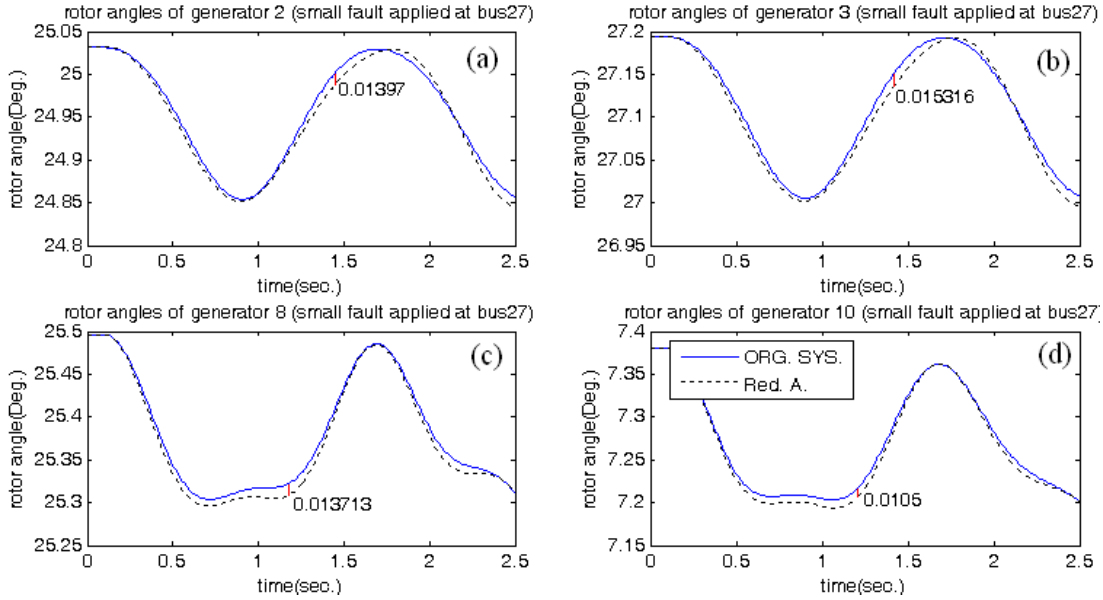

Figure 6.10 Rotor angles of the internal generators from the original system and the reduced system A when the small fault is applied at bus 27 showing the values and the positions of the maximum difference occurred for; (a) generator 2, (b) generator 3, (c) generator 8, and (d) generator 10.

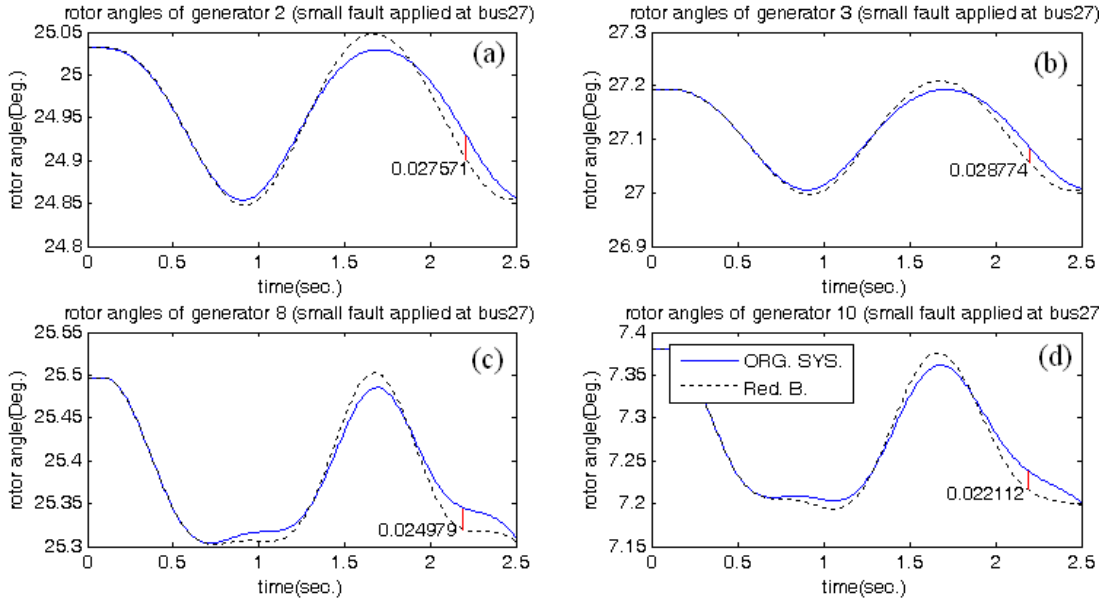

Figure 6.11 Rotor angles of the internal generators from the original system and the reduced system B when the small fault is applied at bus 27 showing the values and the positions of the maximum difference occurred for; (a) generator 2, (b) generator 3, (c) generator 8, and (d) generator 10.

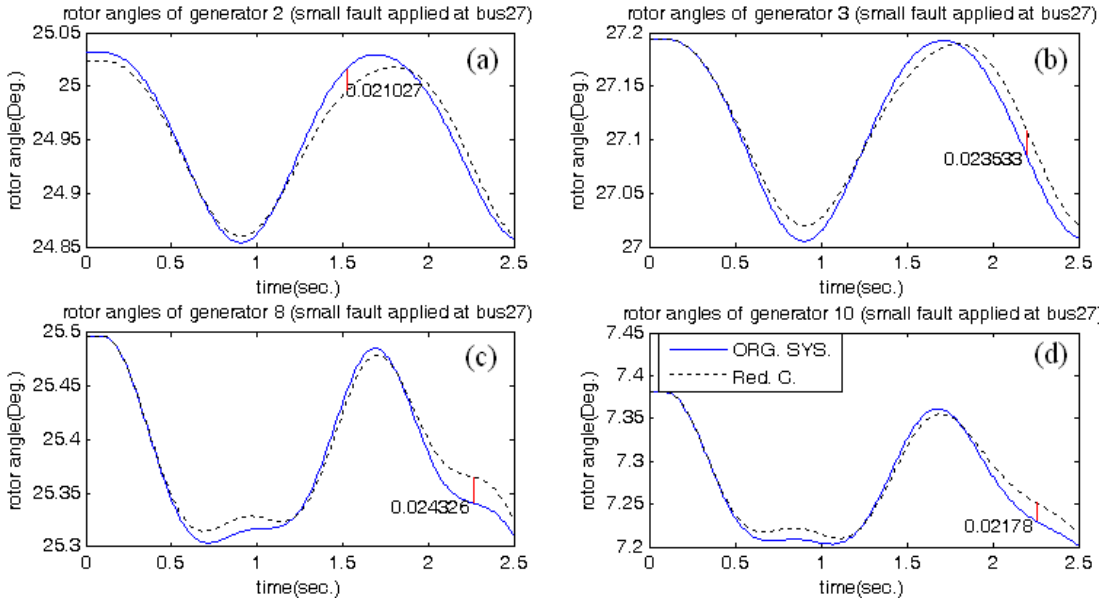

Figure 6.12 Rotor angles of the internal generators from the original system and the reduced system C when the small fault is applied at bus 27 showing the values and the positions of the maximum difference occurred for; (a) generator 2, (b) generator 3, (c) generator 8, and (d) generator 10.

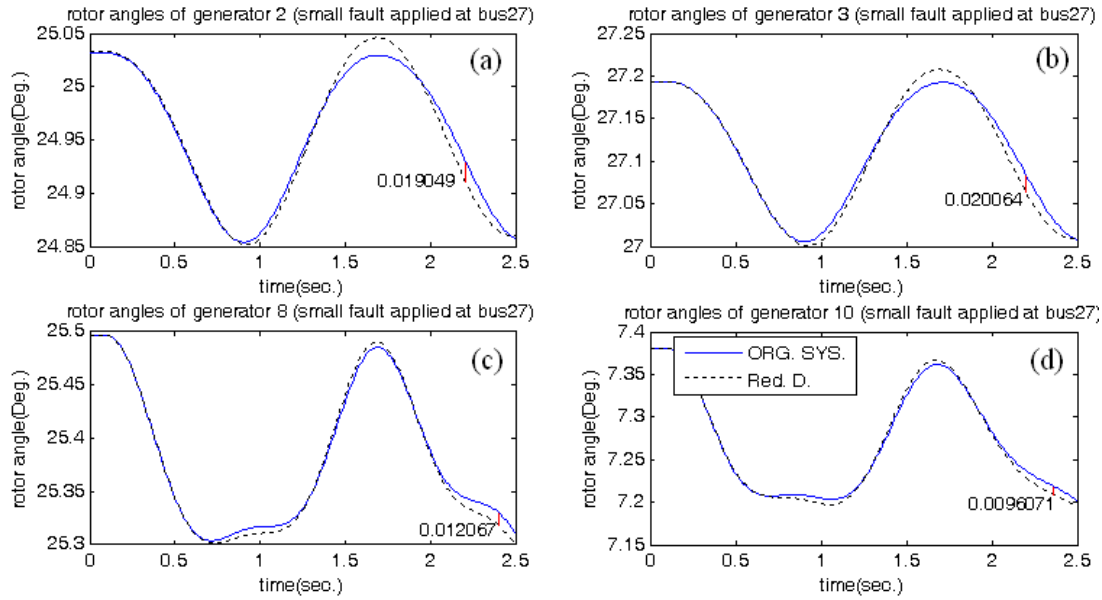

Figure 6.13 Rotor angles of the internal generators from the original system and the reduced system D when the small fault is applied at bus 27 showing the values and the positions of the maximum difference occurred for; (a) generator 2, (b) generator 3, (c) generator 8, and (d) generator 10.

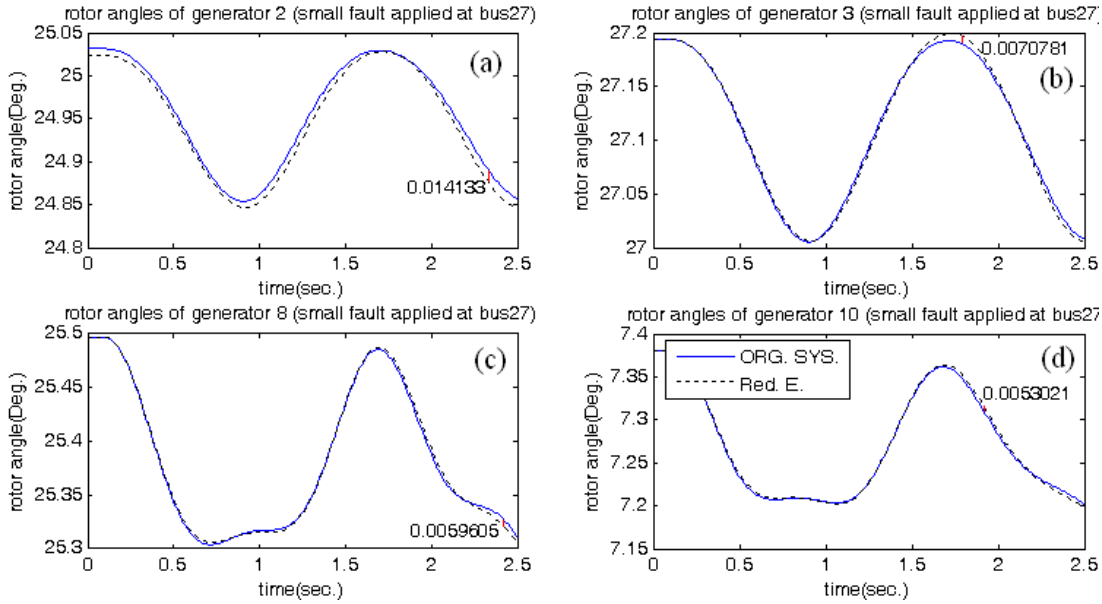

Figure 6.14 Rotor angles of the internal generators from the original system and the reduced system E when the small fault is applied at bus 27 showing the values and the positions of the maximum difference occurred for; (a) generator 2, (b) generator 3, (c) generator 8, and (d) generator 10.

For the large fault with accuracy < 2 degree, the numbers of testing conditions for which the reduced systems A, B, C, D, and E are valid are zero, zero, four, three, and twelve respectively. Although the reduced system B which is constructed from the proposed equivalencing method has none of acceptable testing condition as well as the reduced system A, at the same unacceptable testing condition such as a solid fault at bus 27 (see Figures 6.5(b) and 6.6(b)), the swing curves of the internal generators of the reduced system B (Figure6.16) is quite similar to those of the original system compared to that of the reduced system A (Figure 6.15). The swing curves of internal generators obtained from the reduced systems C and D (Figures 6.17 and 6.18) are also similar to those of the original system for this testing condition (the solid fault at bus 27) even though it is the testing condition for which the reduced systems C and D are invalid. This indicates that the reduced system A may not suitable to represent the external part of the system. By contrast, it also confirms that the proposed equivalencing method provides more reliable dynamic equivalent.

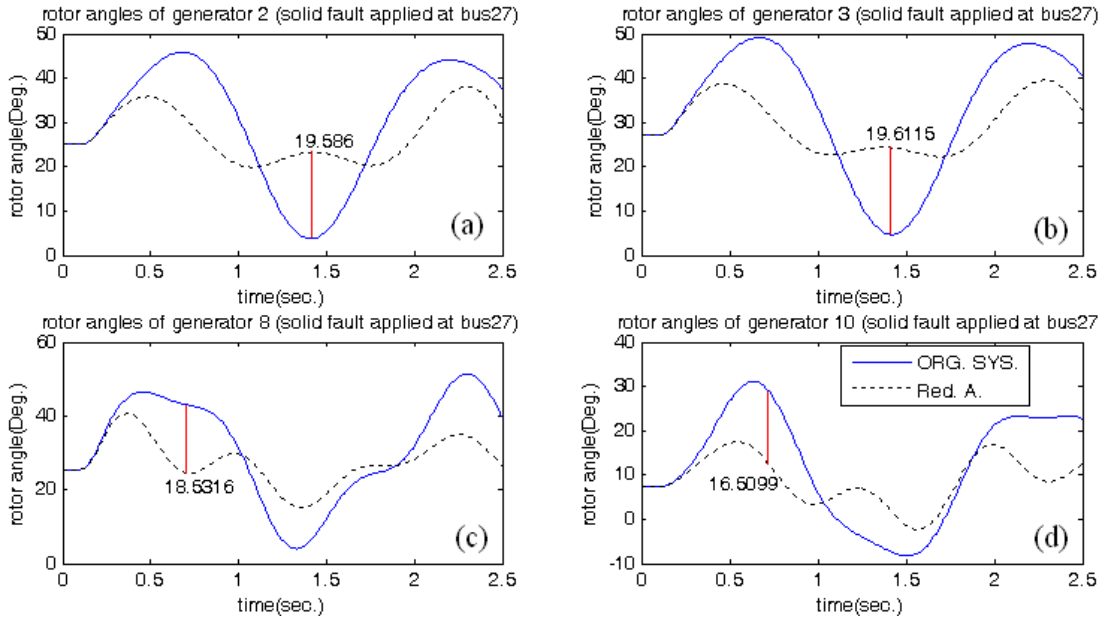

Figure 6.15 Rotor angles of the internal generators from the original system and the reduced system A when the large fault is applied at bus 27 showing the values and the positions of the maximum difference occurred for; (a) generator 2, (b) generator 3, (c) generator 8, and (d) generator 10.

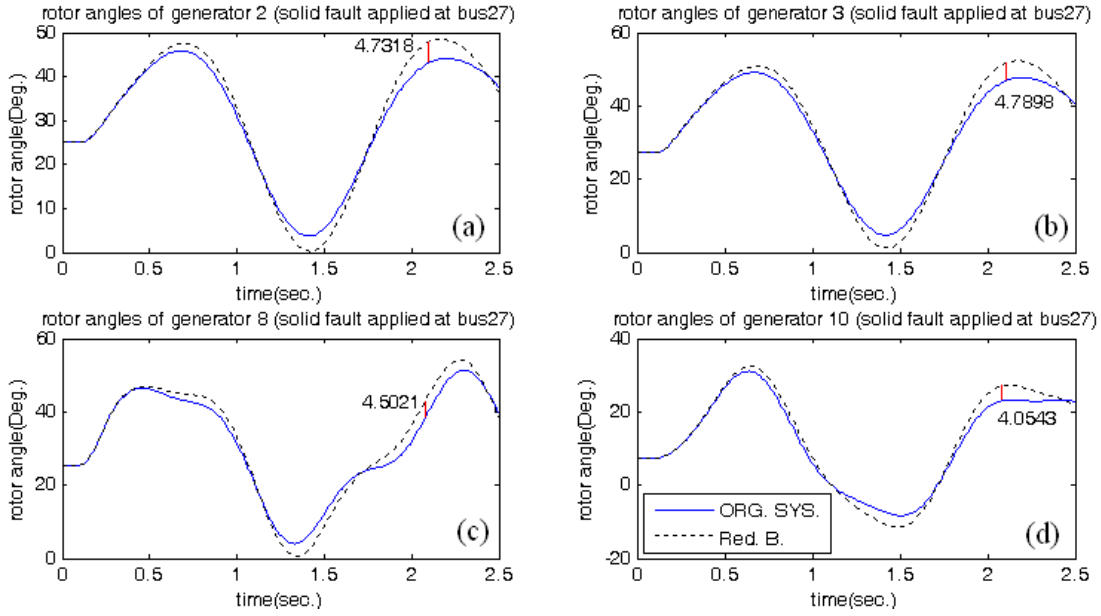

Figure 6.16 Rotor angles of the internal generators from the original system and the reduced system B when the large fault is applied at bus 27 showing the values and the positions of the maximum difference occurred for; (a) generator 2, (b) generator 3, (c) generator 8, and (d) generator 10.

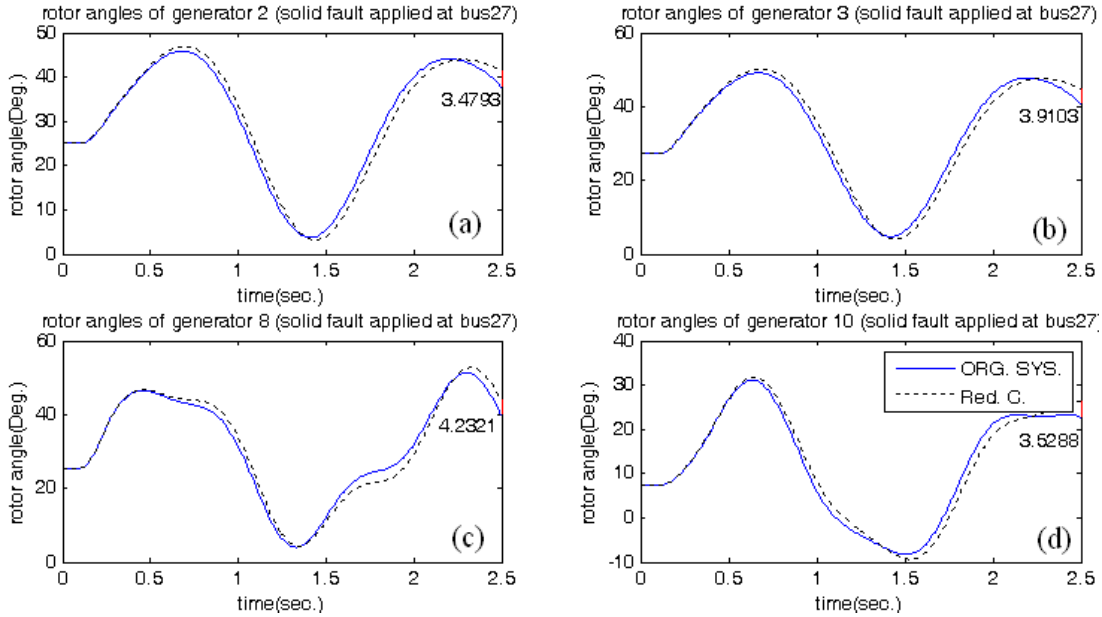

Figure 6.17 Rotor angles of the internal generators from the original system and the reduced system C when the large fault is applied at bus 27 showing the values and the positions of the maximum difference occurred for; (a) generator 2, (b) generator 3, (c) generator 8, and (d) generator 10.

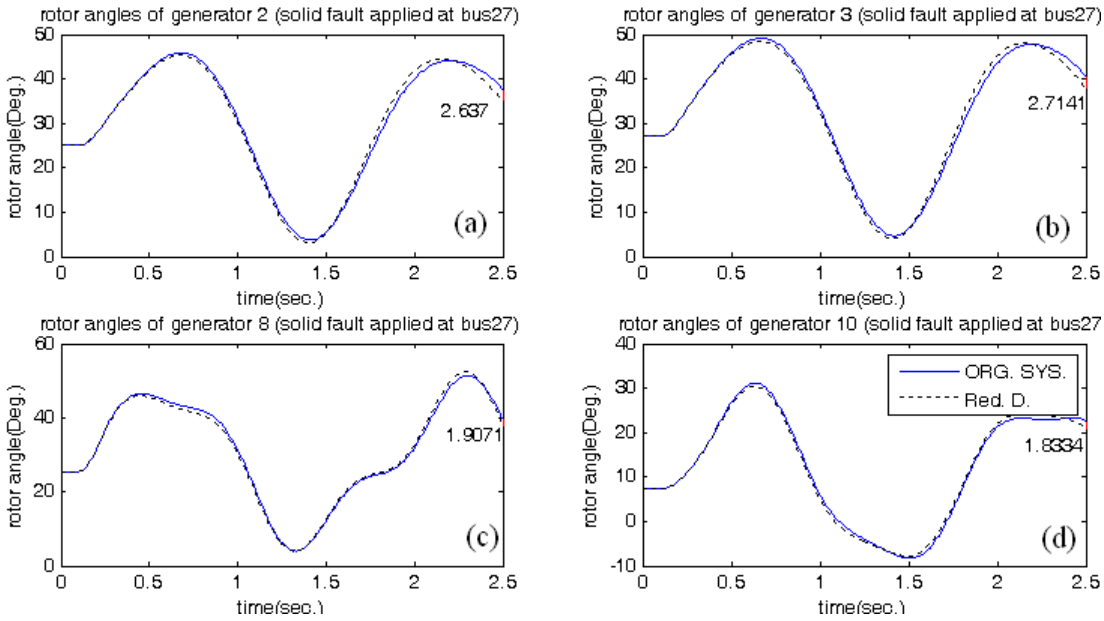

Figure 6.18 Rotor angles of the internal generators from the original system and the reduced system D when the large fault is applied at bus 27 showing the values and the positions of the maximum difference occurred for; (a) generator 2, (b) generator 3, (c) generator 8, and (d) generator 10.

Apart from the evaluation at the specific level of accuracy, the results in Table A1.13 can be presented by bar charts for the performance evaluation of the reduced systems over different levels of accuracy, as shown in Figures 6.19 and Figure 6.20.

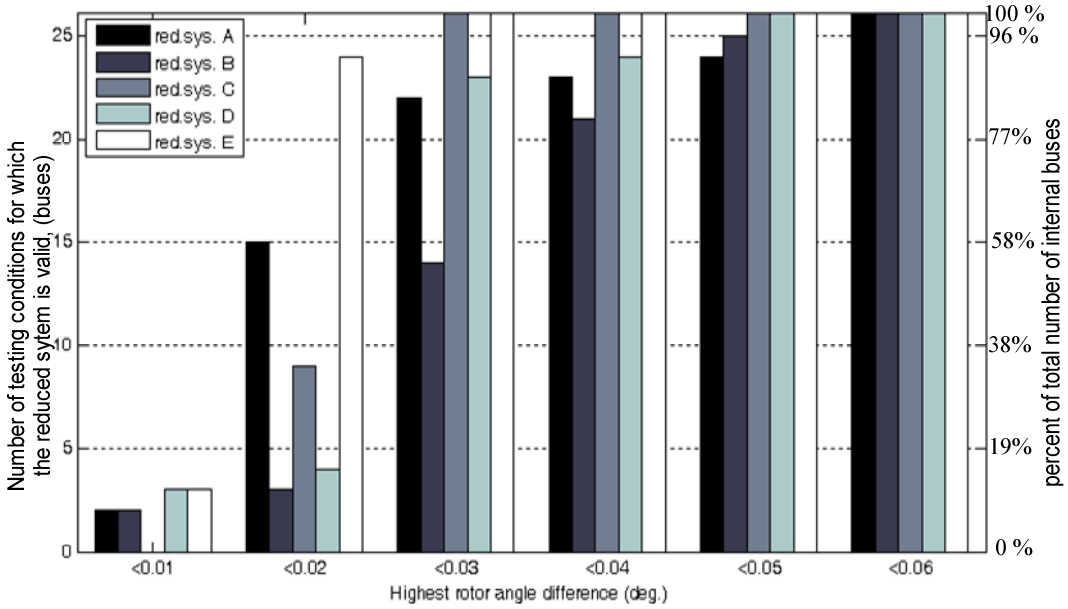

Figure 6.19 Number of testing condition for which the reduced systems A, B, C, D and E of the case study 1.1 (small fault) are valid for different level of accuracy.

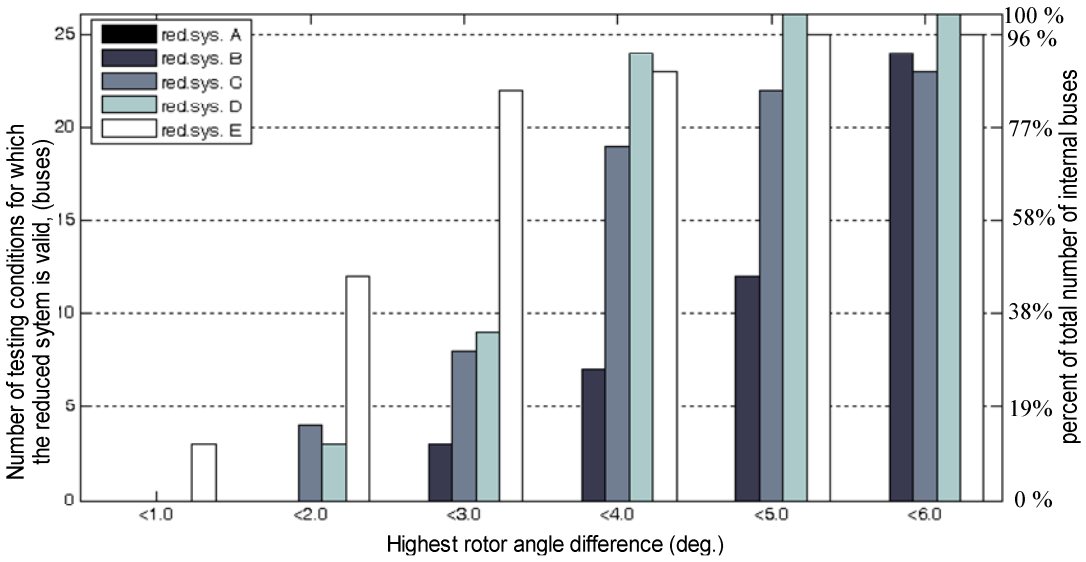

Figure 6.20 Number of testing condition for which the reduced systems A, B, C, D and E of the case study 1.1 (large fault) are valid for different level of accuracy.

The bar charts in Figure 6.19 and Figure 6.20 show the number of testing condition for which the reduced systems are valid over different levels of accuracy for the small and the large faults, respectively. As can be seen from the bar charts, the number of testing condition for which the reduced system A (based on two fictitious generators) is valid does not come in the last for only the small fault case when the accuracy less than 0.04 degrees. However, it is not the best. By contrast, there is no testing condition for which the reduced system A is valid when the large fault is considered. This is totally different from the case of the proposed equivalents (B, C, D, and E). Even thought the loose coherent groups are used, its reduced systems (B and D) still have the valid conditions for the large fault case. This indicates that the proposed equivalent is more reliable than the traditional identification-based dynamic equivalent.

Among the reduced systems based on the proposed equivalents, the reduced system C (or E) constructed by using the identified tight coherent groups have a better performance than the reduced system B (or D) constructed by using the identified loose coherent groups. This can be seen by a comparison between the bar chart of the reduced system C (or E) and the bar of the reduced system B (or D). However, the comparison may not be straightforward for the large fault after the accuracy greater

than 3 degrees are considered. For example, in Figure 6.20, the number of testing condition for which the reduced system D is valid becomes a bit higher than that of the reduced system E. This is because there are three large angle differences occurring at buses 15, 16, and 17, respectively, for the reduced system E (as shown in Figure 6.21). However, in overall, the level of validity for each testing condition of the reduced system E is considerably better than that of the reduced system D.

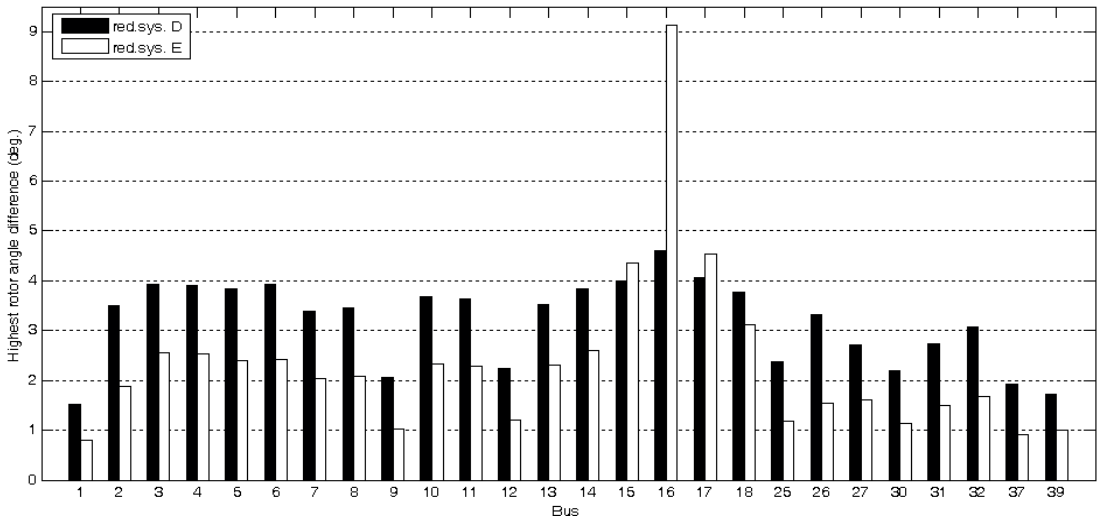

Figure 6.21 Highest rotor angle differences of the reduced systems D and E of case study 1.1(large fault).

Concerning the method of parameter identification, the equivalent (B or C) whose parameters are identified by the method with a full system simulation has reliability better than the equivalent (D or E) whose parameters are identified by the method without a full system simulation. This can be seen by a comparison between the bar charts of the reduced system B (or C) and D (or E) in Figure 6.19 and Figure 6.20. As discussed in Chapter 5, the inputs to the external equivalent are not quite correct for the parameter identification without a full system simulation. Moreover, a number of data points actually used during the parameter identification process of the method without a full system simulation is much less than the case of the method with a full system simulation, even thought they are used the same set of the recorded data. This is because the method with a full system simulation fits the simulated responses from the reduced model to every individual point of the

recorded data, but the method without a full system simulation does fit to the resultant data from a summation of the recorded data (which represents the outputs from the external part). These reasons may cause the identified parameters from the method without a full system simulation less efficient than the identified parameters from the method with a full system simulation. However, its usage time during the parameter identification is much less (as shown in Tables A1.5-A1.9).

6.3.2 Case study 1.2: Generator model order study

6.3.2.1 Description of the test system and the testing scenarios

The test system in this case study is IEEE39 bus system as described in the section 6.3.1.1., except that all generator models (both internal generators and external generators) are resumed to the full details (the fourth order model). In this study, the validity of the reduced system when the equivalent generators are modelled by different model orders is examined. The testing scenarios for the generator model order study are as follows:

Scenario 1: the external equivalent generators are represented by the fourth order generator dynamic model.

Scenario 2: the external equivalent generators are represented by the third order generator dynamic model.

Scenario 3: the external equivalent generators are represented by the second order generator dynamic model.

The parameters of generator according to each model order are given in Table 6.3. The models and their parameters are based on Power System Analysis Toolbox (PSAT) [6] which is the main program for performing the dynamic simulation (i.e. transient stability) in this thesis.

Table 6.3 Set of parameters for different model order

Parameter / Model order	4	3	2
Leakage reactance (X_l)	x	x	x
Armature resistance (r_a)	x	x	x
d-axis synchronous reactance (X_d)	x	x	
d-axis transient reactance (X'_d)	x	x	x
d-axis open circuit transient time constant (T'_{do})	x	x	
q-axis synchronous reactance (X_q)	x	x	
q-axis transient reactance (X'_q)	x		
q-axis open circuit transient time constant (T'_{qo})	x		
Inertia constant (H)	x	x	x
Damping coefficient (D)	x	x	x

6.3.2.2 Test results and discussions

The equivalent model based on the tight coherent groups of the case study 1.1 (Figure 6.3 (a)) is only considered here. The parameters of three equivalent generators are identified according to three different scenarios mentioned above. However, the parameter identification that requires a full system simulation is only employed for this case study since our developed code of parameter identification without a full system simulation is currently available for a classical model of generator with two parameters (i.e. X'd and H). The identified values of the parameters are given in Tables A2.1-A2.3.

The validity test as mentioned in Section 6.2 was conduced on three reduced systems by applying two kinds of faults (a small fault and a large fault) under all 26 internal buses (including the boundary buses). The small fault is a fault with 10 p.u. resistance which is applied at 0.1 second without a clearance. The large fault is a solid fault which is applied at 0.1 second and cleared at 0.2 second. The results are presented in Figure 6.22 and Figure 6.23 for the case of the small fault and the case of the large fault, respectively. The numerical values of the maximum angle difference are given in Tables A2.4.

From Figure 6.22 and Figure 6.23, it is found that the reduced systems based on the third order and the fourth order equivalent generator models, respectively, yield almost similar level of accuracy, while the accuracy of the reduced system based on the second order equivalent generator model is considerably less than those of the two reduced systems. Also, this comparable performance of using the fourth and the third order equivalent generator models could be seen in the results of the reliability test (Figure 6.24 and Figure 6.25). This suggests the third order equivalent generator model would be the suitable choice for equivalencing the system of this case study, when the complexity and the performance of the reduced system are needed to be tradeoff.

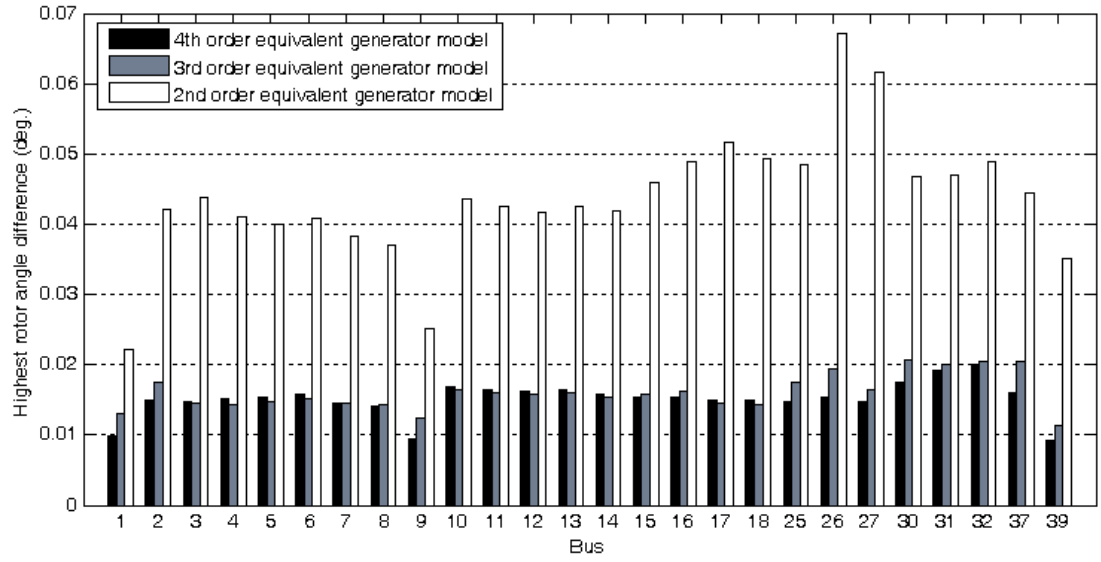

Figure 6.22 Highest rotor angle differences of three reduced systems of case study 1.2 (small fault).

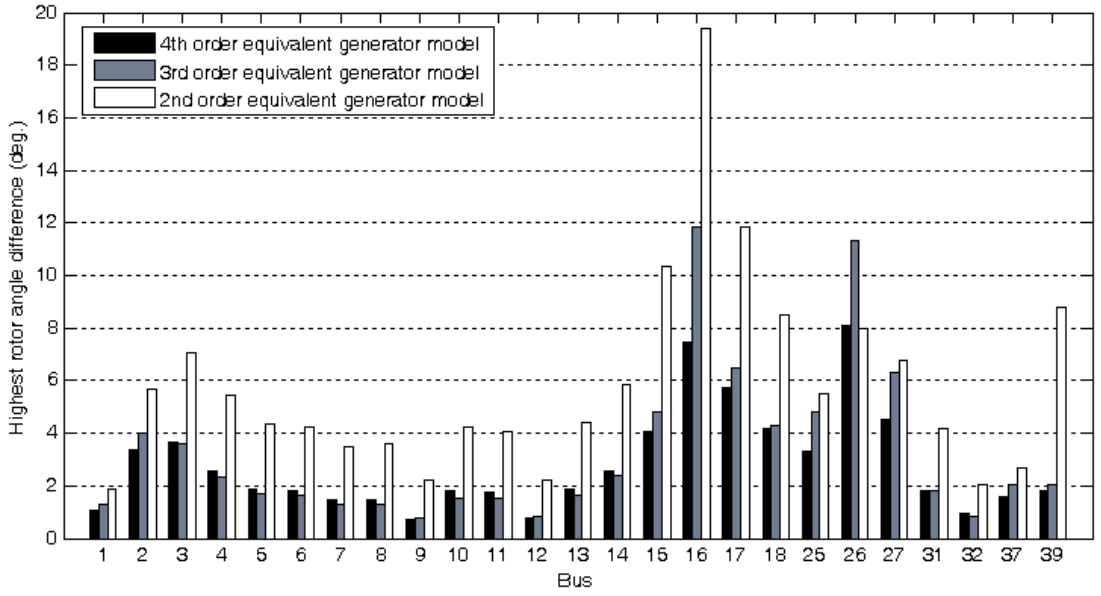

Figure 6.23 Highest rotor angle differences of three reduced systems of case study 1.2 (large fault).

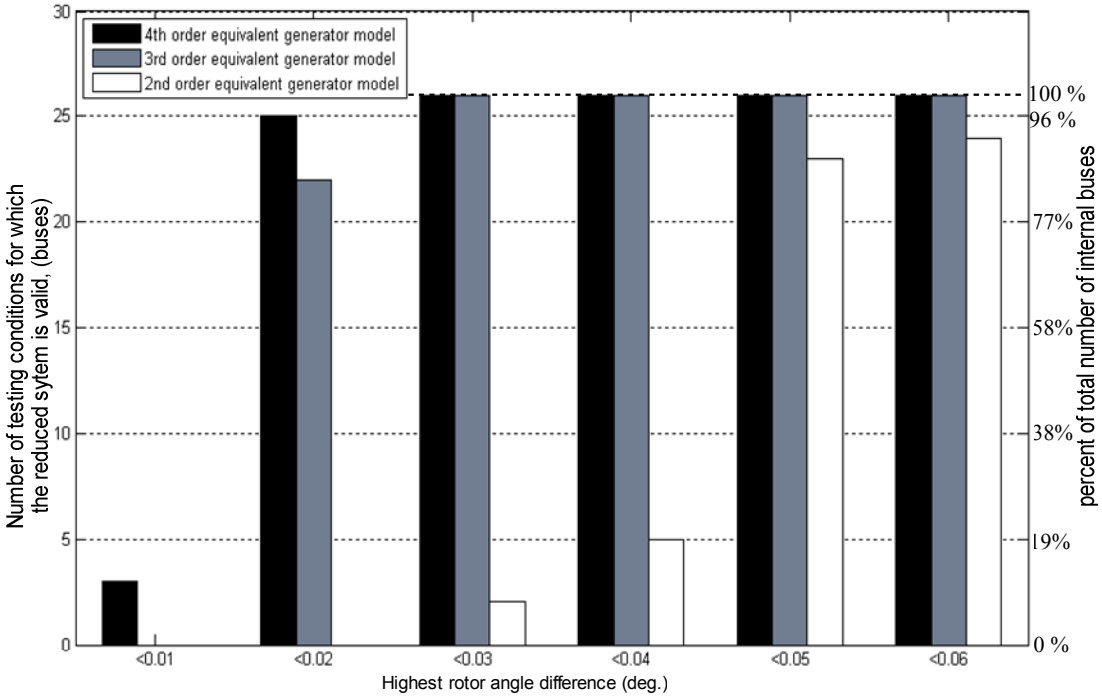

Figure 6.24 Number of testing condition for which the three reduced systems of case study 1.2 (small fault) are valid for different level of accuracy.

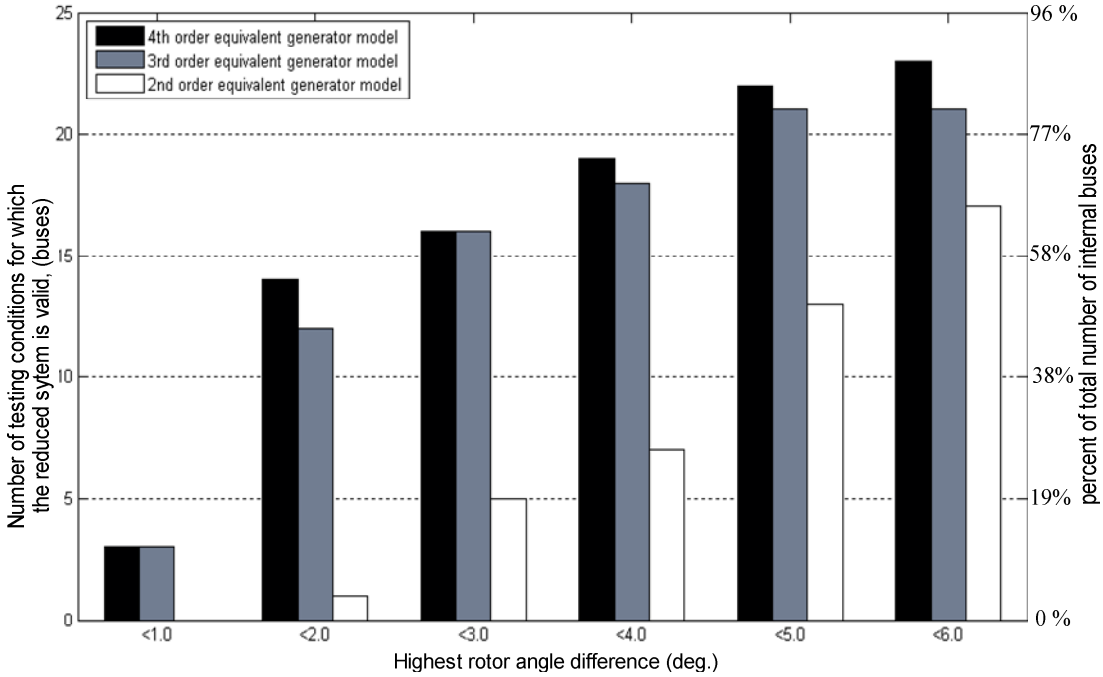

Figure 6.25 Number of testing condition for which the three reduced systems of case study 1.2 (large fault) are valid for different accuracy.

The cost function sensitivity analysis (mentioned in section 4.2.1 of Chapter 4) was also conducted to study the selection of the suitable model order. For this study, eqn. (4.7) was chosen as the cost function for testing of the sensitivity. The values of the parameters of generators were perturbed about their initial values one by one; and, the value of the cost function was recorded at the same time. The plots of the cost function against the values of the perturbed parameters for each model order are given in Appendix A2. These plots show whether the cost function is sensitive to all parameters in the chosen model order or not. For example, in case of using the fourth order model, there are nine insensitivities noticed from the plot. These insensitivity (Figure A2.1) occur when either d-axis open circuit transient time constant (T'_{do}) or q-axis open circuit transient time constant (T'_{qo}) of each equivalent generator are perturbed. Therefore, the fourth order of generator model may not suitable (over parameters). From the results in Appendix A2 (Figures A2.1, A2.2, and A2.3), the perturbed parameters when insensitivity of the cost function is noticed for three different orders of equivalent generator dynamic model could be summarised in Table 6.4 below.

Table 6.4 Perturbed parameters when insensitivity of the cost function is noticed for three different orders of equivalent generator dynamic model

Model order	4			3			2		
Parameter / Equivalent generator	1	2	3	1	2	3	1	2	3
Leakage reactance (X_l)									
Armature resistance (r_a)									
d-axis synchronous reactance (X_d)									
d-axis transient reactance (X'_d)									
d-axis open circuit transient time constant (T'_{do})	x	x	x	x	x	x			
q-axis synchronous reactance (X_q)									
q-axis transient reactance (X'_q)									
q-axis open circuit transient time constant (T'_{qo})	x	x	x						
Inertia constant (H)									
Damping coefficient (D)	x	x	x	x	x	x	x	x	x

From Table 6.4, the second order equivalent generator model has the least number of the parameters causing the insensitivity to the cost function; therefore, it should be the best choice according to the suggestion from [7]. However, the validity (Figures 6.22 and 6.23) test and the reliability test (Figures 6.24 and 6.25) reveal that the performance of using the second order equivalent generator model is worst when compared with the performance of using the third and the forth order equivalent generator models. Hence, the criterion of choosing the suitable model order by using the model order having the least (or none) parameters causing the insensitivity to the cost function would not be practical in this case.

6.4 Case study 2: IEEE118 bus system

The objectives of this case study are twofolds. The first objective is to examine the performances (i.e. validity, reliability, and construction time) of the proposed equivalent on a large system. The second objective is to examine predictability in the performances of the proposed equivalent when an operating condition and topology of the system have changed.

6.4.1 Description of the test system and the testing scenarios

The IEEE118 bus system contains 118 buses, 180 branches, and 20 generators. The generator is represented by a classical dynamic model with two parameters (X'_d and H). The single line diagram of the system and the system data are adapted from [8] and [5]; and they are given in Appendix B2. The internal part and the external part of the system are defined according to Figure 6.26. There are two areas of the external part. The boundary buses for the first external area are buses 24, 33, 34, and 38; and the boundary buses for the second external area are buses 68 and 77.

The first external area contains 35 buses (excluding the boundary buses), 53 branches, and 7 generators. The second external area contains 36 buses (excluding the boundary buses), 55 branches, and 5 generators. The internal area contains 47 buses (including the boundary buses), 72 branches, and 8 generators.

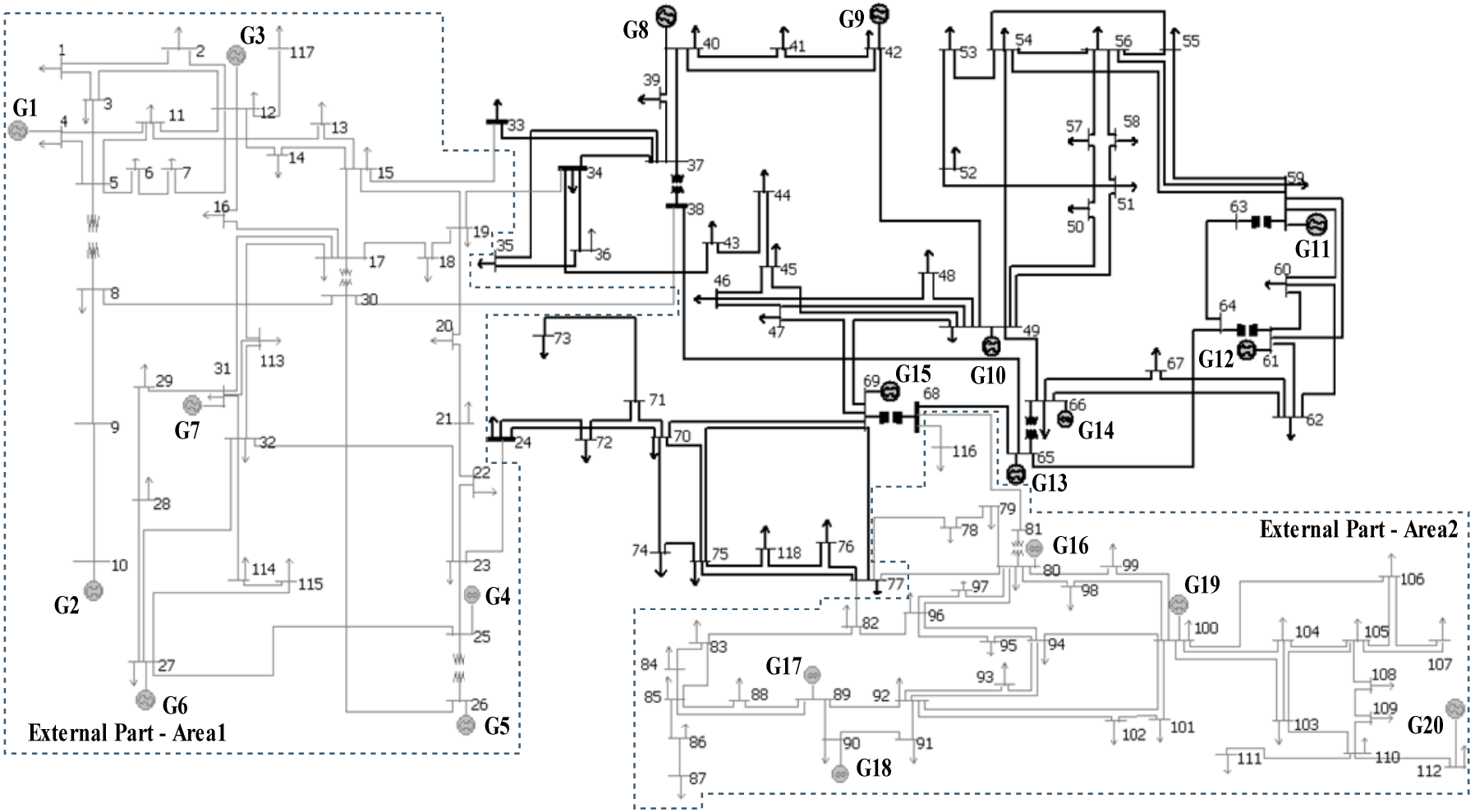

Figure 6.26 Internal part and external parts of the case study 2

There are three conditions of the system in this study, which are:

The first condition: a based case (see Appendix B2 for loads and generations),

The second condition: the base case with 10% loads decreased; and

The third condition: the base case with the following lines simultaneously opened.

-line between bus 17 and bus 30

-line between bus 28 and bus 27

-line between bus 32 and bus 27

-line between bus 90 and bus 89

-line between bus 114 and bus 115

The groups of coherent generators for these three system conditions are identified from their corresponding node-weighted graph model by using the applied epsilon decomposition technique. For the first condition and the second conditions, the identified coherent groups are the same, but they are slightly different for the third condition of the system. The identified groups for different values of epsilon are summarised in Figure 6.27 and Figure 6.28 by using contour lines. The value on the contour line indicates the minimum value of epsilon. The generators contained in each contour are the coherent generators identified by using any values of epsilon which is greater than the value indicated on that contour line. For example, in Figure 6.18, the group of generators1 and 3, the group of generators 4 and 5, the group of generators 6 and 7, the group of generators 16 and 19, and the group of generators 17 and 18 are the groups of coherent generators identified with the epsilon values greater than 0.27 units.

According to these three conditions of the system and their identified coherent groups, six scenarios of reduced system have been conducted in this study as shown in Table 6.5. For each scenario, the conditions of the system where the three tasks (i.e. coherent generator identification, parameter identification, and the reduced system test) were performed are defined.

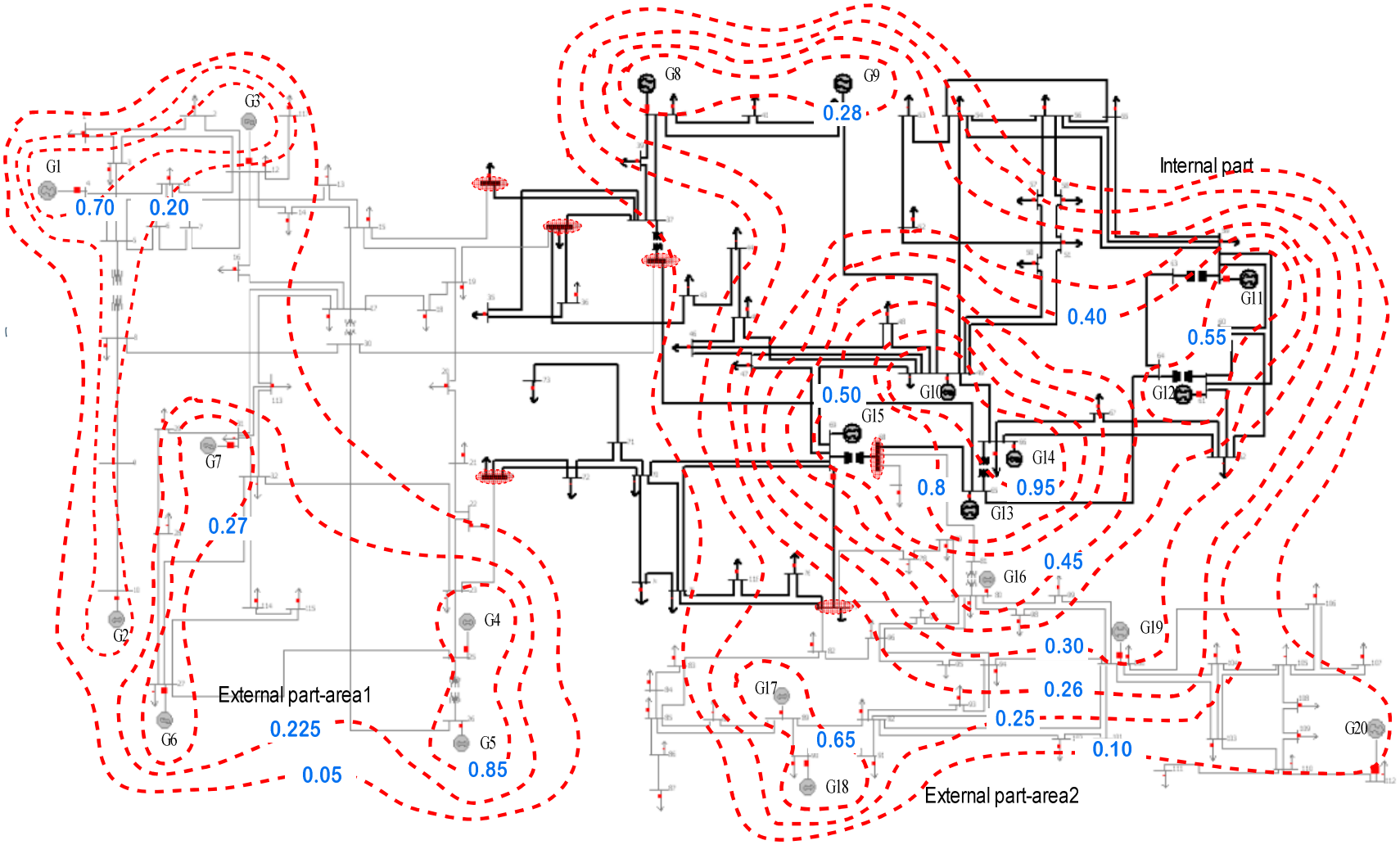

Figure 6.27 Coherent groups of the case study 2 for different values of epsilon at the first and the second system conditions

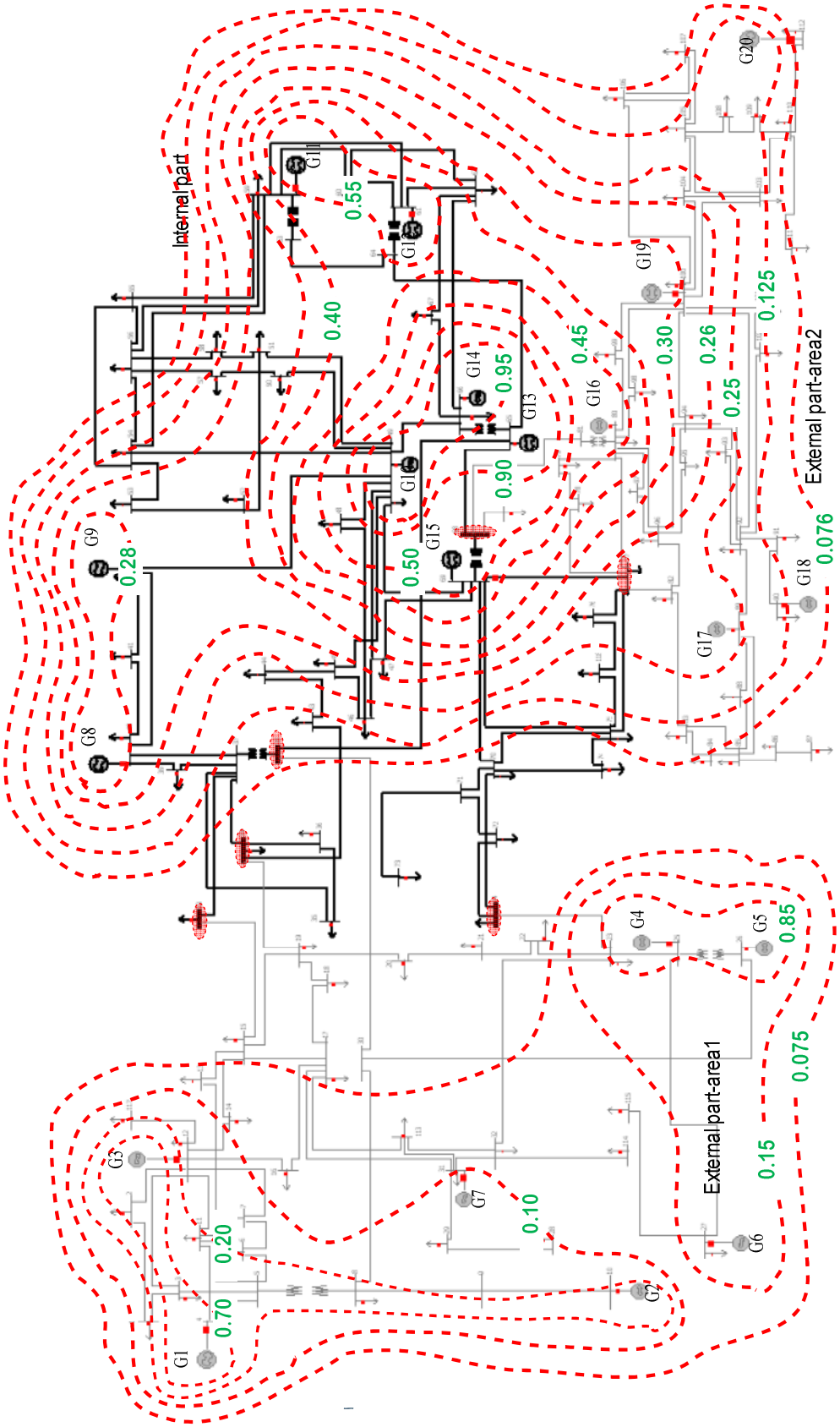

Figure 6.28 Coherent groups of the case study 2 for different values of epsilon at the third system condition

Table 6.5 Six scenarios of the reduced system for the case study 2

scenario	Coherent generator identification				Parameter identification	Reduced system test
	Condition of system	Epsilon	area	Coherent groups	Condition of system	Condition of system
A	1	≥ 0.27	1	(G1-G3), (G4-G5), (G6-G7), (G2)	1	1
			2	(G16-G19), (G17-G18), (G20)		
B	1	≥ 0.20	1	(G1-G2-G3), (G4-G5-G6-G7)	1	1
			2	(G16-G17-G18-G19), (G20)		
C	2	≥ 0.20	1	(G1-G2-G3), (G4-G5-G6-G7)	2	2
			2	(G16-G17-G18-G19), (G20)		
D	2	≥ 0.20	1	(G1-G2-G3), (G4-G5-G6-G7)	1	2
			2	(G16-G17-G18-G19), (G20)		
E	3	≥ 0.20	1	(G1-G2-G3), (G4-G5), G6, G7	3	3
			2	(G16-G17-G19), (G18), (G20)		
F	1	≥ 0.20	1	(G1-G2-G3), (G4-G5-G6-G7)	3	3
			2	(G16-G17-G18-G19), (G20)		

The coherent groups being used for construction of the reduced system are based on the results of Figure 6.27 and Figure 6.28 when the thresholds (under the epsilon column) are specified. The parameter identification without a full system simulation (all at once) is applied for all scenarios. The obtained reduced systems are tested under the system condition shown in the last column.

The first two scenarios (A and B) are to examine the performance of the equivalents when they are constructed by using the tight coherent groups ($\text{epsilon} \geq 0.27$) and using the loose coherent groups ($\text{epsilon} \geq 0.20$), respectively

The scenarios C and D are to examine the performance of the equivalents when their values of parameters are identified from the first system condition and the second system condition, respectively.

The scenarios E and F are to examine the performance of the equivalents when they are constructed by using the coherent groups identified from the third system condition and the first system condition, respectively.

6.4.2 Test results and discussions

The equivalent models and their corresponding reduced systems have been constructed according to the scenarios shown in Table 6.5. The parameter identification without full system simulation (as mentioned in Chapter 5) is applied in this study. For each external area, the parameters (X'_d and H) of all equivalent generators are identified together by fitting the active power responses at boundaries from the external part when a persistent fault with 10 p.u. resistances is applied at bus 44. The values of the identified parameters are given in Tables A3.1 to A3.5. The comparisons of the power flow results of the reduced system for each scenario to that of their original are given in Tables A3.6-A3.10. These results show good agreement for all scenarios.

The validity test has been conducted for all scenarios by applying two kinds of faults (a small fault and a large fault) under all 47 internal buses (including the boundary buses). The small fault is a fault with 10 p.u. resistances which is applied at 0.1 second without a clearance. The large fault is a solid fault which is applied at 0.1 second and cleared at 0.2 second. The results are given in Tables A3.11 and A3.12 for the case of the small fault and the case of the large fault, respectively.

For the scenarios A and B, it is seen that the equivalents based on tight coherent groups provide the reduced system having higher accuracy and having higher reliability as shown by the bar charts of the highest rotor angle differences (Figures 6.29 and Figure 6.30) and the bar charts of the number of testing condition for which the reduced systems are valid (Figures 6.31 and 6.32), respectively. Considering the accuracy when the number of testing condition for which the reduced system is valid is more than half of the total testing conditions (i.e. the number of the internal buses), the equivalent based on tight coherent groups gives the reduced model having an accuracy of 0.03 degree for the small fault and having an accuracy of 1.00 degree for the large fault. These show a good performance of the equivalent. In order to extend

the number of testing condition for which the reduced system is valid but maintaining the same level of the accuracy, another set of parameters may be identified by using a different fault location. For the reduced system obtained by using the equivalent based on loose coherent group, the accuracy would be 0.09 degree for the small fault and 3.00 degree for the large fault. This lower accuracy is a trade-off for a smaller size of equivalent. For example, seven equivalent generators are required for the reduced system of the scenario A; but, only four equivalent generators are required for the reduced system of the scenario B.

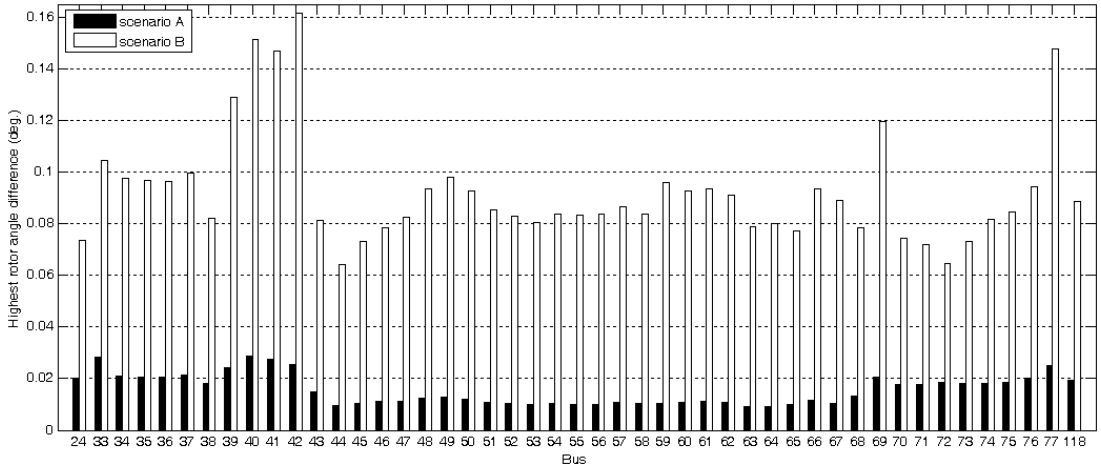

Figure 6.29 Highest rotor angle differences of the reduced systems of the scenarios A and B of the case study 2 (small fault).

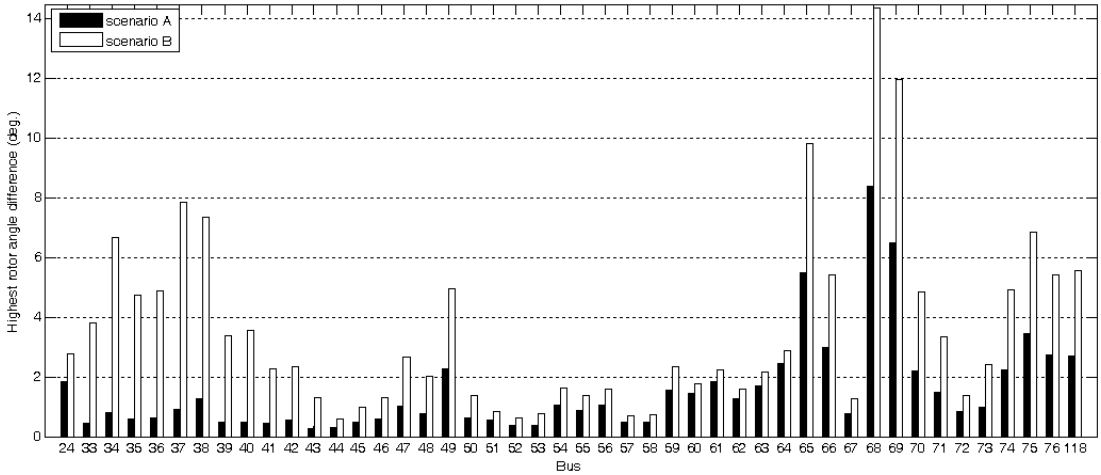

Figure 6.30 Highest rotor angle differences of the reduced systems of the scenarios A and B of the case study 2 (large fault).

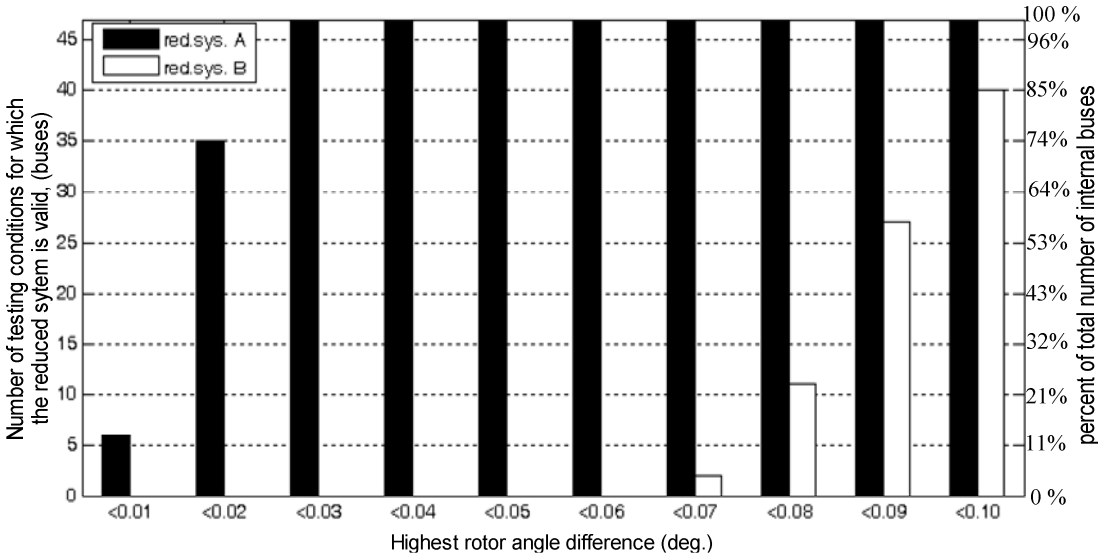

Figure 6.31 Number of testing condition for which the reduced systems of the scenarios A and B of the case study 2 (small fault) are valid for different level of accuracy.

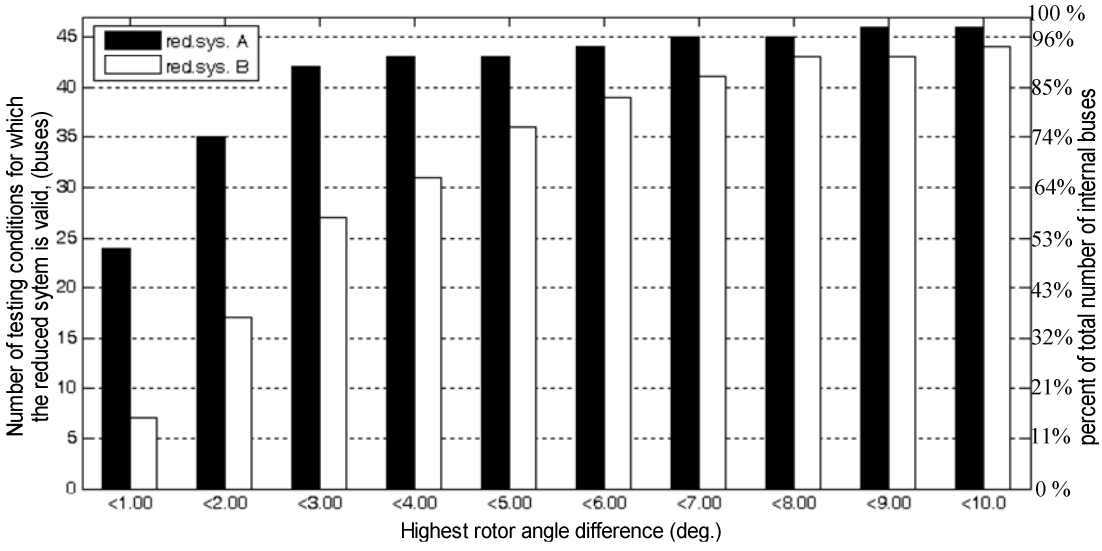

Figure 6.32 Number of testing condition for which the reduced systems of the scenarios A and B of the case study 2 (large fault) are valid for different level of accuracy.

The bar charts of the number of testing condition for which the reduced systems are valid over the different level of accuracy from the results of the scenarios C, D, E, and F are also plotted in order to provide data for an evaluation. For the scenarios C and D, the bar charts (Figures 6.33 and 6.34) show that the reduced system of the scenario C (using identified parameters at the second condition) is a bit better than the reduced system of the scenario D (using identified parameters from the first condition) for the small fault case; but they are comparable for the large fault case. Considering the accuracy when the number of testing condition for which the reduced system is valid is more than half of the total testing conditions, both reduced models have an accuracy of about 0.09 degree for the small (actually 0.08 for scenario C) fault and having an accuracy of 3.00 degree for the large fault.

For scenario E and F, in overall, the bar charts (Figures 6.35 and 6.36) show that the reduce system of scenario E is a bit better than the reduced system of the scenario F for the small fault case; and the reduced system of scenario E is much better for the large fault case. Moreover, the accuracy when the number of testing condition for which the reduced system E is valid is more than half of the total testing conditions for the large fault is 3.00 degree but that of the reduced system F is 4.00 degree.

These would indicate that the same external equivalent could be used with the comparable level of accuracy when the condition of the system is changed, if the identified coherent groups are the same. However, the re-construction of the equivalent would be necessary if the different coherent groups are identified at a new system condition.

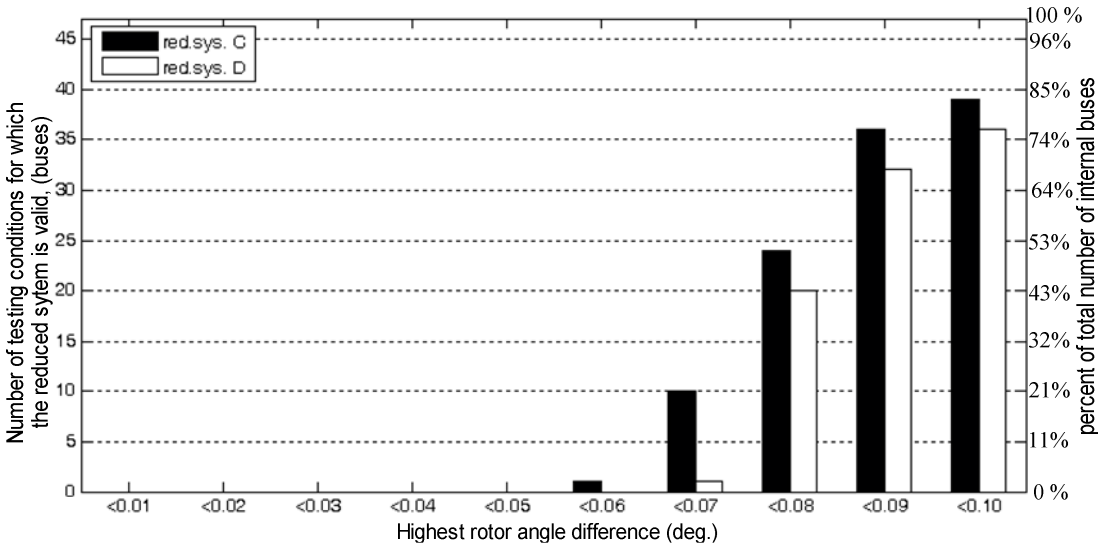

Figure 6.33 Number of testing condition for which the reduced systems of the scenarios C and D of the case study 2 (small fault) are valid for different level of accuracy.

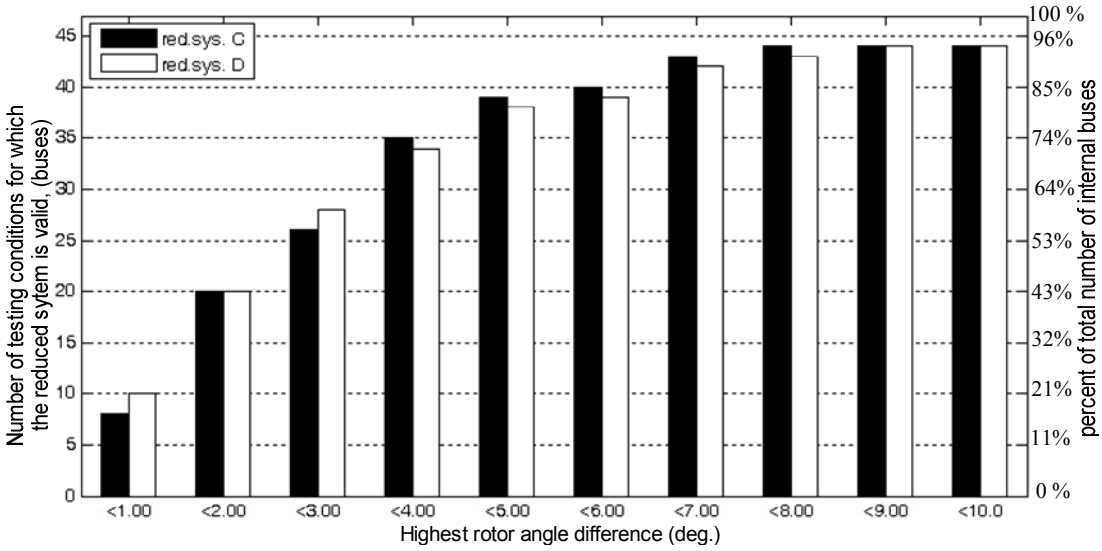

Figure 6.34 Number of testing condition for which the reduced systems of the scenarios C and D of the case study 2 (large fault) are valid for different level of accuracy.

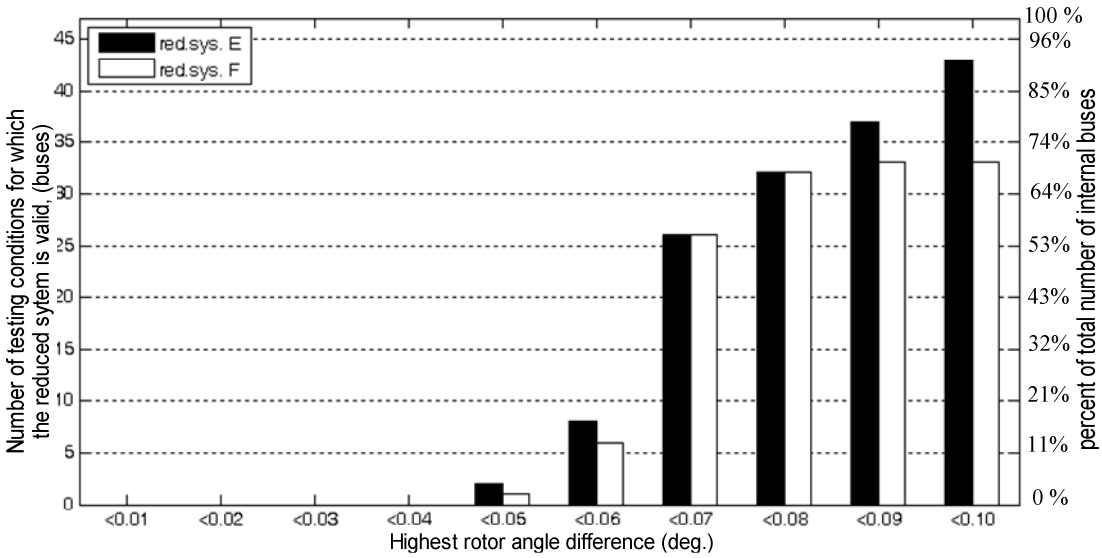

Figure 6.35 Number of testing condition for which the reduced systems of the scenarios E and F of the case study 2 (small fault) are valid for different level of accuracy.

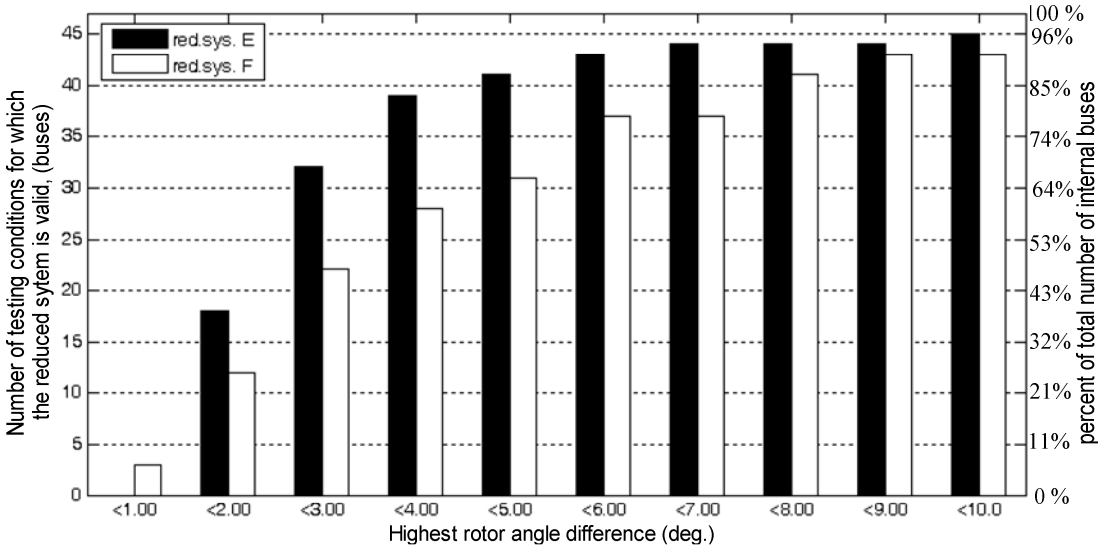

Figure 6.36 Number of testing condition for which the reduced systems of the scenarios E and F of the case study 2 (large fault) are valid for different level of accuracy.

6.5 Conclusion

The method for construction of identification-based dynamic equivalent developed in this thesis is applied to two test systems (IEEE39 bus system and IEEE118 bus system). The test results of three studies – namely, the reliability study, the model order study, and the large system study, were discussed. Based on the results obtained from these studies, it can be concluded as follows:

(a) The proposed equivalencing method can construct the reduced system which can accurately reproduce the steady-state behaviour of the internal part (i.e. power flow solution) and the dynamic behaviour of the internal part (i.e. the rotor angle of the internal generators) for about 2.5 seconds. The computational time for the parameter identification could be much reduced by using the parameter identification method that does not require a full system simulation; but it is a trade-off for the level of accuracy of the reduced model.

(b) The reliability of the proposed equivalent is considerably improved when compares to that of the traditional identification-based dynamic equivalent, which is based on attaching the fictitious generator to each boundary bus. The proposed equivalent is valid for various testing conditions per one construction. Apart from recorded measurements, the power-flow modelling data of the external part is required for the construction of the proposed equivalent.

(c) The higher the order of the equivalent generator model, the more the accuracy is the resultant reduced model. However, an increase in accuracy is not direct in proportion with an increase in model order.

(d) The same equivalent could be used for a new system condition (i.e. a new load setting) with a comparable accuracy if the identified coherent groups are not changed. This would save an overall computation time for construction of the reduced system.

6.6 References

[1] The MathWorks Inc. , "MATLAB Programing," The MathWorks Inc., 2007.

[2] J. M. Ramírez Arredondo, "Obtaining dynamic equivalents through the minimization of a line flows function," *International Journal of Electrical Power & Energy Systems,* vol. 21, pp. 365-373, 1999.

[3] I. A. Hiskens, "Power System Test Cases [online] http://psdyn.ece.wisc.edu/IEEE_benchmarks/index.htm."

[4] G. Rogers and J. H. Chow, "Power System Toolbox [online],http://www.ecse.rpi.edu/pst/PST.html."

[5] PowerWorld Corporation, "PowerWorld Simulator version 11 [Online] Available at http://www.powerworld.com."

[6] F. Milano, "Power System Analysis Toolbox (PSAT) ", 1.3.4 ed, 2006.

[7] M. A. El-Sharkawi, "Choice Of Model And Topology For External Equivalent Systems," *Power Apparatus and Systems, IEEE Transactions on,* vol. PAS-102, pp. 3761-3768, 1983.

[8] V. G. Rau and M. Y. Hussain, *Coherent Generators*: Allied Publishers Limited, New Delhi, 1998.

CHAPTER 7

CONCLUSION AND SUGGESTIONS FOR FUTURE WORK

Although dynamic equivalent have been extensively developed for four decades, the needs for future research are still required especially for an inclusion of power electronics equipments and for an analysis in online environment. This thesis is devoted to the development of dynamic equivalent for online environment which calls for the equivalent featuring high reliability but limited modelling data use. In addition, the equivalent should be compatible with available commercial power system software. This study, therefore, aims to develop the dynamic equivalent based on grey-box approach where recorded responses are used together with partial modelling data to construct the equivalent. A number of studies and literatures have been reviewed and discussed in terms of equivalencing methods and implementation schemes aiming for online application. These results in the proposed identification-based dynamic equivalent consisting of three components: coherent generator identification from power flow modelling data, determination of an appropriate model structure for the equivalent of the external part from the knowledge of coherent generators, and parameter identification of the model structure without a complete system simulation. The attractive features of the proposed dynamic equivalent are as follows:

(1) The obtained equivalent is physically meaningful and it can be implemented directly into commercial power system software as it is modelled by a combination of equivalent generators, equivalent transmission lines, and equivalent shunts.

(2) The validity of the equivalent is more reliable as its model structure is derived from the knowledge of coherent generators. In addition, the derivation of the model structure has a finite step rather than iterative process by trial and error, hence reducing the total usage time for equivalencing process.

(3) The equivalent could be constructed online by using only up-to-date power flow modelling data of the entire power system and recorded transient responses at the boundaries

(4) The proposed identification-based dynamic equivalent can be employed with Coherency-based dynamic equivalent in order to compromise between the needs of generator parameters and measurements.

(5) With the parameter identification that requires no complete system simulation, the total usage time for eqivalencing process is additionally reduced and, therefore, the equivalent could be frequently updated or even reconstructed for different operating conditions.

In relation to this development, the original contributions of this thesis are in four major aspects as mention earlier in Chapter 1. These contributions are:

- Development and verification of a new methodology for coherent generator identification based on graph model
- Development and verification of a new methodology for constructing identification-based dynamic equivalent based on grey-box approach
- Development and verification of a new methodology for parameter identification without full system simulation.

- Application of the developed computer programs based on the above methodologies to IEEE 39 bus system and IEEE 118 bus system.

The details of each contribution are summarised in the following parts.

Coherent generator identification from the node-weighted graph model is the first components of the proposed identification-based dynamic equivalent. It aims to provide information for the derivation of the appropriate model structure for the equivalent of the external part. The theory of coherency in term of a node-weighted graph is employed in order to develop the coherent generator identification from the power flow modelling data. The developed coherent generator identification based on the graph model consists of three successive steps: collecting power flow modelling data and its solution, establishing the node-weighted graph model, and identifying groups of strong-intra linked nodes among weak-inter linked nodes. According to this developed method, three techniques (i.e. two level of line thickness plot, applied weak coupling, and applied epsilon decomposition) to identify of such particular groups of nodes have been studied. Various tests have been conducted on both artificial system and power systems. The most interesting findings are that:

(a) The node-weighted graph model provides an aid to interpretation as it represents dynamic model of power system, in particular a small signal rotor angle dynamics, in the way that parameters of generators and of transmission network are presented in different components of the graph (i.e. different nodes and edges). Therefore it allows making an assumption to identify coherent generator by using only power flow modelling data.

(b) The coherent groups based on the graph theorem are independent to type of disturbance; hence, a reduced model based on them may be valid over a wide range of testing conditions.

(c) The developed coherent generator identification based on the graph model succeeds to identify the coherent generators, in particular the coherent groups that is caused by the structure of strong intra-linked nodes among weak inter-linked nodes.

With the coherent generator identification based on the graph model, the parametric identification of dynamic equivalent using only power flow modelling data and recorded response at boundaries has been developed. The developed method consists of three fundamental steps: coherent generator identification from power flow modelling data, determination of an appropriate model structure for the equivalent of the external part from the knowledge of coherent generators, and parameter identification of the model structure by fitting the responses of the reduced system with the responses of the original system.

The coherency-based aggregation method has been adopted with a minor modification (i.e. avoiding the use of parameters of generators) to determine the appropriate model structure for the equivalent of the external part after the coherent generator are identified from the graph model. Based on this technique, the appropriate model structure for the equivalent is represented as a combination of equivalent generators, equivalent transmission lines, and equivalent shunts. The values of the parameters of the equivalent generators are identified by fitting the responses of the reduced model with that of the original system; and the transient

responses of the active power flows from the internal part to the boundaries are used in this case. The non-linear optimisation is employed in order to keep the parameterisation of the model structure preserving the structure of power system components. The details of each step were demonstrated with nine bus power system and the short performance evaluation was presented. The performance is evaluated by a comparison of the responses of the reduced system formed by the proposed equivalent with the responses of the original system. In addition, another reduced system based on attaching one fictitious generator to each boundary bus is also brought to compare. The results show good validity and reliability of the proposed equivalent. The attractive features of this developed parametric identification of dynamic equivalent cover first four of the five features of our final developed identification-based equivalencing method mentioned in the very beginning of this chapter.

In addition to the parameter identification based on fitting the responses of the reduced system with the responses of the original system, another parameter identification method that requires no simulation of a complete system (i.e. internal part together with external equivalent) is also developed in thesis. The parameter identification method without complete system simulation is based on a re-formulation of the obtained model structure for the equivalent of the external part as the input-output model. According to this input-output formulation of the equivalent, one set of recorded responses (voltages at boundaries) is used as the inputs while another set (active power flows from the external part to boundaries) is used as the original responses for fitting. The fitting of the responses is also based on non-linear optimisation technique. Apart from the details of the derivation of the input-output

model and the algorithm for the parameter identification, two possibilities of implementation, which are the identification of all parameters at once and the identification of parameters for each individual equivalent generator, are also discussed. The parameter identification method without a complete system simulation was tested on IEEE39 bus system to evaluate its performance (i.e. usage time and accuracy). The accuracy of the parameters is assessed by both a comparison with the calculated parameters from the structure preservation technique and a comparison of the swing curves of internal generators of the reduced system using the identified parameters with those of the original system. The interesting findings are that:

(a) This parameter identification method greatly improves the usage time of the whole parameter identification process and saves the memory needed for model storage during the identification process when compares with those requires from the parameter identification with complete system simulation.

(b) The accuracy of the identified parameters is acceptable for both possibilities of implementation.

Based on above developments, a dynamic equivalencing program has been constructed and applied to IEEE39 bus system and IEEE118 bus system for extensive performance evaluation. The extensive performance evaluation includes the reliability study, the model order study, and the large system study. In the first study, the reliability of the equivalent is assessed from the number of testing condition that its reduced system reproduces swing curves of internal generators with acceptable accuracy. Two equivalents are considered in this study, which are the

proposed equivalent and the equivalent based on attaching one fictitious generator to each boundary bus. In the second study, the validity of the proposed equivalent when different orders of generator dynamic model for representing the equivalent generator are used is assessed. The third study is a large system study and it was conducted on IEEE118 bus system to evaluate the performance of the proposed identification-based dynamic equivalencing method over wide range of system conditions (i.e. different operating conditions and different topology of network). With these extensive tests, the following interesting features are found.

(a) The reduced system based on the proposed identification-based dynamic equivalent can accurately maintain the steady-state behaviour of the internal part while the dynamic behaviour of the internal part, in particular the swing curves of the internal generators, can be well preserved over time duration (2.5 seconds) of the tests.

(b) With a compromise between the degree of accuracy and the size of the reduced system, the equivalent can be constructed by using either loose or strong coherent groups and by using either high or low orders of generator dynamic model.

(c) The proposed equivalent has a good validity for various testing conditions, such as different fault locations and different operating conditions that the coherent groups are not changed; and its reliability is considerably improved when compares to that of the identification-based dynamic equivalent based on attaching one fictitious generator to each boundary bus.

Nonetheless, this study has some limitations relating to the development and evaluation stages. In the development stage, the limitations in the developed identification-based dynamic equivalent involve the coherent generator identification based-on the graph model and the parameter identification without a complete system simulation. For the developed coherent generator identification, the identifiable groups of coherent generators are only the coherent groups that are caused by the structure of strong-intra linked nodes among weak-inter linked nodes. It is, therefore, possible that any other stronger coherent groups caused by other factors exist and are not identified. However, this specific-identifiability of the developed coherent generator identification compromises on the required computation power and the required system modelling data.

For the developed parameter identification, the technique has the main drawback of the impracticality to obtain the correct inputs for the simulation of the external model. This is because the correct recorded responses for driving the inputs of equivalent model must be the recorded responses from the reduced system; but such reduced system does not exist beforehand. In addition, the developed parameter identification technique that requires no complete system simulation is limited to only classical equivalent generator dynamic model with two parameters (X'_d and H) due to time constraint of this study. Further work needs to be done to extend this technique for a higher order generator model and to include generating unit controls. A future research in the parameter identification regarding the role of intentional disturbance to the quality of the identified parameters would be great help in providing guidance for practical implementation.

In the evaluation stage, the type of fault applied in the studies is only the faults at bus and the responses of internal part consider only the swing curves of the internal generators. Therefore, the future study could be expanded to other kinds of faults (e.g. line removal) and other internal responses (e.g. voltages at bus and power flows in transmission line) so that it would provide a better assessment of the effectiveness of the reduced system constructed by the proposed method. In addition, a further study investigating the effect of more complex system which includes generating unit controls (e.g. excitation system, turbine-governor system, and power system stabilizer) would be recommended.

APPENDIX A: RESULTS OF CHAPTER 6

A.1 Case study 1.1

Table A1.1 Equivalent transmission lines for the reduced system of case study 1.1 (scenario 1)

From Bus –To Bus	R (p.u.)	X (p.u.)	B (p.u.)
26 – 40 (Geq1)	0.0013	0.0465	0
16 – 41(Geq3)	0.0013	0.0290	0
16 – 42 (Geq2)	0	0.0260	0

Table A1.2 Equivalent shunts for the reduced system of case study 1.1 (scenario 1)

Bus	G (p.u.)	B (p.u.)
16	6.385617	3.016970
26	1.818569	1.643307
40	2.793009	-0.294296
41	5.226109	-3.396020
42	2.347352	-0.960231

Table A1.3 Equivalent transmission lines for the reduced system of case study 1.1 (scenario 2)

From Bus –To Bus	R (p.u.)	X (p.u.)	B (p.u.)
16 – 40 (Geq2)	0.7246	0.00031	0.01369
26 – 38 (Geq1)	0	0.00124	0.04648

Table A1.4 Equivalent shunts for the reduced system of case study 1.1 (scenario 2)

Bus	G (p.u.)	B (p.u.)
16	6.32450	3.13290
26	1.81870	1.64340
38	2.7930	1.0000
40	7.47820	-4.47830

Table A1.5 Identified parameters of the reduced system A of the case study 1.1

Equivalent Parameters	Fictitious Generator1		Fictitious Generator2	
	X'_d (p.u.)	H (kWs/kVA)	X'_d (p.u.)	H (kWs/kVA)
Initial values	0.050	100.00	0.100	50.00
Identified values	0.0933	58.8828	0.0317	168.5065
Computation time	88.25 sec.			
Residual error	0.0012			

Table A1.6 Identified parameters of the reduced system B of the case study 1.1

Equivalent Parameters	Equivalent Generator1		Equivalent Generator2	
	X'_d (p.u.)	H (kWs/kVA)	X'_d (p.u.)	H (kWs/kVA)
Initial values	0.050	50.00	0.040	50.00
Identified values	0.0562	35.0032	0.0152	105.1759
Computation time	5.73 sec.		37.27 sec.	
Residual error	0.00000055		0.0047	

Table A1.7 Identified parameter of the reduced system C of the case study 1.1

Equivalent Parameters	Equivalent Generator1		Equivalent Generator2		Equivalent Generator3	
	X'_d (p.u.)	H (kWs/kVA)	X'_d (p.u.)	H (kWs/kVA)	X'_d (p.u.)	H (kWs/kVA)
Initial values	0.050	50.00	0.050	50.00	0.050	50.00
Identified values	0.0562	35.0032	0.0240	64.2897	0.0557	51.2113
Computation time	5.73 sec.		8.16 sec.		8.22 sec.	
Residual error	0.00000055		0.00006		0.00035	

Table A1.8 Identified parameters of the reduced system D of the case study 1.1

Equivalent Parameters	Equivalent Generator1		Equivalent Generator2	
	X'_d (p.u.)	H(kWs/kVA)	X'_d (p.u.)	H(kWs/kVA)
Initial values	0.050	50.00	0.040	50.00
Identified values	0.0458	36.4267	0.0151	118.3054
Computation time	104.40 sec.			
Residual error	0.00077			

Table A1.9 Identified parameters of the reduced system E of the case study 1.1

Equivalent Parameters	Equivalent Generator1		Equivalent Generator2		Equivalent Generator3	
	X'_d (p.u.)	H (kWs/kVA)	X'_d (p.u.)	H (kWs/kVA)	X'_d (p.u.)	H (kWs/kVA)
Initial values	0.050	50.00	0.050	50.00	0.050	50.00
Identified values	0.0516	36.9102	0.0142	75.6303	0.0584	43.2374
Computation time	197.90 sec.					
Residual error	0.00028					

Table A1.10 Comparison of load flow of the case study 1.1 (the reduced system based on the loose coherent groups).

Bus	Original system voltage		Reduced system voltage			
	Magnitude (p.u.)	Angle (deg.)	Magnitude (p.u.)	Angle (deg.)	$\lvert\Delta V\rvert$ (p.u.)	$\lvert\Delta\theta\rvert$ (p.u.)
1	1.0474	-8.428	1.0474	-8.4288	0	0.0008
2	1.0487	-5.7419	1.0487	-5.7426	0	0.0007
3	1.0302	-8.5867	1.0302	-8.5875	0	0.0008
4	1.0039	-9.5968	1.0038	-9.5975	0.0001	0.0007
5	1.0053	-8.6038	1.0053	-8.6044	0	0.0006
6	1.0077	-7.942	1.0077	-7.9426	0	0.0006
7	0.997	-10.1159	0.997	-10.1165	0	0.0006
8	0.996	-10.6073	0.996	-10.6079	0	0.0006
9	1.0282	-10.3128	1.0282	-10.3135	0	0.0007
10	1.0172	-5.4182	1.0171	-5.4188	0.0001	0.0006
11	1.0127	-6.2757	1.0127	-6.2763	0	0.0006
12	1.0002	-6.2347	1.0001	-6.2353	0.0001	0.0006
13	1.0143	-6.0884	1.0143	-6.089	0	0.0006
14	1.0117	-7.646	1.0117	-7.6467	0	0.0007
15	1.0154	-7.7224	1.0153	-7.7233	0.0001	0.0009
16	1.0318	-6.1725	1.0317	-6.1733	0.0001	0.0008
17	1.0336	-7.2874	1.0335	-7.2882	0.0001	0.0008
18	1.0309	-8.2107	1.0309	-8.2115	0	0.0008
19	1.0499	-1.0077				
20	0.9912	-1.9996				
21	1.0318	-3.7636				
22	1.0498	0.6873				
23	1.0448	0.4903				
24	1.0373	-6.0521				
25	1.0576	-4.3513	1.0576	-4.352	0	0.0007
26	1.0521	-5.5137	1.0521	-5.5144	0	0.0007
27	1.0377	-7.482	1.0377	-7.4828	0	0.0008
28	1.0501	-2.0019				
29	1.0499	0.7574				
30	1.0475	-3.3221	1.0475	-3.3228	0	0.0007
31	0.982	0	0.982	0	0	0
32	0.9831	2.5779	0.9831	2.5774	0	0.0005
33	0.9972	4.2098				
34	1.0123	3.1901				
35	1.0493	5.649				
36	1.0635	8.3432				
37	1.0278	2.4332	1.0278	2.4325	0	0.0007
38	1.0265	7.8208				
39	1.03	-10.043	1.03	-10.0438	0	0.0008

Table A1.11Comparison of load flow of the case study 1.1(the reduced system based on the tight coherent groups).

Bus	Original system voltage		Reduced system voltage			
	Magnitude (p.u.)	Angle (deg.)	Magnitude (p.u.)	Angle (deg.)	$\lvert\Delta V\rvert$ (p.u.)	$\lvert\Delta\theta\rvert$ (p.u.)
1	1.0474	-8.428	1.0474	-8.4249	0	0.0031
2	1.0487	-5.7419	1.0487	-5.7384	0	0.0035
3	1.0302	-8.5867	1.0302	-8.583	0	0.0037
4	1.0039	-9.5968	1.0039	-9.5936	0	0.0032
5	1.0053	-8.6038	1.0053	-8.6012	0	0.0026
6	1.0077	-7.942	1.0077	-7.9395	0	0.0025
7	0.997	-10.1159	0.997	-10.1133	0	0.0026
8	0.996	-10.6073	0.996	-10.6047	0	0.0026
9	1.0282	-10.3128	1.0282	-10.31	0	0.0028
10	1.0172	-5.4182	1.0172	-5.4153	0	0.0029
11	1.0127	-6.2757	1.0127	-6.273	0	0.0027
12	1.0002	-6.2347	1.0002	-6.2318	0	0.0029
13	1.0143	-6.0884	1.0143	-6.0853	0	0.0031
14	1.0117	-7.646	1.0117	-7.6426	0	0.0034
15	1.0154	-7.7224	1.0154	-7.7178	0	0.0046
16	1.0318	-6.1725	1.0318	-6.1674	0	0.0051
17	1.0336	-7.2874	1.0335	-7.2829	0.0001	0.0045
18	1.0309	-8.2107	1.0309	-8.2065	0	0.0042
19	1.0499	-1.0077				
20	0.9912	-1.9996				
21	1.0318	-3.7636				
22	1.0498	0.6873				
23	1.0448	0.4903				
24	1.0373	-6.0521				
25	1.0576	-4.3513	1.0575	-4.3474	0.0001	0.0039
26	1.0521	-5.5137	1.052	-5.51	0.0001	0.0037
27	1.0377	-7.482	1.0377	-7.4781	0	0.0039
28	1.0501	-2.0019				
29	1.0499	0.7574				
30	1.0475	-3.3221	1.0475	-3.3186	0	0.0035
31	0.982	0	0.982	0	0	0
32	0.9831	2.5779	0.9831	2.5808	0	0.0029
33	0.9972	4.2098				
34	1.0123	3.1901				
35	1.0493	5.649				
36	1.0635	8.3432				
37	1.0278	2.4332	1.0278	2.4372	0	0.004
38	1.0265	7.8208				
39	1.03	-10.043	1.03	-10.04	0	0.003

Table A1.12 Comparison of load flow of the case study 1.1 (the reduced system based on the fictitious generators).

Bus	Original system voltage		Reduced system voltage			
	Magnitude (p.u.)	Angle (deg.)	Magnitude (p.u.)	Angle (deg.)	$\lvert\Delta V\rvert$ (p.u.)	$\lvert\Delta\theta\rvert$ (p.u.)
1	1.0474	-8.428	1.0474	-8.4283	0	0.0003
2	1.0487	-5.7419	1.0487	-5.7423	0	0.0004
3	1.0302	-8.5867	1.0302	-8.587	0	0.0003
4	1.0039	-9.5968	1.0039	-9.597	0	0.0002
5	1.0053	-8.6038	1.0053	-8.604	0	0.0002
6	1.0077	-7.942	1.0077	-7.9422	0	0.0002
7	0.997	-10.1159	0.997	-10.116	0	0.0001
8	0.996	-10.6073	0.996	-10.6075	0	0.0002
9	1.0282	-10.3128	1.0282	-10.313	0	0.0002
10	1.0172	-5.4182	1.0172	-5.4185	0	0.0003
11	1.0127	-6.2757	1.0127	-6.276	0	0.0003
12	1.0002	-6.2347	1.0002	-6.235	0	0.0003
13	1.0143	-6.0884	1.0143	-6.0886	0	0.0002
14	1.0117	-7.646	1.0117	-7.6463	0	0.0003
15	1.0154	-7.7224	1.0154	-7.7229	0	0.0005
16	1.0318	-6.1725	1.0318	-6.1731	0	0.0006
17	1.0336	-7.2874	1.0336	-7.2879	0	0.0005
18	1.0309	-8.2107	1.0309	-8.2111	0	0.0004
19	1.0499	-1.0077				
20	0.9912	-1.9996				
21	1.0318	-3.7636				
22	1.0498	0.6873				
23	1.0448	0.4903				
24	1.0373	-6.0521				
25	1.0576	-4.3513	1.0576	-4.3517	0	0.0004
26	1.0521	-5.5137	1.0521	-5.5143	0	0.0006
27	1.0377	-7.482	1.0378	-7.4825	-0.0001	0.0005
28	1.0501	-2.0019				
29	1.0499	0.7574				
30	1.0475	-3.3221	1.0475	-3.3225	0	0.0004
31	0.982	0	0.982	0	0	0
32	0.9831	2.5779	0.9831	2.5776	0	0.0003
33	0.9972	4.2098				
34	1.0123	3.1901				
35	1.0493	5.649				
36	1.0635	8.3432				
37	1.0278	2.4332	1.0278	2.4327	0	0.0005
38	1.0265	7.8208				
39	1.03	-10.043	1.03	-10.0433	0	0.0003

Table A1.13 the highest values of the maximum rotor angle difference of the internal generators for the reduced systems A, B, C, D, and E of the case study 1.1

bus	Highest value of the maximum rotor angle difference (degree)									
	Reduced system A		Reduced system B		Reduced system C		Reduced system D		Reduced system E	
	Small fault	Large fault	Small fault	Large fault	Small fault	Large fault	Small fault	Large fault	Small fault	Large fault
1	0.0089	6.4355	0.009	2.1922	0.0113	1.3606	0.0064	1.5288	0.0092	0.794
2	0.023	18.1773	0.0322	5.0488	0.0207	3.8892	0.0227	3.5115	0.0158	1.8895
3	0.015	20.1821	0.0261	5.4103	0.0191	4.6922	0.0208	3.9288	0.0143	2.5456
4	0.0162	17.5197	0.0252	5.505	0.0181	3.9348	0.021	3.9016	0.0153	2.5368
5	0.0187	15.3909	0.0271	5.4951	0.0181	3.7333	0.023	3.8312	0.0168	2.4045
6	0.0206	15.4685	0.0288	5.5667	0.0187	3.7634	0.0245	3.9199	0.0174	2.4299
7	0.0182	12.415	0.0232	4.8136	0.0165	3.2166	0.0204	3.3891	0.0159	2.0447
8	0.0182	12.5829	0.0214	4.8921	0.0157	3.2729	0.019	3.4512	0.0153	2.074
9	0.0102	6.1359	0.0076	2.8221	0.0114	1.5163	0.0066	2.0564	0.0095	1.0308
10	0.0267	15.4506	0.0349	5.2822	0.0214	3.5772	0.0289	3.6862	0.019	2.3248
11	0.0243	14.8661	0.0327	5.2181	0.0203	3.5374	0.0272	3.6384	0.0184	2.288
12	0.0225	7.4273	0.0317	3.0435	0.0201	1.8353	0.0263	2.2494	0.0179	1.2076
13	0.0225	15.4236	0.0327	5.0755	0.0208	3.5221	0.0269	3.5207	0.0179	2.2981
14	0.0157	17.934	0.0283	5.3323	0.0195	4.138	0.0231	3.8299	0.0156	2.5957
15	0.0145	21.7863	0.0285	5.7626	0.0231	6.0894	0.0221	3.9897	0.0127	4.3597
16	0.0171	31.4681	0.0337	6.586	0.0263	11.3919	0.0254	4.6104	0.0134	9.1208
17	0.0152	25.7821	0.0273	5.5424	0.0241	6.7425	0.0221	4.0646	0.0128	4.5265
18	0.014	21.2848	0.0256	5.2038	0.0219	5.3649	0.021	3.7806	0.0131	3.1291
25	0.0237	16.6657	0.0343	4.771	0.0217	3.5939	0.0241	2.3815	0.0167	1.1716
26	0.0191	21.0731	0.0413	7.022	0.0271	3.4457	0.0206	3.325	0.0171	1.5357
27	0.0153	19.6115	0.0288	4.7898	0.0243	4.2321	0.0201	2.7141	0.0141	1.6064
30	0.0357	9.9049	0.04	3.1815	0.024	2.1544	0.0293	2.1958	0.0183	1.1339
31	0.0506	7.8203	0.0471	3.9862	0.0261	2.367	0.0401	2.7321	0.0248	1.5065
32	0.0559	9.5609	0.0521	4.328	0.0285	2.5883	0.0435	3.0816	0.0259	1.6684
37	0.0487	9.1457	0.0452	3.3012	0.0258	2.0494	0.0301	1.9191	0.0191	0.9037
39	0.0086	6.904	0.0143	2.3122	0.0215	1.0024	0.009	1.7235	0.0095	0.9966

A.2 Case study 1.2

Table A2.1 Identified parameters of the 4-th order equivalent generators

Parameter	Initial values	Identified values		
		Equivalent generator 1	Equivalent generator 2	Equivalent generator 3
Leakage reactance (X_l), p.u.	0.005	0.0307	0.0220	0.0051
Armature resistance (r_a), p.u.	0.005	0.0307	0.0144	0.0055
d-axis synchronous reactance (X_d), p.u.	0.050	0.3183	0.1470	0.1587
d-axis transient reactance (X'_d), p.u.	0.050	0.0500	0.0346	0.0215
d-axis open circuit transient time constant (T'_{do}), p.u.	5.000	4.6283	5.1815	5.0854
q-axis synchronous reactance (X_q), p.u.	0.050	0.2975	0.2148	0.0576
q-axis transient reactance (X'_q), p.u.	0.050	0.0306	0.0490	0.0853
q-axis open circuit transient time constant (T'_{qo}), p.u.	0.500	0.4841	0.9636	0.7407
Inertia constant (H), kWs/kVA	50.00	49.8646	71.6645	48.9040
Damping coefficient (D), p.u.	0.500	0.6680	0.5911	0.5973

Table A2.2 Identified parameters of the 3-rd order equivalent generators

Parameter	Initial values	Identified values		
		Equivalent generator 1	Equivalent generator 2	Equivalent generator 3
Leakage reactance (X_l), p.u.	0.005	0.0302	0.0219	0.0103
Armature resistance (r_a), p.u.	0.005	0.0331	0.00047	0.0051
d-axis synchronous reactance (X_d), p.u.	0.050	0.4764	0.1711	0.0995
d-axis transient reactance (X'_d), p.u.	0.050	0.0473	0.0448	0.0197
d-axis open circuit transient time constant (T'_{do}), p.u.	5.000	4.3079	4.8805	4.9285
q-axis synchronous reactance (X_q), p.u.	0.050	0.0519	0.0946	0.0858
Inertia constant (H), kWs/kVA	50.00	48.7943	52.3164	52.7267
Damping coefficient (D), p.u.	0.500	0.3474	0.6136	0.5254

Table A2.3 Identified parameters of the 2-nd order equivalent generators

Parameter	Initial values	Identified values		
		Equivalent generator 1	Equivalent generator 2	Equivalent generator 3
Leakage reactance (X_l), p.u.	0.005	0.0110	0.0350	0.0052
Armature resistance (r_a), p.u.	0.005	0.0362	0.0014	0.0131
d-axis transient reactance (X'_d), p.u.	0.050	0.0505	0.0436	0.0938
Inertia constant (H), kWs/kVA	50.00	47.0053	64.9797	31.6289
Damping coefficient (D), p.u.	0.500	4.9297	2.1847	2.0097

Table A2.4 Highest values of the maximum rotor angle difference of the internal generators for the reduced system 4th order, 3rd order, and 2nd order of the case study 1.2

Bus	Highest value of the maximum rotor angle difference (degree)					
	Reduced system 4th		Reduced system 3rd		Reduced system 2nd	
	Small fault	Large fault	Small fault	Large fault	Small fault	Large fault
1	0.0099	1.0493	0.0131	1.2831	0.0222	1.8834
2	0.0149	3.3801	0.0174	3.9843	0.0422	5.6765
3	0.0148	3.659	0.0145	3.6275	0.0439	7.0366
4	0.0151	2.5745	0.0143	2.3473	0.0411	5.4488
5	0.0153	1.8727	0.0148	1.6967	0.04	4.3373
6	0.0157	1.7971	0.0152	1.6617	0.0409	4.259
7	0.0145	1.4463	0.0146	1.2708	0.0382	3.4848
8	0.0141	1.4839	0.0144	1.2961	0.037	3.6176
9	0.0095	0.6976	0.0125	0.7941	0.0252	2.2311
10	0.0169	1.8149	0.0165	1.555	0.0436	4.2262
11	0.0165	1.7305	0.016	1.5154	0.0426	4.0582
12	0.0163	0.7912	0.0158	0.8086	0.0417	2.2267
13	0.0165	1.8939	0.0161	1.6553	0.0426	4.3858
14	0.0157	2.5625	0.0153	2.3874	0.042	5.872
15	0.0153	4.0407	0.0158	4.8192	0.0459	10.3699
16	0.0153	7.4384	0.0163	11.8412	0.0489	19.3972
17	0.015	5.7373	0.0145	6.502	0.0517	11.8399
18	0.0149	4.1624	0.0143	4.2962	0.0493	8.5253
25	0.0147	3.2872	0.0174	4.8068	0.0485	5.4834
26	0.0154	8.1173	0.0195	11.3271	0.0671	7.9858
27	0.0148	4.5122	0.0165	6.3008	0.0617	6.7845
30	0.0176	-	0.0206	-	0.0467	-
31	0.0191	1.8035	0.02	1.8304	0.047	4.1925
32	0.02	0.9335	0.0204	0.8123	0.049	2.0185
37	0.016	1.5687	0.0204	2.0509	0.0444	2.6804
39	0.0092	1.8425	0.0113	2.0592	0.0351	8.766

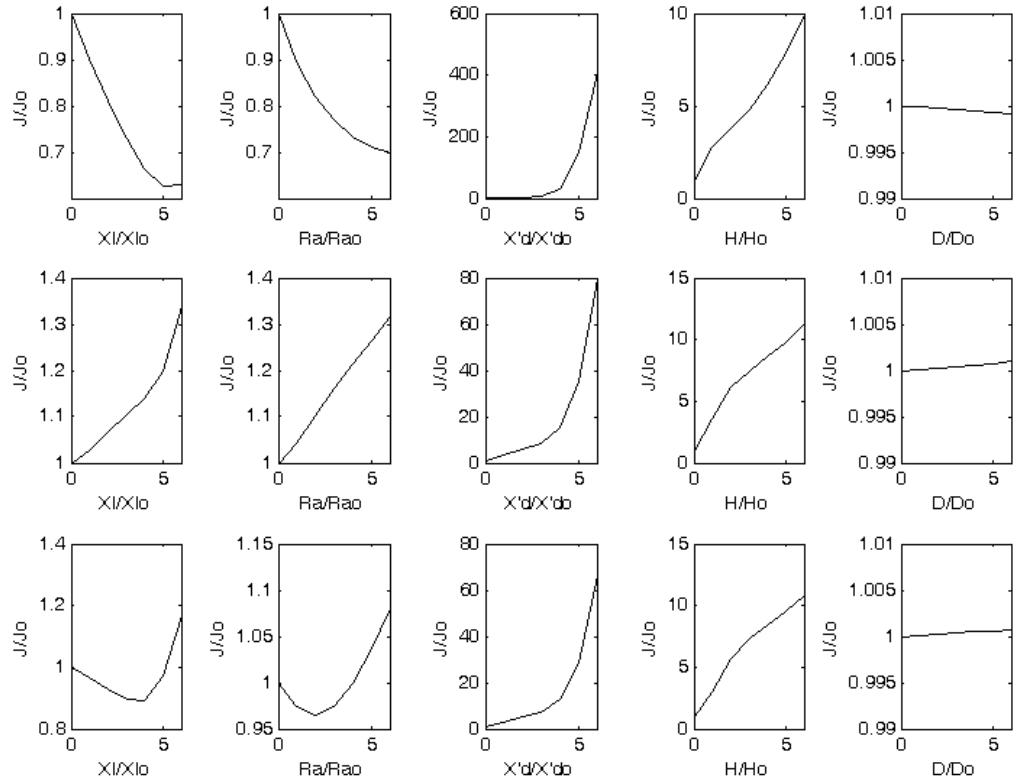

Figure A2.1 Cost function sensitivity of the reduced system based on the second order equivalent generator model

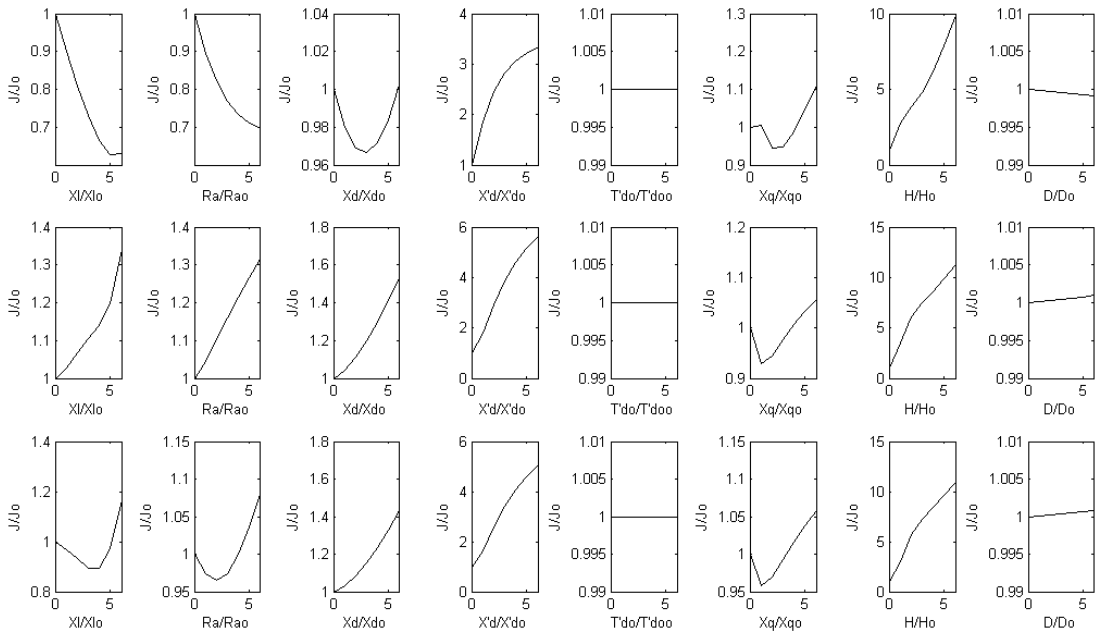

Figure A2.2 Cost function sensitivity of the reduced system based on the third order equivalent generator model

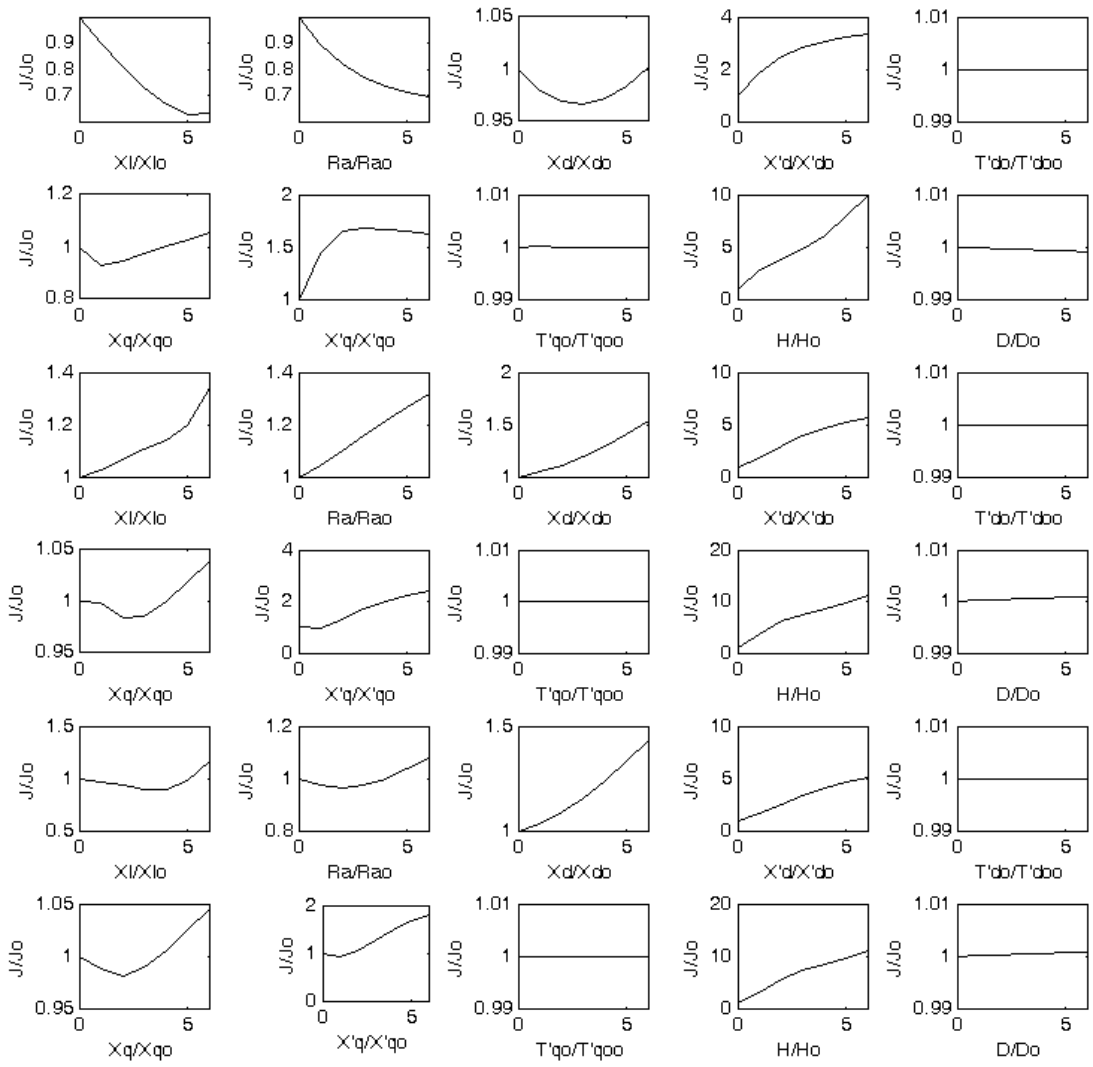

Figure A2.3 Cost function sensitivity of the reduced system based on the fourth order equivalent generator model

A.3 Case study 2

Table A3.1 Identified parameters of the external equivalent generators for the scenario A

Area	Computation time (sec.)	Equivalent generator	Coherent generators	Initial values		Identified values	
				X'_d (p.u.)	H (kWs/kVA)	X'_d (p.u.)	H (kWs/kVA)
1	12.75	1	(G1-G3)	0.05	25	0.0418	20.8640
		2	(G4-G5)	0.05	25	0.0616	26.3781
		3	(G6-G7)	0.05	25	0.0626	25.3138
		4	(G2)	0.05	25	0.0501	24.1189
2	29.58	1	(G16-G19)	0.05	50	0.0651	25.5852
		2	(G17-G18)	0.05	50	0.0691	43.8646
		3	(G20)	0.01	50	0.0978	23.5781

Table A3.2 Identified parameters of the external equivalent generators for the scenarios B and D

Area	Computation time (sec.)	Equivalent generator	Coherent generators	Initial values		Identified values	
				X'_d (p.u.)	H (kWs/kVA)	X'_d (p.u.)	H (kWs/kVA)
1	13.81	1	(G1-G2-G3)	0.05	25	0.0455	29.3182
		2	(G4-G5-G6-G7)	0.05	25	0.0615	46.9025
2	13.88	1	(G16-G17-G18-G19)	0.10	50	0.1303	52.9579
		2	(G20)	0.05	25	0.0862	28.1599

Table A3.3 Identified parameters of the external equivalent generators for the scenario C

Area	Computation time (sec.)	Equivalent generator	Coherent generators	Initial values		Identified values	
				X'_d (p.u.)	H (kWs/kVA)	X'_d (p.u.)	H (kWs/kVA)
1	10.23	1	(G1-G2-G3)	0.05	25	0.0461	28.3679
		2	(G4-G5-G6-G7)	0.05	25	0.0649	44.5425
2	13.73	1	(G16-G17-G18-G19)	0.10	50	0.1179	52.4611
		2	(G20)	0.05	25	0.1050	27.7864

Table A3.4 Identified parameters of the external equivalent generators for the scenario E

Area	Computation time (sec.)	Equivalent generator	Coherent generators	Initial values		Identified values	
				X'_d p.u.	H (kWs/kVA)	X'_d p.u.	H (kWs/kVA)
1	26.55	1	(G1-G2-G3)	0.05	25	0.0722	32.1784
		2	(G4-G5)	0.05	25	0.0265	24.9833
		3	(G6)	0.05	25	0.0354	16.3166
		4	(G7)	0.05	25	0.1141	17.9194
2	15.22	1	(G16-G17-G19)	0.01	50	0.0131	49.6189
		2	(G18)	0.05	25	0.0102	19.2473
		3	(G20)	0.05	25	0.0060	28.6855

Table A3.5 Identified parameters of the external equivalent generators for the scenario F

Area	Computation time (sec.)	Equivalent generator	Coherent generators	Initial values		Identified values	
				X'_d p.u.	H (kWs/kVA)	X'_d p.u.	H (kWs/kVA)
1	14.30	1	(G1-G2-G3)	0.05	25	0.0725	40.1203
		2	(G4-G5-G6-G7)	0.05	25	0.0522	45.2289
2	14.02	1	(G16-G17-G18-G19)	0.10	50	0.1458	56.9878
		2	(G20)	0.05	25	0.0710	28.5453

Table A3.6 Comparison of load flow of the case study 2 (the reduced system based on tight coherent groups of the first system condition).

Bus	Original system voltage		Reduced system voltage			
	Magnitude (p.u.)	Angle (deg.)	Magnitude (p.u.)	Angle (deg.)	$\lvert\Delta V\rvert$ (p.u.)	$\lvert\Delta\theta\rvert$ (p.u.)
24	0.992	-8.2335	0.9919	-8.2325	0.0001	0.001
33	0.9716	-18.1272	0.9716	-18.1282	0	0.001
34	0.986	-17.3372	0.986	-17.3376	0	0.0004
35	0.9807	-17.7564	0.9807	-17.7567	0	0.0003
36	0.98	-17.7535	0.98	-17.7539	0	0.0004
37	0.9921	-16.858	0.9921	-16.8583	0	0.0003
38	0.9633	-12.0945	0.9633	-12.0947	0	0.0002
39	0.9708	-19.4704	0.9708	-19.4708	0	0.0004
40	0.97	-20.1015	0.97	-20.1018	0	0.0003
41	0.9667	-20.2036	0.9667	-20.2038	0	0.0002
42	0.985	-17.6661	0.985	-17.6662	0	0.0001
43	0.9787	-17.5131	0.9787	-17.5133	0	0.0002
44	0.9853	-15.2186	0.9853	-15.2187	0	0.0001
45	0.9869	-13.4579	0.9869	-13.4579	0	0
46	1.005	-10.7198	1.005	-10.7198	0	0
47	1.0173	-8.5782	1.0173	-8.5782	0	0
48	1.0206	-9.2626	1.0206	-9.2625	0	0.0001
49	1.025	-8.2556	1.025	-8.2556	0	0
50	1.0015	-10.1158	1.0015	-10.1158	0	0
51	0.9676	-12.4909	0.9676	-12.4909	0	0
52	0.9576	-13.3713	0.9576	-13.3712	0	0.0001
53	0.9464	-14.1477	0.9464	-14.1476	0	0.0001
54	0.955	-13.0903	0.955	-13.0903	0	0
55	0.952	-13.5063	0.952	-13.5062	0	0.0001
56	0.9546	-13.2624	0.9546	-13.2623	0	0.0001
57	0.9713	-12.3124	0.9713	-12.3124	0	0
58	0.9597	-13.1149	0.9597	-13.1148	0	0.0001
59	0.985	-10.4092	0.985	-10.4091	0	0.0001
60	0.9932	-6.9483	0.9932	-6.9482	0	0.0001
61	0.995	-6.0573	0.995	-6.0572	0	0.0001
62	0.998	-6.7943	0.998	-6.7942	0	0.0001
63	0.969	-7.2215	0.969	-7.2213	0	0.0002
64	0.9839	-5.5593	0.9839	-5.5592	0	0.0001
65	1.005	-2.5555	1.005	-2.5553	0	0.0002
66	1.05	-3.3052	1.05	-3.3051	0	0.0001
67	1.0198	-5.6895	1.0198	-5.6894	0	0.0001
68	1.0032	-2.6181	1.0032	-2.6178	0	0.0003
69	1.035	0	1.035	0	0	0
70	0.984	-7.1097	0.984	-7.1094	0	0.0003
71	0.9869	-7.4878	0.9868	-7.4874	0.0001	0.0004
72	0.98	-8.419	0.98	-8.4184	0	0.0006
73	0.991	-7.6992	0.991	-7.6988	0	0.0004
74	0.9586	-8.0794	0.9585	-8.079	0.0001	0.0004
75	0.9682	-6.8289	0.9682	-6.8284	0	0.0005
76	0.943	-7.8573	0.943	-7.8566	0	0.0007
77	1.0118	-2.9144	1.0117	-2.9125	0.0001	0.0019
118	0.9499	-7.7688	0.9499	-7.7683	0	0.0005

Table A3.7 Comparison of load flow of the case study 2 (the reduced system based on loose coherent groups of the first system condition).

Bus	Original system voltage		Reduced system voltage			
	Magnitude (p.u.)	Angle (deg.)	Magnitude (p.u.)	Angle (deg.)	$\lvert\Delta V\rvert$ (p.u.)	$\lvert\Delta\theta\rvert$ (p.u.)
24	0.992	-8.2335	0.992	-8.2312	0	0.0023
33	0.9716	-18.1272	0.9716	-18.1244	0	0.0028
34	0.986	-17.3372	0.986	-17.3354	0	0.0018
35	0.9807	-17.7564	0.9807	-17.7546	0	0.0018
36	0.98	-17.7535	0.98	-17.7517	0	0.0018
37	0.9921	-16.858	0.9921	-16.8562	0	0.0018
38	0.9633	-12.0945	0.9633	-12.093	0	0.0015
39	0.9708	-19.4704	0.9708	-19.4687	0	0.0017
40	0.97	-20.1015	0.97	-20.0998	0	0.0017
41	0.9667	-20.2036	0.9667	-20.2019	0	0.0017
42	0.985	-17.6661	0.985	-17.6646	0	0.0015
43	0.9787	-17.5131	0.9787	-17.5114	0	0.0017
44	0.9853	-15.2186	0.9853	-15.2173	0	0.0013
45	0.9869	-13.4579	0.9869	-13.4566	0	0.0013
46	1.005	-10.7198	1.005	-10.7187	0	0.0011
47	1.0173	-8.5782	1.0173	-8.5772	0	0.001
48	1.0206	-9.2626	1.0206	-9.2614	0	0.0012
49	1.025	-8.2556	1.025	-8.2544	0	0.0012
50	1.0015	-10.1158	1.0015	-10.1147	0	0.0011
51	0.9676	-12.4909	0.9676	-12.4897	0	0.0012
52	0.9576	-13.3713	0.9576	-13.3701	0	0.0012
53	0.9464	-14.1477	0.9464	-14.1465	0	0.0012
54	0.955	-13.0903	0.955	-13.0891	0	0.0012
55	0.952	-13.5063	0.952	-13.505	0	0.0013
56	0.9546	-13.2624	0.9546	-13.2611	0	0.0013
57	0.9713	-12.3124	0.9713	-12.3112	0	0.0012
58	0.9597	-13.1149	0.9597	-13.1137	0	0.0012
59	0.985	-10.4092	0.985	-10.4079	0	0.0013
60	0.9932	-6.9483	0.9932	-6.947	0	0.0013
61	0.995	-6.0573	0.995	-6.056	0	0.0013
62	0.998	-6.7943	0.998	-6.7931	0	0.0012
63	0.969	-7.2215	0.969	-7.2202	0	0.0013
64	0.9839	-5.5593	0.9839	-5.5581	0	0.0012
65	1.005	-2.5555	1.005	-2.5542	0	0.0013
66	1.05	-3.3052	1.05	-3.304	0	0.0012
67	1.0198	-5.6895	1.0198	-5.6882	0	0.0013
68	1.0032	-2.6181	1.0032	-2.6167	0	0.0014
69	1.035	0	1.035	0	0	0
70	0.984	-7.1097	0.984	-7.1091	0	0.0006
71	0.9869	-7.4878	0.9868	-7.487	0.0001	0.0008
72	0.98	-8.419	0.98	-8.4175	0	0.0015
73	0.991	-7.6992	0.991	-7.6984	0	0.0008
74	0.9586	-8.0794	0.9585	-8.0788	0.0001	0.0006
75	0.9682	-6.8289	0.9682	-6.8283	0	0.0006
76	0.943	-7.8573	0.943	-7.8566	0	0.0007
77	1.0118	-2.9144	1.0117	-2.9128	0.0001	0.0016
118	0.9499	-7.7688	0.9499	-7.7682	0	0.0006

Table A3.8: Comparison of load flow of the case study 2 at the second system condition.

Bus	Original system voltage		Reduced system voltage			
	Magnitude (p.u.)	Angle (deg.)	Magnitude (p.u.)	Angle (deg.)	$\lvert\Delta V\rvert$ (p.u.)	$\lvert\Delta\theta\rvert$ (p.u.)
24	0.9977	-0.3542	0.9976	-0.3518	0.0001	0.0024
33	0.9798	-8.3119	0.9798	-8.3084	0	0.0035
34	0.9941	-8.4162	0.9941	-8.4138	0	0.0024
35	0.9894	-8.7914	0.9894	-8.789	0	0.0024
36	0.9888	-8.7876	0.9888	-8.7853	0	0.0023
37	0.9994	-8.0008	0.9994	-7.9985	0	0.0023
38	0.9695	-3.6328	0.9695	-3.631	0	0.0018
39	0.9741	-10.8278	0.9742	-10.8256	0.0001	0.0022
40	0.97	-11.6857	0.97	-11.6836	0	0.0021
41	0.9676	-11.9944	0.9676	-11.9924	0	0.002
42	0.985	-10.3017	0.985	-10.2999	0	0.0018
43	0.99	-9.2379	0.99	-9.2358	0	0.0021
44	0.9974	-8.1708	0.9974	-8.1692	0	0.0016
45	0.9974	-6.9459	0.9974	-6.9445	0	0.0014
46	1.0121	-4.8944	1.0121	-4.8932	0	0.0012
47	1.021	-3.433	1.021	-3.4319	0	0.0011
48	1.0229	-3.3747	1.0229	-3.3734	0	0.0013
49	1.025	-2.391	1.025	-2.3897	0	0.0013
50	1.0041	-4.0213	1.0041	-4.02	0	0.0013
51	0.974	-6.0908	0.974	-6.0895	0	0.0013
52	0.9652	-6.8605	0.9652	-6.8592	0	0.0013
53	0.9548	-7.5085	0.9548	-7.5071	0	0.0014
54	0.9618	-6.537	0.9618	-6.5357	0	0.0013
55	0.9588	-6.8855	0.9588	-6.8842	0	0.0013
56	0.9612	-6.6774	0.9612	-6.6761	0	0.0013
57	0.9767	-5.9006	0.9767	-5.8993	0	0.0013
58	0.9666	-6.6051	0.9666	-6.6038	0	0.0013
59	0.985	-3.9397	0.985	-3.9384	0	0.0013
60	0.9936	-0.9149	0.9936	-0.9135	0	0.0014
61	0.995	-0.114	0.995	-0.1127	0	0.0013
62	0.9989	-0.8061	0.9989	-0.8048	0	0.0013
63	0.9701	-1.2913	0.9701	-1.2899	0	0.0014
64	0.9847	0.0769	0.9847	0.0783	0	0.0014
65	1.005	2.3019	1.005	2.3033	0	0.0014
66	1.05	2.2031	1.05	2.2044	0	0.0013
67	1.0211	0.1151	1.0211	0.1164	0	0.0013
68	1.0016	0.9597	1.0016	0.961	0	0.0013
69	1.035	0	1.035	0	0	0
70	0.9942	-4.0008	0.9941	-4.0001	0.0001	0.0007
71	0.9965	-3.9394	0.9965	-3.9385	0	0.0009
72	0.9888	-2.7373	0.9888	-2.7357	0	0.0016
73	1.0003	-4.1264	1.0003	-4.1256	0	0.0008
74	0.9719	-5.0499	0.9719	-5.0493	0	0.0006
75	0.9798	-4.0021	0.9798	-4.0014	0	0.0007
76	0.9558	-4.2218	0.9558	-4.2209	0	0.0009
77	1.015	1.1099	1.0149	1.1117	0.0001	0.0018
118	0.9629	-4.5114	0.9629	-4.5107	0	0.0007

Table A3.9 Comparison of load flow of the case study 2 at the third system condition (the reduced system based on coherent groups identified at the third system condition).

Bus	Original system voltage		Reduced system voltage			
	Magnitude (p.u.)	Angle (deg.)	Magnitude (p.u.)	Angle (deg.)	$\lvert\Delta V\rvert$ (p.u.)	$\lvert\Delta\theta\rvert$ (p.u.)
24	0.9728	-11.1156	0.9728	-11.1014	0	0.0142
33	0.9479	-23.6348	0.9479	-23.6161	0	0.0187
34	0.9828	-19.2107	0.9829	-19.1954	0.0001	0.0153
35	0.9783	-19.546	0.9783	-19.5308	0	0.0152
36	0.9774	-19.5673	0.9774	-19.552	0	0.0153
37	0.9904	-18.528	0.9905	-18.5128	0.0001	0.0152
38	0.9682	-12.0914	0.9683	-12.0762	0.0001	0.0152
39	0.9703	-20.9328	0.9703	-20.9191	0	0.0137
40	0.97	-21.4399	0.97	-21.4272	0	0.0127
41	0.9666	-21.435	0.9666	-21.4231	0	0.0119
42	0.985	-18.6046	0.985	-18.595	0	0.0096
43	0.9757	-19.0004	0.9757	-18.9878	0	0.0126
44	0.983	-16.1284	0.983	-16.1197	0	0.0087
45	0.9852	-14.1559	0.9852	-14.1486	0	0.0073
46	1.004	-11.2619	1.004	-11.2558	0	0.0061
47	1.0168	-9.0142	1.0168	-9.009	0	0.0052
48	1.0204	-9.7577	1.0204	-9.7517	0	0.006
49	1.025	-8.739	1.025	-8.733	0	0.006
50	1.0015	-10.5863	1.0015	-10.5804	0	0.0059
51	0.9676	-12.9454	0.9676	-12.9395	0	0.0059
52	0.9576	-13.8217	0.9576	-13.8158	0	0.0059
53	0.9464	-14.587	0.9464	-14.5812	0	0.0058
54	0.9551	-13.5216	0.9551	-13.5158	0	0.0058
55	0.952	-13.9321	0.952	-13.9264	0	0.0057
56	0.9546	-13.6903	0.9546	-13.6845	0	0.0058
57	0.9713	-12.7587	0.9713	-12.7528	0	0.0059
58	0.9598	-13.5581	0.9598	-13.5523	0	0.0058
59	0.985	-10.7919	0.985	-10.7863	0	0.0056
60	0.9932	-7.3124	0.9932	-7.3069	0	0.0055
61	0.995	-6.4186	0.995	-6.4131	0	0.0055
62	0.998	-7.1632	0.998	-7.1576	0	0.0056
63	0.969	-7.5811	0.969	-7.5756	0	0.0055
64	0.9839	-5.9063	0.9839	-5.9009	0	0.0054
65	1.005	-2.8678	1.005	-2.8625	0	0.0053
66	1.05	-3.7038	1.05	-3.6982	0	0.0056
67	1.0198	-6.0746	1.0198	-6.069	0	0.0056
68	1.0032	-2.9163	1.0032	-2.9127	0	0.0036
69	1.035	0	1.035	0	0	0
70	0.9774	-7.9259	0.9774	-7.922	0	0.0039
71	0.979	-8.4831	0.979	-8.4783	0	0.0048
72	0.9663	-10.3269	0.9662	-10.3176	0.0001	0.0093
73	0.9832	-8.6978	0.9832	-8.693	0	0.0048
74	0.9542	-8.7007	0.9542	-8.6979	0	0.0028
75	0.9647	-7.3768	0.9647	-7.3743	0	0.0025
76	0.9406	-8.4612	0.9406	-8.4585	0	0.0027
77	1.0113	-3.5708	1.0113	-3.568	0	0.0028
118	0.9469	-8.3459	0.9469	-8.3433	0	0.0026

Table A3.10 Comparison of load flow of the case study 2 at the third system condition (the reduced system based on coherent groups identified at the first system condition).

Bus	Original system voltage		Reduced system voltage			
	Magnitude (p.u.)	Angle (deg.)	Magnitude (p.u.)	Angle (deg.)	$\lvert\Delta V\rvert$ (p.u.)	$\lvert\Delta\theta\rvert$ (p.u.)
24	0.9728	-11.1156	0.9728	-11.1101	0	0.0055
33	0.9479	-23.6348	0.9479	-23.6271	0	0.0077
34	0.9828	-19.2107	0.9828	-19.2059	0	0.0048
35	0.9783	-19.546	0.9783	-19.5414	0	0.0046
36	0.9774	-19.5673	0.9774	-19.5626	0	0.0047
37	0.9904	-18.528	0.9904	-18.5234	0	0.0046
38	0.9682	-12.0914	0.9683	-12.0876	0.0001	0.0038
39	0.9703	-20.9328	0.9703	-20.9286	0	0.0042
40	0.97	-21.4399	0.97	-21.4361	0	0.0038
41	0.9666	-21.435	0.9666	-21.4314	0	0.0077
42	0.985	-18.6046	0.985	-18.6015	0	0.0048
43	0.9757	-19.0004	0.9757	-18.9964	0	0.0046
44	0.983	-16.1284	0.983	-16.1255	0	0.0047
45	0.9852	-14.1559	0.9852	-14.1534	0	0.0046
46	1.004	-11.2619	1.004	-11.2598	0.0001	0.0038
47	1.0168	-9.0142	1.0168	-9.0123	0	0.0042
48	1.0204	-9.7577	1.0204	-9.7555	0	0.0038
49	1.025	-8.739	1.025	-8.7368	0	0.0036
50	1.0015	-10.5863	1.0015	-10.5842	0	0.0031
51	0.9676	-12.9454	0.9676	-12.9432	0	0.004
52	0.9576	-13.8217	0.9576	-13.8195	0	0.0029
53	0.9464	-14.587	0.9464	-14.5849	0	0.0025
54	0.9551	-13.5216	0.9551	-13.5194	0	0.0021
55	0.952	-13.9321	0.952	-13.93	0	0.0019
56	0.9546	-13.6903	0.9546	-13.6882	0	0.0022
57	0.9713	-12.7587	0.9713	-12.7565	0	0.0022
58	0.9598	-13.5581	0.9598	-13.556	0	0.0021
59	0.985	-10.7919	0.985	-10.7898	0	0.0022
60	0.9932	-7.3124	0.9932	-7.3102	0	0.0022
61	0.995	-6.4186	0.995	-6.4164	0	0.0021
62	0.998	-7.1632	0.998	-7.161	0	0.0022
63	0.969	-7.5811	0.969	-7.5789	0	0.0021
64	0.9839	-5.9063	0.9839	-5.9042	0	0.0021
65	1.005	-2.8678	1.005	-2.8657	0	0.0022
66	1.05	-3.7038	1.05	-3.7017	0	0.0021
67	1.0198	-6.0746	1.0198	-6.0725	0	0.0021
68	1.0032	-2.9163	1.0032	-2.9143	0	0.0022
69	1.035	0	1.035	0	0	0.0022
70	0.9774	-7.9259	0.9774	-7.9242	0	0.0022
71	0.979	-8.4831	0.979	-8.4811	0	0.0022
72	0.9663	-10.3269	0.9662	-10.3233	0	0.0021
73	0.9832	-8.6978	0.9832	-8.6958	0	0.0021
74	0.9542	-8.7007	0.9542	-8.6993	0	0.0021
75	0.9647	-7.3768	0.9646	-7.3753	0	0.0021
76	0.9406	-8.4612	0.9406	-8.4593	0	0.002
77	1.0113	-3.5708	1.0112	-3.5676	0	0
118	0.9469	-8.3459	0.9469	-8.3442	0	0.0017

Table A3.11 the highest values of the maximum rotor angle difference of the internal generators for the reduced systems A, B, C, D, E, and F of the case study 2 (small fault).

Bus	Highest value of the maximum rotor angle difference (degree)					
	A	B	C	D	E	F
24	0.02	0.0734	0.0646	0.0915	0.0756	0.1059
33	0.0282	0.1045	0.1032	0.1096	0.1332	0.1467
34	0.0211	0.0977	0.0985	0.1091	0.0912	0.1334
35	0.0206	0.0967	0.0977	0.1081	0.0905	0.132
36	0.0206	0.0965	0.0975	0.1079	0.0905	0.1317
37	0.0213	0.0997	0.1005	0.1113	0.0903	0.1362
38	0.018	0.082	0.0819	0.0908	0.0668	0.109
39	0.0242	0.1291	0.1296	0.1428	0.0851	0.1762
40	0.0287	0.1512	0.151	0.1653	0.1013	0.2065
41	0.0273	0.1469	0.1472	0.1614	0.101	0.1997
42	0.0255	0.1617	0.1534	0.1608	0.1065	0.1946
43	0.0147	0.0813	0.0839	0.0945	0.0713	0.1083
44	0.0097	0.0642	0.0667	0.0781	0.0528	0.0792
45	0.0104	0.0733	0.0655	0.0724	0.0524	0.0694
46	0.0112	0.0785	0.0699	0.0773	0.0544	0.0616
47	0.0113	0.0823	0.0698	0.08	0.0587	0.0549
48	0.0125	0.0934	0.0841	0.0828	0.0626	0.0758
49	0.013	0.0978	0.0884	0.0845	0.0654	0.0799
50	0.012	0.0927	0.0836	0.0806	0.064	0.0743
51	0.0108	0.0853	0.077	0.075	0.0622	0.0668
52	0.0104	0.0828	0.0748	0.073	0.0613	0.0644
53	0.0099	0.0806	0.0727	0.0712	0.0622	0.0616
54	0.0102	0.0839	0.0755	0.0736	0.0662	0.0631
55	0.01	0.0833	0.0748	0.073	0.0669	0.0622
56	0.0101	0.0839	0.0754	0.0735	0.0668	0.0628
57	0.0107	0.0865	0.0778	0.0757	0.0645	0.0668
58	0.0104	0.0839	0.0756	0.0737	0.0635	0.0644
59	0.0104	0.0959	0.0846	0.0805	0.0863	0.0676
60	0.0109	0.0927	0.0805	0.0814	0.0891	0.0671
61	0.0112	0.0933	0.081	0.0818	0.0909	0.0679
62	0.0106	0.0912	0.079	0.0818	0.0859	0.0662
63	0.0093	0.0789	0.0671	0.0741	0.0751	0.0547
64	0.0093	0.0801	0.0655	0.0744	0.0713	0.0505
65	0.0098	0.0774	0.0623	0.0699	0.0454	0.0477
66	0.0115	0.0937	0.0779	0.088	0.0789	0.0682
67	0.0104	0.0892	0.0773	0.0843	0.0795	0.0658
68	0.0133	0.0783	0.0655	0.0715	0.0423	0.0537
69	0.0207	0.1197	0.1351	0.1374	0.0894	0.1221
70	0.0176	0.0743	0.0821	0.0845	0.0637	0.0639
71	0.0179	0.0721	0.0772	0.08	0.0635	0.0604
72	0.0185	0.0647	0.0525	0.074	0.0653	0.0674
73	0.0181	0.073	0.0773	0.08	0.0636	0.0599
74	0.018	0.0815	0.0779	0.08	0.0595	0.0696
75	0.0185	0.0846	0.0819	0.0833	0.061	0.0787
76	0.0203	0.0943	0.0866	0.0901	0.0622	0.0852
77	0.0249	0.1476	0.1376	0.1288	0.091	0.1453
118	0.0192	0.0886	0.0811	0.0857	0.0596	0.0787

Table A3.12 the highest values of the maximum rotor angle difference of the internal generators for the reduced systems A, B, C, D, E, and F of the case study 2 (large fault).

Bus	Highest value of the maximum rotor angle difference (degree)					
	A	B	C	D	E	F
24	1.8271	2.7748	3.0176	2.7189	3.4553	2.7283
33	0.4403	3.7959	3.5144	3.3828	1.5046	3.7604
34	0.8097	6.6736	6.2244	6.0522	3.5915	7.3852
35	0.5993	4.7575	4.4769	4.3724	2.6247	5.4567
36	0.6173	4.8833	4.5933	4.4996	2.7376	5.6384
37	0.912	7.8467	7.2957	7.1042	4.0686	8.3871
38	1.266	7.3679	6.7365	6.4883	4.9401	8.0035
39	0.4797	3.3771	3.5085	3.523	1.9832	4.3069
40	0.486	3.5699	3.4603	3.3515	2.1106	4.0873
41	0.4494	2.2726	2.588	2.5271	1.8045	3.2479
42	0.5578	2.3451	2.1109	2.0198	2.9795	3.5794
43	0.2729	1.2953	1.2531	1.2812	1.1031	1.7187
44	0.3154	0.5978	0.6209	0.5964	1.0205	0.9616
45	0.4719	0.9711	0.7045	0.6163	1.241	1.3722
46	0.5795	1.3246	0.8345	0.758	1.2711	1.8244
47	1.0045	2.6759	1.6753	1.482	1.735	3.5058
48	0.7739	2.0085	1.3682	1.2463	1.6773	2.799
49	2.2613	4.9568	3.1205	3.1116	5.9711	7.2693
50	0.6149	1.3696	1.0159	0.902	1.3739	2.0314
51	0.5384	0.8258	0.6867	0.6664	1.3575	1.3206
52	0.3938	0.6266	0.5732	0.5883	1.0795	0.7972
53	0.3897	0.7601	0.7608	0.7746	1.2178	0.934
54	1.0403	1.6228	1.507	1.5284	2.739	2.0352
55	0.8857	1.391	1.3327	1.3537	2.3788	1.747
56	1.0488	1.6044	1.4828	1.5039	2.7197	2.0443
57	0.484	0.7155	0.6207	0.5815	1.19	1.158
58	0.4958	0.745	0.6436	0.6616	1.2742	1.0795
59	1.5397	2.355	2.4995	2.2559	3.9372	2.9246
60	1.4411	1.7797	1.9267	1.5345	2.8388	2.614
61	1.8321	2.2528	2.5289	2.0199	3.6158	3.1486
62	1.2837	1.5937	1.6397	1.3062	2.3544	2.6064
63	1.7056	2.1643	2.3513	2.0061	3.4847	2.7182
64	2.4544	2.8707	3.1706	2.4886	3.7753	4.5968
65	5.4946	9.8276	6.453	8.055	5.231	13.05
66	2.9943	5.4192	3.4421	3.3151	6.1662	7.8445
67	0.7614	1.2853	1.0259	0.8594	1.2505	1.9154
68	8.4036	14.3686	-	-	9.1135	14.0235
69	6.5057	11.9593	12.8108	-	11.6316	18.9735
70	2.216	4.8652	3.835	3.9666	2.794	5.169
71	1.4994	3.3471	2.6153	2.5425	2.1836	3.6076
72	0.8311	1.3917	1.1808	1.0031	1.6387	1.6591
73	0.9944	2.4205	1.8064	1.6736	1.5682	2.6287
74	2.221	4.9356	3.9581	4.1256	2.1558	5.0602
75	3.4643	6.8689	5.497	6.982	3.0081	7.0136
76	2.7305	5.4376	4.403	4.9158	2.2142	5.3142
77	12.5938	-	-	-	11.7954	-
118	2.6887	5.5629	4.4987	5.0096	2.3194	5.5431

APPENDIX B: TEST SYSTEMS

B.1 IEEE 39 bus system

1. Single line diagram of the system

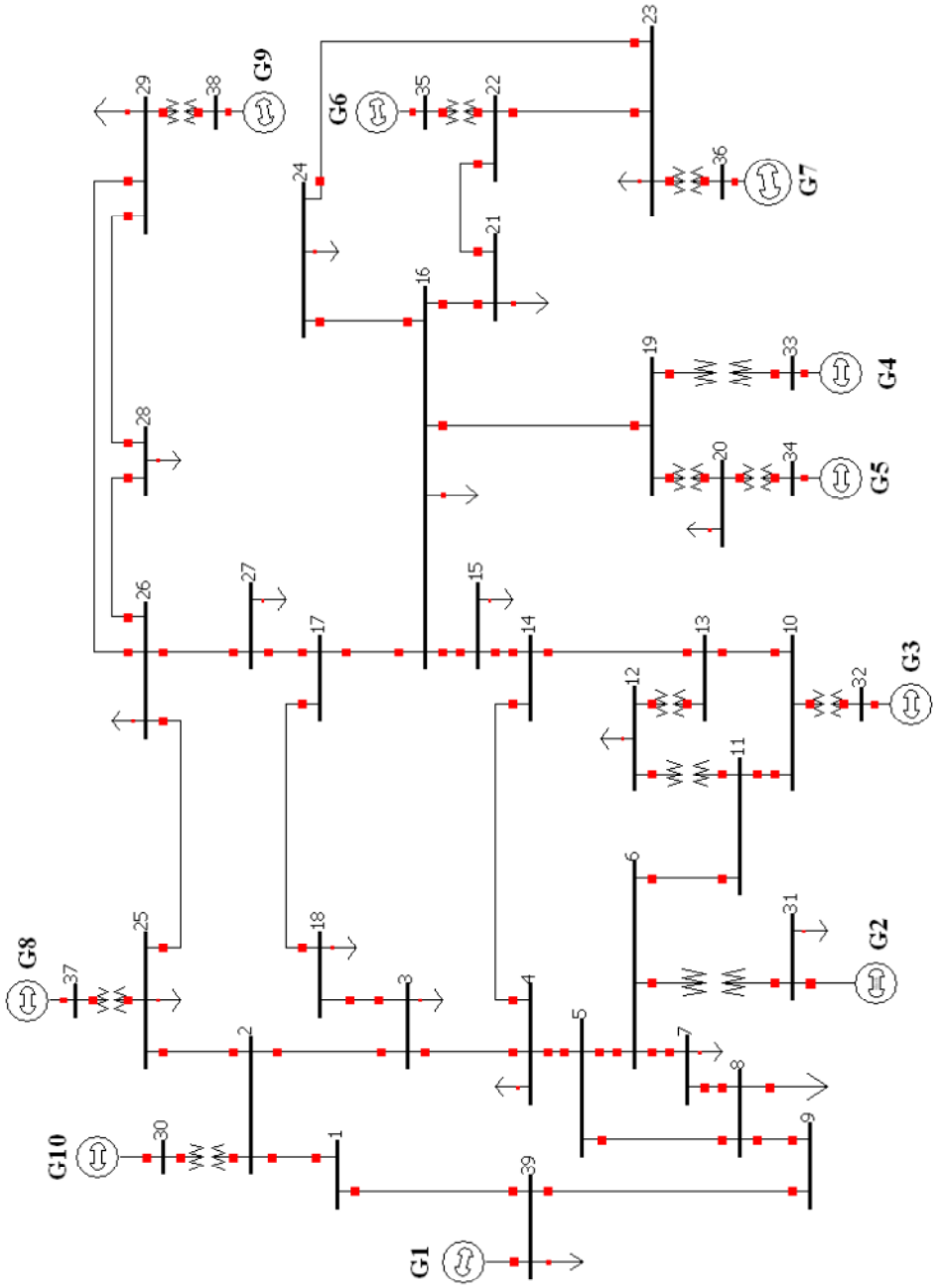

2. System data

Table B.1 Bus data and power flow results

Bus No.	Bus voltage		Generation		Load	
	Magnitude (p.u.)	angle (deg.)	Real (MW)	Reactive (MVAR)	Real (MW)	Reactive (MVAR)
1	1.0474	-8.4280	0	0	0	0
2	1.0487	-5.7419	0	0	0	0
3	1.0302	-8.5867	0	0	322	2.4
4	1.0039	-9.5968	0	0	500	184
5	1.0053	-8.6038	0	0	0	0
6	1.0077	-7.9420	0	0	0	0
7	0.9970	-10.1159	0	0	233.8	84
8	0.9960	-10.6073	0	0	522	176
9	1.0282	-10.3128	0	0	0	0
10	1.0172	-5.4182	0	0	0	0
11	1.0127	-6.2757	0	0	0	0
12	1.0002	-6.2347	0	0	7.5	88
13	1.0143	-6.0884	0	0	0	0
14	1.0117	-7.6460	0	0	0	0
15	1.0154	-7.7224	0	0	320	153
16	1.0318	-6.1725	0	0	329	32.3
17	1.0336	-7.2874	0	0	0	0
18	1.0309	-8.2107	0	0	158	30
19	1.0499	-1.0077	0	0	0	0
20	0.9912	-1.9996	0	0	628	103
21	1.0318	-3.7636	0	0	274	115
22	1.0498	0.6873	0	0	0	0
23	1.0448	0.4903	0	0	247	84.6
24	1.0373	-6.0521	0	0	308.6	-92.2
25	1.0576	-4.3513	0	0	224	47.2
26	1.0521	-5.5137	0	0	139	17
27	1.0377	-7.4820	0	0	281	75.5
28	1.0501	-2.0019	0	0	206	27.6
29	1.0499	0.7574	0	0	283.5	26.9
30	1.0475	-3.3221	250	146.1721	0	0
31	0.9820	0.000	520.3221	198.1765	9.2	4.6
32	0.9831	2.5779	650	205.143	0	0
33	0.9972	4.2098	632	109.9205	0	0
34	1.0123	3.1901	508	165.7704	0	0
35	1.0493	5.6490	650	212.4463	0	0
36	1.0635	8.3432	560	101.1903	0	0
37	1.0278	2.4332	540	0.4395	0	0
38	1.0265	7.8208	830	22.8445	0	0
39	1.0300	-10.043	1000	88.2881	1104	250

Table B.2 Line and transformer data

Line No.	Line data					Transformer Tap	
	From	To	R (p.u.)	X (p.u.)	B (p.u.)	magnitude	Angle
1	1	2	0.0035	0.0411	0.6987	1	0
2	1	39	0.001	0.025	0.75	1	0
3	2	3	0.0013	0.0151	0.2572	1	0
4	25	2	0.007	0.0086	0.146	1	0
5	2	30	0	0.0181	0	1.025	0
6	3	4	0.0013	0.0213	0.2214	1	0
7	18	3	0.0011	0.0133	0.2138	1	0
8	4	5	0.0008	0.0128	0.1342	1	0
9	4	14	0.0008	0.0129	0.1382	1	0
10	5	6	0.0002	0.0026	0.0434	1	0
11	5	8	0.0008	0.0112	0.1476	1	0
12	6	7	0.0006	0.0092	0.113	1	0
13	6	11	0.0007	0.0082	0.1389	1	0
14	6	31	0	0.025	0	1.07	0
15	7	8	0.0004	0.0046	0.078	1	0
16	8	9	0.0023	0.0363	0.3804	1	0
17	39	9	0.001	0.025	1.2	1	0
18	11	10	0.0004	0.0043	0.0729	1	0
19	13	10	0.0004	0.0043	0.0729	1	0
20	10	32	0	0.02	0	1.07	0
21	12	11	0.0016	0.0435	0	1.006	0
22	12	13	0.0016	0.0435	0	1.006	0
23	13	14	0.0009	0.0101	0.1723	1	0
24	15	14	0.0018	0.0217	0.366	1	0
25	15	16	0.0009	0.0094	0.171	1	0
26	17	16	0.0007	0.0089	0.1342	1	0
27	19	16	0.0016	0.0195	0.304	1	0
28	21	16	0.0008	0.0135	0.2548	1	0
29	24	16	0.0003	0.0059	0.068	1	0
30	18	17	0.0007	0.0082	0.1319	1	0
31	27	17	0.0013	0.0173	0.3216	1	0
32	19	20	0.0007	0.0138	0	1.06	0
33	19	33	0.0007	0.0142	0	1.07	0
34	20	34	0.0009	0.018	0	1.009	0
35	21	22	0.0008	0.014	0.2565	1	0
36	22	23	0.0006	0.0096	0.1846	1	0
37	22	35	0	0.0143	0	1.025	0
38	24	23	0.0022	0.035	0.361	1	0
39	23	36	0.0005	0.0272	0	1	0
40	25	26	0.0032	0.0323	0.513	1	0

Line No.	Line data					Transformer Tap	
	From	To	R (p.u.)	X (p.u.)	B (p.u.)	magnitude	Angle
41	25	37	0.0006	0.0232	0	1.025	0
42	27	26	0.0014	0.0147	0.2396	1	0
43	28	26	0.0043	0.0474	0.7802	1	0
44	29	26	0.0057	0.0625	1.029	1	0
45	28	29	0.0014	0.0151	0.249	1	0
46	29	38	0.0008	0.0156	0	1.025	0

Table B.3 Generator data

No.	Bus	H (sec.)	Ra (p.u.)	X'd (p.u.)	X'q (p.u.)	Xd (p.u.)	Xq (p.u.)	T'do (p.u.)	T'qo (p.u.)	Xl (p.u.)
1	39	500	0.00100	0.006	0.008	0.02	0.019	7.0	0.7	0.003
2	31	30.3	0.02700	0.0697	0.170	0.295	0.282	6.56	1.5	0.035
3	32	35.8	0.00386	0.0531	0.0876	0.2495	0.237	5.7	1.5	0.0304
4	33	28.6	0.00222	0.0436	0.166	0.262	0.258	5.69	1.5	0.0295
5	34	26.0	0.00140	0.132	0.166	0.67	0.62	5.4	0.44	0.054
6	35	34.8	0.06150	0.05	0.0814	0.254	0.241	7.3	0.4	0.0224
7	36	26.4	0.00268	0.049	0.186	0.295	0.292	5.66	1.5	0.0322
8	37	24.3	0.00686	0.057	0.0911	0.290	0.280	6.7	0.41	0.028
9	38	34.5	0.00300	0.057	0.0587	0.2106	0.205	4.79	1.96	0.0298
10	30	42.0	0.00140	0.031	0.008	0.1	0.069	10.2	0.0	0.0125

B.2 IEEE118 bus system

1. Single line diagram of the system

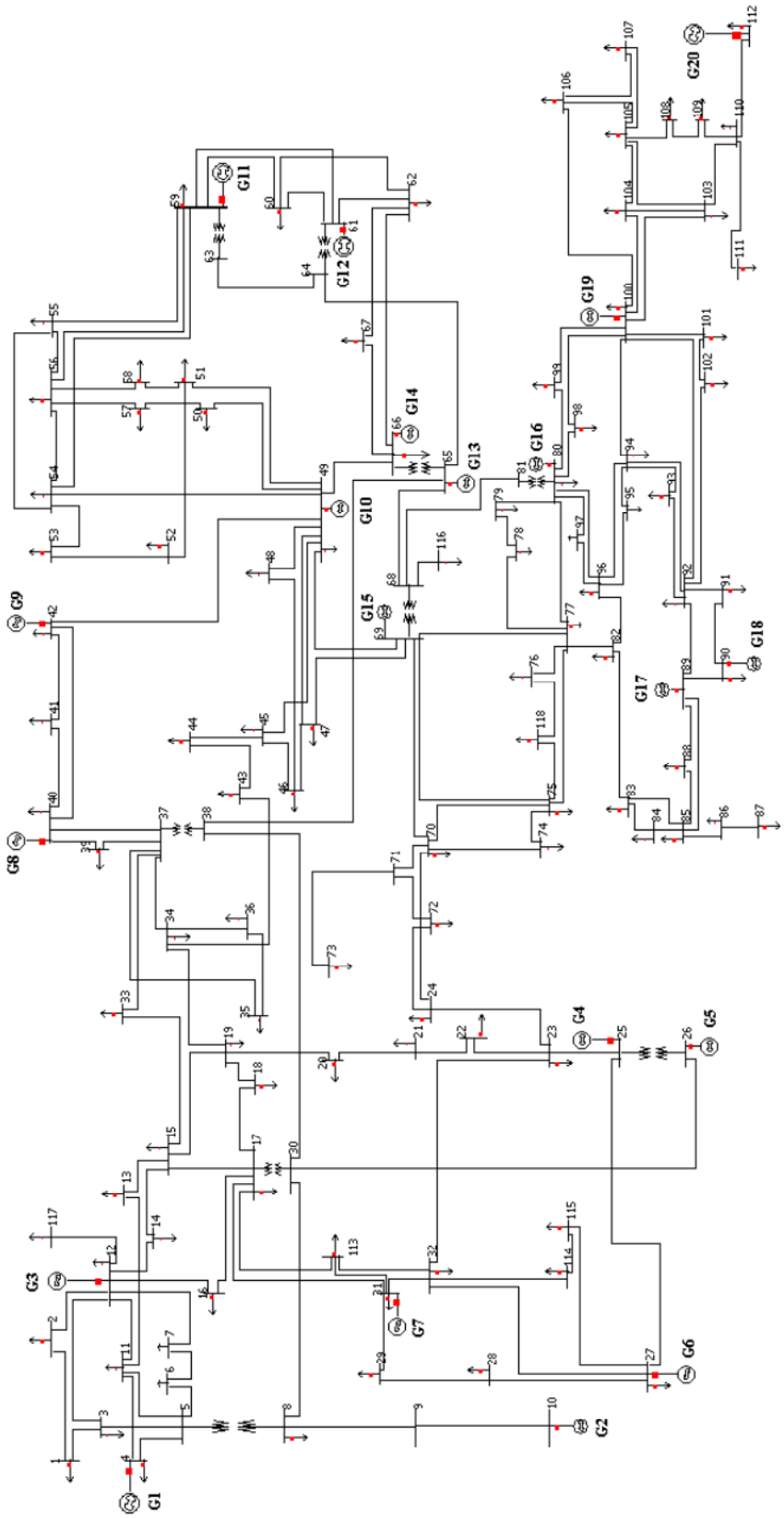

2. System data

Table B.4 Bus data and power flow results

Bus No.	Bus voltage		Generation		Load	
	Magnitude (p.u.)	angle (deg.)	Real (MW)	Reactive (MVAR)	Real (MW)	Reactive (MVAR)
1	0.9572	-18.2207	0	0	51	27
2	0.9722	-17.6608	0	0	20	9
3	0.969	-17.325	0	0	39	10
4	0.998	-13.5944	-9	-15.5133	30	12
5	1.0021	-13.1499	0	0	0	0
6	0.99	-15.8726	0	0	52	6.23
7	0.9893	-16.3159	0	0	19	2
8	1.015	-8.134	0	0	28	-61.61
9	1.0429	-0.8797	0	0	0	0
10	1.05	6.7012	450	-51.0208	0	0
11	0.9851	-16.1566	0	0	70	23
12	0.99	-16.6722	85	88.9666	47	10
13	0.9683	-17.5238	0	0	34	16
14	0.9836	-17.3798	0	0	14	1
15	0.97	-17.6495	0	0	90	27.29
16	0.984	-16.9808	0	0	25	10
17	0.9952	-15.1884	0	0	11	3
18	0.973	-17.3681	0	0	60	8.74
19	0.9634	-17.8209	0	0	45	33
20	0.9581	-16.9691	0	0	18	3
21	0.9588	-15.4019	0	0	14	8
22	0.9698	-12.8712	0	0	10	5
23	0.9997	-7.9878	0	0	7	3
24	0.992	-8.2335	0	0	13	13.87
25	1.05	-1.0004	220	49.566	0	0
26	1.015	0.7774	314	9.5097	0	0
27	0.968	-13.4483	-9	2.3345	62	13
28	0.9616	-15.0845	0	0	17	7
29	0.9632	-15.9783	0	0	24	4
30	0.9859	-10.1523	0	0	0	0
31	0.967	-15.8264	7	3.9701	43	27
32	0.9637	-14.0154	0	0	59	37
33	0.9716	-18.1272	0	0	23	9
34	0.986	-17.3372	0	0	59	34
35	0.9807	-17.7564	0	0	33	9
36	0.98	-17.7535	0	0	31	18.73
37	0.9921	-16.858	0	0	0	0
38	0.9633	-12.0945	0	0	0	0
39	0.9708	-19.4704	0	0	27	11
40	0.97	-20.1015	-46	25.2921	20	23

Bus No.	Bus voltage		Generation		Load	
	Magnitude (p.u.)	angle (deg.)	Real (MW)	Reactive (MVAR)	Real (MW)	Reactive (MVAR)
41	0.9667	-20.2036	0	0	37	10
42	0.985	-17.6661	-59	21.8542	37	23
43	0.9787	-17.5131	0	0	18	7
44	0.9853	-15.2186	0	0	16	8
45	0.9869	-13.4579	0	0	53	22
46	1.005	-10.7198	0	0	9	15.68
47	1.0173	-8.5782	0	0	34	0
48	1.0206	-9.2626	0	0	20	11
49	1.025	-8.2556	204	108.4161	87	30
50	1.0015	-10.1158	0	0	17	4
51	0.9676	-12.4909	0	0	17	8
52	0.9576	-13.3713	0	0	18	5
53	0.9464	-14.1477	0	0	23	11
54	0.955	-13.0903	0	0	65	60.95
55	0.952	-13.5063	0	0	63	20.89
56	0.9546	-13.2624	0	0	84	26
57	0.9713	-12.3124	0	0	12	3
58	0.9597	-13.1149	0	0	12	3
59	0.985	-10.4092	155	83.2454	277	113
60	0.9932	-6.9483	0	0	78	3
61	0.995	-6.0573	160	-41.7222	0	0
62	0.998	-6.7943	0	0	77	13.4
63	0.969	-7.2215	0	0	0	0
64	0.9839	-5.5593	0	0	0	0
65	1.005	-2.5555	391	78.7829	0	0
66	1.05	-3.3052	392	16.8191	39	18
67	1.0198	-5.6895	0	0	28	7
68	1.0032	-2.6181	0	0	0	0
69	1.035	0.0000	503.3161	-84.4974	0	0
70	0.984	-7.1097	0	0	66	13.4
71	0.9869	-7.4878	0	0	0	0
72	0.98	-8.419	0	0	12	11.16
73	0.991	-7.6992	0	0	6	-9.63
74	0.9586	-8.0794	0	0	68	33
75	0.9682	-6.8289	0	0	47	11
76	0.943	-7.8573	0	0	68	35.22
77	1.0118	-2.9144	0	0	61	48
78	1.0085	-3.2964	0	0	71	26
79	1.0131	-3.1619	0	0	39	32
80	1.04	-1.3773	477	126.0545	130	26

Bus No.	Bus voltage		Generation		Load	
	Magnitude (p.u.)	angle (deg.)	Real (MW)	Reactive (MVAR)	Real (MW)	Reactive (MVAR)
81	0.9967	-2.1283	0	0	0	0
82	1.0000	-2.9993	0	0	54	5.14
83	0.9939	-2.0636	0	0	20	10
84	0.9852	0.0755	0	0	11	7
85	0.9883	1.4421	0	0	24	23
86	0.9887	0.1011	0	0	21	10
87	1.0149	0.3772	0	0	-4	-9.95
88	0.9891	4.2017	0	0	48	10
89	1.005	8.006	607	-18.4437	0	0
90	0.985	3.4643	-85	44.2937	78	42
91	0.9799	3.7051	0	0	10	19.06
92	0.9976	4.4391	0	0	65	13
93	0.9911	1.2104	0	0	12	7
94	0.994	-1.1403	0	0	30	16
95	0.9853	-2.2299	0	0	42	31
96	0.9981	-2.5538	0	0	38	15
97	1.0142	-2.3153	0	0	15	9
98	1.0235	-2.7184	0	0	34	8
99	1.01	-2.8864	0	0	42	17.57
100	1.017	-1.7275	252	77.263	37	18
101	0.9946	0.0231	0	0	22	15
102	0.9952	2.8682	0	0	5	3
103	1.0063	-5.3724	0	0	-17	-24
104	0.9882	-8.2567	0	0	38	2
105	0.9824	-9.3476	0	0	31	3
106	0.9726	-9.5027	0	0	43	16
107	0.952	-12.0637	0	0	50	20.68
108	0.9766	-10.4011	0	0	2	1
109	0.9746	-10.7997	0	0	8	3
110	0.9729	-11.5184	0	0	39	38
111	0.98	-9.8755	0	0	-36	1.66
112	0.975	-14.6215	-43	41.7395	25	13
113	0.993	-15.3162	0	0	6	-34.41
114	0.9605	-14.3395	0	0	8	3
115	0.9604	-14.3461	0	0	22	7
116	1.0049	-3.053	0	0	184	-50.34
117	0.9738	-18.2132	0	0	20	8
118	0.9499	-7.7688	0	0	33	15

Table B.5 Line and Transformer data

Line No.	Line data					Transformer Tap	
	From	To	R (p.u.)	X (p.u.)	B (p.u.)	magnitude	Angle
1	1	2	0.0303	0.0999	0.0254	1	0
2	1	3	0.0129	0.0424	0.0108	1	0
3	2	12	0.0187	0.0616	0.0157	1	0
4	3	5	0.0241	0.108	0.0284	1	0
5	3	12	0.0484	0.16	0.0406	1	0
6	4	5	0.0018	0.008	0.0021	1	0
7	11	4	0.0209	0.0688	0.0175	1	0
8	5	6	0.0119	0.054	0.0143	1	0
9	8	5	0	0.0267	0	0.985	0
10	11	5	0.0203	0.0682	0.0174	1	0
11	6	7	0.0046	0.0208	0.0055	1	0
12	7	12	0.0086	0.034	0.0087	1	0
13	8	9	0.0024	0.0305	1.162	1	0
14	30	8	0.0043	0.0504	0.514	1	0
15	9	10	0.0026	0.0322	1.23	1	0
16	11	12	0.006	0.0196	0.005	1	0
17	11	13	0.0222	0.0731	0.0188	1	0
18	12	14	0.0215	0.0707	0.0182	1	0
19	12	16	0.0212	0.0834	0.0214	1	0
20	12	117	0.0329	0.14	0.0358	1	0
21	13	15	0.0744	0.2444	0.0627	1	0
22	14	15	0.0595	0.195	0.0502	1	0
23	15	17	0.0132	0.0437	0.0444	1	0
24	15	19	0.012	0.0394	0.0101	1	0
25	15	33	0.038	0.1244	0.0319	1	0
26	16	17	0.0454	0.1801	0.0466	1	0
27	17	18	0.0123	0.0505	0.013	1	0
28	30	17	0	0.0388	0	0.96	0
29	17	31	0.0474	0.1563	0.0399	1	0
30	17	113	0.0091	0.0301	0.0077	1	0
31	18	19	0.0112	0.0493	0.0114	1	0
32	19	20	0.0252	0.117	0.0298	1	0
33	34	19	0.0752	0.247	0.0632	1	0
34	20	21	0.0183	0.0849	0.0216	1	0
35	21	22	0.0209	0.097	0.0246	1	0
36	22	23	0.0342	0.159	0.0404	1	0
37	23	24	0.0135	0.0492	0.0498	1	0
38	23	25	0.0156	0.08	0.0864	1	0
39	32	23	0.0317	0.1153	0.1173	1	0
40	70	24	0.1022	0.4115	0.102	1	0

Line No.	Line data					Transformer Tap	
	From	To	R (p.u.)	X (p.u.)	B (p.u.)	magnitude	Angle
41	24	72	0.0488	0.196	0.0488	1	0
42	26	25	0	0.0382	0	0.96	0
43	25	27	0.0318	0.163	0.1764	1	0
44	30	26	0.008	0.086	0.908	1	0
45	28	27	0.0191	0.0855	0.0216	1	0
46	32	27	0.0229	0.0755	0.0193	1	0
47	27	115	0.0164	0.0741	0.0197	1	0
48	29	28	0.0237	0.0943	0.0238	1	0
49	31	29	0.0108	0.0331	0.0083	1	0
50	30	38	0.0046	0.054	0.422	1	0
51	31	32	0.0298	0.0985	0.0251	1	0
52	31	113	0	0.1	0	1	0
53	113	32	0.0615	0.203	0.0518	1	0
54	32	114	0.0135	0.0612	0.0163	1	0
55	33	37	0.0415	0.142	0.0366	1	0
56	34	36	0.0087	0.0268	0.0057	1	0
57	37	34	0.0026	0.0094	0.0098	1	0
58	34	43	0.0413	0.1681	0.0423	1	0
59	36	35	0.0022	0.0102	0.0027	1	0
60	37	35	0.011	0.0497	0.0132	1	0
61	38	37	0	0.0375	0	0.935	0
62	39	37	0.0321	0.106	0.027	1	0
63	37	40	0.0593	0.168	0.042	1	0
64	38	65	0.009	0.0986	1.046	1	0
65	39	40	0.0184	0.0605	0.0155	1	0
66	40	41	0.0145	0.0487	0.0122	1	0
67	40	42	0.0555	0.183	0.0466	1	0
68	41	42	0.041	0.135	0.0344	1	0
69	42	49	0.0238	0.1077	0.258	1	0
70	43	44	0.0608	0.2454	0.0607	1	0
71	44	45	0.0224	0.0901	0.0224	1	0
72	45	46	0.04	0.1356	0.0332	1	0
73	45	49	0.0684	0.186	0.0444	1	0
74	46	47	0.038	0.127	0.0316	1	0
75	46	48	0.0601	0.189	0.0472	1	0
76	47	49	0.0191	0.0625	0.016	1	0
77	47	69	0.0844	0.2778	0.0709	1	0
78	48	49	0.0179	0.0505	0.0126	1	0
79	49	50	0.0267	0.0752	0.0187	1	0
80	49	51	0.0486	0.137	0.0342	1	0

Line No.	Line data					Transformer Tap	
	From	To	R (p.u.)	X (p.u.)	B (p.u.)	magnitude	Angle
81	54	49	0.0257	0.0966	0.2206	1	0
82	49	66	0.006	0.0306	0.0744	1	0
83	49	69	0.0985	0.324	0.0828	1	0
84	50	57	0.0474	0.134	0.0332	1	0
85	51	52	0.0203	0.0588	0.014	1	0
86	58	51	0.0255	0.0719	0.0179	1	0
87	52	53	0.0405	0.1635	0.0406	1	0
88	53	54	0.0263	0.122	0.031	1	0
89	54	55	0.0169	0.0707	0.0202	1	0
90	54	56	0.0028	0.0096	0.0073	1	0
91	54	59	0.0503	0.2293	0.0598	1	0
92	56	55	0.0049	0.0151	0.0037	1	0
93	55	59	0.0474	0.2158	0.0565	1	0
94	57	56	0.0343	0.0966	0.0242	1	0
95	58	56	0.0343	0.0966	0.0242	1	0
96	56	59	0.0273	0.0823	0.1672	1	0
97	59	60	0.0317	0.145	0.0376	1	0
98	61	59	0.0328	0.15	0.0388	1	0
99	63	59	0	0.0386	0	0.96	0
100	60	61	0.0026	0.0135	0.0146	1	0
101	60	62	0.0123	0.0561	0.0147	1	0
102	61	62	0.0082	0.0376	0.0098	1	0
103	64	61	0	0.0268	0	0.985	0
104	66	62	0.0482	0.218	0.0578	1	0
105	62	67	0.0258	0.117	0.031	1	0
106	63	64	0.0017	0.02	0.216	1	0
107	64	65	0.0027	0.0302	0.38	1	0
108	65	66	0	0.037	0	0.935	0
109	68	65	0.0014	0.016	0.638	1	0
110	66	67	0.0224	0.1015	0.0268	1	0
111	68	69	0	0.037	0	0.935	0
112	68	81	0.0018	0.0202	0.808	1	0
113	68	116	0.0003	0.004	0.164	1	0
114	70	69	0.03	0.127	0.122	1	0
115	75	69	0.0405	0.122	0.124	1	0
116	69	77	0.0309	0.101	0.1038	1	0
117	70	71	0.0088	0.0355	0.0088	1	0
118	70	74	0.0401	0.1323	0.0337	1	0
119	70	75	0.0428	0.141	0.036	1	0
120	72	71	0.0446	0.18	0.0444	1	0

Line No.	Line data					Transformer Tap	
	From	To	R (p.u.)	X (p.u.)	B (p.u.)	magnitude	Angle
121	71	73	0.0087	0.0454	0.0118	1	0
122	74	75	0.0123	0.0406	0.0103	1	0
123	75	77	0.0601	0.1999	0.0498	1	0
124	75	118	0.0145	0.0481	0.012	1	0
125	77	76	0.0444	0.148	0.0368	1	0
126	118	76	0.0164	0.0544	0.0136	1	0
127	77	78	0.0038	0.0124	0.0126	1	0
128	77	80	0.0066	0.0197	0.1172	1	0
129	77	82	0.0298	0.0853	0.0817	1	0
130	78	79	0.0055	0.0244	0.0065	1	0
131	79	80	0.0156	0.0704	0.0187	1	0
132	81	80	0	0.037	0	0.935	0
133	96	80	0.0356	0.182	0.0494	1	0
134	97	80	0.0183	0.0934	0.0254	1	0
135	80	98	0.0238	0.108	0.0286	1	0
136	80	99	0.0454	0.206	0.0546	1	0
137	83	82	0.0112	0.0366	0.038	1	0
138	82	96	0.0162	0.053	0.0544	1	0
139	83	84	0.0625	0.132	0.0258	1	0
140	85	83	0.043	0.148	0.0348	1	0
141	84	85	0.0302	0.0641	0.0123	1	0
142	85	86	0.035	0.123	0.0276	1	0
143	85	88	0.02	0.102	0.0276	1	0
144	85	89	0.0239	0.173	0.047	1	0
145	86	87	0.0283	0.2074	0.0445	1	0
146	88	89	0.0139	0.0712	0.0193	1	0
147	90	89	0.0124	0.0484	0.2116	1	0
148	89	92	0.0044	0.0218	0.151	1	0
149	90	91	0.0254	0.0836	0.0214	1	0
150	91	92	0.0387	0.1272	0.0327	1	0
151	92	93	0.0258	0.0848	0.0218	1	0
152	92	94	0.0481	0.158	0.0406	1	0
153	92	100	0.0648	0.295	0.0472	1	0
154	92	102	0.0123	0.0559	0.0146	1	0
155	93	94	0.0223	0.0732	0.0188	1	0
156	95	94	0.0132	0.0434	0.0111	1	0
157	96	94	0.0269	0.0869	0.023	1	0
158	94	100	0.0178	0.058	0.0604	1	0
159	96	95	0.0171	0.0547	0.0147	1	0
160	96	97	0.0173	0.0885	0.024	1	0

Line No.	Line data					Transformer Tap	
	From	To	R (p.u.)	X (p.u.)	B (p.u.)	magnitude	Angle
161	98	100	0.0397	0.179	0.0476	1	0
162	99	100	0.018	0.0813	0.0216	1	0
163	101	100	0.0277	0.1262	0.0328	1	0
164	100	103	0.016	0.0525	0.0536	1	0
165	100	104	0.0451	0.204	0.0541	1	0
166	100	106	0.0605	0.229	0.062	1	0
167	102	101	0.0246	0.112	0.0294	1	0
168	104	103	0.0466	0.1584	0.0407	1	0
169	103	105	0.0535	0.1625	0.0408	1	0
170	103	110	0.0391	0.1813	0.0461	1	0
171	104	105	0.0099	0.0378	0.0099	1	0
172	105	106	0.014	0.0547	0.0143	1	0
173	105	107	0.053	0.183	0.0472	1	0
174	105	108	0.0261	0.0703	0.0184	1	0
175	107	106	0.053	0.183	0.0472	1	0
176	108	109	0.0105	0.0288	0.0076	1	0
177	109	110	0.0278	0.0762	0.0202	1	0
178	110	111	0.022	0.0755	0.02	1	0
179	110	112	0.0247	0.064	0.062	1	0
180	114	115	0.0023	0.0104	0.0028	1	0

Table B.6 Shunt capacitor data

Bus	G	B (p.u.)
5	-	-0.40
34	-	0.14
37	-	-0.25
44	-	0.10
45	-	0.10
46	-	0.10
48	-	0.15
74	-	0.12
79	-	0.20
82	-	0.20
83	-	0.10
105	-	0.20
107	-	0.06
110	-	0.06

Table B.7 Generator data

No.	Bus	X'd (p.u.)	H (sec.)
1	4	0.0875	8
2	10	0.0636	22
3	12	0.1750	8
4	25	0.1000	14
5	26	0.0538	26
6	27	0.0875	8
7	32	0.0875	8
8	40	0.0875	8
9	42	0.0875	8
10	49	0.1167	12
11	59	0.1400	10
12	61	0.1167	12
13	65	0.0700	20
14	66	0.0700	20
15	69	0.0467	30
16	80	0.0500	28
17	89	0.0437	32
18	90	0.0875	8
19	100	0.0875	16
20	112	0.0467	15

APPENDIX C: SUPPLEMENT RESULTS

C.1 Rotor angle plot of case study 1.1

The plots in this section show the comparison of the rotor angles of the reduced systems of scenarios A (based on two fictitious generators) and B (based on loose coherent groups), when the large fault is applied at each internal bus, to the rotor angle of the original system. However, the legends on each figure are defined as follows:

OG - Original System
RD.A - Reduced system based on loose coherent groups
RD.B - Reduced system based on two fictitious generators

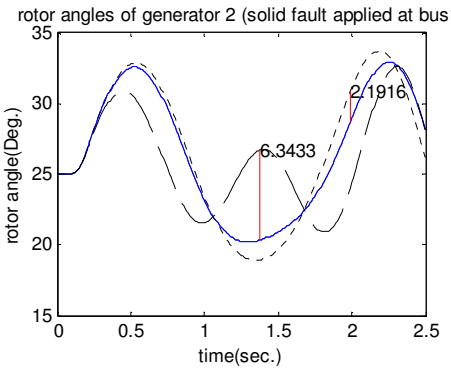
rotor angles of generator 2 (solid fault applied at bus1)
rotor angle(Deg.)
time(sec.)
6.3433
2.1916

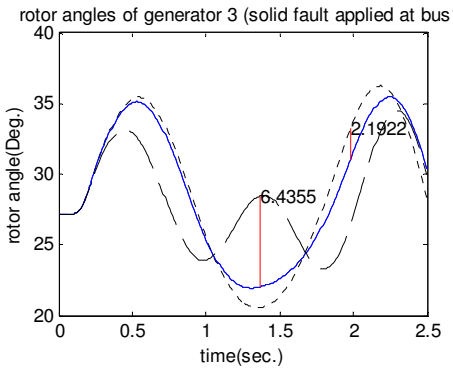
rotor angles of generator 3 (solid fault applied at bus1)
rotor angle(Deg.)
time(sec.)
6.4355
2.1922

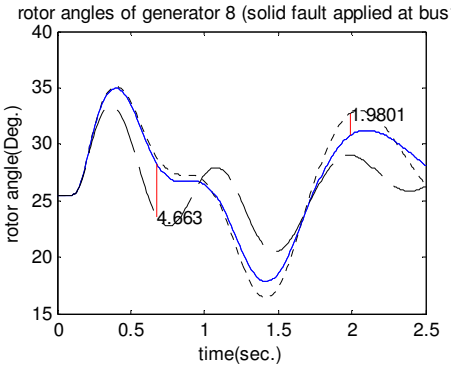
rotor angles of generator 8 (solid fault applied at bus1)
rotor angle(Deg.)
time(sec.)
4.663
1.9801

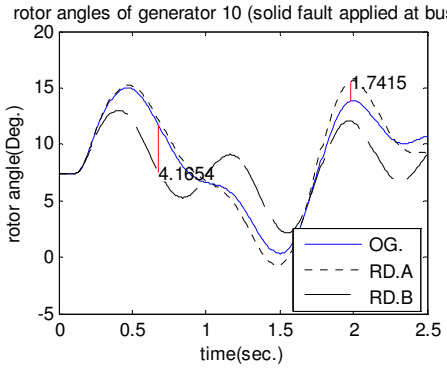
rotor angles of generator 10 (solid fault applied at bus1)
rotor angle(Deg.)
time(sec.)
4.1654
1.7415
OG.
RD.A
RD.B

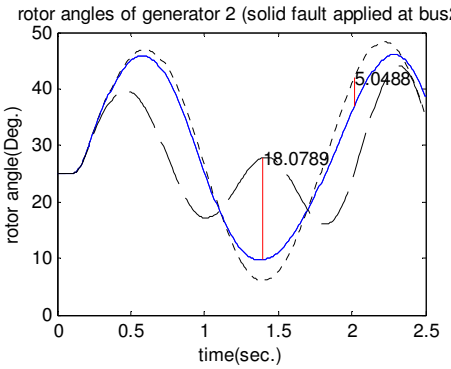
rotor angles of generator 2 (solid fault applied at bus2)
rotor angle(Deg.)
time(sec.)
18.0789
5.0488

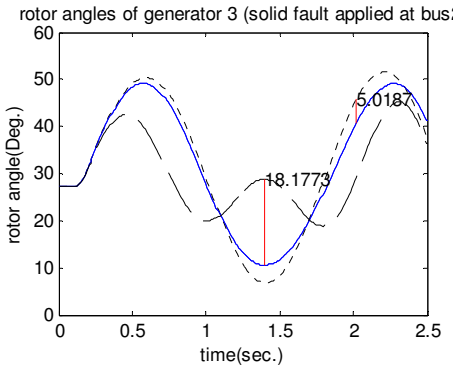
rotor angles of generator 3 (solid fault applied at bus2)
rotor angle(Deg.)
time(sec.)
18.1773
5.0187

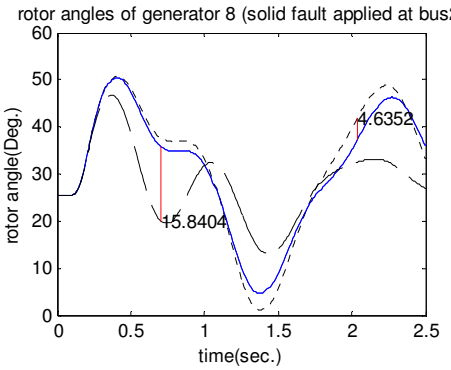
rotor angles of generator 8 (solid fault applied at bus2)
rotor angle(Deg.)
time(sec.)
15.8404
4.6352

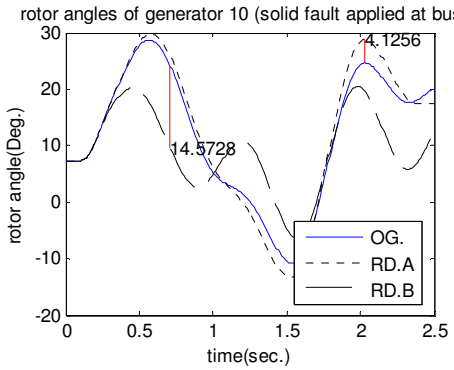
rotor angles of generator 10 (solid fault applied at bus2)
rotor angle(Deg.)
time(sec.)
14.5728
4.1256
OG.
RD.A
RD.B

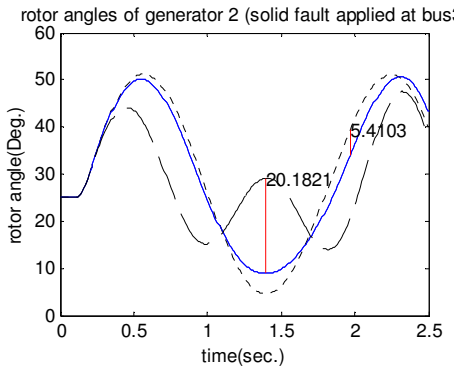
rotor angles of generator 2 (solid fault applied at bus3)
rotor angle(Deg.)
time(sec.)
20.1821
5.4103

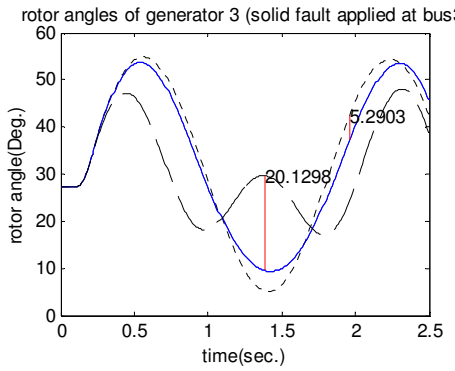
rotor angles of generator 3 (solid fault applied at bus3)
rotor angle(Deg.)
time(sec.)
20.1298
5.2903

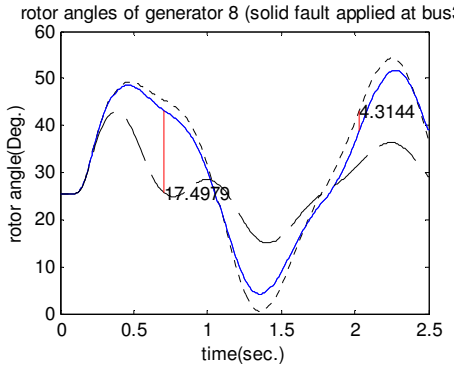
rotor angles of generator 8 (solid fault applied at bus3)
rotor angle(Deg.)
time(sec.)
17.4979
4.3144

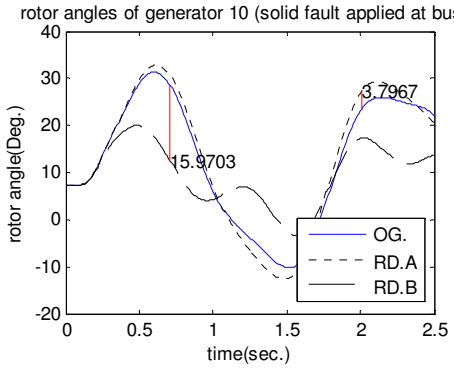
rotor angles of generator 10 (solid fault applied at bus3)
rotor angle(Deg.)
time(sec.)
15.9703
3.7967
OG.
RD.A
RD.B

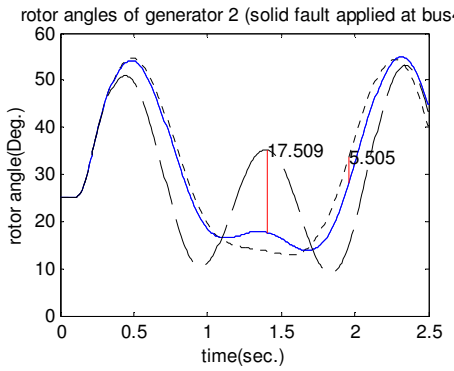
rotor angles of generator 2 (solid fault applied at bus4)
rotor angle(Deg.)
time(sec.)
17.509
5.505

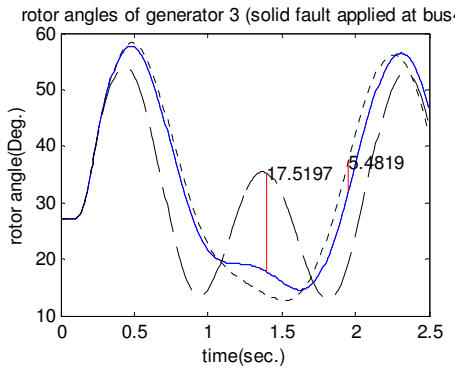
rotor angles of generator 3 (solid fault applied at bus4)
rotor angle(Deg.)
time(sec.)
17.5197
5.4819

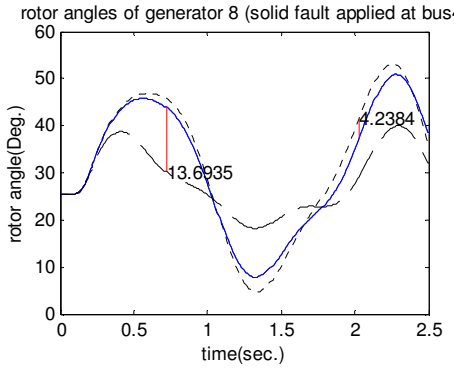
rotor angles of generator 8 (solid fault applied at bus4)
rotor angle(Deg.)
time(sec.)
13.6935
4.2384

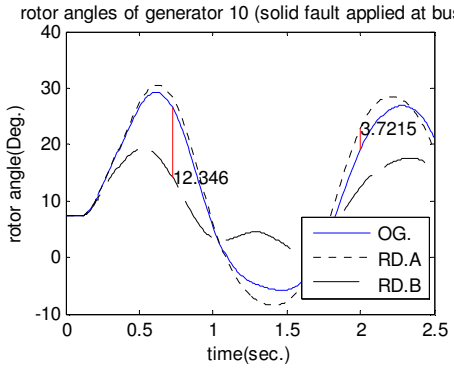
rotor angles of generator 10 (solid fault applied at bus4)
rotor angle(Deg.)
time(sec.)
12.346
3.7215
OG.
RD.A
RD.B

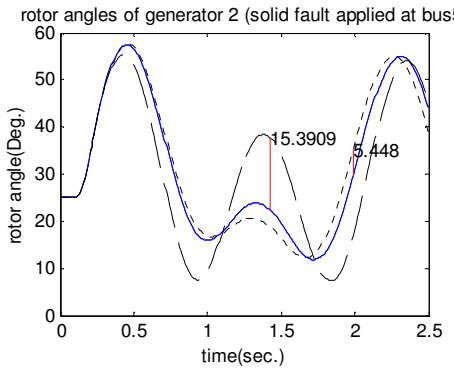
rotor angles of generator 2 (solid fault applied at bus5)
rotor angle(Deg.)
time(sec.)
15.3909
5.448

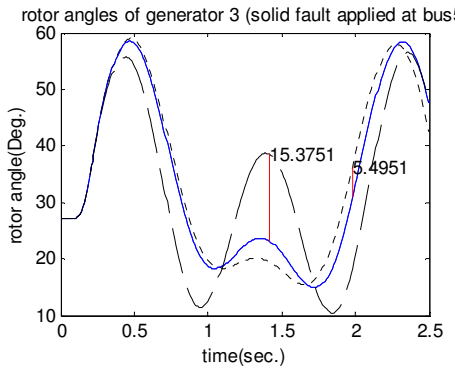
rotor angles of generator 3 (solid fault applied at bus5)
rotor angle(Deg.)
time(sec.)
15.3751
5.4951

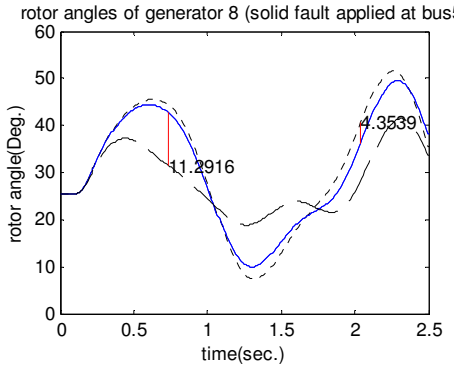
rotor angles of generator 8 (solid fault applied at bus5)
rotor angle(Deg.)
time(sec.)
11.2916
4.3539

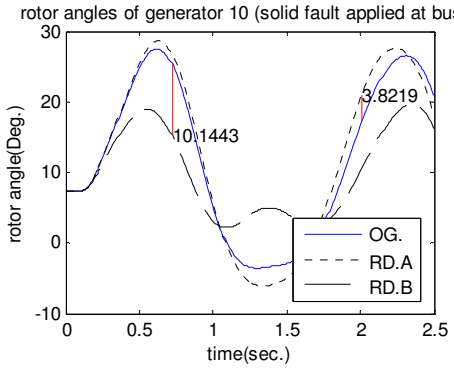
rotor angles of generator 10 (solid fault applied at bus5)
rotor angle(Deg.)
time(sec.)
10.1443
3.8219
OG.
RD.A
RD.B

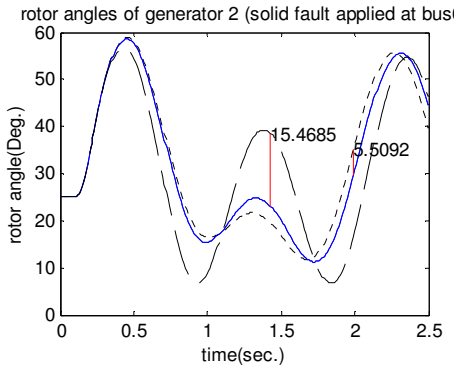
rotor angles of generator 2 (solid fault applied at bus6)
rotor angle(Deg.)
time(sec.)
15.4685
5.5092

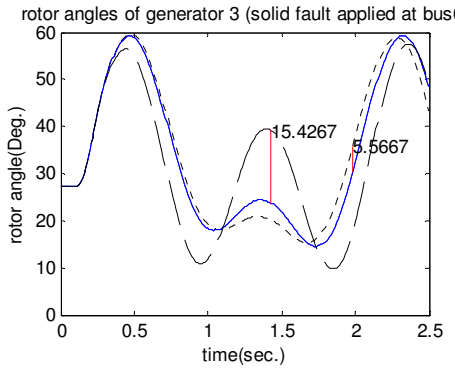
rotor angles of generator 3 (solid fault applied at bus6)
rotor angle(Deg.)
time(sec.)
15.4267
5.5667

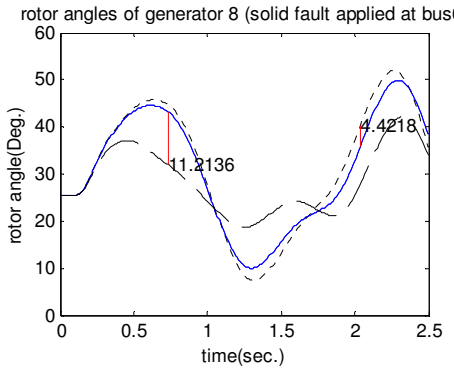
rotor angles of generator 8 (solid fault applied at bus6)
rotor angle(Deg.)
time(sec.)
11.2136
4.4218

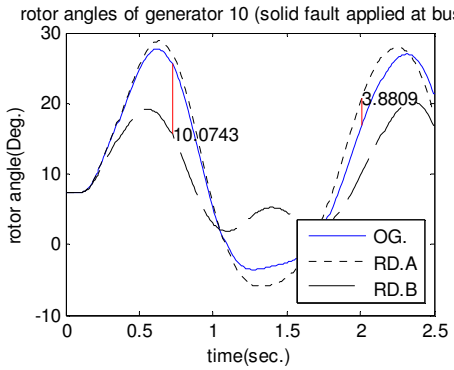
rotor angles of generator 10 (solid fault applied at bus6)
rotor angle(Deg.)
time(sec.)
10.0743
3.8809
OG.
RD.A
RD.B

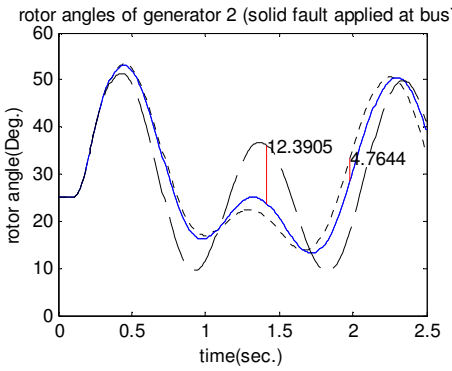
rotor angles of generator 2 (solid fault applied at bus7)
rotor angle(Deg.)
time(sec.)
12.3905
4.7644

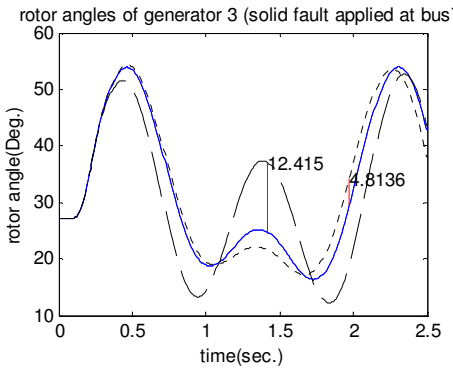
rotor angles of generator 3 (solid fault applied at bus7)
rotor angle(Deg.)
time(sec.)
12.415
4.8136

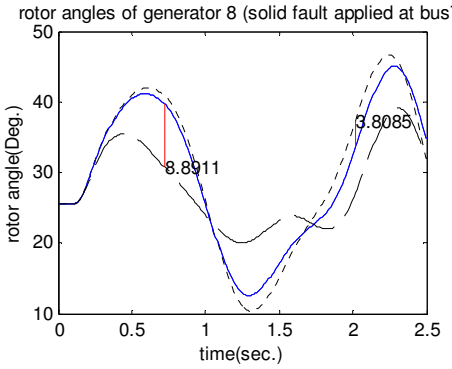
rotor angles of generator 8 (solid fault applied at bus7)
rotor angle(Deg.)
time(sec.)
8.8911
3.8085

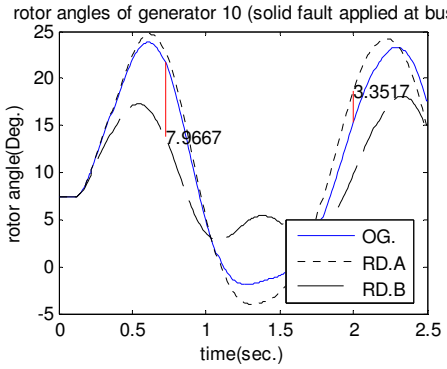
rotor angles of generator 10 (solid fault applied at bus7)
rotor angle(Deg.)
time(sec.)
7.9667
3.3517
OG.
RD.A
RD.B

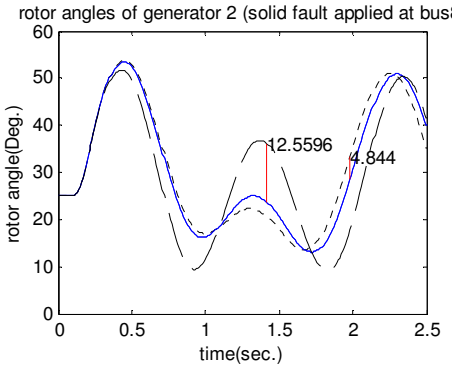
rotor angles of generator 2 (solid fault applied at bus8)
rotor angle(Deg.)
time(sec.)
12.5596
4.844

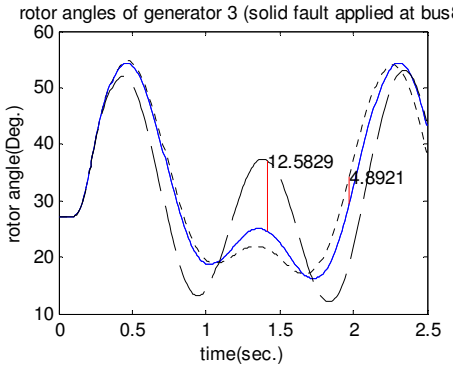
rotor angles of generator 3 (solid fault applied at bus8)
rotor angle(Deg.)
time(sec.)
12.5829
4.8921

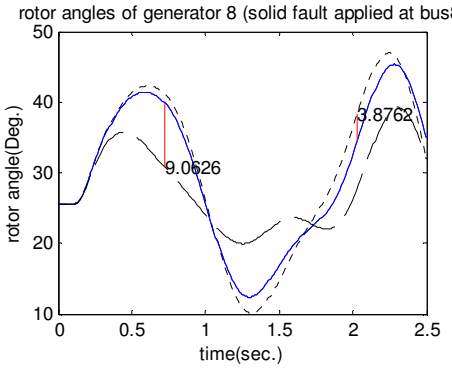
rotor angles of generator 8 (solid fault applied at bus8)
rotor angle(Deg.)
time(sec.)
9.0626
3.8762

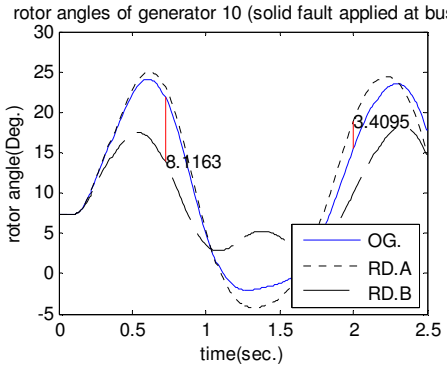
rotor angles of generator 10 (solid fault applied at bus8)
rotor angle(Deg.)
time(sec.)
8.1163
3.4095
OG.
RD.A
RD.B

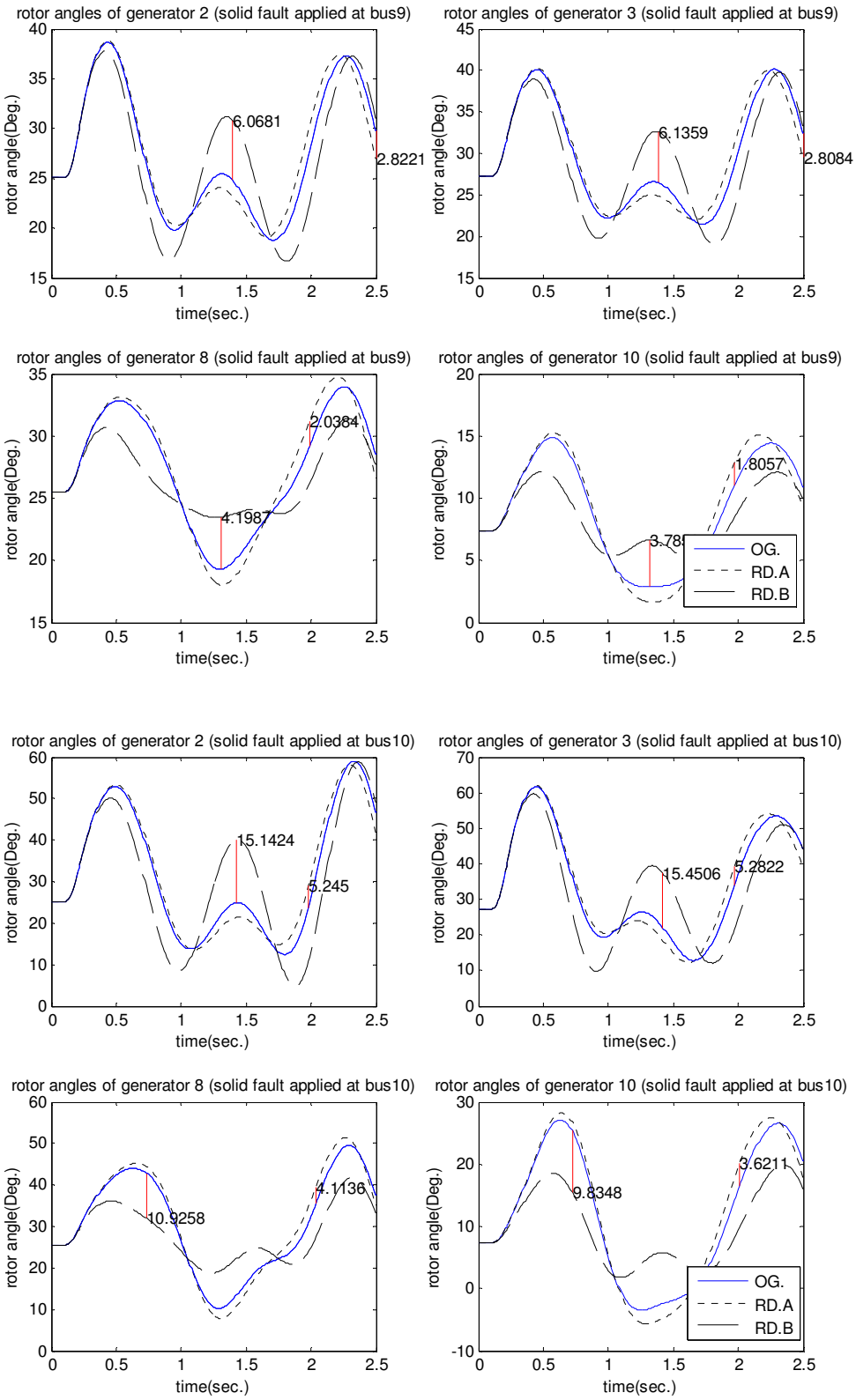
rotor angles of generator 2 (solid fault applied at bus9)
rotor angle(Deg.)
time(sec.)
6.0681
2.8221
rotor angles of generator 3 (solid fault applied at bus9)
rotor angle(Deg.)
time(sec.)
6.1359
2.8084
rotor angles of generator 8 (solid fault applied at bus9)
rotor angle(Deg.)
time(sec.)
2.0384
4.1987
rotor angles of generator 10 (solid fault applied at bus9)
rotor angle(Deg.)
time(sec.)
1.8057
OG.
RD.A
RD.B
rotor angles of generator 2 (solid fault applied at bus10)
rotor angle(Deg.)
time(sec.)
15.1424
5.245
rotor angles of generator 3 (solid fault applied at bus10)
rotor angle(Deg.)
time(sec.)
15.4506
5.2822
rotor angles of generator 8 (solid fault applied at bus10)
rotor angle(Deg.)
time(sec.)
10.9258
4.1136
rotor angles of generator 10 (solid fault applied at bus10)
rotor angle(Deg.)
time(sec.)
9.8348
3.6211
OG.
RD.A
RD.B

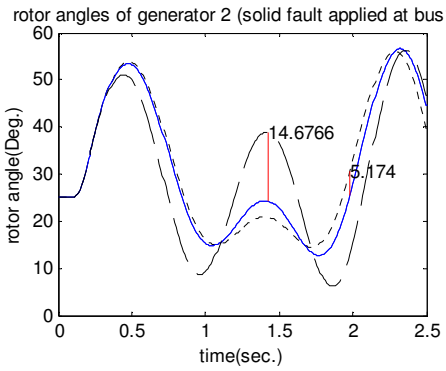
rotor angles of generator 2 (solid fault applied at bus11)
rotor angle(Deg.)
time(sec.)
14.6766
5.174

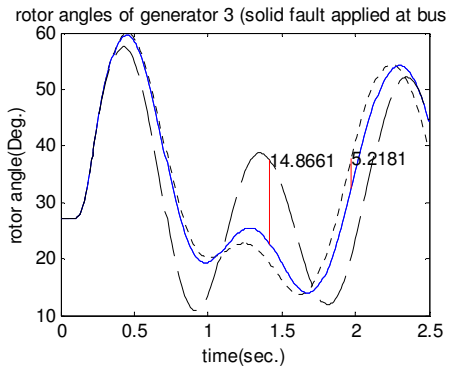
rotor angles of generator 3 (solid fault applied at bus11)
rotor angle(Deg.)
time(sec.)
14.8661
5.2181

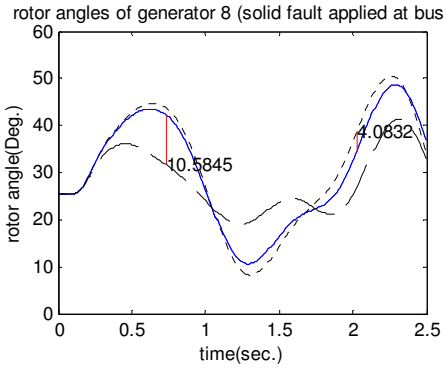
rotor angles of generator 8 (solid fault applied at bus11)
rotor angle(Deg.)
time(sec.)
10.5845
4.0832

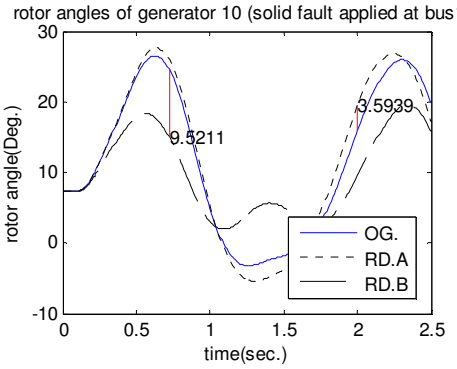
rotor angles of generator 10 (solid fault applied at bus11)
rotor angle(Deg.)
time(sec.)
9.5211
3.5939
OG.
RD.A
RD.B

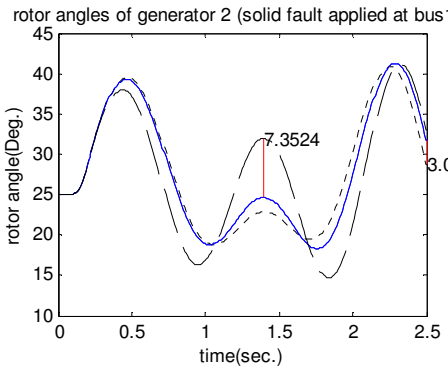
rotor angles of generator 2 (solid fault applied at bus12)
rotor angle(Deg.)
time(sec.)
7.3524
3.0435

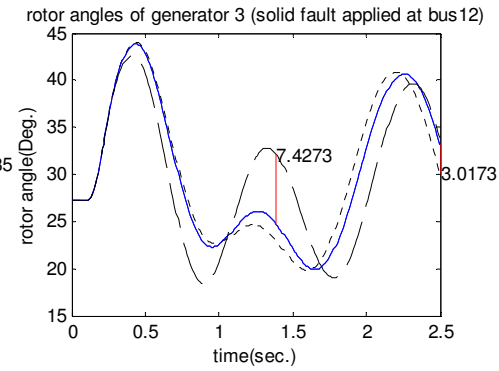
rotor angles of generator 3 (solid fault applied at bus12)
rotor angle(Deg.)
time(sec.)
7.4273
3.0173

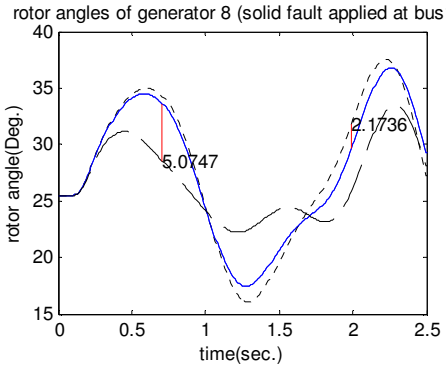
rotor angles of generator 8 (solid fault applied at bus12)
rotor angle(Deg.)
time(sec.)
5.0747
2.1736

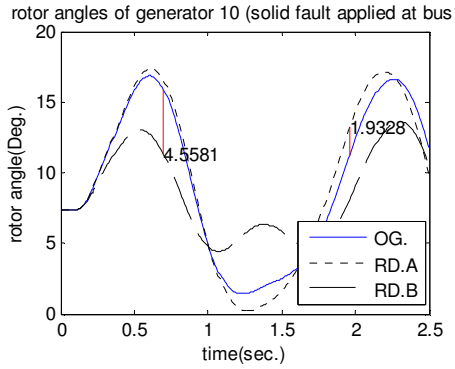
rotor angles of generator 10 (solid fault applied at bus12)
rotor angle(Deg.)
time(sec.)
4.5581
1.9328
OG.
RD.A
RD.B

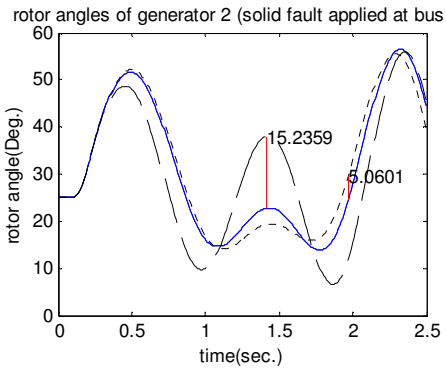
rotor angles of generator 2 (solid fault applied at bus13)
rotor angle(Deg.)
time(sec.)
15.2359
5.0601

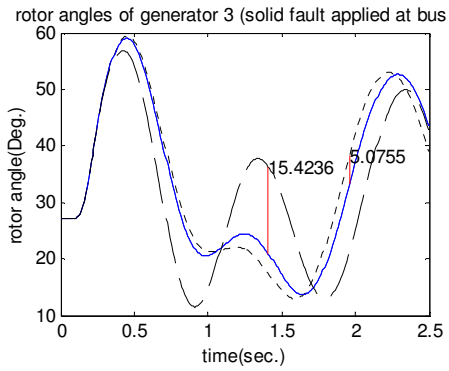
rotor angles of generator 3 (solid fault applied at bus13)
rotor angle(Deg.)
time(sec.)
15.4236
5.0755

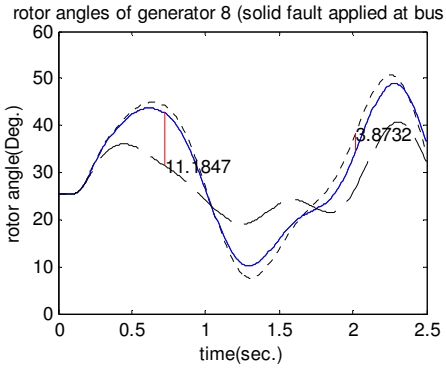
rotor angles of generator 8 (solid fault applied at bus13)
rotor angle(Deg.)
time(sec.)
11.1847
3.8732

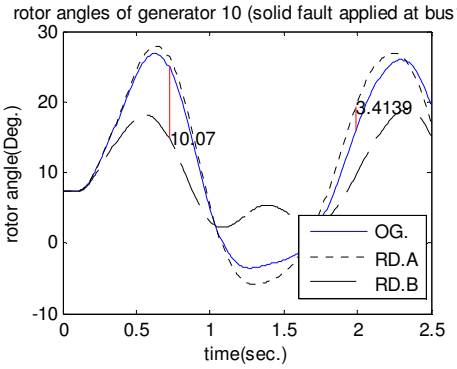
rotor angles of generator 10 (solid fault applied at bus13)
rotor angle(Deg.)
time(sec.)
10.07
3.4139
OG.
RD.A
RD.B

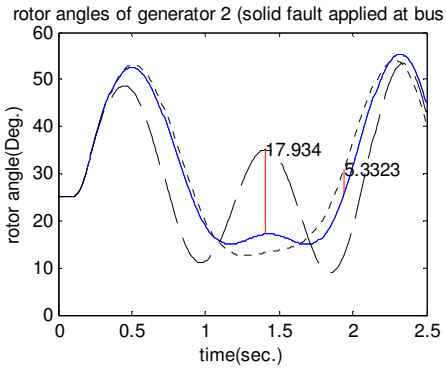
rotor angles of generator 2 (solid fault applied at bus14)
rotor angle(Deg.)
time(sec.)
17.934
5.3323

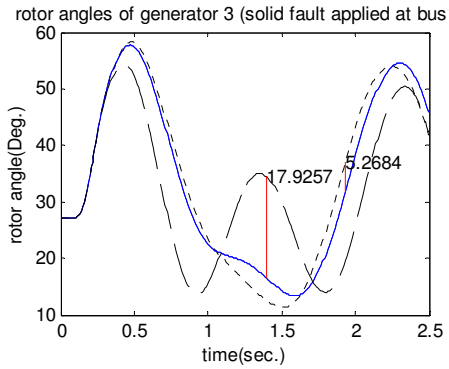
rotor angles of generator 3 (solid fault applied at bus14)
rotor angle(Deg.)
time(sec.)
17.9257
5.2684

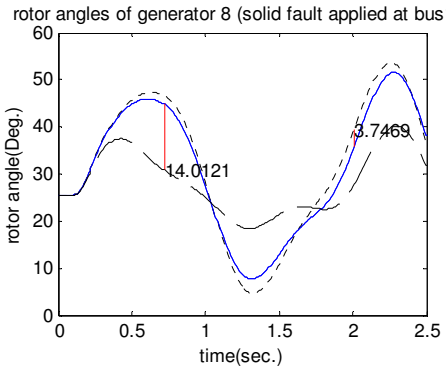
rotor angles of generator 8 (solid fault applied at bus14)
rotor angle(Deg.)
time(sec.)
14.0121
3.7469

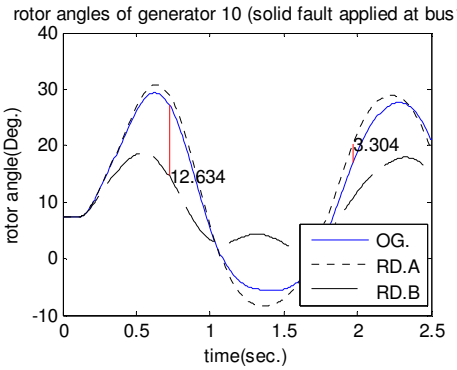
rotor angles of generator 10 (solid fault applied at bus14)
rotor angle(Deg.)
time(sec.)
12.634
3.304
OG.
RD.A
RD.B

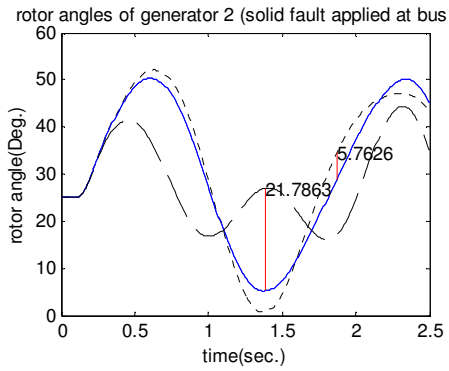
rotor angles of generator 2 (solid fault applied at bus15)
rotor angle(Deg.)
time(sec.)
21.7863
5.7626

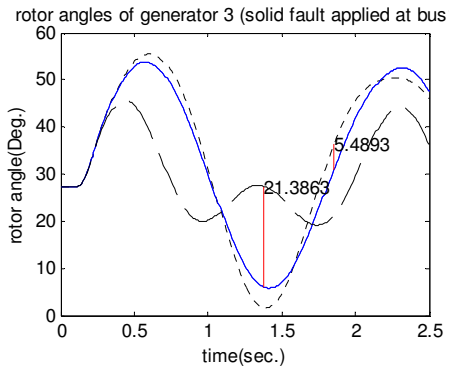
rotor angles of generator 3 (solid fault applied at bus15)
rotor angle(Deg.)
time(sec.)
21.3863
5.4893

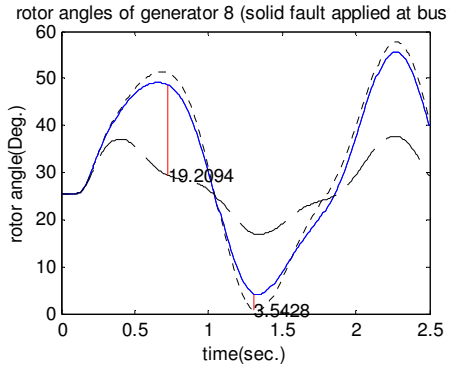
rotor angles of generator 8 (solid fault applied at bus15)
rotor angle(Deg.)
time(sec.)
19.2094
3.5428

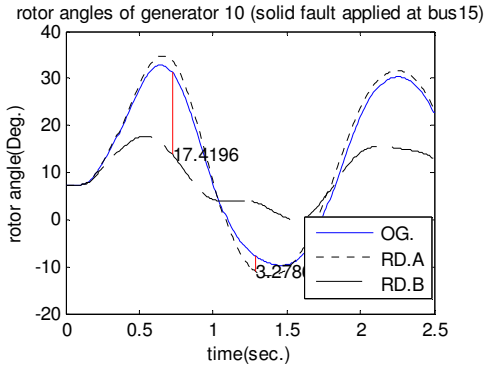
rotor angles of generator 10 (solid fault applied at bus15)
rotor angle(Deg.)
time(sec.)
17.4196
OG.
RD.A
RD.B

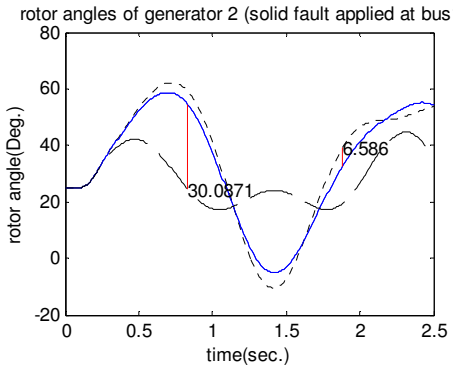
rotor angles of generator 2 (solid fault applied at bus16)
rotor angle(Deg.)
time(sec.)
30.0871
6.586

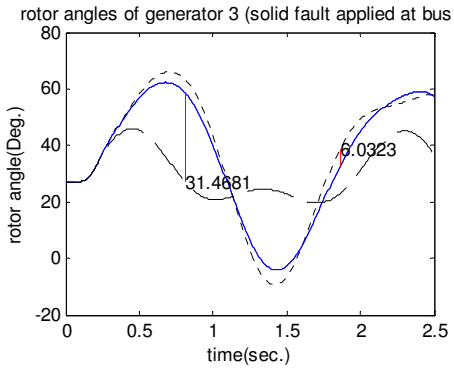
rotor angles of generator 3 (solid fault applied at bus16)
rotor angle(Deg.)
time(sec.)
31.4681
6.0323

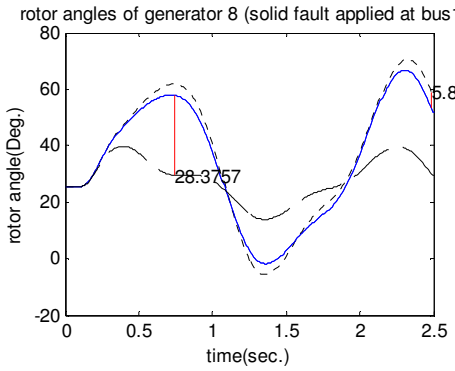
rotor angles of generator 8 (solid fault applied at bus16)
rotor angle(Deg.)
time(sec.)
28.3757
5.8606

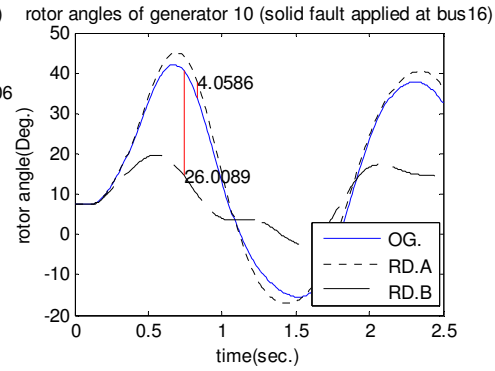
rotor angles of generator 10 (solid fault applied at bus16)
rotor angle(Deg.)
time(sec.)
4.0586
26.0089
OG.
RD.A
RD.B

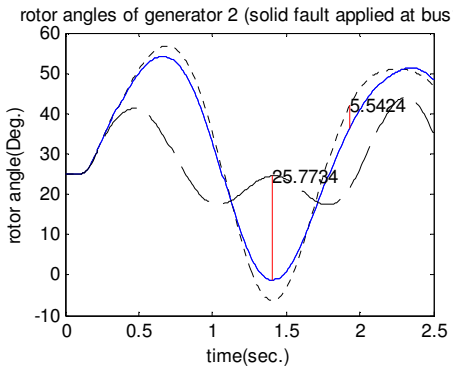
rotor angles of generator 2 (solid fault applied at bus17)
rotor angle(Deg.)
time(sec.)
25.7734
5.5424

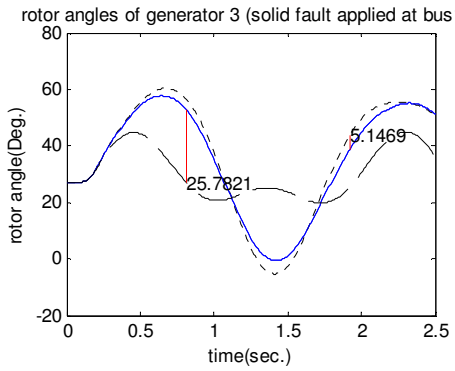
rotor angles of generator 3 (solid fault applied at bus17)
rotor angle(Deg.)
time(sec.)
25.7821
5.1469

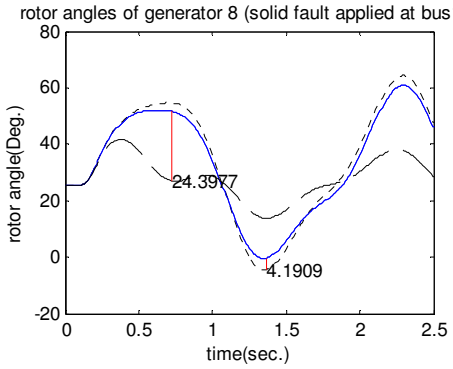
rotor angles of generator 8 (solid fault applied at bus17)
rotor angle(Deg.)
time(sec.)
24.3977
4.1909

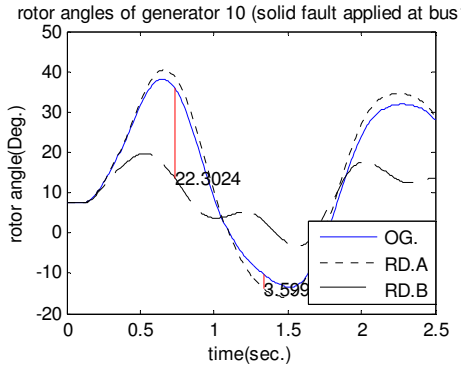
rotor angles of generator 10 (solid fault applied at bus17)
rotor angle(Deg.)
time(sec.)
22.3024
OG.
RD.A
RD.B

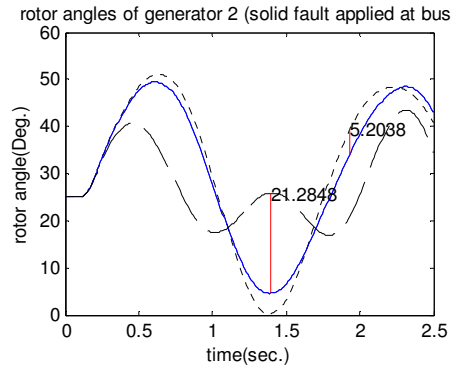
rotor angles of generator 2 (solid fault applied at bus18)
rotor angle(Deg.)
time(sec.)
21.2848
5.2088

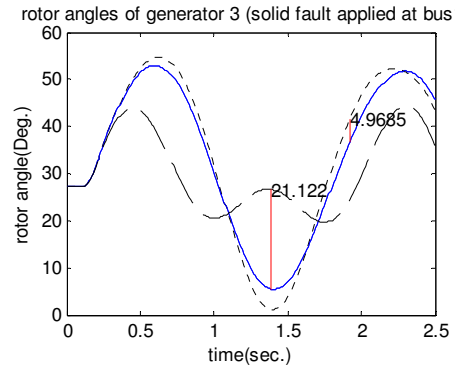
rotor angles of generator 3 (solid fault applied at bus18)
rotor angle(Deg.)
time(sec.)
21.122
4.9685

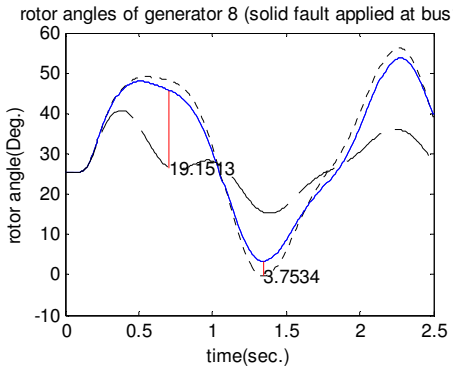
rotor angles of generator 8 (solid fault applied at bus18)
rotor angle(Deg.)
time(sec.)
19.1513
3.7534

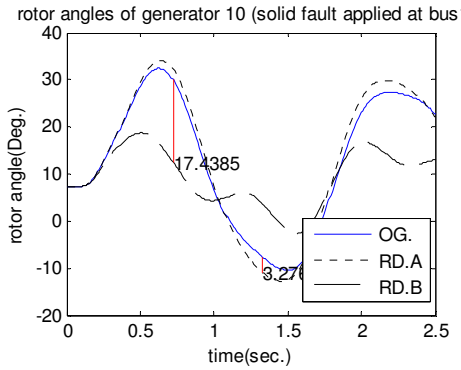
rotor angles of generator 10 (solid fault applied at bus18)
rotor angle(Deg.)
time(sec.)
17.4385
OG.
RD.A
RD.B

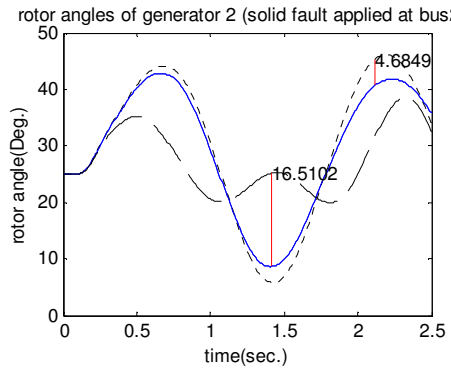
rotor angles of generator 2 (solid fault applied at bus25)
rotor angle(Deg.)
time(sec.)
4.6849
16.5102

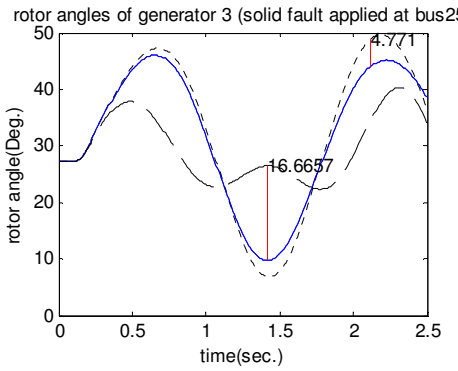
rotor angles of generator 3 (solid fault applied at bus25)
rotor angle(Deg.)
time(sec.)
4.771
16.6657

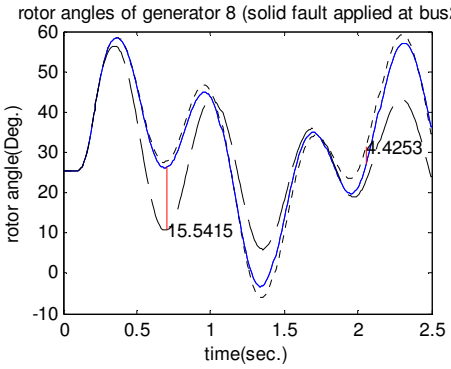
rotor angles of generator 8 (solid fault applied at bus25)
rotor angle(Deg.)
time(sec.)
4.4253
15.5415

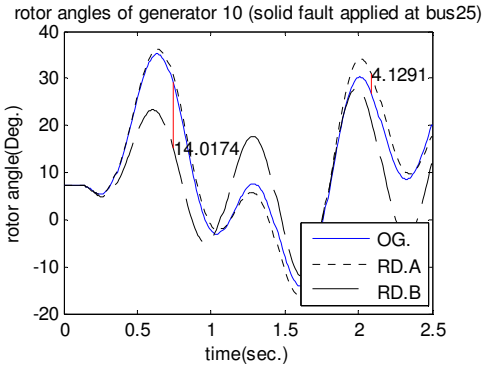
rotor angles of generator 10 (solid fault applied at bus25)
rotor angle(Deg.)
time(sec.)
4.1291
14.0174
OG.
RD.A
RD.B

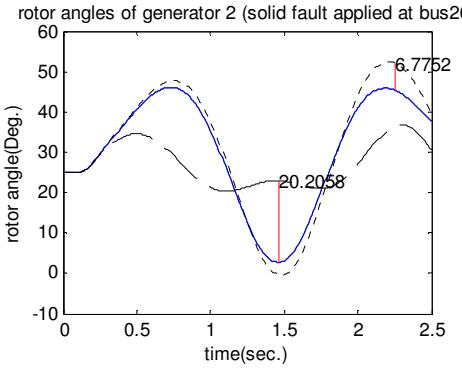
rotor angles of generator 2 (solid fault applied at bus26)
rotor angle(Deg.)
time(sec.)
6.7752
20.2058

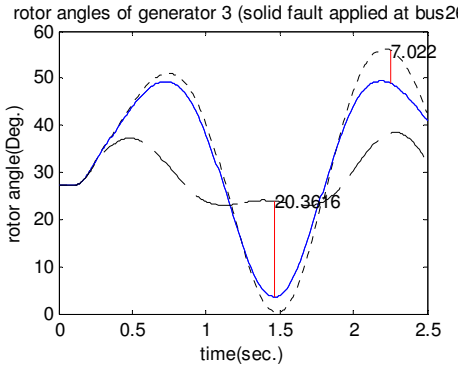
rotor angles of generator 3 (solid fault applied at bus26)
rotor angle(Deg.)
time(sec.)
7.022
20.3616

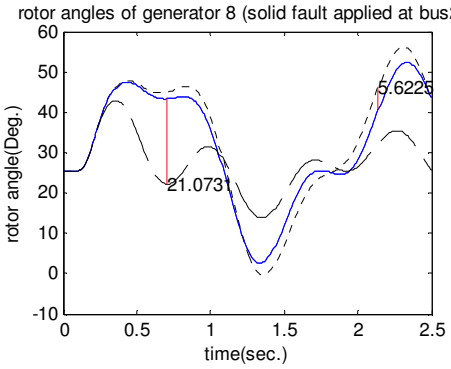
rotor angles of generator 8 (solid fault applied at bus26)
rotor angle(Deg.)
time(sec.)
5.6225
21.0731

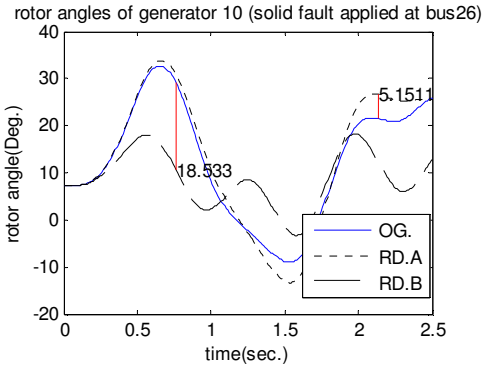
rotor angles of generator 10 (solid fault applied at bus26)
rotor angle(Deg.)
time(sec.)
5.1511
18.533
OG.
RD.A
RD.B

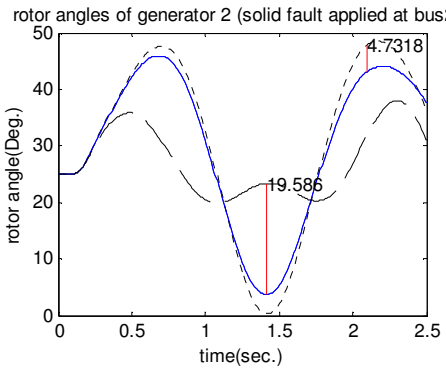
rotor angles of generator 2 (solid fault applied at bus27)
rotor angle(Deg.)
time(sec.)
4.7318
19.586

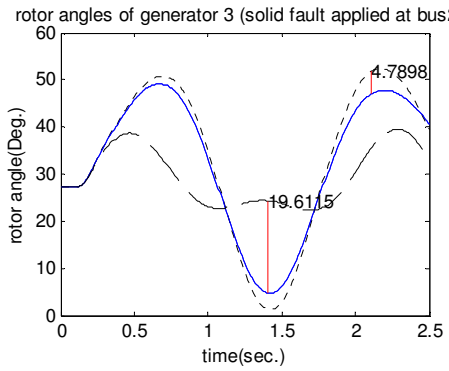
rotor angles of generator 3 (solid fault applied at bus27)
rotor angle(Deg.)
time(sec.)
4.7898
19.6115

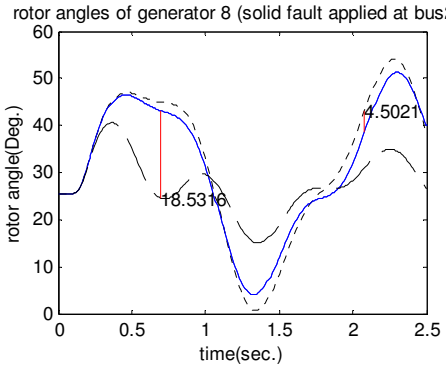
rotor angles of generator 8 (solid fault applied at bus27)
rotor angle(Deg.)
time(sec.)
4.5021
18.5316

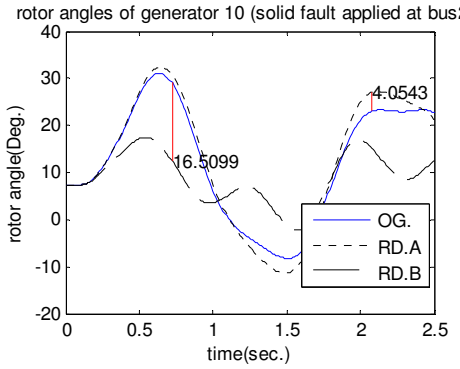
rotor angles of generator 10 (solid fault applied at bus27)
rotor angle(Deg.)
time(sec.)
4.0543
16.5099
OG.
RD.A
RD.B

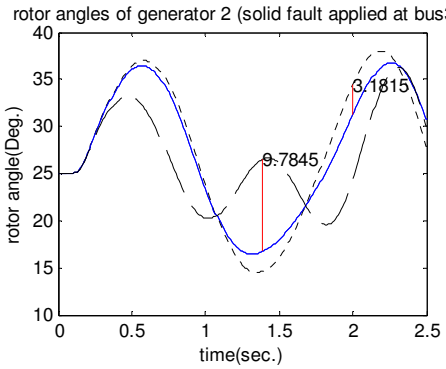
rotor angles of generator 2 (solid fault applied at bus30)
rotor angle(Deg.)
time(sec.)
3.1815
9.7845

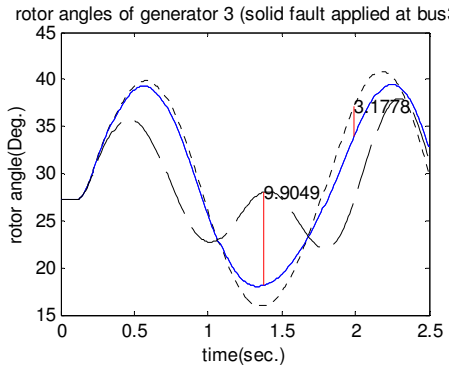
rotor angles of generator 3 (solid fault applied at bus30)
rotor angle(Deg.)
time(sec.)
3.1778
9.9049

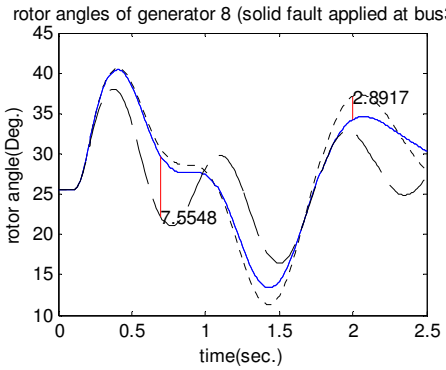
rotor angles of generator 8 (solid fault applied at bus30)
rotor angle(Deg.)
time(sec.)
2.8917
7.5548

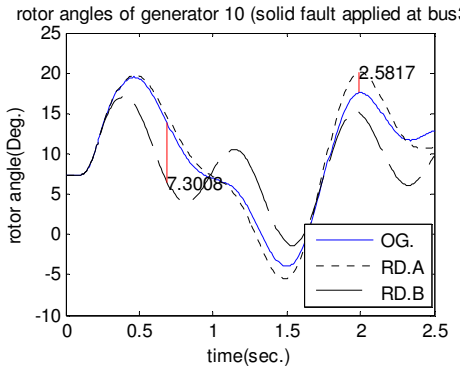
rotor angles of generator 10 (solid fault applied at bus30)
rotor angle(Deg.)
time(sec.)
2.5817
7.3008
OG.
RD.A
RD.B

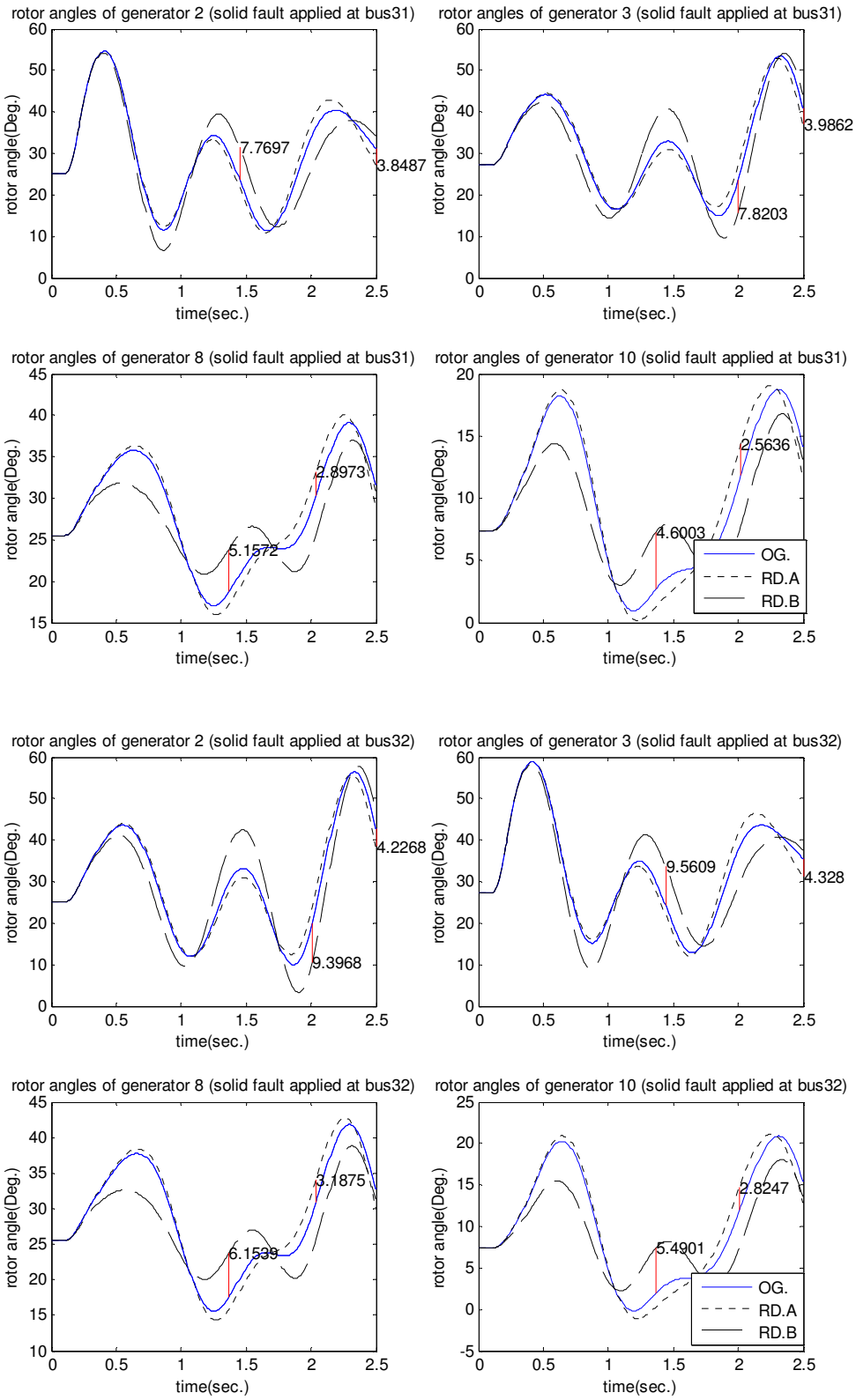
rotor angles of generator 2 (solid fault applied at bus31)
rotor angle(Deg.)
time(sec.)
7.7697
3.8487
rotor angles of generator 3 (solid fault applied at bus31)
rotor angle(Deg.)
time(sec.)
3.9862
7.8203
rotor angles of generator 8 (solid fault applied at bus31)
rotor angle(Deg.)
time(sec.)
2.8973
5.1572
rotor angles of generator 10 (solid fault applied at bus31)
rotor angle(Deg.)
time(sec.)
2.5636
4.6003
OG.
RD.A
RD.B
rotor angles of generator 2 (solid fault applied at bus32)
rotor angle(Deg.)
time(sec.)
4.2268
9.3968
rotor angles of generator 3 (solid fault applied at bus32)
rotor angle(Deg.)
time(sec.)
9.5609
4.328
rotor angles of generator 8 (solid fault applied at bus32)
rotor angle(Deg.)
time(sec.)
3.1875
6.1539
rotor angles of generator 10 (solid fault applied at bus32)
rotor angle(Deg.)
time(sec.)
2.8247
5.4901
OG.
RD.A
RD.B

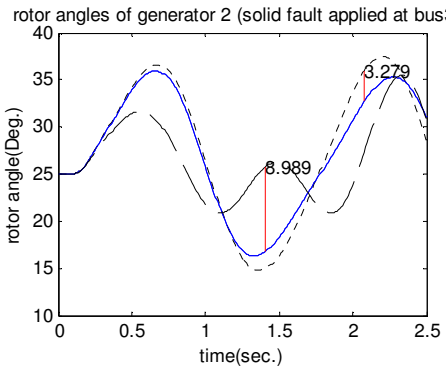
rotor angles of generator 2 (solid fault applied at bus37)
rotor angle(Deg.)
time(sec.)
8.989
3.279

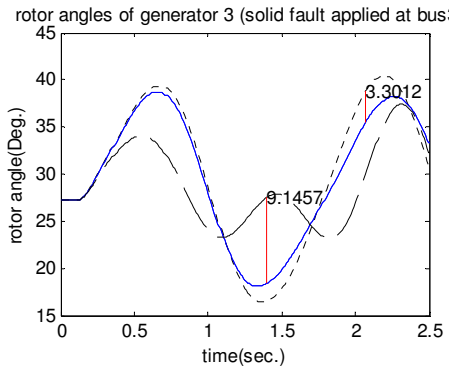
rotor angles of generator 3 (solid fault applied at bus37)
rotor angle(Deg.)
time(sec.)
9.1457
3.3012

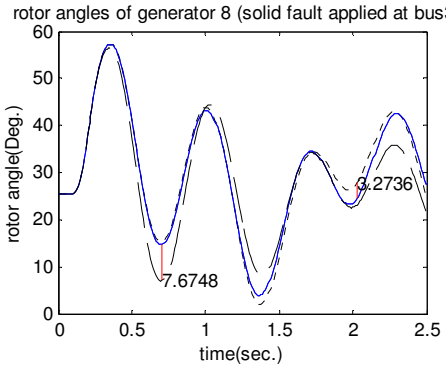
rotor angles of generator 8 (solid fault applied at bus37)
rotor angle(Deg.)
time(sec.)
7.6748
3.2736

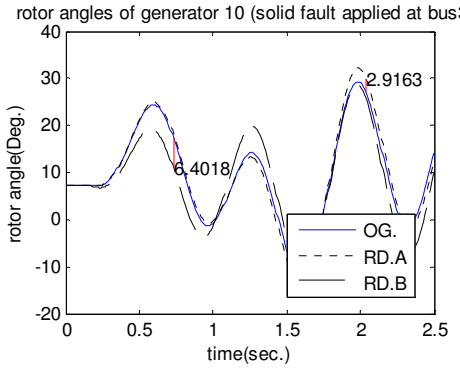
rotor angles of generator 10 (solid fault applied at bus37)
rotor angle(Deg.)
time(sec.)
6.4018
2.9163
OG.
RD.A
RD.B

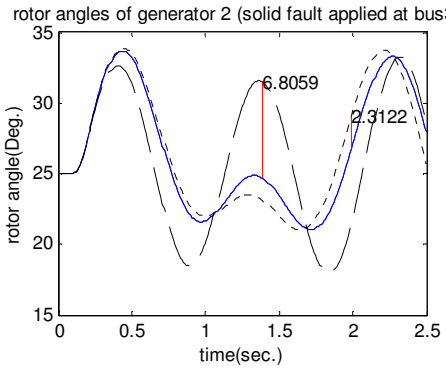
rotor angles of generator 2 (solid fault applied at bus39)
rotor angle(Deg.)
time(sec.)
6.8059
2.3122

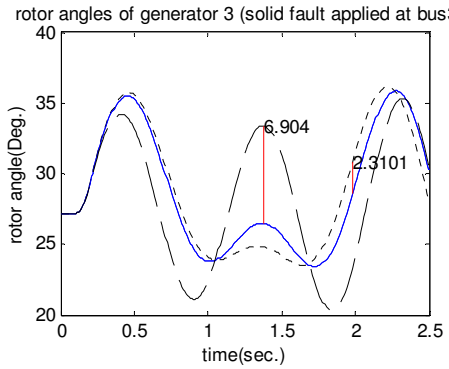
rotor angles of generator 3 (solid fault applied at bus39)
rotor angle(Deg.)
time(sec.)
6.904
2.3101

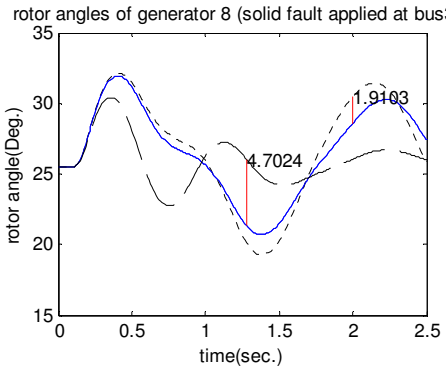
rotor angles of generator 8 (solid fault applied at bus39)
rotor angle(Deg.)
time(sec.)
4.7024
1.9103

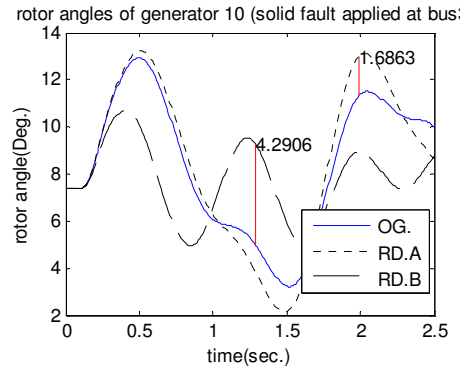
rotor angles of generator 10 (solid fault applied at bus39)
rotor angle(Deg.)
time(sec.)
4.2906
1.6863
OG.
RD.A
RD.B

C.2 Rotor angle plot of case study 1.2

The plots in this section show the comparison between the rotor angle of the original system and the rotor angle of the reduced system of each scenarios of case study 1.2, when the large fault is applied at each internal bus. The details for each scenarios are repeated here.

Scenario 1: the external equivalent generators are represented by the fourth order generator dynamic model.

Scenario 2: the external equivalent generators are represented by the third order generator dynamic model.

Scenario 3: the external equivalent generators are represented by the second order generator dynamic model.

Case study 1.2: Scenario 1

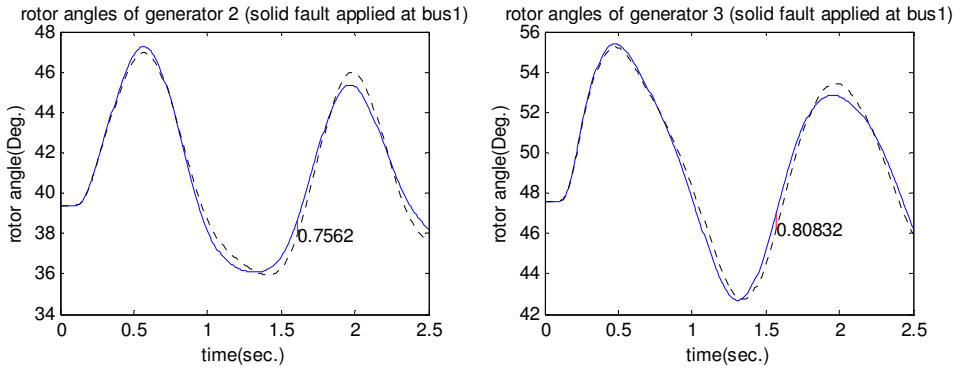

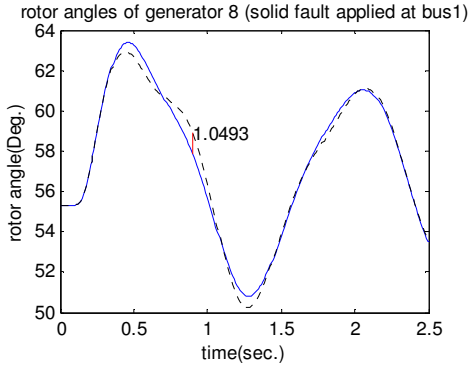

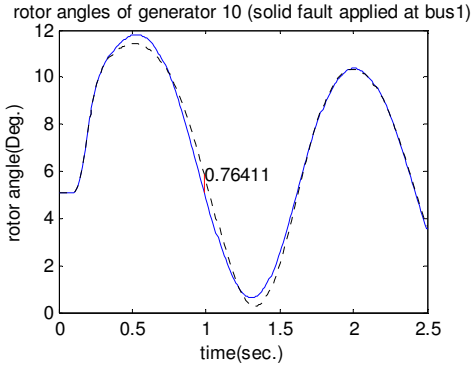

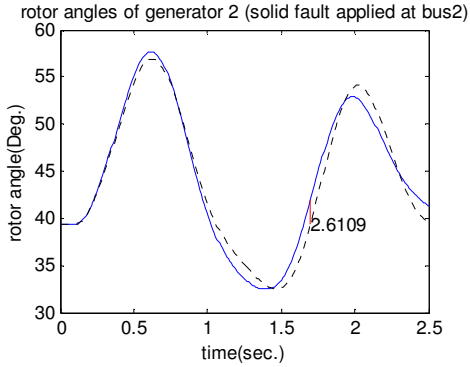

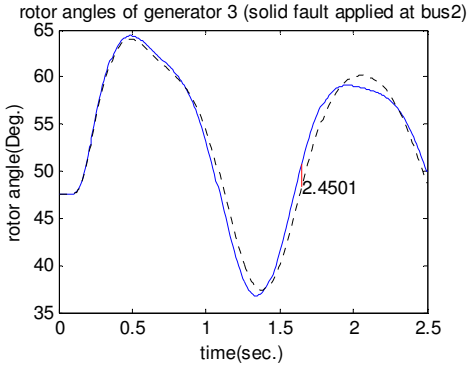

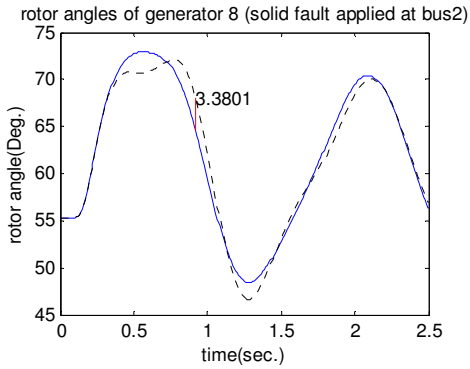

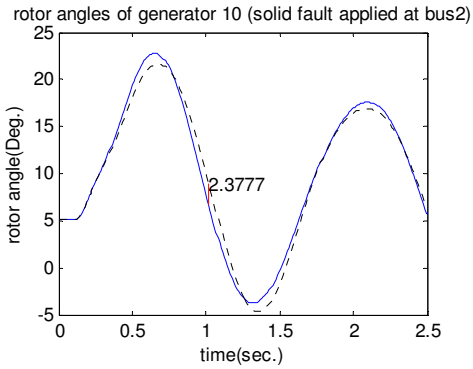

Case study 1.2: Scenario 1

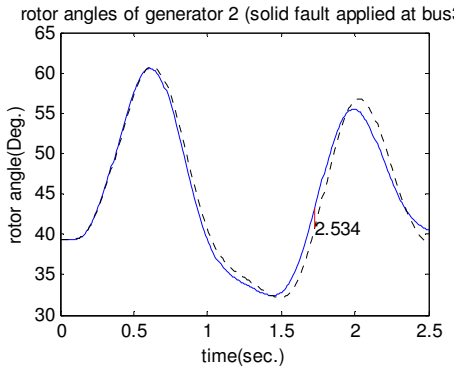

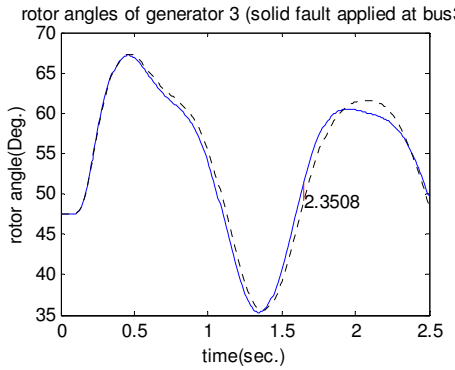

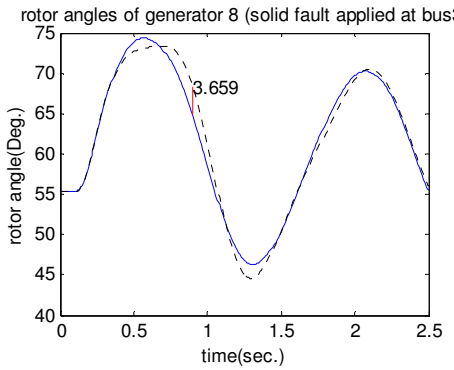

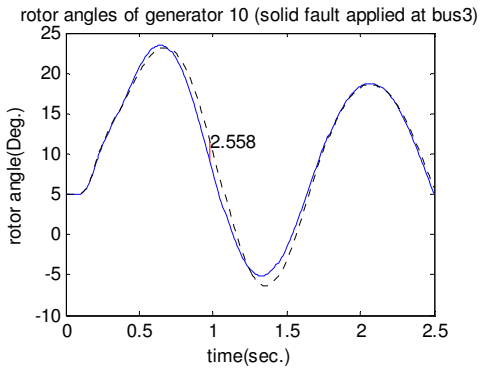

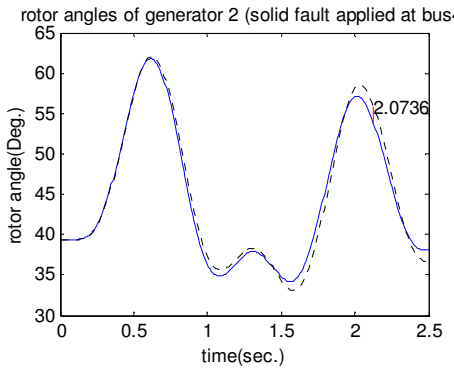

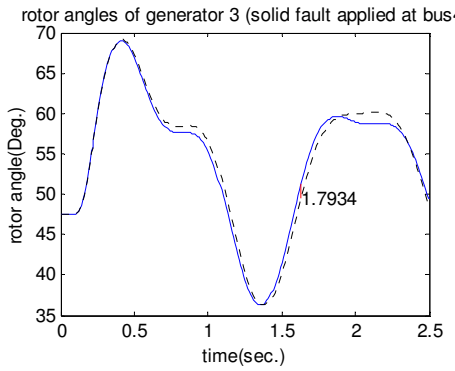

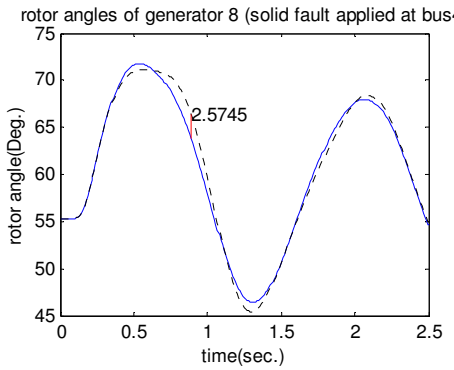

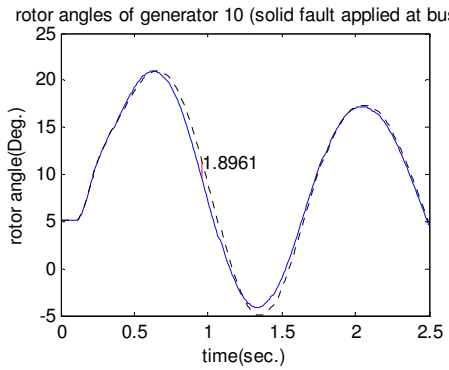

Case study 1.2: Scenario 1

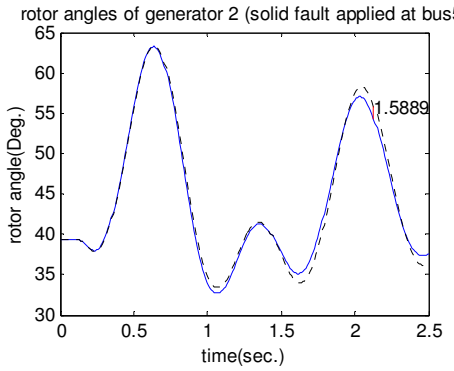

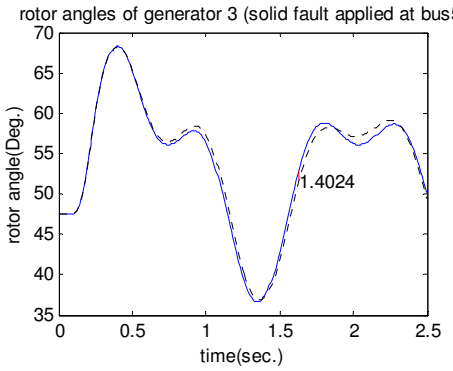

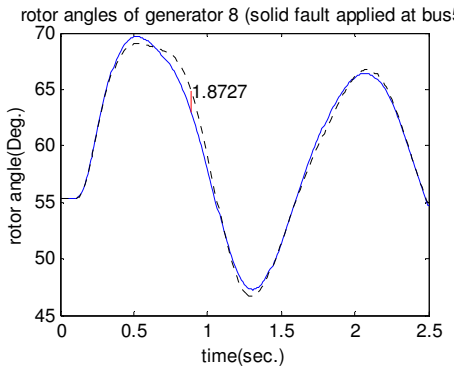

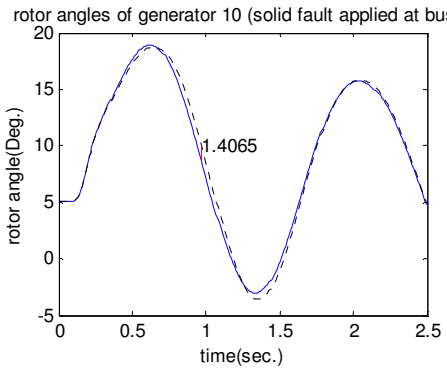

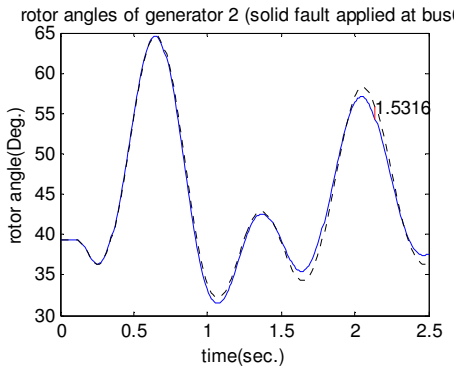

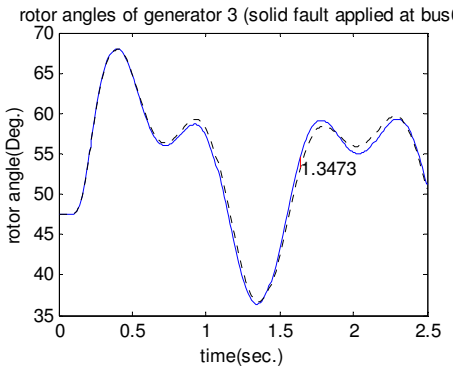

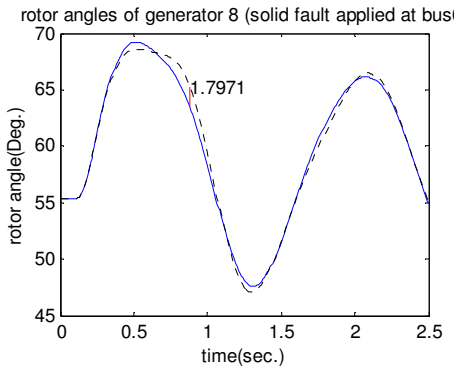

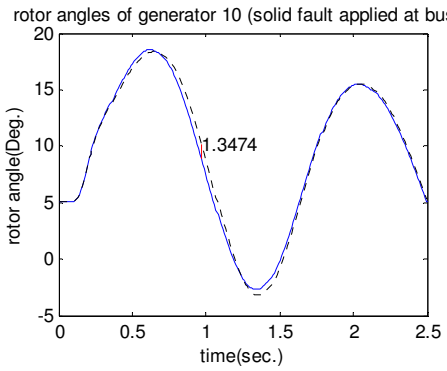

Case study 1.2: Scenario 1

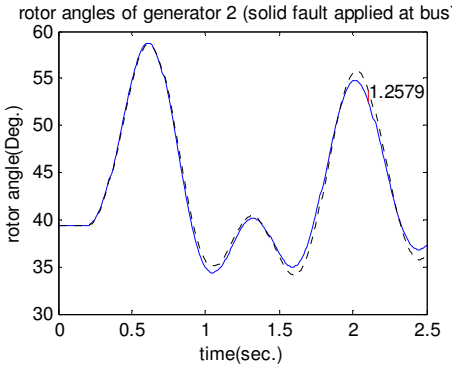

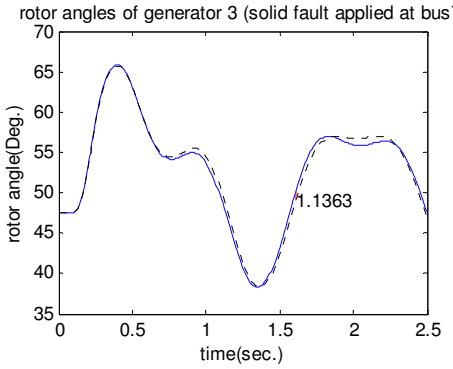

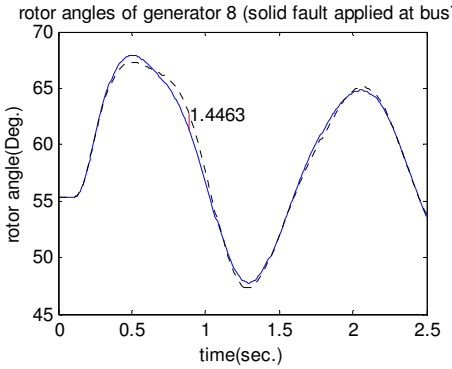

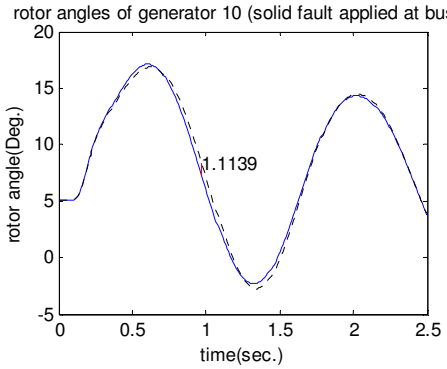

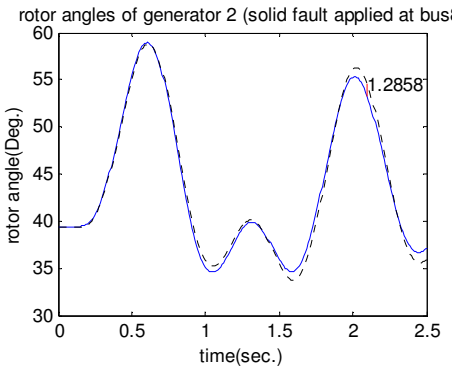

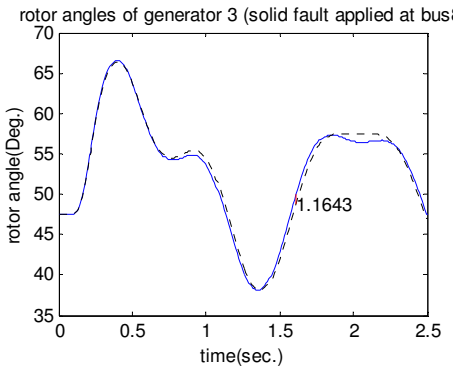

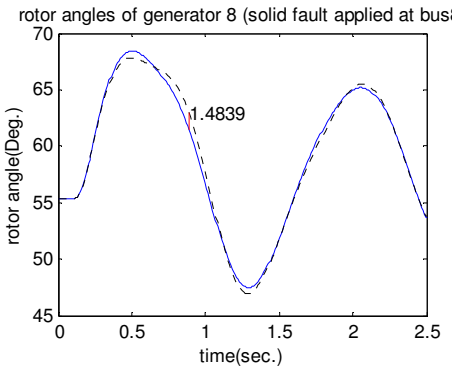

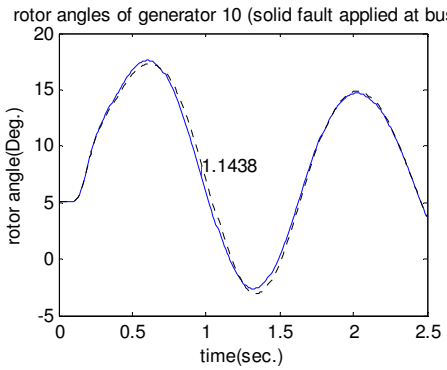

Case study 1.2: Scenario 1

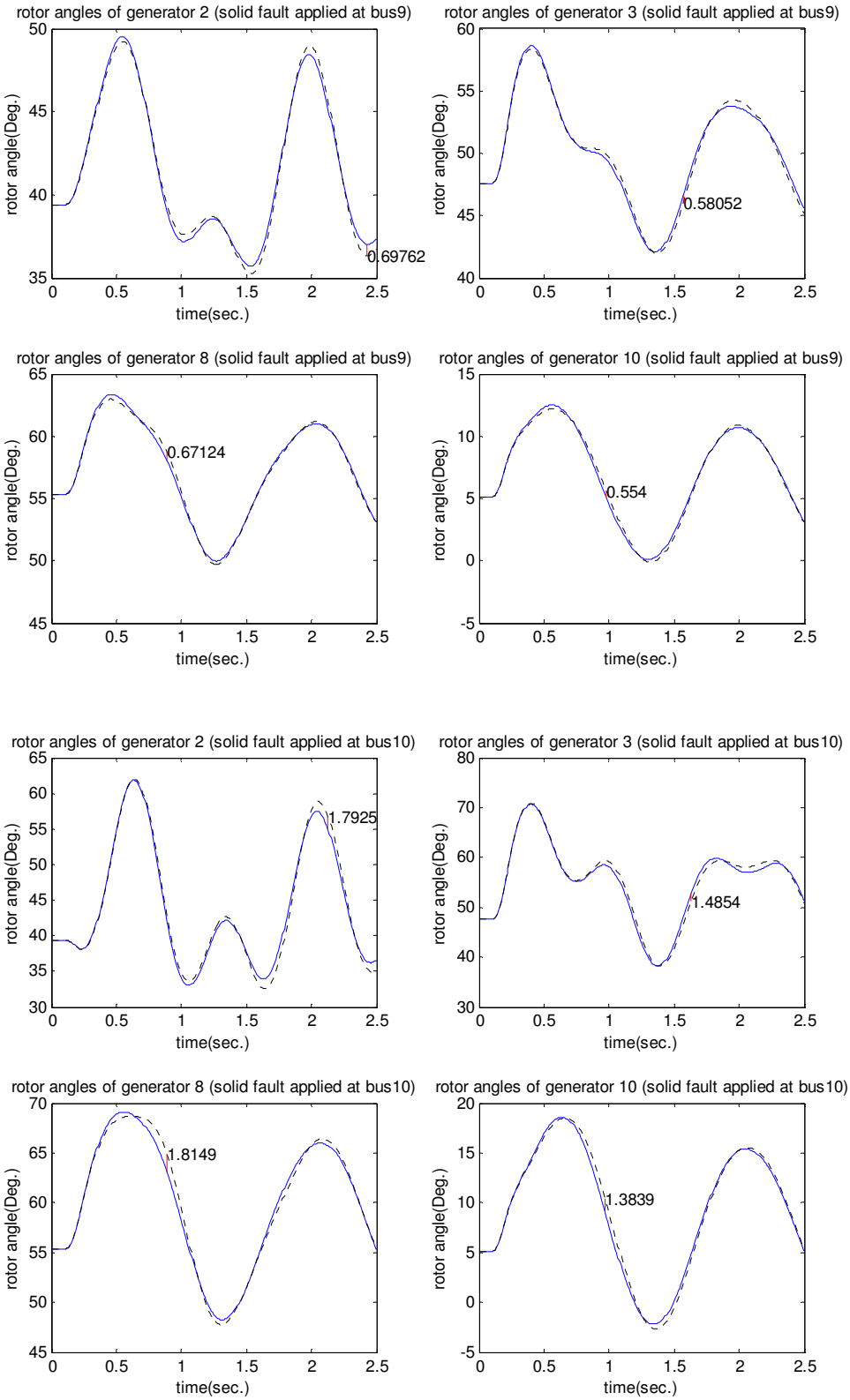

Case study 1.2: Scenario 1

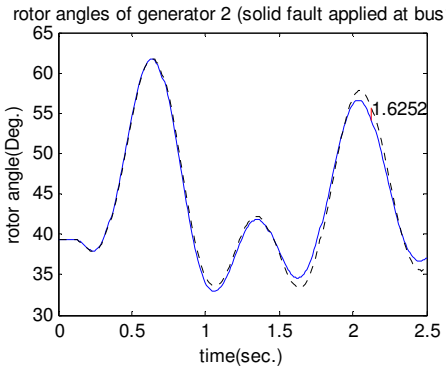

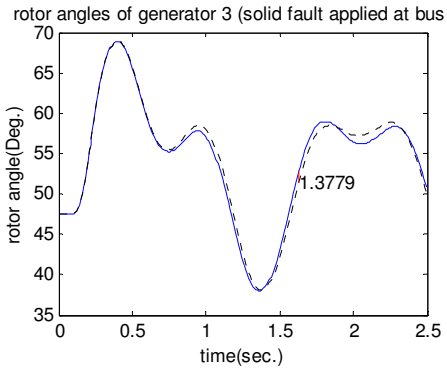

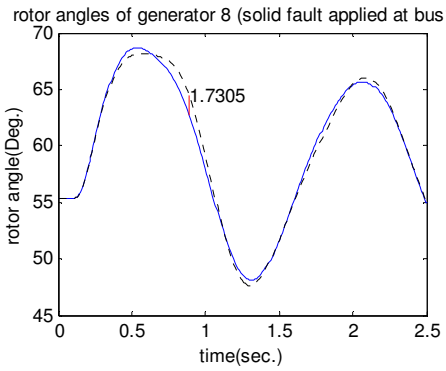

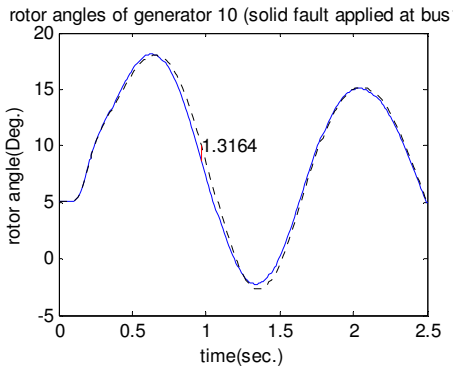

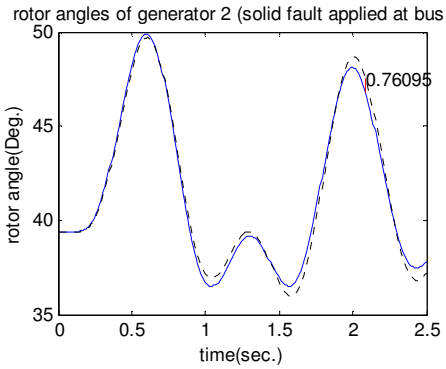

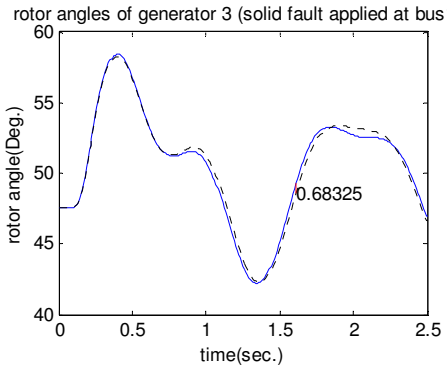

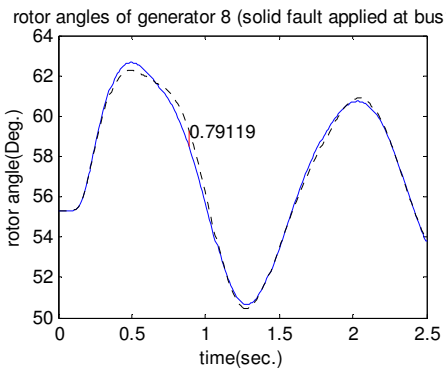

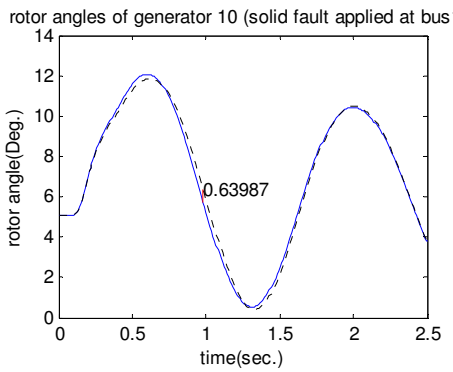

Case study 1.2: Scenario 1

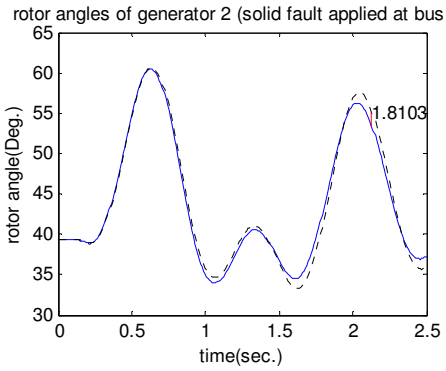

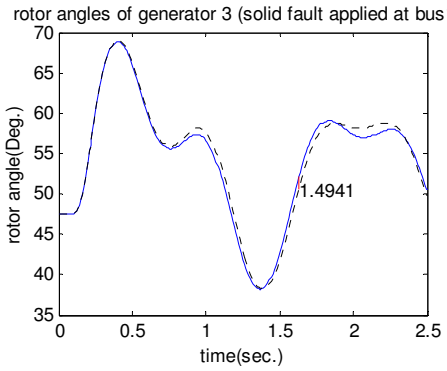

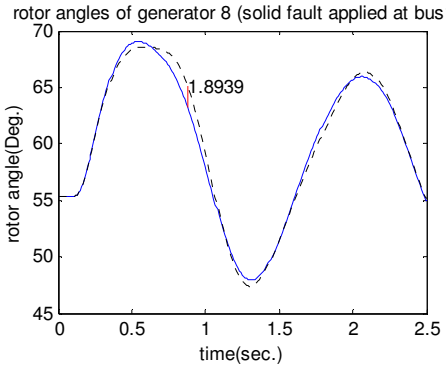

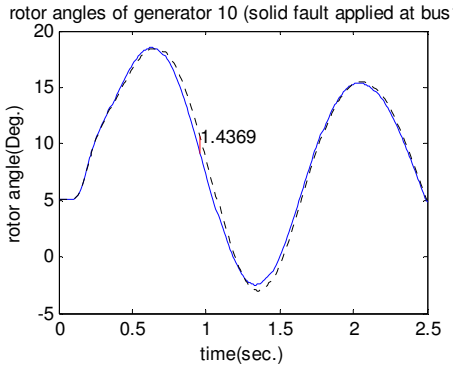

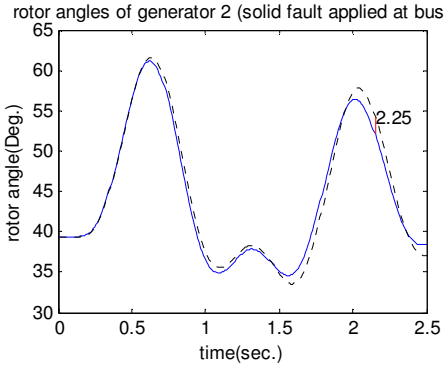

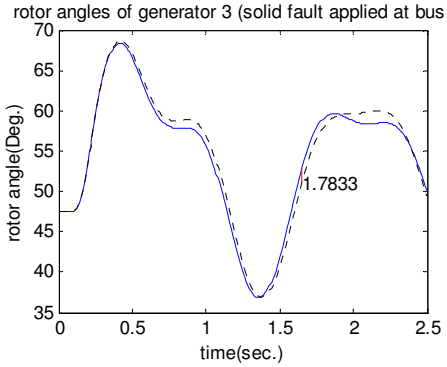

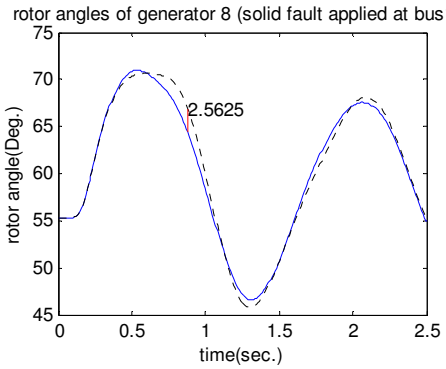

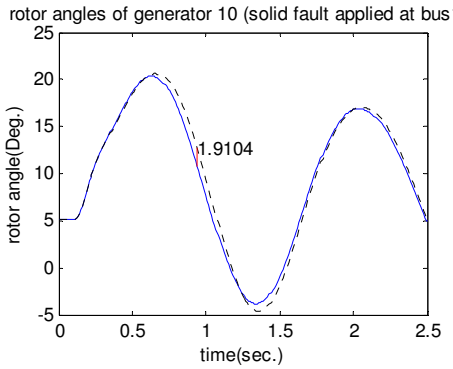

Case study 1.2: Scenario 1

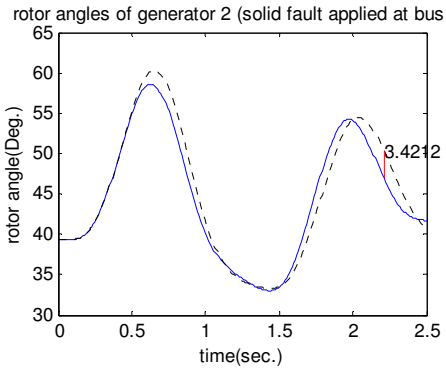

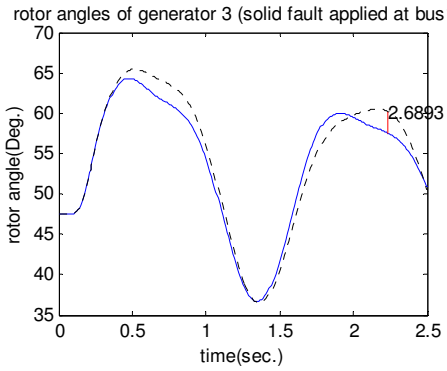

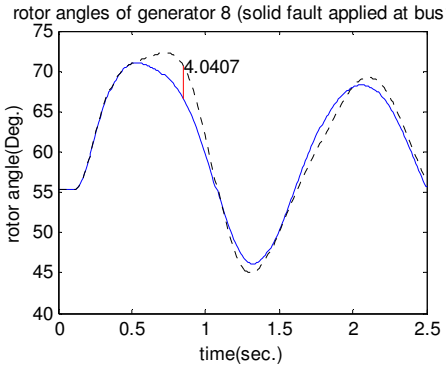

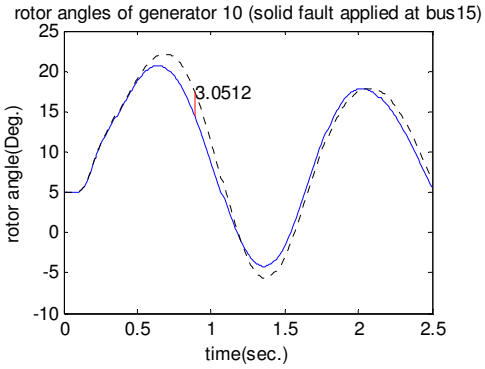

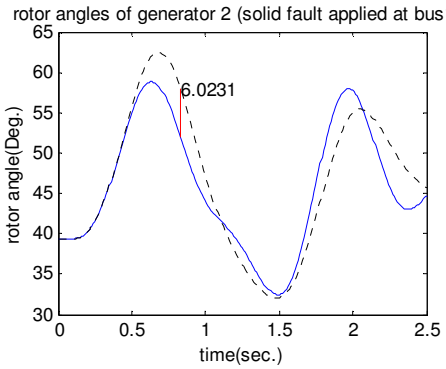

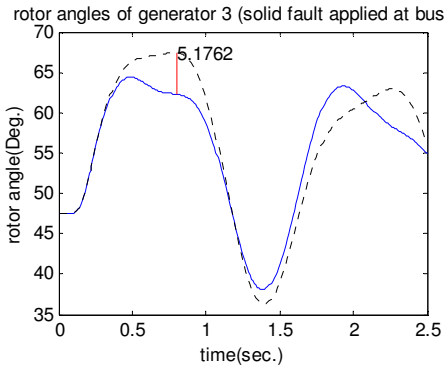

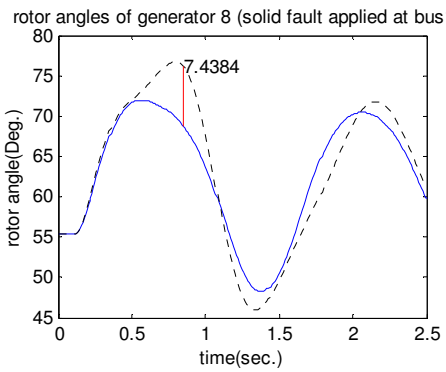

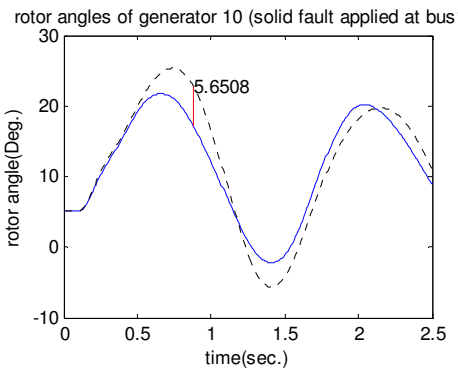

Case study 1.2: Scenario 1

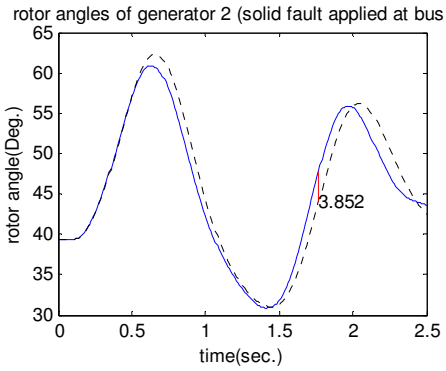

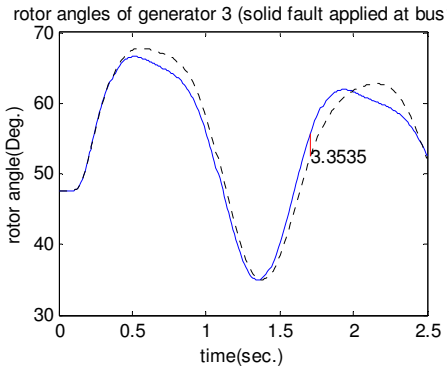

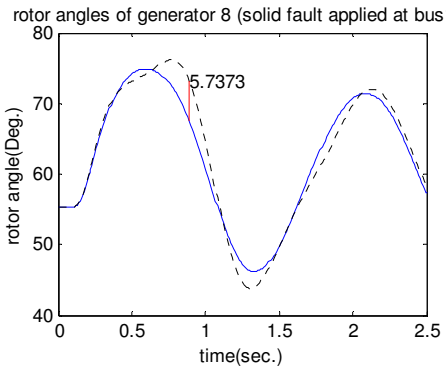

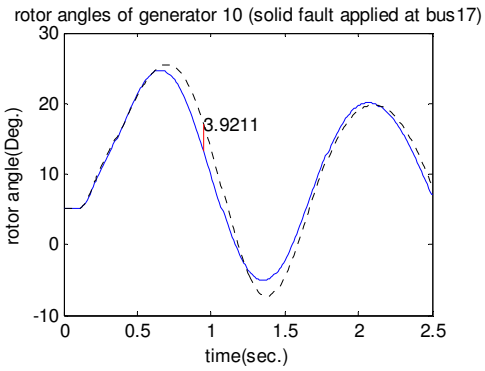

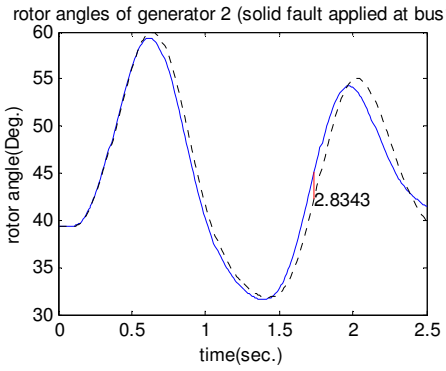

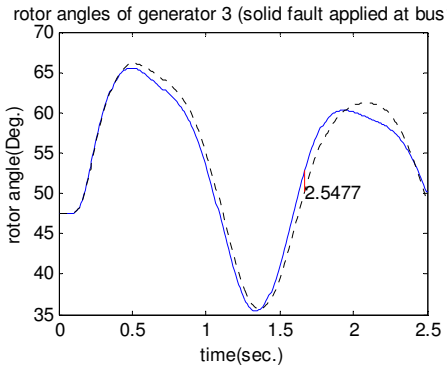

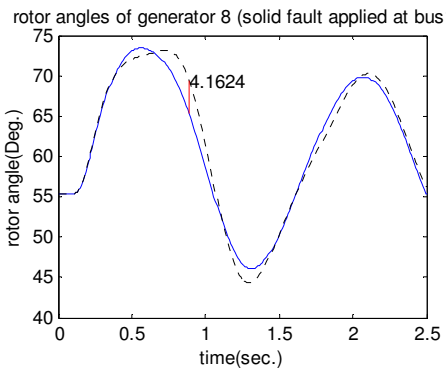

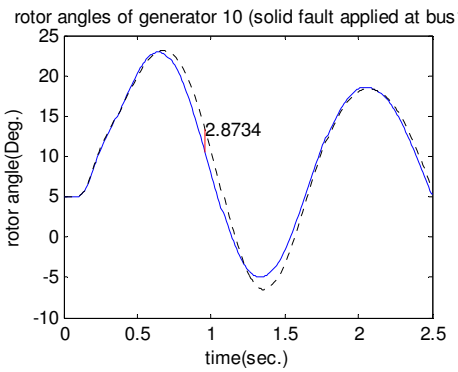

Case study 1.2: Scenario 1

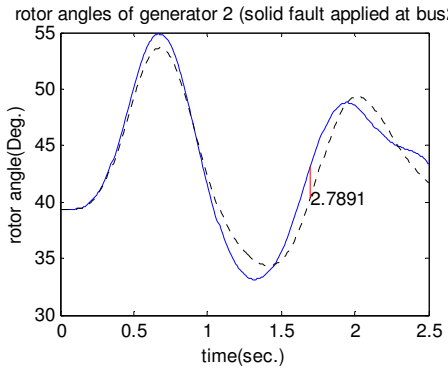

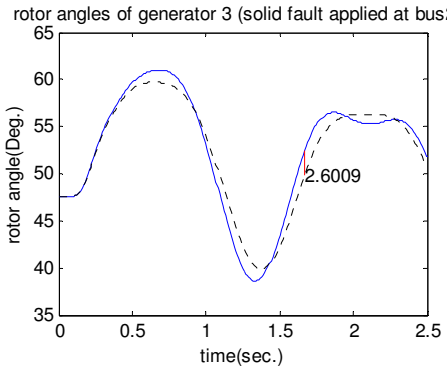

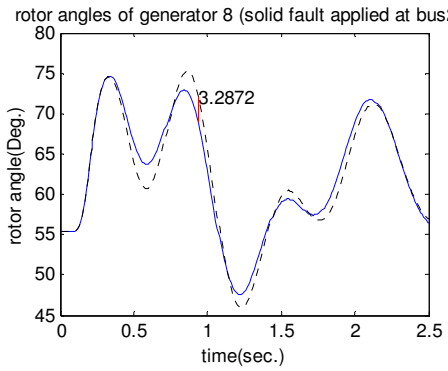

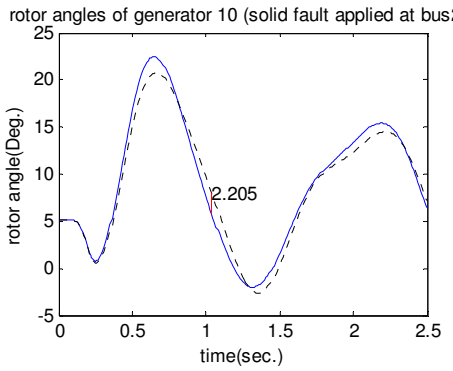

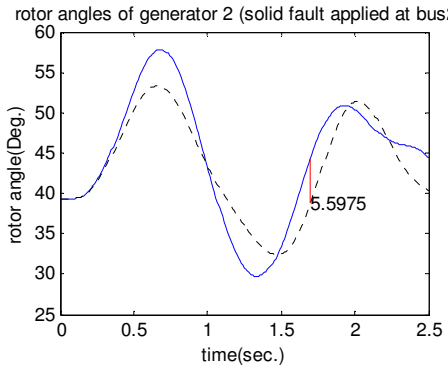

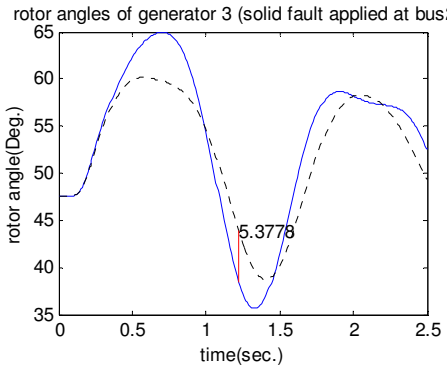

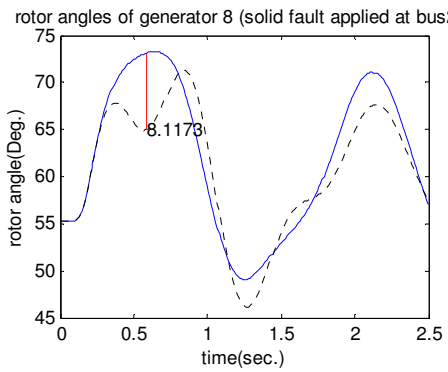

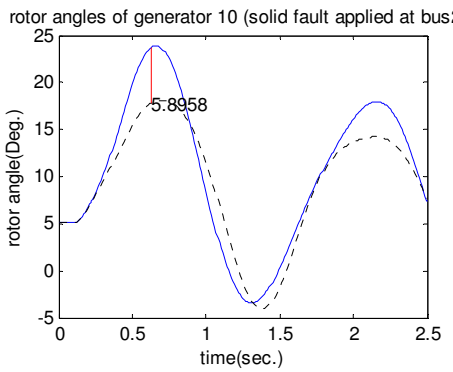

Case study 1.2: Scenario 1

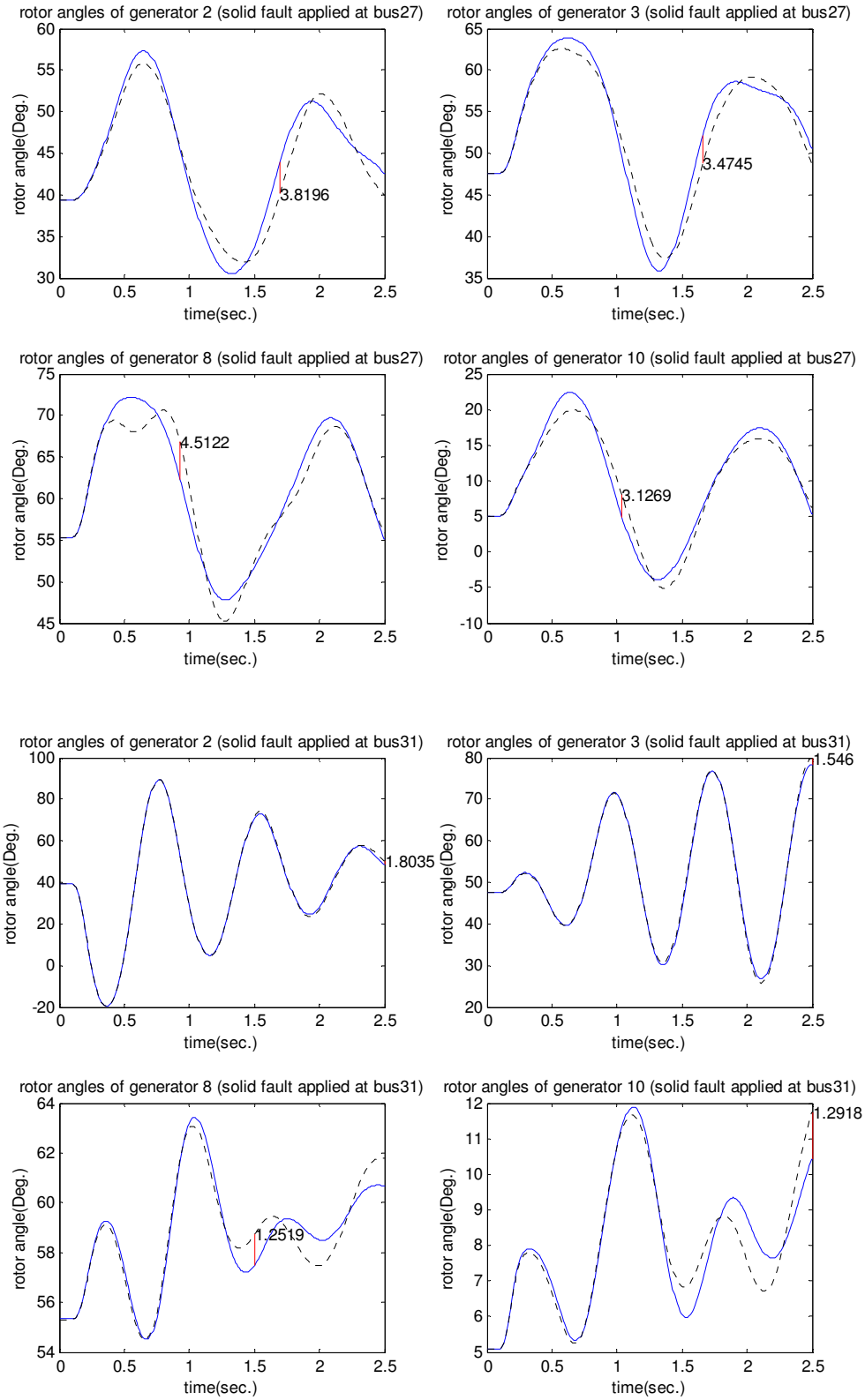

Case study 1.2: Scenario 1

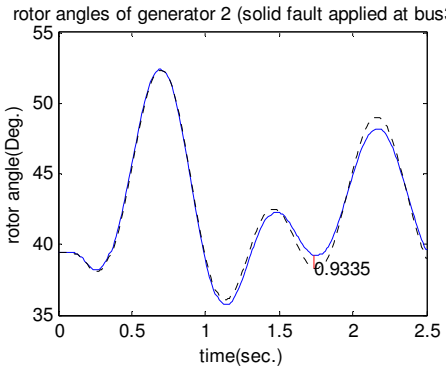

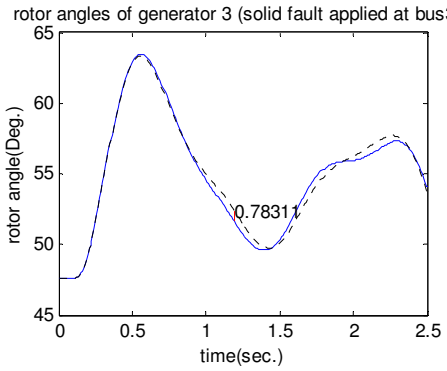

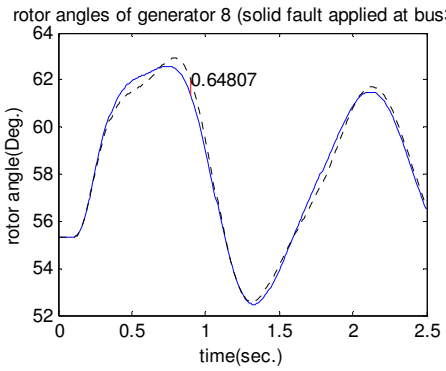

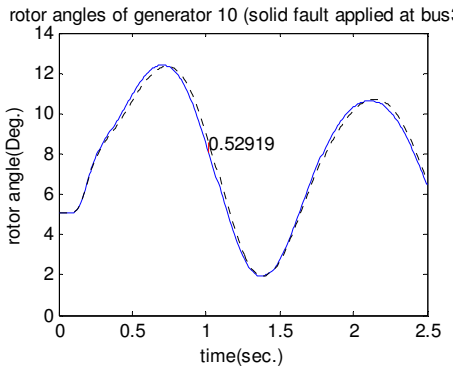

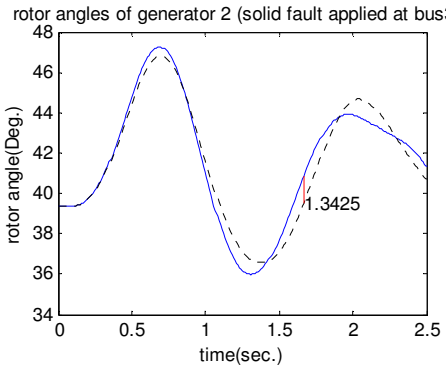

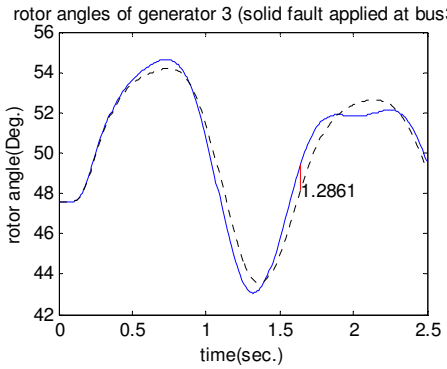

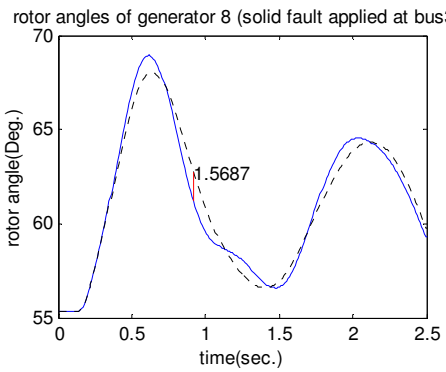

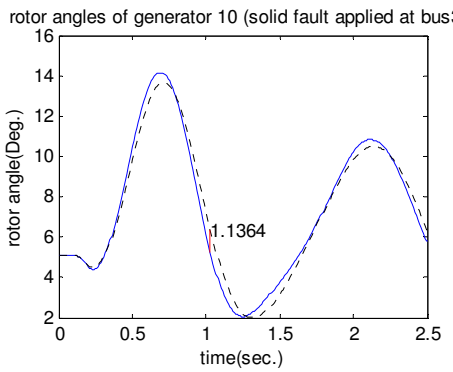

Case study 1.2: Scenario 1

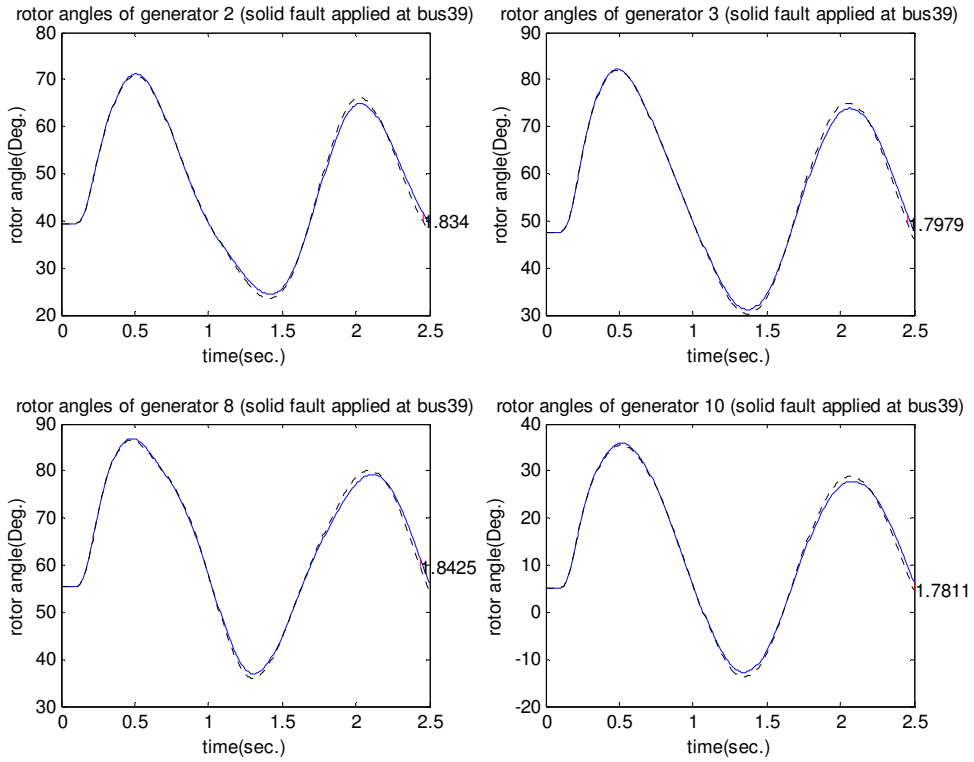

Case study 1.2: Scenario 2

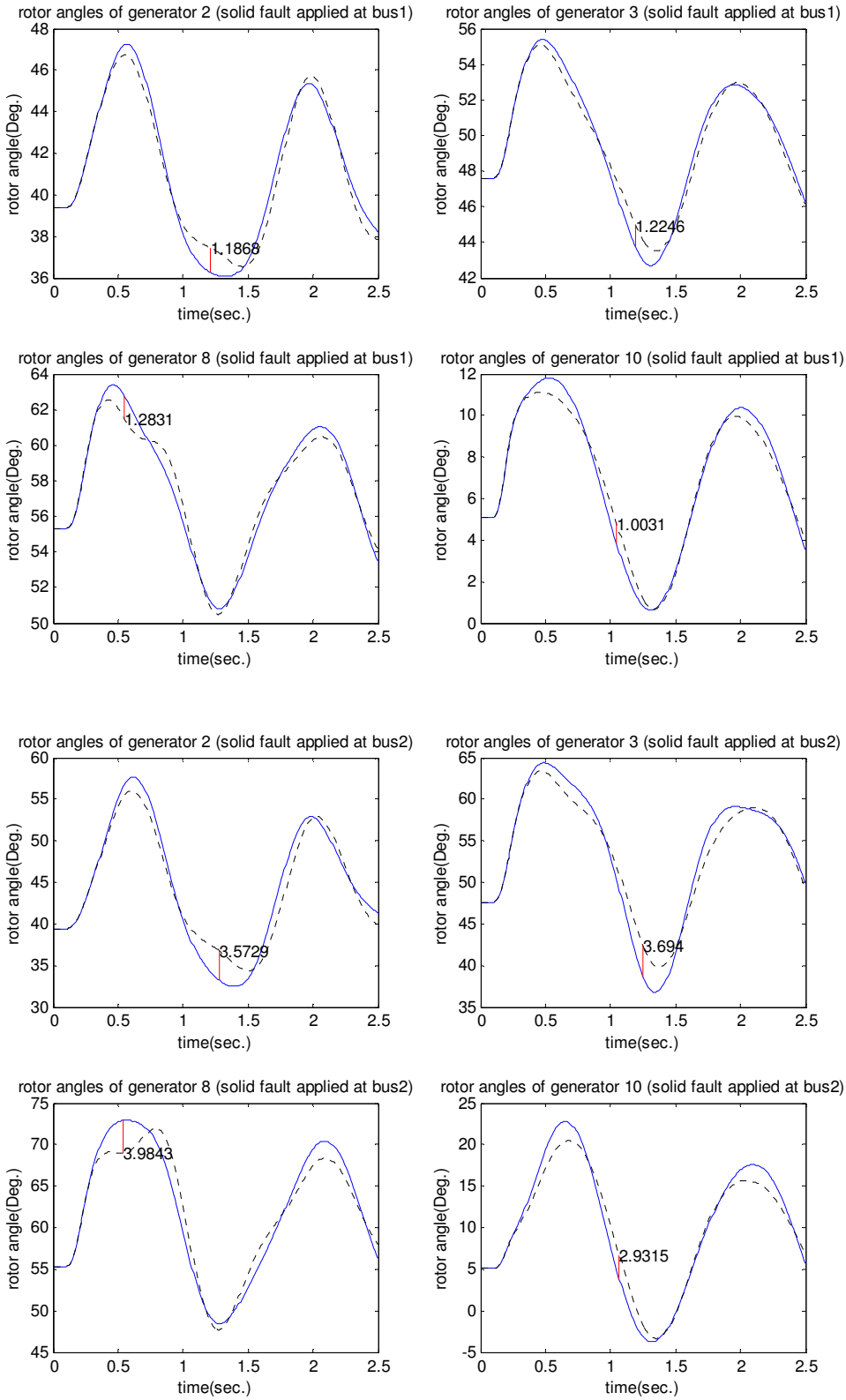

Case study 1.2: Scenario 2

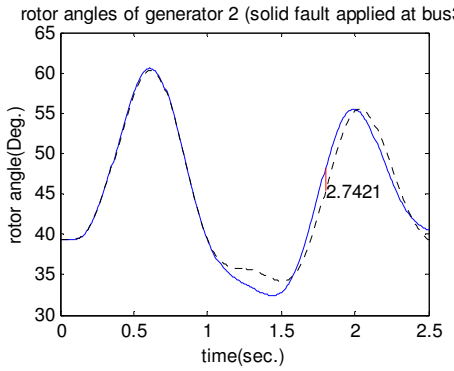

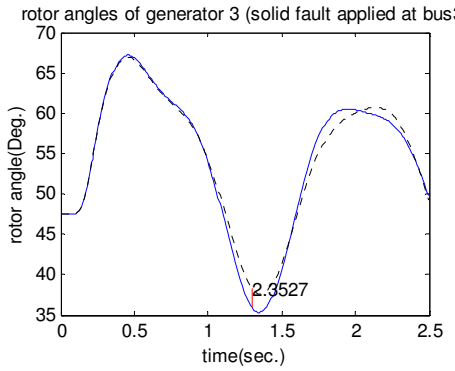

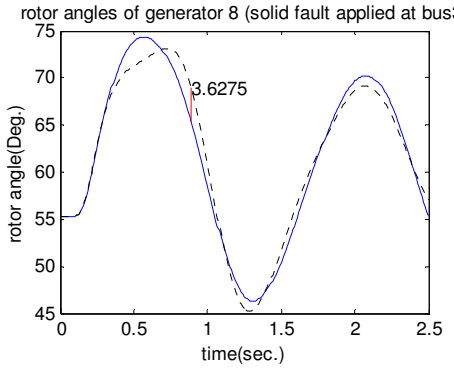

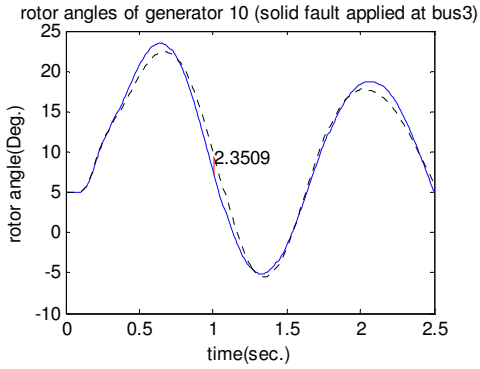

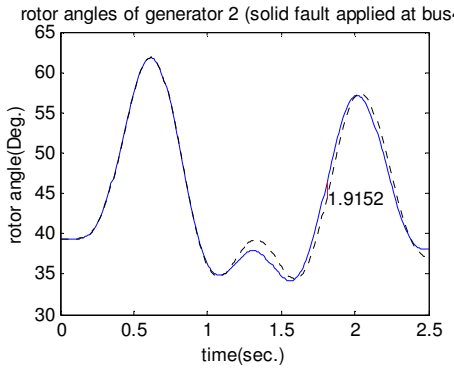

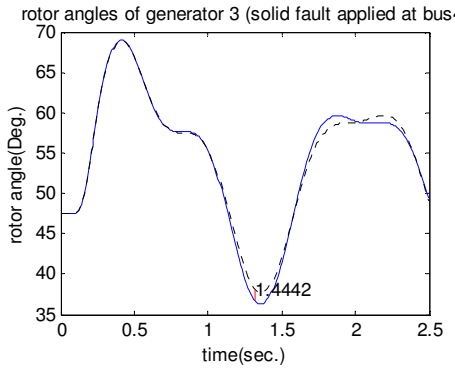

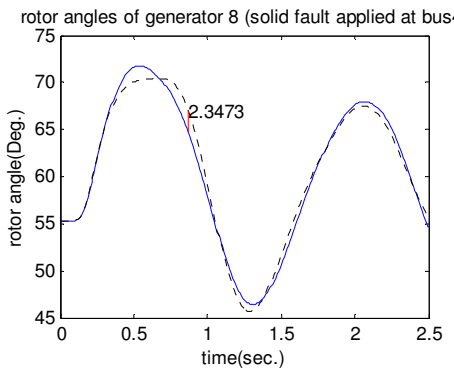

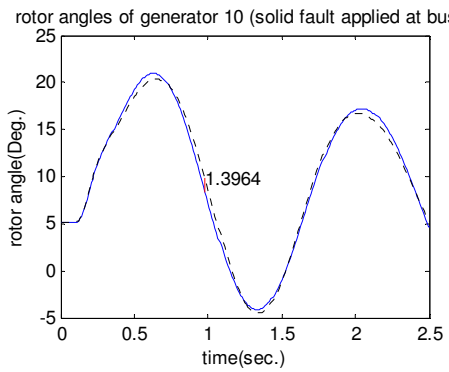

Case study 1.2: Scenario 2

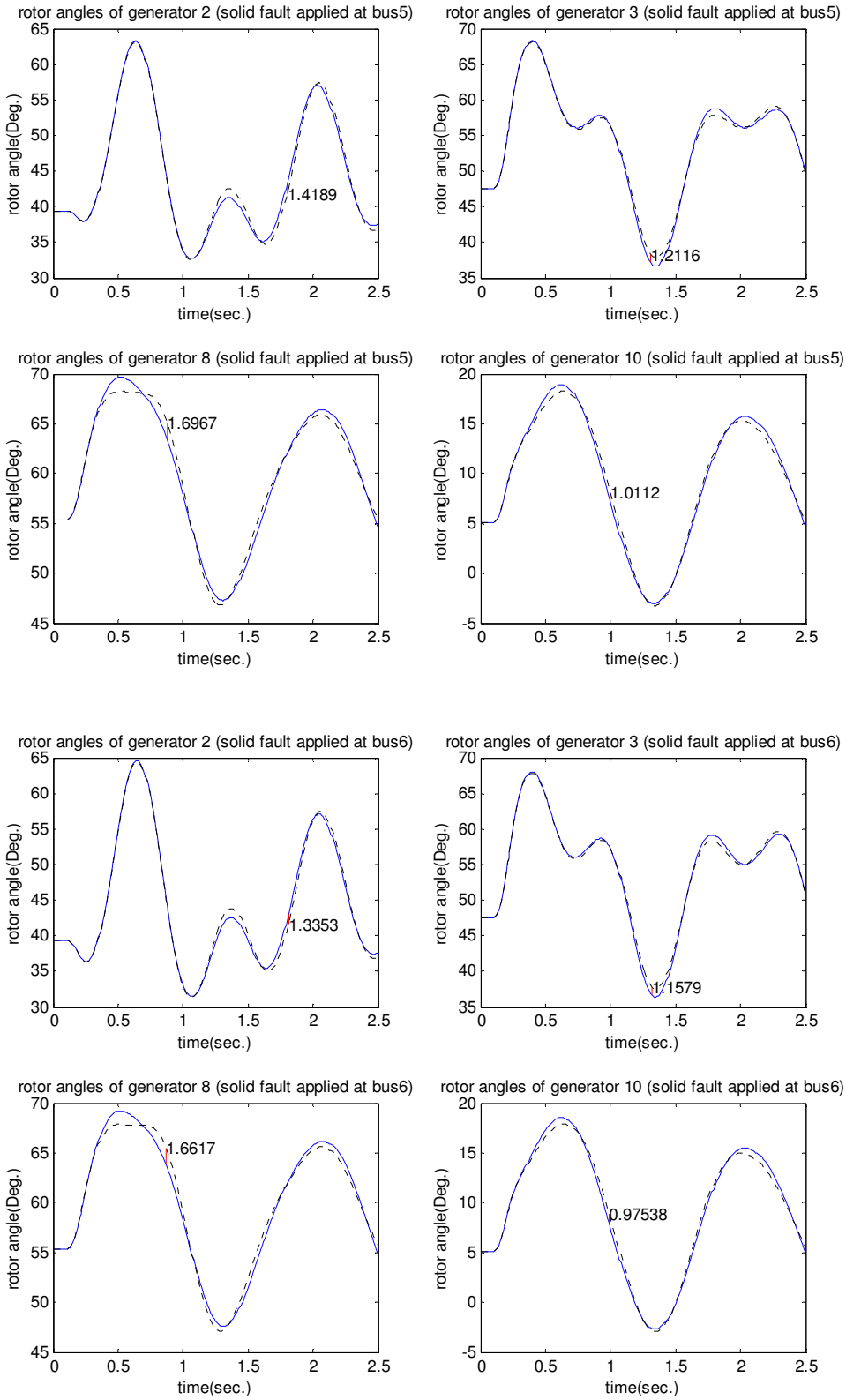

Case study 1.2: Scenario 2

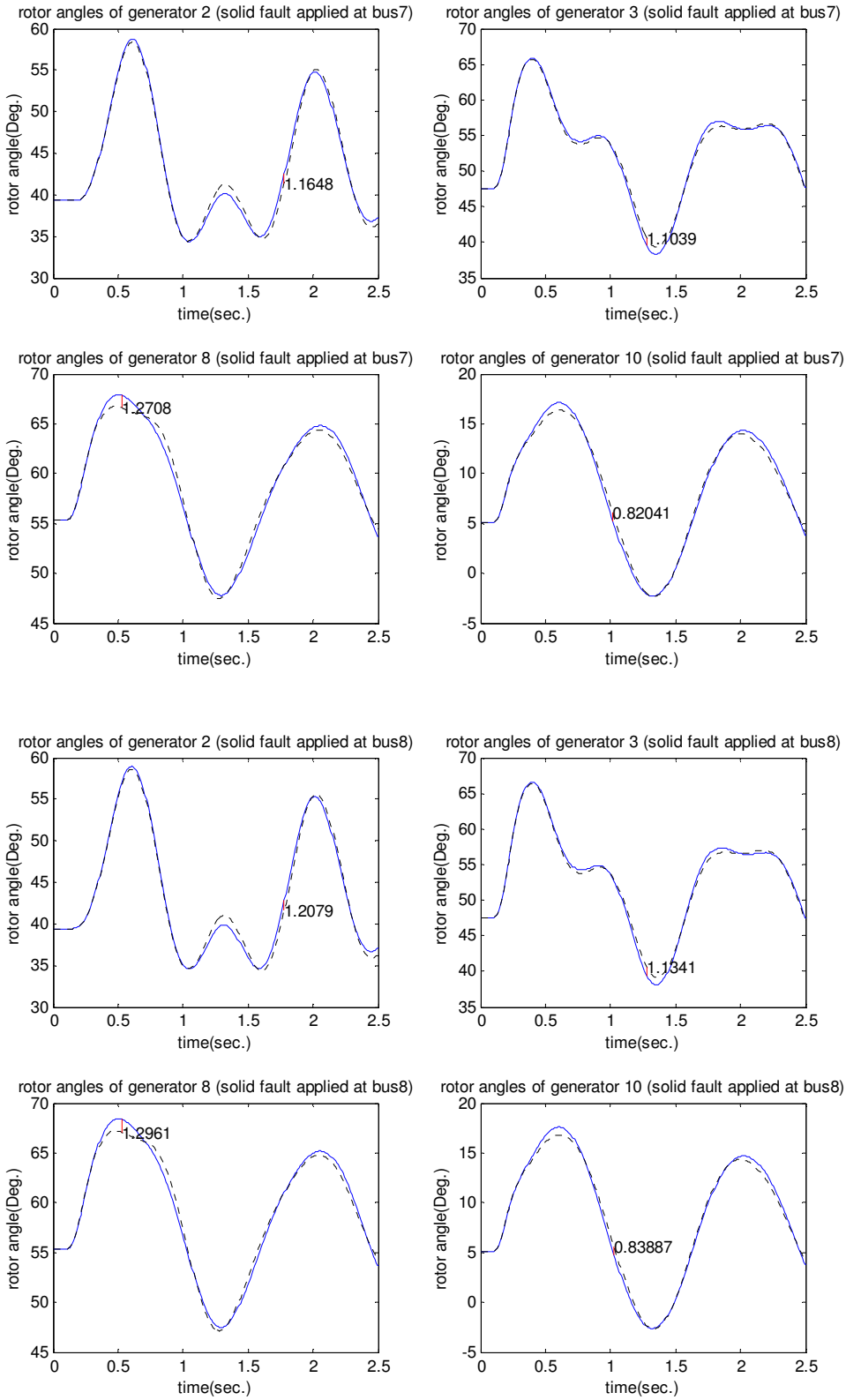

Case study 1.2: Scenario 2

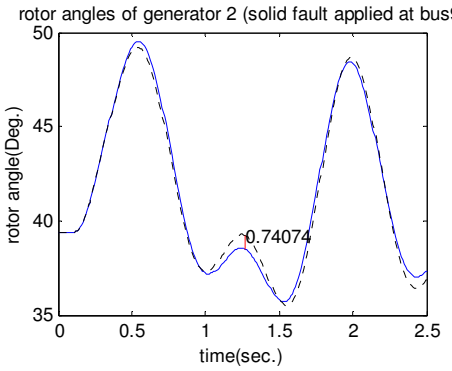

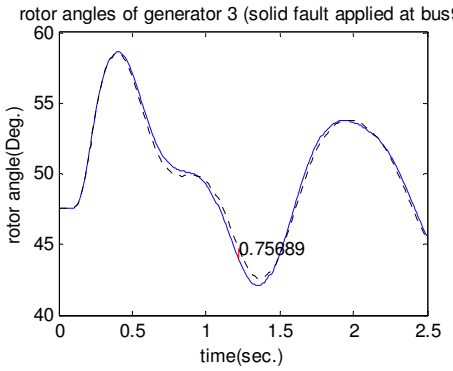

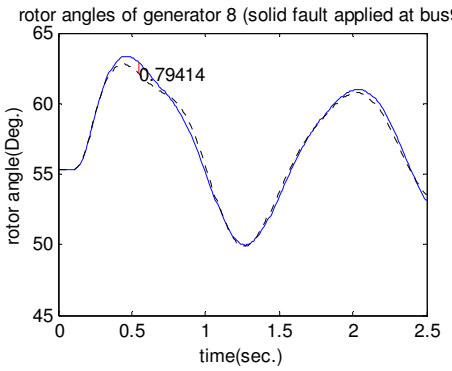

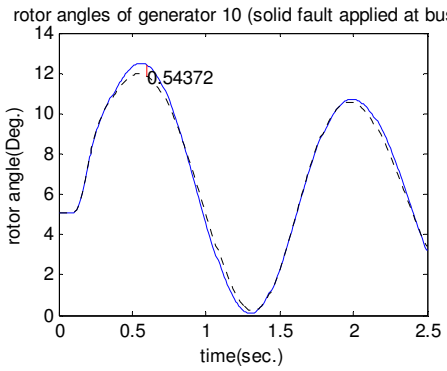

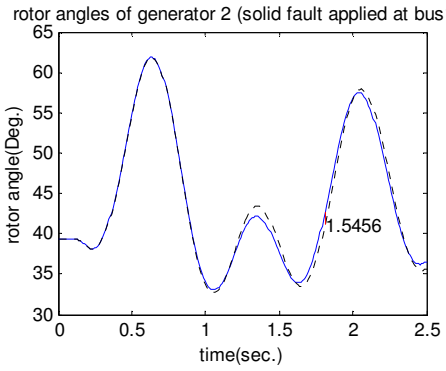

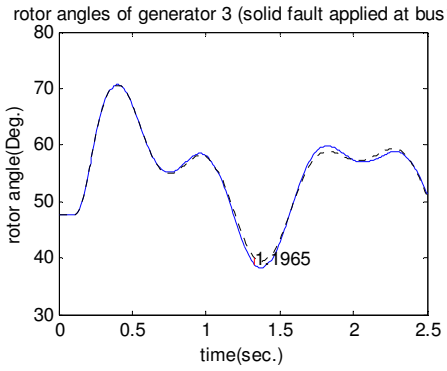

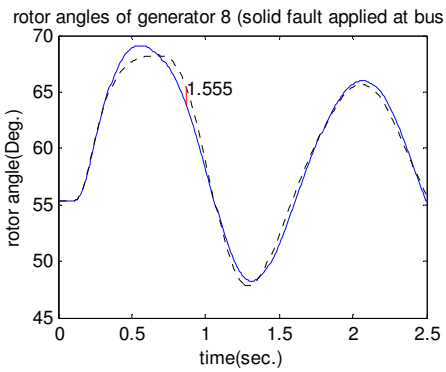

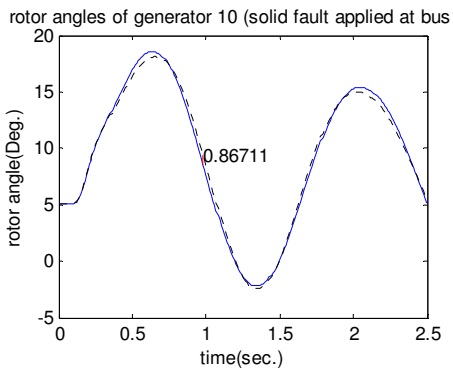

Case study 1.2: Scenario 2

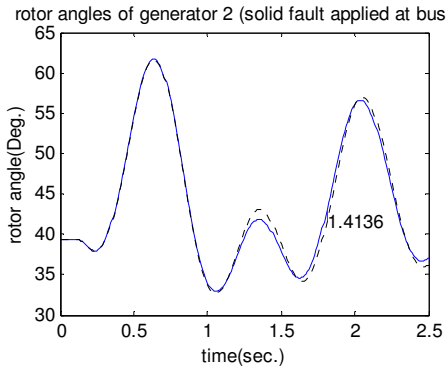

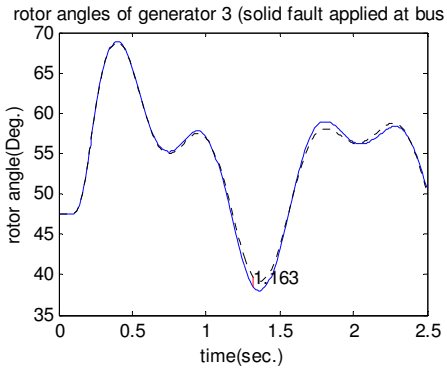

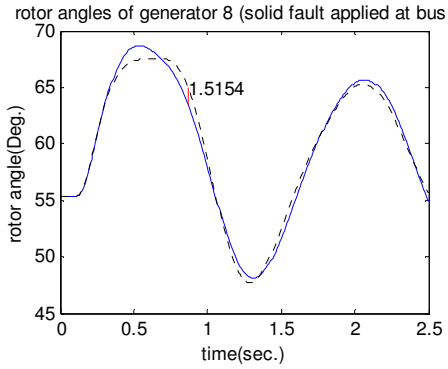

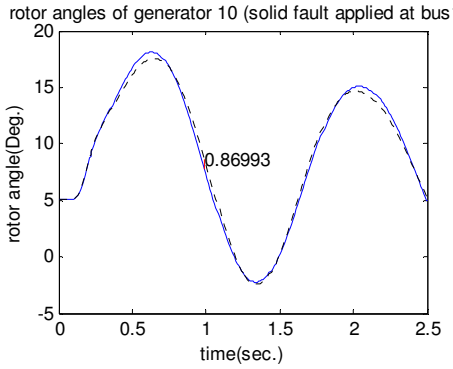

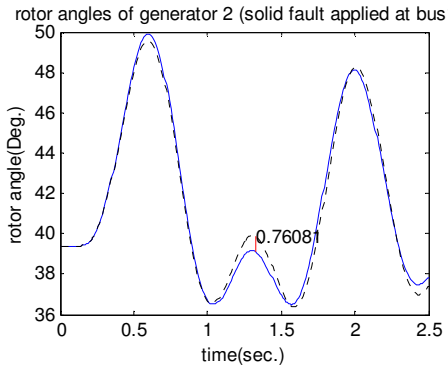

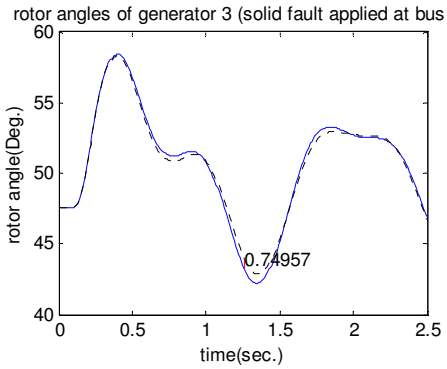

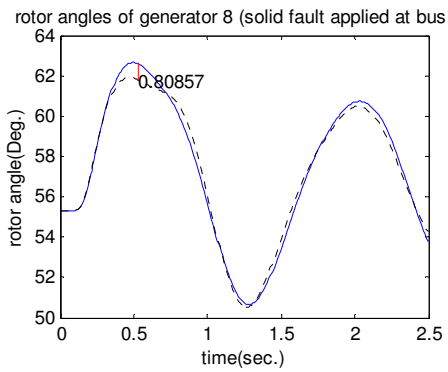

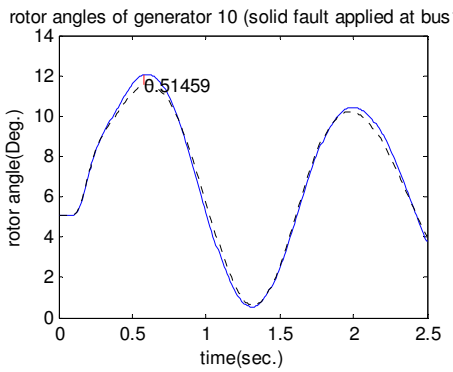

Case study 1.2: Scenario 2

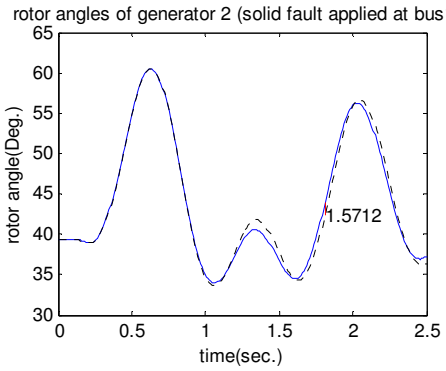

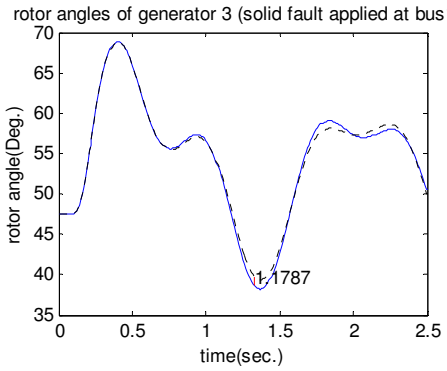

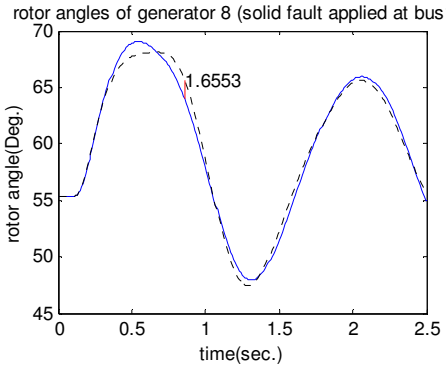

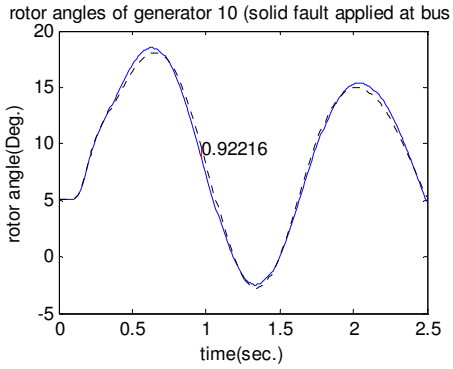

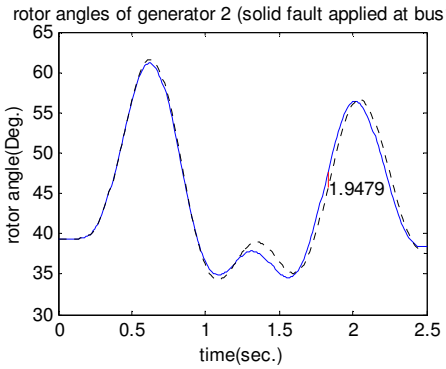

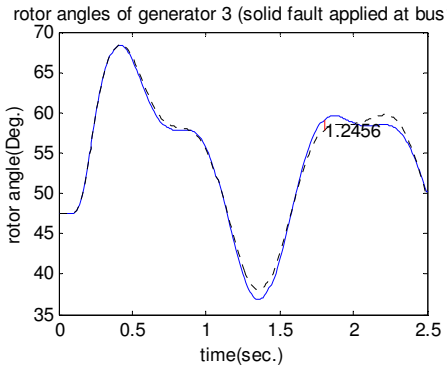

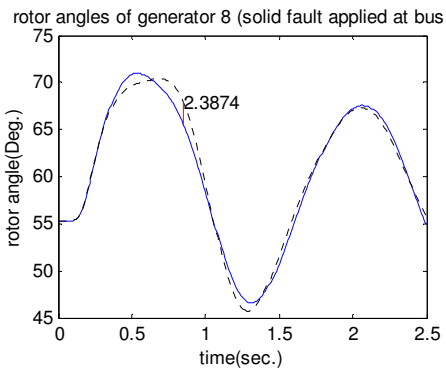

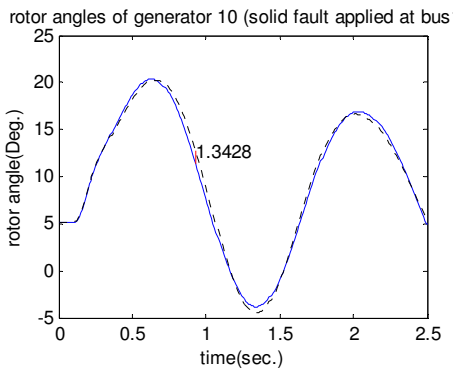

Case study 1.2: Scenario 2

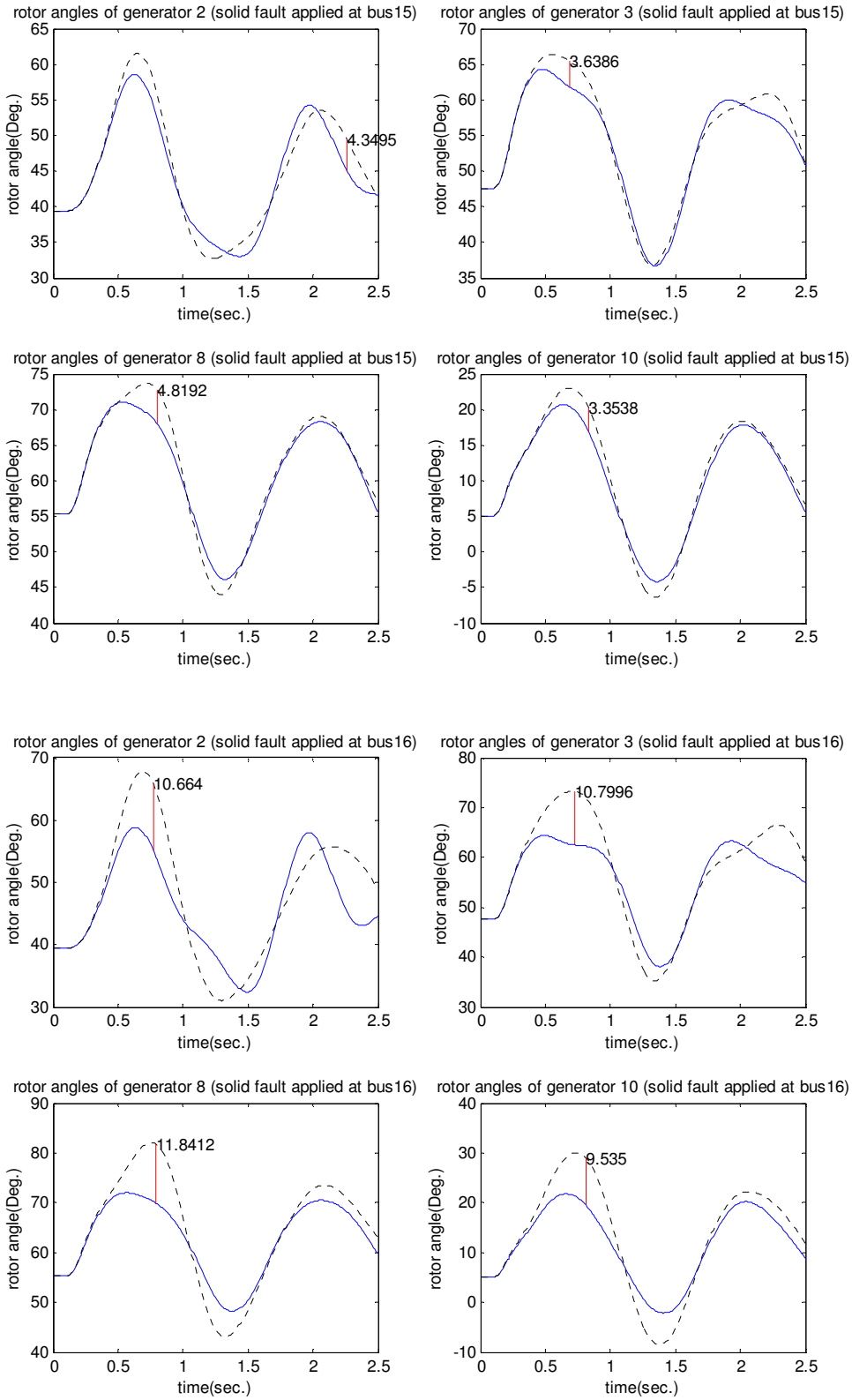

Case study 1.2: Scenario 2

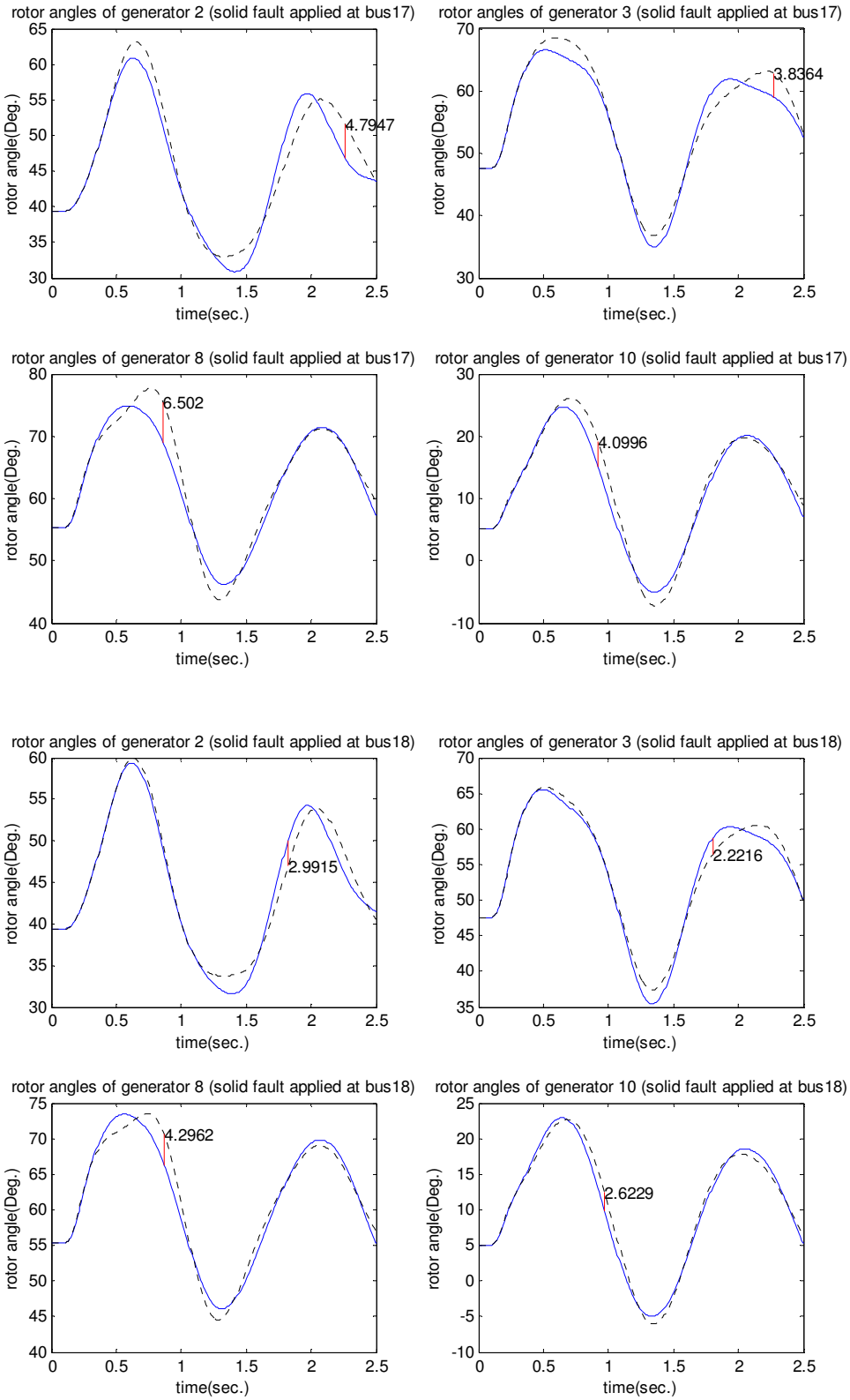

Case study 1.2: Scenario 2

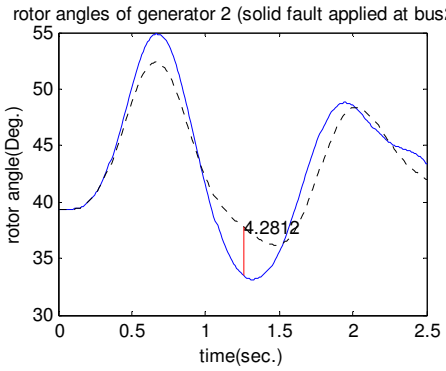

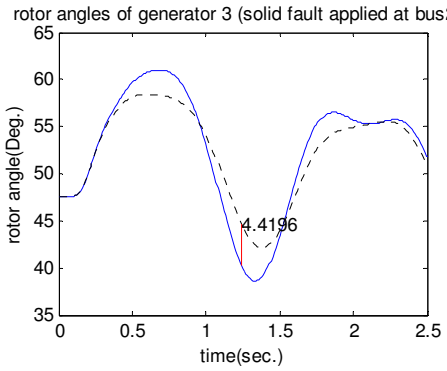

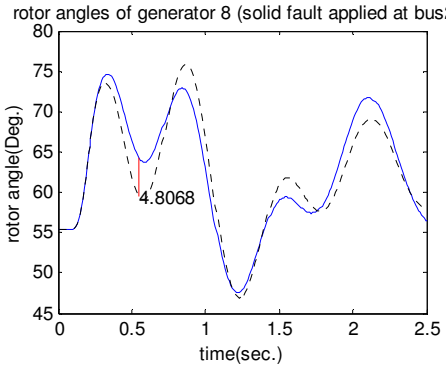

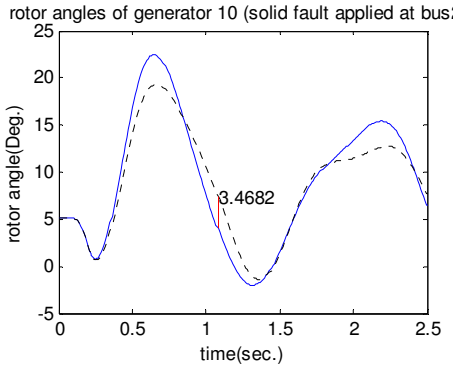

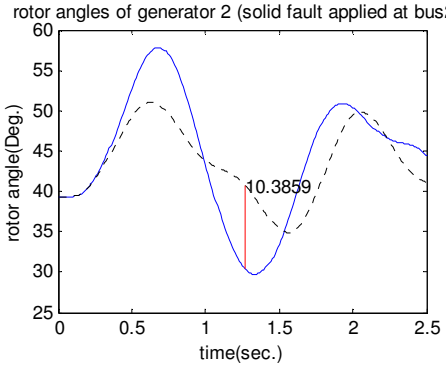

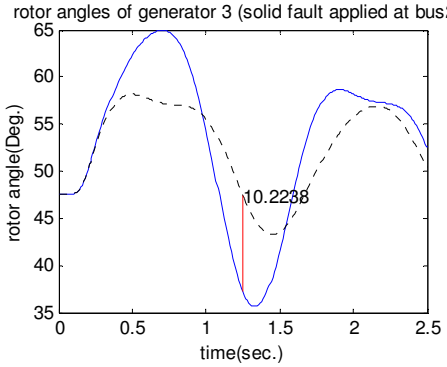

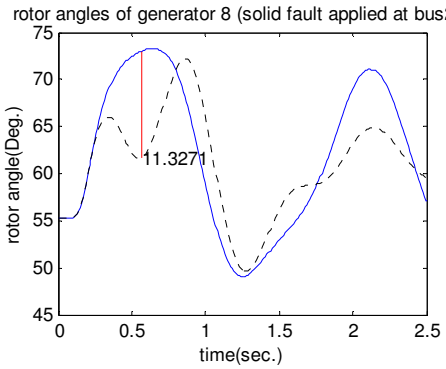

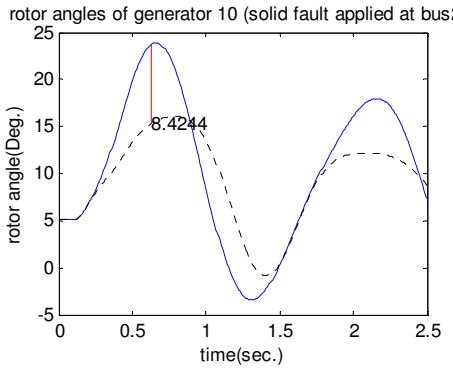

Case study 1.2: Scenario 2

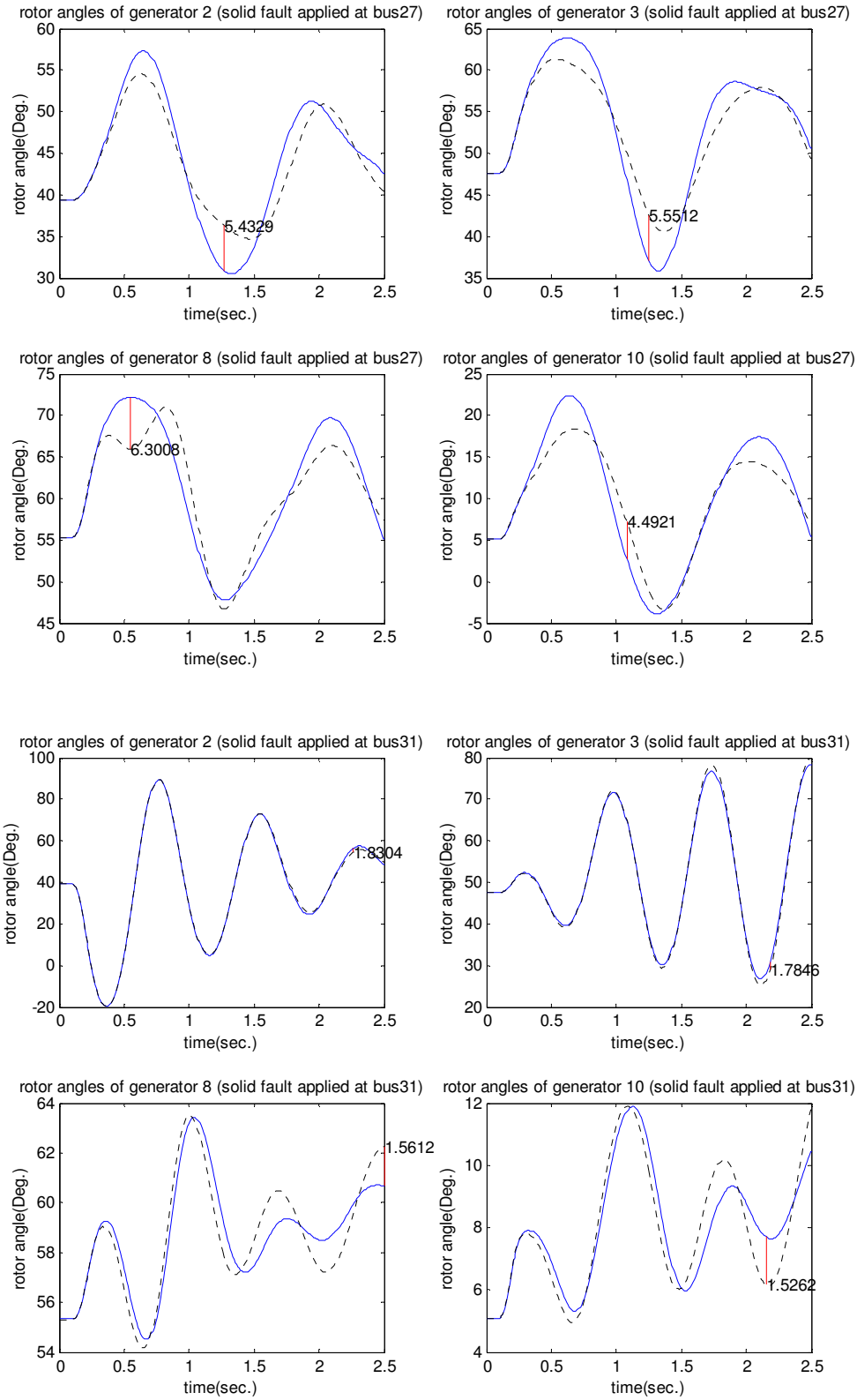

Case study 1.2: Scenario 2

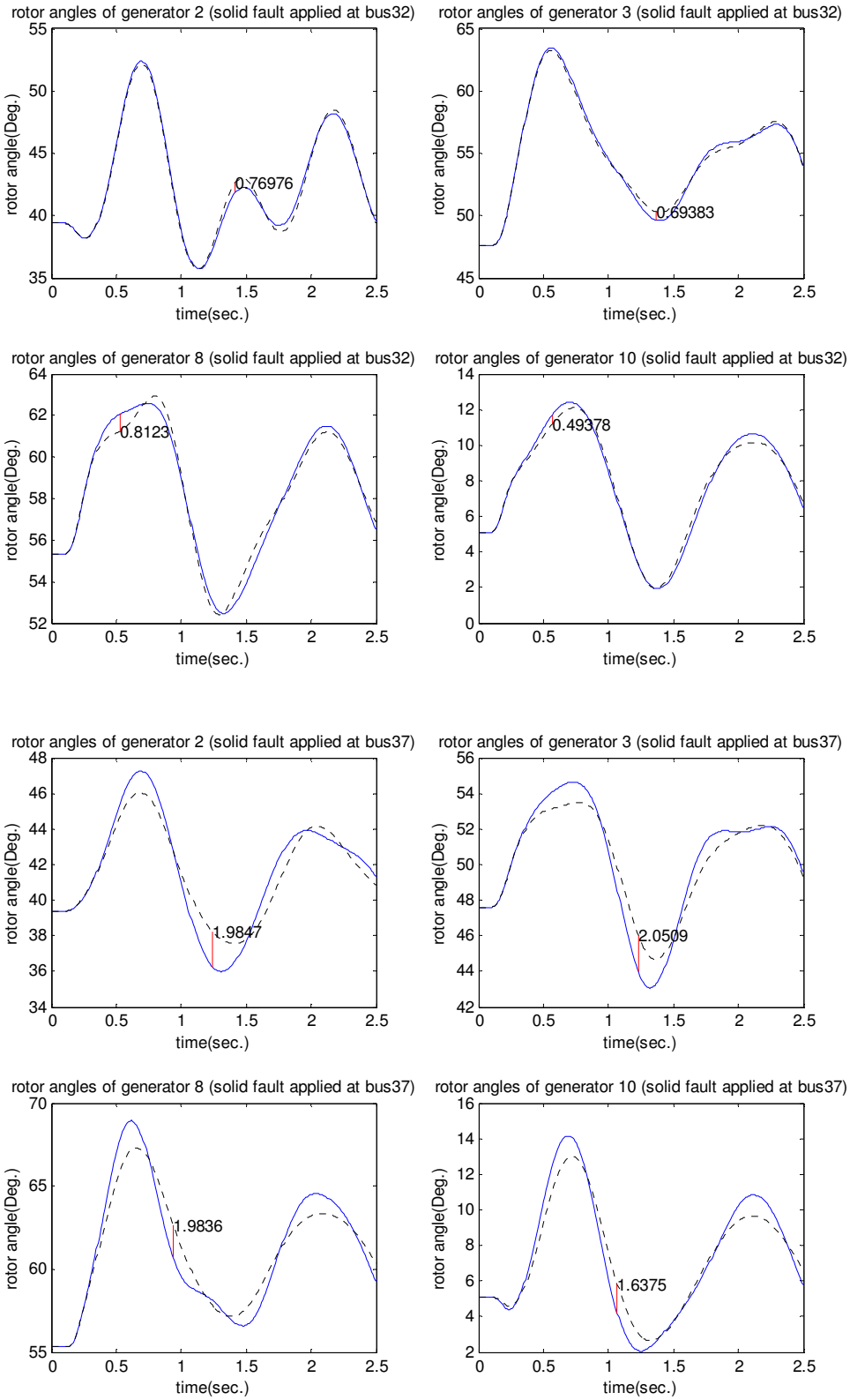

Case study 1.2: Scenario 2

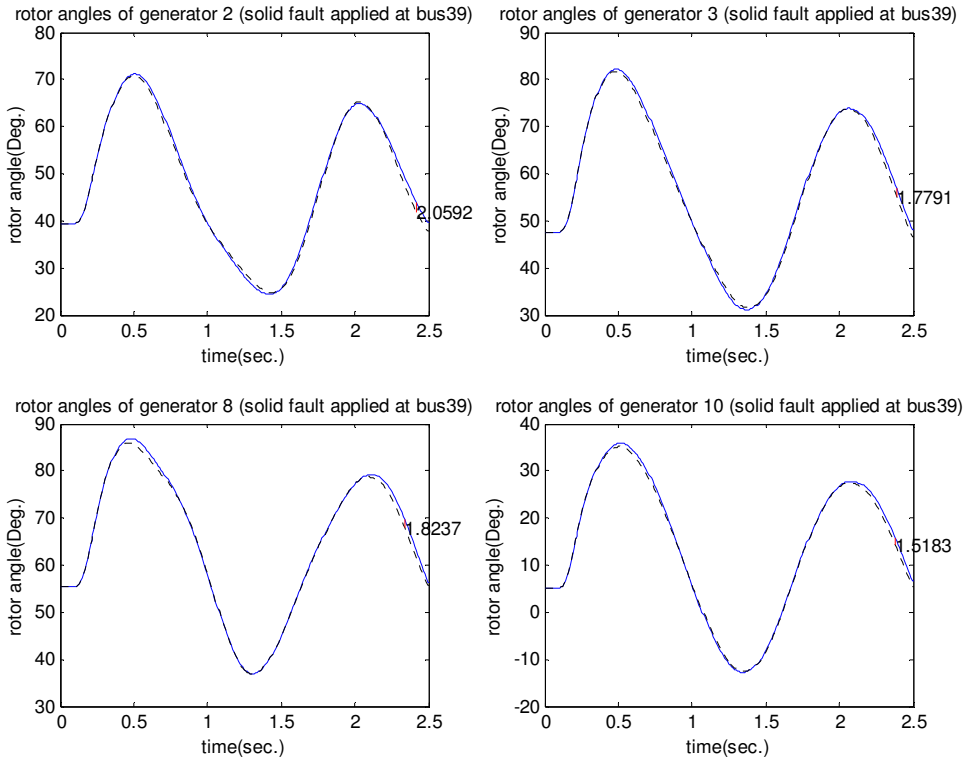

Case study 1.2: Scenario 3

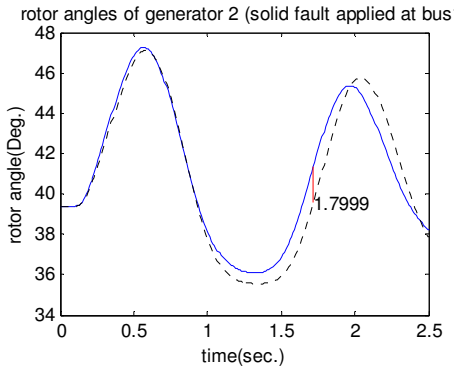

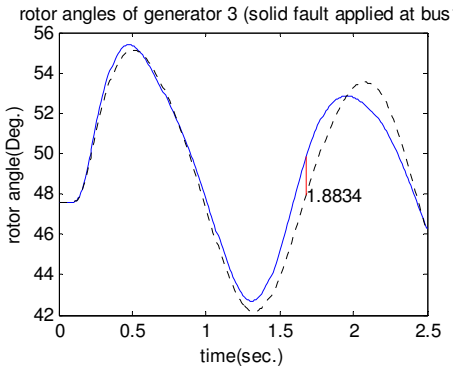

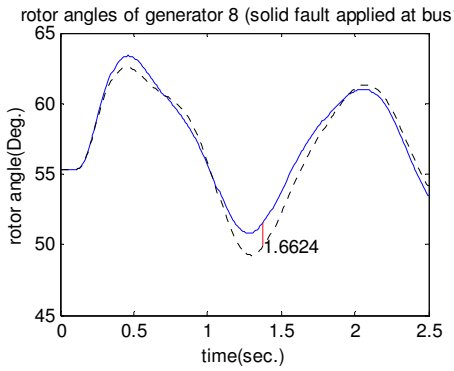

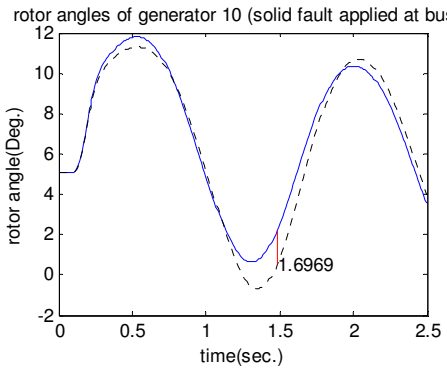

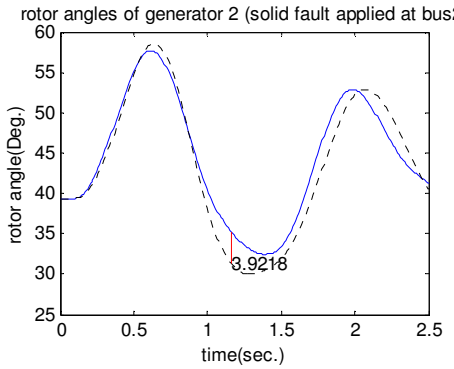

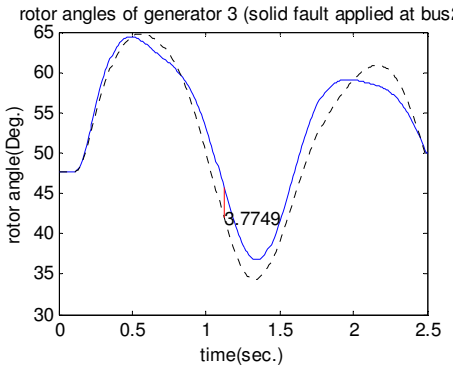

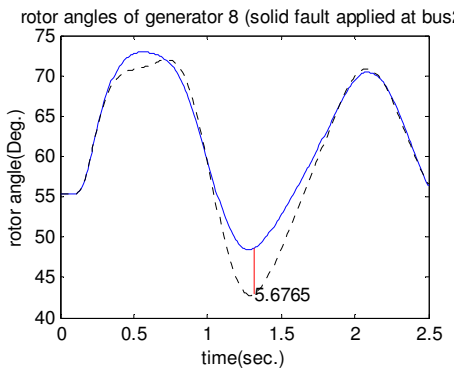

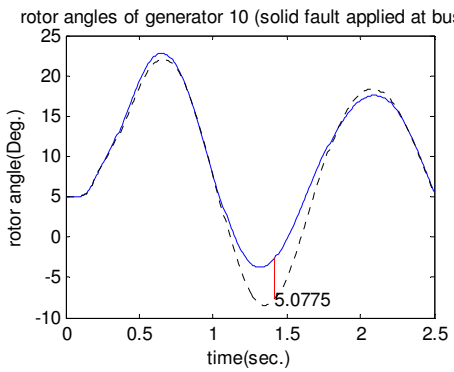

Case study 1.2: Scenario 3

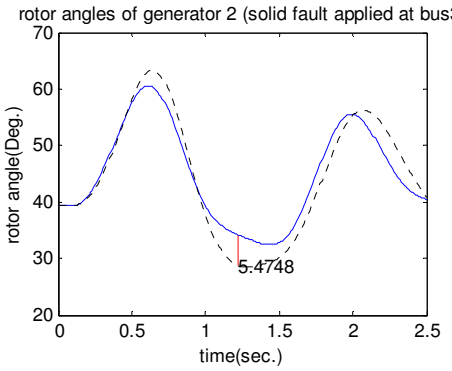

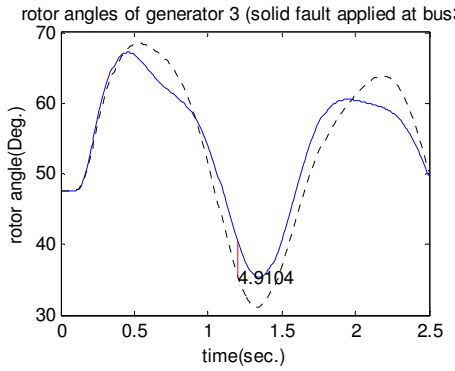

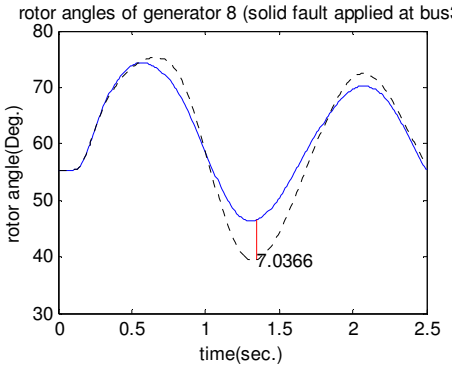

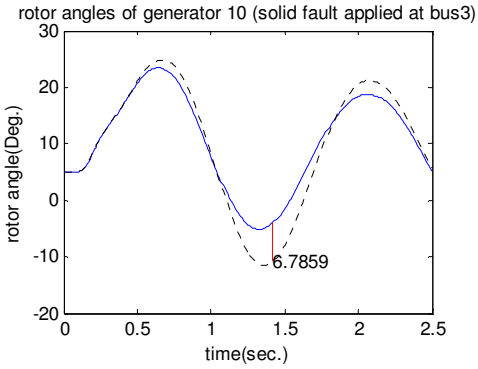

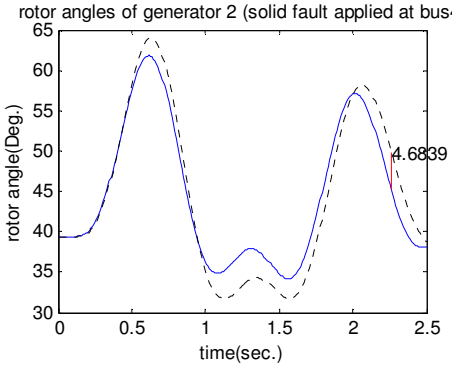

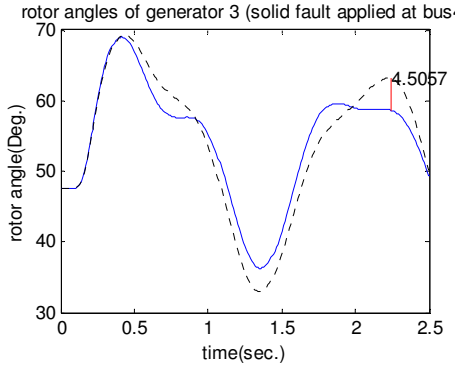

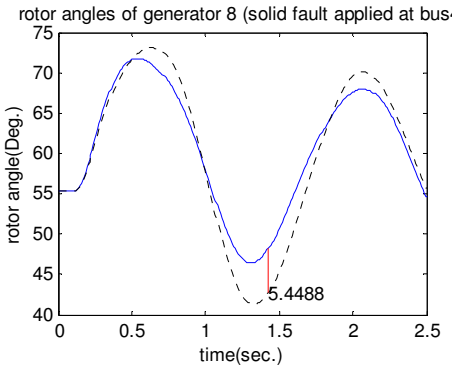

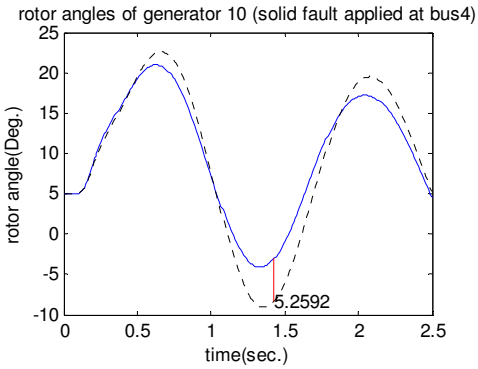

Case study 1.2: Scenario 3

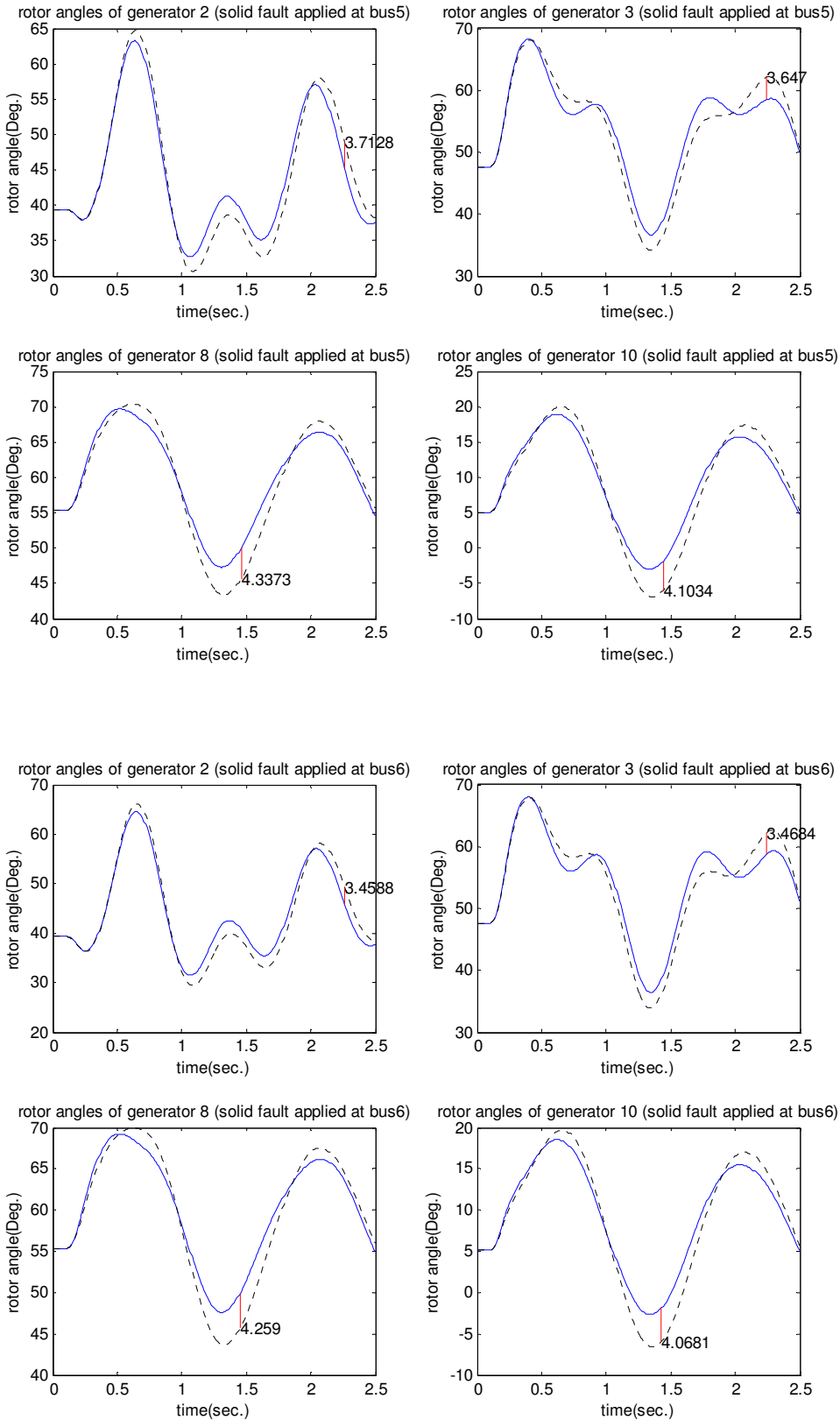

Case study 1.2: Scenario 3

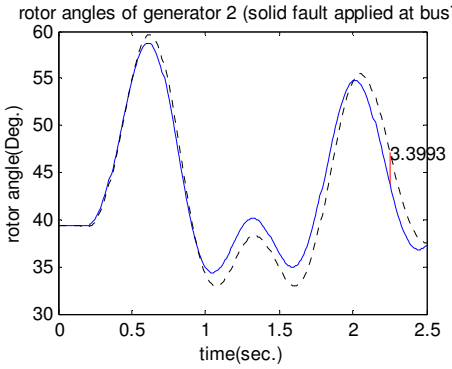

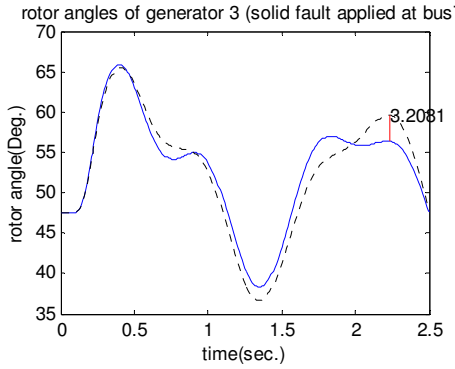

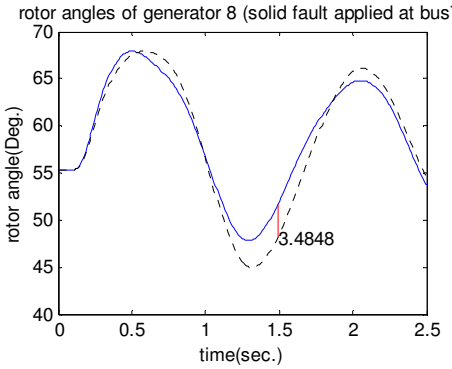

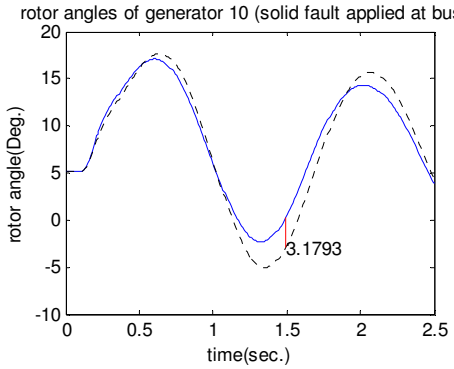

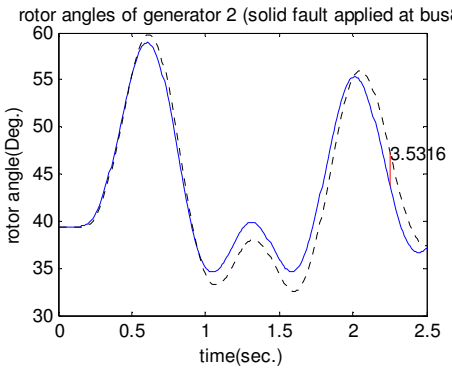

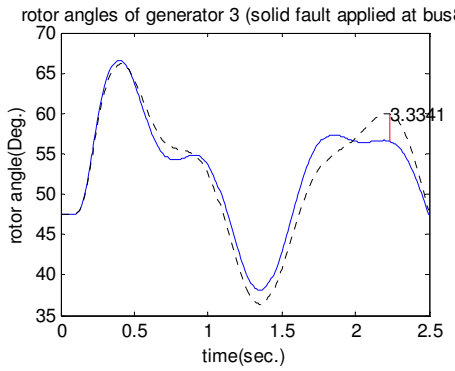

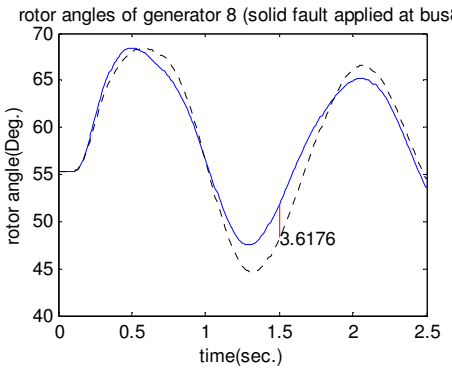

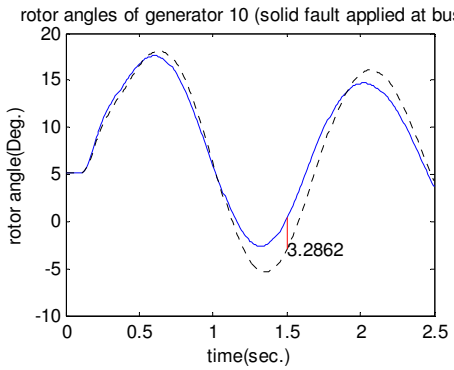

Case study 1.2: Scenario 3

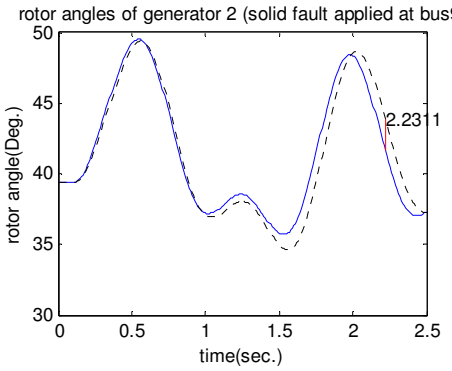

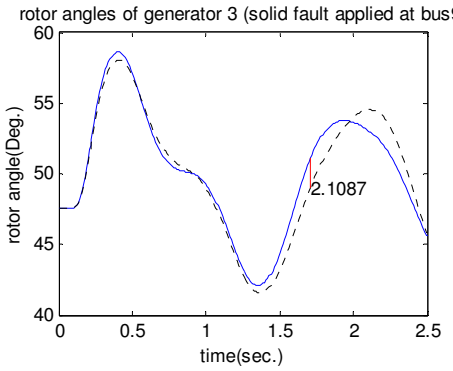

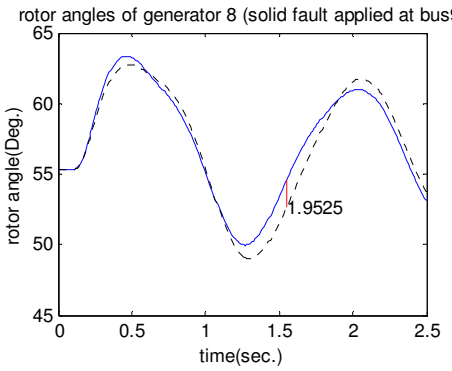

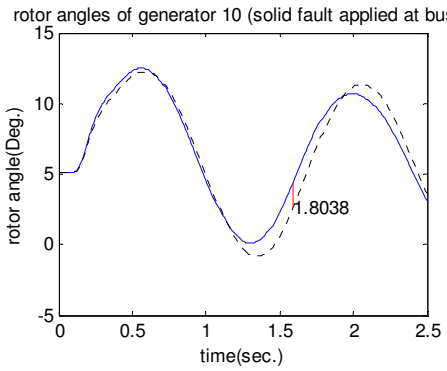

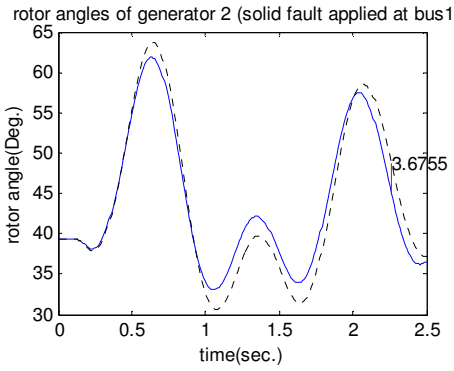

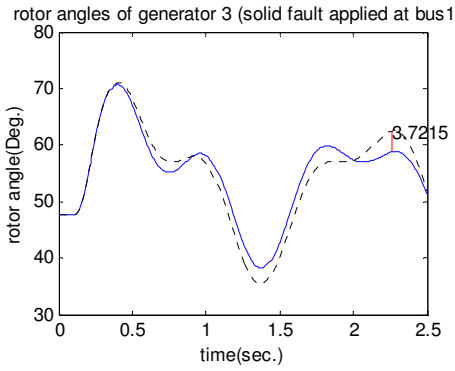

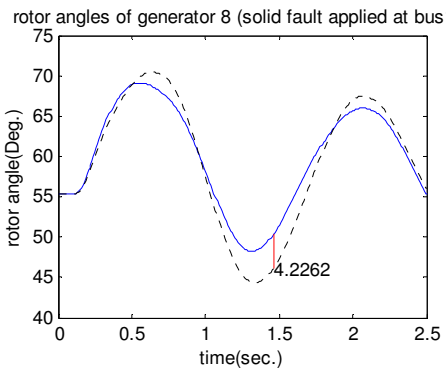

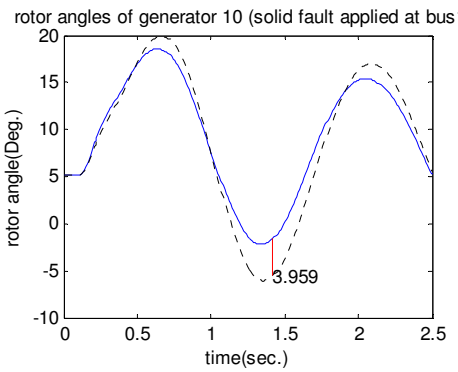

Case study 1.2: Scenario 3

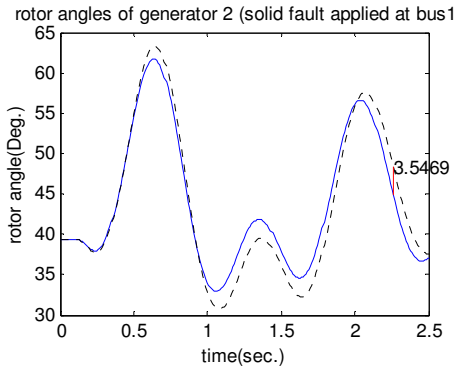

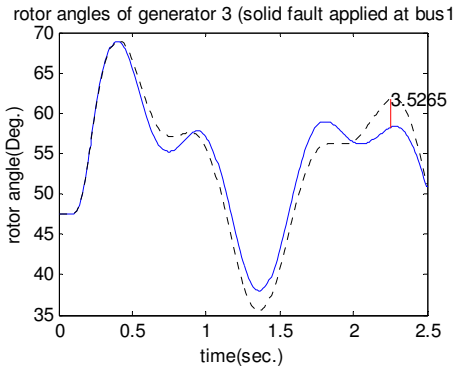

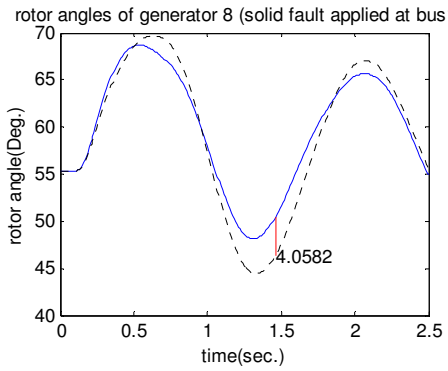

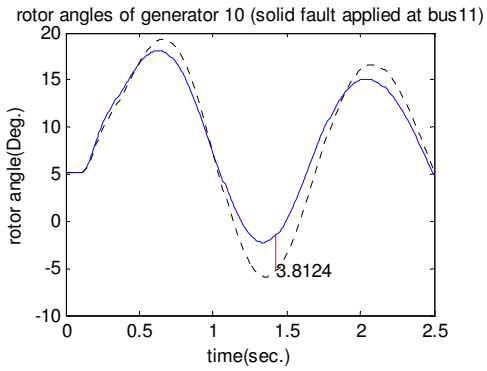

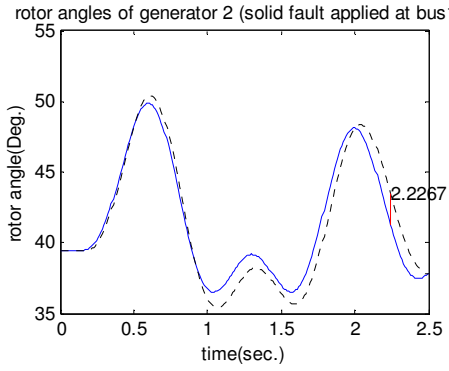

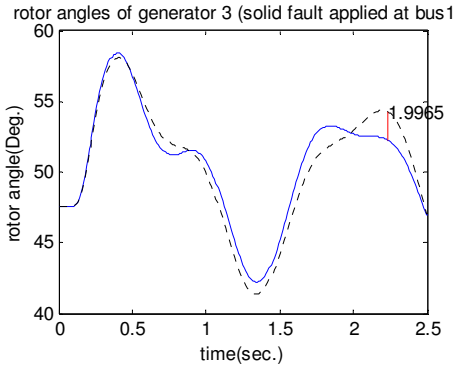

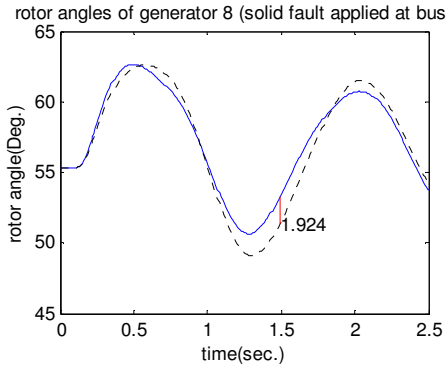

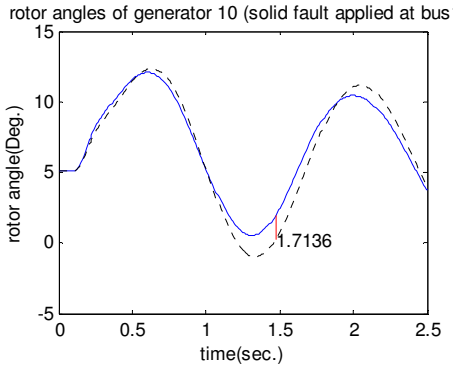

Case study 1.2: Scenario 3

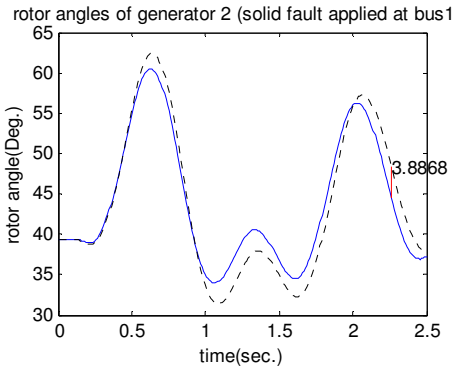

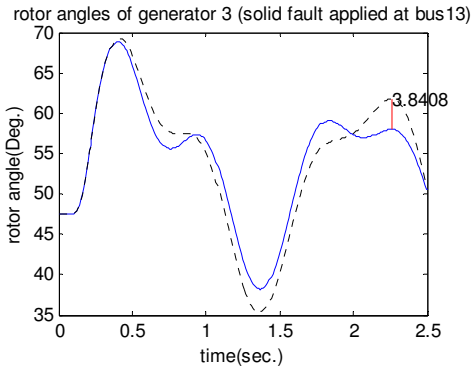

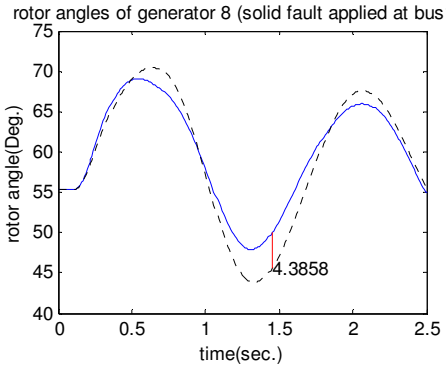

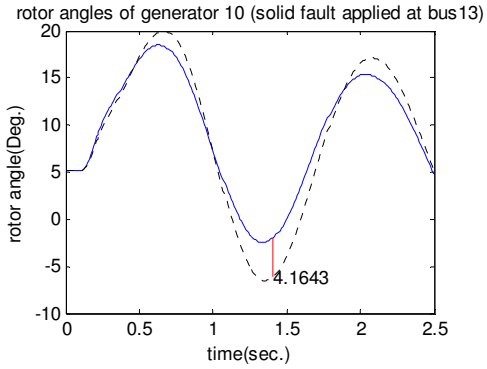

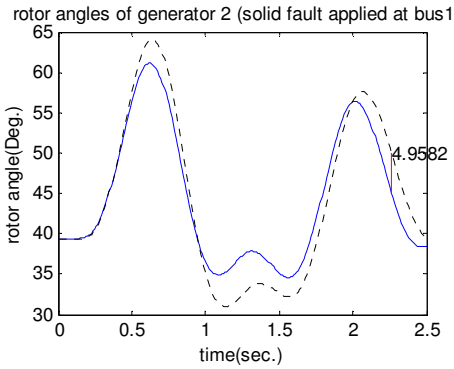

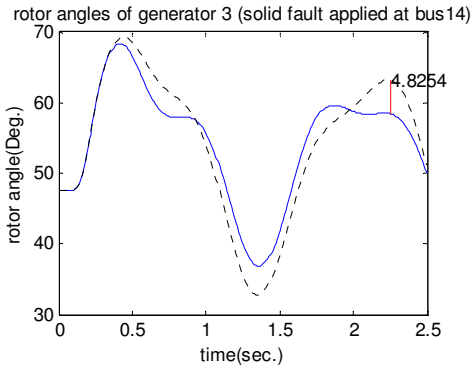

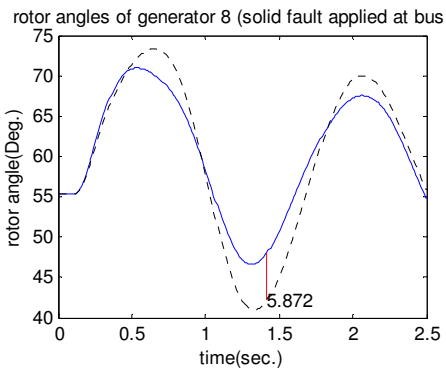

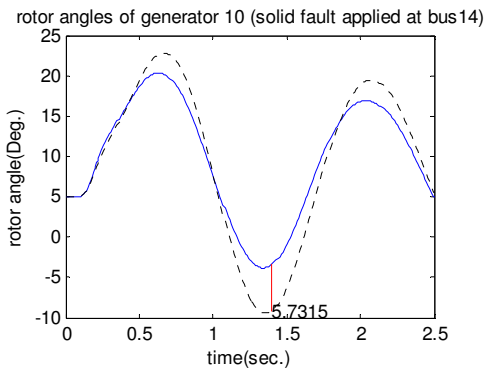

Case study 1.2: Scenario 3

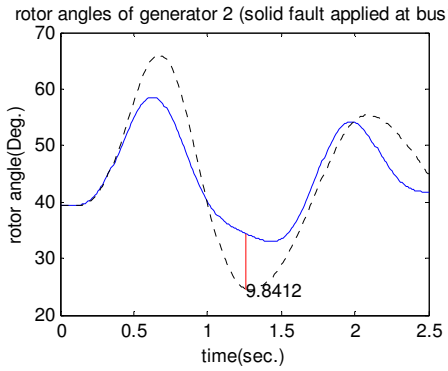

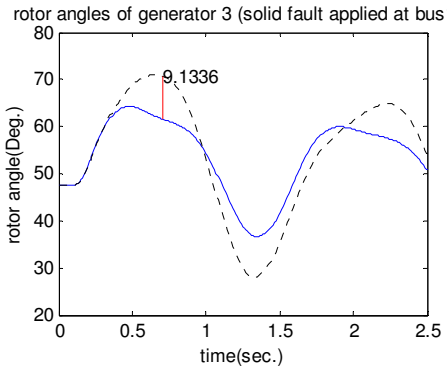

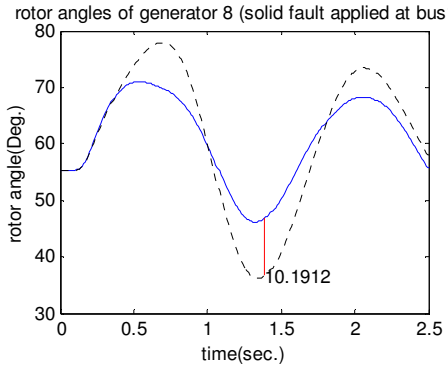

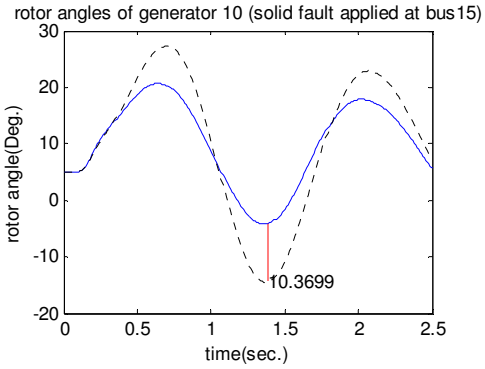

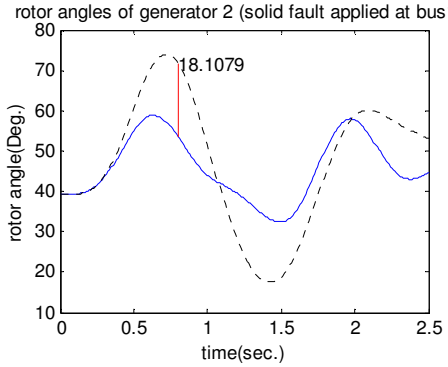

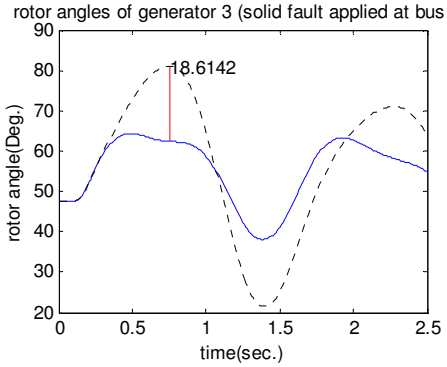

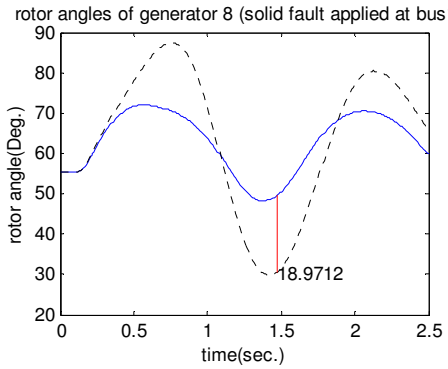

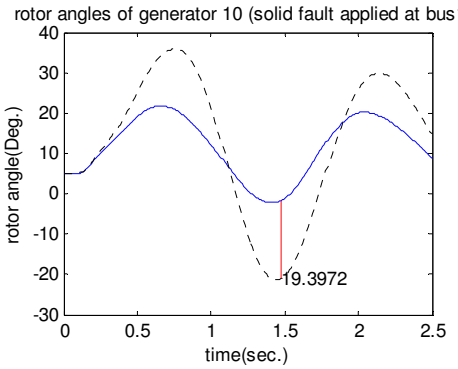

Case study 1.2: Scenario 3

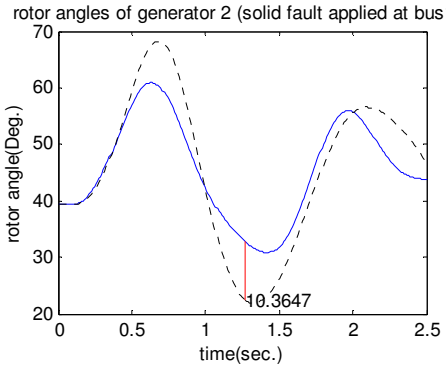

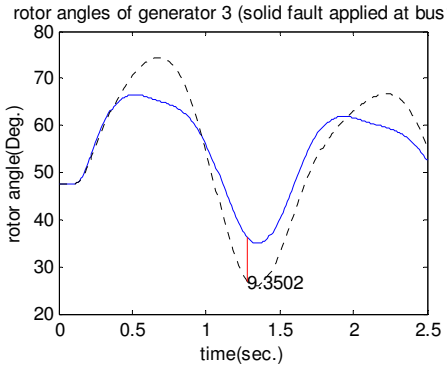

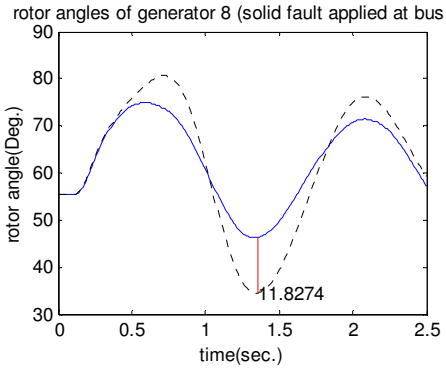

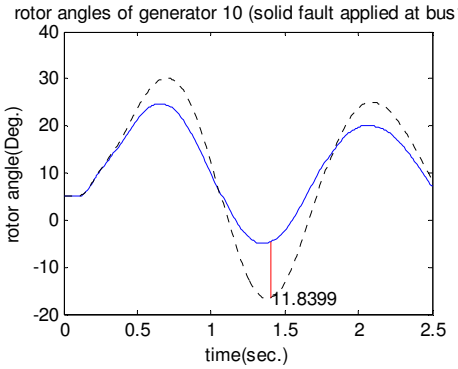

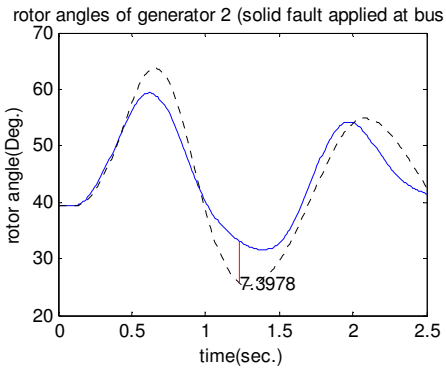

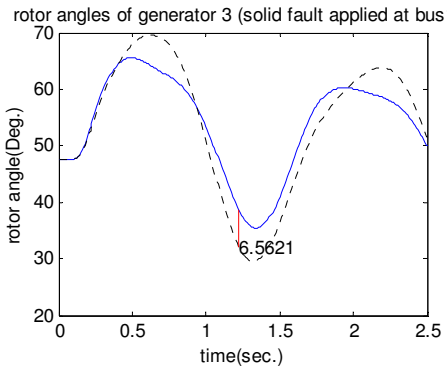

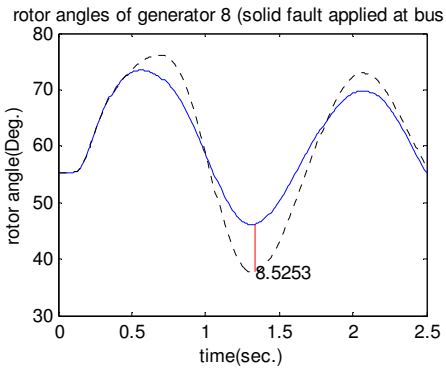

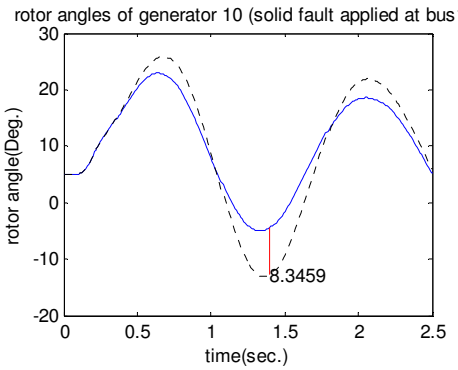

Case study 1.2: Scenario 3

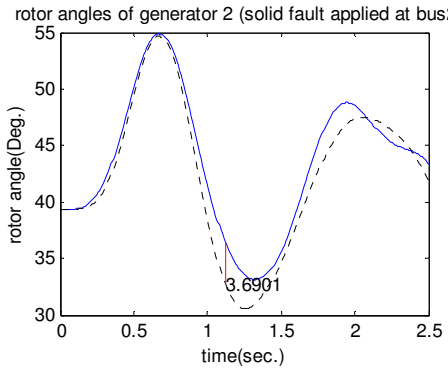

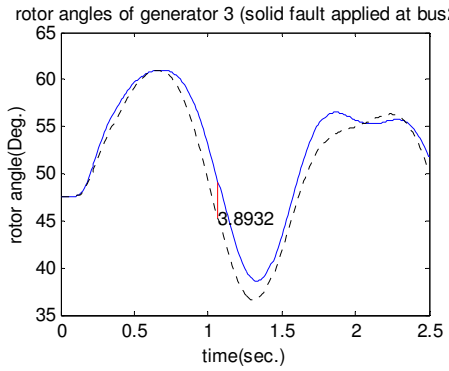

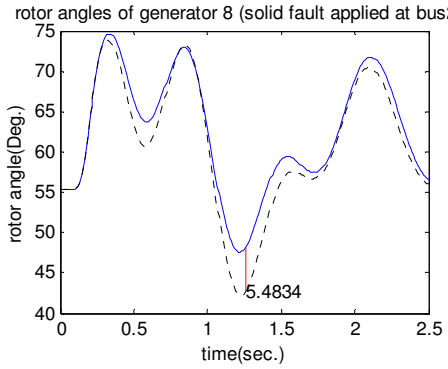

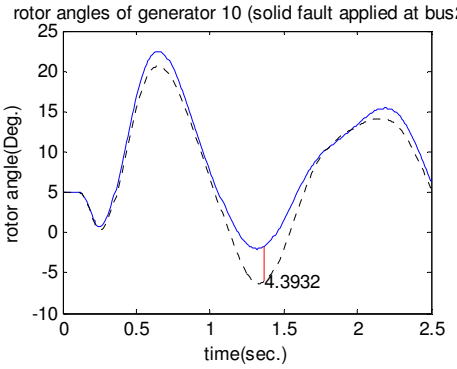

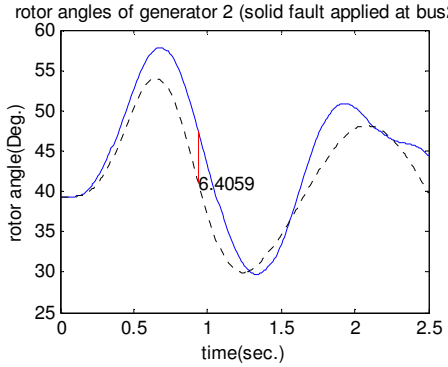

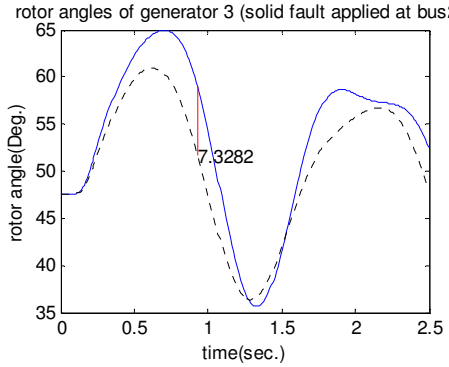

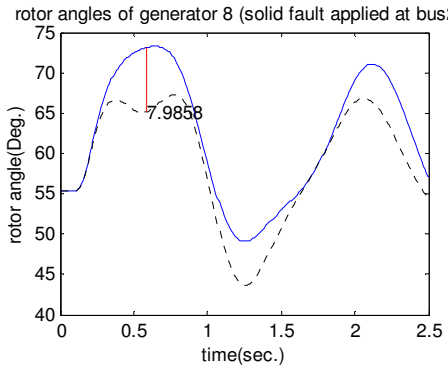

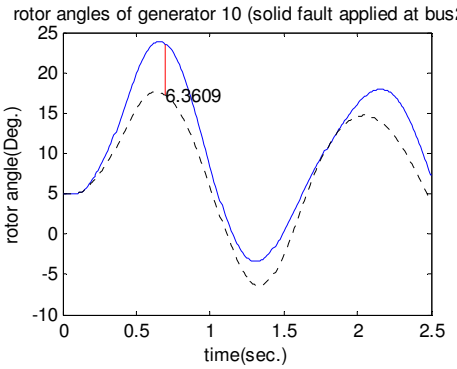

Case study 1.2: Scenario 3

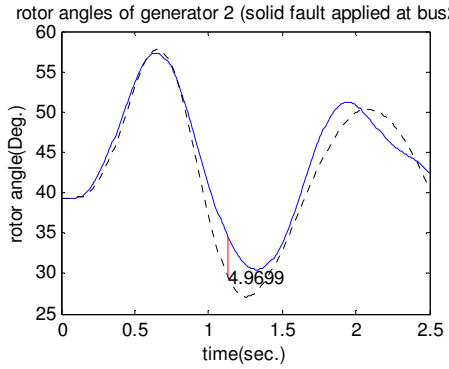

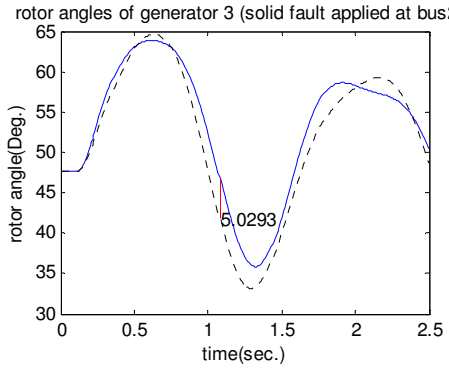

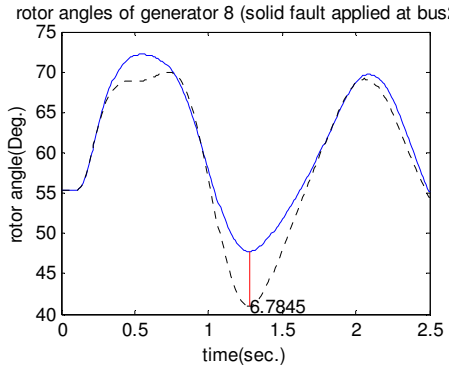

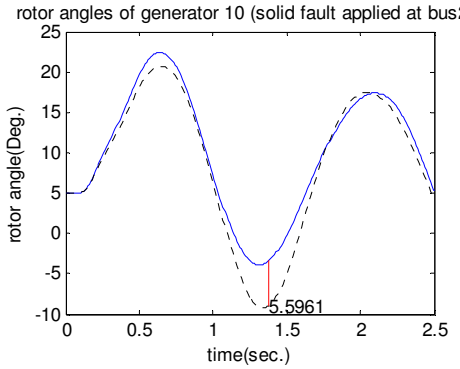

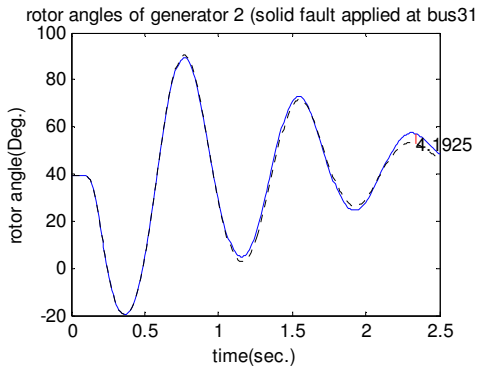

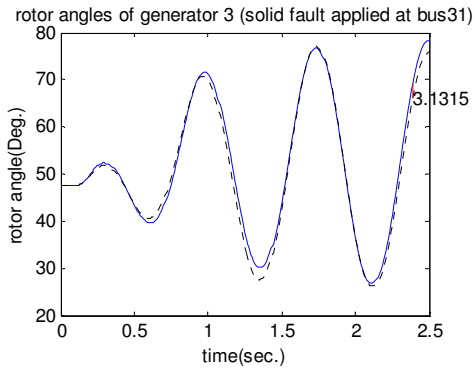

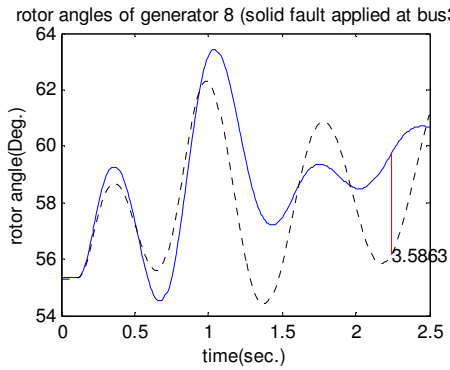

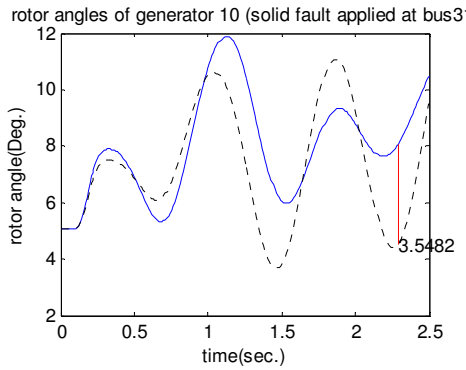

Case study 1.2: Scenario 3

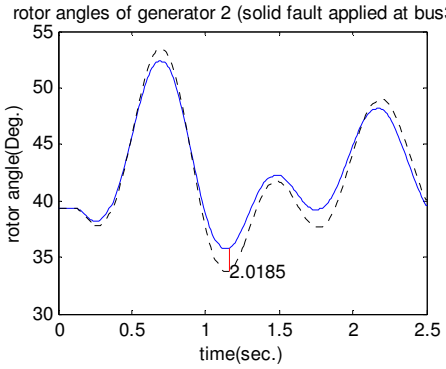

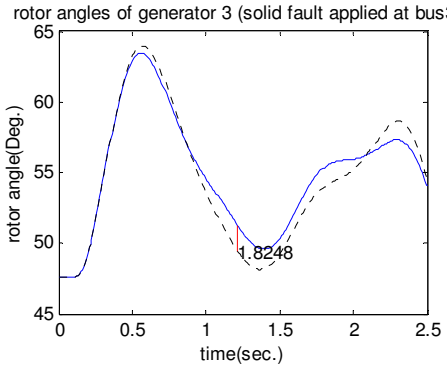

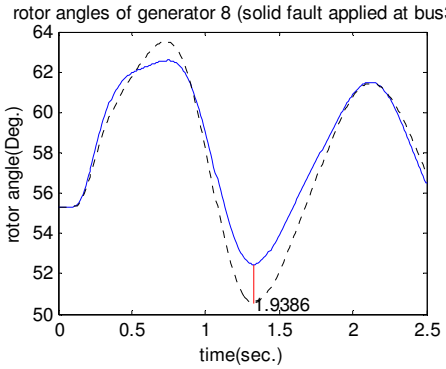

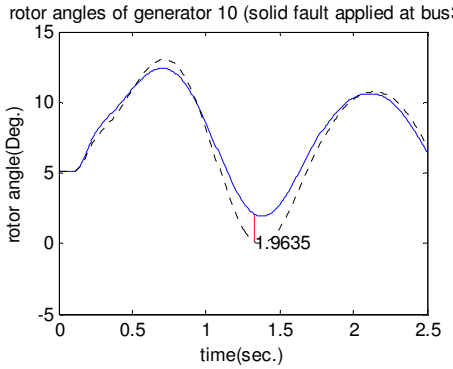

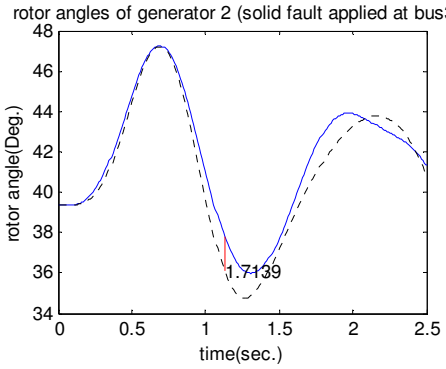

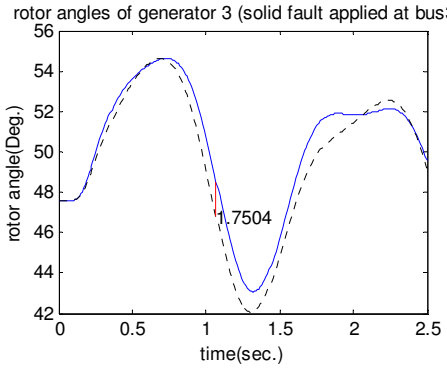

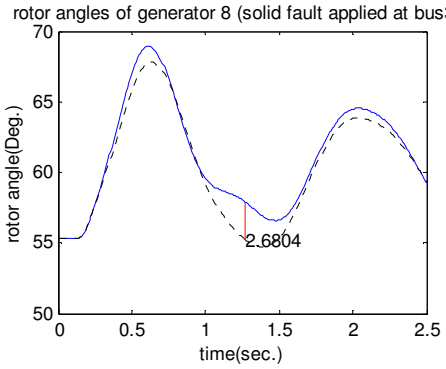

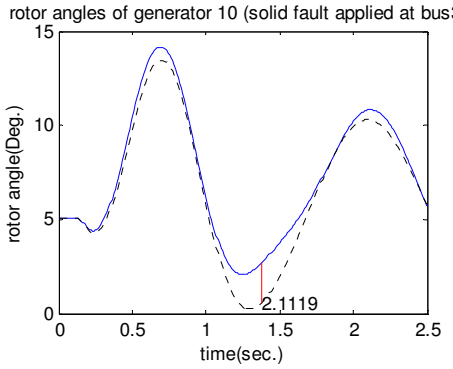

Case study 1.2: Scenario 3

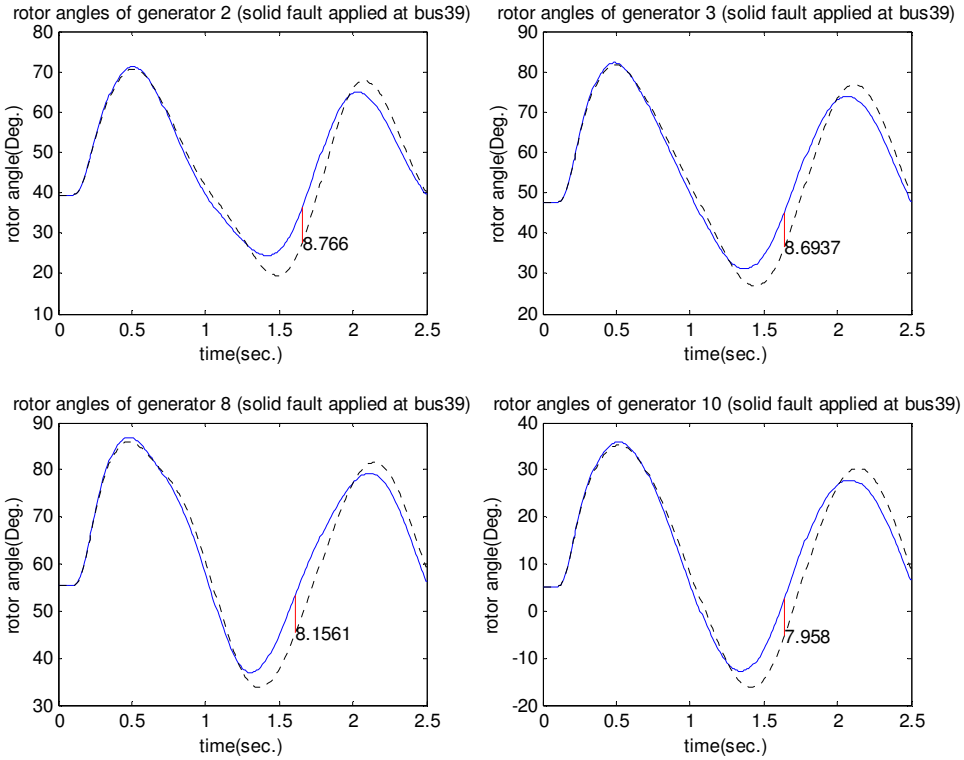

C.3 Rotor angle plot of case study 2

The plots in this section show only the comparison between the rotor angle of the original system and the rotor angle of the reduced system of each scenarios of case study 2, when the large fault is applied at bus 44. The details for each scenario are repeated here.

Table 6.5 (repeated) Six scenarios of the reduced system for the case study 2

scenario	Coherent generator identification				Parameter identification	Reduced system test
	Condition of system	Epsilon	area	Coherent groups	Condition of system	Condition of system
A	1	≥ 0.27	1	(G1-G3), (G4-G5), (G6-G7), (G2)	1	1
			2	(G16-G19), (G17-G18), (G20)		
B	1	≥ 0.20	1	(G1-G2-G3), (G4-G5-G6-G7)	1	1
			2	(G16-G17-G18-G19), (G20)		
C	2	≥ 0.20	1	(G1-G2-G3), (G4-G5-G6-G7)	2	2
			2	(G16-G17-G18-G19), (G20)		
D	2	≥ 0.20	1	(G1-G2-G3), (G4-G5-G6-G7)	1	2
			2	(G16-G17-G18-G19), (G20)		
E	3	≥ 0.20	1	(G1-G2-G3), (G4-G5), G6, G7	3	3
			2	(G16-G17-G19), (G18), (G20)		
F	1	≥ 0.20	1	(G1-G2-G3), (G4-G5-G6-G7)	3	3
			2	(G16-G17-G18-G19), (G20)		

Case study 2: scenario A

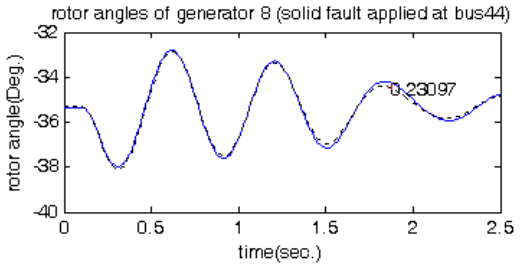

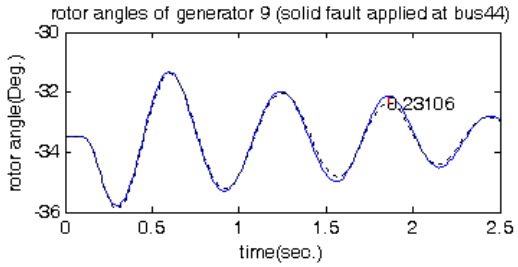

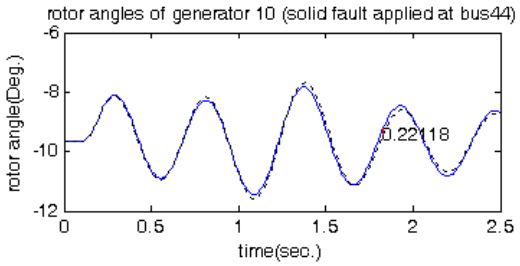

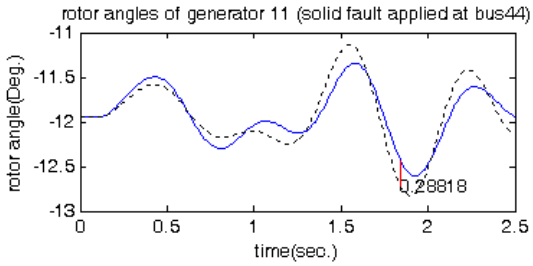

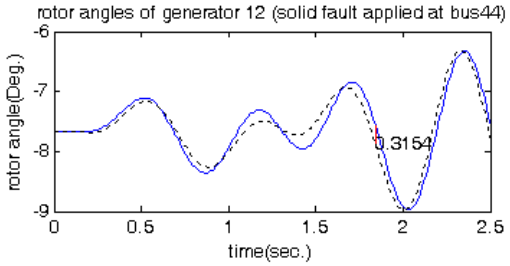

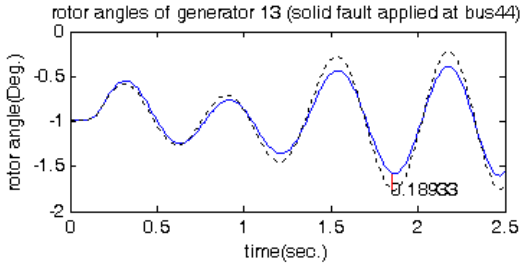

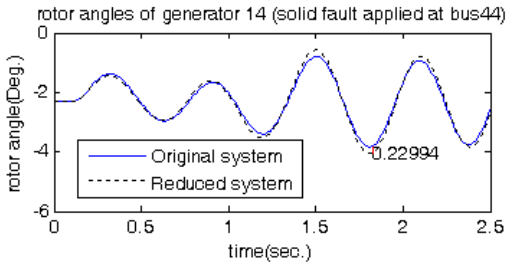

CASE: A -- OPP1

Reduced system:
-the coherent generators of OPP1(tight-group)
-the parameters identified from OPP1

Case study 2: scenario B

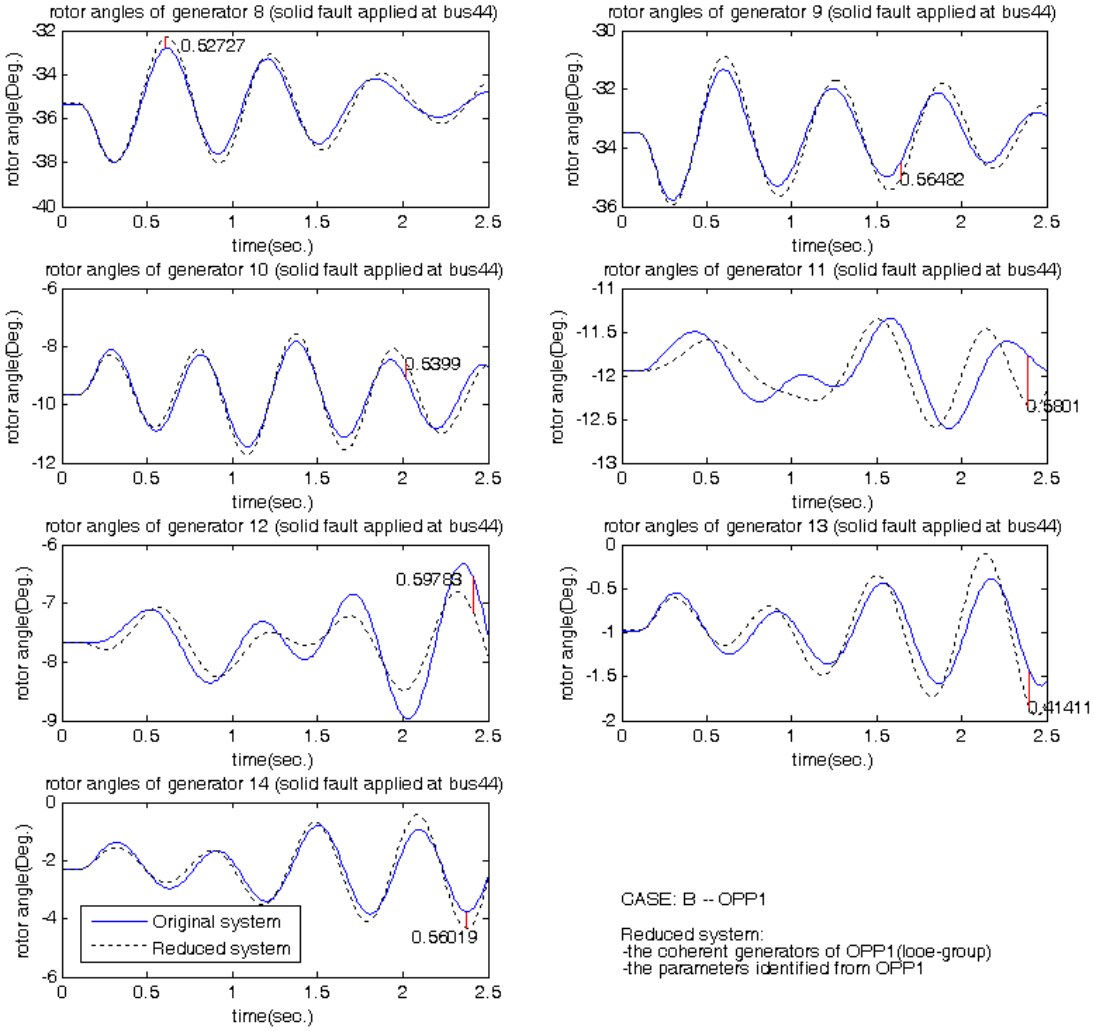

Case study 2: scenario C

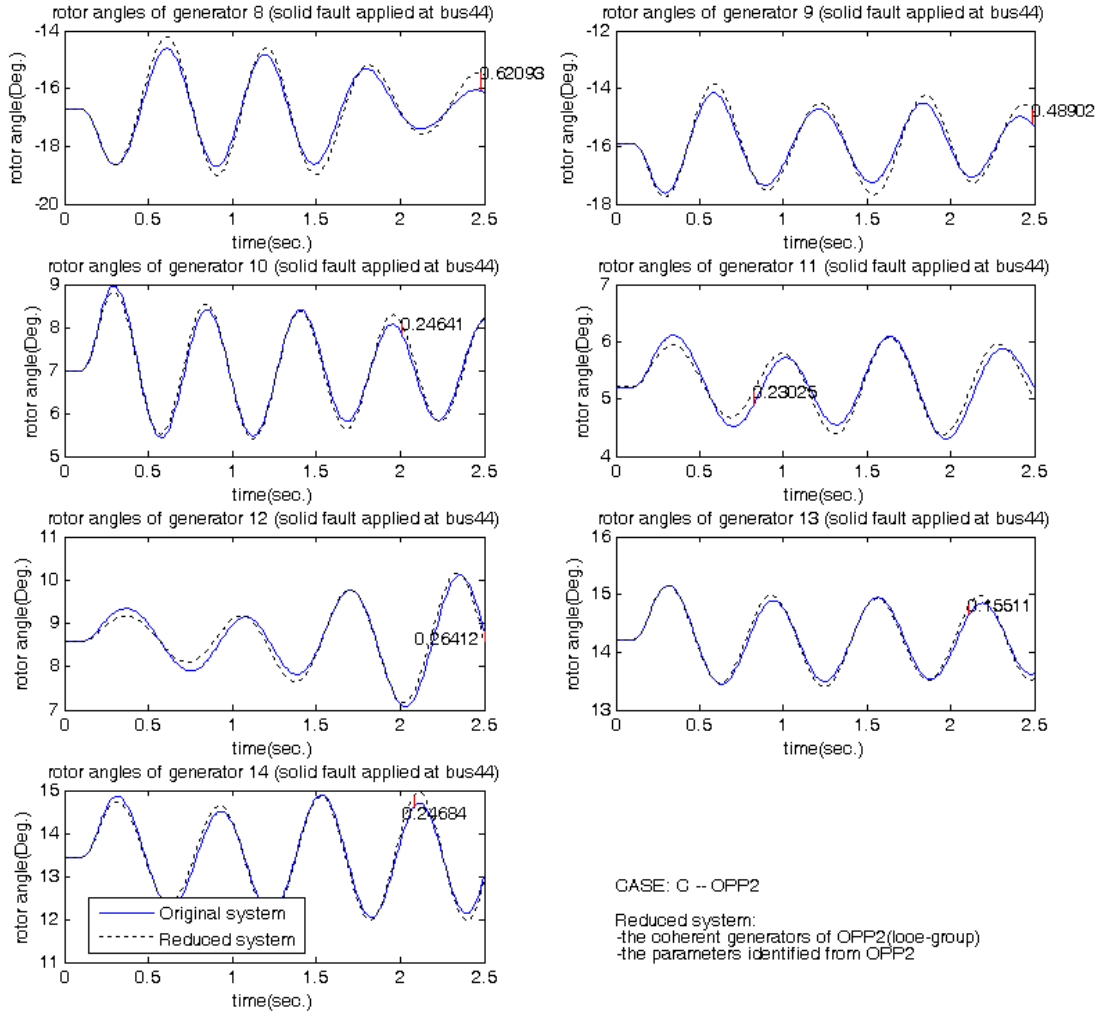

Case study 2: scenario D

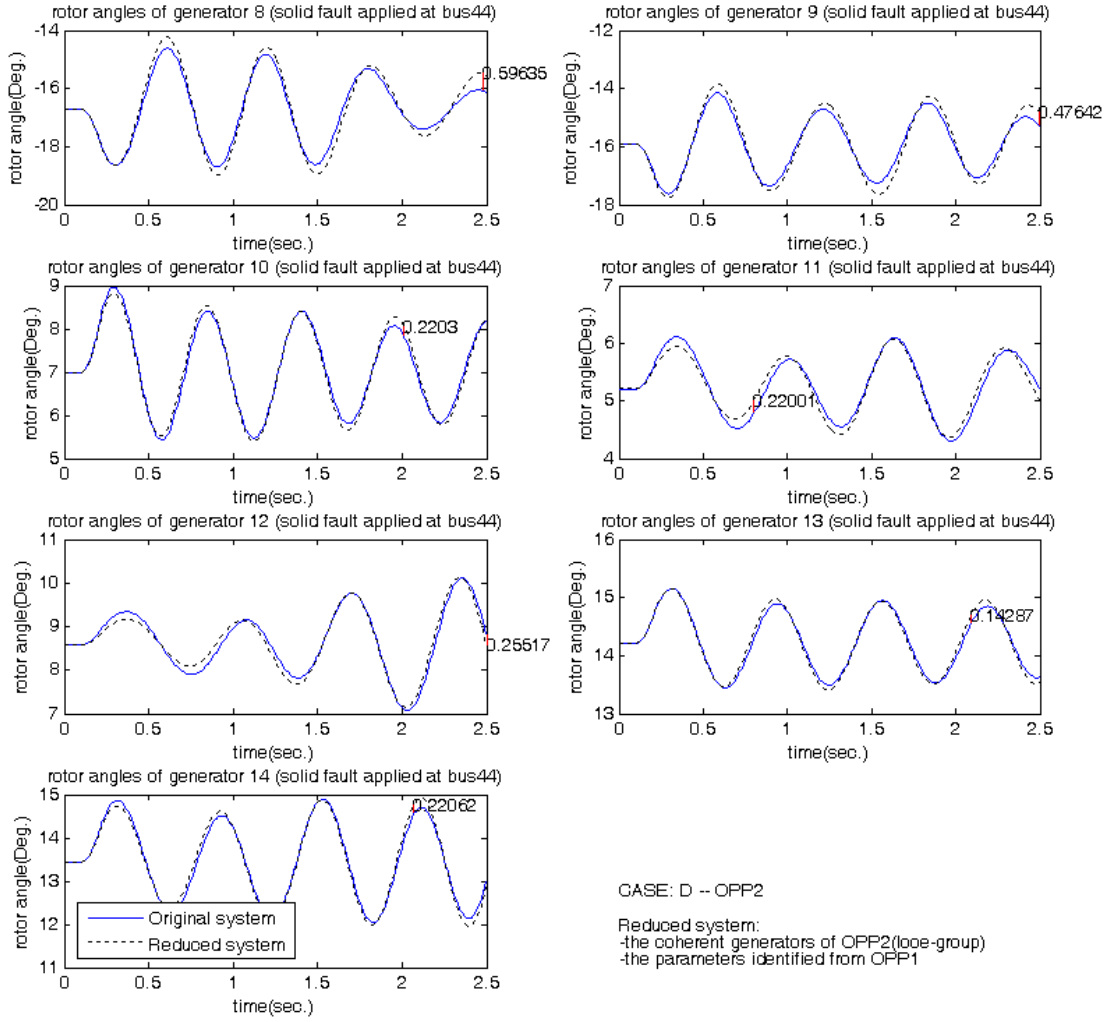

Case study 2: scenario E

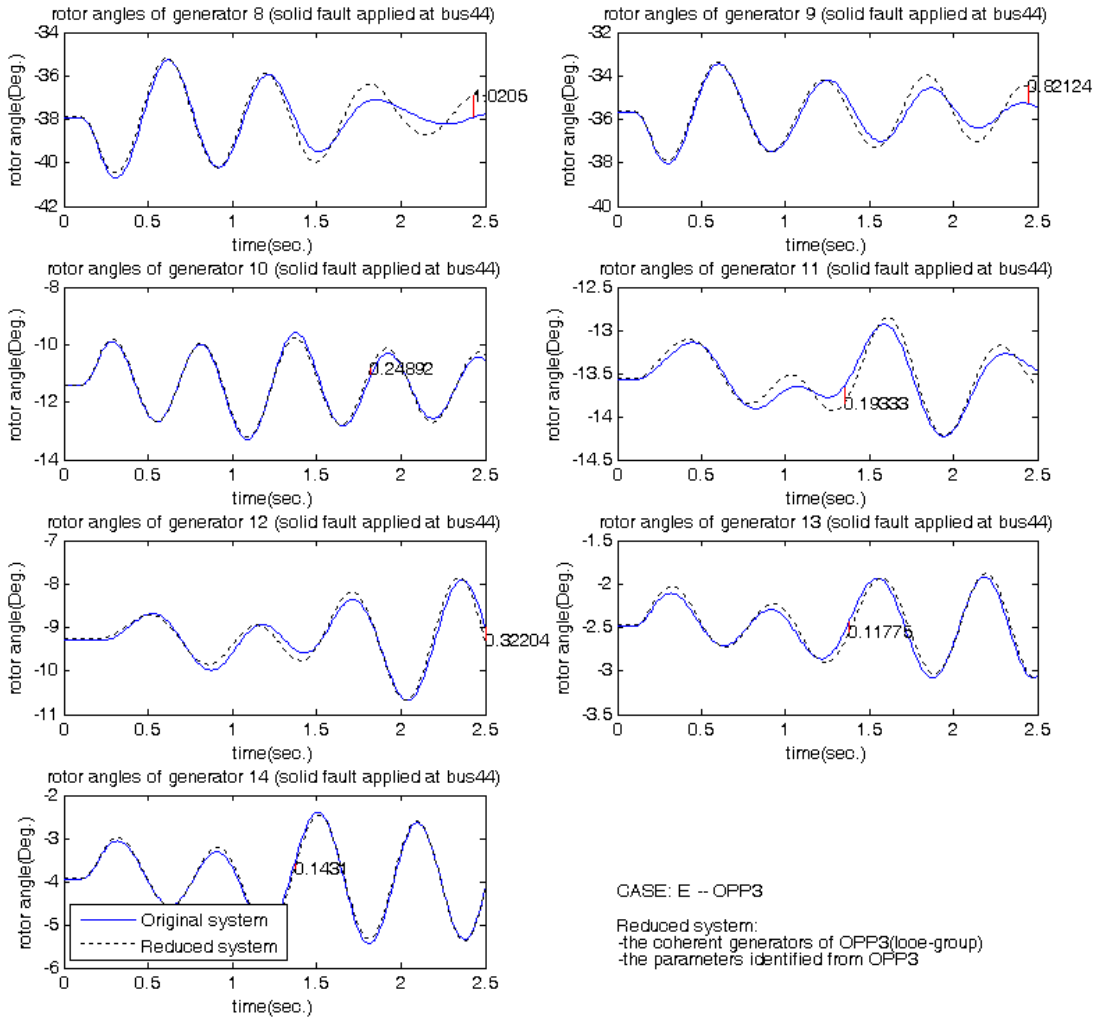

Case study 2: scenario F

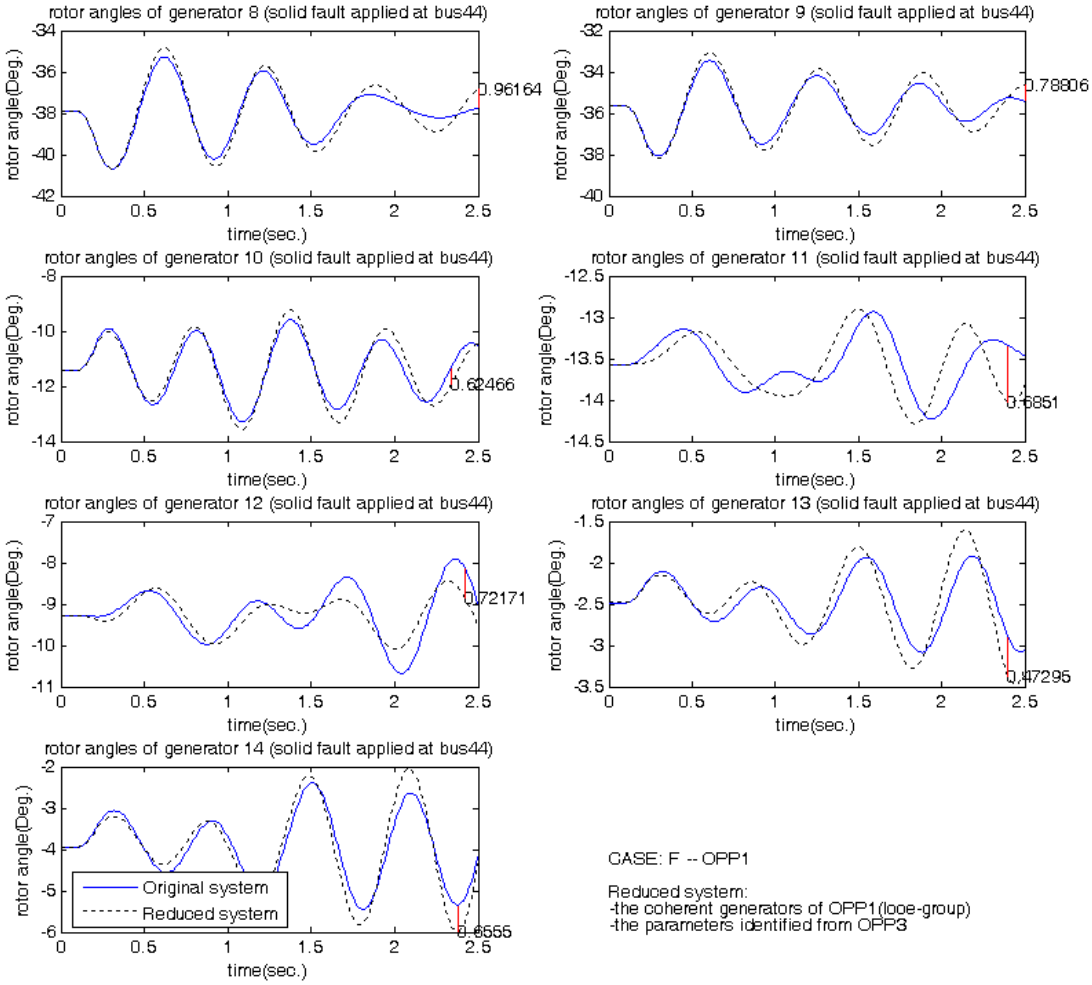

APPENDIX D: EXACT COHERENCY THEOREM

'*Consider a graph G described by the matrix pair (**L**, **M**), having modes ($\boldsymbol{\Lambda}$, **U**), where* $\boldsymbol{\Lambda}$ *=diag (* $\lambda_1,\ldots,\lambda_n$ *) and* $\mathbf{U}=[\ \mathbf{u}_1,\ldots,\mathbf{u}_n\ ]$*. Let* $\nu_q=\{V_1,\ldots,V_q\}$ *be a q-partition of G where each area* V_i *has size* n_i*, with* $n_1+\cdots+n_q=n$*. Let* $\boldsymbol{X}$*=diag (* $\mathbf{1}_{n_1},\ldots,\mathbf{1}_{n_q}$ *) be the corresponding* $n\times$ *q partition matrix. Let the aggregate graph* $G[\nu_q]$ *be described by the matrix pair (*$\boldsymbol{L}_{[q]}$, $\boldsymbol{M}_{[q]}$ *) given by*

$$\boldsymbol{L}_{[q]}=\boldsymbol{X}^T\boldsymbol{L}\boldsymbol{X}=\begin{bmatrix}\delta_1 & -\xi_{12} & \cdots & -\xi_{1q}\\ -\xi_{21} & \delta_2 & \cdots & -\xi_{2q}\\ \vdots & \vdots & \ddots & \vdots\\ -\xi_{q1} & -\xi_{q2} & \cdots & \delta_q\end{bmatrix}\qquad \boldsymbol{M}_{[q]}=\boldsymbol{X}^T\boldsymbol{M}\boldsymbol{X}=\begin{bmatrix}M[1] & & \\ & \ddots & \\ & & M[q]\end{bmatrix}$$

having modes ($\boldsymbol{\Theta},\mathbf{C}$*), where* $\boldsymbol{\Theta}=diag(\theta_1,\ldots,\theta_q)$ *and* $\mathbf{C}=[\ \mathbf{c}_1,\ldots,\mathbf{c}_q\ ]\in R^{q\times q}$*. Let* $F=\{\ \theta_1,\ldots,\theta_q\}$ *be the chord of frequencies of interest. And let* $\mathbf{L}=\hat{\mathbf{L}}+\tilde{\mathbf{L}}$ *be the* ν_q*-induced splitting of the Laplacian matrix* $\boldsymbol{L}$*.*

Then the graph $\boldsymbol{G}$ *is (*ν_q*, F)-coherent if, and only if,*

$$\tilde{\mathbf{L}}_i=\frac{\delta_i}{M[i]}\mathbf{M}_i, \qquad i=1,\ldots, q$$

and

$$\tilde{\mathbf{L}}_{ij}\mathbf{1}_{nj}=-\frac{\xi_{ij}}{M[i]}\underbrace{\mathbf{M}_i\mathbf{1}_{ni}}_{\mathbf{m}_i}=-\frac{\xi_{ij}}{M[i]}\mathbf{m}_i\ ,$$

Theorem 5.16, p.114-115, Ayazifar[9]

APPENDIX E: SLOW COHERENCY ALGORITHM

"In the slow coherency algorithm, the user selects the number r of coherent groups. Then the eigenvector matrix $\mathbf{V}_S$ *of the r lowest frequency modes is computed. Coherency is determined by comparing the angles between the row vectors* $\mathbf{v}_i$ *of* $\mathbf{V}_S$*. The machines corresponding to the 'most' linearly independent vectors* $\mathbf{v}_i$ *are selected as the reference machines. A non-reference machine with the vector* $\mathbf{v}_j$ *is then grouped with the reference machine whose* $\mathbf{v}_i$ *makes the smallest angle with* $\mathbf{v}_j$*."*

EPRI, p.2-2 [18]

"Step1: Choose the number of groups and the slow modes σ_a

Step2: Compute a basis matrix $\mathbf{V}_S$ *of the* σ_a*-eigenspace for a given ordering of the state variables.*

Step3: Apply Gaussian elimination with complete pivoting to $\mathbf{V}_S$ *and obtain the set of reference states.*

Step4: Compute $\mathbf{L}_d$ *for the set of reference states chosen in step 3.*

Step5: Construct the matrix $\mathbf{L}_g$ *which defines the states in each area"*

Chow, p.120 [2]

Where $\mathbf{L}_d = \mathbf{V}_2 \mathbf{V}_1^{-1}$

$\mathbf{V}_1$ *- the matrix of reference vectors (* $\mathbf{v}_i$ *)*

$\mathbf{V}_2$ *- the matrix of non-reference vectors (* $\mathbf{v}_i$ *)*

$\mathbf{L}_g$ *is found to minimize* $\left\| \mathbf{L} - \mathbf{L}_g \right\|$

APPENDIX F: TOLERANCE-BASED SLOW COHERENCY ALGORITHM

In the tolerance-based algorithm, two machines are coherent if the angle made by their corresponding $\mathbf{v}_i$ *are less than* $\cos^{-1}(\gamma)$. *The procedure starts by computing a coherency matrix*

$$\mathbf{C_m}(i,j) = \mathbf{v}_i \mathbf{v}_j^T \Big/ \left(\|\mathbf{v}_i\| \|\mathbf{v}_j\| \right) \quad - \gamma$$

Where the tolerance, $\gamma < 1$, *is selected by the user. Machine i and j are said to be coherent if* $\mathbf{C_m}(i,j) > 0$.

The key idea in the tolerance-based algorithm is the concept of loose coherent areas and tight coherent areas. In a loose coherent area, a machine is coherent to at least on other machine. In a tight-coherent area, the coherency of machines is larger, on the average, than the tolerance. Unlike the slow coherency algorithm, the number of loose or tight areas is not limited to be the same as ***r****, the number of columns in* $\mathbf{V}_S$. *The total number of coherent groups found from the algorithm may be several times larger than* ***r****.*

The loose and tight coherent areas are determined using a set of coherency rules. The rules are listed in the following. Let $\mathbf{C_m}$ *be the coherency matrix and* J_α *be the machines in coherent area* α.

1. *Machines i and j are coherent if* $\mathbf{C_m}(i,j) > 0$.
2. *If machines i and j are coherent and machines j and k are coherent, then machines i and k are also coherent.*
3. *A loose coherent area is formed by machines that are coherent under Rules 1 and 2.*
4. *Extract a submatrix* $\mathbf{C_{m\alpha}}$ *from* $\mathbf{C_m}$ *for all the machines in a coherent area* J_α. *Under Rule 2, some* $\mathbf{C_{m\alpha}}(i,j)$ *may be negative.*

5. *If all entries of $\mathbf{C}_{\mathbf{m}\alpha}(i, j)$ are positive, then J_α is a packed area.*
6. *If the column sums of $\mathbf{C}_{\mathbf{m}\alpha}(i, j)$ excluding the diagonal entries are all positive, then J_α is a tight coherent area. In a tight coherent area, a machine is coherent, on the average, to every other machine in the same area. From Rule 5, a packed area is also a tight area.*
7. *If any of the column sums of $\mathbf{C}_{\mathbf{m}\alpha}$ excluding the diagonal entries is negative, then J_α should be decomposed into tight areas.*
8. *The least coherent machine in a loose-coherent group is the one corresponding to the columns of $\mathbf{C}_{\mathbf{m}\alpha}$ with the smallest off-diagonal sum.*
9. *The coherency of an area may be improved by removing the least coherent machine from the area and reassigning it to a different area to achieve a tighter coherency.*
10. *Given two partitions I1 and I2 of a loose-coherent area, the partition I1 is tighter than I2 if the sum of the off-diagonal entries of $\mathbf{C}_{\mathbf{m}\alpha}$ corresponding to I1 is smaller than that of I2.*

Based on these coherency rules, the following algorithm for tight coherency is coded in DYNRED:

1. *Find the loose coherent area using Rules 1-3.*
2. *For each coherent area,*
    (a) *Use Rule 6 to determine tight area, which requires no further decomposition.*
    (b) *If the area is not tight, decompose the area into tight coherent areas. Start by identifying the least coherent machine in the area using Rule 8 and reassigning it to improve the coherency using Rule 10. Repeat the process until no improvement is possible.*

As an illustration of finding the tight coherent areas from the loose coherent areas, consider the following example. Let $\mathbf{C}_{\mathbf{m}\alpha}$ denote a loose coherent area

$$C_{m\alpha} = \begin{bmatrix} + & + & + & - & - & - \\ + & + & + & + & - & - \\ + & + & + & + & + & - \\ - & + & + & + & + & + \\ - & - & + & + & + & + \\ - & - & - & + & + & + \end{bmatrix}$$

Where positive and negative numbers are denoted by + and - , respectively. Find the off-diagonal row sum of each row. Suppose row 1 yields the smallest sum which is negative. Then a partition of $\mathbf{C}_{m\alpha}$ *into 2 areas yields a tighter coherency*

$$C_{m\alpha} = \left[\begin{array}{c|ccccc} + & + & + & - & - & - \\ \hline + & + & + & + & - & - \\ + & + & + & + & + & - \\ - & + & + & + & + & + \\ - & - & + & + & + & + \\ - & - & - & + & + & + \end{array}\right].$$

In the next step, for each area, find the least coherent machine, which we assume to be machine 2. At this point, there are three possibilities:

1. *Leave machine 2 with the same group,*
2. *Let machine 2 form a single-machine area,*
3. *Move machine 2 to be coherent with machine 1.*

For each of the possibilities the off-diagonal block sums are computed as illustrated in the following expressions

$$(C_{m\alpha})_1 = \left[\begin{array}{c|ccccc} + & \oplus & \oplus & \ominus & \ominus & \ominus \\ \hline + & + & + & + & - & - \\ + & + & + & + & + & - \\ - & + & + & + & + & + \\ - & - & + & + & + & + \\ - & - & - & + & + & + \end{array}\right].$$

$$(C_{m\alpha})_2 = \left[\begin{array}{cc|ccc} + & \oplus & \oplus & \ominus & \ominus & \ominus \\ + & + & \oplus & \oplus & \ominus & \ominus \\ \hline + & + & + & + & + & - \\ - & + & + & + & + & + \\ - & + & + & + & + & + \\ - & + & + & + & + & + \end{array}\right].$$

$$(C_{m\alpha})_3 = \left[\begin{array}{cc|ccc} + & + & \oplus & \ominus & \ominus & \ominus \\ + & + & \oplus & \oplus & \ominus & \ominus \\ \hline + & + & + & + & + & - \\ - & + & + & + & + & + \\ - & - & + & + & + & + \\ - & - & + & + & + & + \end{array}\right].$$

The off-diagonal block elements to be added are circled. Since the matrix $\mathbf{C}_{m\alpha}$ *is symmetric, the low triangular part need not be added. Of three possibilities, the partition with the smallest sum yields the tight coherency. The iterative shifting process terminates if the partition does not change further.*

EPRI, p.2-3, 2-4, 2-5 [18]**.**

APPENDIX G: ESTABLISHING A-MATRIX OF A LINEARISED POWER SYSTEM MODEL

A-matrix of a linearised power system model

Step 1: Perform Power-flow analysis

Step 2: Calculate the generator internal bus voltages (i.e. magnitude and angle)

Step 3: Record an admittance matrix (Ybus) and all bus voltages (including the generator internal buses).

Step 4: Convert a PQ-load to a constant admittance and add it to the recorded admittance matrix (Ybus).

Step 5: Build a new admittance matrix of power system including the generator internal buses from the recorded admittance matrix and the generator D-axis transient reactance.

Step 6: Eliminate all buses excluding the generator internal bus in the new admittance matrix by using Kron reduction.

Step 7: Build a Laplacian matrix whose entries are calculated according to equation (5) in the section 3.3.1 from an imaginary part of the reduced admittance matrix and the record voltages.

Step 8: Build a normalised generator inertia matrix

Step 9: Calculate A-matrix by multiplying the Laplacian matrix (step 7) by an inverse of the normalized generator inertia matrix (step 8).

APPENDIX H: ESTABLISHING LAPLACIAN MATRIX FOR A GRAPH MODEL OF A POWER SYSTEM

Laplacian matrix for a complete graph (i.e. up to the generator internal bus)

Step 1: Perform Power-flow analysis

Step 2: Calculate the generator internal bus voltages (i.e. magnitude and angle)

Step 3: Record an admittance matrix (Ybus) and all bus voltages (including the generator internal buses).

Step 4: Convert a PQ-load to a constant admittance and add it to the recorded admittance matrix (Ybus).

Step 5: Build a new admittance matrix of power system including the generator internal buses from the recorded admittance matrix and the generator D-axis transient reactance.

Step 6: Go to step 8 if a full graph is required, otherwise continue step 7

Step 7: Eliminate all buses excluding the generator internal bus in the new admittance matrix by using Kron reduction.

Step 8: Build a Laplacian matrix whose entries are calculated according to equation (5) in the section 3.3.1 from an imaginary part of the latest admittance matrix and the record voltages.

Laplacian matrix for a partial graph (i.e. up to the generator terminal bus)

Step 1: Perform Power-flow analysis

Step 2: Record an admittance matrix (Ybus) and all bus voltages (i.e. magnitude and angle).

Step 3: Convert a PQ-load to a constant admittance and add it to the recorded admittance matrix (Ybus).

Step 4: Go to step 6 if a full graph is required, otherwise continue step 5

Step 5: Eliminate all buses excluding the generator terminal bus in the admittance matrix by using Kron reduction.

Step 6: Build a Laplacian matrix whose entries are calculated according to equation (5) in the section 3.3.1 from an imaginary part of the latest admittance matrix and the record voltages.